DOCTOR OF PHILOSOPHY

Suspended sediment dynamics and flux in the macrotidal Taf estuary, South Wales.

Ishak, Abdul Kadir

Award date:
1997

Awarding institution:
Bangor University

SUSPENDED SEDIMENT DYNAMICS AND FLUX IN THE MACROTIDAL TAF ESTUARY, SOUTH WALES

By

Abdul Kadir bin Ishak

A thesis submitted to the University of Wales

for the Degree of Doctor of Philosophy

School of Ocean Sciences
University of Wales,
Bangor

August 1997

SOME PARTS
EXCLUDED
UNDER
INSTRUCTION
FROM THE
UNIVERSITY

ABSTRACT

Vertical profiles of suspended sediment concentration (using transmissometers), current velocity, salinity, and temperature were measured over neap-spring tidal cycles at various locations in the macrotidal Taf estuary, South Wales. These measurements were supplemented by spatial surveys carried out during high water along the longitudinal axis of the estuary

The measurements reveal that a turbidity maximum with maximum suspended sediment concentrations over 600 mg/l occurs at the limit of salt water intrusion in the upper estuary. This turbidity maximum forms as a result of resuspension of bottom sediment by fast tidal currents as the flood tide sweeps through the estuarine channel and over the intertidal flats. This maximum is however an ephemeral feature as it grows and decays with the increase and decrease of the tidal prism over a lunar cycle.

Sediment transport across the estuary profile shows large variations with the greatest transport in the main channel and least transport on the intertidal sand flats. These variabilities reflect the strength of the tidal currents operative in different parts of the estuarine cross section. Flood transport is dominant over ebb transport during both spring and neap tides. Of the three transport equations tested for their reliability, the Engelund and Hansen (1967) equation gives a good overall agreement with the measured transport rate, followed by the Hardisty (1983) equation, while the Jago and Mahamod (1997) equation shows the most inconsistent results compared to the measured transport. All equations overestimate transport at high flow velocities. The Jago and Mahamod equation has been improved by varying the value of the exponent n depending on current velocity; a lower value for fast currents and a higher value for slow currents.

Central to this study was the measurement of sediment flux at two transects across the lower estuary. A balanced water flux which is a prerequisite for the calculation of sediment flux was obtained for both transects. The tidal prism varies linearly with tidal range. The sediment flux (mostly of fine sand) varies exponentially with tidal range and the gross flood flux is 10 - 30 % higher than the gross ebb flux; thus there is a net sediment (fine sand) accumulation in the estuary. The annual sand sedimentation rate estimated from the flux measurement is 1.2 - 1.6 cm/year. These values are very similar to the accumulation rates (1.8 cm/yr) previously obtained from the long term measurement of the sand budget by estimating the volumetric change of the sand body by regular transect surveys.

The accretion rate of the salt marsh has been determined using ^{137}Cs radioisotope dating. The ^{137}Cs peaks which correspond to 1963 (the peak fallout from the nuclear weapon testing) and 1986 (the Chernobyl nuclear accident) can be recognised in the sediment cores. The mean accretion rate calculated from these peaks is 1.0 cm/yr.

To my wife Rohaya, sons Muhammad Akram and Muhammad Shafiq, and daughters Maisarah and Anisah for their enduring patience.

It is He Who has let free the two bodies of flowing water: one palatable and sweet, and the other salt and bitter; yet has He made a barrier between them, a partition that is forbidden to be passed.
(Al-Quran, XXV, 53)

He has let free the two bodies of flowing water, meeting together. Between them is a barrier which they do not transgress.
(Al-Quran LV, 19-20)

Nor are the two bodies of flowing water alike, - The one palatable, sweet, pleasant to drink, and the other, salt and bitter. Yet from each (kind of water) do ye eat flesh fresh and tender, and ye extract ornaments to wear; and thou seest the ships therein that plough the waves, that ye may seek (thus) of the Bounty of God that ye may be greatful.
(Al-Quran, XXXV, 12)

ACKNOWLEDGEMENT

IN THE NAME OF ALLAH, THE MOST GRACIOUS, THE MOST MERCIFUL

There are many people to whom I am indebted for their advice, assistance and support, which has enabled me to bring this thesis into reality.

My principal thanks go to my supervisor, Dr. Colin Jago; both for his major input to the work, and for his patience and support throughout my study period. His help, encouragement and critical assessment have been invaluable, and is reflected in both completion and content of this thesis. I also wish to thank the help and support given by other members of my supervisory committee; Dr. Sarah Jones, Dr. Garry Reid and Dr. Dew Huws.

My thanks also go to all the members of the technical staff who helped brilliantly in the field work and in the laboratory, in particular Alan Nield, Gwyn Jones and Geraint Wiliams.

I wish to acknowledge many students of the School of Ocean Sciences for their help and assistance in sampling programmes.

I wish to thank my colleagues who helped me at various stage of my study, in particular to Joseph Cheok (Dr) who taught me many tricks in data processing and brought them into nice plots, and to Chris Bull and Paul Rampling who helped with particle size analysis and field data collection.

I am also grateful to Dr. David Assinder for access to the radioisotope counting facilities and for help in the interpretation of caesium results.

The river discharge data for the Taf have been provided by Environmental Agency (previously National River Authority) and is gratefully acknowledged.

Most of all I would like to thank my parents and all my family who have stood behind all my education and career. I could not have achieved this without their guidance, support and prayers.

Finally, I wish to acknowledge the study leave given by Malaysian Institute for Nuclear Technology Research (MINT) and the financial support from Public Service Department of Malaysia, which enabled me to carry out and complete my study.

CONTENTS

Notations and Symbols

A	Area
B	Dimensionless property of the flow near the bed
c	Beam attenuation coefficient
C	Suspended sediment concentration
C_D	Drag coefficient
C_L	Coefficient in lift force expression
C_{100}	Drag coefficient at 100 cm above the bed
d	Ripple's height
D	Grain diameter
D_{gr}	Dimensionless grain diameter
F	Froude number
F_D	Drag force
F_G	Gravity force
F_{gr}	Sediment mobility number
F_L	Lift force
g	Gravitation acceleration
G_{gr}	Sediment transport parameter
h	Water depth
H	Cross sectional area
I_o	Light intensity at the source
I_r	Light intensity at distance r from the source
K	Efficiency factor
k_1	Proportionality coefficient (Equation 2.33)
k_2	Empirical constant (Equation 2.37)
k_3	Entrainment function (Equation 2.48)
m	Exponent in sediment transport equation (Equation 2.42)
n	Exponent number
q	Transport rate of sediment
Q_e	Total mass transport for the ebb tide
Q_f	Total mass transport for the flood tide
Q_t	Instantaneous mass transport
Q_T	Total suspended sediment flux
r	Path length of beam transmittance.
R	Coefficient in sediment transport equation (Equation 2.42)
Re	Reynolds number
Re_*	Grain or boundary Reynolds number
S	Dimensionless access shear stress (Equation 2.34)
t	Beam transmission
T	Initial motion parameter
u	Horizontal velocity
u_0	Horizontal velocity near the bed (at z_0)
u_{100}	Velocity at 100 cm above the bed
u_*	Friction or shear velocity
W_s	Particle settling or fall velocity

z	Vertical coordinate component
z_o	Bed roughness length
β	Constant
δ	Boundary layer thickness
δ_L	Viscous sublayer thickness
Φ	Dimensionless sediment discharge
κ	Von Karman's constant
λ	Ripple's wave length
θ	Shield's Entrainment Function
θ_c	Threshold value of Shield's Entrainment Function
μ	Molecular viscosity
ν	Kinematic viscosity of fluid = μ/ρ
Ξ	Yalin parameter
ρ	Water density
ρ_s	Density of sediment particles
τ	Shear stress
τ_{100c}	Critical shear stress at 100 cm above the bed
τ_0	Bed shear stress
ω	Stream power
ζ	Horizontal area
Δt	Time interval
Δx	Depth function

List of Figures

APPENDIX C

List of Tables

CHAPTER ONE

INTRODUCTION

1.1 Motivation for estuary studies

Estuaries are of considerable interest to mankind, due to their great social and economic importance. Many cities and industries are located on their shores, and harbours are built within estuaries for commerce and pleasure. Estuaries are also important as a source of food supply and therefore are areas of special conservation value. As natural water systems, estuaries serve to supply transport facilities within a small geographical area. With increasing development, larger human communities are situated on the banks of the lower reaches of estuaries. These communities exert changes in the hydrodynamics and quality of estuarine waters due to local coastal defence works, dredging of harbours and estuarine waterways, and discharges of industrial effluent and sewage. The construction of dams in the upper part of catchment areas can also introduce changes in hydrodynamic regime and water quality by reducing flow, dilution, and subsequent flushing of the sediment onto the adjacent shelf. The influence of man on estuaries can thus be very strong and increasingly it is becoming necessary to achieve a balance between the demand for human progress and the need to preserve the natural and unique features of estuaries.

Estuaries are a distinct environment, with their unique physical, chemical and biological complexity and variability. They mark the transition between the fluvial and marine regimes and, as part of the sedimentary cycle, they function either to trap or convey sediment between the land and the sea. Therefore sediment forms a crucial link in estuarine processes; it silts up harbours and navigation channels, and influences pollutant transport. Water motion in estuaries is determined by tides, river discharge, wind and waves. Chemical processes are influenced by variations in salinity, pH and dissolved oxygen concentration, while biological processes can be modulated strongly by hydrodynamics, chemistry and interaction between particles (West, 1994). The dynamics and flux of sediments,

particularly suspended sediments, therefore play a crucial role in a range of biogeochemical processes.

Much of the previous research in estuary studies has concentrated on a need to resolve a certain human requirement, for example for shipping and waste disposal as opposed to use as a recreational outlet or food sources. Far more effort has gone into detailed engineering, fishing, and pollution studies than into generalizing and understanding estuaries as a sedimentary environment (Nicholls and Biggs, 1985). The importance of integrated estuaries studies has been recognised, at least in the U.K. since 1983, when NERC (Natural Environment Research Council) produced a handbook designed to tackle a multidisciplinary approach to elucidate the fundamental processes that characterise the estuarine ecosystem (NERC, 1983).

Another fully-integrated estuarine study is within the framework of LOIS (Land-Ocean Interaction Study) funded by NERC (NERC, 1994). The main objective of this project is to improve the present understanding of multidisciplinary processes in catchments, estuaries and coastal oceans by developing a modelling capability incorporating sediment and solute transport. The main focus of this project is in the Humber estuary where the measurement and modelling of sediment flux through its mouth is being undertaken. This should provide a major contribution to the quantitative understanding of estuarine and coastal zone processes in transporting particle fluxes and other biologically important elements and contaminant from land sources to the coastal zone. However, there are 134 estuaries (excluding 30 or so sea lochs on the west coast of Scotland) of length greater than 5 km in the U.K. (Gameson, 1973). Most of these estuaries appear to be well-mixed or partially stratified, with replacement times that range from approximately one tidal cycle for the smallest one to greater than 200 days for the largest (Severn), under low flow condition (Morris, 1983). There is therefore considerable variation in the nature and scale of processes within estuaries.

There is thus a need for measurements of dynamics and fluxes in several estuaries of different type if the scale and variation of processes in the estuarine and coastal zone is to be understood.

1.2 Background and objectives of the study

A small, macrotidal, sandy estuary was chosen for this study. The Taf estuary was selected for several reasons: (1) there is a basic data set which shows that the estuary is presently infilling with sand from offshore; (2) the dynamics of the estuary are dominated by tidal currents, with the influence of river flow and waves being of secondary importance; (3) the sediment infill is predominantly sand of very uniform texture. This estuary therefore presented a relatively simple dynamic and sedimentological case study for a sediment flux experiment.

The first major study of the Taf estuary was carried out by Jago (1974) where changes in estuarine bed profiles, variations in sediment textures, and various aspect of estuarine hydrodynamics were reported. Subsequent studies (Jago, 1980) have shown that the estuary is being infilled with sand and periodically-levelled transects within the estuary indicate that there has been a net rise in volume of sand within the estuary since 1968. The texture, mineralogy and composition of these estuarine sands are identical to those of Carmarthen Bay, and it is proposed that they were brought into the estuary mouth by south-westerly storms and pumped subsequently into the estuary by strong tidal currents (Jago, 1980). Since then the area has been resurveyed frequently and a pilot study of suspended sediment fluxes has been carried out to determine the subsequent volumetric change of estuarine sediment. Based upon these measurements, the following infilling rates have been proposed (Jones and Jago, 1994; Jago *et al.*, 1996):

1. From measurement of sand budget (from surveys of cross-estuary profiles, 1968-90): 0.02 m/year

2. From measurement of suspended sediment flux over a few tidal cycles: 0.04 m/year

3. From calculation using a total load sediment transport formula (Mahamod, 1989): 0.26 m/year

These studies suggested that it would be possible to make flux measurements over tidal cycles of sufficient accuracy to provide a meaningful estimate of the rate of sediment infill; this estimate could be checked against the known infill rate derived from the long-term surveying of cross-estuary profiles.

The overall aim was therefore to reconcile flux and budget measurements on different time scales, which has not been previously achieved. Therefore, the study attempted to demonstrate whether the net sediment flux from short-term flux measurement can be extrapolated meaningfully over time to give the net annual flux. Specific objectives were:

1. To assess the role of various parameters and processes, including the turbidity maximum, that control sedimentation in the Taf Estuary.

2. To measure and/or calculate the net mass transports of suspended and bedload sediment over tidal cycles.

3. To determine a sediment budget from sediment flux and sedimentation rate measurements, and to compare these with known long-term sedimentation rates of the sand flats.

4. To determine the accretion rates of salt marsh sediment that borders the margins of the estuary.

This study involved the measurement of sediment transport, sediment flux, and sedimentation rate, through the estuarine cross section over tidal cycles at different times of the year. The measurements provided hydrographic data for an accurate estimation of sediment flux, sediment budget and sedimentation rate. Furthermore, it provided data that may be used for a later calibration of a predictive numerical model of sedimentation in the estuary.

The particular hypotheses to be tested by measurement of fluxes were therefore: (1) the

estuary is infilling with marine sand from offshore; (2) the rate of infilling is of the order of 0.02 m/year.

1.3 The field site

The River Taf is located on the south coast of Wales and drains into Carmarthen Bay where it meets the rivers Towy and Gwendraeth (Figure 1.1). The estuary is fed by two main rivers, the Taf and the Cywyn. The Taf drains a basin area of about 217 km^2. The river discharge data obtained from NRA (National River Authority) for the period of 1991-1995 as measured at Clog-y-fran (Figure 1.1) gauging station showed that the daily average freshwater discharge for the Taf is 7.0 m^3/s, with extreme values of 60 m^3/s during winter months and 0.6 m^3/s during summer months. No gauging station is available for the Cywyn, but its fresh water contribution is much less than the Taf from its smaller catchment area.

The estuary is about 1.5 km at the widest point near the mouth, narrowing down to less than 40 m wide at the upper reaches near St Clears. The spring-tidal saline water penetrates up to about 15 km upstream from the mouth and forms a well-defined estuarine environment. At high water, the estuary covers an area of approximately 7.5 km^2. The lower part of estuary between Laugharne and Ginst Point it can be classified as a bar-built estuary in which the eastward extension of Pendine Sands form the coastal barrier or spit; above Laugharne, the estuary is a drowned river valley or a coastal plain type. Bordering the estuary are extensive salt marshes, mudflat and rocky headlands.

The tides are semi diurnal and show pronounced asymmetry, particularly on springs (Jago, 1980). The estuary is macro-tidal with mean tidal ranges of 7.5 m for springs and 3.7 m for neaps. Associated with the high tidal range are strong tidal currents with peak values reaching 2.2 m/s; they provide for strong mixing of salt and fresh water. Thus, the Taf estuary is generally well mixed vertically. The tidal influence in the River Cywyn reaches up to Pont-ddu, 4 km north of Laugharne, and to 3 km above St Clears in the River Taf.

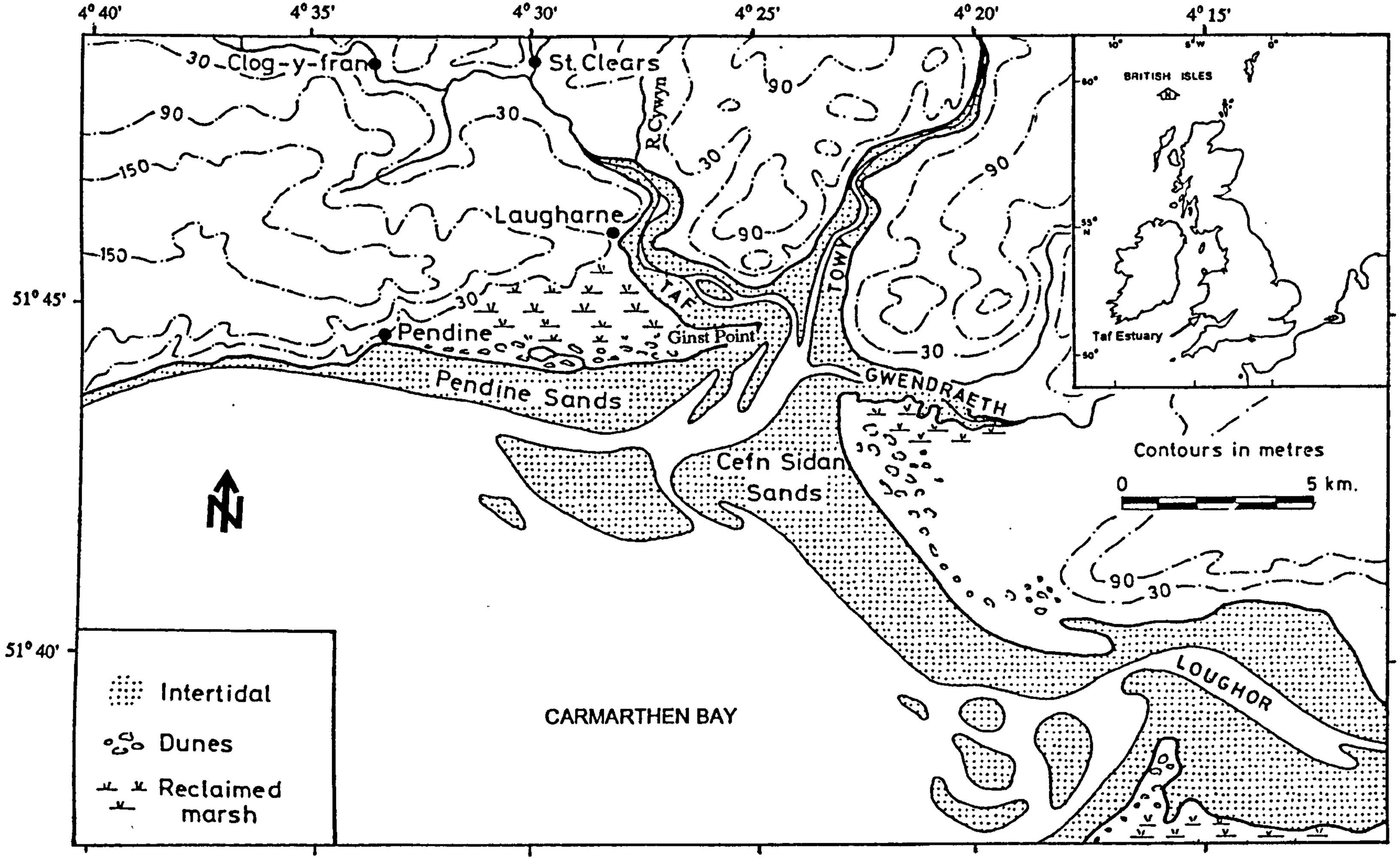

Figure 1.1 Location map of the study area.

As a result of large tidal ranges, water depth at high water during mean spring tides exceeds 6 m at the mouth, but at low tide the water in the main channel is only a few tens of centimetres deep when the salt water is totally excluded and only the river water is flowing. At low tide the estuary is effectively an intertidal flat with saltmarshes and mudflats fringing low lying sandbanks, which are dissected by a complex pattern of shallow drainage channels.

Within the estuary itself, several sub-environments are recognised; these are the sand flat, mud flat, and salt marsh (Figure 1.2), which can be differentiated by their sediment type, vegetation cover and surface and sub-surface fauna (Jago, 1974). The salt marsh occupies the highest part of the intertidal zone, followed by mudflat and sand flat in the lowest part. The salt marsh is characterised by vegetation cover, dominated by short sward and grass of *Glyceria* and *Spartina* species. The salt marsh occurs on both sides of the estuary at its upper reaches but predominantly on the right bank in the lower estuary. The width of the salt marsh varies along the estuary, ranging from tens to several hundred metres. A major part of the western side of the lower estuary has been reclaimed for agriculture purposes, but some portions of the marsh bordering the estuary still exist where it extends to a maximum width of 500 m. The sediment in the salt marsh is generally muddy; however, in the lower estuary where the marsh traps wind-blown sand from the dunes of the coastal barrier, the sediment is predominantly sandy. Numerous dendritic creeks cut thought the marshland before joining the main channel to form a distinctive feature of the salt marsh physiography.

The mud flat is defined by the absence of vegetation cover and is most developed near Laugharne; it forms a transition zone between the saltmarsh and the sand flats and normally occurs as narrow bands of 10-50 m width between the two physiographic units. The most extensive physiographic unit is the sand flat which is distributed throughout the estuary; it is characterised by low sand banks, separated by meandering ebb channels. This sand flat is exposed during the ebbing tide and is too unstable to support vegetation. Due to active sand transport, the main channel frequently changes its course, particularly off and above Laugharne where the sharp bend causes the straight current streamlines to impinge on

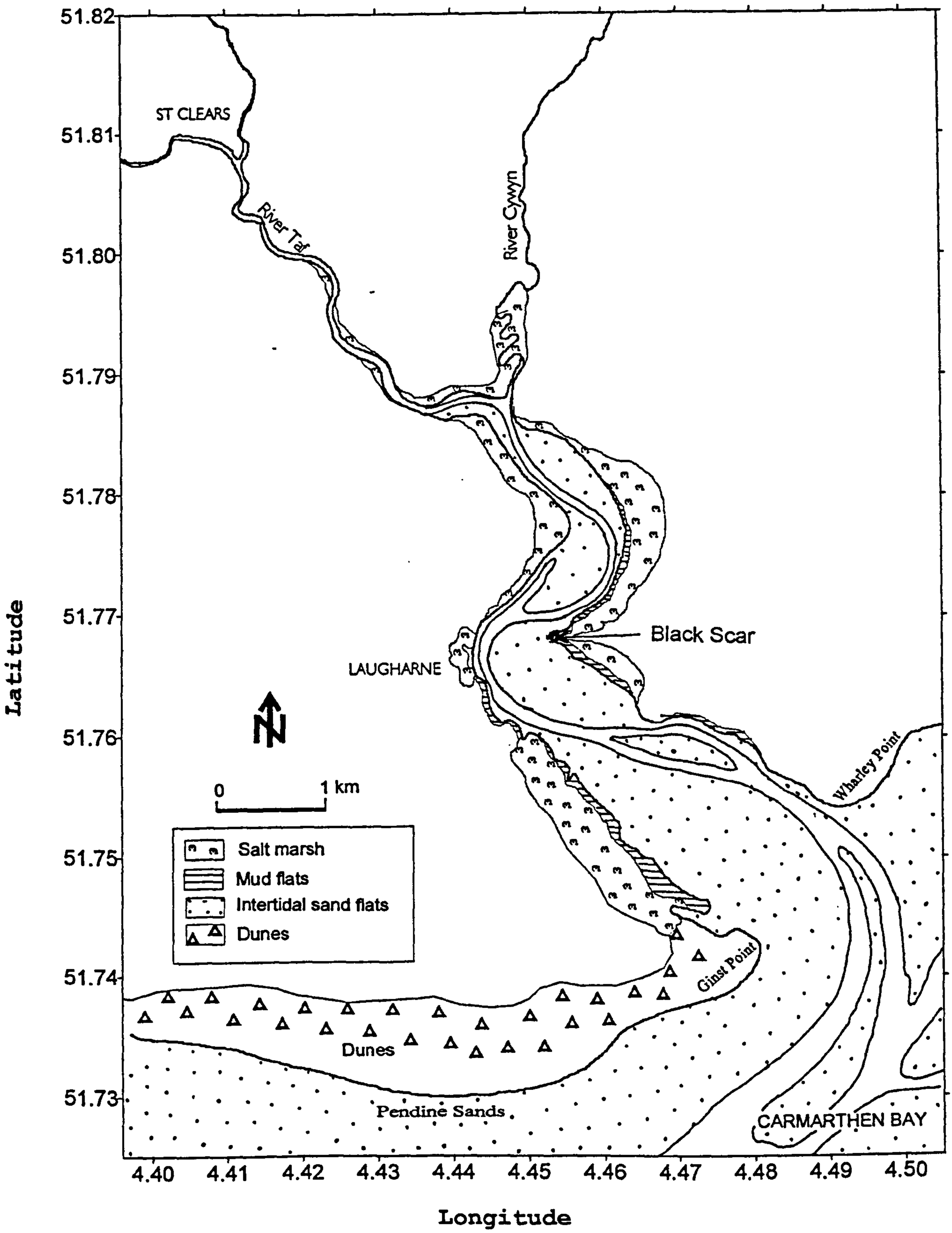

Figure 1.2 The Taf estuary, showing different physiographic units.

curved channel sides and banks. These channel migrations are described in some detail in Jago (1974), who suggests that there might be a cyclic change of the main channel from left to right banks. In the lower estuary the main channel is more stable and tends to hold to the northern side of the estuary as might be expected from consideration of the Coriolis effect. The continuous development of the sand spit near Ginst Point is also a factor where the building up of sand on the western side of the estuary prevents the main channel from changing its course. The evolution of the barrier complex on the western side of the estuary (from Pendine to the Taf estuary) was studied recently by Walley (1996). He concludes that the barrier complex which rests on a ridge of Pleistocene glacigenic sediment was formed during early Holocene (*ca* 8,000-7,000 BP), in response to the drowning of the antecedent topography by rapidly rising relative sea levels.

1.4 Geological history

The geology of South Wales has been discussed by Neville George (1970) and, more recently, has been summarised in the volume edited by Duff and Smith (1992). The geology of South Wales is dominated by a thick sequence of Palaeozoic rocks, but limited rock outcrops of Pre-Cambrian and Mesozoic ages are also present (Figure 1.3). The lower part of the Taf estuary is bordered by Old Red Sandstone of Devonian age whilst the upper estuary and the drainage basin of the Taf river consists of a low-lying Ordovician rocks which are made up of an admixture of grits, sandstones, mudtones, shales and limestone with sequence of localised volcanic tuffs and lavas of acid to basic composition. The Old Red Sandstone that borders and forms the rocky headlands of the Taf estuary is made up of tough red quartzites, often conglomeratic, with pebbles and mineral constituents of metamorphic and igneous rocks, vein quartz and greywacke, lie in sandy matrix rich in detrital feldspars. These rocks were deposited under fluviatile and deltaic conditions as apposed to the older Ordovician rocks which were deposited in a marine environment.

The most important geological event that have some relevant to the study of sediment dynamics is the glaciation in the Pleistocene period. During the Pleistocene, South Wales

was affected by two major glacial phases (Bowen, 1970; Neville George, 1970) which deposited unconsolidated glacial deposits that mask the solid rocks over much of the upland and the greater part of the lowland areas. The deposits from these two ice invasions are known as the Older Drifts and the Newer Drifts - each can be subdivided into local (Welsh) and foreign (Irish Sea) drifts. The Irish Sea Ice which deposited the Older Drifts originated from south-west of Scotland, filled the Irish Sea Basin before overflowing south-east across Pembrokeshire and came in contact with local Welsh Ice pouring southwards. The two ice sheets coalesced in the region of the Taf valley around St Clears. The limit of these drifts was traced up to Gower and reached at least as far as Cardiff (Griffiths, 1939). The second Devensian glaciation which deposited the Newer Drifts was much less extensive than the first one, and occur between about 20,000 - 18,000 BP (Cambell and Bowen, 1989). The drifts of this advance are recorded along the eastern fringe of Gower to the north of Mumbles Head, therefore just encroaching on the north-eastern and eastern flanks of Carmarthen Bay (Bowen, 1970; 1981). Griffiths (1940) suggested that the deposits in this region had lithological characteristics of the Older Drifts (mixed Irish Sea and Welsh provinces), but had been substantially reshaped by the Newer Drift Welsh Ice.

The Pleistocene glaciations created undoubtly a significant sediment accumulation in the Bristol Channel region which includes Carmarthen Bay. Within the lower Taf estuary the thickness of the Pleistocene material is between 0-20 m above the bedrock, and it shelves rapidly toward the Old Red Sandstone cliffline on the eastern side of the estuary from the south western portion (Walley, 1996). An exposure of this glacial material, known as Black Scar, can be seen on the eastern side of the estuary (Figure 1. 2) and is thought to represent either a halt stage or a slight readvance during the retreat of the Towy glacier in the late Devensian (Griffiths, 1939; Bowen, 1970). On the top of this deposit are the unconsolidated sands which have been deposited by recent processes, presumably from the reworking of the glacial sediments of the area.

1.5 Structure of the thesis

To address the objectives outlined in Section 1.2, the rest of this thesis is organised as follows:

Chapter 2 describes the fundamental physics of fluid flow, followed by a discussion on the threshold of movement for non-cohesive sediment grains. Also considered are some of the sediment transport equations used commonly for predicting transport rates in the shelf seas and intertidal environments. In the second part of the Chapter, a review is given on the source, transport, deposition and flocculation processes of estuarine sediment. Chapter 3 details the field experimental and data collection procedures. A range of instrumentations used in the study are described. Also described are the techniques employed for the processing of the data available for further analysis. The calibration of the Sea-Tech transmissometer which was the key instrument to this investigation is presented in the final section of this Chapter. Chapter 4 presents the general hydrodynamic conditions operative within the estuary. The characteristics of the tidal current velocities, estuarine water salinities, and water temperature are described. Estuarine classification based on the model proposed by Hansen and Rattray (1966) is attempted, followed by a short summary on the various factors that control the hydrodynamics of the Taf Estuary. In Chapter 5, the general characteristics of the velocity profiles within the bottom boundary layer are presented and factors affecting the observed profiles are discussed. The associated roughness length, shear velocity and drag coefficient are obtained for different bed topographies. The results of the spatial surveys where a zone of turbidity maximum was found are presented in Chapter 6; this is followed by a discussion on the dynamics of the suspended sediment over spring-neap tidal cycles. In Chapter 7 the water and sediment fluxes calculated for the two survey transects in the lower estuary are presented. A net annual sediment flux is estimated for both transects, and this is used to calculate the annual sedimentation rate of the estuary. Sediment transport rate calculations in the study area are presented in Chapter 8. The results of the measured transport rates are given in the first part of the chapter, while the sediment transport rates estimated using several transport equations are given in the second part of the chapter. The data available have given a

unique opportunity whereby the predictive capability of these equations can be tested by comparing the measured rates with rates calculated by the different formula. The data was also used to calibrate a newly formulated sediment transport equation of Jago and Mahamod (1997). Chapter 9 outlines the methodology and results of caesium analysis of sediment cores collected from the estuary saltmarsh area. Accretion rates of the marsh sediment are calculated based on the peak activity of the caesium concentration found in sediment cores. Chapter 10 concludes the thesis by summarising the main findings of the study, followed by some suggestions for future work in the area.

CHAPTER TWO

TRANSPORT PROCESSES IN TIDAL CHANNELS

2.1 Introduction

This review chapter is divided into a number of sections. After this introductory section, the basic physics of the fluid flow is described in Section 2. This is followed by a discussion on the threshold of sediment motion in Section 3. Measurement techniques of bed load and suspended load transports, and some transport equations are highlighted in Section 4. The last Section of this chapter contains a review on the estuarine sedimentary processes where the source, transport, deposition and flocculation processes are discussed. As the sediment type found in the study area is essentially well-sorted fine sands, the main focus of this review is on the non-cohesive sediment. However where appropriate, references are also made on the behaviour of cohesive sediment in the estuarine environment.

The hydraulics and mechanics of sediment transport have been the subjects of much research in laboratories, open channels and in the sea. As a result, the flow characteristic and its interaction with the bottom sediment particles that make up the loose boundary are now fairly well understood. There is a voluminous literature concerning the hydrodynamic behaviour of cohesionless granular sediment in the flow field and no review can be exhaustive. Standard texts include those of Graf (1971), Yalin (1972), Sleath (1984) and Dyer (1986). Many expressions have been developed describing the threshold of grain motions (see Komar and Miller, 1973; Miller *et al.*, 1977) and the subsequent sediment transport rates (summarised in Raudkivi, 1976), both under unidirectional and oscillatory flow, and combined wave-current interactions. The description of threshold for sediment motion and some commonly-used transport equations are discussed further in Sections 2.3 and 2.4. However, the general applicability of equations purporting to quantify sediment transport is still open to question (eg. Heathershaw, 1981; Crickmore *et al.*, 1990).

Many theoretical or empirical relationships pertaining to sediment entrainment and transport may be related to a concept of fluid stress exerted on the bed which will be discussed in the following sections.

2.2 Boundary layer flow structure

2.2.1 Water flow in the boundary layer

The nature of the motion in a moving fluid can either be laminar i.e. all particles passing a point will follow the same path and that will be the same as a stream-line, or turbulent i.e. the stream-line breaks and the particles move in random eddies within the fluid with intense lateral mixing. Turbulence results whenever there is a tangential shear at the fluid boundary, and spreads to other parts of the fluid if the Reynolds number of the flow is sufficiently large (Inman, 1963). The Reynolds number, Re is a dimensionless criterion expressing flow intensity in the zone close to the surface of the moving fluid, and is given by:

$$Re = uh/\nu \qquad [2.1]$$

where u is the flow velocity, h is the depth and ν is the fluid kinematic viscosity and $\nu = \mu/\rho$ where μ is the molecular viscosity and ρ is the density of the fluid. The Re can be thought of as the ratio of the inertial forces, which represent the resistance of the fluid mass to accelerations, to the viscous forces which resist deformation of the fluid. The critical value of Re defines the transition from laminar to turbulence condition. For pipe flow, Re has a value of about 2000 when condition ceases to be laminar, but full turbulence is not developed until an Re of about 4000 (Dyer, 1986). In rivers, turbulence develops at much lower Re values due to local disturbance (Komar, 1978).

When a fluid passes over a boundary in a laminar flow, there is a frictional drag between the fluid and the boundary. The influence of the friction extends upwards some way towards the surface of the fluid. The effect of this friction is to slow down the flow such that a

velocity gradient is created near the boundary. This produces a shear stress (designated as τ) on the successive fluid layers parallel to the boundary, whose magnitude depends on the fluid viscosity and the velocity gradient. The velocity of the moving fluid, u, increases with distance from the boundary, z, and thus the shear stress caused by fluid molecules in their movement passing between higher velocity layers and lower velocity layers can be expressed as:

$$\tau = \mu \frac{du}{dz} \qquad [2.2]$$

where μ is the fluid molecular viscosity. Fluids that conform to Equation 2.2, are called Newtonian fluids. However, flows in all natural waters are almost always turbulent; laminar flow occurs only for slow currents or for very small depths.

Because of the development of eddies in turbulent flow, fluid particles are able to move in all directions about the net direction of flow. The velocities can be separated into three orthogonal components; the u-component is horizontal, parallel to the flow direction; the v-component is horizontal but at right angle to the net flow direction; the w-component is vertical. The resulting turbulent shear stress is much greater than the shear stress that exists in the laminar flow, and has been experimentally shown to be proportional to the square of the time averaged velocity u, thus:

$$\tau \propto u^2 \qquad [2.3]$$

It is convenient to express shear stress in a term that has the units of velocity. This term is called the friction velocity u_*, and is derived from bed shear stress τ_0 and the fluid density ρ such that:

$$u_* = \sqrt{\frac{\tau_0}{\rho}} \qquad [2.4]$$

or $$\tau_0 = \rho u_*^2 \qquad [2.5]$$

The concept of fluid flow in pipes is equally applicable to the water flow in channels. When water flows over sediment lying on a bed, there is a frictional drag caused by the sediment which acts to retard the flow velocity towards the surface of the water. This retardation is greatest near the bed, but gets less further away into the body of the flow. The lower part of the flow which experiences frictional retardation is known as the boundary layer which in the shelf seas has a thickness (δ) of typically a few tens of metres. In water that is sufficiently shallow such as on continental shelves or in estuaries, the boundary layer occupies the entire water depth ($\delta = h$) and it is said to be fully developed (Figure 2.1a). The current speed increases with height from zero at the bed to its value at the water surface. In deeper water, with weaker currents, the boundary layer thickness δ, is less than the water depth h (Figure 2.1b). The current speed increases systematically with height z until at about $z = \delta$, it attains the frictionless free-stream velocity, u_∞, within which the vertical velocity gradient is zero up to the water surface.

The boundary layer can be subdivided into a number of layers (Figure 2.1a). Very close to the bed is the viscous (laminar) sublayer. The layer is typically of the order of a few millimetres thick but varies according to the current speed and the size of the roughness element present at the bed. Over a relatively smooth, flat bed, the flow in the viscous sublayer is laminar (but the vertical profile of mean velocity is linear) and the molecular viscosity dominates the dynamics. In the presence of roughness elements, the sublayer breaks and the turbulent conditions extend right down to the bed. Above the viscous layer and below the overlying fully turbulent layer is a transitional or buffer, layer. Above this is the logarithmic layer in which the velocity profile is logarithmic with height and neither the details of the bed nor the nature of the free stream flow affect the local dynamics. It generally extends a few metres above the bed. Above this again is the outer layer, in which the velocity and turbulence profiles depend strongly on the nature of the free stream flow, and are thus not universal. Reviews of the benthic boundary layer have been made by Wimbush and Munk (1970), Bowden (1978), Komar (1978), and Soulsby (1983; 1990).

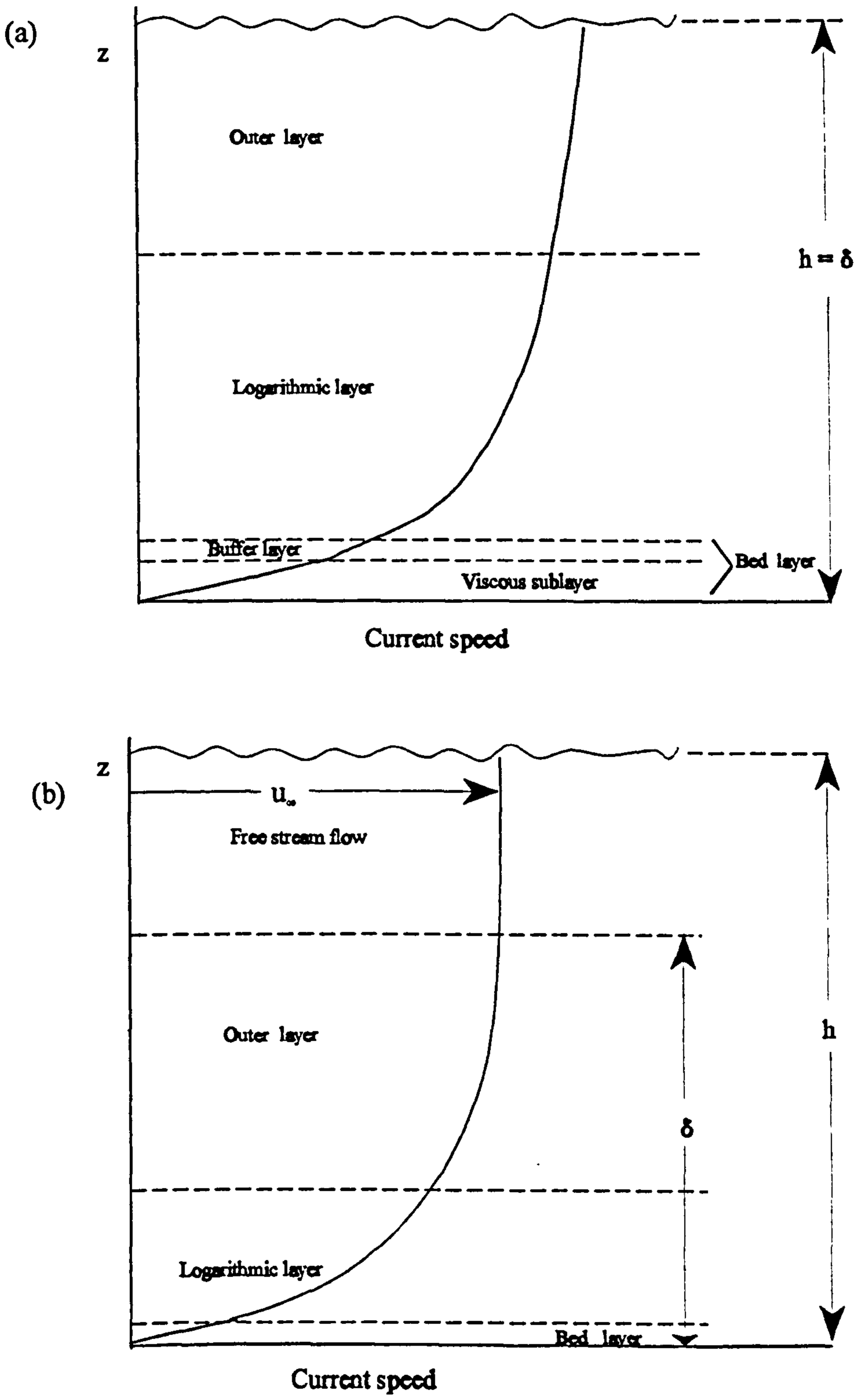

Figure 2.1 Schematic diagram of the sub-division of the boundary layer for smooth bed. (a) The shallow case in which the boundary layer occupy the entire water depth. (b) The deep case in which the water is deeper than the boundary layer thickness. The thicknesses of the layers are not to scale (After Soulsby, 1983).

The shear stress within the viscous sublayer is constant and the flows are dominated by viscous forces. Inserting the definition of the friction velocity in Equation 2.2, gives:

$$u_*^2 = \nu \frac{du}{dz} \qquad [2.6]$$

where ν is kinematic viscosity $= \mu/\rho$, and by integration Equation 2.6 gives:

$$\frac{u}{u_*} = \frac{zu_*}{\nu} \qquad [2.7]$$

The ratio of kinematic viscosity to friction velocity is a length scale that is used to described the thickness of the laminar sublayer $\delta_L = \nu/u_*$. The viscous sublayer becomes thinner as the velocity gradient increases.

Any mechanical quantity related to the near bed flow is a dimensionless function of four independent variables: the water density ρ, water molecular viscosity μ, shear velocity u_* and sediment grain diameter, D forming the bed roughness (Yalin, 1972). These can be combined to produce a dimensionless variable Re_*, the shear or boundary Reynolds number:

$$Re_* = \frac{u_* D}{\nu} = \left(\frac{\tau_0 D}{\rho \mu}\right)^{1/2} \qquad [2.8]$$

Re_* is important in describing the flow property in the near bed layer which can also be equally described by the ratio of size D to the thickness of the viscous sublayer (D/δ_L).

In the turbulent layer the friction velocity or shear velocity is related to the distance from

the bed by:

$$\frac{du}{dz} = \frac{1}{\kappa}\frac{u_*}{z} \qquad [2.9]$$

where the constant κ is known as the von Karman constant. The value of κ has been measured in the sea by several experimenters (see Soulsby, 1983). The results do not differ significantly from those found in the laboratory, and a general purpose figure can be taken as $\kappa = 0.40$. It was suggested some years ago that the value of κ is reduced by the presence of suspended sediment (eg. Gust and Walger, 1976), but the modern interpretation is that modifications to the velocity profile can be explained in terms of density stratification while retaining the value $\kappa = 0.40$ (Soulsby, 1990). Integration of Equation 2.9 over the interval z_0; z gives:

$$\frac{u}{u_*} = \frac{1}{\kappa}\ln\frac{z}{z_0} + \frac{u_0}{u_*} \qquad [2.10]$$

where u_0 is the value of u at z_0, i.e. the roughness height of the boundary. The behaviour of Equation 2.10 for different values of Re_* can be predicted for small and large values of D/δ_L (Yalin, 1972). A more general form of Equation 2.9 can be written as:

$$\frac{u}{u_*} = \frac{1}{\kappa}\ln\frac{z}{D} + B \qquad [2.11]$$

The quantity B is a dimensionless property of the flow near the bed and its value depends on the magnitude of D/δ_L or Re_*. The value of B was obtained from pipe flow experiments by Nikuradse (1933) as shown in Figure 2.2. It shows that the flow in the near bed layer can

be classified into three regimes:

i. smooth turbulent regime : when $u_*D/\nu < 5$

ii. rough turbulent regime: when $u_*D/\nu > 70$

iii. transitional regime: when $5 < u_*D/\nu < 70$

For $Re_* > 70$ the value of $B = 8.5$ and for $Re_* = 0.0$, the value of $B = 5.5$. For the case of transitional regime the values of B is an unknown function of Re_* and can be estimated from the curve in Figure 2.2. The slope of the straight line in Figure 2.2 is equal to $1/\kappa$, thus giving the von Karman constant $\kappa = 0.40$.

Figure 2.2 Nikuradse's experimental relation between B and log Re_* (Yalin, 1972).

In the smooth regime, the roughness elements are completely immersed within the viscous sublayer. The velocity distribution is independent of the size and nature of the roughness and is given by:

$$\frac{u}{u_*} = \frac{1}{\kappa} \ln \frac{zu_*}{\nu} + 5.5 \qquad [2.12]$$

The thickness of viscous sublayer δ_L may be estimated from the intersection of the profiles given by Equations 2.7 and 2.10, hence;

$$\delta_L = 11.6\frac{\nu}{u_*} \qquad [2.13]$$

In the rough regime, turbulence extends into the spaces between the roughness elements and no viscous sub-layer is present. This is termed fully developed turbulent flow. The bed shear stress is transmitted by form drag and skin friction on the individual roughness elements. The mean velocity distribution is given by:

$$\frac{u}{u_*} = \frac{1}{\kappa}\ln\frac{z}{D} + 8.5 \qquad [2.14]$$

However, the value of B in fully developed turbulent flow over a rough boundary varies with the type of surface roughness (Raudkivi, 1976). Using the roughness criterion in terms of u_*, z_0 and ν, Sternberg (1968) found that the boundary may be considered rough when $u_* z_0/\nu > 5$.

2.2.2 Velocity gradient and current shear at the bed

Within the boundary, layer the profile of the time mean velocity u(z) is a function of the height z above the bed. The velocity generally increases with z from zero at the bed to its value at the water surface if the boundary layer occupies the entire water depth, or to a free steam velocity at the edge of the boundary layer in water which is deeper than the boundary layer thickness. Because of shearing forces caused by layers of water moving over each other, a shear stress τ is created over each layer of the flow and ultimately acts on the bed.

If the value of the shear stress operating on the bed (τ_0), exceeds a threshold value it may move the bottom sediment.

Several different methods are available for estimating the bed shear stress due to a unidirectional fluid flow. The most common ones are the velocity profile method and the quadratic stress law (Sternberg, 1972). The logarithmic velocity profiles were described with respect to a form of the Karman-Prandtl equation which relates the mean velocity, u at distance, z from the boundary to the boundary shear stress:

$$\frac{u}{u_*} = \frac{1}{\kappa} \ln \frac{(z + z_0)}{z_0} \qquad [2.15]$$

where z_0 is the roughness length. The term for velocity u, denotes the mean horizontal velocity averaged over a period of time, taking into account the fluctuations in water particle directions caused by turbulent eddies. Equation 2.15 gives the average velocity as a straight line function when plotted against the logarithm of $z + z_0$ and enables u_* and z_0 to be obtained from the slope of the velocity gradient and the z-axis intercept, respectively. If κ is assumed to be 0.40, z_0 is assumed to be small compared with z, and converting ln to $\log_{10}$, Equation 2.15 can be written as:

$$\frac{u}{u_*} = 5.75 \log \frac{z}{z_0} \qquad [2.16]$$

Equation 2.16 above was derived on the assumption that the shear stress within the boundary layer was constant. The boundary shear stress τ_0 may be obtained from the slope of the velocity profile from the equation:

$$\tau_0 = \rho \frac{u_{z_2} - u_{z_1}}{5.75(\log z_2 - \log z_1)} \qquad [2.17]$$

which allows τ_0 to be determined from two mean velocity measurements u_1 and u_2 at levels z_1 and z_2.

Figure 2.3 shows a typical Karman-Prandtl velocity profile plot (Equation 2.16) obtained from measurements in tidal streams. The plot is used to obtain u_* (and hence τ_0) from the slope, and z_0 from the intercept, of the regression line of u on log(z). A least squares technique is used to fit the field measurement data after averaging over a 10-15 minutes period to minimise random errors. Some problems have been considered by Heathershaw and Simpson (1978). The logarithmic profile has become so well established in the literature that it is tempting to fit it to any near bed velocity profile. However this can be misleading as a slight curvature in the profile, due to perhaps topography, acceleration or stratification can easily be missed , which can cause the apparent u_* and z_0 to be very different form their true values (Soulsby, 1983). Estimation of errors in u_* and z_0 obtained from a log profile is given by Wilkinson (1984).

Figure 2.3 Example of velocity profile plot obtained from logarithmic layer - Karman-Prandtl profile of Equation 2.17 (Dyer, 1986).

An alternative technique of predicting τ_0 is based on the quadratic stress law. In the turbulent flow the shear stress has been shown experimentally, to be proportional to the fluid density ρ, and the square of the mean velocity u:

$$\tau_0 \propto \rho u^2 \qquad [2.18]$$

or, introducing a proportionality coefficient:

$$\tau_0 = \rho C_D u^2 \qquad [2.19]$$

where C_D is called the drag coefficient assumed to be a constant value for a given bed configuration and a given level z when the flow is in the rough regime.

For a large sea area, the drag coefficient in Equation 2.19 is usually taken as a constant over the area, with $C_D = 0.0025$ being the generalised figure. In practice and for sediment transport purposes the measured value of C_D will vary with water depth and bed composition. Thus, a spatially varying C_D, such as the Manning-Strickler law (Soulsby, 1990), which is a function of relative roughness (z_0/h) can be used such that:

$$C_D = 0.0474\left(\frac{z_0}{h}\right)^{1/3} \qquad [2.20]$$

where h is the water depth. Alternatively, a relation of the form:

$$C_D = \left[\frac{\kappa}{\beta + \ln(z_0/h)}\right]^2 \qquad [2.21]$$

can be used. If the logarithmic velocity profile is assumed to hold throughout the water depth, then the constant $\beta = 1$. For the velocity measured at the standard distance from

the bed (100 cm), Equation 2.19 becomes:

$$\tau_0 = C_{100}\rho u_{100}^2 \qquad [2.22]$$

or, since $\tau_0 = \rho u_*^2$, Equation 2.22 can be written in terms of friction velocity:

$$u_*^2 = C_{100}u_{100}^2 \qquad [2.23]$$

For fully rough turbulent flows, the quadratic stress law offers the advantages of simplicity of measurement and application. Given a representative value of C_{100} the boundary shear stress can be estimated from a single measurement of mean velocity within the boundary layer. Measurements by Sternberg (1968) in various tidal channels in Puget Sound, Washington indicated that a logarithmic profile occurred 62% to 100% of a time, averaging about 85%. For this reason, the velocity profile method is recommended because multiple velocity measurements will indicate the existence of a logarithmic velocity profile.

2.2.3 Roughness length

The roughness length, z_0 is the height above the bed at which the mean velocity is zero. The roughness length z_0 is directly related to the nature of the seabed (Soulsby, 1990), namely the grain size of the sediment and upraised features such as ripple marks, where these occur. Its value increases as the grain size of the bed sediment or the size of the ripples increases. So the velocity profiles constructed from current meter data can also provide an idea of the roughness of the bed beneath the flow.

An estimate of the bed shear stress τ_0 often has to be made from a current velocity measurement made at a single height, most commonly that at 100 cm above the bed, u_{100}. This can be done either by using the logarithmic velocity profile (Equation 2.17) or the

quadratic stress law (Equation 2.22). In the former case it is necessary to know the value of the value of z_0, and in the latter the drag coefficient C_{100}. The two are directly related via Equation 2.24:

$$C_{100} = \left[\frac{\kappa}{\ln(100/z_0)}\right]^2 \qquad [2.24]$$

An appropriate value of z_0 or C_{100} can be assigned provided the nature of the underlying bed is known (Table 2.1). The largest values of z_0 are found for rippled sand, where form drag

Table 2.1 Typical values of roughness length z_0 and drag coefficient C_{100} for different bottom types (after Soulsby, 1990).

Bottom Type	z_0(cm)	C_{100}
Mud	0.02	0.0022
Mud/sand	0.07	0.0030
Silt/sand	0.005	0.0016
Sand (unrippled)	0.04	0.0026
Sand (rippled)	0.6	0.0061
Sand/shell	0.03	0.0024
Sand/gravel	0.03	0.0024
Mud/sand/gravel	0.03	0.0024
Gravel	0.3	0.0047

over the ripples is the major source of roughness. The rather small values obtained for mixtures of sand/gravel and mud/sand/gravel are due to fine sediment filling the space between the coarser grains. The mobility of sand over rippled beds and changes in flow direction can cause variation in z_0 through tidal cycles. For smooth turbulent flow, laboratory experiments show that $z_0 = v/9u$. For rough turbulent flow Nikuradse quoted the value $z_0 = D/30$, while Kamphuis (1974) gave the value $z_0 = D/15$. In an alluvial channel with a movable sand or gravel bed, the roughness elements depend on the flow as well as on the bed material. Such natural channels seldom have plane boundaries. In the

appropriate circumstances they develop ripples, megaripples, sandwaves or antidunes. These bed features have a much greater spacing than the Nikuradse sand roughness and exert appreciable form drag which can overshadow the surface roughness of the bed forms (Raudkivi, 1976).

2.3 Threshold of sediment motion

2.3.1 Introduction

The sediment found in natural stream beds varies in chemical composition, size, shape, density and surface texture. These variabilities influence to varying degree the erodibility of individual grain particles. Grains may be moved not only by the fluid motion but also by being struck by other grains. The present of very fine particles in the sediment mixture further complicates the erosion process due to the electrochemical forces that cause intergranular cohesion. This cohesiveness results mainly from the present of clay minerals in the sediment. The circumstances necessary to initiate sediment motion are a function of the characteristic of the sediment, the fluid, and the flow condition (Miller *et al.*, 1977).

The most commonly-used quantity to describe the potential of sediment movement by a moving fluid is the bed shear stress, τ_0. A stationary grain on the seabed will begin to move when the bed shear stress reaches a critical or a threshold value, τ_c. The expression for the critical stress may be derived by equating the weight (gravity) force which hold the sediment particles on the bed to the fluid forces which cause the particles to move and be transported if the flow velocity exceeds the threshold value. Figure 2.4 illustrates the forces acting on the grains resting on the flow boundary. The gravity force, F_G acting on a single spherical grain vertically downwards is given by:

$$F_G = \frac{\pi}{6}(\rho_s - \rho)gD^3 \qquad [2.25]$$

where ρ_s is the density of the grain immersed in the fluid of density ρ, g is gravitational acceleration and D is a representative mean diameter of the grain.

Figure 2.4 Forces acting on static grains resting on the bed (Fredsoe and Deigaard, 1992).

For most natural streams, the channel slopes are small enough that the component of gravitational forces in the direction of flow can be neglected as compared with other forces acting on a spherical sediment particle (Yang, 1973). The fluid forces on a sediment particle resting on the bed may be resolved into two vector components; a lift force, F_L acting normal to the bed and a drag force, F_D acting horizontally, parallel to the bed.

The lift force F_L, is primarily due to the grain particles which, by sitting on the boundary, disturb the flow stream lines. The stream lines over the top of the grain are compressed and the flow accelerates causing a lowering in pressure (the Bernoulli's effect). Thus, near the upper part of the grain the pressure will locally decrease below the hydrostatic pressure, while an excess pressure will be created at the lower part of the grain. This pressure difference acts to lift the grain up into the flow. The lift force, F_L is given by:

$$F_L = \frac{1}{2}\rho C_L A u^2 \qquad [2.26]$$

where C_L is a non-dimensional coefficient for the lift force, and A is the projection area exposed to the flow and can be adequately represented (Dyer, 1986) by $A = \pi D^2/4$.

The drag force F_D is caused by the tangential drag of the moving fluid relative to the bed. It consists of a skin friction acting on the surface of the grain and a form drag due to a pressure different on the up- and down-stream sides of the grain because of flow separation. The point of application of the drag force depends on the magnitudes of the lift and drag components. These in turn are the function of the shape and location of the exposed grain and the local Reynolds number. The F_D is given by the similar expression as F_L, thus:

$$F_D = \frac{1}{2}\rho C_D A u^2 \qquad [2.27]$$

where C_D is drag coefficient.

The mobility of the grains depends upon the relative size of the forces F_D, F_L and F_G. Thus, the threshold of grain motion will be reached when the resultant of the lift and drag forces about a point of contact balances the moment of the gravity force.

2.3.2 The Shields Diagram

A number of competency curves, defining the threshold condition for grain motion have been proposed. These curves were derived mainly from laboratory investigations which indicate that the movement will not take place until the critical shear stress, which is a function of grain diameter, is exceeded. The most significant result of these was obtained

by Shields (1936). Based on dimensional analysis, he combined the parameters of fundamental importance into a non-dimensional relationship. These parameters are the density of the sediment ρ_s, the grain diameter D, the density of fluid ρ, the kinematic fluid viscosity ν, and the shear stress of the fluid flow τ, as well as the acceleration of gravity g. The combination of these parameters takes the form:

$$\theta = \frac{\tau}{(\rho_s - \rho)gD} = f(\frac{u_* D}{\nu}) \qquad [2.28]$$

The parameter θ in the equation is termed as the Shields entrainment function. At the threshold condition, it is denoted by θ_c and is called the Shields criterion which represents the ratio of the fluid forces to the gravitational force acting on the grain. The term u_*D/ν on the right-hand-side of Equation 2.28 is the dimensionless grain Reynolds number denoted by Re_*. The functional dependence on Re_* is an expression of the importance of the ratio of grain size to the thickness of viscous sub-layer δ_L, and it describes whether the fluid condition involves the transmission of shear stress to the bed by the fluid forces. The plot of Sheilds diagram which relates θ_c to Re_* (Equation 2.28) is shown in Figure 2.5. Note that the original plot is represented by a narrow band rather than a single curve (added by later workers) as the data used showed considerable scatter. This curve therefore marks the critical limit between grain movement if the values of θ fall above the line, and bed stability if they fall below the line.

The Shields curve has three distinct zones whose limit correspond to three boundary layer flow regimes. Below Re_* values of about 5, smooth boundary flow exists and the grains are completely embedded in the viscous sublayer. Shields predicted that at this region, θ_c is independent of grain diameter and plotted the curve negatively sloping at -45^0 based on speculation that $\theta_c = 0.1\ Re_*^{-1}$. Above Re_* of about 70 is the rough turbulent regime. Viscosity should be unimportant and thus θ_c would be independent of Re_* and has a constant value of between 0.04 to 0.06. For $5 < Re_* < 70$ is known as the transition zone, where the bed is influenced by both viscous and fluid forces. In this region, θ_c reaches its minimum value of about 0.03.

Figure 2.5 The original Shields threshold curve of the grain Reynolds number Re_* versus Shields threshold criterion θc. The solid line was added later by other investigators (Miller *et al.*, 1977).

Figure 2.6 The improved and extended Shields diagram, based on additional selected data (Miller *et al.*, 1977).

The availability of additional data has allowed Miller *et al.* (1977) to extend the Shield diagram by three orders of magnitude of Re_* (Figure 2.6). This diagram shows that in the lower Re_* region, the curve follows the trend proposed by Shields but arises at less steeper slope which indicate that the grain size is still an important factor in the threshold relationship. Independent experiments by Mantz (1977) and later by Unsold and Walger (1987) at lower Re_* region reached the same conclusion. Mantz found that only a small percentage of grains greater than 10μm in diameter exhibited cohesion and proposed the following relationship for the extended Shields curve based on his work and data of others at the lower Re_* region:

$$\theta_c = 0.1(Re_*)^{-0.3} \qquad [2.29]$$

Thus, the -45° extrapolation originally proposed by Shields now is definitely shown to be invalid.

For large Re_* values, θ_c increases to 0.06. This was found to be much too high by Neill (1968). Using additional data, Miller *et al.*, (1977) indicate that θ_c levels out at about 0.045. Due to the scatter of the available empirical data, the existence of a transition zone as suggested by Shields and speculated by other workers has not been conclusively established (Mantz, 1977). It might suggest that θ_c becomes constant at Re_* greater than about 10.

The data plotted in Shields diagram shows considerable scatter, even when data are 'carefully selected' (Miller *et al.*, 1977). The main reasons for this scatter can be attribute to the difficulty encountered in defining the critical threshold condition and to the influence of flow turbulence. Many workers have simply defined the critical conditions at some arbitrary point in the initial movement process. This is because the onset of grain movement occurs gradually over a large range of shear stress as the flow velocity increases. It is then difficult to relate such qualitative observations between different investigators which results in systematic differences between data sets. The difficulties of defining the threshold condition are discussed by Lavelle and Mofjeld (1987) who question the very existence of a threshold

given that as long as a flow is turbulent, there will exist bursts capable of lifting sediment from the bed, even if the mean flow does not posses enough energy. Another source of scatter is the lack of grain uniformity used in the different experiments. Ideally the relationship should relate materials of uniform sizes and near-spherical shapes, and on flat beds. The results of Mantz (1977) show that fine mica flakes plot slightly lower than usual on a Shield's diagram

The Shields curve is a general curve since the characteristics of the fluid and the grain are included in both parameters, making it independent of fluid type and grain density. The inclusion of shear stress and grain diameter in both the ordinate and abscissa make the Shields curve difficult to use. Yalin (1972) has overcome this difficulty by introducing different dimensionless parameters. He combined θ_c and Re_* in a manner so as to eliminate u_* from the equation to give the Yalin parameters as :

$$\Xi = \frac{Re_*^2}{\theta_c} = \frac{(\rho_s - \rho)gD^3}{\rho\nu^2} \qquad [2.30]$$

The plot of θ_c against Ξ (Figure 2. 7) have an advantage over the Shields curve in that $\sqrt{\Xi}$ can be calculated from known fluid and grain parameters, and thus the threshold θ_c can be determined directly, whereas the Shields diagram requires indirect calculation.

Other threshold curves, more limited in their applications, are the Inman curve (Figure 2.8) and the Sundborg curve (Figure 2.9) (see Miller *et al.*, 1977). The curve of u_{100} versus D in Figure 2.9 could be described very closely as two straight-line segments that intersect at D= 0.2 cm. These lines can be represented by the following linear equations:

$u_{100} = 122.6\ D^{0.29}$ for $D < 0.2$ cm,

$u_{100} = 160.0\ D^{0.45}$ for $D > 0.2$ cm.

In both relationships D must be measured in centimetres and the u_{100} value obtained will be

Third Party Material excluded from digitised copy.
Please refer to original text to see this material.

Figure 2.7 The Yalin parameter $\sqrt{\Xi}$ versus the Shields threshold criterion θc (Miller *et al.*, 1977).

Third Party Material excluded from digitised copy.
Please refer to original text to see this material.

Figure 2.8 The grain diameter D versus the friction velocity U_* for grain density 2.65 g/cm^3 at 20^{0}C (Miller *et al.*, 1977).

in cm/sec.

It has been shown that different threshold relationships exist, and they are limited to certain

Figure 2.9 The grain diameter D versus the flow velocity u_{100} for grain density 2.65 g/cm^3 at 20^{0}C (Miller *et al.*, 1977).

sediment properties and water densities. The Shield curve for example does not account for boundary conditions such as bedforms, slope and the grain size non-uniformity. Despite this limitation it is generally accepted that the Shield's curve is adequate for predicting the entrainment velocity for cohesionless sediment of a given grain size situated on a flat bed (Sternberg, 1972; Nichols and Biggs, 1985) and the term threshold is usually taken to represent the motion of the bed and not of single particles. For cohesive sediments there still exists much ambiguity as to the nature of the threshold and there is no entirely satisfactory way to predict the critical shear stress or erosion rates as a function of erosion resistance for a range of flow conditions. So far no single alternative, universally-accepted criterion has emerged (Dade *et al.*, 1992). As suggested by Sundborg (1956) and Postma (1967), the erosion resistance of cohesive sediment depends on its concentration and consolidation history. The presence of microbes can exert significant influence on erosion resistance, and the degree to which microbes can alter flow properties of clay-rich muds

remain unclear (Dade *et al.*, 1992). Therefore it is very difficult to predict the changing character of cohesive sediments and the erosion characteristics at the sediment-water interface.

Another widely used entrainment curve is shown in Figure 2.10 from Bagnold (1966). It is seen from the figure that material of diameter less than 0.17 mm will be largely transported in suspension as soon as the threshold of movement is exceeded. Bagnold has suggested that for sediment to remain in suspension the upward-directed component of the turbulent eddy velocity fluctuation must exceed its settling velocity. On this basis Bagnold

Figure 2.10 Curve for the onset of suspension, based on Equation 2.30. The 0.4 curve is that given by Bagnold (1966), and the 0.19 curve is that suggested by McCave (1971). Also shown is the curve for threshold of sediment motion (Komar, 1978).

derived the suspension criterion as:

$$\theta = \frac{\tau}{(\rho_s - \rho)gD} > 0.4\left(\frac{w_s^2}{gD}\right) \qquad [2.31]$$

where D is the grain diameter, w_s is the settling velocity and 0.4 is the proportionality coefficient. McCave (1971) argues that the suspension criterion should be determined relative to the lower levels of the flow where the turbulence eddy is larger rather than taking a mean value as Bagnold did. He plotted a suspension curve based on the proportionality coefficient equal to 0.19 (Figure 2.10). Using the 0.19 coefficient of McCave, material with diameter finer than 0.23 mm would be transported in suspension at the threshold of movement.

2.3.4 Threshold condition over a rippled bed

The threshold condition for grain movement under unidirectional flow on a smooth bed is given by the Shields curve (Section 2.3.3). However, naturally occurring stream and sea beds are more often rippled than flat. Ripples are normally formed when sediment grains are under continuous movement and they occur only if the grains are smaller than about 0.7 mm diameter (Bagnold, 1963; Inman, 1963). Sediment grains exceeding about 1 mm in diameter do not spontaneously form ripples under fully developed flow and it has been shown that for this diameter the critical Shields entrainment function θ_c has a fairly constant value of between 0.04 and 0.06.

The threshold curve for sediment motion on a rippled bed has been provided by Bagnold (1963) (Figure 2.11, curve B), but with no experimental verification. The curve was drawn based on the fact that the form drag exerted by the bed features caused τ_c to increase from 0.04 to more than 0.25 with decreasing grain size. Beside the skin friction that causes sediment motion, a rippled bed has an additional resistance to the flow due to the form drag of the ripples; thus it has a much higher value of θ_c than a smooth bed. Bagnold has estimated that the total drag is between 2 to 5 times the skin friction, while laboratory measurements by Kapdasli and Dyer (1986) suggest a form drag component between 5 to 12 times the skin friction. The flume results of Kapdasli and Dyer (*op. cit.*) for well sorted sand of 0.137 - 0.50mm diameter show that the total drag fits the equation, $\theta_c = 0.026D^{-0.82}$ when $D < 0.9$ mm. (Figure 2.11, curve C).

Since it is only the skin friction that causes the sediment to move, the threshold of movement on the ripple will occur when the total drag over the bedforms produces a skin friction at the crest equals to the Shields's value (Kapdasli and Dyer, 1986) .

Figure 2.11 Threshold entrainment function. (A) Shields curve for flat bed; (B) Curve for rippled bed (Bagnold, 1963); (C) Curve from flume studies (Kapdasli and Dyer, 1986).

Sternberg (1966) did the first field measurement to study the threshold of sediment movement over a rippled bed. His later measurements (Sternberg, 1971) for sediment sizes 0.33 - 0.50mm show good agreement with Bagnold's curve (Figure 2.11). Other field estimates were reported by Dyer (1980) for finer bed material (0.125mm). The results of

Dyer were somewhat higher than Bagnold's proposed curve and he attributed the differences as due to the present of the ripples on the sea bed.

2.4 Measurement of sediment transport

2.4.1 Movement of grains over a bed

Once the threshold for motion is exceeded, grains are lifted from the bed and transported by the flow. Sediment can be transported in several ways. The first grain movement will be by rolling and sliding over the surface of the bed when the shear stress just exceeds the threshold value. With a small increase in the bed shear stress, these grains will hop up from the bed and jump into the flow, executing short ballistic-like trajectories before falling back; this is saltation. As the flow velocity increases, there come a stage where the shear velocity of the moving fluid is higher than the settling velocity of the grain. At this stage the form of trajectories change and the grains are lifted higher and longer into the flow, supported by the turbulent fluctuations. They follow an irregular path into the interior of the fluid to be transported in suspension mode. These different transport modes have been observed and studied by a number of workers (eg. Francis, 1973; Abbot and Francis, 1977; Bagnold, 1973; and Wiberg and Smith, 1985). Within these transport modes, sediment carried by water flow can be sub-divided into two main categories according to their transport mechanisms: the bed load; the suspended load.

The bed load is defined as the part of the total load that is in almost continuous contact with the bed during transport. It comprises primarily grains that roll, slide or saltate, moving slowly (relative to the fluid stream velocity) along the bed. Its size grading is the same as the bed sediment and it largely determines the rate of propagation of slow moving bedforms. Thus the bed load must be determined almost exclusively by the effective bed shear acting directly on the sand surface.

The suspended load is the part of the total load that is moving completely within the flow

without continuous contact with the bed, as the result of the agitation of fluid turbulence. It occurs when the vertical component of the turbulent velocity is sufficient to overcome the effect of gravity on the sediment grains. Once in suspension the sediment particles move at a velocity comparable with local flow velocity. In well developed suspension transport, the suspended material moves in clouds or billows in a random manner rather than a uniform and constant concentration (Inman, 1963). Generally, medium sand and larger grains tend to be transported as bedload, while silt and clays are transported as suspended load. Therefore the median size of the suspended load is finer than the median size of the bed sediment.

The demarcation line between bedload and suspended load transport is not so clear (see eg. Bagnold, 1973; Soulsby, 1977; Bridge, 1981; Crickmore *et al.*, 1990). For a given steady turbulent flow, there must be every gradation between the two modes in terms of their distance from the boundary, speed, and mechanics of movement (Bridge, 1981). When the flow velocity is small but above the critical shear stress τ_c, the sediment particles will begin to move, remaining in contact with the boundary as bed load. As the shear velocity increases with increasing flow speed, particles are lifted into the turbulent flow region where they will be carried as suspended load if the vertical upward velocities in the eddies balance the settling velocity of the particles; however the threshold of suspension is much less well documented.

Figure 2.12 shows the dependence of threshold conditions for bedload and suspended load for sand particles. The flow intensity is plotted as shear velocity (u_*) which is a measure of the vertical velocity gradient ($du_z/d\log z$). The figure shows that the suspension threshold curve crosses the bedload curve at a diameter of 0.2mm, indicating that for sand particles smaller than this size, suspension occurs at threshold of the movement, and they do not move as bed load. The minimum value of u_{100} at which suspension of sand may occur is about 0.2 m/s. The coarser particles however, will first move as bedload and only later as suspended load when the drag force increases and is capable of promoting suspension.

Figure 2.12 Threshold values of shear velocity for bed load movement, and for suspension. Values for u_{100} shown assume a logarithmic velocity with a roughness length of 5 mm (Soulsby, 1977).

2.4.2 Measurement of bedload transport

Direct measurement of bedload sediment transport may be obtained by means of sediment traps, by studying the bedform migrations, by using sediment tracers to simulate the movement of natural sediments, or by acoustic recordings of self-generated noise. Sediment traps are normally set up by the creation of a pit or trench across a river or estuary bed, or by using a portable trap. The building of trenches is too costly, while the use of these mechanical bed-load samplers often give unreliable estimates of bedload transport as the sediments captured by the samplers are highly erratic, and when fine sand predominates, unknown amount of suspended particles will also be trapped (Dyer, 1988; Van den Berg, 1987; Crickmore *et al.*, 1990).

The use of radioactive tracers to predict bedload transport has been reported by many workers (eg. Crickmore and Lean, 1962a, 1962b; Caillot, 1973, 1983; Heathershaw, 1981; Davison, 1984). The tracers are normally ^{46}Sc (half-life 84 days) or ^{192}Ir (half-life 74 days) incorporated into a special glass melt which can then be graded to match the size of the natural sediment. The radioactive particles are then deposited on the sea bed and their movement and distribution are mapped at regular intervals by dragging scintillation counters along the sea bed from a survey boat. Such an approach has been used by Heathershaw (1981) to measure sand transport rates in Swansea Bay.

In addition to radioactive tracers, fluorescent tracers have been used for sand and gravel movement studies. Fluorescent substances such as rhodamine, kiton yellow and uvitex are normally used to coat the sand or shingle grains. Unlike radioactive tracers where concentration measurement can be done *in-situ*, fluorescent tracers rely on sampling and subsequent time-consuming particle counting to obtain concentration. Lees (1981; 1983) has used fluorescent coated sand as the tracer to study sand transport rates and directions off the East Anglian coast, U.K.

Bedform tracking is one of the common technique employed to estimate sediment transport rates. Kachel and Sternberg (1971) and Wilkinson *et al.*,(1984) used underwater cameras

to survey along a line of moving bedforms. By comparing the photographs taken at intervals the ripple migration rates can be converted to mass transport. Side-scan sonar and echo sounder surveys were used by McCave and Langhorne (1982), McLean (1983) and Van den Berg (1987) to track the migration of megaripples and sandwaves which can be shown as evidence of sediment transport. Langhorne (1982) used divers to measure changes in the crest elevations of sandwaves, hence their movement relative to a series of sea bed reference stakes. The shortcoming of the technique is that there is uncertainty as to the amount of sediment in motion that has become lodged (temporarily) in the bedform as compared to the amount remaining in motion and bypassing the bedform (Ludwick, 1989). The observed bedform migration rate can give information only on the former.

Another approach is to measure bedload transport using acoustic techniques. A technique has been used in the field by Tywoniuk and Warnock (1973) and Jonys (1976) and is particularly useful for monitoring movement of coarse sand and gravel. Recently, improvements have been made on the technique to obtain a more accurate estimate of bedload transport (Thorne, 1986; Thorne *et al.*, 1989; Williams *et al.*, 1989). A hydrophone was used to record self-generated noise (SGN) from the collisions of moving particles as bed load transport took place. The acoustic intensity of the generated noise was found to be related to bed load transport rate (Heathershaw and Thorne, 1985). The results can be compared with simultaneous measurement made visually using an underwater television camera and a video recorder.

As an alternative to direct measurement, one can use empirical relationships to estimate the transport rates. A large number of sediment transport equations have been proposed over the last 100 years, since Du Boys (Leeder, 1983; Reid and Frostick, 1994). Faced with such a large number of transport equations, the most sensible way is to select one or more formulae that give good results for conditions similar to those in the area of interest. Most of these equations were derived based upon results obtained in laboratory conditions, but some were derived from basic principles of physics such as those proposed by Bagnold (1966, 1973) and Einstein (1950). These empirical relationships indicate that the greater the flow magnitude above the threshold, the greater the transport rate. The transport

formulae may be a function of several parameters such as the flow speed, sediment grain size, water and sediment densities, viscosity and bed roughness. In practice however only a few of these are included in the formula but the rest are difficult to measure accurately and are normally combined as a constant to be determined experimentally in the laboratory. Some of the most frequently used transport equations are briefly reviewed in the following section.

2.4.3 Sediment transport equations

There is a wide range of sediment transport equations to choose from. Some of these equations are concerned only with bedload but others include both bedload and suspended load. Many of these equations have been developed from theoretical and empirical models which were based on mean, time-averaged steady flows in open channels. Some of the most quoted ones are those of Meyer-Peter and Muller (1948); Bagnold (1963,1966); Einstein (1950); Yalin (1963); Engelund and Hansen (1967); Sternberg (1972); Ackers and White (1973); and Hardisty (1983). A threshold condition for sediment entrainment has been included in some of the formulae, but others predict transport at all flow velocities. A number of workers have evaluated their applicability in marine and inter-tidal conditions conditions (eg. Gadd *et a*l., (1978); Collins *et al.*, (1981); Heathershaw (1981); Lees (1981); Mahamod (1989); and Williams *et al.*, (1989)).

2.4.3.1 Bagnold bedload equation

Bagnold's (1963) theory relates the bedload sediment transport rate q, to the stream power ω, and an efficiency factor, *K*. This relationship is expressed as:

$$q = \frac{\rho_s}{(\rho_s - \rho)g}\omega K \qquad [2.32]$$

The power expended by fluid per unit of bed area ω, can be expressed as $\omega = \tau u_*$ or $\omega = \rho u_*^3$ since $\tau = \rho u_*^2$. K is a constant which depends primarily on the characteristics of the transported sediment. Observations by Bagnold suggest K is a function of relative roughness h/D where h is the flow depth and D is the sediment mean diameter. However, Kachel and Sternberg (1971) demonstrate that K depends not only on the sediment characteristics but also on the excess shear stress $(\tau - \tau_c)/\tau_c$. They later show that the modified Bagnold's equation predicts best both the field data and some data from the flume experiments of Guy *et al.*, (1966). Using the data of Guy *et al.*, Gadd *et al.*, (1978) have removed the efficiency coefficient in Equation 2.32 and expressed the equation in terms of the near bed flow velocity (u_{100}) and a threshold velocity u_c. The new transport equation thus becomes:

$$q = k_1(u_{100} - u_{100c})^3 \qquad [2.33]$$

where k_1 is the proportionality coefficient obtained from the flume data. $k_1 = 7.22 \times 10^{-5}$ $gcm^{-4}s^2$ for 180 μm sand and $k_1 = 1.73 \times 10^{-5}$ $gcm^{-4}s^2$ for 450 μm sand.

2.4.3.2 Yalin bedload equation

Yalin's (1963) transport equation was derived from a dimensional analysis and an analysis of the mechanics of grain motions. In this derivation particles are assumed to move over the bed by saltation once the threshold condition is exceeded. Yalin found that the bed load mass transport rate q, is related to the boundary layer fluid flow by:

$$q = 0.635\,\rho_s D u_* S \left[1 - \frac{1}{aS}\ln(1 + aS)\right] \qquad [2.34]$$

where

$$a = 2.45\left(\frac{\rho}{\rho_s}\right)^{0.4}\left(\frac{\rho u^2}{(\rho_s - \rho)gD}\right)^{1/2} \qquad [2.35]$$

and S is dimensionless access shear stress given by:

$$S = \frac{(\tau - \tau_c)}{\tau_c} \qquad [2.36]$$

The constant value of 0.635 in Equation 2.34 was obtained from experimental data. Gadd *et al.* (1978) apply the Yalin bedload equation to the Guy *et al.* flume data for grain sizes 190μm and 450μm. They find that the grain size 450 μm gave good agreement at velocities near threshold, but at higher flow velocities the predicted rates were less than those predicted by the flume experiments. Using the same equation, Williams *et al.* (1989) found the estimated transport was in moderate agreement with the acoustic measurement (where hydrophones are used to record the sediment generated noise arising from interparticle collisions of mobile bedload materials, and an underwater television camera and video recorder are used to monitor the movement) for the gravel size sediments.

Yalin's bedload equations are applicable only to rough plane beds, fully developed turbulent flow, and where there is a large flow-depth to particle-diameter ratio (h/D). Also since it was assumed that the bed roughness exceeded the thickness of a laminar sublayer, the result is applicable only to grains exceeding about 200μm (Dyer, 1986).

2.4.3.3 Hardisty bedload equation

Hardisty's (1983) transport formula for bedload was based on the original equation of

Bagnold (1963) which gives the mass transport per unit width q, in terms of stream power, ω and efficiency factor, K (Equation 2.32). The shortcoming in the Bagnold equation is that it has no threshold condition and predicts sediment motion at all flow speeds. Following a suggestion by Vincent *et al.*, (1981), Hardisty modified the equation to relate the stream power to the flow velocity at the standard height of 100 cm above the bed, u_{100} and to include the threshold term, u_{100c} in the new formula such that:

$$q = k_2 (u_{100}^2 - u_{100c}^2) u_{100} \qquad [2.37]$$

k_2 is the constant related to the grain size of the sediment and has been calibrated for grain diameter ranges between 0.18 mm to 0.45 mm using the flume data of Guy *et al.*, (1966). k_2 is given by:

$$k_2 = (1/6.6D^{1.23}) \times 10^{-5} \text{ gm cm}^{-4} \text{ s}^2 \qquad [2.38]$$

where D is the grain diameter in millimetres.

This form of transport equation is close to the first part of the Yalin (1972) bedload transport equation.

2.4.3.4 Ackers and White total load equation

The general sediment transport function of Ackers and White (1973) is expressed in terms of three dimensionless groups:

i. *Sediment mobility number*, F_{gr}

This is the ratio of the appropriate unit area of the bed to the immersed weight of the grains.

F_{gr} is given by:

$$F_{gr} = \frac{u_*^n}{\sqrt{gD\frac{(\rho_s-\rho)}{\rho}}}\left[\frac{u}{2.46\ln(10h/D)}\right]^{1-n} \qquad [2.39]$$

ii. *Dimensionless grain diameter*, D_{gr}

This expression can be derived by eliminating shear stress from the drag coefficient, and Reynolds Number of a settling particle by eliminating the settling velocity. It is generally applicable to coarse, transitional and fine sediments, and is the cube root of the ratio of immersed weight to viscous forces:

$$D_{gr} = D\left[\frac{(\frac{\rho_s-\rho}{\rho})}{g\frac{}{\nu^2}}\right]^{1/3} \qquad [2.40]$$

D_{gr} ranges between 1 for fine sediment (D=0.04 mm)and 60 for coarse sediment (D=2.5 mm).

iii. *Sediment transport*, G_{gr}

This dimensionless expression for sediment transport was based on the stream power concept. For the coarse sediment, the product of net grain shear and stream velocity as the power per unit area of the bed is used, and for fine sediment the total stream power is used, which in both cases takes account of the different modes of transport. The hypothesis is also made that the efficiency is dependent on the mobility number F_{gr}. The general transport

parameter is given by:

$$G_{gr} = \frac{qg\rho h}{\rho_s D}\left(\frac{u_*}{u}\right)^n \qquad [2.41]$$

The transport rates G_{gr} are related to F_{gr} by:

$$G_{gr} = R\left(\frac{F_{gr}}{T} - 1\right)^m \qquad [2.42]$$

where R, T, m and n all vary with sediment size.

For coarse sediment (D>2.5 mm);

$$T = 0.17;\ R = 0.025;\ \ m = 1.5;\ \text{and}\ \ n = 0.0$$

For intermediate fine sediment (40μm < D < 2.5 mm);

$$T = 0.23(D_{gr})^{-1/2} + 0.14$$

$$\log R = 2.86 \log D_{gr} - (\log D_{gr})^2 - 3.53$$

$$m = 9.66/D_{gr} + 1.34$$

$$n = 1 - 0.56 \log D_{gr}$$

The equation does not cater for sediments finer than 40μm as generally they exhibit cohesive properties and the law of erosion and accretion are far more complex. The expression may be applied to plain, rippled, and dune configuration for Froud number, F≤0.8. The expression was developed based on nearly 1000 flume experiments using graded and well

sorted sediments in flow depths up to 0.4 m.

2.3.4.5 Engelund and Hansen total load equation

The Engelund and Hansen's (1967) equation for total load transport in alluvial streams is given by:

$$f\Phi = 0.1\,\theta^{5/2} \qquad [2.43]$$

where f is a friction factor defined by:

$$f = 2\frac{u_*^2}{u} \qquad [2.44]$$

Φ is a dimensionless sediment discharge defined by:

$$\Phi = \frac{q}{\rho_s\left[\frac{(\rho_s-\rho)}{\rho}gD^3\right]^{1/2}} \qquad [2.45]$$

and θ is a dimensionless bed shear stress, commonly referred to as the Shields entrainment function and defined as:

$$\theta = \frac{\tau}{(\rho_s-\rho)gD} \qquad [2.46]$$

By substituting f, Φ and θ in Equation 2.43, the total discharged load becomes:

$$q = 0.05\,\rho_s\,u^2\left[\frac{D}{g(\rho_s-\rho)}\right]^{1/2}\left[\frac{\tau}{(\rho_s-\rho)gD}\right]^{3/2} \qquad [2.47]$$

The equation has some limitations in that its applications are only valid for dune-covered beds with sediment size coarser than 150 μm and boundary Reynolds number R_e greater than 12 (Raudkivi, 1976). Despite these limitations, both Graf (1971) and A.S.C.E. (1975) recommend its general use for predicting sediment transport in rivers.

2.3.4.6 Jago and Mahamod total load equation

A new equation for total load transport has been proposed by Jago and Mahamod (1997). The equation was derived from reanalysis of the Guy *et al.*, (1966) flume data and takes a similar form to those of the Gadd *et al.*, (1978) and Hardisty (1983) equations for bed load transport. The total sand flux is given by:

$$q = k_3 \left(\frac{u_{100} - u_{100c}}{u_{100c}} \right)^n \qquad [2.48]$$

Where k_3 is an entrainment function, u_{100} and u_{100c} are the current velocity and the threshold current velocity at standard height 100 cm above the bed, and n is an exponent. Both k_3 and n depend on the grain diameter. The functions of k_3 and n have been calibrated using Guy *et al.*, (1966) flume data for sands with grain diameter range from 190- 930 μm which give the following polynomial fits:

$$\log_{10} k_3 = (2973 \cdot 10^3) D^2 - 1163 D - 2.465 \qquad [2.49]$$

and

$$n = (3225 \cdot 10^3) D^2 - 5564 D + 5.028 \qquad [2.50]$$

where D is the grain diameter in metres.

This equation has taken a slightly different form from that proposed by Gadd *et al.* (1978) and Hardisty (1983) in that instead of having a fixed value for the entrainment function, k_3 increases with larger grain diameter, and the exponent n varies from smaller than three for coarser sand to greater than four for fine sand which indicates suspension becoming more dominant with decreasing grain diameter.

The above equation have been calibrated against low and fast flow velocities (0.2 - 1.5 m/s) thus making it suitable for application in fast tidal current environments such as in macrotidal estuaries.

2.4.4 Measurement of suspended sediment concentration

Two standard techniques for measuring suspended sediment concentration in estuarine studies are by gravimetric analysis of water samples and by using optical instruments. Reviews of the techniques and some other techniques have been given by McCave (1979), Huntley (1982), Van Rijn (1986), Sternberg *et al.* (1989), and Eisma (1993).

The gravimetric technique is a direct method for measuring suspended sediment concentration in natural waters. This common and simple method involves collecting a known volume of water sample, filtering it, and determining the weight of the material retained on the filter. The gravimetric analysis is capable of producing accurate suspended sediment concentration, but has the disadvantages of being slow, labour intensive both in the field and in the laboratory and cannot provide a rapid temporal variation of sediment concentration in the field. The most commonly used filters are: cellulose ester membrane (eg. Millipore filters); perforated polycarbonate (Nuclepore filters), and glass microfibre (Whatmann GF/F, GF/C filters). Filters with 47 mm diameter with a nominal pore size of 0.4 μm are easy to handle and most commonly used for marine as well as estuarine applications. Weighing and pre-weighing of the filters to determine the suspended sediment concentration can be done in any electronic balance that gives reading to 10^{-5} g.

In many estuary studies, *in-situ* measurement of suspended sediment concentration is now almost exclusively made using an optical instrument. The measurement of suspended sediment concentration using optical instruments is possible because suspended particles in water scatter light and the amount of scattering depends on their concentration but also on their size, shape, and transparency (Dawning *et al.*, 1981; Baker and Lavelle, 1984; Wells and Kim, 1991; Conner and De Visser, 1992). Two different types of optical instrument widely used are the transmissometer and the nephelometer. The transmissometer measures the attenuation of a light beam projected to a sensor, while the nephelometer measures at an angle the light scattered (reflected and refracted) by the suspended particles. Because of the fast time response and relatively low power requirements, optical sensors are ideal for obtaining continuous vertical or horizontal time series measurements of suspended particulate from moorings or sensors attached to a structure within a water column (Sternberg, 1989).

i. Transmissometer

The optical beam transmissometer has been used widely as the replacement to the direct measurements of mass or volume concentration of particles in natural waters. The instrument can be used at a single depth deployment on a mooring, or as a profiling instrument mounted on a CTD frame. The advantages of the technique are its speed, simplicity, low cost and general availability, and with technological advances, the storage of large quantities of data set can be done without difficulty. The suspended sediment concentration measurement is based on the assumption that there is a linear relationship between the beam attenuation and the particle concentration. This relationship is valid only if the effects of variations in the particle size, shape, refractive index are either negligible, mutually compensating, or can be quantitatively corrected (Baker and Lavelle, 1984; Spinrad, 1986; Wells and Kim, 1991).

The beam attenuation coefficient, c from a collimated monochromatic light beam is obtained through the relationship:

$$I_r = I_o\, e^{-cr} \qquad [2.51]$$

where I_o and I_r are the light intensities at the source and at distance r - the path length (in m) from the source. Beam transmission, the ratio of received to source light intensity, I_r/I_o, is given by;

$$t = I_r/I_o = e^{-cr} \qquad [2.52]$$

and the attenuation coefficient c, is thus determined from beam transmission by the relationship:

$$c = -1/r\ (\ln t) \qquad [2.53]$$

The transmission values depend on the absorption and scattering from pure water, suspended particles and dissolved organic material (Wells and Kim, 1991). Certain types of transmissometer, such as the Sea Tech, which was used in this study (see Chapter 3) has a 660 nm wavelength LED source that eliminates the absorbtion from dissolved organic matter so that any attenuation is due to water and sediment only.

The optical transmissometer must be calibrated in order to establish the empirical relationship between the suspended matter concentration and the attenuation coefficient. A laboratory calibration is normally good enough if the actual properties of the particle in suspension are known. But as suspended sediments are very rarely homogenous in composition and concentration and their nature varies in time and space, a separate field calibration must be made for each particular environment. Field calibration is carried out by measuring suspended material concentration and beam transmission simultaneously (Krause and Ohm, 1984; Wells and Kim, 1991). The calibrations are usually done by taking water samples and determining the sediment concentration using a standard gravimetric technique. The calibration diagram is established through linear regression of the sediment concentration against the attenuation coefficient. With careful calibration, transmissometers are capable of measuring sediment concentrations down to a fraction of a milligram per

litre. The principal disadvantage of the transmissometer is that it is prone to fouling by biological matter which can grow on the instrument housing and interfere with the optical path. This may be overcome by frequent checking on the calibration and cleanness of the optical path.

ii. Nephelometer

Instruments for measurements of angular light scattering are called nephelometers. The measurements are more complicated than transmittance technique and calibration is more difficult since the scattering is more sensitive to interference from the present of biological materials and air bubbles in the water column (Downing *et al.*, 1983; Osborne *et al.*, 1994). Generally, measurement can be made at any angle from 0° - 180° , but most instruments are designed to measure the forward scattering at an angle 45° or 90°, and the back scattering. The OBS (Optical Back Scatterence) sensors which measure backscattering at angles between 140° -165° are claimed to have greater sensitivity to changes in particle concentration and size (D&A Instruments, 1989). The OBS's have poorer resolution than the transmissometers. They do however have a linear response to a much wider range of particle concentration and can measure approximately 5 - 15,000 mg/l concentration in muddy environments (Sternberg, 1989), and therefore they tend to be used in regions of high turbidity. The OBS sensors are also relatively insensitive to bubbles and plankton which are strong forward scatterers (Downing *et al.*, 1983; D&A Instruments, 1988). As with the transmissometer, the OBS does not provide any information about the grain size of the suspended particles.

2.5 Sedimentary processes in estuaries

2.5.1 Introduction

The term estuary is commonly referred to the region where a river meets an inlet of the sea.

This definition gives no indication of how far up-river an estuary extends, or of the interaction between the fresh river water and the saline sea water. Consequently, Fairbridge (1980) has proposed that "an estuary is an inlet of the sea, reaching into a river valley as far as the upper limit of tidal rise". Another commonly used definition for an estuary is given by Pritchard (1967) as "a semi-enclosed coastal body of water which has a free connection with the open sea and within which the sea water is measurably diluted with fresh water derived from land drainage". Pritchard has defined the estuary in oceanographic terms, whereas Fairbridge defined it in geomorphic terms. The difference between the two lies in the definition of the upper limit of an estuary. Pritchard's landward boundary is a chemical one (the presence of sea water) whereas Fairbridge's landward boundary is physical (the upstream limit of a measurable tide). For some estuaries, the difference is trivial, but for others the Fairbridge estuary may extend 100 km landward of the Pritchard estuary (Nichols and Biggs, 1985).

From a sedimentological and stratigraphical standpoint, the following definition was given by Howard and Frey (1980): "An estuary is a complex of intertidal and shallow subtidal intercoastal facies dominated by tidal processes, exhibiting conspicuous variations in sediment texture, composition, and provenance, and in physical and biogenic sedimentary structures. Individual depositional environments comprising this complex of intercoastal facies may be as varied as: tidal deltas and shoals, protected beaches and spits, washover fans, swash and point bars, tidal flats and salt marshes, and stream banks and channels". Compared with the previous definitions, this definition places more emphasis on the processes and products than upon salinity and physiography. It includes the domination of salt water and the prospect of freshwater influences in the development of various estuarine facies.

Most estuaries are geologically very young and relatively short-lived geomorphic features which are subjected to rapid and continuous natural changes. They were formed as a result of the drowning of coastal areas and mouths of river valleys during the latest eustatic rise of sea level associated with the melting of the Pleistocene ice sheet (Officer, 1981). This process, which began about 15,000 years ago, caused the sea level to rise 100 -130 m to its

present position (Nichols and Biggs, 1985). This sea level rise became comparatively stable only about 3,000 to 5,000 years ago and most modern estuaries are less than about 6,000 years old (Postma, 1980). They are now being progressively infilled with sediment. Sedimentation in some kept pace with the gradual inundation where the sediment supply was high such as the Mississippi, but others where sediment discharge is lower and faster currents associated with a high tidal range occur (thereby keeping the estuary clear of sediment) may be still slowly adjusting to a new equilibrium. An estuary is regarded as stable when sediment input balances the output (Dyer, 1972).

2.5.2 Classification of estuaries

Estuaries are far from uniform in character and the differences are mainly due to variations in tidal range and river discharge, which affect the extend to which saline sea water mixes with fresh river water. Different types of mixing result in different estuarine circulation, and thus the behaviour of sediment load. On this basis, most estuaries found in the coastal plain areas can be divided into three main types: salt wedge, partially mixed, and well-mixed estuaries. Detailed description on the estuarine classification and their physical characteristics are given by Dyer (1973; 1986), Officer (1976), and Bowden (1980).

Salt wedge estuaries develop where a high river flow discharges into a virtually tideless sea. Here, the water circulation is dominated by the river flow, and tides play a negligible role. The less dense river water spreads out on top of denser, saline sea water and thins seaward. The underlying layer is wedge shaped and thins landward. Between the freshwater and seawater, there are very sharp density and salinity gradients so that a stable halocline develops and the two water masses do not mix easily. However, because one layer of the water is moving over another, a shear stress occurs, producing turbulence at the base of the fresh-saline water interface. The turbulence generates a series of internal waves which cause the upward advection of salt water along the interface. The position of the salt wedge is dependent on the river flow. When the discharge is low the salt wedge can penetrate further inland than when discharge is high. An example of the salt wedge estuary is the

Mississippi. In this estuary the salt wedge penetrates 150 km inland at low inflow, but extends only a kilometre or so above the mouth at high inflow.

Partially mixed estuaries occur where rivers discharge into a sea with a moderate tidal range. Tidal currents are significant, so that the river flow does not dominate the circulation. The whole water mass moves up and down the estuaries with the flood and ebb tides. Consequently, in addition to the current shear at the salt water-freshwater interface, friction at the estuary bed creates shear stress there, and generates turbulence which causes even more effective mixing of the water column than that caused by waves at the fresh water/salt water interface. This tidal mixing removes the sharp boundary between the two water layers and make it much less well defined as both salt water and fresh water are transferred upwards and downwards. Towards the head of the estuary, the net landwards bottom flow of salt water diminishes and the net seawards upper flow of fresh river water increases. The depth at which there is no net landward or seaward movement of water increases until eventually it coincides with the bed of the estuary where it is called the null point of the estuary. The actual position of the null point fluctuates up and down the estuary depending on the tidal cycle and river discharge. Examples of the partially mixed estuaries are the Mersey and Thames (UK), and the James River in Virginia.

In the well-mixed estuaries, the tidal range and the tidal currents velocities are large enough to break down the vertical salinity stratification completely. The salinity hardly varies with depth, although it may vary considerably across the width of the estuary, being higher on the right (viewed landward) than on the left. This is due to the Coriolis force which tends to swing the incoming tidal flow and the seawards-flowing river water to the right in the Northern Hemisphere and to the left in the Southern Hemisphere. There is little landward flow but mainly lateral movement. The mixing takes place laterally from right to left so that a horizontal rater than vertical, residual circulation developed. Sometimes the ebb dominated and flood dominated parts of the circulation can be separated into topographically distinct ebb-and-flood channels, with a bank between (Dyer 1986). The Severn in UK and the Gironde in France are examples of well-mixed estuaries.

Estuaries and related coastal environments can also be classified according to their tidal ranges. Such a classification has been suggested by Davies (1973) and Hayes (1975). They suggest that where the spring tide range is less than 2 m, the estuary is termed micro-tidal; between 2 and 4 m, meso-tidal; and more than 4 m, macro-tidal. This classification may be considered as approximately- equivalent respectively to the three types of estuaries described previously.

2.5.3 Source of estuarine sediments

Sediments in estuaries range all the way from granular sand common on most beaches to very fine colloidal materials in suspension. In most estuaries there is a gradation in size of the bed sediment, with sandy material near the mouth giving way to muddier sediments near the head of the estuary (Ippen, 1966; Dyer, 1988). Estuarine sediments are derived from a number of sources including the watershed, the continental shelf, the atmosphere, erosion of estuarine margins and bottom, as well as from biological activity within the estuaries. A particular estuarine deposit usually consists of various proportions of materials from these different sources. The relative importance of these sources will vary between estuaries and will depend to a great extent on the seasonal cycle of river discharge, the particular geological and social history of the estuary and its hinterland, as well as on the dynamic of erosional, transportation, and deposition processes.

River inflow can supply a significant amount of sediment to an estuary. The river input consists of sand, silt and clay size material, and substantial amount of organic matter. These different materials are supplied by tributaries, from bank erosion, and from sheet-wash on slopes. There is normally a close correlation between the river discharge and sediment input (Buller *et al.*, 1975), although the reverse may occur (eg. Meade, 1969). The presence of dams or lakes can serve as sediment traps, especially for the coarser materials and reduce the supply of fluvial sediment. River flooding may supply more material into an estuary in a few days than normal run-off in years.

Entrainment of marine sediment into the estuaries has been described by a number of workers. Meade (1969) provides evidence for the landward transport of beach sands into estuaries in the U.S. Atlantic Coast. The sediment heavy mineral assemblages suggest its offshore derivation. Buller *et al.* (1975) working in the Tay estuary describes the heavy mineral assemblages found in sand banks and sand flats and show that they are of marine origin. Evidence from sediment texture and mineralogy show that the primary source of sand found in the Taf estuary, a macrotidal estuary in southwest Wales, is from the nearby Carmarthen Bay (Jago, 1980). In Minas Basin, Canada, the mud that accumulates in the tidal mudflat is derived mainly from coastal erosion but in other regions, the main source of mud is from the open sea which in turn derived its mud mainly from major rivers (Middleton, 1980). The fine sediment sources in the Chignecto Bay, Bay of Fundy, Canada are from wave erosion of the cliffs and current scouring of the seabed (Amos, 1987).

The *in-situ* reworking sources include the marginal input derived from the erosion of supra-tidal cliffs and slopes, and the resuspension of bottom material by waves and currents. This may be an under-estimated source in many areas, for example slumping and rainwashing of preglacial material in mid- to upper latitude estuaries such as those of Brittany (Buller *et al.*, 1975) and sliding and dry shore erosion of loosely consolidated masses in the marshlands of Northern Chesapeake Bay in the United States (Biggs, 1969). Some of the material dredged from the estuary and discharged too close to the estuary entrance may find its way back and contribute as a new source of sediment deposit.

The biogenic contribution is mainly in the form of organic materials as a result of the biological cycles of estuarine flora and fauna and are of secondary importance. Ippen (1966) reported that in Charleston Harbour, the organic component has been identified as contributing up to 15% of the finer sizes of sediment found in shoals. Another significant contribution to the total suspended sediment in estuaries is from anthropogenic sources which is derived from the discharges of sewage and industrial wastes. There is an increased contribution from these sources as industrial activity and global population increase.

Beside quartz, micas, feldspars, chlorite particles and various clay minerals that make up

the bulk of the inorganic constituents of the estuarine mud, there are also biological and organic phases within the sediment. Plant fragments, pollen spores, foraminifera and diatom tests, spicules, rods and tube fragments have been reported from muddy, inter-tidal sediment (Johnson, 1974; 1976). In addition, the sediment contains biota, bacteria, and other microbes which produce secrete mucus that bind the sediment together, making it more resistance to erosion. Useful reviews on the roles of these various organic components in binding the fine-grained sediments, and their relation to erosion resistance are due to Montague (1986) and Heinzelmann and Wallisch (1991).

2.5.4 Flocculation of sediment grains

Estuaries contain considerable amounts of suspended matter which consist of mineral particles mainly clays, quartz, feldspar and carbonate, as well as organic matter. They are present as single mineral grains or they form flocs of mineral grains and organic matter strongly bound together. There are two main types of flocs recognised in estuaries; microflocs and macroflocs (Eisma, 1986; Dyer, 1994). The microflocs with diameters up to 125 μm consist of mineral particles and organic matter and are strongly bonded. The microflocs together with single mineral particles interact with increasing order of aggregation to form macroflocs. The macroflocs, up to a few millimetres diameter, are loosely bound and fragile, easily broken up by turbulent shear to form microflocs eventually (Glasgow and Lueke, 1980) but are stable in flowing water of up to 1.5 m/s (Eisma, 1986).

For the formation of flocs (also termed as aggregates), there must be collisions between the particles and the colliding particles must stick to each other (Krone, 1978). The cohesion of mineral particles is largely due to the presence of a significant proportion of clay minerals, usually less than 2μm in diameter (Dyer, 1972; Owen, 1977) . These clay minerals are formed as the product of chemical weathering of pelitic rocks and are predominantly kaolinite, illite, chlorite and montmorillonite. Due to their small size and large specific area, the surface physico-chemical forces become dominant in comparison to the gravitational force acting on each clay particle. These cause the particles to interact electrostatically and

stick together rather than stay as separate individual particles.

Clay minerals are hydrated silicates of aluminium and exist as an interlayered crystal structure and carry negative charges on their faces (Partheniades, 1986). This negative charge is due to exposed oxygen atoms at the edge of the broken intermolecular bonds of the clay crystal lattice and to cationic substitution within the lattice (Dyer, 1986). In river water where cation concentration is low, the clay particles repel each other due the repulsive forces of the negative charges. However, in a solution with high ion concentrations like seawater, the free cations will interact and neutralise the negative charges on the clay particles. If they are sufficiently close, the particles are attracted to each other by a molecular attraction force known as the London-van der Waals force to form flocs. The flocculation of clay particles tends to very quickly reach an equilibrium situation at a comparatively very low salinity, although this varies for each mineral species. With adequate particle concentrations, flocculation of illite and kaolinite is complete above a salinity of about 4‰; however, for montmorillonite it varies over the entire range of salinity up to 35‰ (Dyer, 1972).

The three most important mechanisms which bring and facilitate the collisions between particles are Brownian motion, differential settling of the particles and fluid shear (Dyer, 1986; Krone, 1978; 1986; van Leussen, 1988). Brownian motion results from the random movement of thermally agitated water molecules and is an importance mechanism when sediment concentration is high (~10 g/l); it produces weak aggregates that are easily dispersed by shearing or crushed during deposition. The settling of suspended particles at different speeds also results in collisions. There is little stress on particles colliding by differential settling, and the resulting flocs are usually of low density, ragged and relatively weak. In fluid shearing the suspended particles moving at different speed overtake one another, collide and form flocs. The flocs formed by fluid shear are relatively dense and strong. However, fluid shear is also an effective process for breaking up aggregates. In conclusion the first two processes produce weak, very open aggregates having densities near of that the suspending water and they are readily redispersed by the fluid shear or turbulence, while flocs formed by fluid shear are relatively dense and strong because only

particles with inter-particle cohesive bonds survive the local fluid stresses.

Repeated collision can produce flocs of much bigger sizes than the individual suspended particles. A typical floc diameter is between 60 μm to 150 μm and each one would contain around 10^5 to 10^6 particles (Dyer, 1986), though *in-situ* measurements made by Wells (1989) showed much bigger aggregate sizes, being average from 290 μm to 470 μm. The flocs have settling velocities up to four orders of magnitude larger than the primary particles (Owen, 1971; Krone, 1972; McCave, 1979; van Leussen, 1988). This explains the presence of clay grains in tidal sediments (Pethick, 1984). The rate of floc formation, their average sizes and the size distribution in estuarine waters depend on the suspended sediment concentration, the strength of inter-particle bonds formed and on the maximum fluid shear stress they can withstand (Owen, 1977; Partheniades, 1986; Mehta and Dyer, 1990). Under the hydraulic condition found in estuaries, turbulence helps flocculation initially by promoting contact, while more turbulence causes internal shearing that breaks the flocs apart (Ippen, 1966; Eisma, 1986; Pejrup, 1988).

The presence of organic matter and micro-organisms in suspension increase the probability of particles sticking together, hence significantly enhancing flocculation (eg. Zabawa, 1978; Krank, 1981; 1984, Eisma *et al.*,1991). Particles of organic material, themselves electrically charged, can act as nuclei, and attract clay minerals, forming clay-organic-clay particles. Certain organisms can produce sticky organic compounds that can form coatings on the particles. Organic binding increases flocs settling velocities (Pethick, 1984) and makes the floc aggregates very much harder to break up (Dyer, 1986). There is also evidence that the formation of flocs and settling is most efficient at a certain organic-inorganic ratio. Krank (1984) found for three estuaries in eastern Canada that 65% organic matter as an optimum composition for floc formation.

In the turbulent flow field, the flocs will be in a continuous state of formation and breakup. The flow-induced shear stress limits the growth of the flocs into a higher order or breaks higher order flocs into lower ones. As the flocs settle to the bed, their fate is determined by the maximum velocity gradient which occurs close to the bed. If the interparticle bonds are

high enough to withstand the maximum shear stress operating near the bed (Partheniades, 1986), the floc will stay there permanently; or else will be broken up and re-entrained back into the flow.

2.5.5 Sedimentary processes

2.5.5.1 Controlling factors

Estuaries offer an effective shelter against strong waves and meteorological currents that make them a more favourable environment for sediment deposition than the more exposed open shelf. Within the estuaries there are three main contributing factors that affect transport and accumulation of sediment, as well as their depositional pattern and sequences. These factors are tides, the estuarine circulation, and waves which can act simultaneously or independently to supply and distribute varying kinds of amounts of sediment. An evaluation of each of these factors and their interaction are very important in the studies of sedimentary processes prevail in estuaries.

i. Effect of tides

In many estuaries, tides are the major energy source for mixing fresh and salt water, for resuspending sediment from the bed, and for transporting suspended sediment seaward or landward. Sedimentary processes respond to two characteristics of tides: tidal wave deformation with distance landward; and fluctuations of tidal amplitude during the neap-spring tidal cycle (Allen *et al.*, 1980; Castaing and Allen, 1981; Nichols and Biggs, 1985).

In tide-dominated estuaries, the tidal wave becomes increasingly deformed as it propagates upstream in the estuary (Allen *et al.*, 1980; Nichols and Biggs, 1985; Wright, 1985). This deformation is due to the fact that the tidal-wave celerity is a direct function of water depth. The effect of this deformation is to shorten the flooding phase and extend the ebbing phase

so that in shallow estuaries the flood crest propagates faster than the ebb trough. Because of this pronounced tidal asymmetry, average flood velocities become increasingly stronger towards the head of estuary, significantly exceeding average ebb velocities. The greater flood velocities produce higher bed shear stresses, which cause greater bottom erosion and transport than the ebb, thus favouring a net landward transport of suspended sediment near the bed (Allen *et al.*, 1980; Castaing and Allen, 1981; Dyer, 1988), this is termed 'tidal pumping'. The few calculations of suspended sediment fluxes which have been made in the Seine and Orne estuaries, France have shown an up-estuary transport caused by the ebb-flood asymmetry (Avoine and Larsonneur, 1987). Such asymmetry creates a tidal sediment trap, thereby explaining the existence of a turbid zone within such estuaries, especially during periods of low river flow. In the upper tidal reaches of the estuary, where the tidal waves and currents damp out, the flood-velocity predominance disappears, and net transport is directed downstream by the seaward flowing river water.

In response to a landward increase of tide wave asymmetry, bedforms migrate upstream in the channel under the influence of flood currents. In the Ord, Australia (a macro-tidal estuary), flood currents cause the largest bedforms to be transported landward and extensive sand accumulation occurs within the channel (Wright, 1985). Another effect of ebb-flood asymmetry is to favour sedimentation at high water slack. This results from the deformation of the tidal wave which induces a longer lasting high water slack than low water slack (Postma, 1967).

The flood-ebb tidal current fluctuation is particularly important in macrotidal estuaries. A change in tide range from spring to neap is normally accompanied by a marked change in current velocity. Greater erosion and resuspension occur at high current velocities during spring tides than neap tides. Therefore concentrations vary with tide range during a fortnightly cycle.

The neap-spring tidal cycle is one of the main mechanisms that control sediment accumulation. There will be more sedimentation than erosion during the period of decreasing tidal amplitude, while the reverse process occurs at the period of increasing

tides. A certain amount of cohesive sediment deposited during neap gets sufficiently consolidated and may resist erosion during the following spring tides, so that a thin lamination of mud accumulates permanently in the estuary bed after each tidal cycle. This fortnightly sedimentation-erosion cycle can also induce sediment escape onto the shelf by a surface seaward density flow, particularly during high river run-off (Castaing and Allen, 1981).

Settling and scour lag effects are other mechanisms that control sediment transport and accumulation over tidal cycles in estuaries (Postma, 1980). These transport mechanisms were first introduced by Van Straaten and Kuenen (1957, 1958) and Postma (1961, 1967), is explained in more detailed by Dronkers (1986). Settling lag is the time taken for a particle to reach the bed after the decreasing tidal velocity can no longer hold it in suspension while scour lag is the delay due to the difference in velocity required to keep sediment in suspension, and that required to lift it into suspension. At high water, because of the settling lag, sediment is carried and deposited further landwards from the point where it start to sink. At the turn of the tide during the ebb, however, due to scour lag the deposited sediment will not be resuspended until the currents have attained a higher velocity than when it was deposited. The overall result of the settling and scour lag effects is that around high water the sediment undergoes a net landward movement whereas at low water, due to the shorter period of slack water no corresponding outward shift occurs. The constant shifting of sediment during flood and ebb with settling and scour lags, and the landward diminishing velocity trend, result in a distance velocity asymmetry whereby the sediment has a net landward transport at each tidal cycle. Consequently the sediment gradually migrates further upstream to deposit in areas where the maximum velocity equals the grain's threshold velocity. Settling and scour lags also could lead to the sediment sorting whereby the grain size progressively decreases towards the estuary head (Dyer, 1988).

ii. Effect of estuarine circulation

The different water movements in the three types of estuaries (salt wedge, partially-mixed,

and well-mixed) result in a different behaviour of their suspended sediment loads. In salt wedge estuaries, most of the suspended material is fluviatile and dispersed through the upper layer. Since upstream water movements are slow, the bottom layer is filled up with sediment that settles through the halocline. If the tidal and wave regimes are mild, and the sediment load is high, it tends to accumulate to form a delta adjacent to the estuary mouth. In partially mixed estuaries, the landward flow is sufficiently strong to transport suspended sediment to the upper limit of salt intrusion. This sediment which may be fluviatile material that has settled from the upper layer or may be of marine origin will accumulate to form a turbidity maximum. In well mixed estuaries, the suspended sediment is dispersed away above the bed by tidal resuspension. Because of the Coriolis force, the flow in a well-mixed estuary leads to the deposition of marine sediments on the left-hand bank, and deposition of fluviatile sediments on the right-hand bank (facing down-stream) in the Northern Hemisphere.

It appears from the above discussion that the three main mechanisms are responsible for transporting and accumulating different sediment sizes within estuaries and their near shore zone. Waves act mainly on coarse material such as sand, shell remains and pebbles; tides acts on fine grain sand and silt; and the estuarine circulation accumulates silt and mud (Postma, 1980). One difficulty that remains paramount when discussing estuarine sediment is that extreme conditions are often more important than the average. One river flood can discharge more sediment in days than normally appears in years. Under extreme flow conditions, the estuary as defined above may not exist and the deposits of a long period can be flushed into the open sea.

Although hydrodynamic processes are generally the primary factor, this is not to ignore the fact that aggregation of fine particles is a very important factor in sediment transport in estuaries (Hunt, 1986; Dyer, 1988; Van Leussen, 1988). This aggregation process has been discussed in Section 2.5.4. There would be little accumulation of fine-grained material if the suspended fine sediment particles were not co-agulated as flocs, aggregates and faecal pellets. Without aggregation there would be hardly any deposition during the short periods of slack water.

The neap-spring cycle also modulates the ratio of river flow to tidal volume, which in turn causes large variation in mixing. The Gironde for example, a macro-tidal estuary with extensive intertidal flats, changes from a well-mixed state during spring tides to a partially-mixed or well stratified state during neap tides (Allen *et al.*, 1980). From their measurements in the Gironde and Aulne, it was shown that tidal effects can be as important as the density circulation in trapping fine sediment.

iii. Effect of waves

Although estuaries are often considered protected environments, waves can have significant sedimentological effects by eroding shores, stripping substrates, and suspending sediments so that they can be dispersed by currents. These waves are either generated externally in the ocean and penetrate estuary mouth or generated internally within the estuary.

Ocean waves often carry high energy that can erode sand from the beach or shoreface and transport it via longshore or drift currents toward the estuary entrance. These result in the development of various sedimentary features such as sand spits, intertidal bars and shoals at the entrance and also cause migration of inlets. The bars and spits function as natural training walls, necessary to maintain a free connection for channels between the estuary waters and the open sea, and protect the inner estuary by reducing the waves' power and erosive capacity (Buller *et al.*, 1975). The effect of waves depends on the fetch length, wind strength and the exposure time. Generally, strongest wave action occurs in estuaries oriented in diagonal directions along the maximum fetch.

Due to their short fetch, estuary waves are shorter and have smaller amplitudes compared to the ocean waves. However, they have significant effect in resuspending fine sediments especially over intertidal flats, drying sandbanks and channel margins. Such waves increased suspended sediment concentration three times more than in calm conditions in the Great Bay estuary, New Hampshire (Anderson, 1972; 1983). Thus, wind-induced waves, despite being damped inside the estuaries, are important erosive agents and may, in

extremely shallow estuaries modify or destroy circulation patterns. Waves hold the material in suspension while the prevailing tidal currents transport it into the estuary or out into the sea.

2.5.5.2 Turbidity maximum

Most estuaries, particularly partially and well-mixed estuaries, show the presence of a zone of high suspended sediment concentration near the limit of salt water intrusion. This feature, termed as turbidity maximum, contains suspended sediment concentrations that are much greater than those in the adjoining river or further seaward in the estuary, and is an important sedimentary feature indicative of fine sediment transport in estuaries (Dyer, 1988; 1994).

The peak suspended sediment concentration in the turbidity maximum varies between wide limits from around 100-200 mg/l in estuaries of low tidal range, up to 1000 - 10,000 mg/l in estuaries with high tidal range (Dyer, 1986). This is 10 - 100 times higher than the concentration found elsewhere in the estuary. These concentrations also vary during the tidal cycle and during the spring-neap cycle. On a neap tide when the current is weaker, the turbidity maximum is less well-developed and sediment concentration is generally low (Avione and Larsonneur, 1987). The grain size of suspended sediment is generally less than 10 μm (Postma, 1967; 1980), but can be larger (20 -30 μm) during peak currents (West *et al.*, 1990).

The location of the turbidity maximum zone in estuaries varies seasonally with river inflow and tidal range (Postma, 1980; Castaing and Allen, 1981 ; Avione and Larsonneur, 1987; Dyer, 1988). During the period of low river discharge, the turbid zone is maintained within the estuary. In the Gironde, the maximum is between 90 and 110 km upstream from the mouth during a normal river flow (Castaing and Allen, 1981). During high river flow, the combined effect of ebb tidal currents and river discharge cause the turbidity maximum to migrate down-estuary. When the migration is sufficiently large, the down-stream end of

the maximum may be extruded out of the estuary at low water. Under such conditions, suspended sediment can escape from the estuaries onto the adjacent shelf (Castaing and Allen, 1981; Avione and Larsonneur, 1987). In general the location of the turbidity maximum coincides with the upper limit of the salt intrusion region, and shifts longitudinally along the estuary as a function of seasonal river flow as the upper limit region moves landward or seaward.

The primary deposition in turbidity maximum region is in the form of silt. Further upstream and downstream fine sand predominates. In other words, the turbidity maximum, governed by the salinity distribution tends to act as a filter within the estuary. According to Postma (1967) and Markofsky *et al.* (1986), the magnitude of a turbidity maximum depends on a number of factors. The most important one is the amount of suspended matter, followed by the strength of estuarine circulation and the settling velocity of the available material.

In some estuaries with a high sediment concentration, the end product of the sediment circulation is the formation of fluid mud close to the bed. This is a layer of low density mud with very large sediment concentrations in the range of 10,000 - 100,000 mg/l (Officer, 1981) and several metres thick (Owen, 1977). A fluid mud layer may be formed from the settling of the homogenous mobile sediment suspension in the turbidity maximum as the current velocity decreases (Odd, 1988; Mehta and Dyer, 1990) . During neap tides a certain amount of the fluid mud becomes compacted, so that as tidal range and currents increase again some of the sediment is able to resist erosion and will be permanently deposited.

One of the important sedimentological effects of the estuarine circulation is to trap suspended sediment in the node, retarding the escape of sediment to the open sea. According to Officer (1981) a well developed estuarine circulation forms an effective sorting mechanism where the coarser silt size particles would be expected to be deposited in the middle to lower reaches of the estuary and the finer, clay-size particles to be carried to the upper limit of the salinity intrusion to form the turbidity maximum.

The turbidity maximum is maintained by a number of processes. In partially mixed estuaries

the mean estuarine circulation has been recognised as the main mechanism for maintaining the turbidity maximum (Schubel, 1969, 1971a; Schubel and Carter, 1984). Postma (1967, 1980) has also proposed a similar model in that the suspended sediment brought into the estuary by the river sinks to the bottom layers in the lower estuary, and is carried back upstream together with particles brought in from lower down the estuary by the landward flowing saline bottom waters to be accumulated at the convergence (a null point) near the head of salt intrusion between the landward bottom residual flow and the seaward surface residual flow. Consequently, the maximum concentration of suspended sediment occurs at the bottom near the null point in salinity of about 1-5‰. This circulation process has been investigated by Feasta and Hansen (1978) using a steady state two-dimensional numerical model. They showed that the magnitude and location of a turbidity maximum depends on particle size, the amount of suspended particle available and the strength of the estuarine circulation. The sediment that recycles many times in the estuarine circulation becomes uniform in size and mineralogy because very fine and less dense sediment is swept out to sea and relatively dense coarse sediment comes to rest.

In British and western European estuaries where tidal ranges are large, tidal pumping due to erosion and suspension of sediment by the tide is a major factor in generating and supporting the turbidity maximum. This tidal transport has been the main mechanism for maintaining the turbidity maximum in the Gironde and Aulne (Allen *et al.*, 1980) , and in the Tamar (Uncles and Stephens, 1989; 1993), particularly during low river discharge. In these estuaries, strong tidal currents during the flood and ebb erode the bed mud and cause the maximum to grow, but near slack water part of the sediment settles and the maximum decays. The net upstream transport of suspended sediment is brought about by the increasing tidal wave deformation further up estuary. This tidal asymmetry results in higher flood-tide velocity which will bring about greater bottom erosion and transport than during the ebb, and could engender a net upstream movement of suspended sediment near the bed (Allen *et al.*, 1980).

2.5.5.3 Sediment deposition

An important aspect of sediment transport is the deposition of sediment particles. This is determined by the their settling velocities, denoted as w_s. The settling of smooth spherical grains is well understood but not so for non-spherical grains. When a spherical grain is settling at a constant velocity through a fluid, the settling velocity is then the terminal velocity attained by the particle when the gravitational force is balanced by the drag force acting on the grain. This terminal velocity is given by the well known Stokes Settling Law:

$$W_s = \frac{(\rho_s - \rho)}{18\mu} g D^2 \qquad [2.54]$$

where ρ_s and ρ the grain and water density, μ is molecular viscosity of water, g is acceleration due to the gravity, and D is the grain diameter. As can be seen the settling velocity varies with the square of the grain diameter. However Stokes Law only valid for grain diameter smaller than ~ 0.1 mm, because small grains have relatively small mass and the main opposing force is only the viscous resistance of the water. At higher grain diameters the settling velocity varies with the square root of the grain diameter following the Impact Law as shown by Equation 2.55 below:

$$W_s = \left[\frac{4}{3}\frac{1}{C_D}\frac{\rho_s - \rho}{\rho} g D\right]^{1/2} \qquad [2.55]$$

where C_D is the drag coefficient and is found empirically to be a function of the Reynolds number as shown in Figure 2.13. These changes in the drag and settling law are linked to a progressive alteration in the pattern of flow around the settling particles. At higher grain diameters the particles are affected by boundary layer separation which occurs behind the

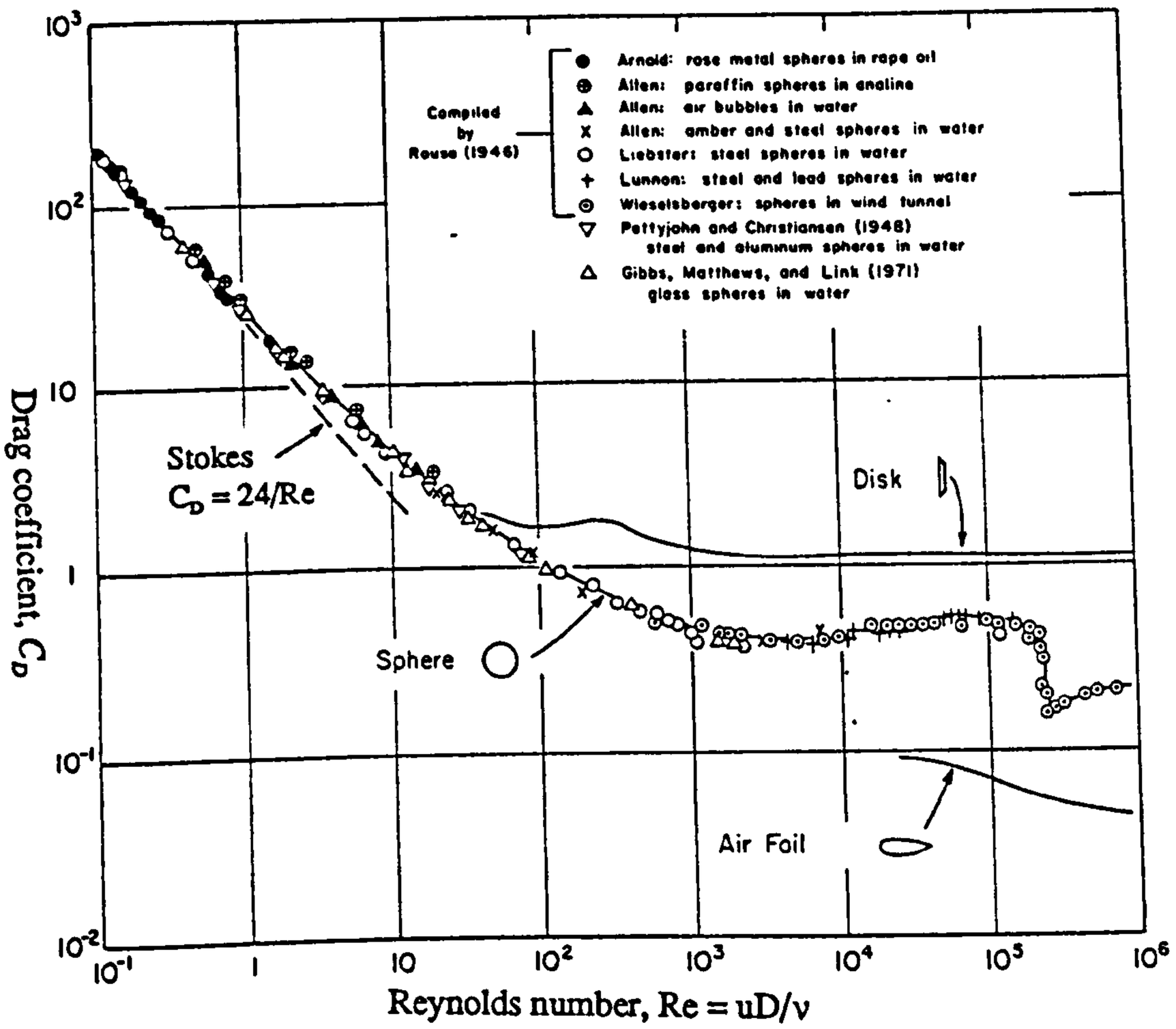

Figure 2.13 Dependence of drag coefficient, C_D on Reynolds number, Re for the steady settling of a smooth, spherical particle. At Reynolds number in excess of Stokes range, the relationship is based on the experimental results. Also shown are the curves for a disk and air foil without the data bases (After Komar, 1981).

falling grains at increased rates of fall velocity.

Two other factors affecting the settling velocity of particles are their shapes and the total particle concentration. The natural occurring grains are rarely spherical in their shapes as assumed in Stokes Law. The effect of departure from a perfectly spherical form is to increase the drag coefficient and to reduce the settling velocity relative to the equivalent sphere. A flat shaped particle settles slower than a sphere or a needle-like particle because it offers more drag. Shape effects are normally included in empirical relations through the use of a shape factor such as the Crey Shape Factor (eg. Komar and Reimers, 1978). At sufficiently high concentrations, the settling velocity is also a function of concentration. Data from various estuaries (Dyer 1989; 1994) show that if the concentration is less than about 2-5000 mg/l, the settling velocity w_s depends on the concentration according to $w_s \propto c^n$ where n varies between 0.6 - 2.2. At very high concentrations (10-20 g/l) the settling of particle interfere with each other and hindered settling occurs (Dyer 1988).

The considerable differences in the settling velocity-concentration relationship between estuaries may be the result of variations in floc density and organic carbon content, as well as differences in the tidal state (Dyer, 1989). Therefore, particle flocculation introduces further complication to the settling velocity of sediment grains.

CHAPTER THREE

OBSERVATIONAL TECHNIQUES

3.1 Introduction

The observational programmes were designed to quantify suspended sediment dynamics and flux in the Taf estuary. The measurements were planned to include spring-neap tidal cycles at different seasons of the year. To achieve this, arrays of instrumented moorings were deployed to obtain time series of data, while boat surveys were carried out to establish a spatial context.

In the following, the two main data collection programmes i.e. fixed mooring (anchor station) surveys and the spatial surveys employed to measure the mean flow and water column properties including suspended sediment concentrations will be described. Other measurements to supplement the above survey programmes will also be discussed. The basic processing of the data sets and transmissometer calibration will be described.

3.2 Data acquisition

3.2.1 Anchor station surveys in the lower estuary

To estimate the suspended sediment flux in the Taf, an array of fixed measurement stations were set up across the estuary. The original plan to set up these stations across the estuary mouth along transect T11 (Figure 3.1) had to be abandoned due to rough sea states particularly during periods of strong winds. Subsequently, the flux measurements were carried out further up the estuary at survey transect T9, and later at transect T5. These transect numbers are referred to the already established survey transects described in Jago (1974; 1980). Between four to seven stations were set up across each transect and at

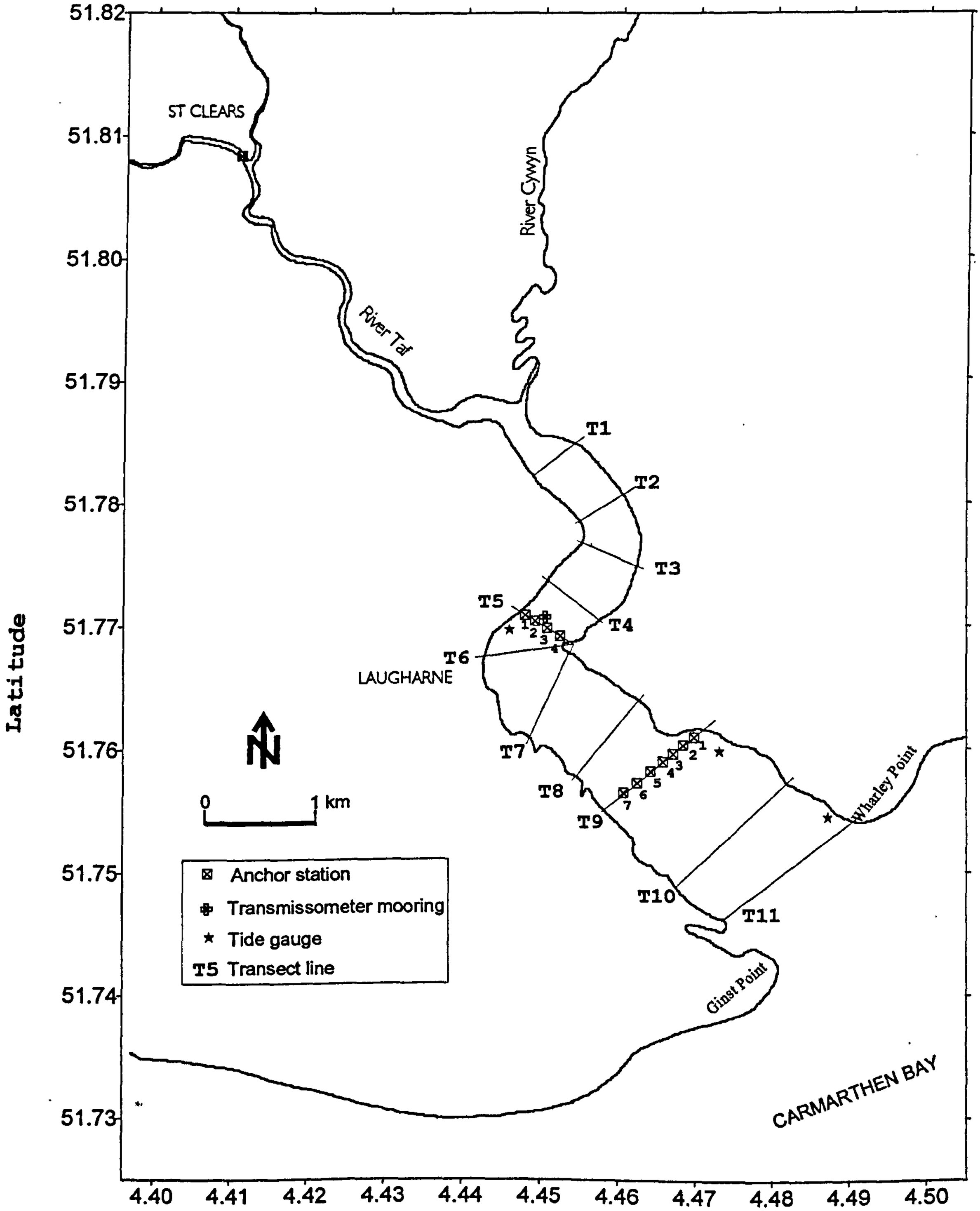

Figure 3.1 The Taf estuary showing the two transects (T9 and T5) for the anchor station surveys. Other transects used in previous studies are also shown.

each station, measurements of salinity, temperature and suspended sediment concentration within the water column were made using CTD and transmissometer casts, while the current velocities at each station were measured using various current meters. These measurements were made over neap-spring tidal cycles at both transects. The instrumentation used for the anchor station surveys is described in more detail in Sections 3.2.2 and 3.2.3.

In order to study the seasonal variation of suspended sediment flux and estuarine circulation, the data collection programme along these transects was carried out at different times of the year. Three data collection campaigns were conducted between October 1994 and September 1995 at T9 and T5 as shown in Table 3.1. Surveys of the cross-sections at the transect lines were carried out (see Section 3.2.9) and the results are shown in Figure 3.2.

Table 3.1 Summary of the three data collection campaigns undertaken between October 1994 - September 1995.

Sampling phase no.	Time	Monthly average river discharge (m^3/s)	Number of tidal cycle measured	Survey transect	Number of anchor station across the transect
I	October 1994	7.1	2	T9	5
II	July 1995	0.75	4	T9	7
III	September 1995	0.52	4½	T5	4

(a) Phase I

The surveys were carried out on the 5 and 6 October 1994 covering two spring tidal cycles. Five monitoring stations spaced about 150 m apart were set up across the estuary (Figure 3.2a). Station 1 was located within the main ebb channel, but all other stations were on the intertidal sand flat and became dry at low water. Fixed moorings were set up at stations 1 and 3. On both dates, the measurement started at HW and continued until HW of the following tide. For a few hours during LW no measurements were made as the estuary was

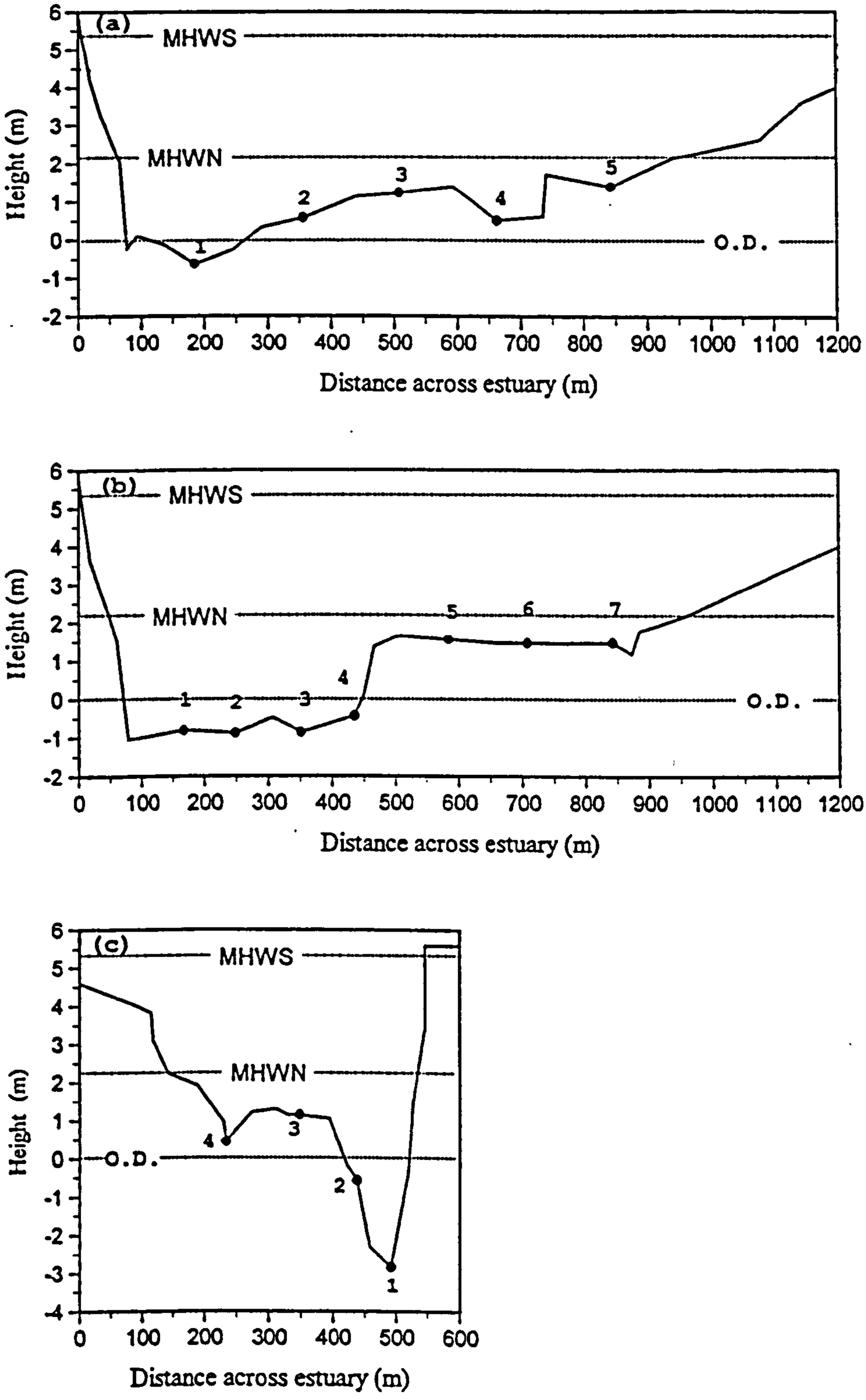

Figure 3.2 Cross section profiles at anchor station transects: (a) transect T9, October 1994; (b) transect T9, July 1995; and (c) transect T5, September 1995.

dry. The river discharges and tidal heights for 5 and 6 October (four different tides) are shown in Table 3.2 .

Table 3.2 Tidal height and daily river discharge for duration of hydrographic measurements in October 1994.

Date	Duration of measurements	River Discharge (m^3/s)	Tidal Range (m)
5 Oct. 1994 (Ebb)	4hrs. 40min.	4.29	8.20
5 Oct. 1994 (Flood)	4hrs. 40min.	4.29	8.62
6 Oct. 1994 (Ebb)	5hrs. 10min.	4.13	8.78
6 Oct. 1994 (Flood)	3hrs. 30min.	4.13	8.98

(b) Phase II

The second sampling campaign was carried out at transect T9 in a summer month (July 1995) when the fresh water discharge was low (the monthly averaged discharge = 0.75 m/s). During this sampling campaign the main ebb channel at transect T9 had changed, and a bed with a wider channel had developed (Figure 3.2b). Within this main channel, there were two small channels through which the rest of the flow was channelised at the end of the ebb. A 2.5 m height sand flat had developed on the right bank of the estuary (looking down estuary) creating a steep slope between the main channel and the sand flat.

Seven anchor stations were set up across the estuary to represent properly the new bed configuration (Figure 3.2b). Stations 1, 2, 3 and 4 were located within the main channels and spaced about 100 m apart, whereas stations 5, 6 and 7 were on the sand bank were spaced about 150 m apart. The fixed moorings were set up at stations 1 and 3. The CTD-transmissometer profiling and current metering for all the stations were undertaken for four complete tidal cycles between 14 - 20 July 1995. The monitoring started before the onset of the flood tide and stopped when the tidal prism was expelled out of the estuary. On 14 July, the CTD data for the last 3 hours of the measurement time were lost because the built-in memory of the CTD unit was saturated. However the temperature and salinity data for

stations 1 and 3 were obtained from other independent instruments used to measure the current velocities. The summary of the measurement times and details of the tidal heights and river discharges are given in Table 3.3.

Table 3.3 Tidal height and mean river discharge for duration of hydrographic measurements in July 1995.

Date	Duration of measurements	River Discharge (m/s)	Tidal range (m)
14 July 1995	9 hrs. 15 min.	2.11	8.47
16 July 1995	9 hrs. 40 min.	0.86	8.01
18 July 1995	9 hrs. 40 min.	1.30	6.43
20 July 1995	11 hrs. 20 min.	0.81	4.52

(c) Phase III

In September 1995 the measurement of sediment flux was made at transect T5. The river discharge for the month (0.52 m/s) was lower than the monthly average for September (4.62 m/s) due to the continued drought since the summer 1995. At this transect the estuary channel was narrower; thus 4 anchor stations were set up across the estuary, and stations 1 and 4 were set up as the mooring stations (Figure 3.2c). Station 1 was located in the main channel and at this location the channel was the deepest part of the estuary and water in the channel remained about 2 m deep at low water. The stations were occupied for 4½ tidal cycles between 12 - 19 September 1995 during a falling spring tide sequence (Table 3.4). On 12 September, the measurements were made only for ebb tidal cycle, and it was the third tidal cycle after the highest spring tide.

Table 3.4 Tidal height and mean river discharge for duration of hydrographic measurements in September 1995.

Date	Duration of measurements	River Discharge (m^3/s)	Tidal range (m)
12 Sept. 1995 (ebb)	4 hrs. 30 min.	0.60	8.15
13 Sept. 1995	7 hrs. 55 min.	0.53	7.58
14 Sept. 1995	7 hrs. 50 min.	0.62	6.75
15 Sept. 1995	7 hrs. 50 min.	0.64	5.79
19 Sept. 1995	7 hrs. 45 min.	0.35	2.97

3.2.2 CTD and suspended sediment measurement.

The vertical profile measurement of salinity, temperature, and suspended sediment concentration were carried out using a combined profiler made up of an Applied Microsystems Limited STD-12, and a Sea Tech transmissometer with a 10 cm transmission beam path length. The STD-12 was a self-logging CTD instrument and was capable of recording 8 data per second. The transmissometer was a compatible unit and was coupled to the CTD during the measurement. The instrument was set to record at 10 cm depth increments. The accuracy of the transmissometer was ± 0.5% of the transmitted beam. Measurements were made at each station from an inflatable boat which traversed to- and fro- across the estuary for the whole tidal cycle. During the measurement, the combined CTD-Transmissometer profiler was slowly lowered into the water until the probe touched the bottom, and slowly raised up to the surface at an average rate of 0.2 m/s to give continuous records of salinity, temperature, and water transmissivity both during downward and upward movements of the profiler. Between 5 to 15 minutes were required to complete each run (i.e. to do CTD-Transmissometer casts at all stations across the transect at any per-set time interval), depending on the number of accessible stations across the estuary and also the water depth. After each total survey, the data were transferred from the CTD unit to a portable micro-computer and the internal memory of the

profiler was cleared for the next survey. The data were then converted into engineering units for further processing.

3.2.3 Current velocity measurement

It was desirable to measure current velocities and other physical parameters simultaneously at each anchor station across the estuary. Due to limited manpower and resources, three and sometimes up to five different types of current meters were employed to measure the tidal flow velocities at these stations at any one survey. Each type of current meter used is briefly described below.

(a) ALEC Electronic EM current meter

This current meter was deployed at Station 1 during the October 1994 sampling campaign. It is a two component electromagnetic current meter and compass for current speed and direction. Current speeds and directions were measured at 0.5 m depth-increments and at 15 minutes intervals. The measurements were made from the survey boat moored at the station. One advantage of this instrument is its instantaneous response that reduced the time lapses required to read at each level, thus increasing the compatibility of the results between each level. The instrument provides a 10 second running average; this was manually averaged over 1 minute.

(b) Valeport Limited direct reading CM (Model 108 Mk III)

This current meter which was also fitted with conductivity, temperature and pressure sensors was deployed at Station 3 (October 1994), Station 1 (July 1995) and Station 4 (September 1995). The measurements were made from the boat moored at these stations during each sampling campaign. The current meter was attached to a stainless steel tackle and weight with a streamlined mass. The whole assembly was raised up and down by a hand operated winch attached to the boat's derrick. The one minute averaged current speed and direction, temperature, salinity and depth (given by pressure in dBar) were recorded for every 0.5 m (1.0 m when water depth was deeper than 3 m) depth increment. The measurement was repeated every 15 minutes. Readings were recorded from the Control

Display Unit which were accurate to 0.001 m/s for current, 0.001 °C for temperature, 0.001 ppt for salinity and 0.001dBar for pressure. Operational difficulties with this current meter increased the time for measurement at each depth increment. One disadvantage arising from this technique was the time taken for readings at each level so producing time lapses between observations and reducing their comparability in this tidally changing system.

(c) Velocity Gradient Unit (VGU)

The VGU is an array of current meters which measure current velocities at fixed heights above the bed. The VGUs were deployed at stations 2 and 4 in both October 1994 and July 1995, and at stations 2 and 3 in September 1995. At these stations the VGU masts were constructed using a steel pole hammered into the bed. An extra stability of the mast was provided by four guy ropes tied to four metal stakes driven into the bed.

Each VGU unit consists of an array of 10 Ott current meters on the steel mast which was bolted to the steel pole. Five of the current meters faced the ebb direction and the other 5 faced the flood direction. The current meters were logarithmically spaced between 0.1m to 2.0 m above the bed. The current meters were connected to a data logger which was buried into the sand bed at 3 m from the mast (to minimise interference with the tidal flow). The logger was programmed to record a 1 minute-averaged current velocity from each current meter at 10 minutes intervals. The VGUs were deployed continuously for a period of 2 weeks, thus they provided current data not only during those tidal cycles where the CTD-Transmissometer casts were made, but also for every tidal cycle during the deployment period. The Ott's height above the bed were measured every day during low water. Scouring at base of the mast and deposition by the active sand bank migration caused the Ott heights to vary during neap-spring tidal cycles. On many occasions, when fast built up of sand was taking place, the bottom rotors were buried, and the VGU mast had to be lifted, or even relocated for the next tide.

The readings of the Ott current meters were affected by fouling by seaweed and debris, so they were cleaned during low water. Sand grains sometimes trapped in gaps between the impeller and the main body of the current meter, giving faulty readings. Thus, not all the data were recoverable and the time-series are fragmented.

(d) NBA direct reading current meter

The NBA current meter (N.B.A. (Controls) Limited, model DNC-3) measured current velocities at Station 3 on 14and 16 July 1995 from a moored boat. When there was enough water for the boat to travel across it was also used to measure currents at Stations 5, 6 and 7. The velocities were recorded as numbers of impeller revolution per minute. Currents were recorded at 0.5 m (1.0m when water depth was deeper than 3m) depth increments from the deck readout unit. As the work boat had to travel between the four stations, the measurements could not be repeated every 15 minutes as intended, instead up to 30 minutes were required. The accuracy of the instrument was ±2% F.S.D. (Full Scale Deflection). In the early hours of its deployment on 18 July 1995, the NBA current meter was found to be malfunctioning and had to be replaced by a small BFM 002 Braystoke current meter.

(e) Braystoke BFM 002 miniature current flow meter and Braystoke BFM 008 current meter

The Braystoke BFM 002 current meter was employed at Station 5 in October 1994 and at Stations 3, 5, 6 and 7 on 18 and 20 July 1995 while the BFM 008 Braystoke current meter was used at Station 1 in September 1995. In October 1994, only surface and bottom readings were measured, but in July and September 1995, the currents were measured every 0.5 m depth increment. The readings were given as the number of impeller revolution per 50 second period.

3.2.4 Time-series measurement of suspended sediment concentration

In addition to the anchor Stations surveys, fixed mooring high resolution measurement of suspended sediment concentration were made during September 1995 and September 1996. The measurement in September 1995 was made using a single CTD-Transmissometer probe (Applied Microsystems Limited STD-12 and Sea Tech transmissometer) fixed at 0.25 m above the bed on the VGU mast. The probe also recorded the temperature, salinity and the height of the water column. The measurement was made at anchor Station 2 (transect T5) over 3 consecutive neap tidal cycles on 16 and 17 September 1995, on two deployments.

On the first deployment, when the probe was orientated parallel to the flow, erroneous salinity readings were obtained due to sand becoming trapped within the conductivity cell, most probably during the early stage of the flood. This problem was overcome by repositioning the probe perpendicular to the flow direction on the second deployment. The instrument was set to record the changes in temperature, salinity and suspended sediment concentration at one minute intervals. The current velocity at this station was provided by the 5 Ott current meters on the VGU which recorded the tidal flow velocity at 10 minute intervals.

In September 1996 the suspended sediment concentration measurements were made over neap-spring tidal cycles from 10 - 25 September 1996. Three self-logging transmissometers with 10 cm path length were positioned at 0.25 m, 0.5 m and 1.0 m above the bed close to the main ebb channel upstream of Transect T5 (Figure 3.1). These instruments, developed at the University of Wales, Bangor, have a similar design to that of a Sea Tech transmissometer; they were set to record transmittance at one minute intervals over the whole period of their deployment. The current velocities were measured by the VGU located at 5 m distance from the transmissometer mast.

3.2.5 Anchor station survey in the upper estuary.

In addition to the multi-station profiling at the lower estuary, a single station measurement was made at St Clears, 11 km upstream of the estuary mouth (Figure 3.1). This station was occupied during a spring tidal cycle, on 12 July 1995. The tidal range was 7.76 m while the river discharge was 0.56 m/s. At this station, depth profile measurement of temperature, salinity and current velocity were made at 15 minutes intervals using the Valeport Mark III combined current meter-CTD probe, while the suspended sediment concentration was determined by taking surface water samples over the same time interval. Additional water samples at the bottom and mid-depth were also collected using an NIO sampling bottle. The combined CTD-Transmissometer profiler was not used at this station as the instrument was being used for the spatial survey.

Similar measurements for a neap tide were not carried out as saline water does not reach St. Clears during the neap.

3.2.6 Spatial surveys

To characterise the suspended sediment distribution in the estuary, spatial surveys were made along the longitudinal axis of the estuary over the neap-spring lunar cycle. These surveys were undertaken during three different data sampling campaigns between September 1994 and September 1996 (Table 3.5). In each survey, vertical profile measurements of temperature, salinity and suspended sediment concentration were made

Table 3.5 Tidal condition and river discharge for the spatial surveys

Sampling phase no.	Date	River discharge (m^3/s)	Tidal range (m)
I	28/09/94	5.59	3.88
	30/09/94	4.99	3.58
	01/10/94	4.90	4.40
	02/10/94	6.37	5.58
	03/10/94	4.96	6.82
II	13/7/95	0.86	8.28
	17/7/95	0.91	7.31
	19/7/95	0.94	5.46
III	10/9/96	0.75	5.13
	11/9/96	0.79	5.90
	13/9/96	0.70	6.81
	15/9/96	0.68	7.58

at fixed stations along the estuary axis within one hour either side of high water starting from the estuary head in the fresh water region and finished at the mouth. The same CTD-Transmissometer probe as used in the anchor station surveys was used in the spatial surveys. The measurements were made at the 32 stations set up along the deepest part of the estuary channel (Figure 3.3). However, the actual number of stations measured in each survey varied according to the upstream limit of the tidal intrusion. The distance between the measurement stations was about 200-400 m in the upper reaches of the estuary but further apart (400-800 m) in the lower reaches of the estuary. In the upper estuary, these stations were established from the known landmarks, while at the lower section, the locations of the stations were obtained from GPS fixes.

3.2.7 Water sampling

To calibrate the tranmissometer during the anchor station surveys, surface water samples were collected each time the CTD-Transmissometer casts were made at one of the mooring stations (Station 3 in October 1994, and Station 1 in July and September 1995). The water samples were normally obtained from 0.2 m below the surface and kept in clean 1300 ml plastic bottles for later determination of suspended sediment concentration and particle size analysis in the laboratory. In July and September 1995, additional water samples were also collected at the other mooring stations during the early stages of the flood and the end of the ebb. At these times, the water depth in the channels was too shallow for the survey boat to make CTD-Transmissometer casts, thus the suspended sediment concentration could be determined directly from these samples.

For spatial surveys, water samples were also collected for suspended sediment determination and transmissometer calibration. These samples were collected randomly at the sampling stations as the survey was conducted from the upper to the lower estuary so that the whole range of sediment concentration was obtained. During September 1996, water samples were collected at all stations within the turbidity maximum zone. At these stations the transmissometer was normally saturated, thus the suspended sediment concentrations could be obtained only from these samples.

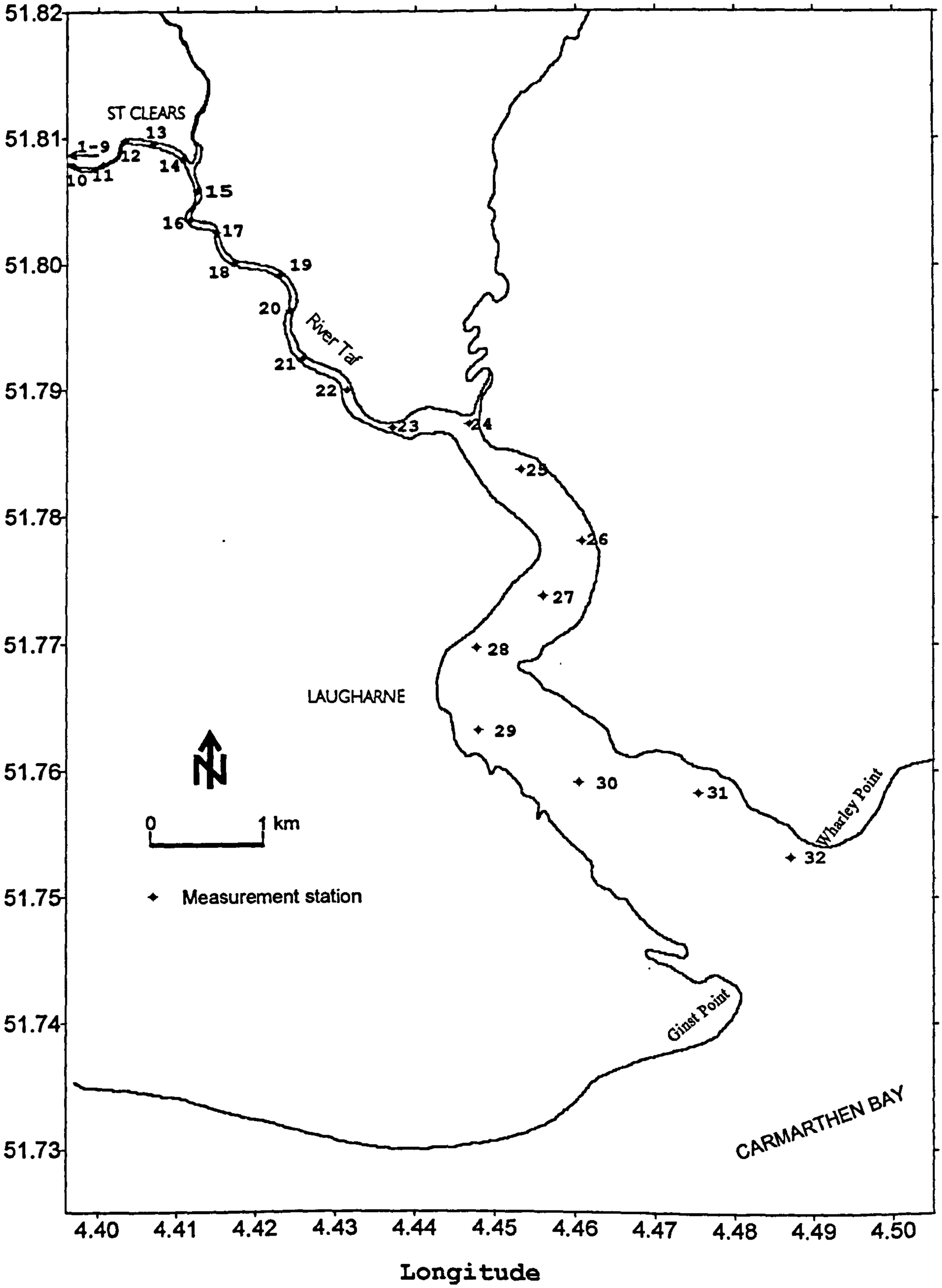

Figure 3.3 The Taf estuary showing the locations of spatial survey stations.

3.2.8 Tidal measurements

Continuous records of the water levels were obtained from tide gauges installed at selected locations within the estuary. Two Aanddera Water Level Recorders were deployed during each survey campaign (Figure 3.1). In October 1994 they were deployed at Wharley Point and by the Boat House near Laugharne. The Boat house deployment was maintained during all three sampling campaigns. The Wharley Point location was shifted to just downstream of the transect T9 in July 1995, but again it was moved back to Wharley Point during September 1995. These tide gauges recorded water level every 15 minutes interval. In each deployment both tide gauges were levelled to the established Ordnance Datum bench marks at Laugharne. No tide gauges were installed during the period of spatial surveys in September 1996.

During the second sampling campaign, the tide gauge at Transect T9 was not switched on, thus failed to function. In September 1995 the tide gauge deployed at Laugharne gave erroneous water level records, thus water level was obtained from the other tide gauge at Wharley Point.

The tidal ranges for Carmarthen Bay area have been estimated using POLPRED tidal prediction software supplied by Proudman Oceanographic Laboratory, at the Bidston Observatory.

3.2.9 Surveys of estuary cross-section

A precise profile of the estuary cross section was required for the determination of cross sectional area which is used in the sediment and water fluxes calculation. It was also important to know the exact positions of the anchor stations set up across the estuary. The estuarine profiles along the transects were obtained by levelling surveys at low tide. In October 1994 and September 1995 (transects T9 and T5, respectively), the surveys were carried out using a microptic level (Nikon Auto-level AP-3) and staff. In July 1995 the estuary profile (transect T9) was surveyed using an EDM (Electronic Distance Measurer).

All the surveys were carried out during low water when the estuary was dry (except in the main channels). At transect T9, the water in the deepest part of the ebb channel was less than 0.5 m during both sampling campaigns, thus the whole section of the estuary cross section could be surveyed. At (transect T5) the water in the main channel was almost 2 m deep, thus the depth of the channel at this transect was estimated by using a graduated measurement pole.

Permanent steel poles used in previous studies (Jago, 1974) were used as the reference marks (temporary bench marks) for the transect surveys. The height of these poles were levelled to the established Ordnance Datum bench marks at Laugharne.

3.2.10 Sediment core

Another independent measurement made in this study was the radiometric dating of salt marsh sediment cores. Details of core sampling and dating techniques used to estimate the sedimentation rate of the salt marshes are given in Chapter 9.

3.3 Data processing and sample analysis

3.3.1 CTD and transmissometer data

The raw data from the CTD-Transmissometer output were processed using a BASIC (GENSPLIT.BAS) despiking and splitting programme (S.E. Jones, pers. com.). Using this programme the data of temperature, salinity and beam transmission were split into individual cast numbers. Each cast was then viewed individually and spikes were removed. The output from the programme were the averaged values of temperature, salinity and beam transmission for every 0.5m depth interval. Both the data from the spatial surveys and anchor station surveys were processed in this manner.

3.3.2 Current meter data

Data recorded by the Ott current meters were the number of impeller revolution in a 60 seconds period. They were converted to current velocities in metres per second using the following calibration factors which were provided by the manufacturer:

for $n \leq 0.91$, $v = 0.2416n + 0.016$, and

for $n \geq 0.91$, $v = 0.2578n + 0.001$

where n is number of revolution per second, and v is current speed in m/s.

The NBA , Valeport and Braystoke current meters, which all gave the current speed in number of impeller revolutions in either 60 or 50 seconds time periods were all converted into current speed in metres per seconds using their respective calibration factors as recommended in the operation manuals.

No attempt has been made to inter-calibrate each type of current meters used in the study. The values were assumed to be correct within their respective limitations.

3.3.3 Gravimetric analysis of water samples

Water samples were brought to the laboratory for the determination of suspended sediment concentration by the standard gravimetric technique. Depending on the amount of solid in the samples, known volumes (between 100 - 500 ml) of water were filtered onto preweight Whatman GF/C glass microfibre filters under negative pressure. The filters were rinsed four times with distilled water to remove any residual salt. The filters with the sediment were then dried in the oven at 60 °C for 12 hours and allowed to equilibrate with the atmosphere before being reweighed for calculation of sediment concentration. Blank filters were used to determine the overall accuracy of the procedures adopted. 500 ml of distilled water was passed through the blank filters, dried and reweighed. The error from this exercise was less than 0.3 %.

3.3.4 Particle size analysis of suspended sediment

Attempts were made during the first data collection campaign to determine the particle size of suspended sediments *in-situ* using a Par-tec100 laser reflectance particle sizing instrument (Lasentec Inc., Redmont, WA 98052) belonging to Plymouth Marine Laboratory. Owing to instrument failure during the deployments, no data were obtained. However, water samples were collected during the anchor station and spatial surveys and brought back to the laboratory for the calibration of the transmissometer. Apart from the gravimetric analysis for the determination of suspended sediment concentration, the water samples were also analysed for particle size distribution using a Galai CIS-100 Particle Size Analysis system. The instrument is a combined system of a laser-based size analyzer and a video-based shape analyzer that provides fast and accurate particle size distributions and shape characterizations. However, for the purpose of this study we were concerned only with the size distribution of the suspended particles. The instrument was set to analyse particle size between 2 - 600 μm.

The water samples were subjected to inevitable agitation during sampling, handling and transportation which breaks any loosely bound flocs, while during storage prior to the analysis, flocs undoubtly formed again with different sizes and characteristics. Thus, the particle size distributions of the fine fraction of suspended sediment determined in the laboratory will not exactly represent the size distribution in the field; however, the coarser fraction (sand) of the suspended particles would not be affected by floc formation and rough handling of the samples prior to the analysis.

The main objectives of this size analysis were to determine the percentages of fines (mud) and coarse particles (sand) present in the upper water column at different stages of the tidal cycle. It might also be possible to look at any relationship between the modes of particle size present in the samples at different stages of the tide. About 500 ml of the water samples were passed through laser particle sizer. Pumping rate was maintained at 0.7 ml/sec. Before the analysis, the samples were vigorously shaken and during the analysis the samples were continuously stirred in the sample reservoir to break up any flocs.

As the instrument was connected to a video monitor, it was possible to observe the particles that passed through the analysing cell. Plankton were found in some samples in variable proportions. Samples collected from Station 4 (September 1995) had more plankton than those collected from Station 1 i.e. from the middle of the channel.

3.4 Calibration of transmissometer

The transmissometer was calibrated separately for anchor station surveys and spatial surveys, and for separate sampling campaigns. For each sampling campaign, the data for all surveys were combined to give a single calibration curve. A simple least square linear regression analysis was employed to find the relationship between the beam attenuation coefficient measured by the transmissometer and the suspended sediment concentration obtained from the gravimetric analysis of the water samples. Where the transmissometer was saturated (negative transmittent), the data was omitted in the regression analysis.

The beam attenuation coefficient, c can be determined from the following relationship:

$$c = \frac{-1}{r} \ln\left(\frac{T}{100}\right) \qquad [3.1]$$

where r is the beam path length (in metres), and T is the percent of light transmission. Thus, for a transmissometer with a path length of 10 cm, the light attenuation is calculated as:

$$c = \frac{-1}{0.1} \ln\left(\frac{T}{100}\right) = -10 \ln\left(\frac{T}{100}\right) \qquad [3.2]$$

The suspended sediment concentration can then be calculated from the relationship given by the calibration curve as:

$$concentration = \frac{c-N}{M} \qquad [3.3]$$

where N is the intercept, and M is the slope.

From this relationship all values of beam attenuation were converted to sediment concentrations (mg/l)

3.4.1 Calibration for spatial surveys

The calibration curves for the three survey campaigns are shown in Figure 3.4. The calibration differed slightly between sampling campaigns but highly significant correlation coefficients ($R^2 > 0.83$) were obtained for all three sampling times, despite some scatter at higher suspended sediment concentration. The consistently good correlation coefficient in each sampling campaign suggests that the suspended material was very homogenous in composition and size distribution throughout the longitudinal axis of the estuary. The scatter observed at higher SPM concentration might be a result of inaccuracy in the gravimetric analysis as only small quantities (100 - 200 ml) of the total sample could be passed through the filter. Suspended sediment is also known to move in clouds of variable concentration particularly in high concentration zones, so reducing the representativeness of the water samples collected for calibration. Saturation of beam attenuation at high sediment concentration is also another source of scatter at high concentrations.

3.4.2 Calibration for anchor station surveys

There was a large variation in SPM concentration in water samples collected during the anchor station surveys. Highest concentrations (up to 1000 mg/l) were normally found in samples collected during the early stage of the flood and at the end of the ebb when the tidal current was strongest, but these reduced to about 10 mg/l around the time of HW.

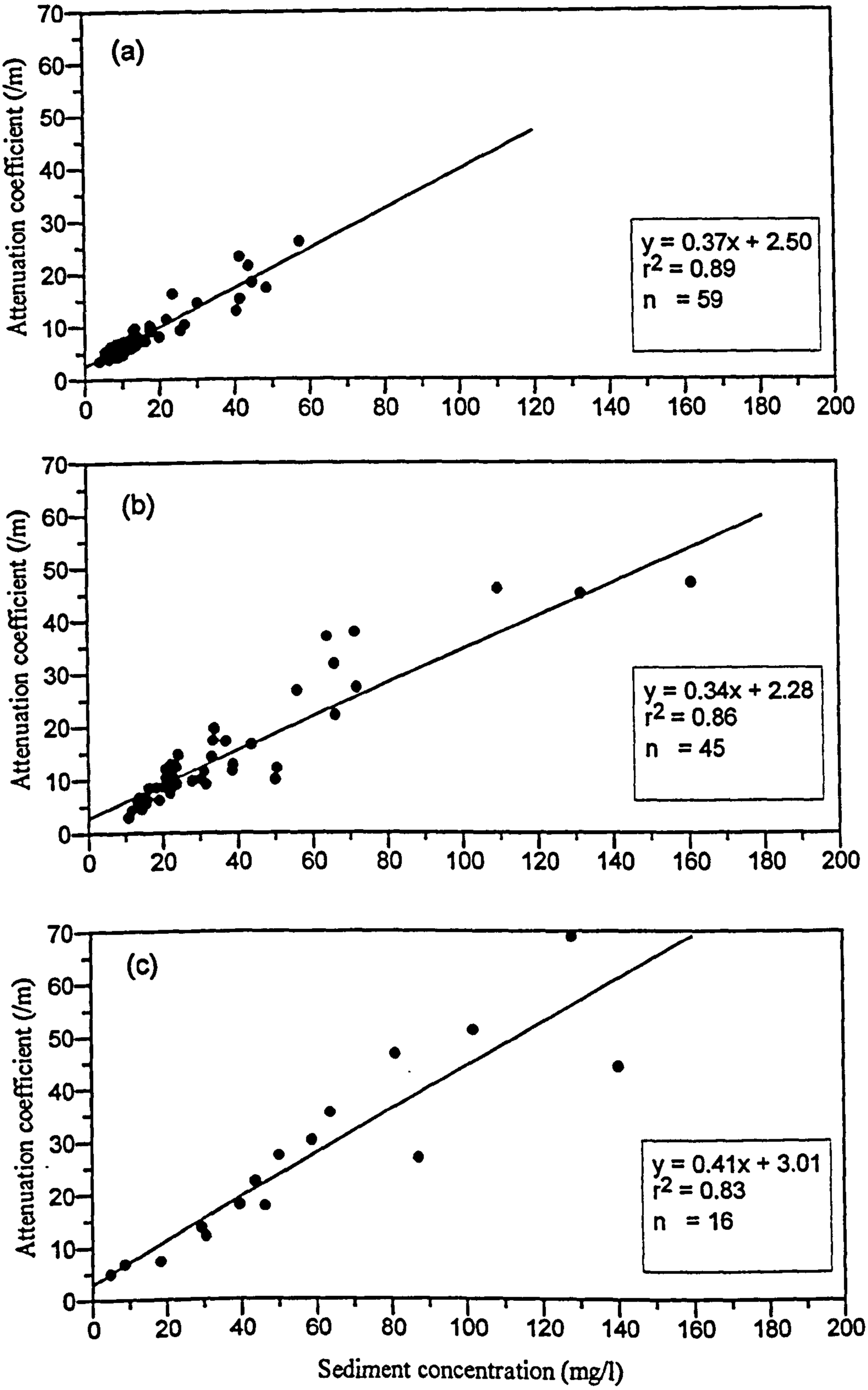

Figure 3.4 Transmissometer calibration for three spatial surveys carried out in; (a) September-October 1994, (b) July 1995, and (c) September 1996.

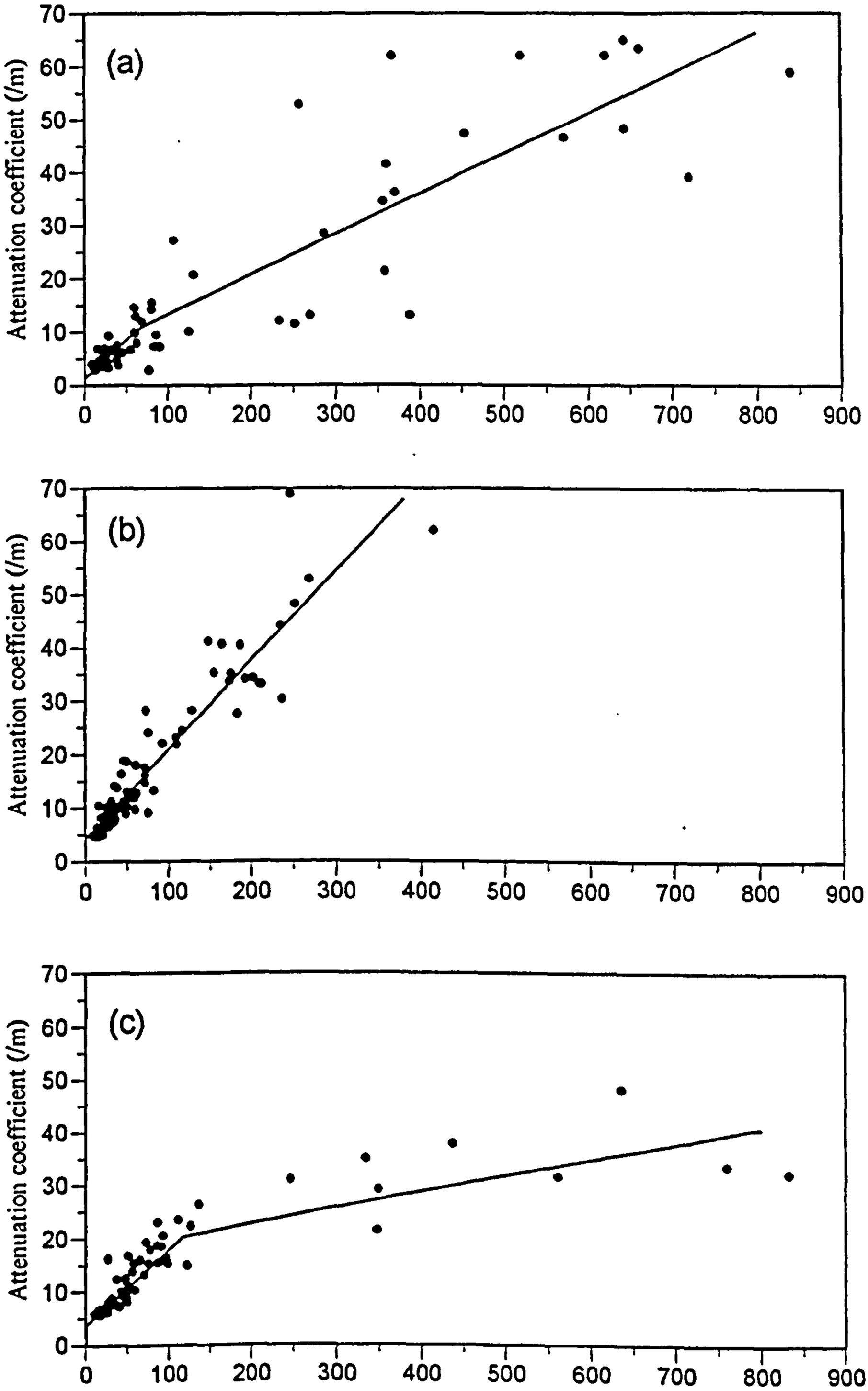

Figure 3.5 Transmissometer calibration for anchor station surveys occupied in; (a) October 1994, (b) July 1995, and (c) September 1995. See Table 3.6 for regression statistics.

There was more than two orders of magnitude difference between the lowest and the highest concentrations and this posed some problem in the transmissometer calibration. Not only does it effect the conversion of the beam transmittance into concentration but it causes uncertainties in the calculation of sediment flux from the concentration data.

The particle size distribution analysis indicated that more than 80 % of suspended sediment collected during fast tidal currents was made up of sand particles; however, at HW slack, the sand fraction was almost absent and the SPM was made up mainly of very fine material (mode = 20μm). For this reason two calibration curves, one for the silt fraction and another for the sand fraction were prepared for each sampling campaign; however, for July 1995, both fractions could be represented by a single calibration curve (Figure 3.5 and Table 3.6). The silt fraction shows a better correlation ($R^2 > 0.68$) than sand fraction (R^2 between 0.58 - 0.65). As expected the coarser fraction has a lower calibration slope than the smaller fraction. The calibration for the sand fraction was complicated by localised and temporal variations in particle population characteristics, particularly the proportion of fines, causing a large scatter of the data points. The scatter was also caused by spatial and temporal variations between transmissometer measurements and water samplings in this tidally active sediment transport.

Table 3.6 Least squares linear regression between beam attenuation and mass concentration for three anchor station survey campaigns.

Date	Sediment size	Sample size	Intercept	Slope	R^2
October 1994	Silt fraction	42	1.33	0.14	0.68
	Sand fraction	23	5.79	0.08	0.58
July 1995	All data	88	4.25	0.17	0.88
September 1995	Silt fraction	43	3.69	0.14	0.74
	Sand fraction	26	16.86	0.03	0.65

CHAPTER FOUR

ESTUARINE HYDRODYNAMICS

4.1 Introduction

Estuaries are a highly dynamics environment caused by the interaction of fluvial water and tidal water. This interaction brings about various types of mixing and water circulation that control the transport and deposition of sediment, and other dissolved substances. Understanding of these circulations is needed to predict the pattern of sediment distribution and the processes that determine it.

The water circulation in estuaries is governed by several factors. Some of these vary periodically, but others vary on a random basis. In the first category we have the periodic flooding and ebbing of the tide during the fortnightly lunar cycle; the fresh water discharge from the river and the meterological forces such as wind and waves, which all vary seasonally but may also change rapidly on a daily basis. The wind stress on the surface may change the net surface flow direction, while waves can intensify vertical mixing. Included in the second category is channel morphology which can vary over one or more tidal cycles. Another principle agent is solar radiation whereby the heated layer of the water surface tends to reduce vertical mixing. Though estuaries experience similar physical, chemical and biological processes, it is the way in which these different factors interact that makes each estuary exhibit some degree of uniqueness.

Estuarine circulation varies both spatially and temporally. The tidal influence is strongest in the lower estuary but diminishes towards the head. The rise and fall of the water surface is accompanied by a horizontal current that varies in strength with location. The changing of channel topography through the formation and destruction of banks, bars and saltmarsh erosion will all be reflected in the pattern of the flow dynamics of the estuary, while the amount of river discharge will alter density stratification and the up-estuary limit of salt

water intrusion.

Many authors have classified estuaries in terms of their mixing processes e.g. Pritchard (1955), Hansen and Rattray (1966). These classifications were based on studies in large estuaries in North America where the tidal depth fluctuations are minimal compared to the depths of the estuaries; thus fresh-saline interaction is a dominant factor in controlling the estuarine circulation. However in many UK (and NW Europe) estuaries which have large tidal ranges, the fresh-saline interaction is a secondary factor compared to the variation in water depth. In many of these estuaries, salt water is totally flushed out with the ebb tide and for several hours during low water only river flow may remain until the next tidal inundation. In such condition the most important factor in controlling the estuarine circulation is the changing in water depth which may vary from a few tens of centimetres to as much as 6-7 metres within a few hours of a tidal cycle.

Previous accounts on the dynamics and circulation of the Taf estuary have been given by Jago (1974, 1980). Description of the estuarine circulation has been based on single station measurements along the estuary channel over a number of tidal cycles. The focus of the present study is on multi-station measurements made across the estuary channel over spring- neap tidal cycles, with variable inputs of fresh water discharge. Thus a full spectrum of estuarine dynamics may be deduced. In addition, the measurements made during HW along a longitudinal profile further enlighten our understanding of the extent of salt water intrusion and thus the transport and deposition of sediment during changing tidal cycles and river flow conditions.

4.2 Measurements

The foregoing descriptions and discussions on the dynamics of Taf estuary are based on the measurements made during the three sampling campaigns described in more detailed in Chapter 3. The tidal velocity, salinity, and temperature were made at four or more anchor stations across two transects (T9 and T5) and at St. Clears (see Chapter 3 and Figure 3.1).

Over the study period, the water levels in the estuary were gauged at the estuary mouth (by Wharley Point) and at Laugharne (Figure 3.1). The variations of salinity and water temperature along the estuary longitudinal axis were obtained from the spatial survey measurements made at 32 stations along the estuary channel (Section 3.2.6, Figure 3.3).

4.2.1 Tidal wave characteristics

Tide gauge measurements at two stations; one at the estuary mouth (Wharley Point) and the other at 4 km upstream (Laugharne) give the general characteristics of the tidal wave propagation in the estuary (Figure 4.1). At the mouth, the tide ranges from 3.0 m during a neap to 6.3 m during a spring. These tidal ranges are smaller than the ranges in Carmarthen Bay. During a spring, the tide must rise over two metres in the bay before it enters the estuary mouth. The predicted mean tidal ranges in the bay for the same tides are 8.4 m for the spring tide and 3.5 m for the neap tide. The curves show tidal asymmetry characterised by a faster rise and a slower fall of the water level. The degree of tidal asymmetry increases with increasing tidal range and with increasing distance from the mouth. During a spring tide, this asymmetry is already pronounced at the mouth, and increases further up-estuary. During a spring, the flood incursion takes less than three hours to reach HW but the time is increased to approximately 4.5 hours during a neap. It takes just over 4 hours for the saline water to be flushed out of estuary during a spring tide and about 6 hours during a neap tide. Due to the shallowness of the estuary, for a few hours during low water only river flow remains with some late drainage of saline water retained by the salt marsh.

Due to this tidal asymmetry, the tidal rise is delayed at the upper estuary. At St. Clears the time of HW during a spring tide occurs 45 minutes later than at the mouth. This delay is just 10 minutes at Laugharne. The tidal rise becomes shorter in the upper estuary (St. Clears), to just over two hours compared to nearly three hours at the lower estuary. Similarly the ebb period is shortened to 2 hours and 45 minutes in the upper estuary compared to over 4 hours at the mouth.

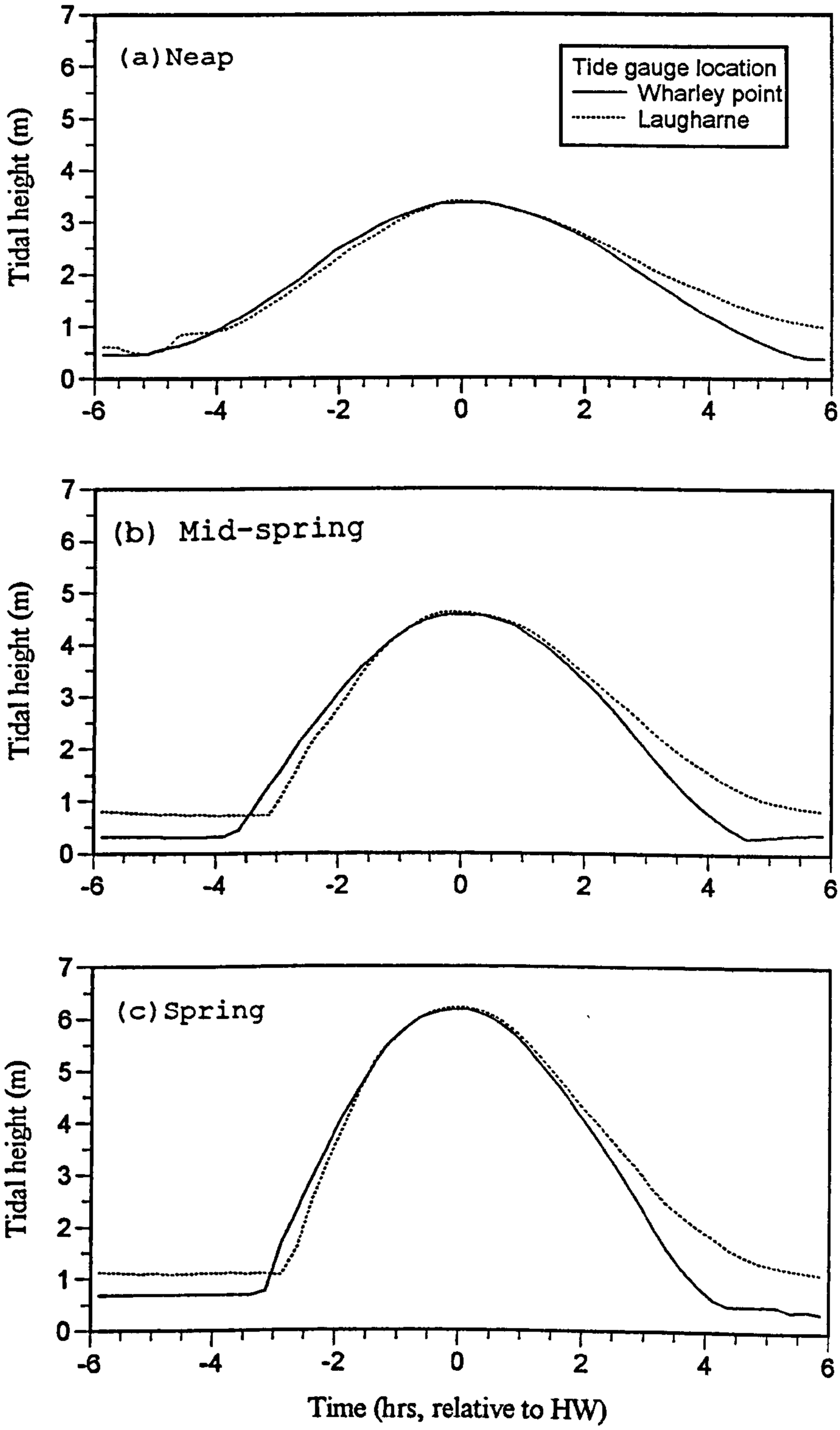

Figure 4.1 Tidal curves for different tidal ranges at the river mouth (Wharley Point) and at 4 km upstream (Laugharne) showing the increase distortion of the tide with increase tidal range and distance from the mouth.

The time of low water in the estuary can be taken as the time when most of the sea water has been flushed out of the estuary and there is very little drop in water level in the main ebb channel. This time does not correspond to the time of low tide in Carmarthen Bay. During the ebb, flow continues for several hours as a river runoff after the tide has left the estuary, and during the flood, the tide is rising several hours in the bay before reaching the estuary. This phenomenon results in a much shorter flood rise and a prolonged ebb fall.

When the tidal waves propagate into shallow water estuaries, the frictional effect causes the crest to travel faster than the trough. This effect deforms the tide waves so that the duration of the tidal rise will be much shorter than that of the fall. This tidal asymmetry is enhanced in macrotidal estuaries where the tidal wave amplitude is large relative to the water depth (cf. Dyer, 1973; Nichols and Biggs, 1985). This produces greater flood velocities than the ebb, thus favouring a net landward sediment transport. In the Taf estuary, however, the tidal asymmetry is already observed at the estuary mouth even though the tide in the near shore zone in Carmarthen Bay is quite symmetrical (Carling, 1978; Jago, 1980). Thus the frictional effect is of a secondary importance in the Taf; and as explained by Jago (1980), the asymmetry is mainly caused by sedimentation which has raised the estuary profile relative to sea level. Due to this sedimentation, the spring tide has to rise some 2 metres in the bay before penetrating the lower reaches of the estuary, by which time the tide is already rising quickly and a fast flood current is already flowing as the tide pours in . But within the estuary, the asymmetry is controlled by the frictional effect as tides propagate towards the head, as illustrated by an increasing distortion of the tidal curve with increasing distance from the estuary mouth. Thus the Taf asymmetry differs from many coastal plain estuaries where the asymmetry results solely from the frictional modification of the tidal wave. During neaps, the tide at the estuary mouth is quite symmetrical. The mean low water level during a neap is higher than the level of the estuary profile at the mouth. Thus the tidal wave deformation during a neap is due only to friction as it propagates up the estuary.

The development of a sand spit at the mouth and the sedimentation within the estuary also affect the tidal wave characteristics. As a result, the time for tidal rise during springs is

shorter than during neaps. This is in contrast to the finding of Carling (1978) in the nearby Bury Inlet, whereby the flood runs longer during springs than during neaps though the ebb is of longer duration than the flood. On large spring tides small bores are produced on the early flood (Jago, 1980), though this was not observed during this study. Bores are produced by the increased steepening of the tidal wave entering the estuary to such a degree that the wave `overshoots' to produce a bore (Buller *et al.*, 1975; Dyer, 1986)

4.2.2 Tidal current characteristics

4.2.2.1 General features

The data recorded by the VGU (Velocity Gradient Unit) provides a continuous record of current velocity over tidal cycles. A typical VGU data recorded by Ott current meters in the lower estuary is shown in Figure 4.2. During a spring tide, the maximum flood currents occur immediately after the tide enters the estuary and the maximum ebb currents occur just before the tide goes out of estuary. During a neap tide, the peak flood velocity is slightly delayed, occurring approximately one hour after the tide enters the estuary. The maximum ebb current during a neap occurs earlier i.e. in the mid stage of the ebb. The maximum flood velocities are greater than the maximum ebb velocities during both springs and neaps.

Figure 4.2 also shows that during spring tides the flood velocity exhibits two peaks during the early stage of the flood with another less pronounced third peak just before high water. There is one peak velocity during the ebb with another small ebb peak about 0.5 hours after high water. During a neap, the flood current shows only one peak velocity, the second and third peaks becoming less obvious due to the much slower pace of the tidal inundation, caused by a much lower volume of the tidal prism.

The first flood velocity peak is associated with a steep pressure gradient created by the fast rising tide in the Carmarthen Bay and a slower rising tide (due to friction) in the estuary.

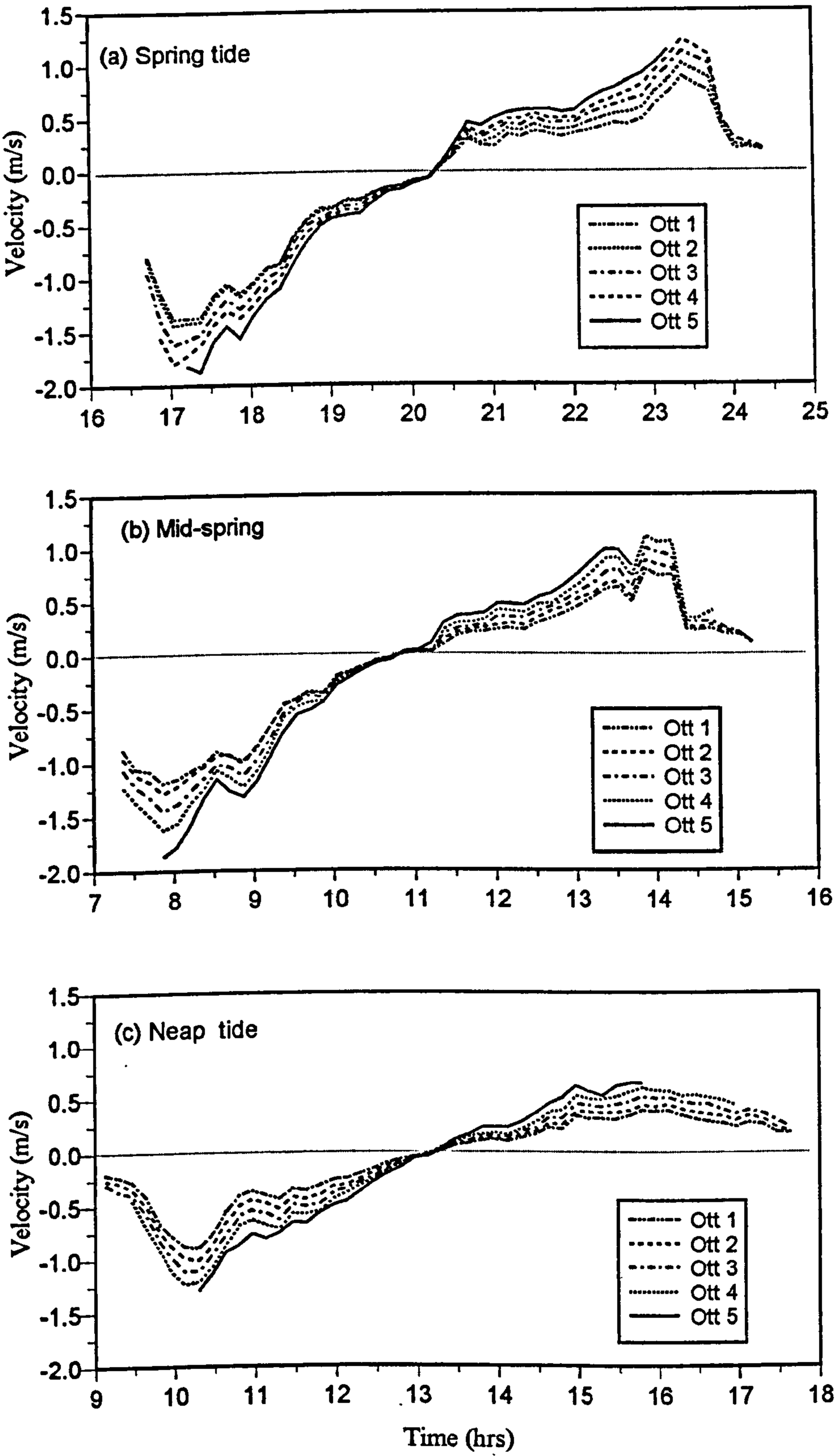

Figure 4.2 Tidal currents during spring, mid- and neap tides at station 2, transect T9 as measured by Ott current meters placed between 0.1 and 2.0 m from the bed on the VGU mast (flood -ve, ebb +ve).

The second flood velocity peak is probably associated with the swift inundation of the sand flat area while the less pronounced third flood velocity peak is associated with the tidal inundation into the salt-marsh area. These inundations result in a sudden increase of the discharge, thereby forcing higher flood-velocity along the channel (see also French and Stoddart, 1992; Lessa and Masselink, 1994), as the current speed reduces approaching HW.

4.2.2.2 Tidal velocity profiles at T9, October 1994

Current velocity measurements were made on 5 and 6 October 1994 during spring tidal cycles at five stations across the estuary. Station 1 was located in the main ebb channel while four other stations were on the intertidal sand flats (see Figure 3.2a). The maximum velocities at all the stations are summarised in Table 4.1. The velocities vary markedly across the estuary. The strongest currents were recorded at station 1 with a peak flood velocity of 2.68 m/s and a peak ebb velocity of 1.84 m/s recorded during the highest spring tide on 6/10/94. Peak current velocity reduced across the tidal channel with the lowest current found at station 5. At this station, the peak current was reduced to just over 0.55 m/s for the flood and 0.44 m/s during the ebb. The peak flood velocity measured at station 5 on 6 October was lower than on 5 October despite 6 October was a bigger tidal height

Table 4.1 Maximum current velocity (m/s) measured at stations 1-5, transect T9 on 5 & 6 October 1994 (T.H. = tidal height above O.D.)

Date	Tide	Station number				
		1	2	3	4	5
5/10/94 ($T.H._{flood}$= 5.4m) ($T.H._{ebb}$= 5.2 m)	Flood	2.20	1.44	1.43	0.69	0.55
	Ebb	1.96	0.58	0.81	1.16	0.35
6/10/94 ($T.H._{flood}$= 5.5m) ($T.H._{ebb}$= 5.4m)	Flood	2.68	1.46	1.51	0.77	0.37
	Ebb	1.84	0.84	1.08	1.42	0.44

than on 5 October. This was because the measurement of tidal velocity at station 5 on 6 October was slightly delayed due to an unforseen circumstance, but was started 45 minutes after the tide had reached the station. Therefore causing a slight underestimate, as during a spring tidal rise the peak flood velocity occurs at the beginning of the tidal surge. Except for Station 4, flood velocities were dominant over ebb velocities at all stations. At Station 4 the maximum ebb velocity was almost double the maximum flood velocity. Station 4 was located at the centre of the estuary within a small depression of the ebb channel. Thus, at this station the local deepening boosted the fresh water discharge particularly when water was shallow towards the end of ebb tide, gave rise to a stronger ebb velocity.

The time-series contour plots of velocity distribution for Stations 1-4 are shown in Figures 4.3 and 4.4. The flood currents are negative and ebb currents are positive. No plots were prepared for Station 5 as data were limited by the shallow water depth and only top and bottom velocities were measured at this station. The water height used in the plots was obtained from the nearby tide gauge. The maximum water depths in each cast were usually affected by the boat swinging on its mooring and local scouring of the ebb channel, so these were not used in the plots. The tidal wave showed a very pronounced asymmetry. In the main channel (Station 1), the flood reached its maximum level in just over 3 hours and low water was reached about 5 hours later (Figures 4.3a and 4.4a). The flood tide energy was thus concentrated into a small time interval as evidenced by the very dense contour lines. The maximum flood current occurred immediately after the tide entered the estuary when water was very shallow (less than 2 m). The maximum ebb current occurred at the end of the ebb before the effective withdrawal of the tidal prism some 4.5 hours after high water by which time the water depth in the channel was reduced to about one metre. The ebb current then declined to a minimum approaching the velocity of the seaward flow of the river water. Maximum currents were always maintained near the surface. During the flood the velocity contours are nearly vertical, but some degree of velocity shear is generated during the ebb.

The above explanations for anchor station 1 are also applicable to the other stations across the estuary (Figures 4.3b-d and 4.4b-d). The time of tidal influence however was

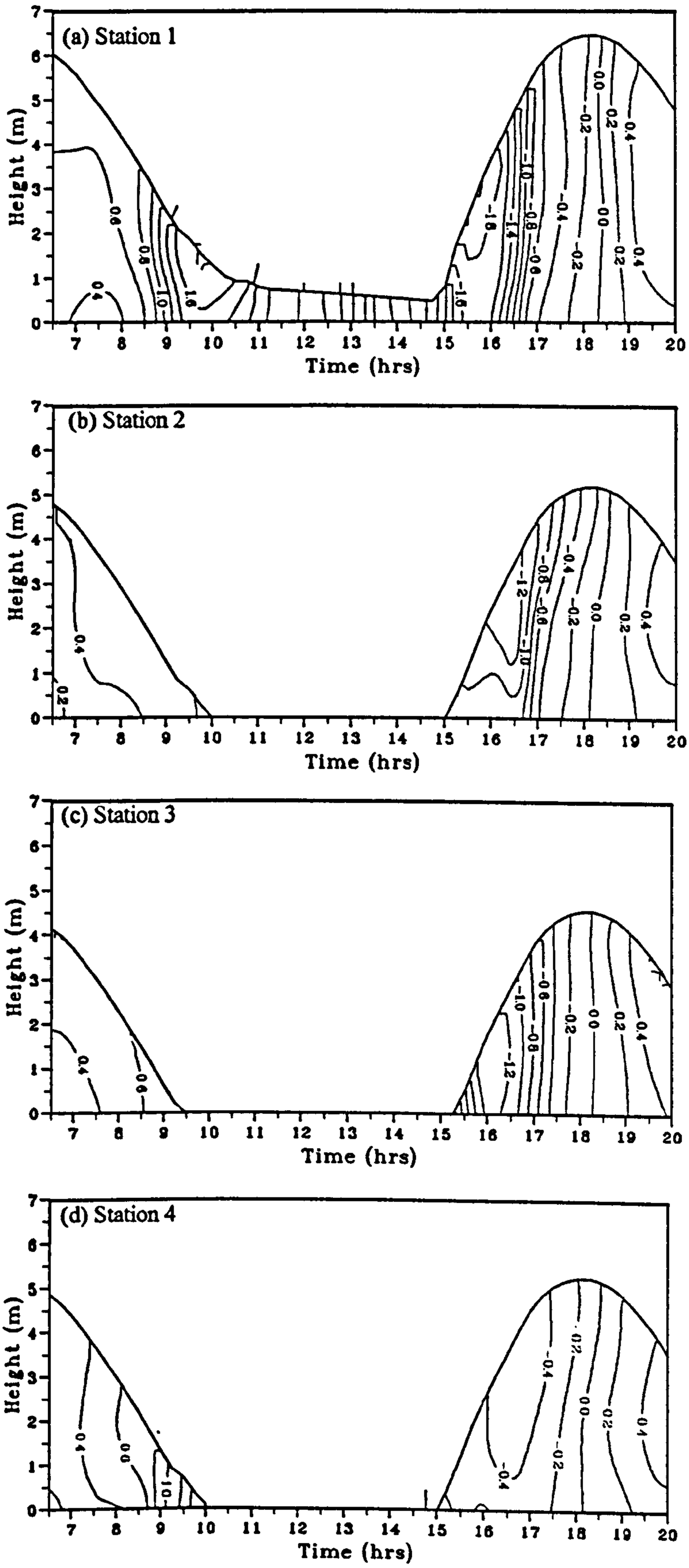

Figure 4.3 Time series contour plots of tidal velocity (m/s) at stations 1-4, 5 October 1994.

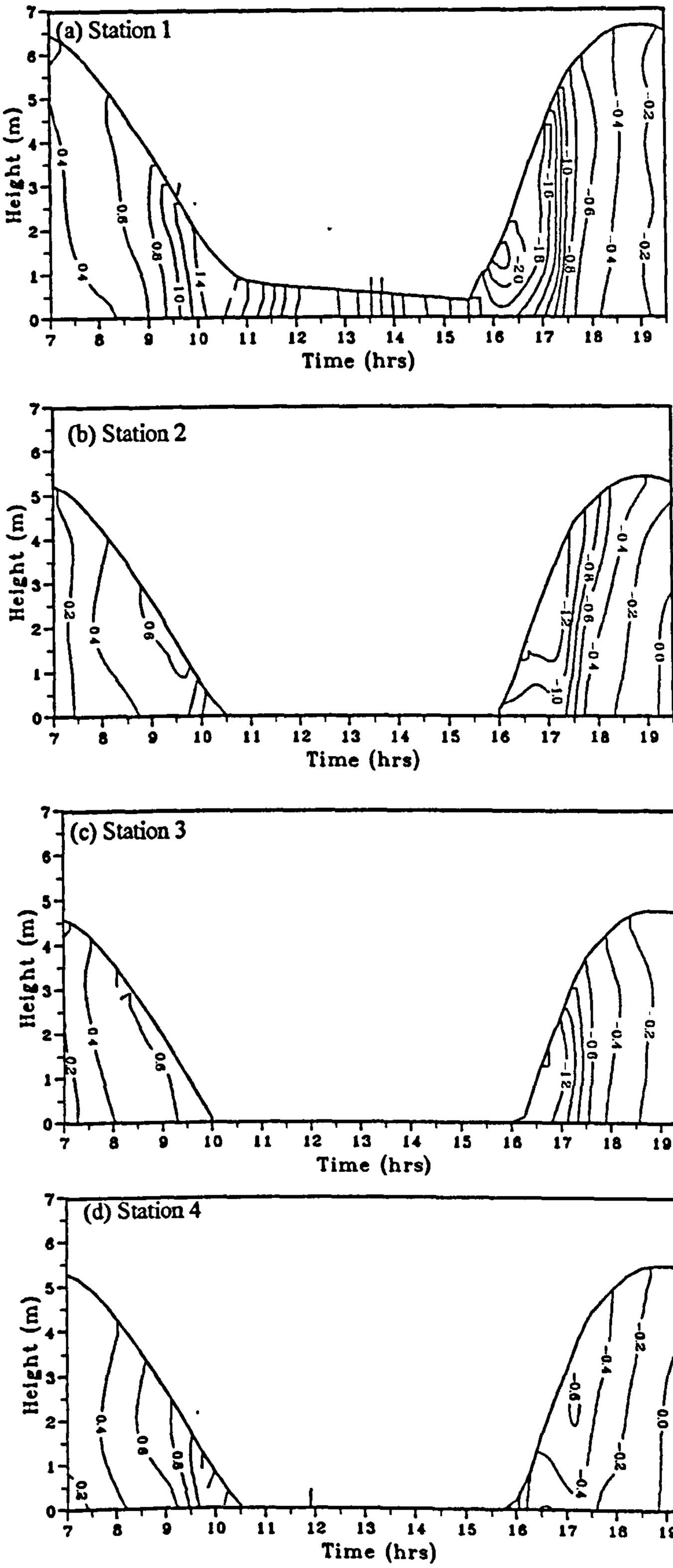

Figure 4.4 Time series contour plots of tidal velocity (m/s) at stations 1-4, 6 October 1994.

reduced further away from the main channel as these stations were located at higher elevations than Station 1. At Station 3 for example, the flood rise took only 2.5 hours , and it took 3.2 hours for the station to dry out during the ebb.

4.2.2.3 Tidal velocity profiles at T9, July 1995

During July 1995, seven stations were set up across the estuary at T9 to accommodate the new bed topography. Stations 1-4 were located in the main channels while Stations 5-7 on the inter-tidal sand flats (see Figure 3.2b). Stations 1 and 3 were located in deeper ebb channels than Stations 2 and 4, and at the end of the ebb all flow diverted into these channels. Currents were measured at these stations for four tidal cycles from 14 July (spring tide) to 20 July (neap tide). The maximum velocities recorded at each stations are summarised in Table 4.3. The maximum flood velocity reached 1.80 m/s during the spring tide but was reduced to 1.29 m/s during the neap. During the ebb, the current velocity was less, reaching just 1.32 m/s during the spring tide and 0.90 m/s during the neap. The current was strongest in the main channel (stations 1-4), but much weaker on the sand bank

Table 4.2 Maximum current velocity (m/s) measured at stations 1-7 across the estuary on 14 - 20 July 1995. (n.d. = not determined; T.H. = tidal height above O.D.)

Date	Tide	Station number						
		1	2	3	4	5	6	7
14/7/95 (T.H.= 5.1 m)	Flood	1.80	1.72	1.72	1.38	n.d.	0.54	n.d.
	Ebb	1.32	1.31	1.46	1.67	n.d.	0.92	n.d
16/7/95 (T.H.= 4.5 m)	Flood	1.58	1.57	1.68	1.29	1.00	0.40	0.38
	Ebb	1.40	1.23	1.59	1.60	0.71	0.62	0.38
18/7/95 (T.H.= 3.8 m)	Flood	1.25	1.51	1.34	1.04	n.d.	n.d	n.d
	Ebb	1.02	0.91	1.10	1.24	0.50	0.54	0.27
20/7/95 (T.H.= 2.8 m)	Flood	0.95	1.29	1.01	0.46	0.20	0.18	0.13
	Ebb	0.86	0.65	0.90	0.74	0.34	0.39	0.18

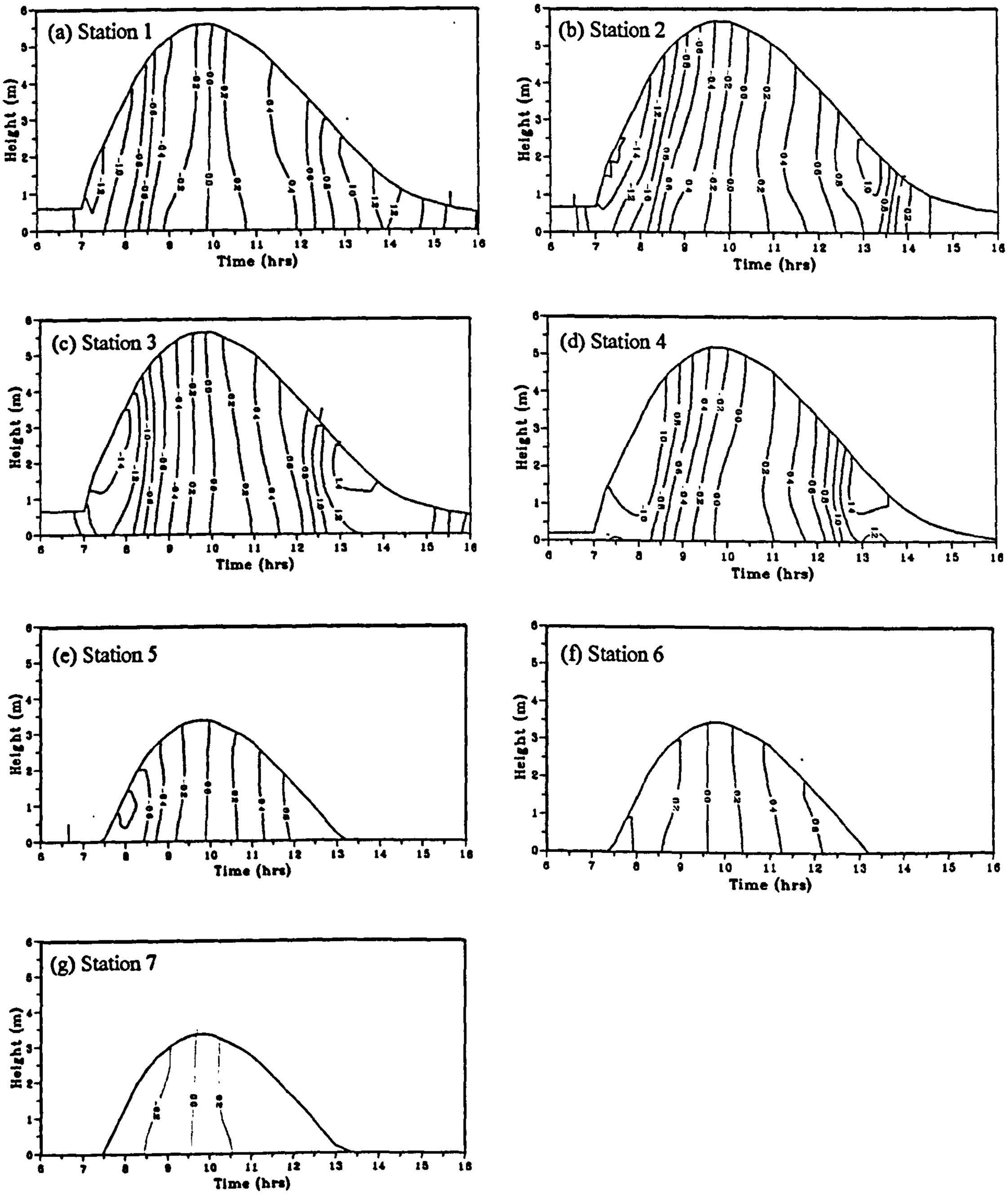

Figure 4.5 Time series contour plots of current velocity (m/s) at stations 1- 7, 16 July 1995.

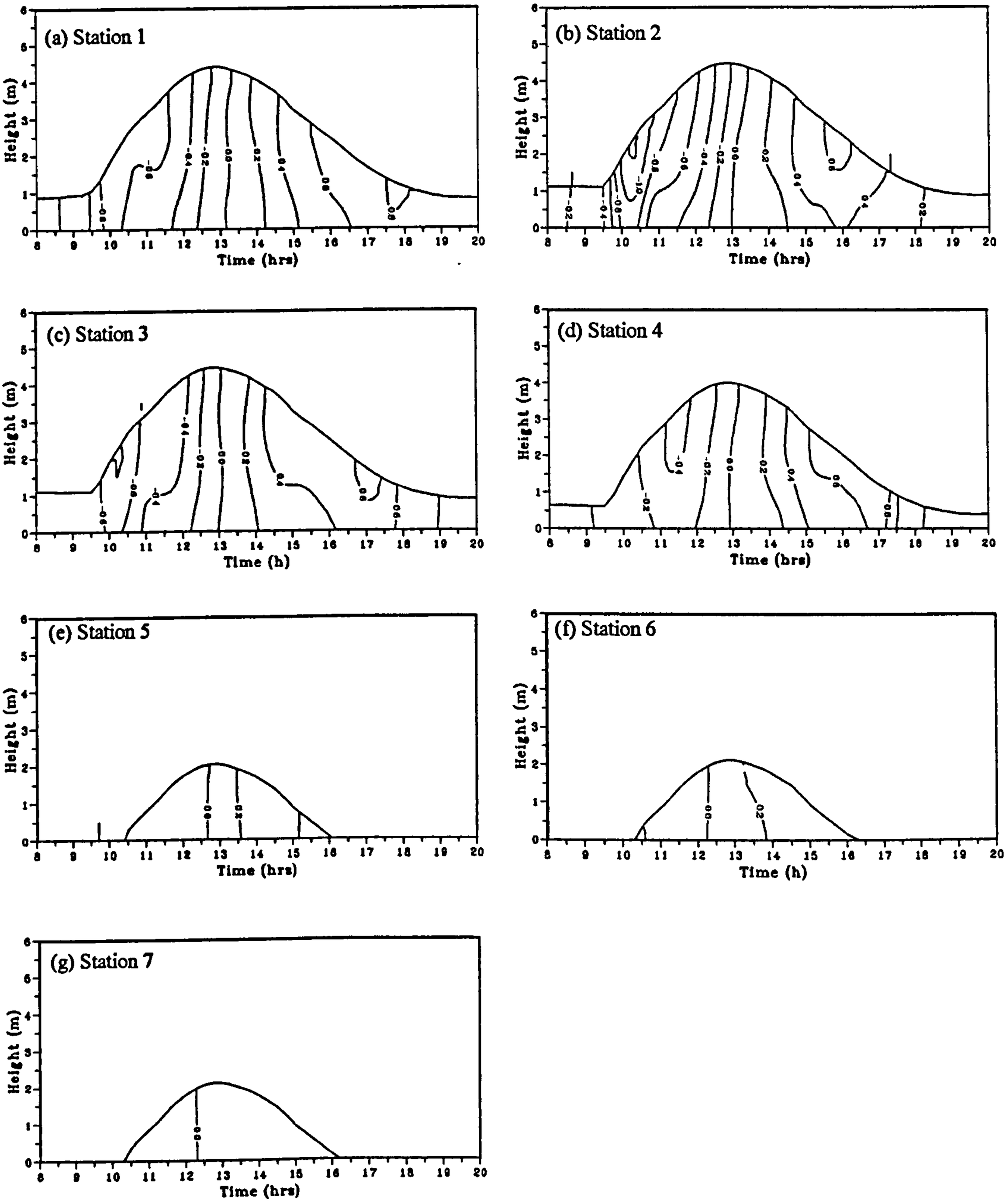

Figure 4.6 Time series contour plots of current velocity (m/s) at stations 1-7, 20 July 1995.

(Stations 5-7) - about half of that measured in the channel. The currents at Stations 4 and 6 were ebb dominant, at other stations the currents were flood dominant.

Contour plots for 16 and 20 July are shown in Figures 4.5 and 4.6. The spring tide plots show similar features as observed during previous surveys but with much reduced maximum flood and ebb velocities. The tidal wave was strongly asymmetry, with the spring rise achieved in 3.5 hours and nearly 5 hours for the ebb. During the neap, the velocity was less and less asymmetrical than the spring, with the flood taking 4. 2 hours and the ebb 5.5 hours. The maximum flood current occurred one hour after the tide reached the station, and the maximum current during the ebb occurred about three hours after high water.

4.2.2.4 Tidal velocity profiles at T5, September 1995

In September 1995, 4 anchor stations were set up across transect T5. Station 1 was in the main channel; Station 2 was on the tidal flat at the edge of the channel, station 3 on the inter-tidal flat, and Station 4 in the shallow depression of an abandoned ebb channel (see Figure 3.2c). Tidal velocities were measured for 4.5 tidal cycles between 12 and 19 September 1995. The results are summarised in Table 4. 3. The current was strongest in the main channel but much weaker on the sand bank. At Station 1, the maximum flood velocity reached over 1.90 m/s during the spring tide but it reduced to 0.72 m/s on the neap tide. During the ebb, the velocity was less reaching just 1.2 m/s on the spring tide and 0.4 m/s on the neap. Flood currents were more dominant than ebb currents at stations 1, 2 and 3 while the current at station 4 was ebb dominant.

The velocity contour plots for all the stations are shown in Figure 4.7 for the spring tide (13 September 1995) and Figure 4.8 for the neap tide (19 September 1995). The plots for 12, 14 and 15 September 1995 are shown in Figures A.01-A.03 (in Appendix A). The spring tidal curve was strongly asymmetrical with the flood rise taking only 3 hours and the ebb fall more than 5 hours. The tidal velocity showed a very pronounced asymmetry particularly at stations 1 and 2 during the spring tide. The maximum flood current

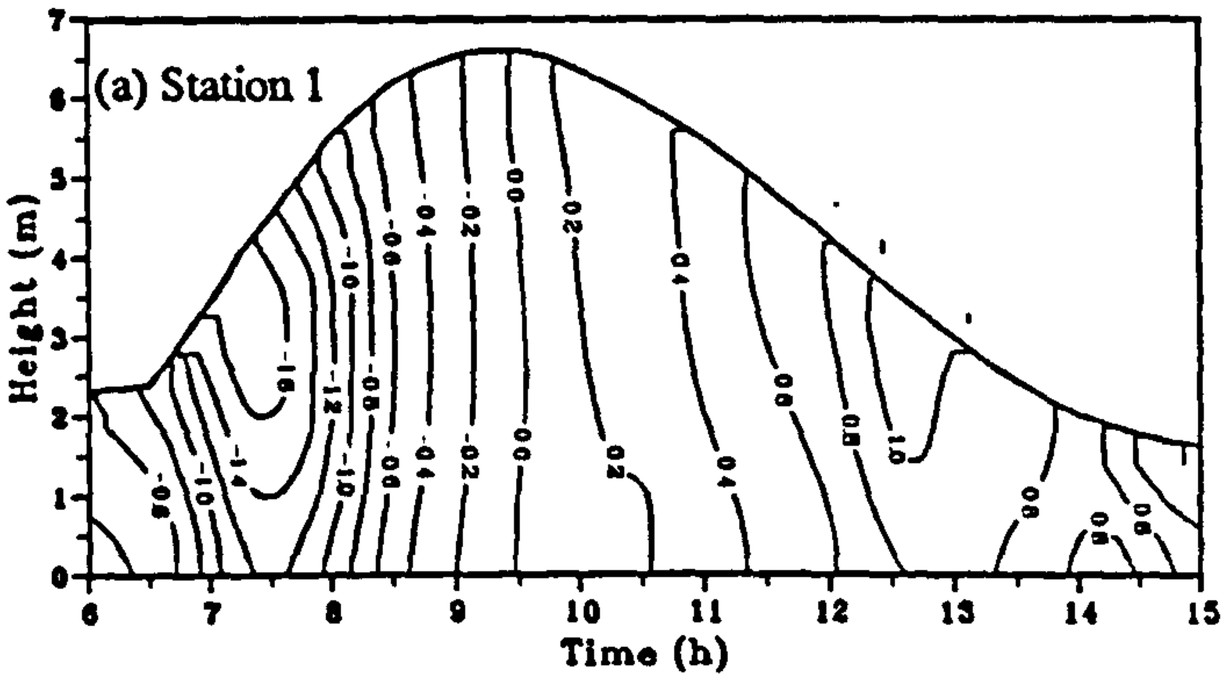

Figure 4.7 Time series contour plots of current velocity (m/s) at stations 1- 4, 13 September 1995.

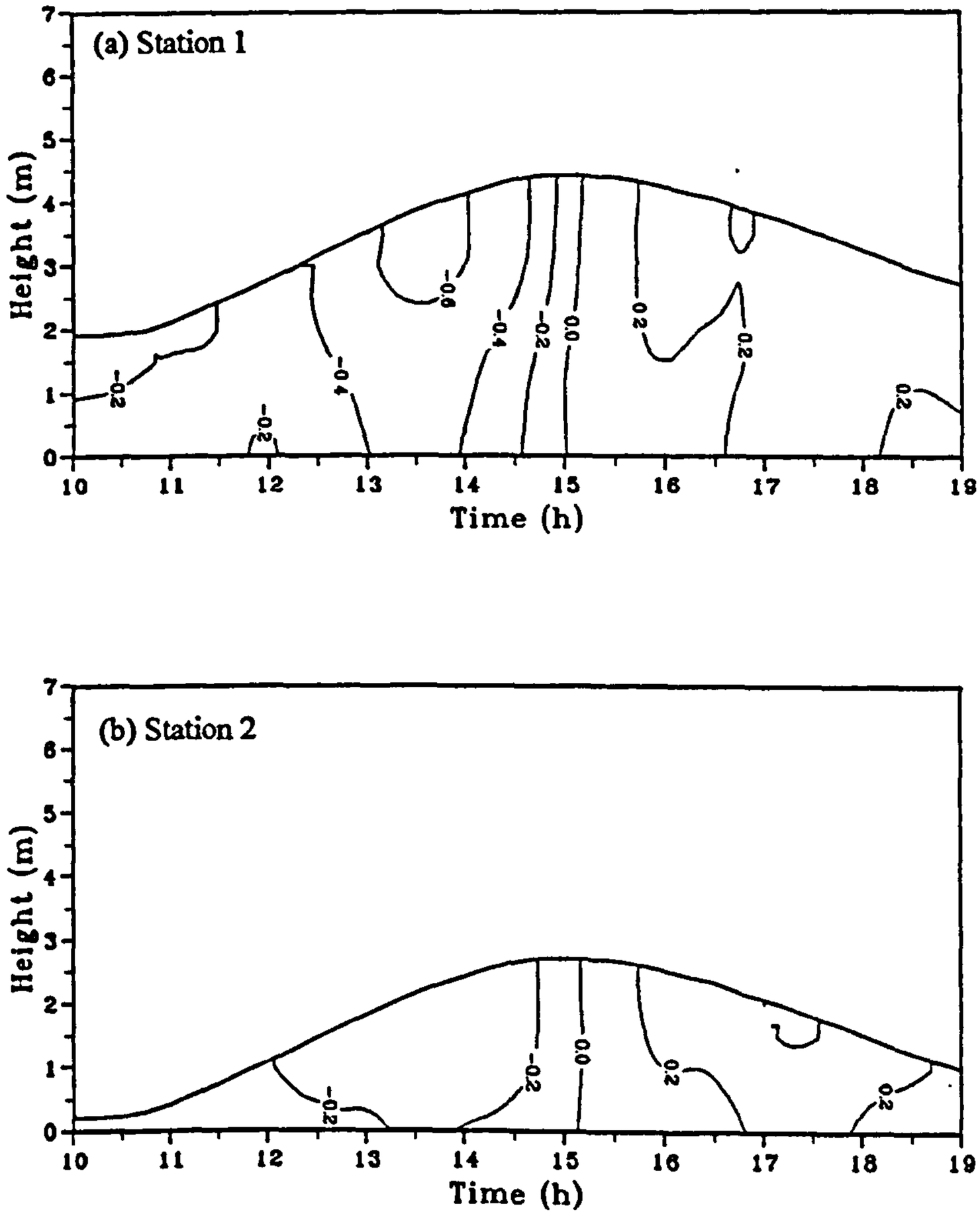

Figure 4.8 Time series contour plots of current velocity (m/s) at stations 1 and 2, 19 September 1995.

occurred 0.75 hours after it reached the stations and the maximum ebb currents occurred 3 hours after high water. During the neap the maximum flood and ebb currents were recorded about 2 hours either side of high water.

Table 4.3 Maximum current velocity (m/s) measured at stations 1-4, transect T5, 12 - 19 September 1995 (n.d. = not determined; T.H. = tidal height above O.D.).

Date	Tide	Station number			
		1	2	3	4
12/9/95 (T.H.= 5.0 m)	Flood	n.d.	n.d.	n.d.	n.d.
	Ebb	1.30	0.99	0.60	0.73
13/9/95 (T.H.= 4.7 m)	Flood	1.88	1.65	1.41	0.41
	Ebb	1.21	0.88	0.58	0.60
14/9/95 (T.H. = 4.4 m)	Flood	1.68	1.34	1.21	0.40
	Ebb	1.13	0.76	0.48	0.52
15/9/95 (T.H.= 3.7m)	Flood	1.35	0.91	0.57	0.28
	Ebb	0.99	0.81	0.50	0.46
19/9/95 (T.H.= 2.7 m)	Flood	0.72	0.48	0.24	0.29
	Ebb	0.42	0.46	0.25	0.27

4.2.2.5 Tidal velocity profiles at St. Clears, 12 July 1995

The measurements at St. Clears were made on 12 July 1995 during a spring tide. The variations of current velocity are shown in Figure 4.9. The maximum current velocities were recorded at the beginning of the flood and at the end of the ebb (Figure 4.9a). This is similar to observations in the lower estuary. The flood velocity was dominant over the ebb velocity, the peak velocities for the flood and ebb being 1.35 m/s and 0.82 m/s, respectively. During the flood, the flow was strongest during the first 30 minutes of the tidal incursion after which the velocity abruptly dropped to less than 0.5 m/s. During the ebb, the current gradually increased until it reached maximum velocity at the end of the ebb before dropping again to the river flow velocity. The biggest difference between surface

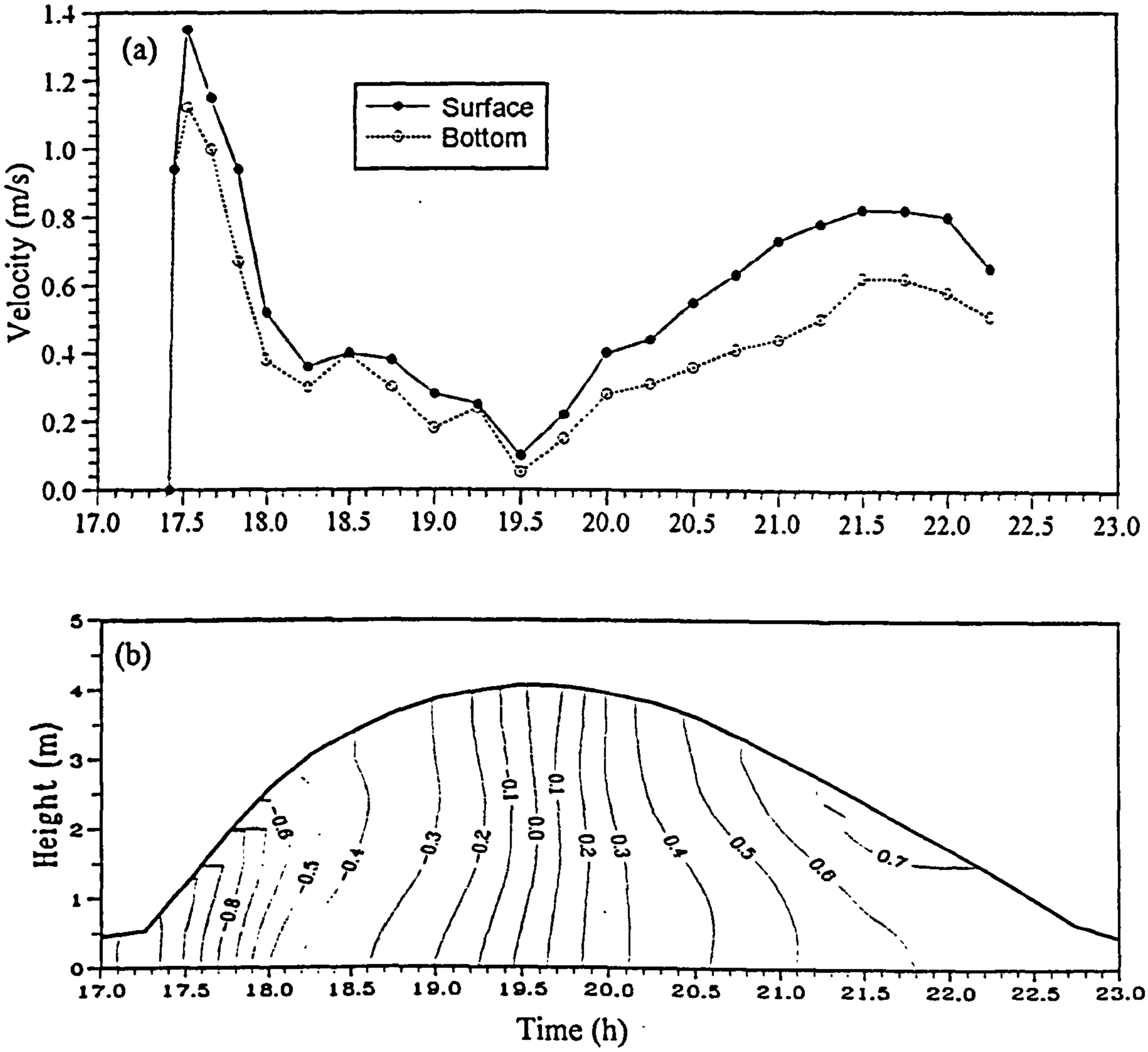

Figure 4.9 (a) Surface and bottom velocity, and (b) Time series contour plots of current velocity (m/s) at St. Clears, 12 July 1995.

and bottom velocities occurred during the accelerating phase of the ebb. Some vertical velocity shear was observed during the ebb but not during the flood (Figure 4.9b).

4.2.2.6 Lateral velocity variation in the lower estuary

It has been demonstrated in the preceding sections that tidal velocities vary quite considerably across the estuary profile. The currents are strongest in the main channel and weaker further away from the channel and on the intertidal sand flats. These variations can be seen in Figure 4.10 (and Figures A.04 & A.05 in Appendix A) which shows the tidal velocity across the estuary at different stages of the tide. During the flood, the currents are maximum in the deepest part of the channel cross section, and the flow reduces further away from the main channel on the intertidal sand flat where the water is shallower (Figure 4.10a-e). The maximum current in the main channel is about twice that on the sand flats. Towards high water the current across the estuary does not vary very much (Figure 4.10f-k). Similarly during the early part of the ebb, the current varies very little across the estuary (Figure 4.10l-n). This shows that during this stage, the ebb current tends to avoid the main channel and flows straight to the sea across the intertidal flats as evidenced by the isovel contours and the presence of velocity shear. The influence of bed topography in changing the flow pattern and velocity becomes more important as the ebb progresses and the water gets shallower, when the main flow is diverted towards the ebb channel (Figure 4.10o-t). At the end of the ebb the flow is confined within the main ebb channel as the sand flats emerge. This increases the ebb current to its maximum values just before the expulsion of the tidal prism (Figure 4.10u-v).

4.2.3 Estuarine salinities

In this section, the salinity data for spatial and anchor station surveys during three sampling campaigns will be presented. As with the velocity profiles, time series contour plots for the salinity have been prepared for each measurement station across the estuary. These plots

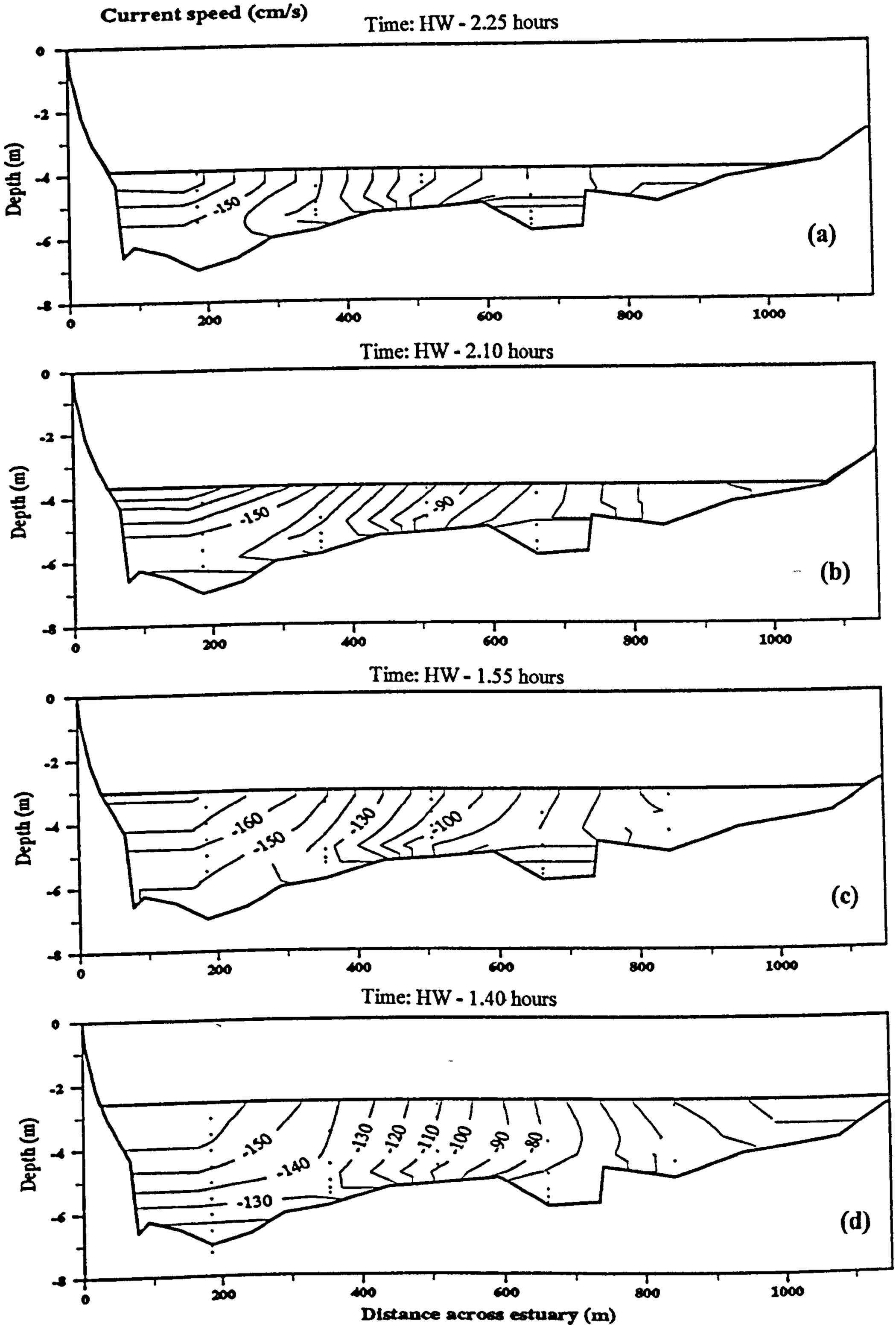

Figure 4.10 Cross estuary contour plots of current velocity (cm/s) at different stages of the tide, 5 October 1994.

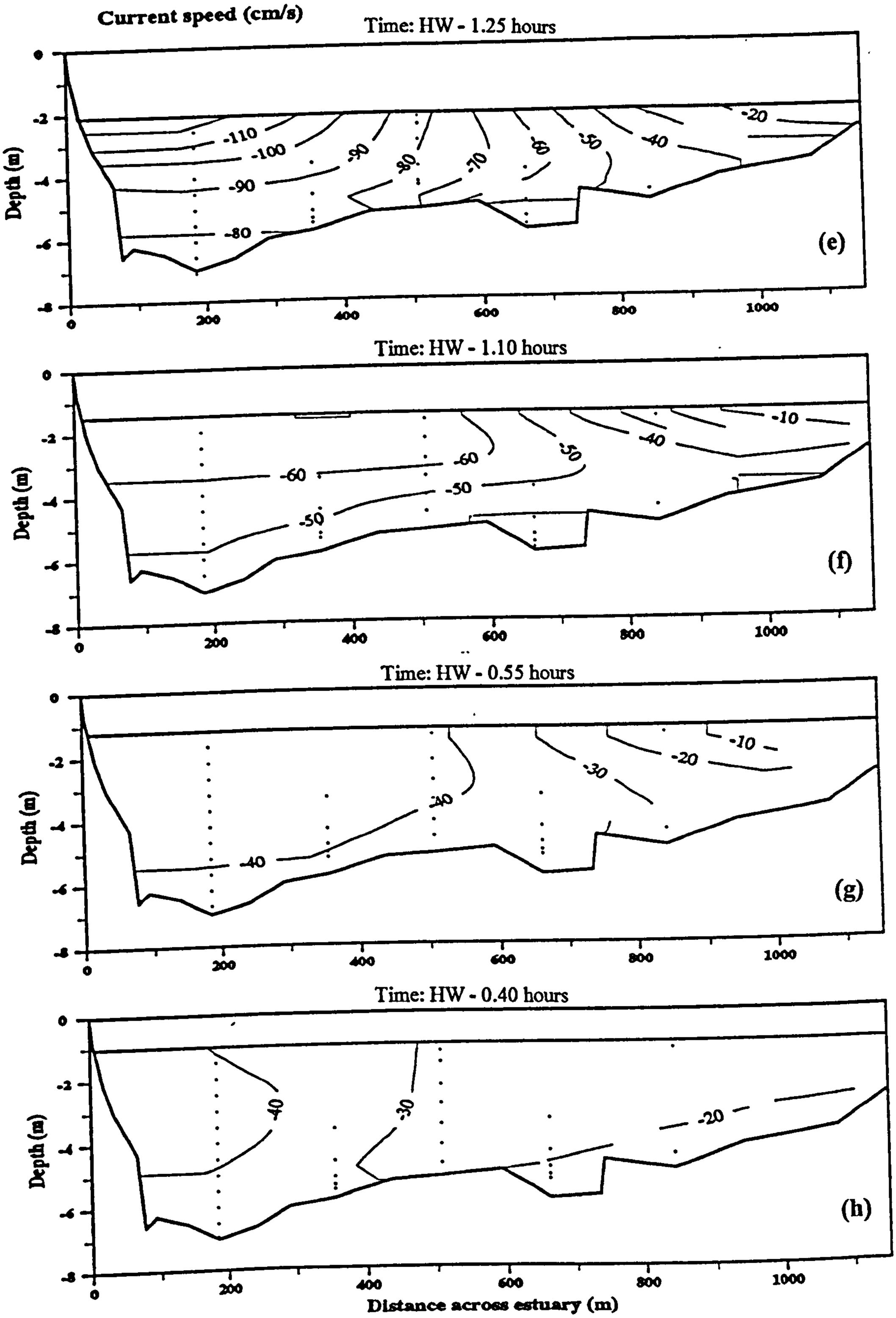

Figure 4.10 (continued)

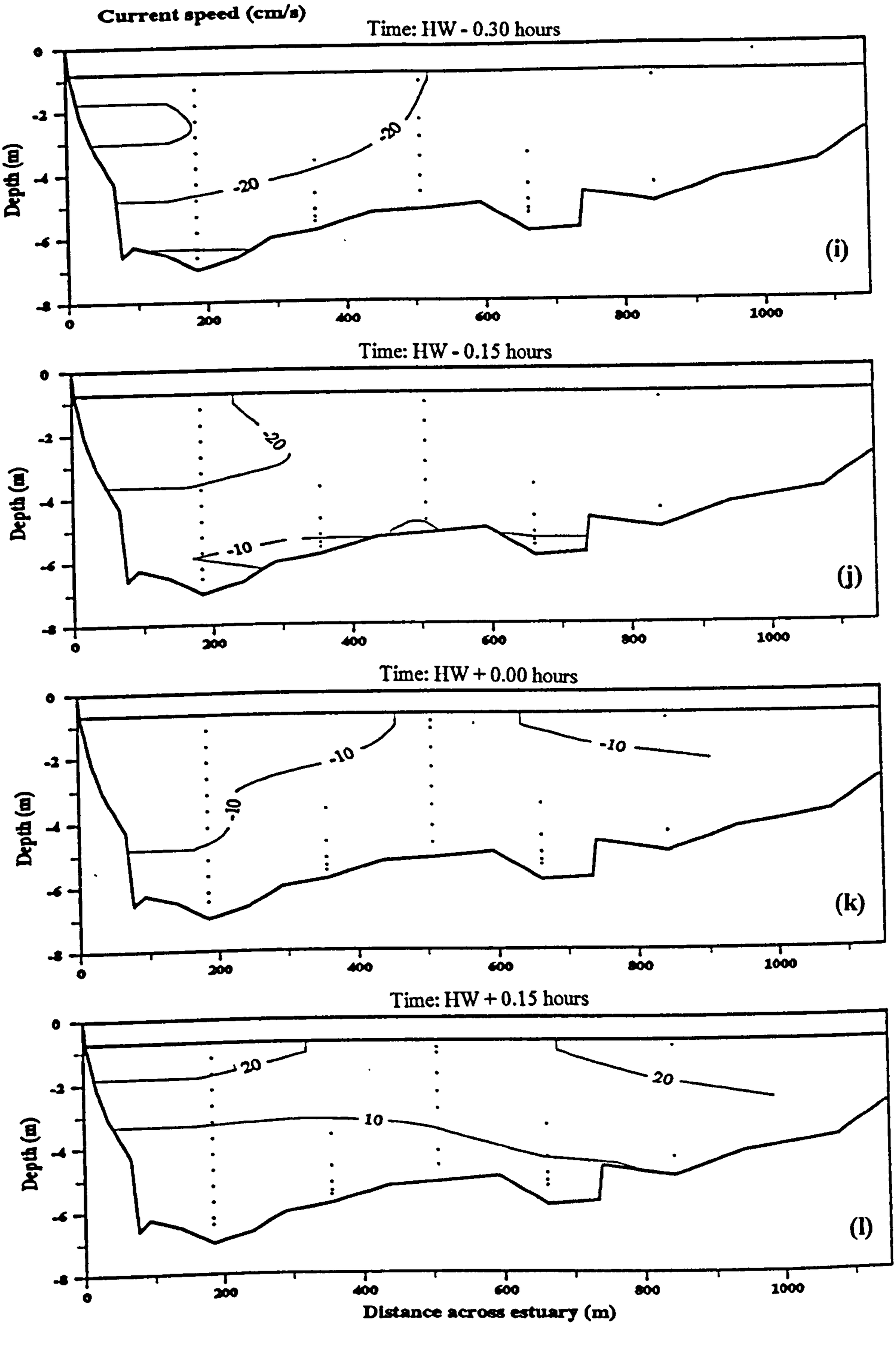

Figure 4.10 (continued)

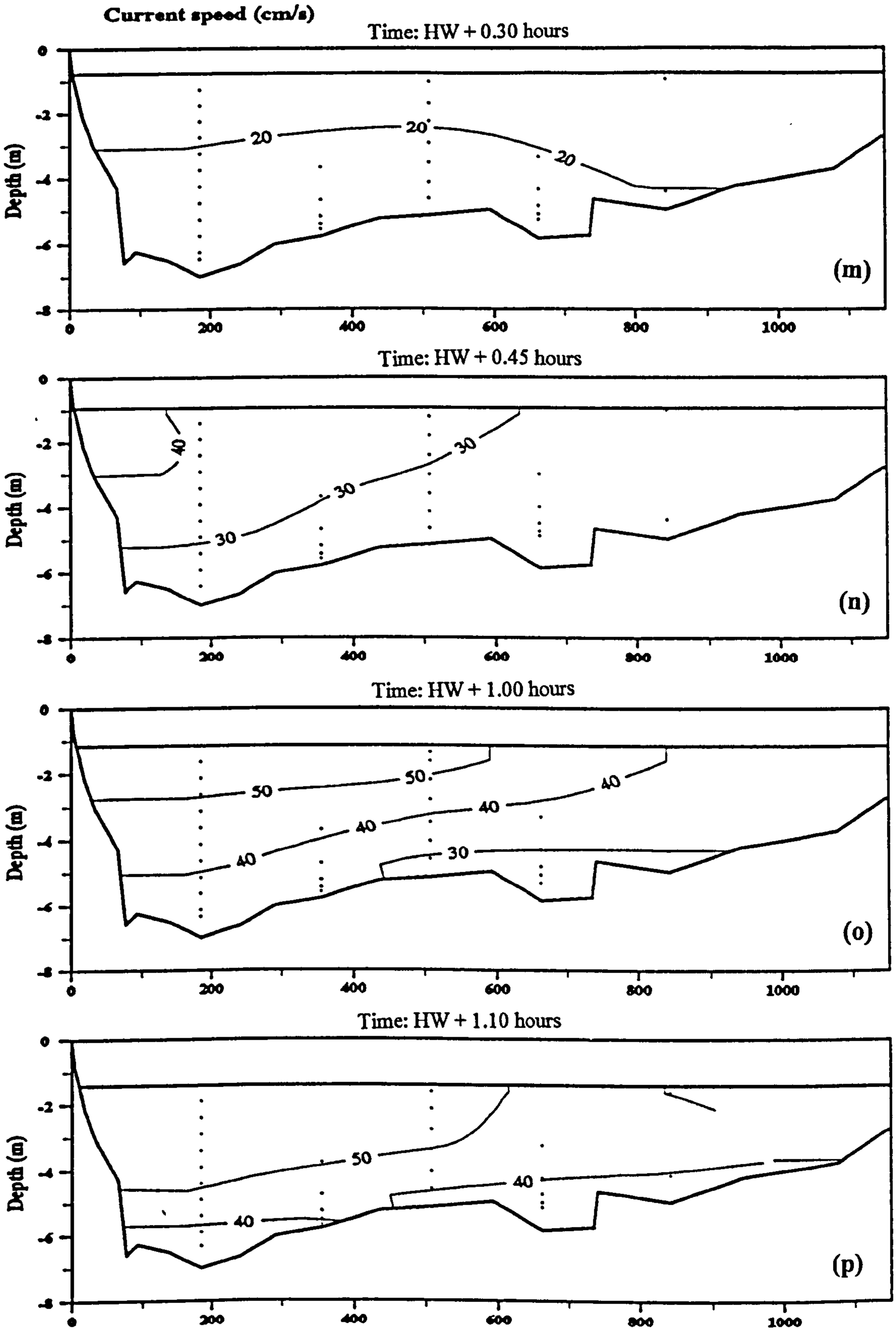

Figure 4.10 (continued)

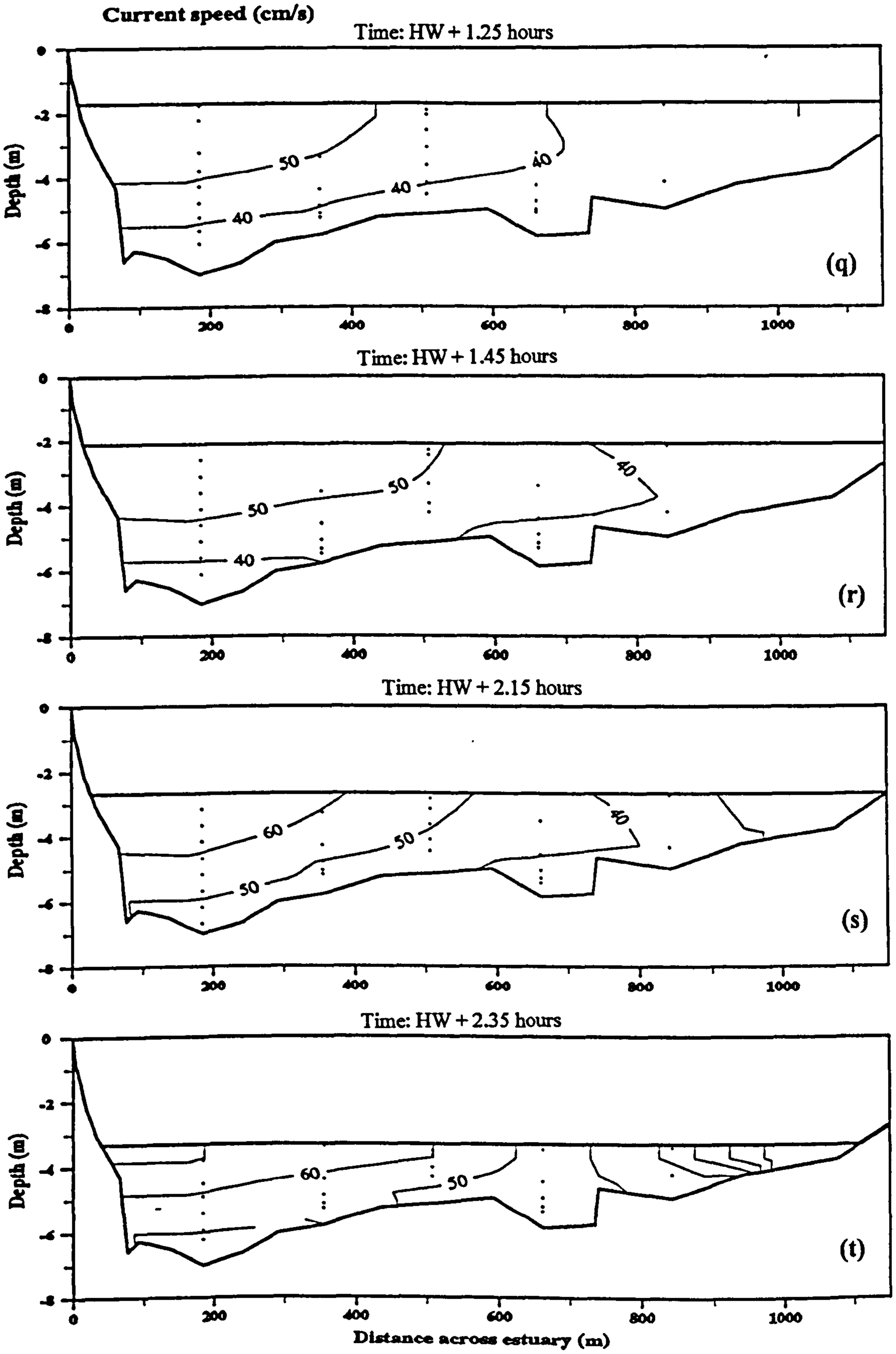

Figure 4.10 (continued)

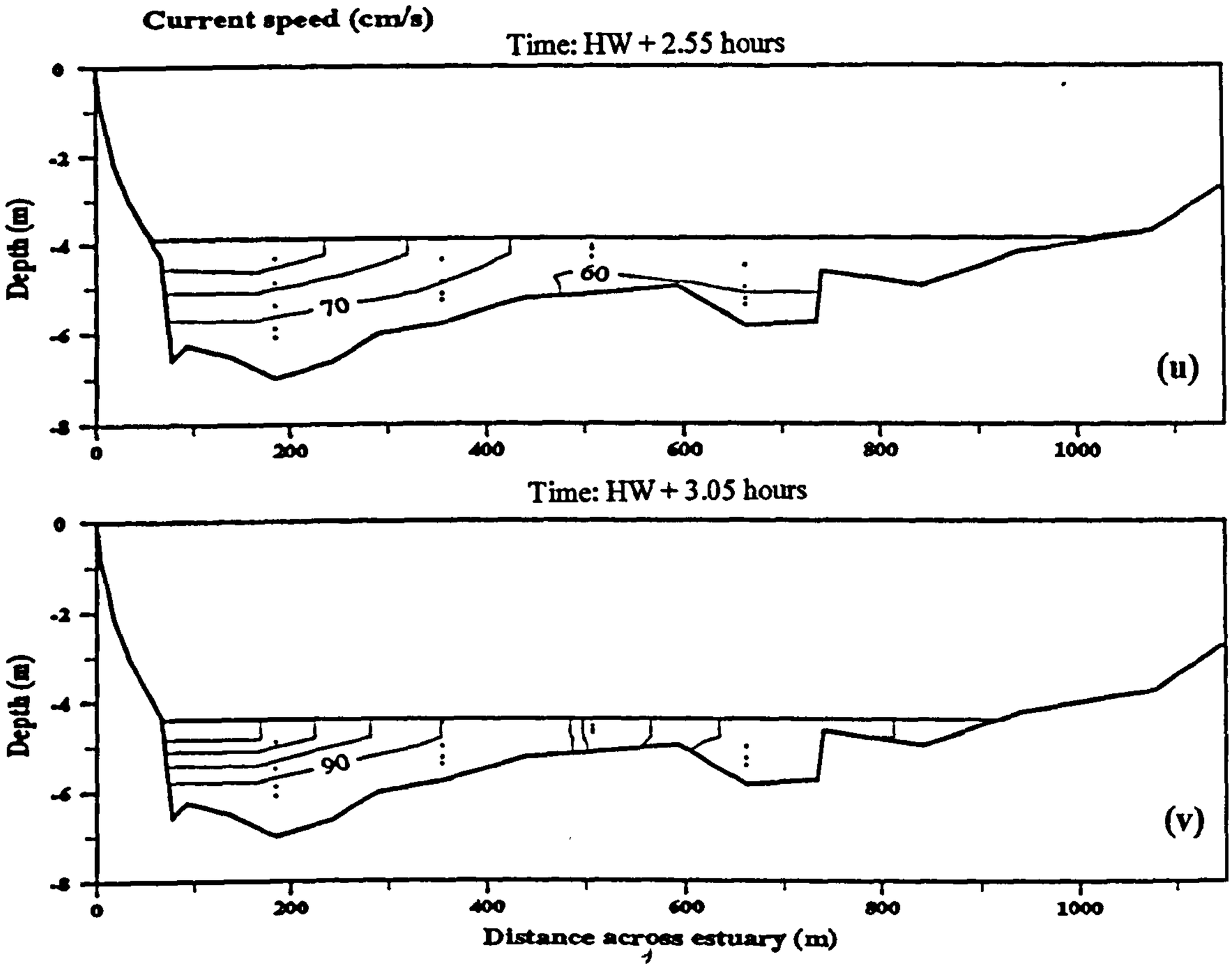

Figure 4.10 (continued)

are repeated for each tidal cycle. On selected tidal cycles, cross-estuary plots have been prepared based on each completed run of the CTD casts.

4.2.3.1 Longitudinal salinity variation

Salinity and stratification varied considerably both during the fortnightly spring-neap cycle and in response to variable fresh water input. Figures 4.11 and 4.12 show typical examples of these variabilities as revealed by the axial surveys during high water. During a spring tide and low river discharge, the salinity maximum (33‰) reached up to 8 km distance from the mouth; up-estuary of this maximum, salinity rapidly diminished (Figure 4.11a). The limit of salt water intrusion (salinity 1 ‰) reached some 14.5 km distance from the mouth. Along this longitudinal axis, the waters were very well mixed. Near the mouth there was only 0.2‰ difference between the surface and bottom salinities. Similarly near the head, where salinity became less than 5‰, the surface-bottom difference was only 0.5‰. During high river discharge, the salinity maximum (33‰ isohaline) was located 1 km from the mouth as the limit of the salt water intrusion was pushed down to just 11 km distance from the mouth (Figure 4.11b). The waters near the head were well mixed but some stratification was observed in the lower estuary with a maximum surface and bottom salinity difference of 1.7‰.

At low river discharge, the neap tide salinity maximum (33‰) was at 3 km distance from the mouth; however, the limit of salt water intrusion was seen as far as 11.5 km from the mouth (Figure 4.12a). The water at the lower and upper estuary were well mixed with less than 0.5 ‰ difference between top and bottom salinities. Stratification was observed only when a neap tide coincided with a high river discharge (Figure 4.12b). During this time, the maximum salinity observed at the lower estuary was 25‰, and the high river flow depressed the salt water intrusion to just 7 km distance from the mouth. The difference between bottom and surface salinities was 14‰ in the lower estuary and 6‰ in the upper estuary.

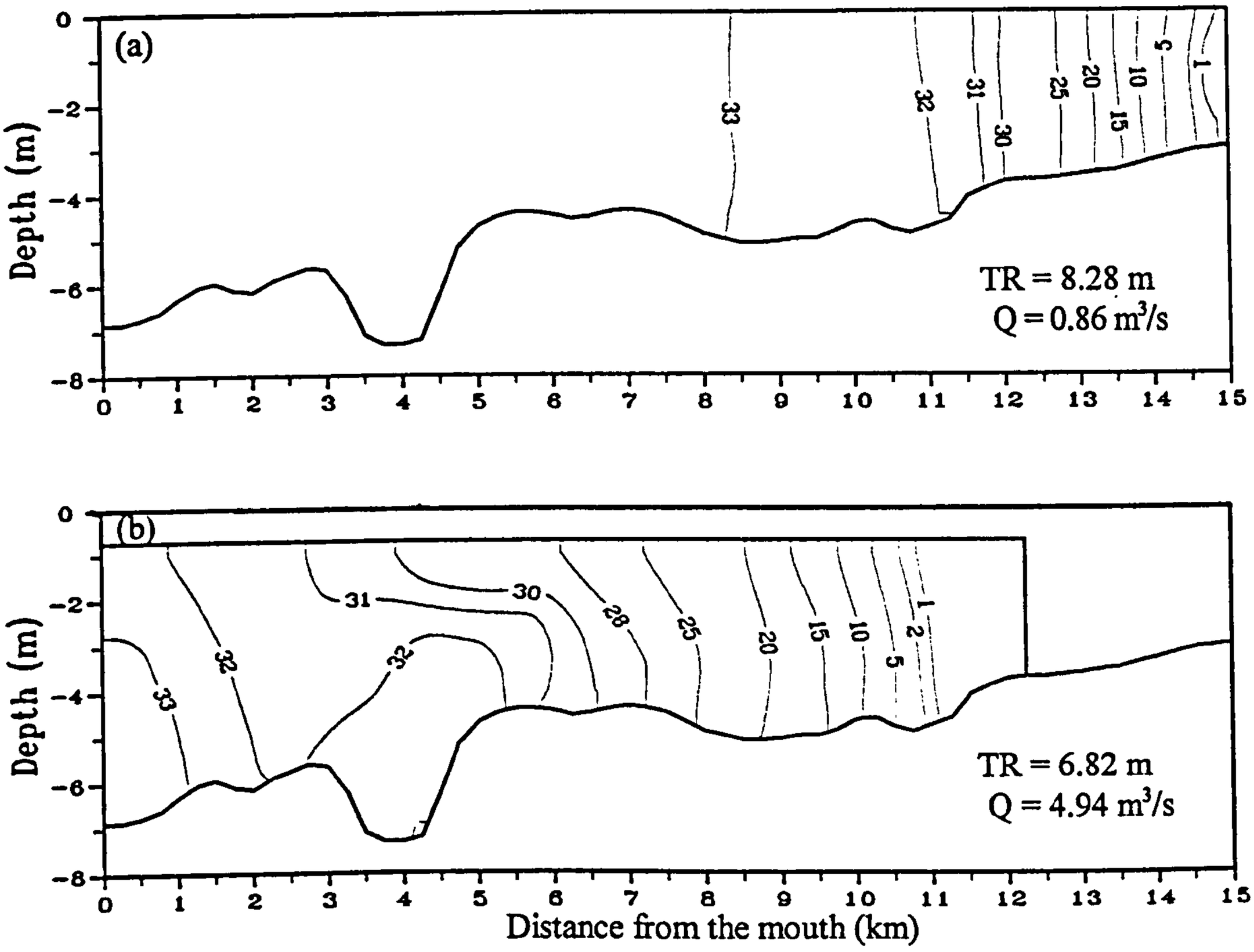

Figure 4.11 Longitudinal variation of salinity (ppt) during spring tides (a) low river discharge, and (b) high river discharge (TR = tidal range, Q = river discharge).

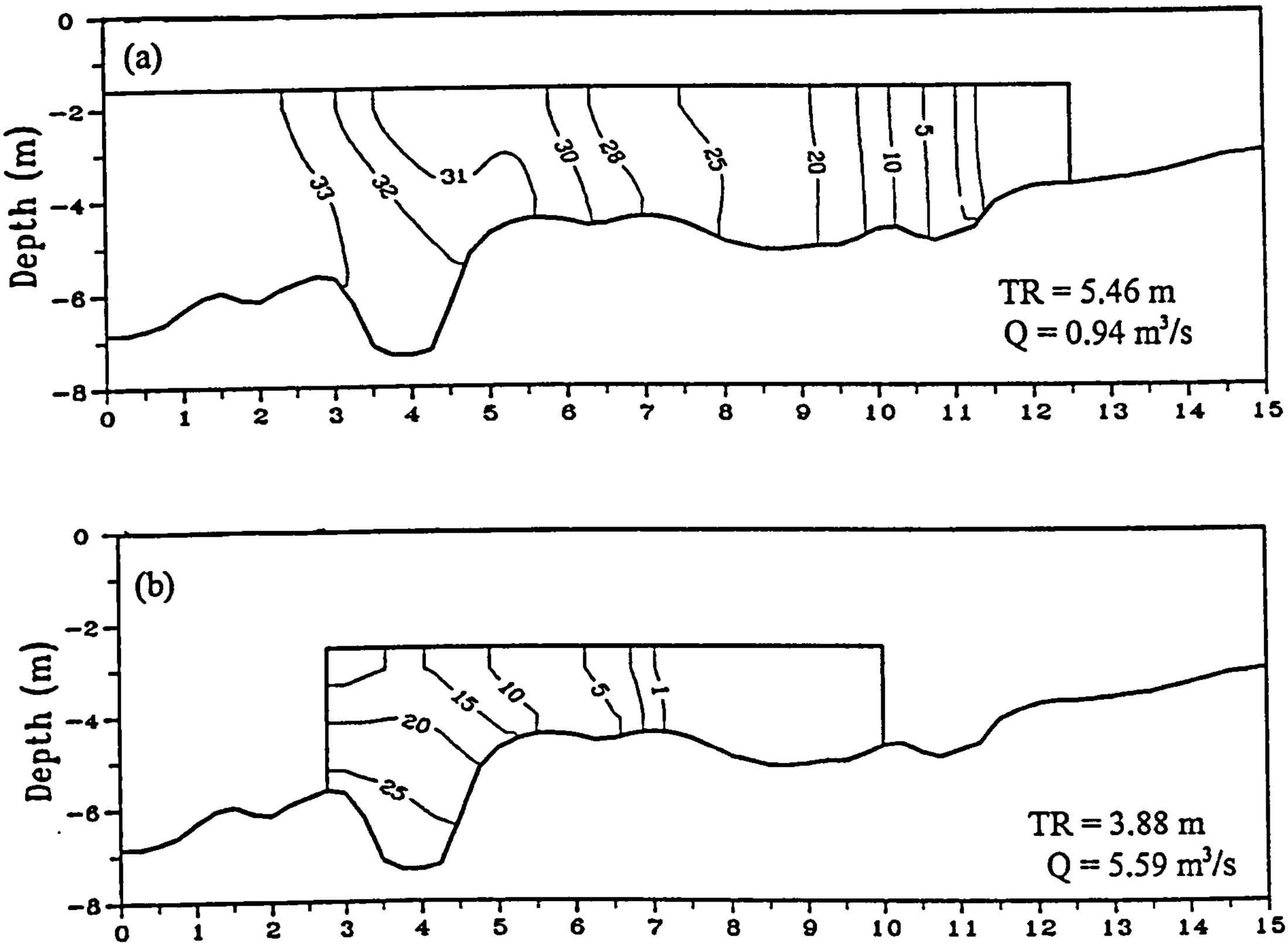

Figure 4.12 Longitudinal variation of salinity (ppt) during neap tides (a) low river discharge, and (b) high river discharge, (TR = tidal range, Q = river discharge).

It appears that the estuarine circulation is very much mediated by the fresh water input. At low river discharge, the water column is uniformly mixed up to the limit of salinity intrusion, during both springs and neaps. At neap tides, the 30‰ isohaline was able to penetrate up to 6 km distance from the mouth. High river flow results in some degree of stratification particularly in the lower estuary. Maximum stratification occurs when high river flows coincide with neap tides. The increase river flow also markedly suppressed the salinity intrusion. There was some 4 km shift of the interface between high and low discharge during a neap tide and about 3 km shift in the interface during a spring tide. As the high river discharge referred to here was just about 5 m^3/s, which is still less than the yearly average, the limit of salinity intrusion would be further depressed when the discharge exceeds 10 m^3/s.

4.2.3.2 Salinity variation in the lower estuary

Contour plots for the salinity measurements made in October 1994 for all stations across the estuary are shown in Figures 4.13 and 4.14. The salinity variation during this observation is best described by the measurement made at anchor Station 1 on 5 and 6 October 1995 (Figures 4.13a 4.14a). This station was located in the main ebb channel. The salinity varied from a minimum value of 5.2‰ during LW to a maximum of 34.1‰ during HW. The minimum salinity was reached just before the flood surge. The salinity slowly decreased during the ebb to a minimum value, as all the salt water was flushed out of estuary. The ebb measurement was stopped 5.5 hours after HW, by which time the salinity fell below 14 ‰. The water remained slightly saline due to the late draining of seawater retained by the marsh. Tidal asymmetry is reflected in the salinity contour plots with a rapid rise and a slower fall in the salinity values, with 33‰ salinity reached after less than 0.5 hour of tidal incursion. A slight salinity stratification was developed just before and after HW with surface water about 1.5‰ less saline than the bottom water. The stratification was strongest at station 1 but became less developed at other stations across the estuary. At all other times, the water was well-mixed with almost uniform salinity throughout the water column.

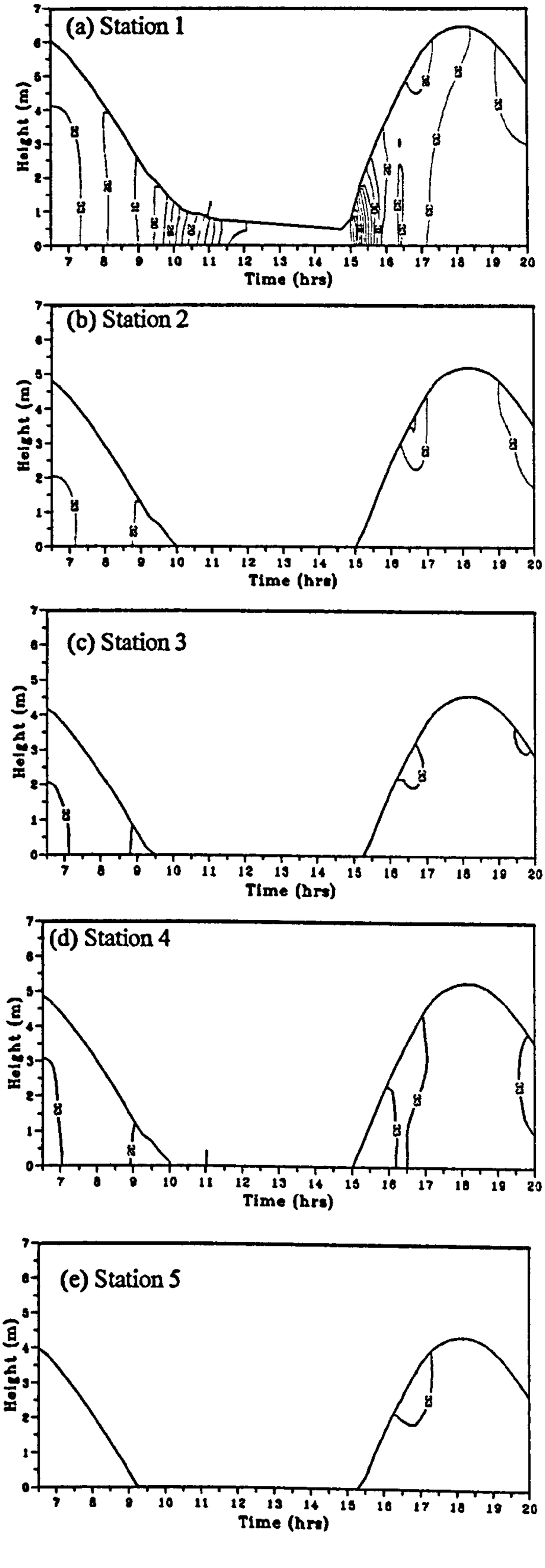

Figure 4.13 Time series contour plots of salinity (ppt) at stations 1- 5, 5 October 1994.

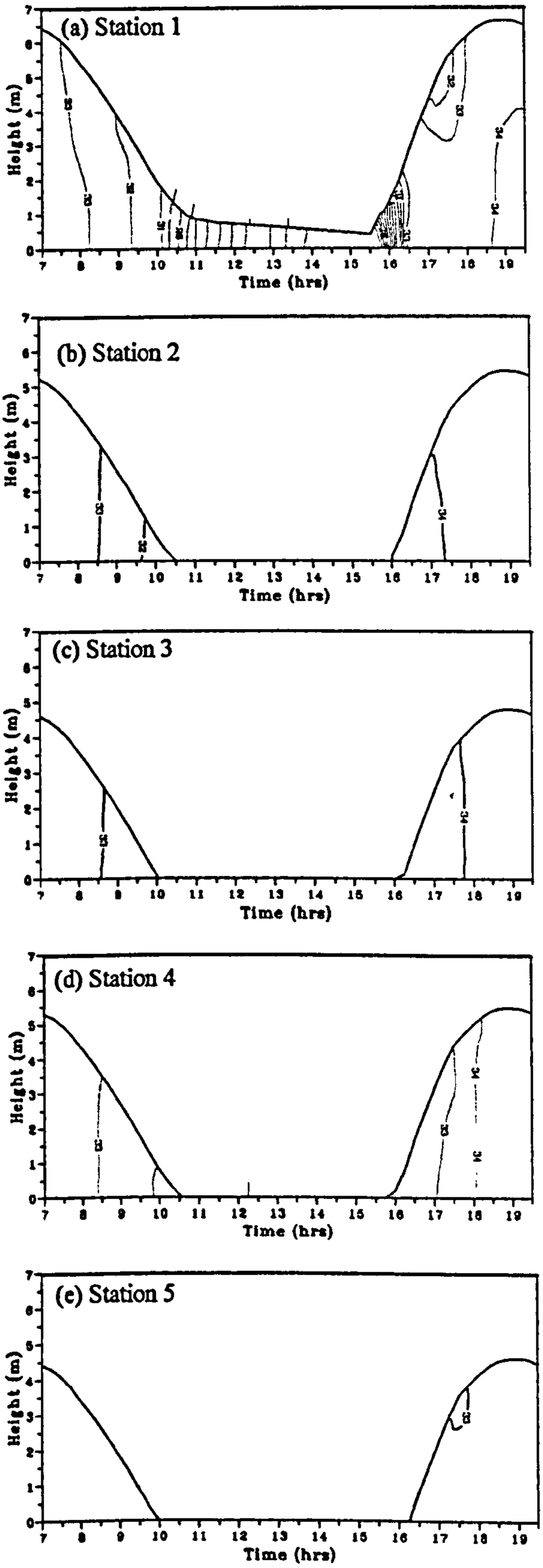

Figure 4.14 Time series contour plots of salinity (ppt) at stations 1- 5, 6 October 1994.

In July 1995, the salinity measurements were made during low river discharges at seven anchor stations across the estuary. Figure 4.15 shows the salinity variation over depth and time at the anchor stations during the spring tide. During the flood, salinity increased from a minimum value of 17.6 ‰ to a maximum of 33.4‰ at HW (Figure 4.15a). The salinity then decreased during the ebb to a value of 22.1‰ when the measurement ceased some 6 hours after HW. The near vertical contour lines show that the water column was well-mixed with less than 1‰ difference between bottom and surface salinities for the whole tidal cycle. The plot also shows the salinity asymmetry with rapid rise in the salinity values during the flood and a slower fall during the ebb. Similar features were observed at other stations across the estuary (Figure 4.15b-g). However, for Stations 5-7 which were on the intertidal sand flat, the minimum values during the flood and the ebb were much higher. For these stations the flood water was already at its maximum salinity (> 33‰) when it reached the station. During the ebb the minimum salinity recorded at these stations was about 32.5‰. The contour plots for the neap tide are shown in Figure 4.16. The maximum salinity reached 33.2‰ at HW, but its values were less asymmetrical than on the spring tide. The plots show that slight stratification developed at high water and for one and half hours after HW.

In September 1995, the salinity measurement was made at 4 stations along transect T5. Typical salinity contour plots are shown in Figures 4.17 for a spring tide and 4.18 for a neap tide. No plots have been prepared for stations 3 and 4 on the neap tide, as the water was very shallow (< 0.5 m deep) and only a few measurements could be made. During the spring tide, the salinity increased from a minimum value of 17.1‰ in the early flood to a maximum value of 34.2‰ at HW (Figure 4.17). The water remained salty (24.4‰) when the measurement was stopped 5 hours after HW. At station 1, the water column was well mixed throughout the tidal cycle, but at stations 2-4 a slight stratification occurred near the surface during the first hour of the ebb, with a surface to bottom salinity difference of 0.6-1.0‰. The water column was relatively well-mixed for the rest of the ebb. The salinity contour plots show tidal asymmetry with a steep rise and slower fall in the salinity values. During a neap tide, a strong stratification developed at the early stage of the flood with a surface to bottom salinity difference up to 10.7‰ (Figure 4.18). Stratification slowly

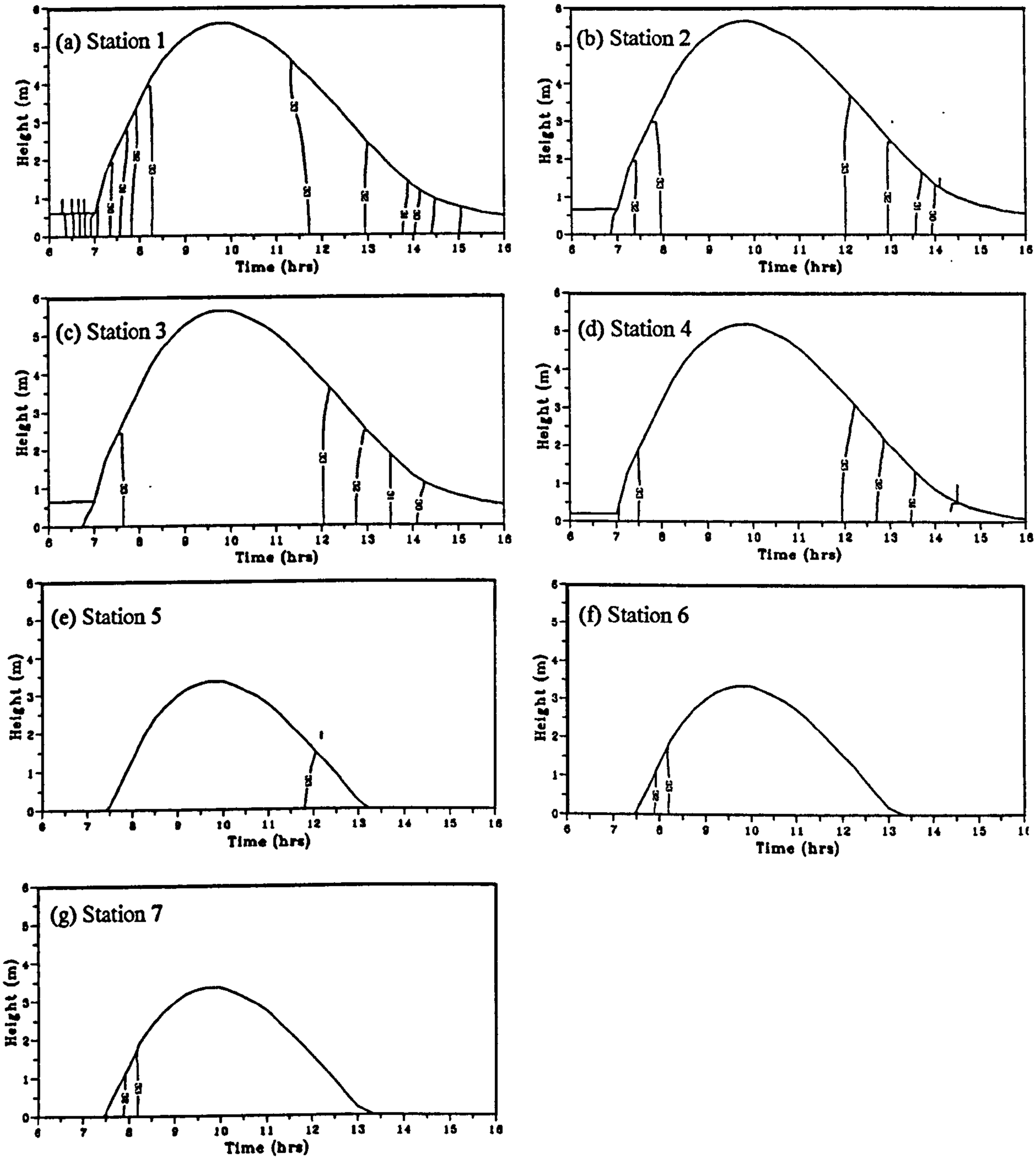

Figure 4.15 Time series contour plots of salinity (ppt) at stations 1 - 7, 16 July 1995.

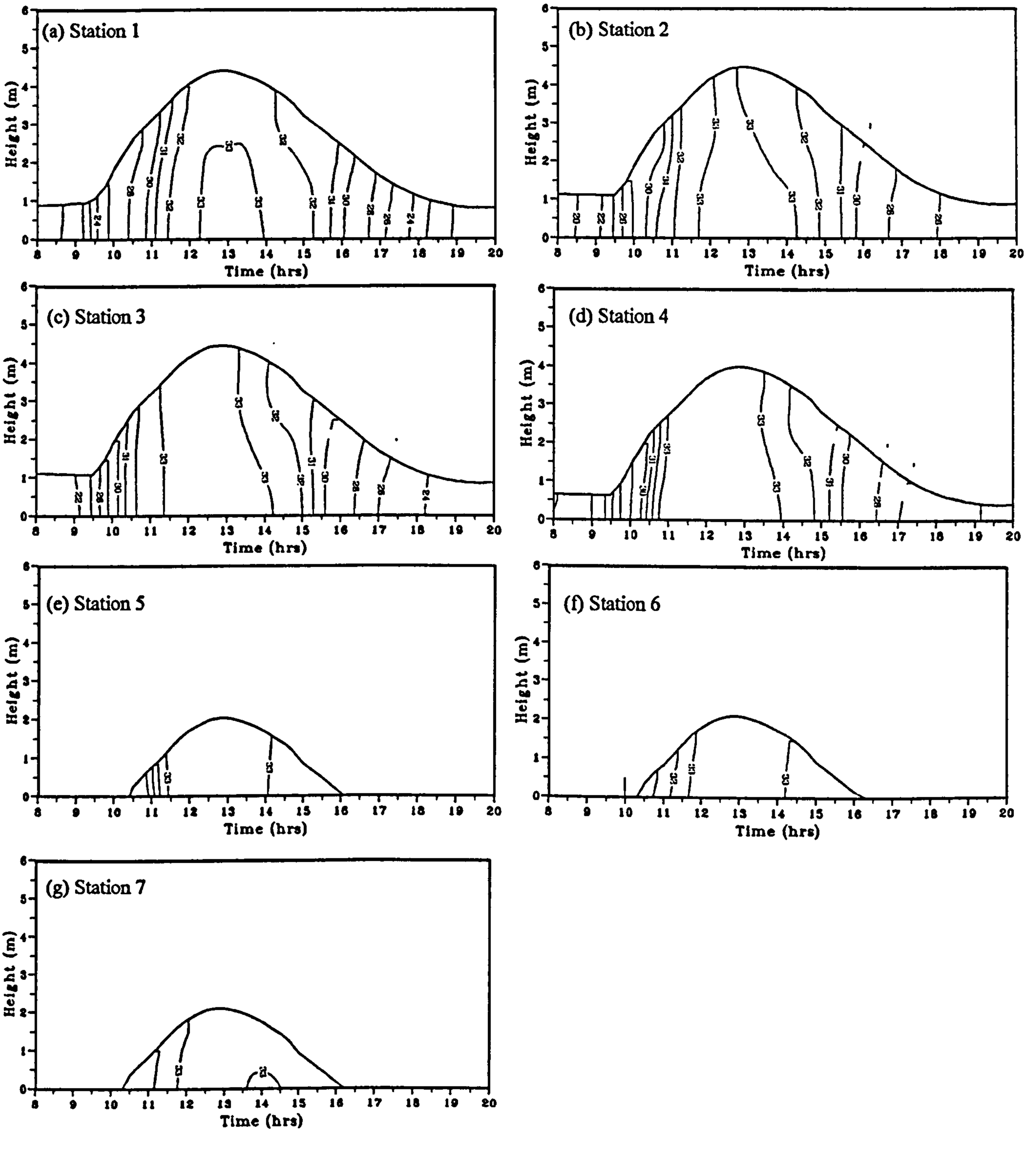

Figure 4.16 Time series contour plots of salinity (ppt) at stations 1-7, 20 July 1995.

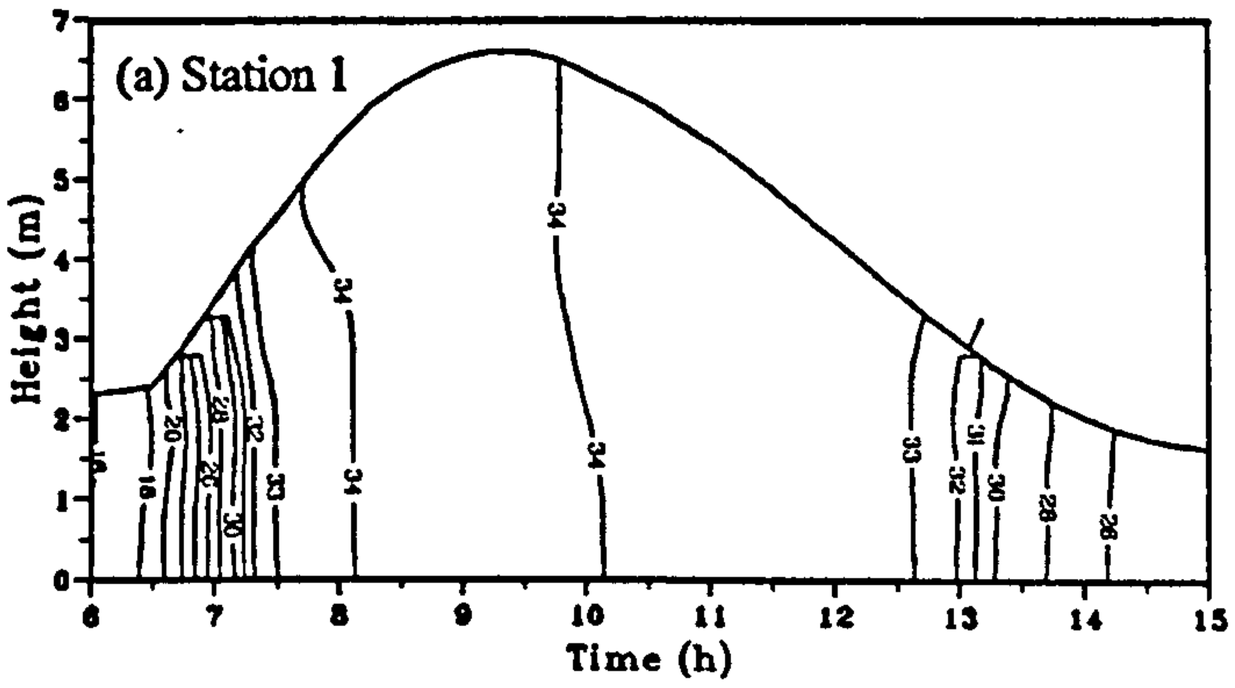

Figure 4.17 Time series contour plots of salinity (ppt) at stations 1-4, 13 September 1995.

broke down and the water column was fairly mixed around HW with a surface to bottom salinity difference less than 0.5‰. At HW, salinity reached a maximum value of 31.7‰. Stratification started to appear again at the late stage of the ebb with a surface to bottom salinity difference of 2.1‰ at the end of the measurement time.

4.2.3.3 Salinity variation in the upper estuary

At St. Clears, the salinity measurement was made during a spring tide. The salinity increased from zero at low water to a maximum of 29.6 ‰ at HW (Figure 4.19). The water column was well-mixed with less than 1‰ difference between the surface and bottom salinity throughout the tidal cycle. The tidal asymmetry at this station is shown by the salinity curve with a rapid rise in the values during the flood and a slower fall during the ebb. The flood was reached in 2 hours 10 minutes while the ebb continued to almost 3 hours when the salinity values dropped to below 1‰ .

4.2.3.4 Lateral salinity variation

The salinity data from each station at transect T9 were combined according to their common measurement time. The cross-estuary contour plots were prepared for each complete run of the CTD casts. This is illustrated in Figure 4.20 (and Figures A.06- A.08 in Appendix A). The plots show the lateral as well as the vertical salinity variations at different stages of the tide. The bottom boundary of the plot is the bed topography while the upper boundary is the water surface, that changes with time in relation to HW.

Figure 4.20 shows this lateral variation during a spring tide and relatively high river discharge. At the early stage of the flood the water was well mixed and no significant lateral and vertical variations were observed (Figure 4.20a-d). A brief stratification developed during mid-flood with a maximum difference between surface and bottom salinity of 1.5‰ (Figure 4.20e), followed by some lateral variation up to the time of high water (Figure

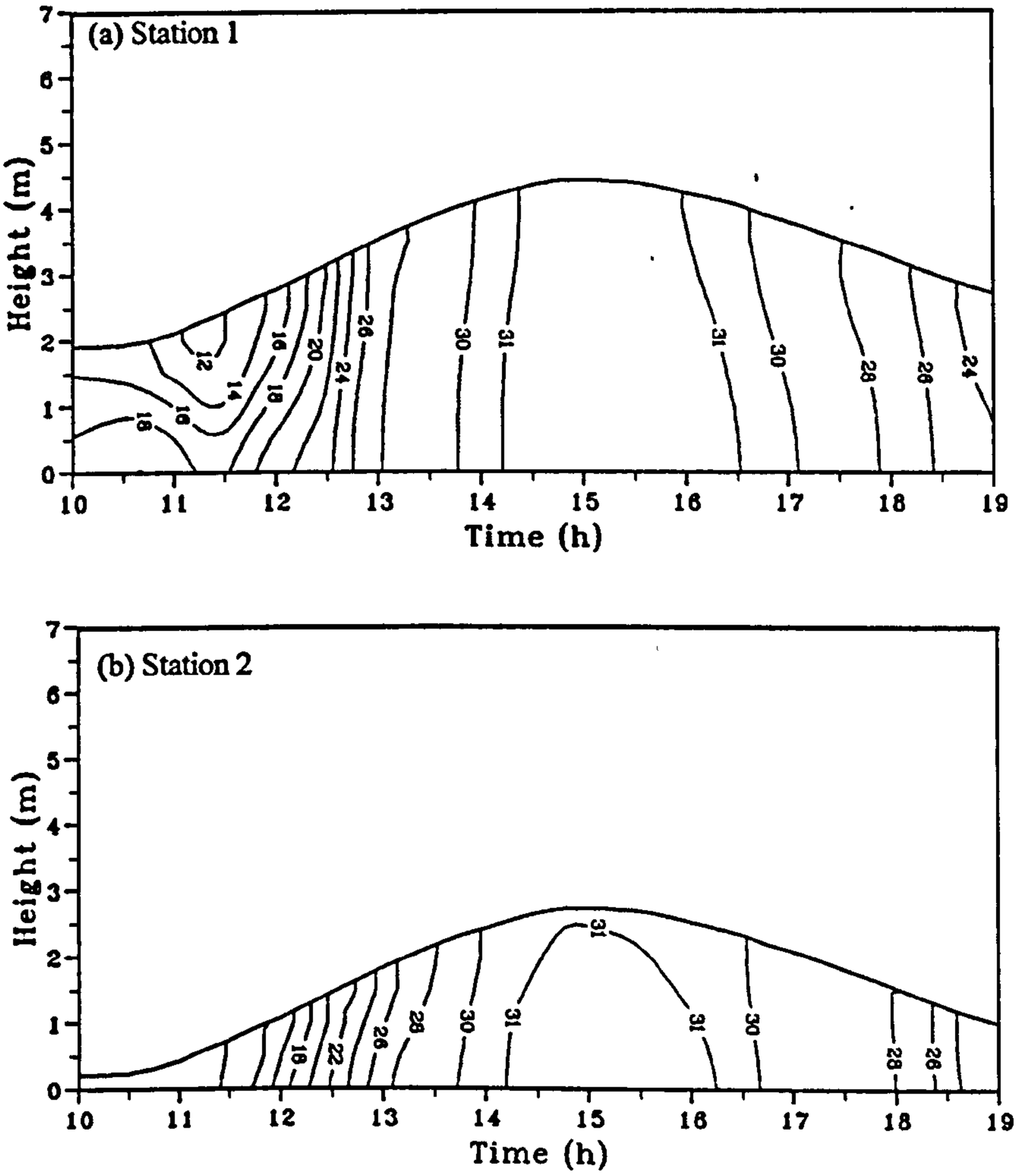

Figure 4.18 Time series contour plots of salinity (ppt) at stations 1 and 2, 19 September 1995.

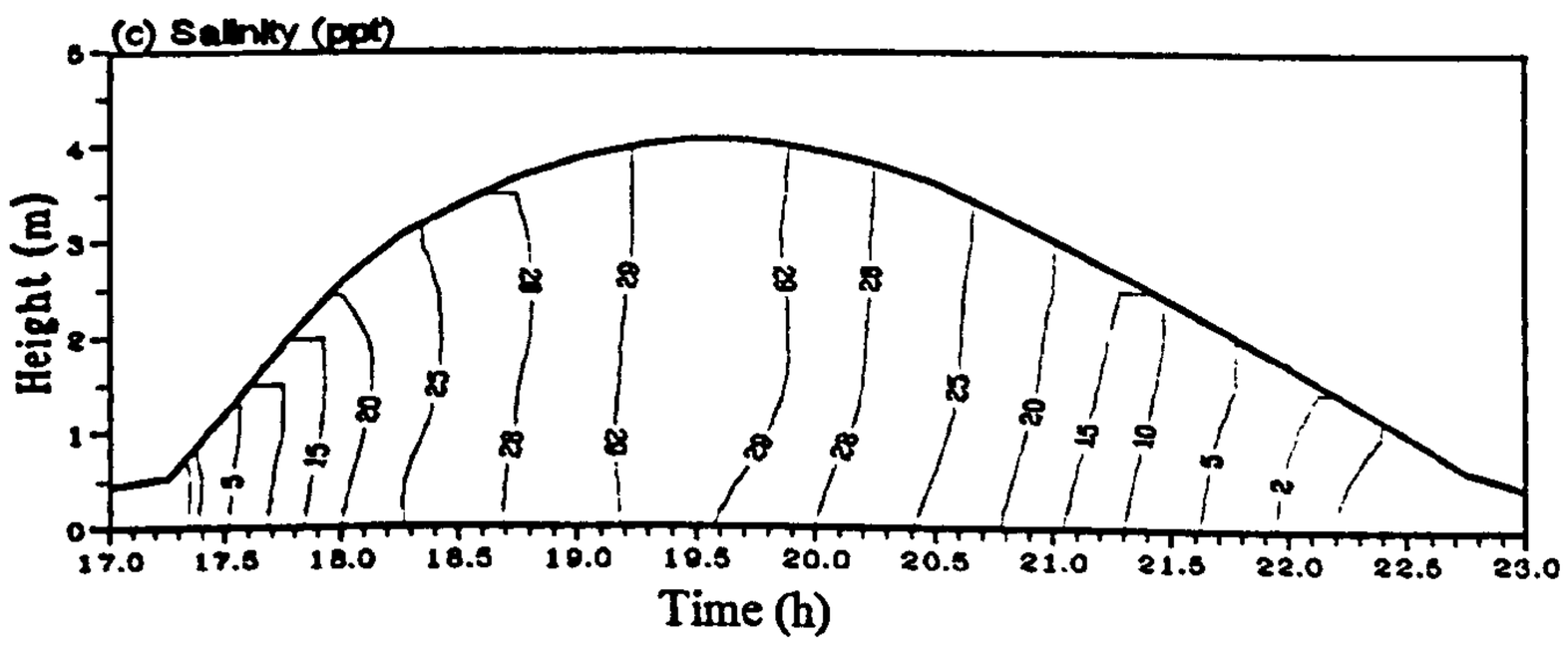

Figure 4.19 Time series contour plot of salinity (ppt) at St. Clears, 12 July 1995.

4.20f-k). At the beginning of this lateral variation, the more saline water was in the centre of the estuary and the less saline water was pushed to the sides. Ebb stratification began shortly after HW and remained for more than 1 hour (Figure 4.20l-q). Ebb stratification was stronger than flood stratification with a maximum difference of 2.5‰ between the surface and bottom salinity. This stratification was then destroyed as the ebb current became stronger and water the column was vertically and laterally mixed (Figure 4.20r-t). A lateral salinity gradient again appeared at the end of the ebb when the fresher water was concentrated in the deeper part of the channel and the more saline water on the shallower part of the channel (Figure 4.20u-x). All the above features were repeated on the measurements made on 6 October 1994 (Figure A.06 in Appendix A).

The existence of a lateral salinity gradient is better illustrated by Figures A.07 and A.08 (Appendix A) which show the cross estuary plots for spring and neap tidal cycles during a period of low river discharge. For a spring tide, a small variation in salinity was observed across the estuary during the first hour of tidal incursion, though vertically the water was well-mixed (Figure A.07a-c). There was about 2‰ salinity difference across the estuary cross section as the saline water entered the estuary on the right hand side (looking seaward), pushing the less saline water to the left hand side. This lateral variation continued during the flooding period but the lateral gradient diminished at high water (Figure A.07d-i). The water was slightly stratified during the first hour of the ebb (Figure A.07j-l), this was destroyed when flows become stronger as the ebb progressed. A lateral salinity variation was again observed towards the end of the ebb with fresher water flowing out of estuary at the right hand side and more saline water at the left hand side (Figure A.07m-r).

During the neap tide on 20 July 1995, a strong lateral salinity gradient was observed in the early stage of the flood tide when the flow was confined to the main channel and the salinities varied from 29.6‰ on the left bank to 33.1‰ on the right bank (Figure A.08a-d). This salinity gradient was maintained during the flood with the lateral variation reduced to 0.6‰ at high water (Figure A.08e-j). As the ebb progressed, the lateral variation was destroyed but vertical salinity stratification began to develop (Figure A.08k-l). This became well developed at mid-ebb when the water near the surface was about 1‰ fresher than the

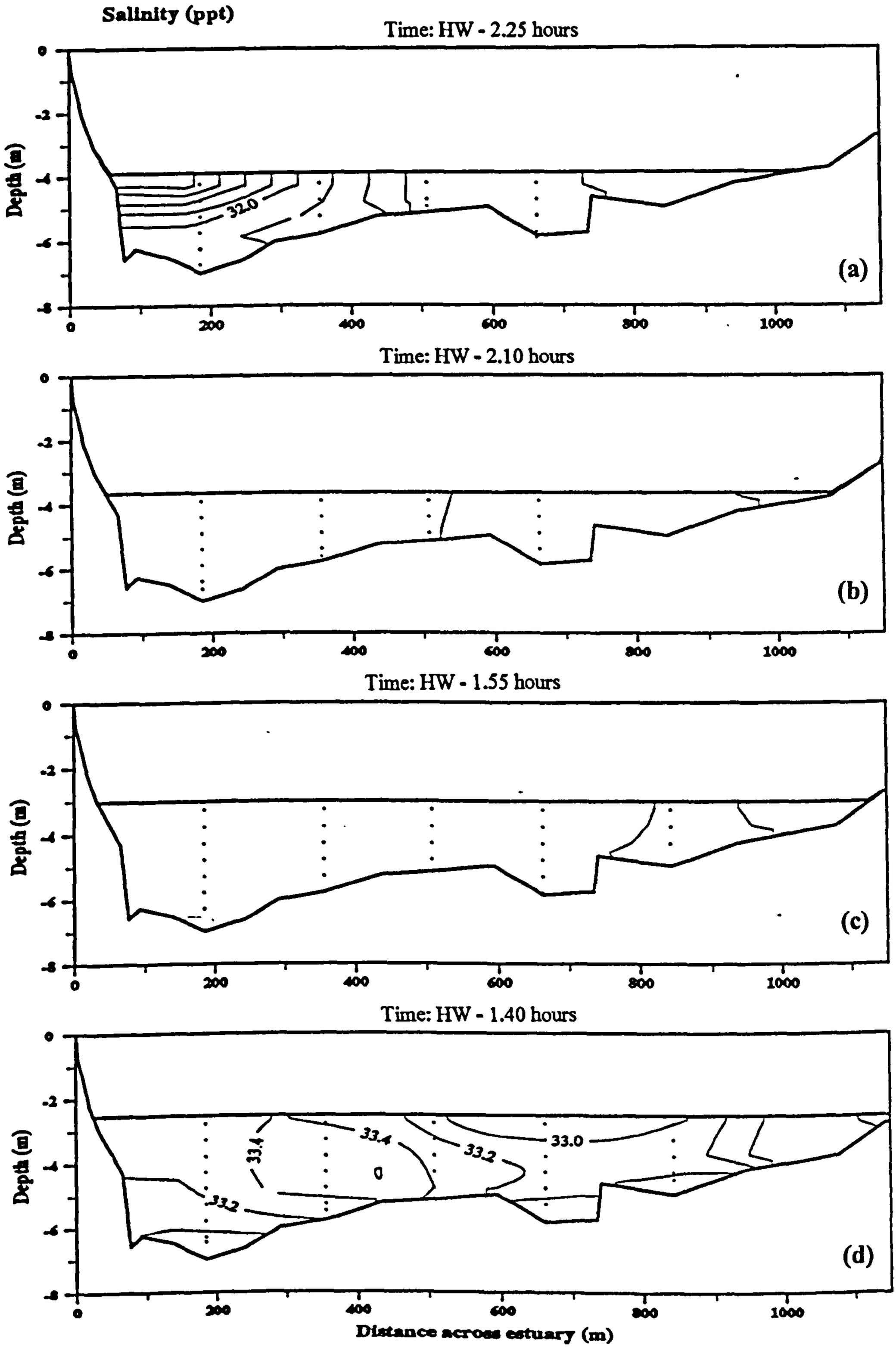

Figure 4.20 Cross estuary contour plots of salinity (ppt) at different stages of the tide, spring tide, 5 October 1994.

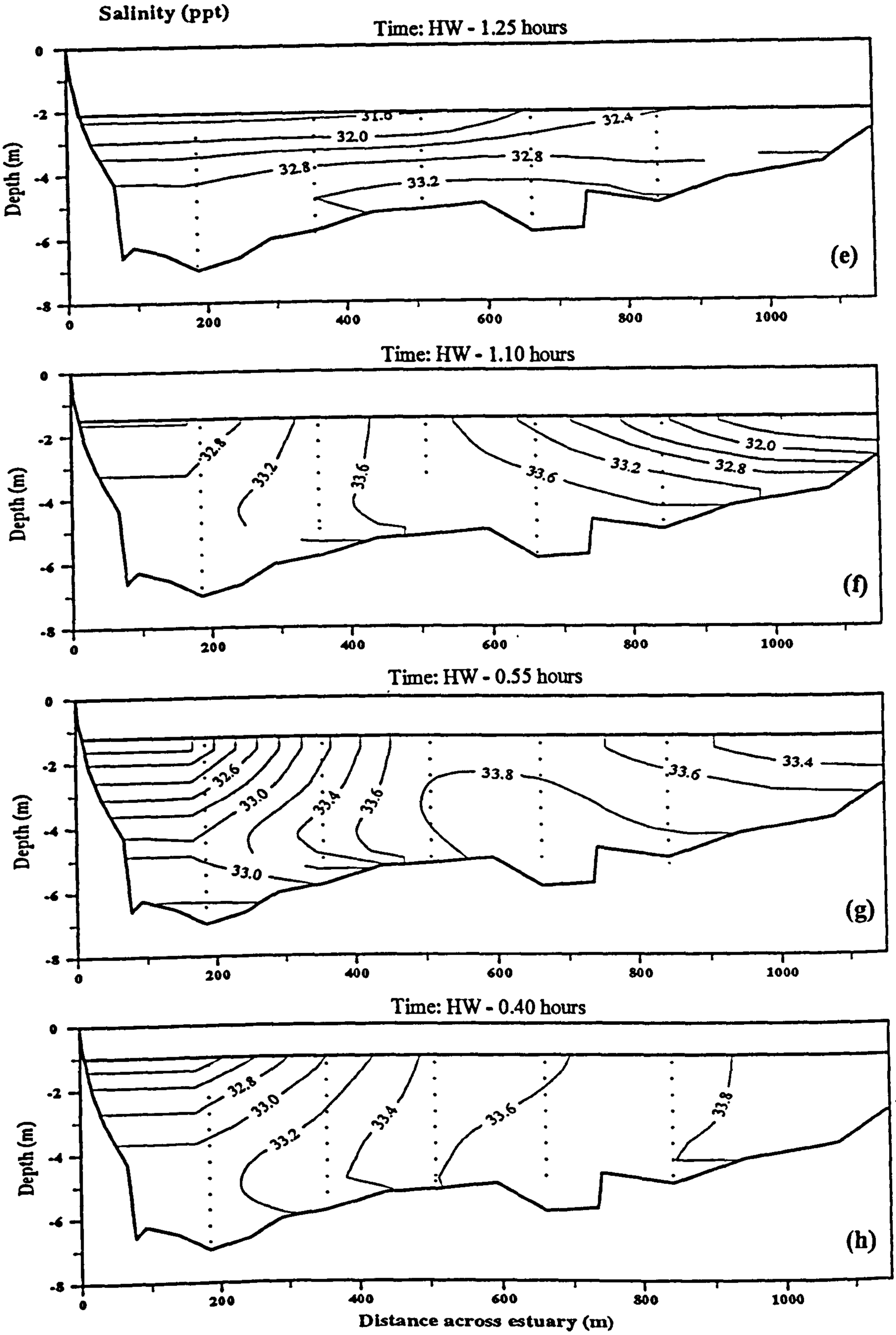

Figure 4.20 (continued).

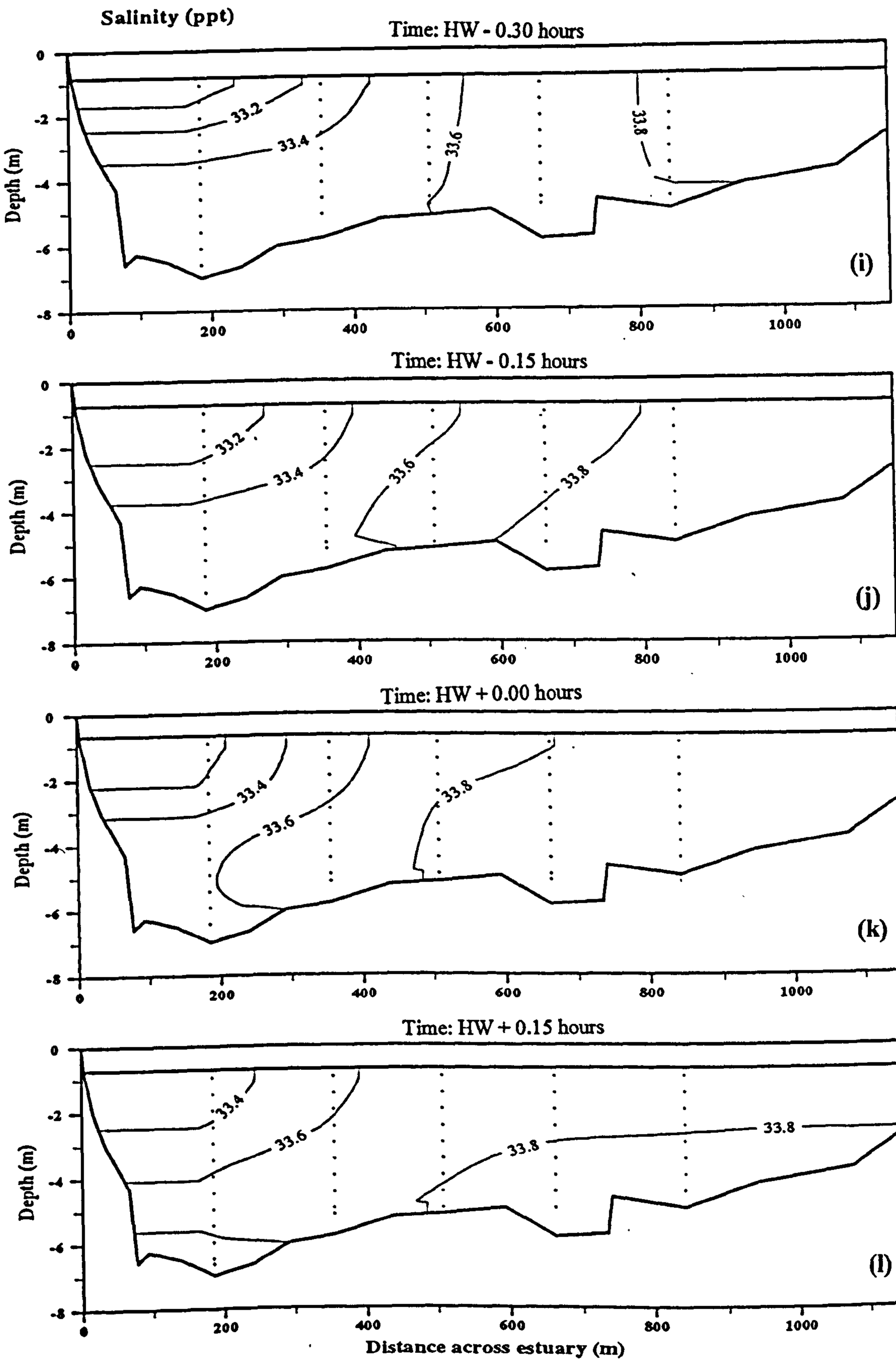

Figure 4.20 (continued).

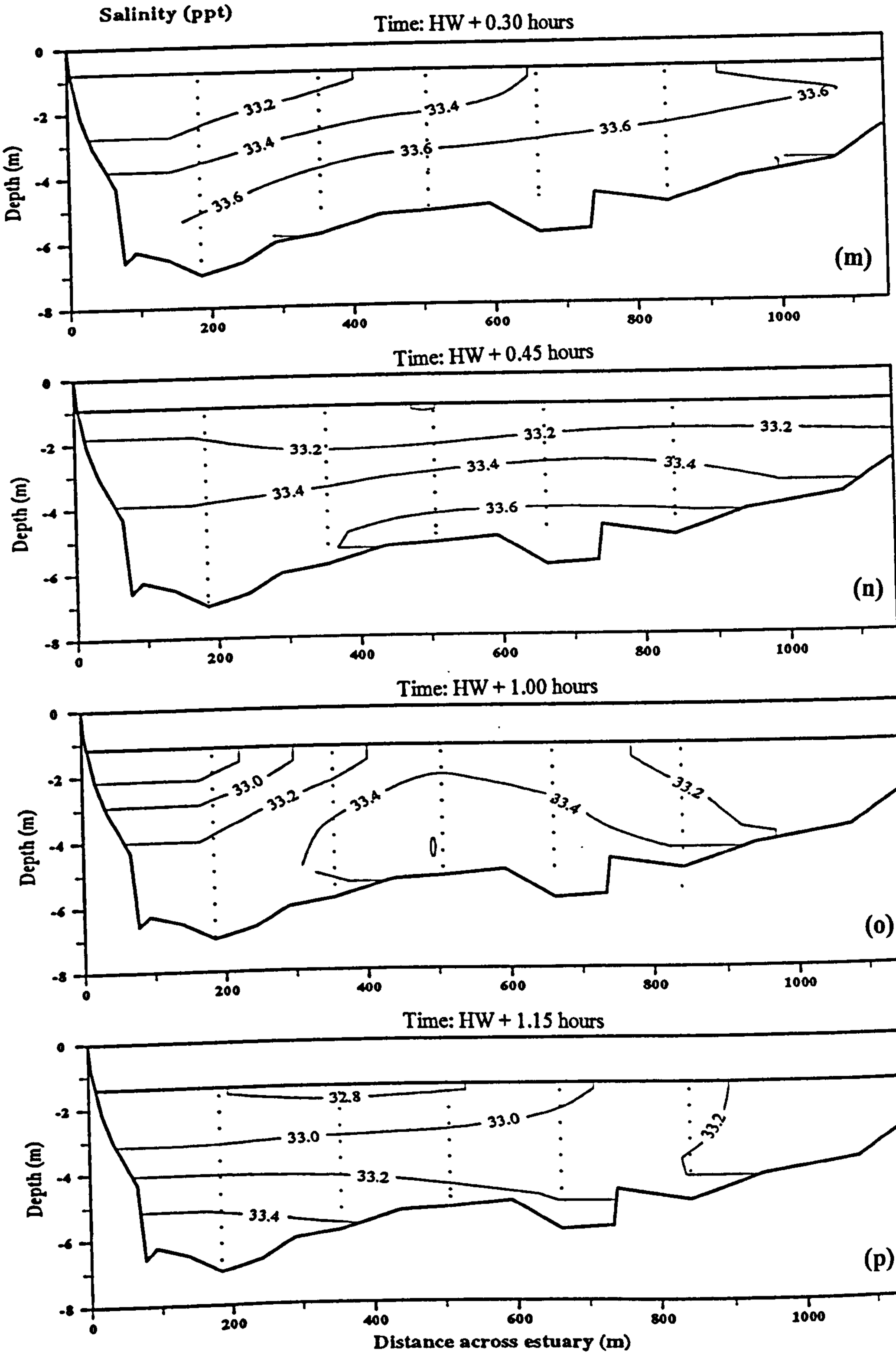

Figure 4.20 (continued).

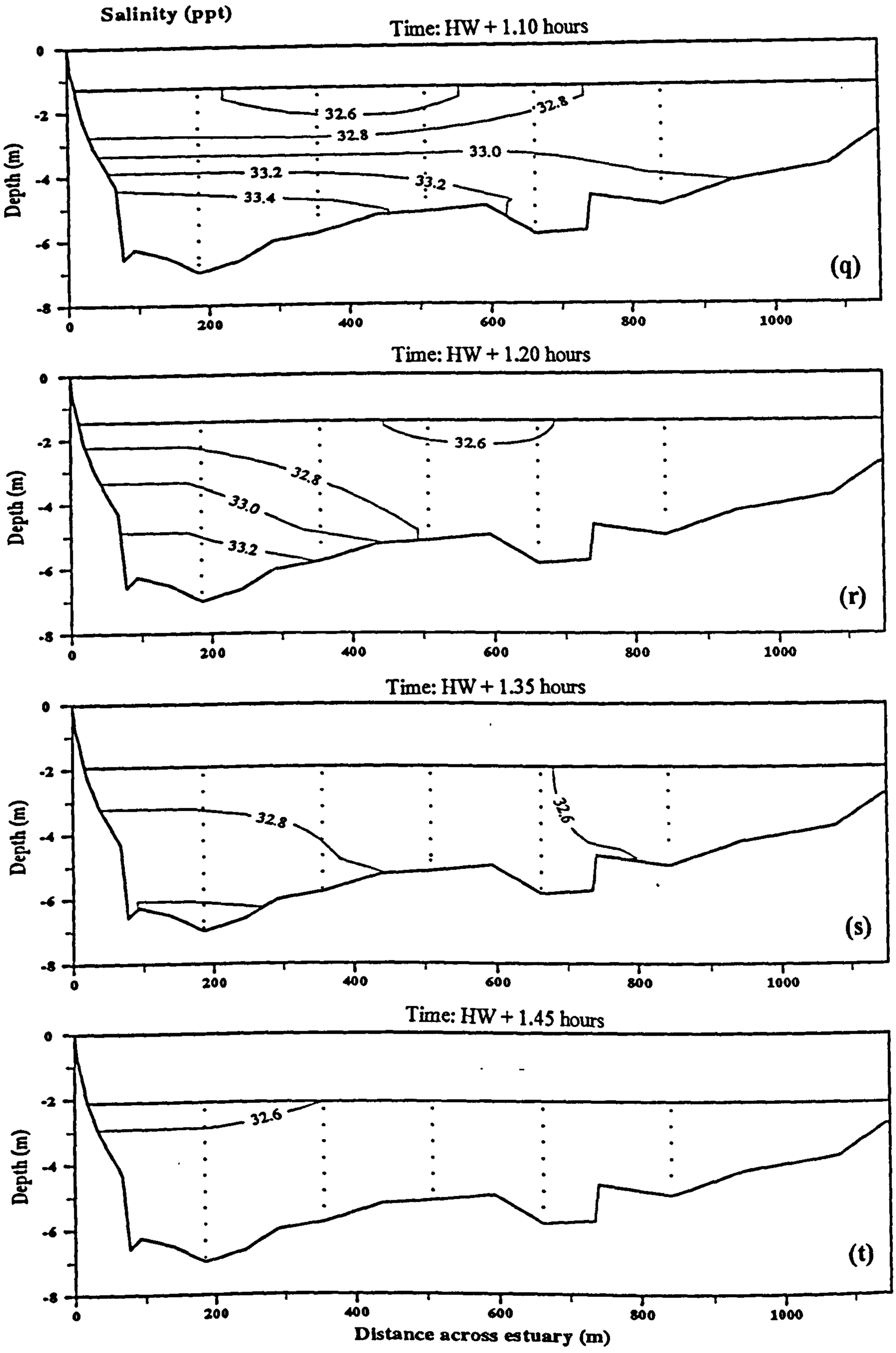

Figure 4.20 (continued).

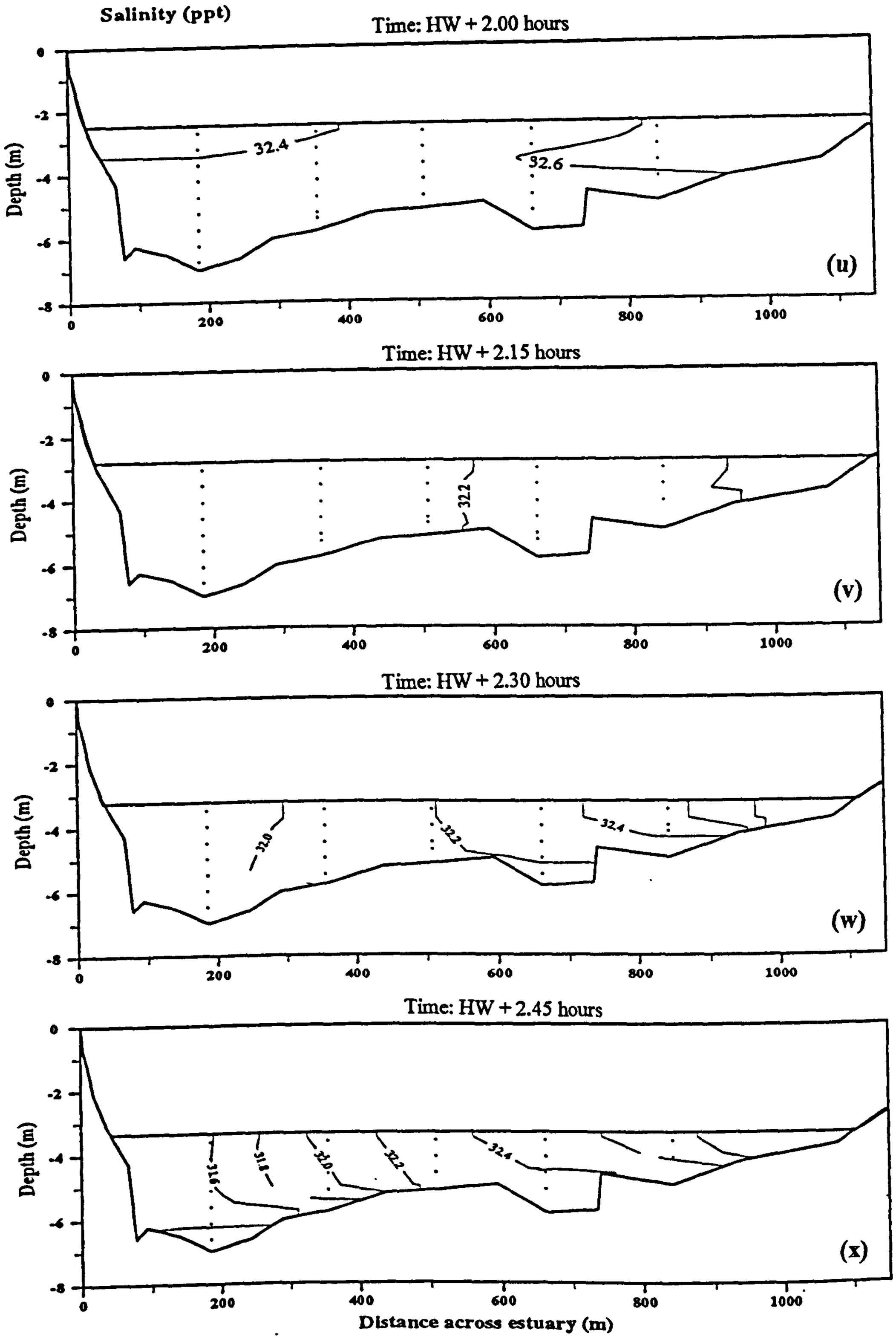

Figure 4.20 (continued).

water at the bottom (Figure A.08m-p). This stratification was well developed in the deeper water; on the intertidal sand flats where the water was shallow, the water was well-mixed. The stratification disappeared when the sand flats became exposed and the ebb flow was confined to the main channel (Figure A.08q-t). At this stage, salinity varied laterally across the estuary cross section with fresher water flowing out on the right hand side and more saline water on the left hand side. It appears that the stronger flow velocity destroyed the vertical stratification at the end of ebb tide with the combined effect of Coriolis force and bottom topography (the presence of the ebb dominant channel) causing the lateral salinity variation.

4.2.4 Estuarine water temperature

River water temperature closely follows the ambient air temperature which is falling at night and rising during the day. In an estuary, the water temperature depends primarily on the temperature of the freshwater and the temperature of the seawater with which it mixes. Due to its greater heat capacity and its slower response to the heating and cooling processes (Bowden, 1980), the seawater temperature is generally warmer than the water temperature of the incoming river. During the day the water temperature can also increase dramatically in value on the first phase of the flood as the flow advances across the sediment surface which has been subjected to solar heating during the period of exposure during low water.

Despite some seasonal variation, the water temperatures of the Taf have several common features as shown by Figure 4.21. The water temperatures are always at a minimum at the beginning of the flood tide and increase steadily with the flooding tide. During the ebb the water temperature can either increase or decrease; it increases due to the warming up of the water surface by solar radiation (Figure 4.21b&c); it decreases on a cloudy day and during early morning due the mixing with colder and a greater proportion of river water at the end of the ebb (Figure 4.21a). The water near the surface is generally warmer during the day and cooler during the night than the water at the bottom. Figure 4.21c shows that during the summer period, a stable thermocline can develop due to heating up of the water

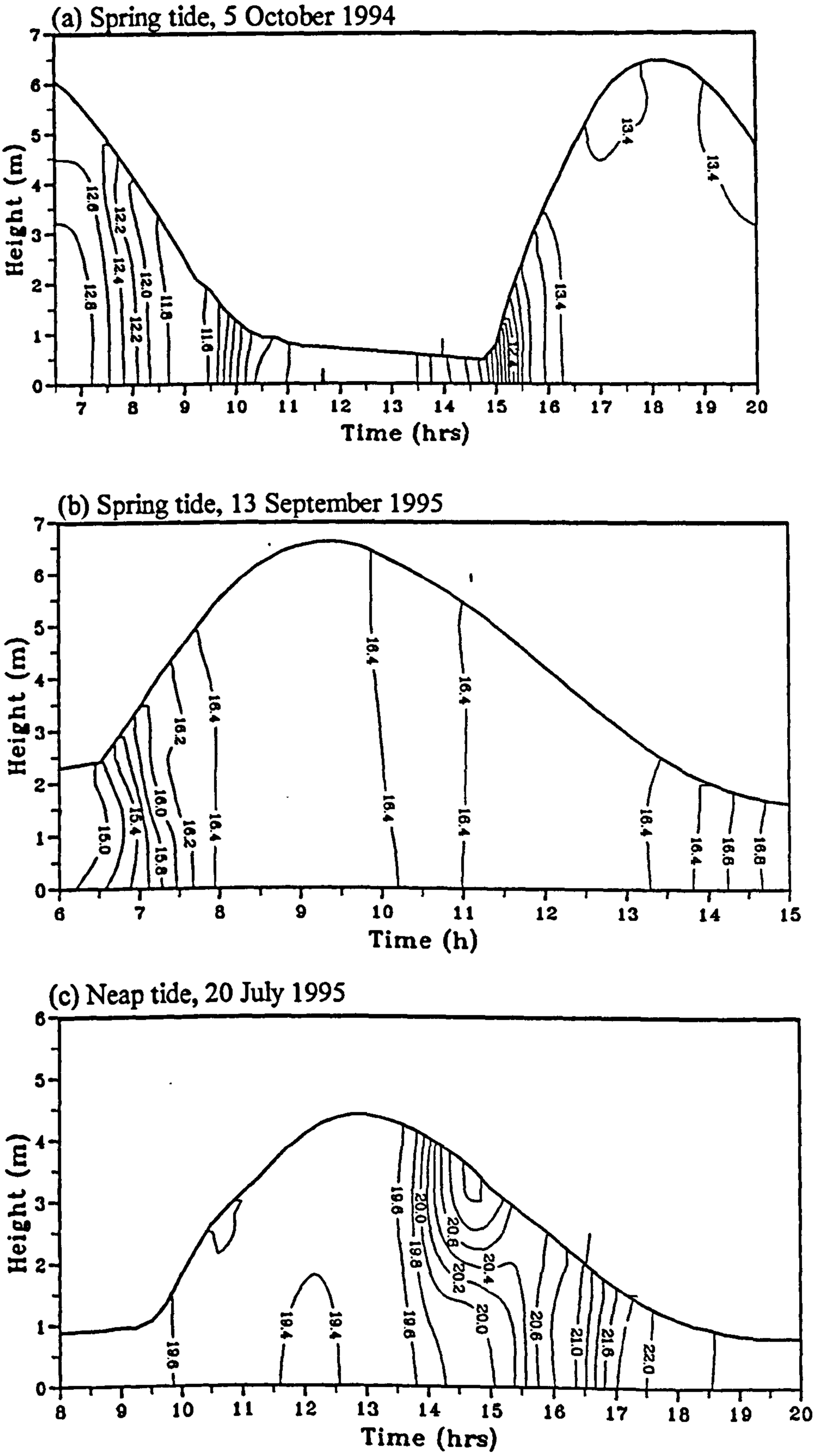

Figure 4.21 Time series contour plots showing typical variations of estuarine water tempetature (°C) over different tidal cycles.

surface by solar radiation.

The thermocline development due to the surface heating by solar radiation is more clearly illustrated by Figure A.09 (Appendix A) which shows the cross estuary temperature plots at different stages of tidal cycles for a neap tide. In the early stage of the flood, the temperature varies very little laterally and vertically (Figure A.09a-i). The high turbulence intensity during the early flood as the tide poured in creates this near homogenous water temperature. Reduction in turbulent mixing at high water and the early stage of the ebb enables a stable thermocline to develop as can be seen in Figure A.09j-p. This thermocline is broken due to intensified turbulent mixing towards the end of the ebb as the current becomes stronger and the flow is confined to the main channel (Figure A.09q-t).

The distribution of water temperature is generally affected by the same factors that control salinity. The variation in the temperature is however less regular and may be modified by heating and cooling within the channel.

4.3 Discussion

4.3.1 Vertical velocity profiles

The velocity data measured over tidal cycles have been used to provide time-averaged vertical velocity values for non-dimensionalised depths. As discussed by Kjerfve (1975), this averaging technique conserves the shape of the profiles, and allows net profiles to be constructed even when the tidal range is an appreciable fraction of the mean water depth. The mean values for non dimensionalised depth $z/h = 0.1, 0.2, \ldots .$ and 0.9 (where z = depth of measurement from the surface, and h = depth of water column) were computed for each 15 minutes cast interval using a cubic spline interpolation method. Using this averaging technique, the mean velocities were calculated for the flood, ebb, and for the whole tidal cycle. The data used for these calculations were those from the velocity measurements made at stations in the main channel. At these stations, the velocity records

were obtained for a complete tidal cycle and represent the total time of the tidal incursion in the estuary. For the tidal mean velocity, flood currents were considered negative, and ebb currents positive, and all flow was taken to be parallel to the estuary margins.

In the calculation of mean velocity, it is important not to include the river flow component, particularly in the calculation of the mean values for the ebb period. This is due to the fact that at low water a significant period of time occurs when only river water is flowing seawards; thus taking the ebb as the total duration of seaward flow will certainly introduced bias in the calculated values. During this period of low water, the velocity (and salinity) has no effect on estuary circulation. Furthermore, water depth at this time is only a small fraction compared to the water depth when the tidal prism is present in the estuary.

At St. Clears, the ebb period was taken as the time from HW (tide turned) to the time when salinity fell below 1‰ . In the lower estuary, salinity values at low water were always greater than 3‰ during high river runoff and 10‰ during low river runoff due to the late drainage of saline water retained by the marsh. The ebbing stage in the lower estuary was taken as the time from HW to the time when the water level at the estuary mouth dropped very little as determined from the tide gauge records i.e. the total expulsion of the tidal prism.

4.3.1.1 Vertical velocity variation along the estuary axis

The mean vertical profiles for flood and ebb velocities for three stations at three different locations along the estuary axis during spring tidal cycles are shown in Figure 4.22. These stations are located at the upper estuary (St. Clears), the middle estuary (transect T5) and the lower estuary (transect T9). The three stations were selected because they show similar bed topography in that all of the flow was concentrated in the main channel at the beginning of tidal intrusion and at the end of tidal expulsion. The figure illustrates the spatial variability of current strength along the estuary. As can be seen the magnitude of mean velocity decreased upstream reflecting less tidal domination and the increase influence of

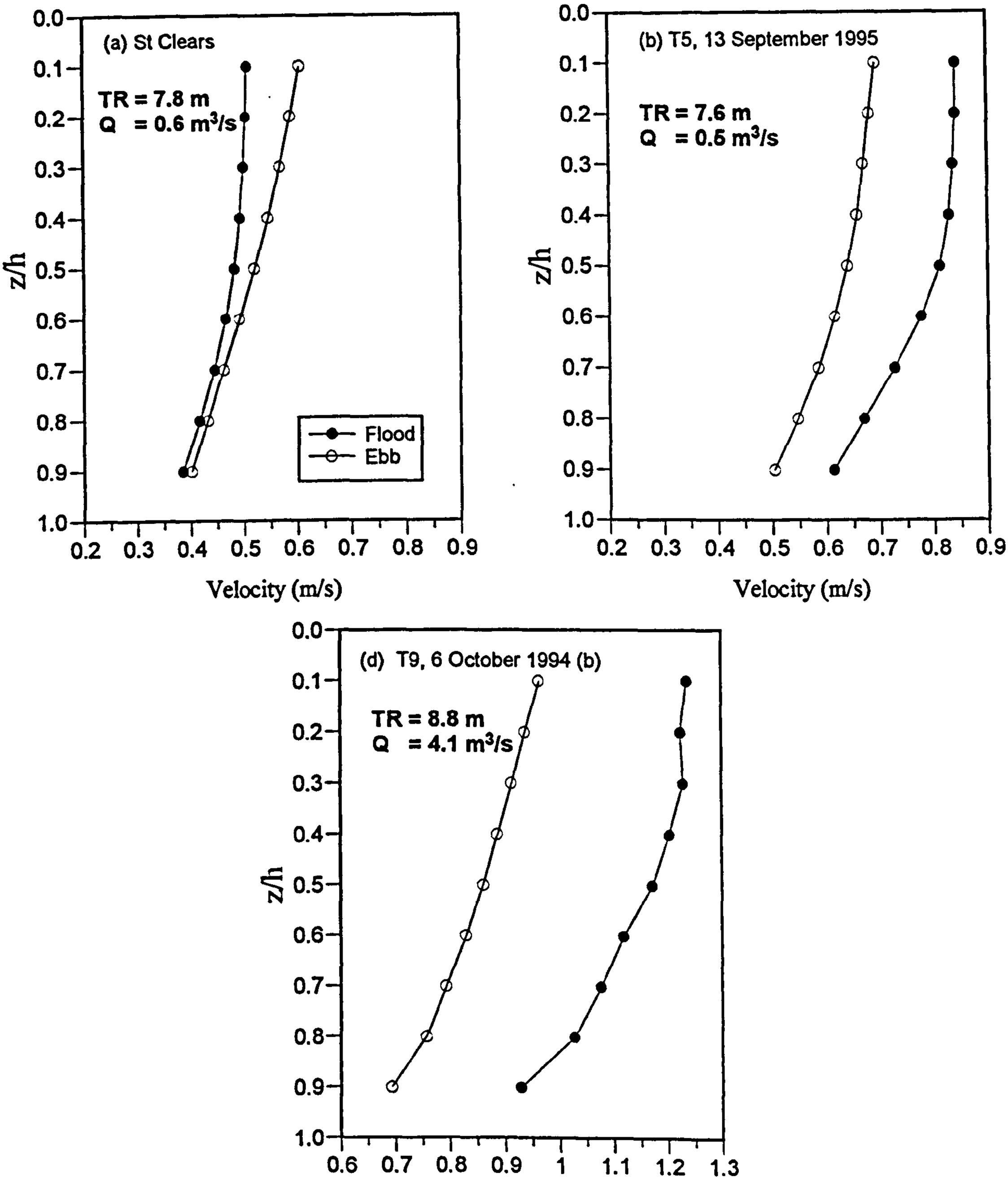

Figure 4.22 Vertical profiles of mean flood and mean ebb velocity at three different stations during spring tides (TR= tidal range, Q = river discharge).

upland flow. Therefore at the upper estuary the mean ebb velocity is dominant over mean flood velocity at all depths, while in the middle and the lower estuary, the reverse occurs.

The mean ebb velocity varies almost linearly with depth, with a maximum flow at the surface and decreasing with depth. This type of profile is produced by the combined effect of river flow at the surface and bed friction at the bottom. The mean surface ebb velocity is amplified by flow stratification. As the tide turns at high water, the ebb begins at the surface before the deeper layers, and the turn of the tide then progresses downstream. Thus early in the ebb, the water at the surface is flowing at a greater velocity than the water at the bottom. The much stronger mean velocities observed at T9 was due to larger tidal ranges but the mean ebb may have been boosted by a higher fresh water discharge. The mean ebb velocity was less at T5 at a time of very low river discharge.

The mean velocity profiles for the flood show a slight variation from the mean ebb profiles. The flood profiles show a near vertical trend from the surface to mid depth but at the bottom the mean velocity reduces rapidly to a minimum. Jago (1974) showed that the mean velocity for the flood is influenced by two factors i.e. near surface salinity stratification and bed friction. During the early part of the flood, opposition from river flow reduces the surface current, while bed friction decreases the current at the bottom. These effects can be seen in the shape of the mean flood velocity profiles which are concave towards the surface.

The mean velocity profiles for complete tidal cycles are shown in Figure 4.23. At St. Clears the mean profile shows a net flood direction near the bottom and a net ebb direction at the surface with increasing net ebb velocity towards the surface. The mean velocity in the mid (T5) and lower estuary (T9) has a net flood direction. At T5 and T9 the net velocity was generally strongest at mid depth, minimum at the bottom and decreasing near the surface. The velocity profiles suggest that the estuary is well-mixed at the lower estuary as the net flow is directed only in one particular direction at all depth but the estuary is slightly stratified at the upper reaches as the mean flow was flood directed at the bottom and ebb directed near the surface.

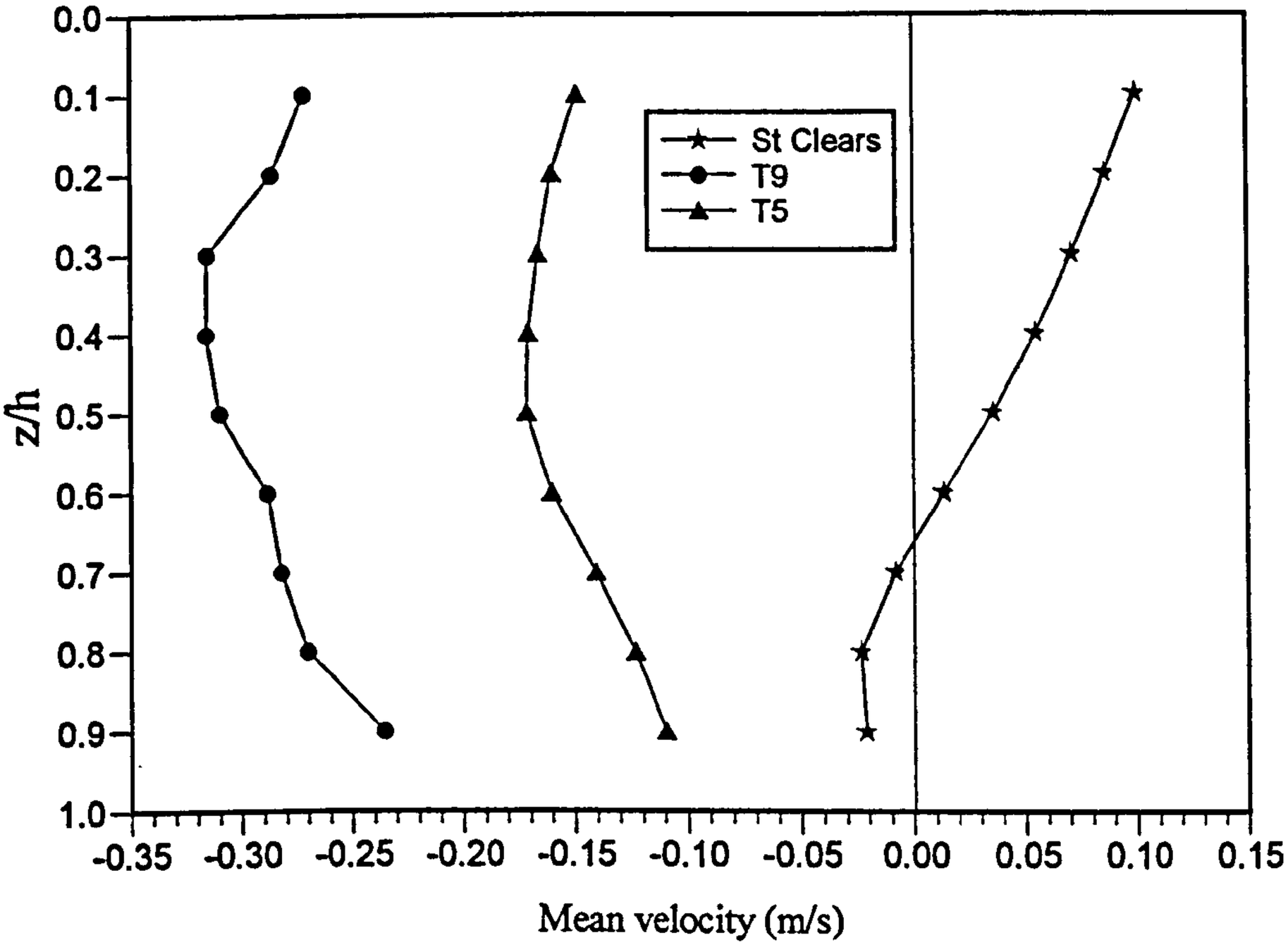

Figure 4.23 Vertical profile of mean velocity at three locations along the estuary channel.

4.3.1.2 Vertical velocity variation over neap and spring cycles

The vertical velocity profiles of mean flood and mean ebb currents at different stations across the estuary for a spring and a neap tides are shown in Figures A.10 and A.11, respectively (see Appendix A). The figures are for the velocity measurement made at stations 1-7, transect T9 on 16 July 1995 (Spring tide) and 20 July 1995 (neap tide). The mean velocities are strongest at stations 1, 2 and 3 which were located in the main ebb channels, but weakest at stations 5, 6 and 7 that were located on the intertidal sand flats. The plots show that during the spring (Figure A.10), flood velocity is dominant over the ebb velocity at stations 1, 2, 3 and 5 but at stations 4, 6 and 7, ebb velocity is dominant over the flood velocity, therefore the mean currents averaged over the tidal cycle have a net flood direction at stations 1, 2, 3 and 5, and a net ebb direction at stations 4, 6 and 7 as shown in Figure 4.24. The maximum velocities occur near the surface at all stations during both flood and ebb. Stations 5, 6 and 7 which were located on the inter-tidal sand flats show very little different between surface and bottom velocities, most probably due to the shallowness of the water (< 3 m at HW), and at most of the times only bottom and surface velocities were measured. During the neap tide (Figure A.11), ebb velocities are dominant over flood velocities except at stations 2 and 3, therefore the mean currents averaged over the tidal cycle have a net flood direction at stations 2 and 3, and a net ebb direction at other stations as shown in Figure 4.25. This indicates that during neap tides, the seaward discharge of freshwater is importance in opposing the flow during the flood and boosting the velocities during the ebb.

The profiles show that the velocity varies across the estuary due to interaction with the freshwater flow, flow confinement in the channels, channel cross section, and the presence of bends and banks. All these alter the hydraulic geometry so as to bring about an increase and decrease in velocities for a given river discharge.

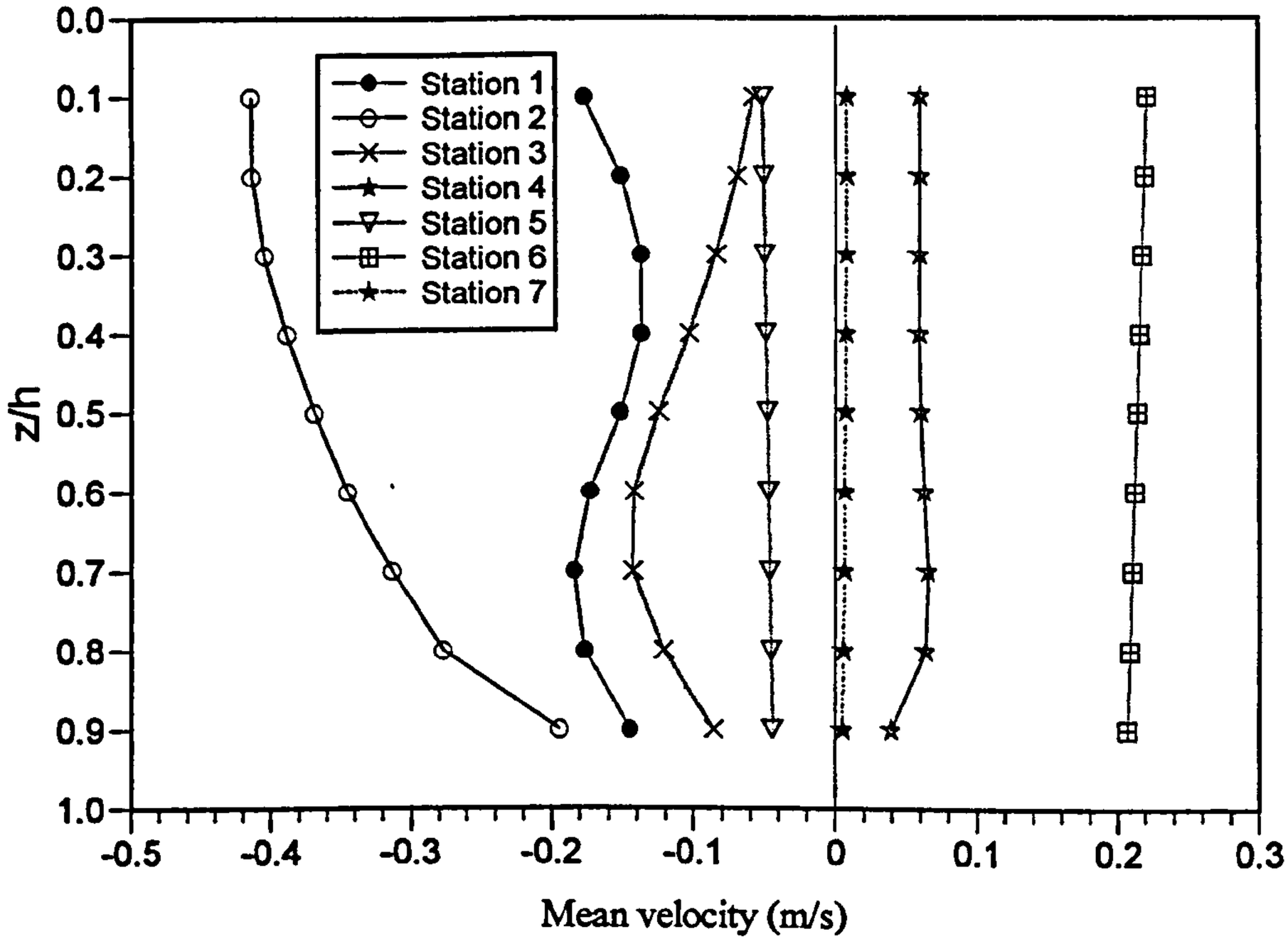

Figure 4.24 Vertical profiles of mean velocity at stations 1-7, 16 July 1995.

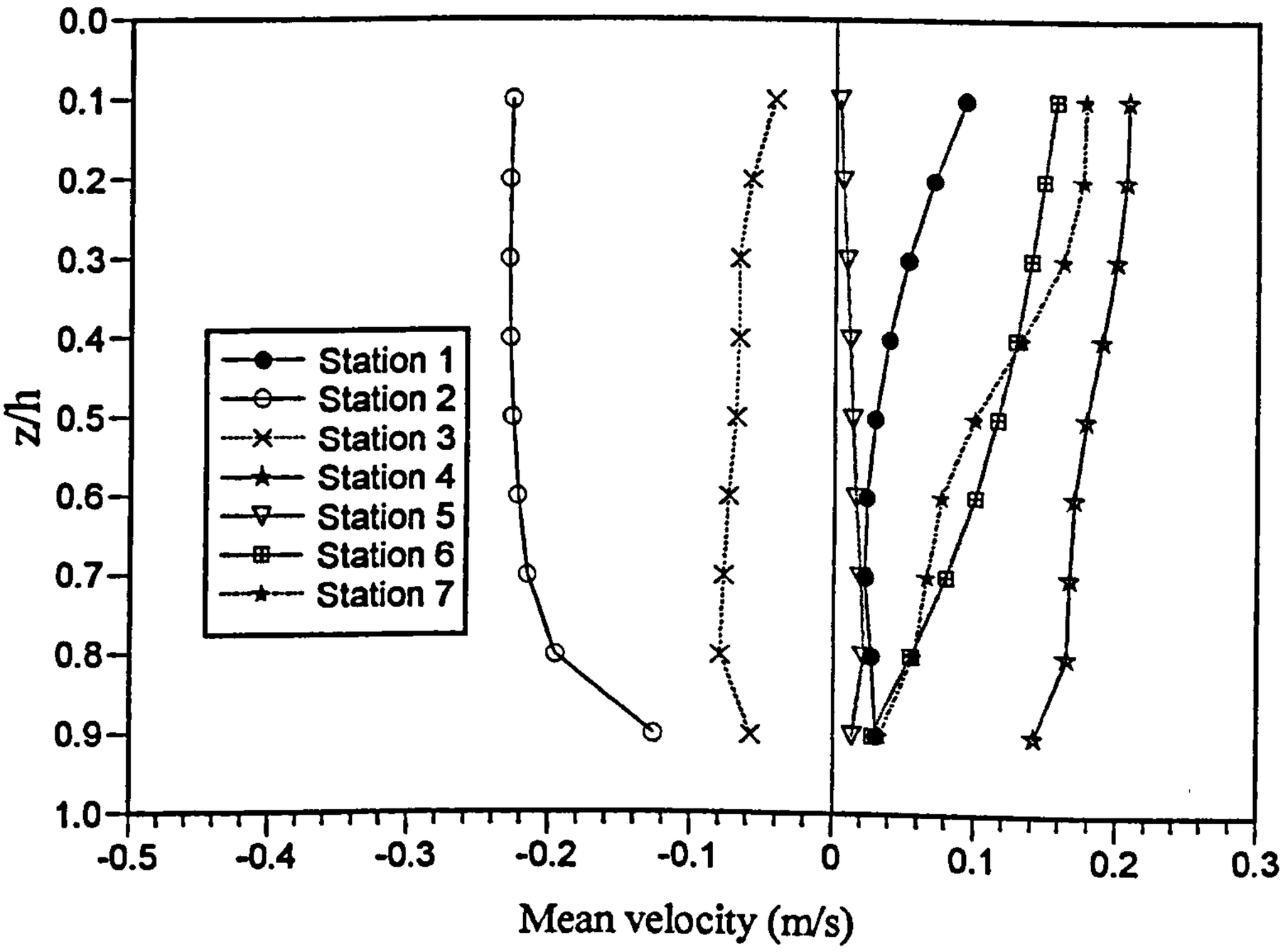

Figure 4.25 Vertical profiles of mean velocity at stations 1-7, 20 July 1995.

4.3.2 Vertical salinity profiles

Time-averaged vertical salinity values for non-dimensionalised depths have been calculated for all stations across the estuary, and for all the complete tidal cycles. The time for one tidal cycle is taken as the time when the tidal prism is present in the estuary. The salinity values for z/h = 0.0, 0.1, 0.2, ... and 0.9 (where z = depth of measurement, and h = depth of water column) were computed for each 15 minutes cast interval using a cubic spline interpolation method. The mean values for each non-dimensionalised depth were computed for all the anchor stations.

The mean salinities for the measurement made in October 1994 (spring tides, average discharge) are shown in Figure 4.26. At station 1 the profile shows that the mixing is most complete in the bottom water with a small degree of stratification near the surface. At stations 2 - 5, the water column is almost well-mixed. For 5/10/94, the difference between surface and bottom salinity is 0.2‰ at stations 2-5 and 0.58‰ at station 1. The mixing is more advanced on a bigger tide of 6/10/94 as shown by smaller difference between surface and bottom salinities i.e. 0.05-0.13‰ for stations 2-5 and 0.35‰ at station 1. The dilutions provided by the river discharge reduced the salinity values at station 1.

For the measurement made in July 1995 (a period of very low river discharges), the mean salinity profiles show a very homogeneous mixing at all stations and on both springs and neaps (Figure 4.27). The difference between bottom and surface salinities varies between 0.00 ‰ and 0.38 ‰, being smallest for the spring tide and largest for the neap tide. The stations in the main ebb channel show greater surface and bottom salinity differences than stations located on the intertidal sand flats. Strong turbulence produced by the thrusting tide encouraged the mixing vertically up to the surface layers. During this exceptionally low river discharge the upland flow was too small to suppress this turbulence, even during a neap tide.

The mean salinity profiles for September 1995 also represent the condition for a dry season and very low river discharge (Figure 4.28). The water column is very well mixed, with a

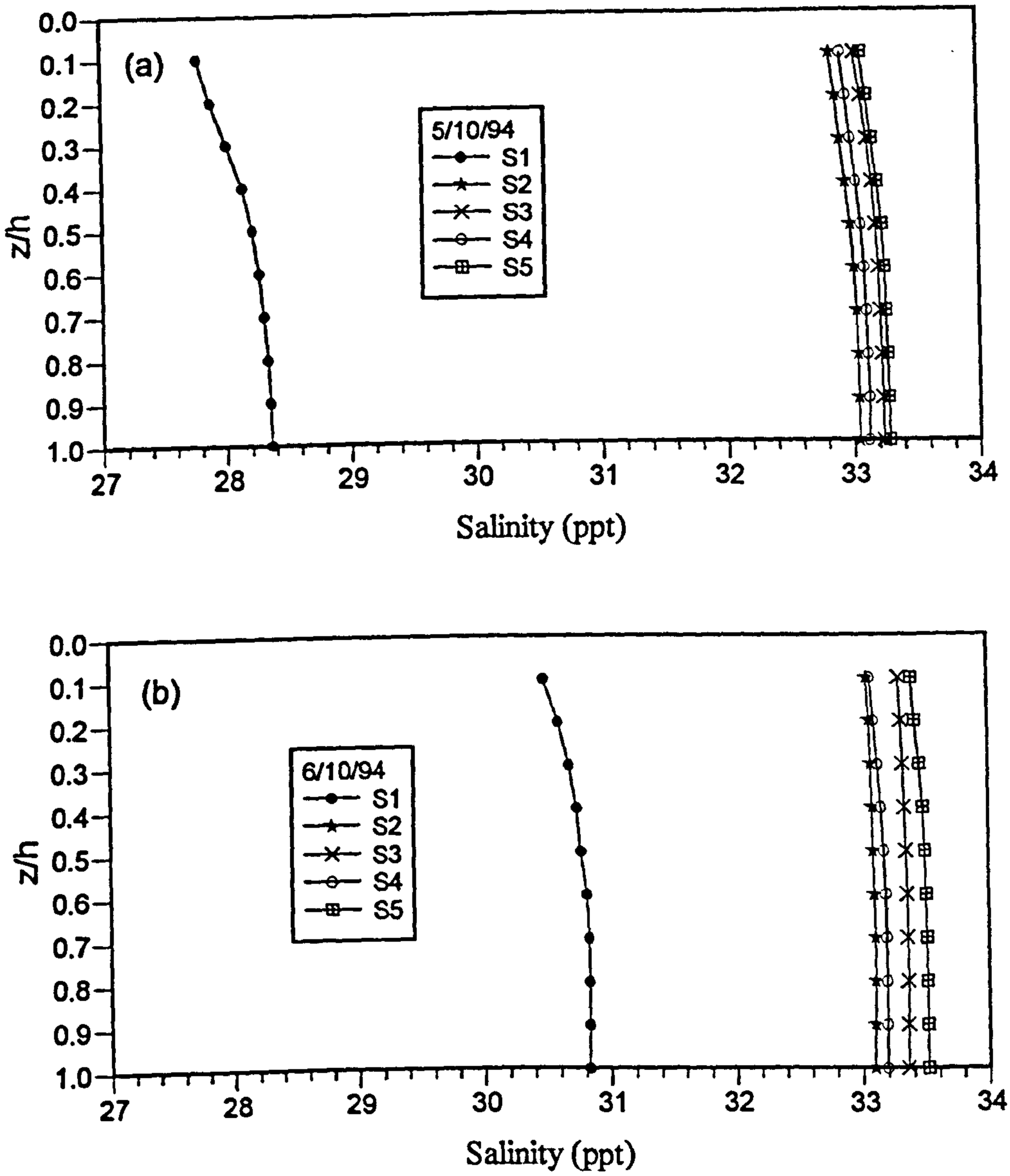

Figure 4.26 Mean salinity profiles at stations 1 - 5, transect T9, on 5 and 6 October 1994 - spring tides.

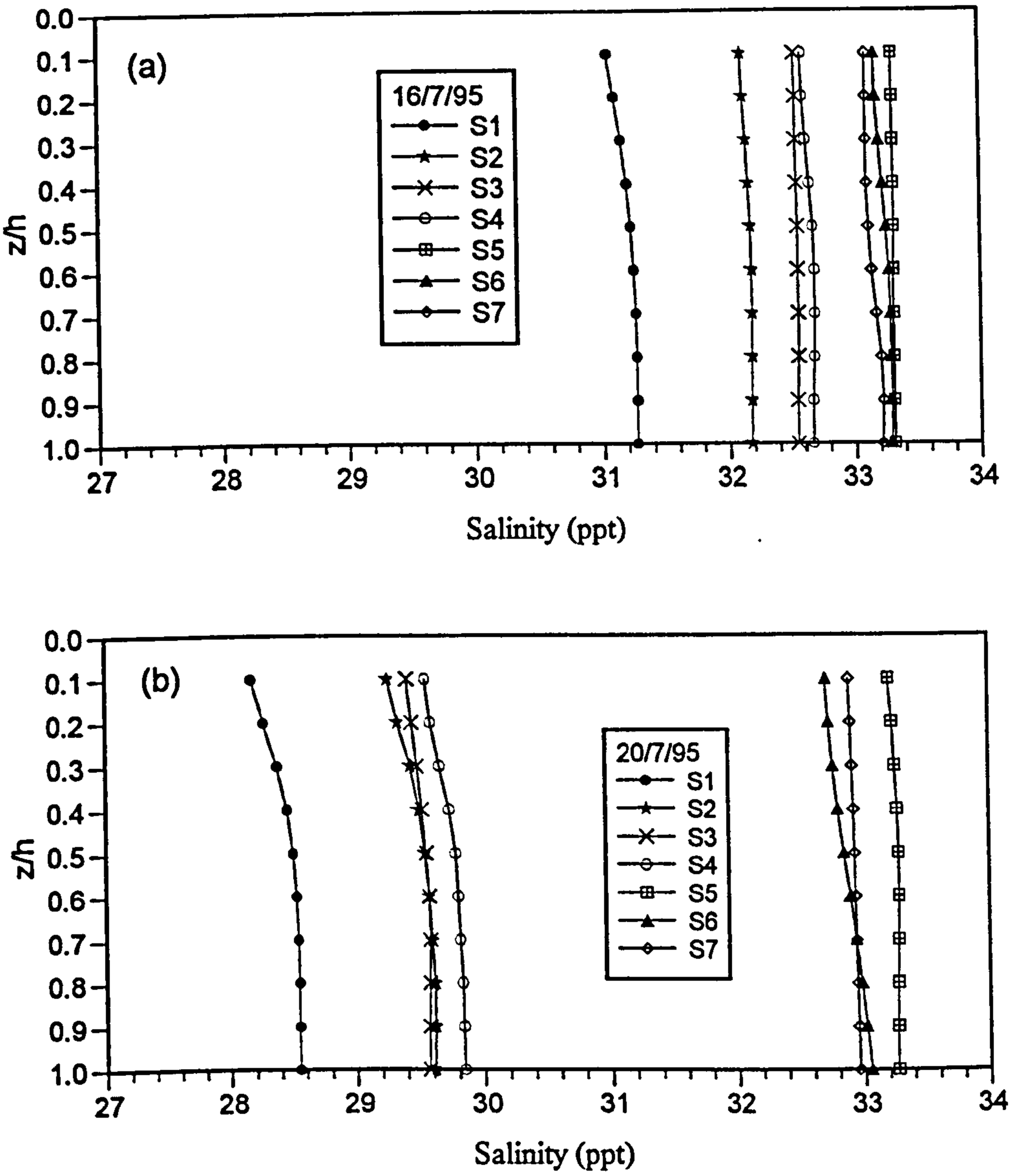

Figure 4.27 Mean salinity profiles at stations 1 - 7, (a) 16 July 1995- spring tide, and (b) 20 July 1995 - neap tide.

very small (0.08 - 0.26 ‰) difference between top and bottom salinity on 13 September 1995, a spring tide (Figure 4.28a). Stations 3 and 4 located on the intertidal sand flats have greater mean salinities values at all depths compared to stations 1 and 2 which were located in the main channel. This shows that on the sand bank the influence of fresh water in controlling mixing is negligible.

The effect of fresh water flow on the estuarine circulation becomes more important towards neaps, as turbulence reduces. During the neap tide on 19 September 1995, the vertical salinity variation is much greater than during the spring tide, the difference between surface and bottom values being 2.21 ‰ at station 1 and 1.55 ‰ at station 2 (Figure 4.28b). Stratification is greater in the top half of the water column. Greater bottom friction and turbulence causes more complete mixing of the water column near the bottom. At this station, stratification is maintained partly due to the fresh water outflow but mainly because the water was quite deep at this station(> 1.0 m during LW). Under similar conditions (neap tide, low discharge) at Station 1, transect T9 on 20 July 1995 (Fig. 4.27), stratification was less developed as the water was shallow (< 0.5 m during LW), and bottom friction and turbulence encouraged vertical mixing.

The mean salinity profile on a spring tide at St. Clears is shown in Figure 4.29 which shows a near-homogenous vertical profile. At this station the difference between bottom and surface salinities is 0.23 ‰. This strong mixing is produced by strong turbulence as the tide advances through this narrow and shallow part of the estuary.

In a well mixed estuary, the water column mostly vertically homogenous, but salinity varies laterally. The main cause of this variation is the Coriolis effect (Pritchard, 1955). In the northern hemisphere the Coriolis force will deflect the flowing water to the right. Thus as the tide enters the estuary the sea water flows up estuary on the left hand side (looking seaward) and the river water flows down estuary on the right hand side, causing horizontal rather than vertical mixing. Therefore, there exists lateral salinity gradient whereby the higher salinity water will be on the left hand side of the estuary, and lower salinity water on the right hand side of the estuary.

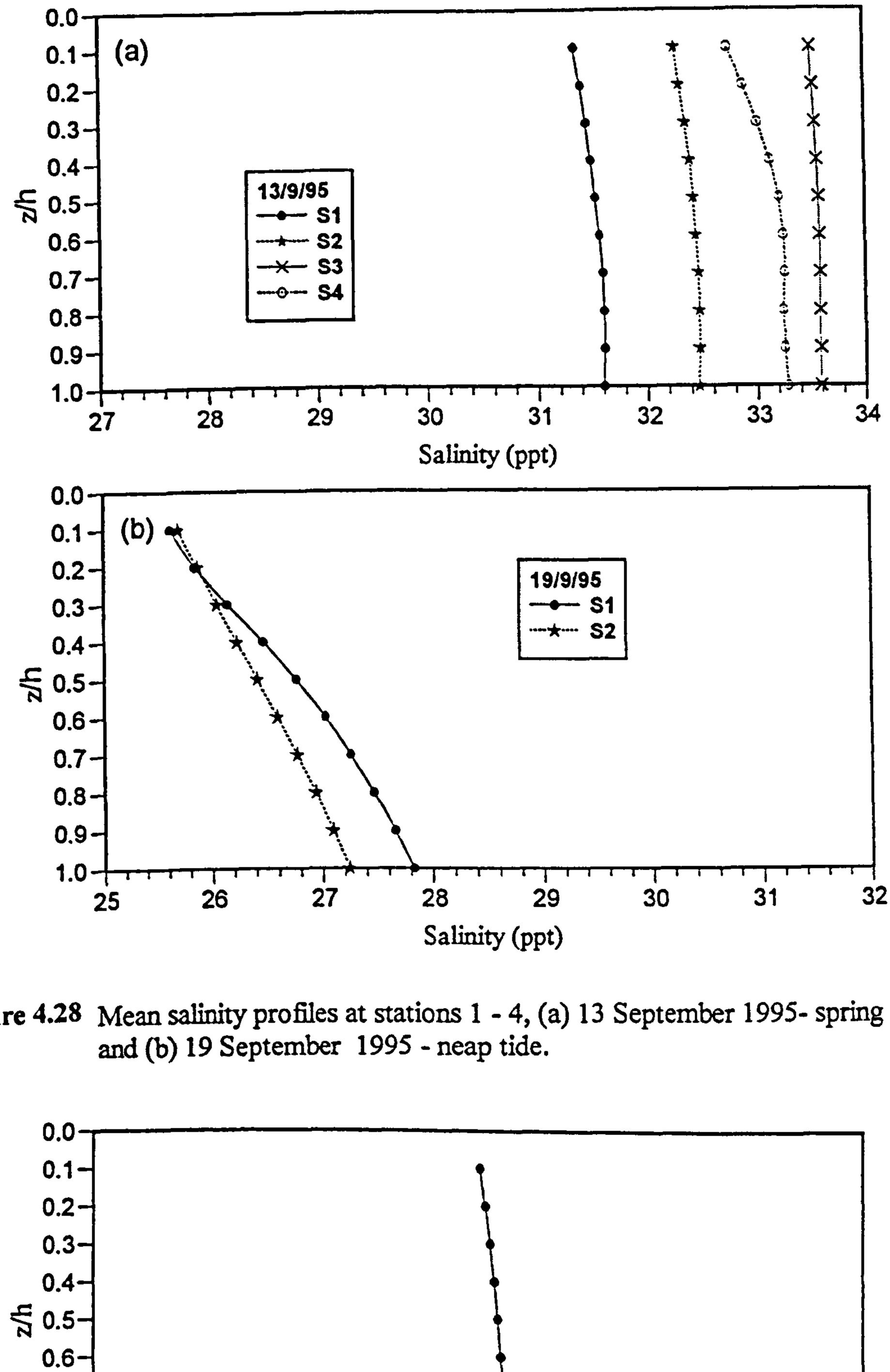

Figure 4.28 Mean salinity profiles at stations 1 - 4, (a) 13 September 1995- spring tide, and (b) 19 September 1995 - neap tide.

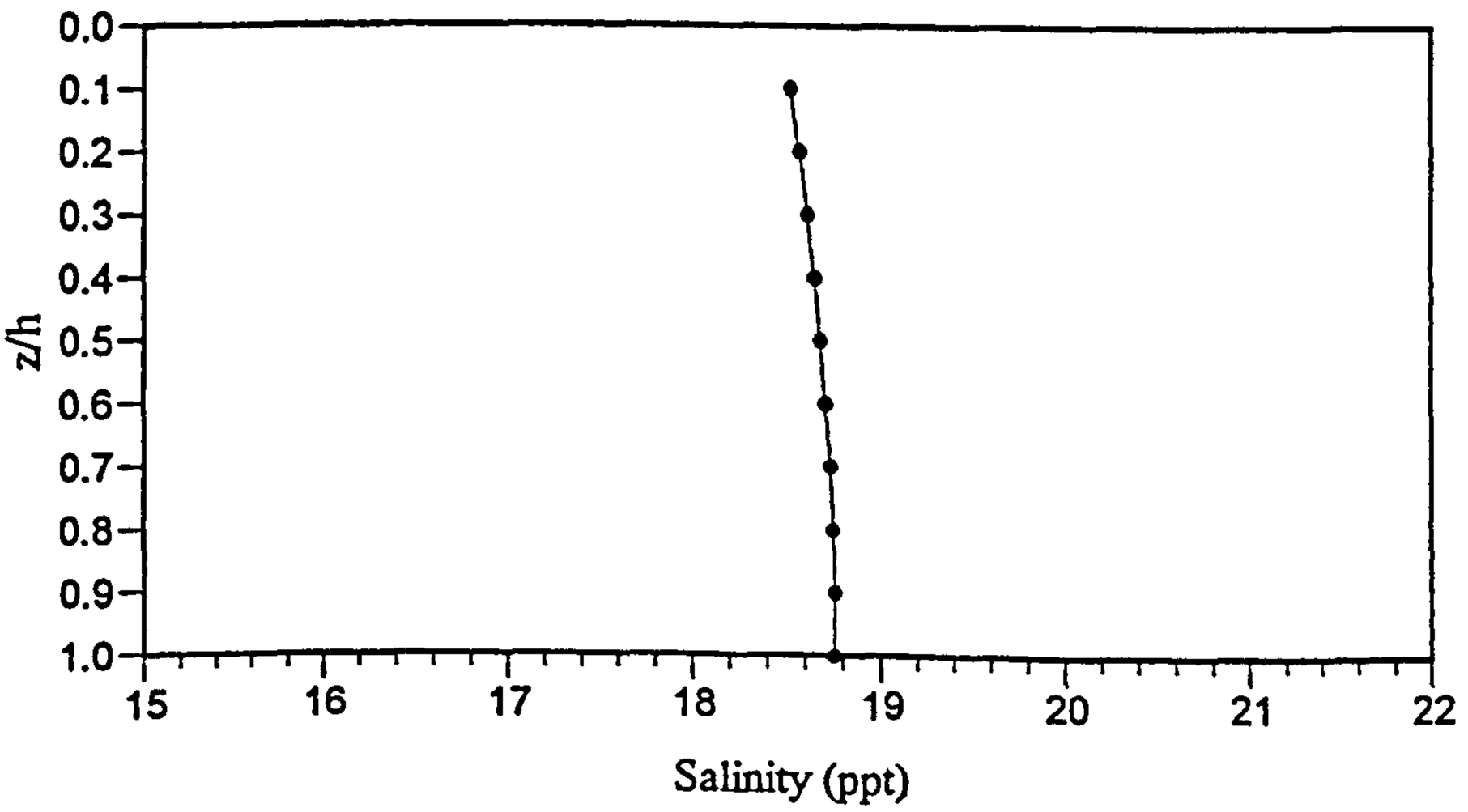

Figure 4.29 Mean salinity profile at St Clears, 12 July 1995.

This lateral salinity gradient was observed in the Taf during the early flood and late ebb in the measurements made in July 1995. During the ebb, the fresher water flowed out on the right hand side of the estuary with the more saline water on the left hand side, as would be expected. The lateral gradient during the flood however reversed from the expected gradient for a northern hemisphere estuary. The higher salinity water was encountered on the right hand side of the estuary with fresher water on the left hand side of the estuary. Vertically the water was well-mixed, but there was a 3 ‰ gradient across the estuary. This shows that factors other than the Coriolis effect are more dominant in controlling the horizontal salinity gradient in the Taf. In a small estuary of less than 400 m across (the width of the main channel), the Coriolis force may not be significant though according to Pethick (1984), it is possible see the effect of geostrophic forcing in shallow estuaries with a cross section about 0.5 km. In the Taf, it is the local bed topography which is more dominant in controlling the horizontal salinity gradient during the flood. As stated by Dyer (1977) and Bowden (1978), if there is variation in the depth across an estuary, the upstream flow tends to be concentrated in the deeper part, while in the shallower part the flow is seaward at all depths. In this case, the channel at the right hand side is more flood dominant than the channel at the left hand side due to the variation in the channel depth. Therefore the variation in bed topography is one of the major factors in controlling water circulation in the Taf.

The effect of fresh water discharge on the salinity intrusion is quite considerable. At low discharge and spring tides, the interface between fresh and salt water was located 15 km from the mouth; at high discharge and neap tide, the interface was just 7 km distance from the mouth. Between these extremes the estuary experiences large salinity variations where it changes from a well-mixed to a stratified type. The stratification is most developed when high river discharge coincides with neap tides. At low river discharge, the estuary is relatively well mixed even at neap tides. Under averaged flow conditions, the estuary is relatively well-mixed during spring tides and partially stratified during neap tides. Except for the winter months, the discharge is relatively low for most of the year. This makes the Taf a predominantly tide-dominated estuary whereby mixing processes destroy stratification.

Wave and wind-induced mixings were not measured in this study, but they undoubtly occur during stormy weather. Measurement made by Jago (1974) shows that during south-westerly storms, the flood tide surges into the estuary earlier than is usual, produces faster flood currents and delays the early stage of the ebb. This intensifies turbulent mixing particularly in the surface layers of the water column and maintains it during the extended slack water period. The effectiveness of the wind-induced flows in modifying the estuarine circulation however would depend upon its direction and the depth of the estuarine waters. In estuaries in general, an up-estuary wind direction frequently generates an upstream surface flow which more than compensates for the normal seaward movement, giving a net surface flow pattern (Bowden, 1980).

4.3.3 Fresh water discharge

The major fresh water input into the estuary is the river Taf itself. The river discharge data were obtained from the NRA (National River Authority) gauging station at Clog-y-fran for the period of January 1991- September 1995. For the period 1991-1994, the seasonal variation ranged from monthly average values of 15.6 m^3/s in January to 2.1 m^3/s in July. The daily average for the same period was 7.0m^3/s with the extreme values of 70 m^3/s and 0.82 m^3/s.

The seasonal variation of fresh water input during the study period is shown in Figure 4.30. The monthly averages for September and October 1994 i.e. the first data collection campaign, were 6.7 m^3/s and 7.1 m^3/s, respectively which were average condition for the river. During summer and autumn 1995, South Wales experienced an extremely long period of drought. The monthly average river discharges for July and September 1995 i.e. the second and third data collection campaigns, were 0.75 m^3/s and 0.52 m^3/s respectively. This is indeed very minimal in comparison to the tidal incursion of salt water of about 1800 m^3/s on average spring tides and and 620 m^3/s on average neaps. This huge difference in the river and tidal inputs has a great influence on estuarine hydrodynamics, as discussed in Section 4.4; it explains the general homogeneity of the estuarine water masses observed

during this study.

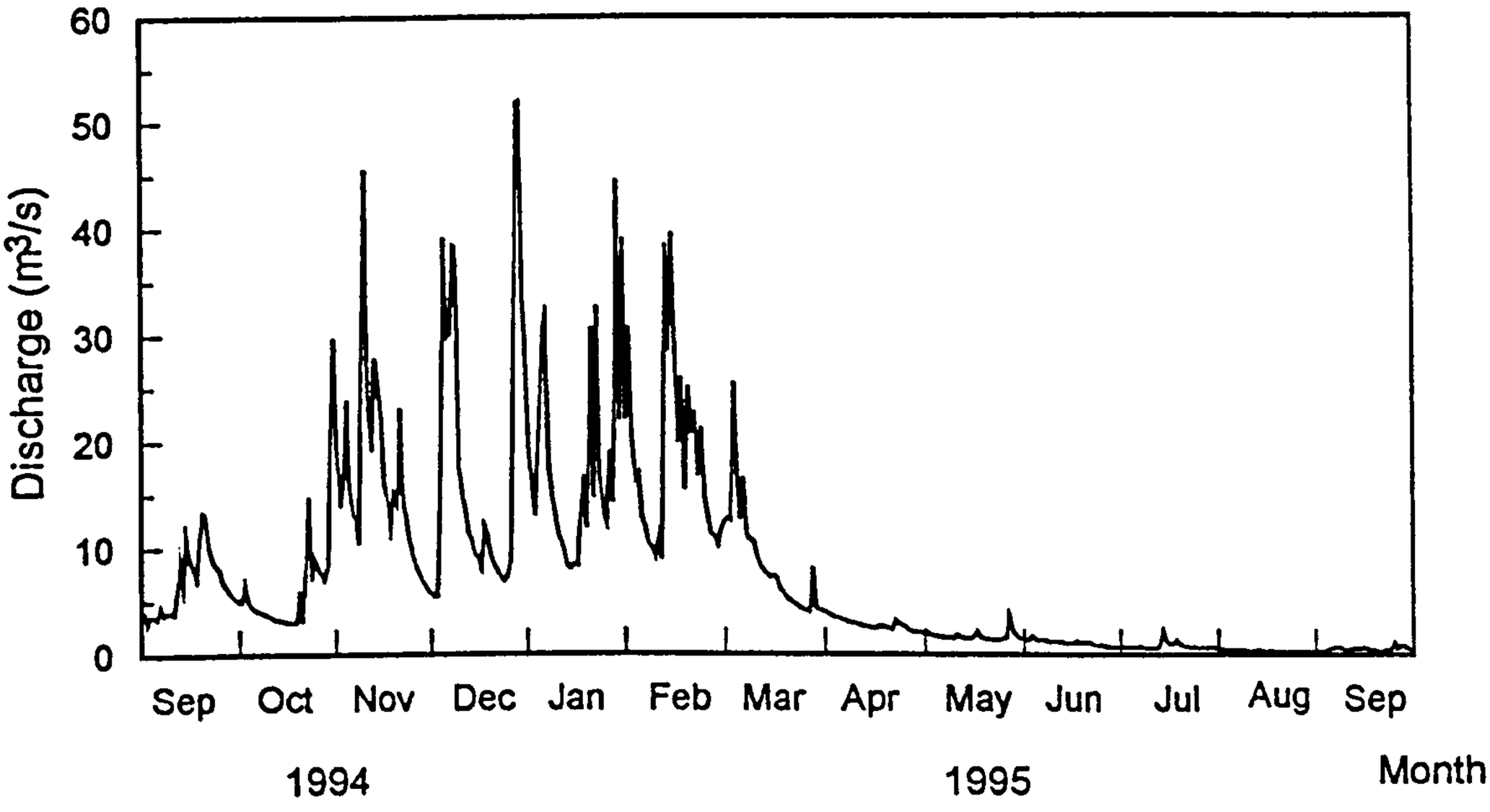

Figure 4.30 River discharge during the main study period as measured at Clog-y-fran.

4.3.4 Tidal prism and flow ratio

The tidal prism i.e. the volume of water entering the estuary from the sea during a flood tide has been calculated for the Taf estuary over spring-neap tidal cycles for the two survey transects; T9 and T5 (see Chapter 7 and Figure 3.1). Using these values, the flow ratio i.e. the ratio of the volume of upland water entering the estuary during a tidal cycle to its tidal prism have been calculated for all the measured tidal cycles. The results are presented in Tables 4.4 and 4.5 for transects T9 and T5, respectively. These flow ratios have been calculated using the river discharge data measured at Clog-Y-Fran for the respective measurement dates.

The tidal prism for estuary can be represented by Table 4.4 where measurements were made closer to the estuary mouth at transect T9. The table shows that the tidal prism varies from 0.67 x 10^7 m^3 during the neap tide to 1.86 x 10^7 m^3 during the spring tide.

Measurements made at transect T5 indicate that the tidal prism is an order of magnitude lower then at transect T9. As expected the tidal prism diminishes up-estuary.

Table 4.4 Tidal prism and flow ratio during neap-spring tidal cycle at transect T9.

Date	Tidal height above O.D. (m)	Tidal prism (m^3)	Flow ratio
5/10/94	5.36 (Spring)	1.74×10^7	0.0071
6/10/94	5.46 (Spring)	1.96×10^7	0.0061
14/7/95	5.13 (Spring)	1.90×10^7	0.0032
16/7/95	4.46	1.42×10^7	0.0017
18/7/95	3.75	1.07×10^7	0.0034
20/7/95	2.78 (Neap)	0.67×10^7	0.0035

Table 4.5 Tidal prism and flow ratio during neap-spring tidal cycle at transect T5.

Date	Tidal height above O.D. (m)	Tidal prism (m^3)	Flow ratio
12/9/95	4.96 (Spring)	0.52×10^7	0.0033
13/9/95	4.73	0.46×10^7	0.0033
14/9/95	4.35	0.41×10^7	0.0044
15/9/95	3.74	0.28×10^7	0.0066
19/9/95	2.66 (Neap)	0.13×10^7	0.0078

The mean value for a spring tidal prism calculated in this study is 1.86×10^7 m^3 . This figure is slightly higher than 1.4×10^7 m^3 from Jago (1980) and 1.7×10^7 m^3 from Philpott (1993) for an average spring tide. For a mean neap tide, Jago (1980) quotes a value of 0.4×10^7 m^3 against 0.69×10^7 m^3 calculated in this study. The differences rely on the method of calculation and accuracy of measurement made in each case. More detailed measurements

made during this study have allowed a more accurate estimate of sediment and water fluxes.

Flow ratios for the Taf have also been calculated using two extreme river discharge values i.e. 50 m^3/s for of maximum flow, and 1 m^3/s for minimum flow for the two survey transects (T9 and T5). In contrast to the tidal prism which decreasing up-estuary, the flow ratios increase further up the estuary. The flow ratio varies from between 0.001-0.08 during spring tides to 0.004 - 0.26 during neap tides in the lower estuary (transect T9). These ratios increase to between 0.004 - 0.29 during spring tides and 0.018 - 1.18 during neap tides in the middle estuary (transect T5). The up-estuary increase in flow ratio indicates the increasing importance of fresh water input in controlling the estuary circulation. During average river discharge, the flow ratio varies from 0.01 during spring tides to 0.03 during neap tides.

Flow ratios have been used by several workers to characterise the estuarine mixing type (eg. Schultz and Simmons, 1957; Bowden, 1980). If a flow ratio is about 1.0 or greater the estuary is more likely to be stratified; if the ratio is of the order of 0.25 the estuary is partially mixed; and when the ratio is appreciably less than 0.1 the estuary is a well-mixed type. The values in Tables 4.4 and 4.5 indicate that during the measurement period, the Taf estuary was relatively well-mixed during both springs and neaps. These very low flow ratios (0.002-0.008) were due to the very low river discharge rates experienced during the study period. However, during extreme river flow conditions, the estuary may change from well-mixed to partially-stratified as suggested by the calculated values of the flow ratios.

Another useful estuarine parameter is the mixing index, defined as the ratio between the volume of fresh water discharge into estuary during a half tidal cycle to the volume of the tidal prism (Schubel, 1971b). This may be used to classify estuaries according to Pritchard's (1955) categories. Under its average flow condition of 7.0 m^3/s, the calculated mixing index for the Taf is 0.005 for an average spring tide. This value places the Taf into Pritchard's Type D estuaries. These estuaries have very low mixing index (< 0.05) and very high width to depth ratios; the mixing energy is very high and the dominant mixing force is due to the tide. Even during neap tides when the tidal prism is small, the mixing index is

0.017 which also places the Taf into type D estuaries.

The mixing index obtained for the Taf may be compared to the values quoted for other Welsh estuaries. The mixing index for the Dwyryd was 0.009 during a spring tide (Mahamod, 1989), and for the Dovey estuary, Haynes and Dobson (1969) obtained a mixing index of 0.016 for an average spring tide. The value for the Dwyryd is greater than the Taf. Though the Dwyryd has a similar river discharge rate (8.7 m^3/s), its tidal range is smaller (3.5m) than the Taf (7.5m). The Dovey estuary has a higher discharge rate (of 22.5 m^3/s) which results in a higher mixing index than for the Taf and the Dwyryd.

4.3.5 Estuarine classification

A more quantitative way to classify an estuary is through the stratification-circulation diagram proposed by Hansen and Rattray (1966). Here, estuaries are characterised by two non-dimensional parameters:

i. A stratification parameter which is computed as the difference between the net bottom and surface salinity (S_b - S_s) relative to the depth-mean salinity (<S>), and
ii. A circulation parameter which is computed as the net surface velocity U_s, relative to the mean cross sectional velocity U_f, i.e. the rate of river discharge R divided by the cross sectional area A.

Based on these parameters, Hansen and Rattray have classified estuaries into 4 mixing types (Figure 4.31). Type 1 is a well-mixed estuary and has mean flow seawards at all depths, and upstream salt transfer is by diffusion alone. Type 2 is the partially-mixed estuary in which the mean flow reverses at depth, and upstream salt transfer is by both diffusion and advection. Type 3 is distinguished from type 2 by having the salt transfer primarily by advection. Type 4 is the salt-wedge estuary with a thick upper layer flowing out over a thin lower salt layer with little interaction. The suffixes a and b in types 1, 2 and 3

correspond, respectively, to the conditions of weak and strong stratification, each subdivided rather arbitrarily.

There are different approaches in obtaining the circulation parameter. In the calculation of the circulation parameter for the Taf, the depth-mean velocity (<U>) was used instead of U_f since the cross sectional area varies greatly during the tidal cycle. Kjerfve (1979), Mahamod (1989) and Larcombe (1992) all used <U> instead of U_f in contrast with Jago (1980), who used a weighted average cross-sectional area to compute the circulation parameter.

For this purpose the stratification and circulation parameters have been calculated using the salinity and velocity data measured at station 1 only except on 12 July 1995 where the measurement was made at St. Clears; and on 19 September 1995, the data for station 2 was used. The velocity measurement at Station 1 on 19 September 1995 was not made at the full water depth and there was inconsistency in the values within a single profile. Station 1 was the mooring station located in the main channel of the estuary where both salinity and velocity were measured simultaneously at 15 minute intervals over a full tidal cycle. Salinity and velocity data for other stations across the estuary (except where VGUs were installed) were less complete due to restricted boat accessibility particularly during the early flood and late ebb. The result are tabulated in Table 4. 4 and plotted in Figure 4.31. In the diagram, different symbols are used for different series of measurement.

The Hansen and Rattray diagram indicates that the lower (T9) and the middle (T5) parts of the estuary is well- to partially-mixed. At the upper part (St. Clears), the estuary is partially-mixed. The mixing is stronger near the mouth but gets weaker towards the head of the estuary. Similarly, stronger mixing was observed during the spring than during the neap. The data for July 1995 and September 1995 indicate the effect of tides on the types of circulation and show stronger stratification toward the neap. In October 1994, no measurement was made during the neap tide, but the results for the two tidal cycles also

Table 4.6 Hansen and Rattray classification of Taf Estuary

Date	Location	$S_b - S_s / \langle S \rangle$	$U_s / \langle U \rangle$	Classification
5/10/94	Station 1	0.021	1.62	well-mixed
6/10/94	Station 1	0.011	1.32	well-mixed
12/7/94	St.Clears	0.011	3.24	partially-mixed
14/7/95	Station 1	0.001	2.00	partially-mixed
16/7/95	Station 1	0.007	1.96	partially-mixed
18/7/95	Station 1	0.009	2.46	partially-mixed
20/7/95	Station 1	0.016	2.13	partially-mixed
13/9/95	Station 1	0.009	1.68	well-mixed
14/9/95	Station 1	0.011	2.37	partially-mixed
15/9/95	Station 1	0.023	3.96	partially-mixed
19/9/95	Station 2	0.059	3.65	partially-mixed

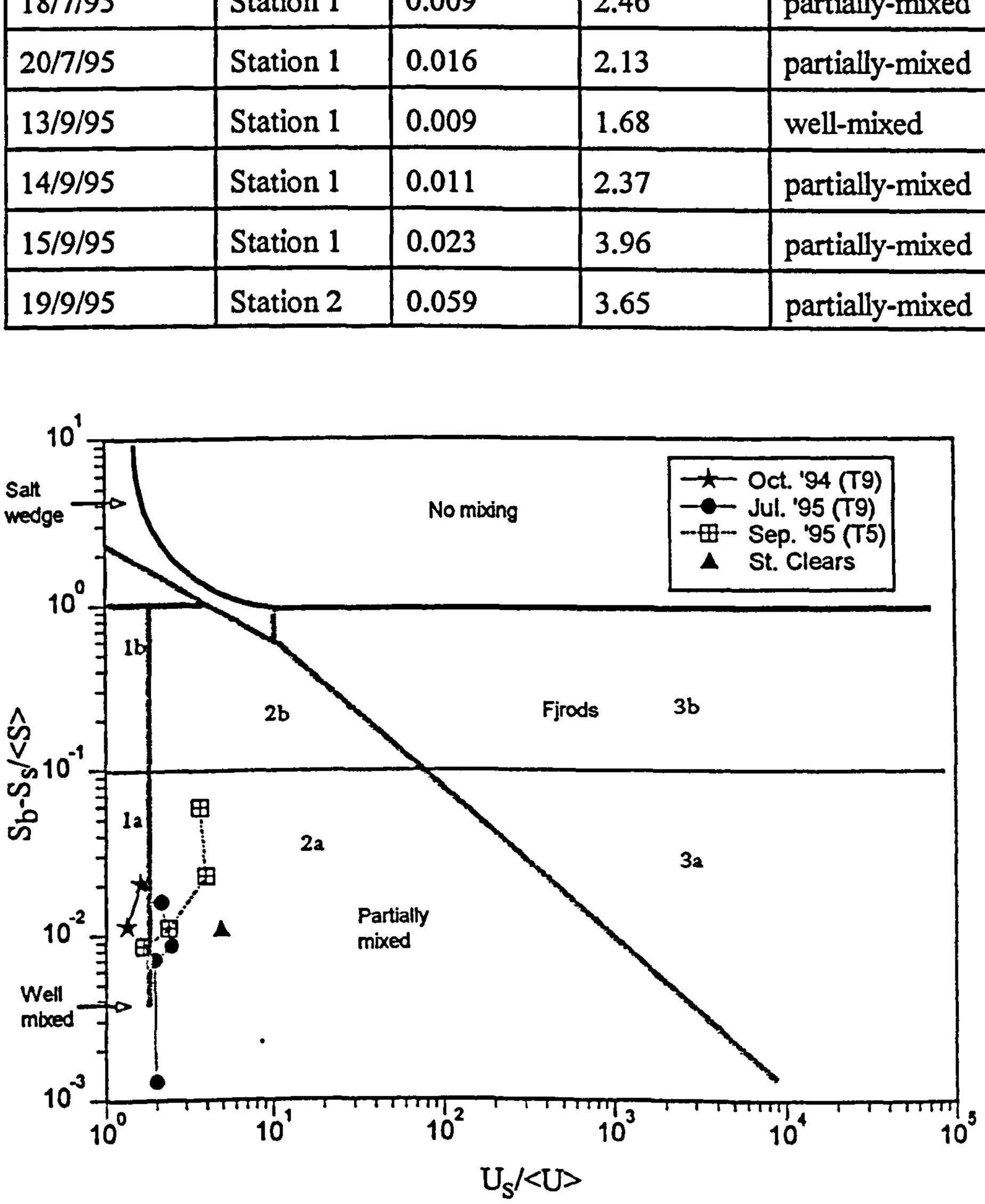

Figure 4.31 Classification of Taf estuary according to Hansen and Rattray (1966).

suggests an increasing stratification towards the neap. Within the limit of this study, river flow (which ranges from 0.5 m^3/s to 5.6 m^3/s) seems to have very little control on the estuarine circulation. A much higher rate of river discharge is required for it to have any significant effect on the estuarine circulation. This normally happens during river floods or during the winter months where the river input can increase tenfold. Jago (1980) observes that the estuary changes from well-mixed when river flow is low to stratified when river flow is high (>10.0 m^3/s) and coincides with neap tides.

The effect of bed geometry on the water circulation may be seen from the measurements made on 5 October 1994 and 14 July 1995. Despite having a much higher river discharge in October 1994, this was compensated for by a smaller main channel cross-section which increased the tidal flow velocities, hence the vertical mixing. In July 1995, the main channel became wider than in October 1994; this resulted in weaker flow velocities, but the low river discharge experienced in July 1995 resulted in a similar degree of mixing intensity.

The application of the Hansen and Rattray diagram to shallow and intertidal estuaries is limited. In these estuaries the tidal effect is a transient one, as for long periods of time the estuary bed is dry with only some channelised river flow remaining. This is in marked contrast to deeper estuaries where tidal effects are continuous. Thus comparison of the Taf estuary with these deep and big estuaries such as the James River, Columbia River, Mississippi River mouth and Mersey estuary on which the Hansen and Rattray classification was conceived and developed, is not truly applicable. Despite these limitations, the Hansen and Rattray diagram has been used to classify some Welsh estuaries where large areas of sand- and mudflats are exposed during low water, e.g. the Conwy (Jenkins, 1976), the Taf (Jago, 1980), the Dwyryd (Mahamod, 1989), and the Mawddach (Larcombe, 1992).

4.4 Conclusions

The study investigates the flow dynamics and the salinity stratifications across the estuary cross section as well as along the estuary axis. Factors affecting their variabilities are emphasised, and their effects on the transport of sediment are noted.

One characteristic of tidal intrusion into the estuary is the asymmetry of the tidal wave as illustrated by a faster rise and a slower fall of the water level. The tidal wave asymmetry is most pronounced during a spring tide but becomes less asymmetrical during neap tides. As a result of tidal wave asymmetry, the flood tide duration is shorter than the ebb on all tides and at all locations within the estuary. The degree of tidal wave deformation increases in the landward direction with the flood duration becoming shorter towards the head of the estuary; for example, during a spring tide the flood took about 3 hours at the mouth but just 2 hours 10 minutes in the upper reaches (at St. Clears). The tidal asymmetry in the Taf is caused by sedimentation which has elevated the estuarine topography relative to sea level. Due to this sedimentation, the water has to rise 2 m before it enters the estuary on a spring tide. The time of HW is progressively delayed up-estuary, indicating the tidal wave is of a standing nature with an increasing progressive nature up-estuary.

The tidal wave asymmetry produces greater flood velocities than the ebb velocities at most measured stations in this estuary, during both springs and neaps. The tidal velocities in the main channel during a spring tide reach a value of 2.7 m/s for the flood and 1.9 m/s for the ebb. The maximum flood currents consistently occurs immediately after the onset of the flood tide, while the maximum ebb current is reached before the expulsion of the tidal prism when flow is confined to the main channel. The current is strongest in the main channel but reduces further away from the channel and on the intertidal sand flats. Across the estuary, however, there exist ebb dominated channels where the ebb current is stronger than the flood current. The very fast flood current and the tidal wave deformation means that the tidal energy is concentrated within a short period of flood time, favouring a net landward sediment transport.

The tidal wave asymmetry is also reflected in the salinity curves where there is a steep rise in salinity values during the flood and a slower fall during the ebb. On a spring tide, the salinity maximum is reached within one hour of tidal incursion; salinity remains high (greater than 10‰) even 5 hours after high water, mainly due to the late drainage of saline water retained by the salt marsh. The salinity maximum occurs at high water and the minimum occurs just before the flood surge. High current speeds and high turbulent intensities during the flood produces an almost complete vertical mixing.

The Taf estuary exhibited variable mixing processes both temporally and spatially during the study period. It has been shown that the dynamics of the observed estuarine circulation are a result of a complex interaction between the tides, river flow and channel morphology. The very high tidal range i.e. 8.4 m during a spring tide produces fast currents that mix the water column and destroy the vertical salinity gradient during early flood and late ebb when the flow is confinement within the narrow main channel. At high water and on the early ebb, stable stratification develops due to reduction in turbulent mixing. Stronger stratification develops during smaller tides and also during an increased river flow. The vertical salinity gradient increases with increasing river flow and decreasing tidal range.

The estuary shows a strong lateral salinity gradient particularly during neap tides, even though vertically the water column shows almost complete mixing. The lateral gradient is controlled by the local channel morphology rather than the geostrophic force. However during inflated river flow, the geostrophic effect may be important as evidence from the existence of foam-lines separating different water masses at the mid stage of the flood tide in the lower estuary. Off Laugharne, the river bend causes strong horizontal eddying and bed friction. Just upstream of this bend, a strong lateral salinity gradient exists as the saline intrusion is maintained in the main channel while fresher water occurs in shallower parts of the estuary channel.

The landwards penetration of saline waters varies with tidal range and the magnitude of river discharge. The salt water intrusion reaches at least 3 km further inland on springs than on neaps, and a further 4 km shift occurs between high and low river discharges. The combined

effect of the two factors means that the estuary experiences a large salinity variation over lunar cycles and changes in the fresh water input. The fortnightly spring-neap tidal cycle modifies the flow ratio and thus the intensity of the mixing in the estuary. The very low flow ratios as determined in this study placed the Taf as a well-mixed estuary during both springs and neaps. From the mixing index value, the Taf falls into Type D category according to Pritchard's categories. Using the classification of Hansen and Rattray (1966), the estuary is well-mixed during spring tides but changes to partially-mixed during neap tides. Mixing is stronger in the lower reaches and weaker in the upper reaches. Similarly, stronger stratification occurs when neap tides coincide with high river discharge. The river discharge however is low for much of the year, making the Taf a tide dominated estuary where the upstream salt transport is by diffusive processes. The Taf shows a comparable hydrodynamics and morphologic characteristics to those of well studied Welsh estuaries which are on the stage of infilling.

The estuarine water temperature depends on the degree of mixing between a warmer sea water and a cooler fresh water (in summer) which results in the general decrease of temperature towards the head. However for a tidal estuary like the Taf, this is not always the case. The time of flooding as well as the sun's insolation also have some effect on the estuary water temperature. On warm sunny days the heating up of the exposed inter-tidal mudflats and sandflats during low water period, can elevate the water temperature to a few degrees as the water floods the intertidal sand flats. During early morning the flooding water can lose heat through conduction to the cooler inter-tidal flats or cooler air, or by radiation from water to air. Both situations have been observed to occur in the Taf.

CHAPTER FIVE

BOUNDARY LAYER STRUCTURES

5.1 Introduction

A fundamental control of sediment transport is the nature of flow in the boundary layer. The shear stress that is generated to move sediment is determined by factors such as flow strength, bed sediment size, and bedform geometry. Interaction of flow strength and bed roughness determines the nature of the boundary layer and the magnitude of bed stress.

This chapter details the structure of the tidal currents described in Chapter 4. The analysis of the boundary layer has been mainly based on velocity profile measurements made by the Velocity Gradient Unit (VGU) in the lower Taf estuary. This array of current meters provided detailed data on the velocity profiles of the tidal flow within a two-metre above bed region of the bottom boundary layer. Spring and neaps tidal currents were compared, and the relationships between roughness length, shear velocity and drag coefficient with the spring-neap currents were evaluated. A principal focus of this analysis is the examination of density stratification which effects the velocity profiles and the associated shear velocity and roughness length values.

The velocity measured near the sea-bed can be represented by the von Karman-Prandtl logarithmic profile equation

$$u = \frac{u_*}{\kappa} \ln\left(\frac{z}{z_0}\right) \qquad [5.1]$$

where u is the mean flow velocity at height z above the bed, κ is the von Karman constant

equals to 0.4, u_* is the shear velocity and z_0 is the roughness length. The equation is valid for steady, unstratified flows, and if z is much greater than z_0, which is often the case for the velocity measurement made in field conditions.

Given logarithmic velocity profiles of the form described by the Karman-Prandtl equation for the bottom 2 meters of the boundary layer (Equation 5.1), shear velocity (u_*) and roughness length (z_0) have been calculated for each profile that has two or more data points. The correlation coefficient (R^2) for the same profile has been calculated using linear regression of log z and u. A fortran program, VGU.FOR (Appendix B) has been used to calculate R^2 , u_* and z_0 for each profile from the VGU records. The number of data points available for the regression analysis and for the calculations u_* and z_0 were less at the beginning of the flood and at the end of the ebb when water levels were low and only the bottom current meters submerged in the water. The velocity at 100 cm above the bed (u_{100}), has also been calculated for each velocity profile using a cubic spline interpolation method.

5.2 Measurements

5.2.1 Current velocity profiles

Tidal currents obtained by the VGU at Station 2, transect T9 from the measurements made in July 1995 were selected for detailed observations of the boundary layer structure. This data set was selected for a number of reasons; (1) it covers a long period over a lunar tidal cycle, between 11-20 July 1995; (2) the data were most complete i.e. the current meter readings were less affected by fouling of the current meters by seaweeds and sand grains; (3) the measurement was made within the main channel (see Figure 3.2), thus would constitute of full ranges of flow strength for a full tidal cycle, providing a more representative picture of the boundary layer structure.

A total of 809 velocity profiles, measured over 17 tidal cycles have been examined. Almost all the profiles were logarithmic as shown by high values (>0.8) of the correlation coefficient,

R^2 . Using this criterion, the data for the 17 tidal cycles showed that 95 % of the velocity profiles conformed to the logarithmic law. For individual tidal cycles however, logarithmic profiles occurred between 90 - 100 % of the time. Typical variations of R^2 over a spring and a neap tidal cycles are shown in Figure 5.1. The figures show that except around high water, excellent correlations with R^2 values > 0.94 were obtained for all the measured profiles. The high R^2 values are not necessarily indicative of logarithmic profiles. Using logarithmic and linear scales, velocity profiles over flood and ebb tidal periods for a spring tidal cycle are plotted in Figures 5.2 and 5.3 for comparison. As revealed by their corresponding R^2 values, the flood velocity profiles can equally be explained by adapting the linear model (Table 5.1), but all the ebb velocity profiles follow the logarithmic law (Table 5.2).

Table 5.1 Calculated values of regression coefficient of the velocity profiles shown in Figure 5.2 (flood tide) using linear fit and logarithmic fit.

Time during flood (hour)	Regression coefficient (R^2)	
	Linear fit	Logarithmic fit
16:42	0.982	0.929
16:52	0.973	0.973
17:02	0.982	0.968
17:12	0.874	0.976
17:22	0.987	0.951
17:32	0.941	0.982
17:42	0.948	0.980
17:52	0.975	0.967
18:02	0.940	0.975
18:12	0.938	0.973
18:22	0.960	0.954
18:32	0.970	0.970
18:42	0.987	0.954
18:52	0.811	0.968
19:02	0.904	0.988
19:12	0.920	0.988
19:22	0.886	0.977
19:32	0.946	0.958
19:42	0.793	0.893
19:52	0.934	0.958

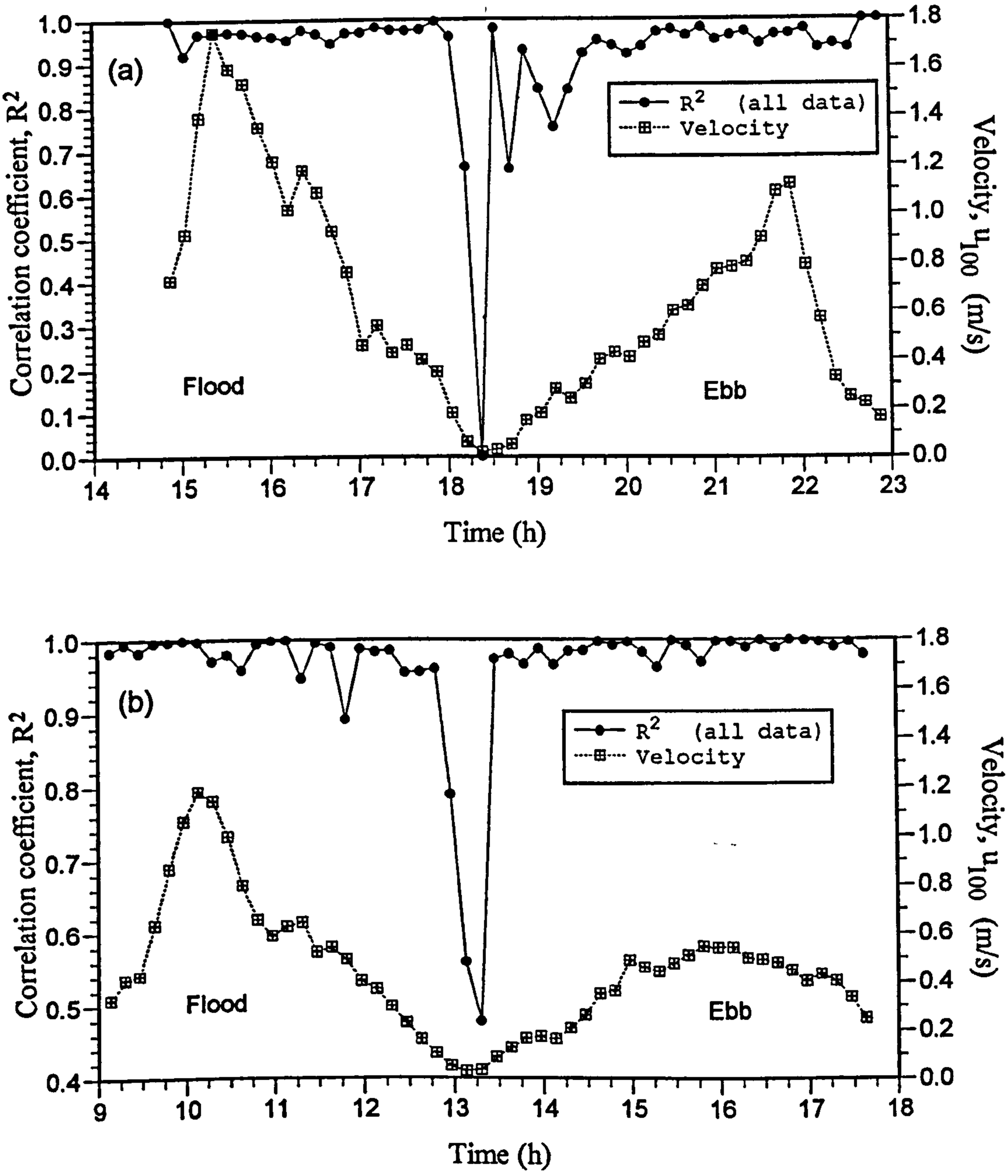

Figure 5.1 Typical variations of correlation coefficient, R^2 and velocity at 100 cm above the bed, u_{100}, (a) spring tide, and (b) neap tide.

Table 5.2 Calculated values of regression coefficient of the velocity profiles shown in Figure 5.3 (ebb tide) using linear fit and logarithmic fit.

Time during flood (hour)	Regression coefficient (R^2)	
	Linear fit	Logarithmic fit
20:22	0.940	0.902
20:32	0.961	0.993
20:42	0.872	0.991
20:52	0.968	0.985
21:02	0.875	0.989
21:12	0.882	0.990
21:22	0.915	0.999
21:32	0.769	0.948
21:42	0.936	0.999
21:52	0.832	0.977
22:02	0.909	0.994
22:12	0.868	0.987
22:22	0.885	0.993
22:32	0.891	0.995
22:42	0.860	0.986
22:52	0.877	0.993
23:02	0.788	0.958
23:12	0.795	0.962
23:22	0.933	0.995
23:32	0.920	0.991
23:42	0.898	0.982
23:52	0.778	0.912
0:02	0.787	0.916
0:12	0.986	1.000
0:22	0.980	0.999

The velocity profiles, averaged over 1 minute, show that vertical variation extends up to 2 m at least (Figures 5.2a and 5.3a), and in all probability it extends right up to the water surface. This shows that the tidal boundary layer is depth-limited here throughout the tidal cycle, so that its thickness is equal to the water depth. Despite having a high R^2 value, some of the velocity profiles measured over a spring tidal cycle show slight deviations from straight log lines; these profiles are curved either upward or downward (Figures 5.2a and 5.3a). For the

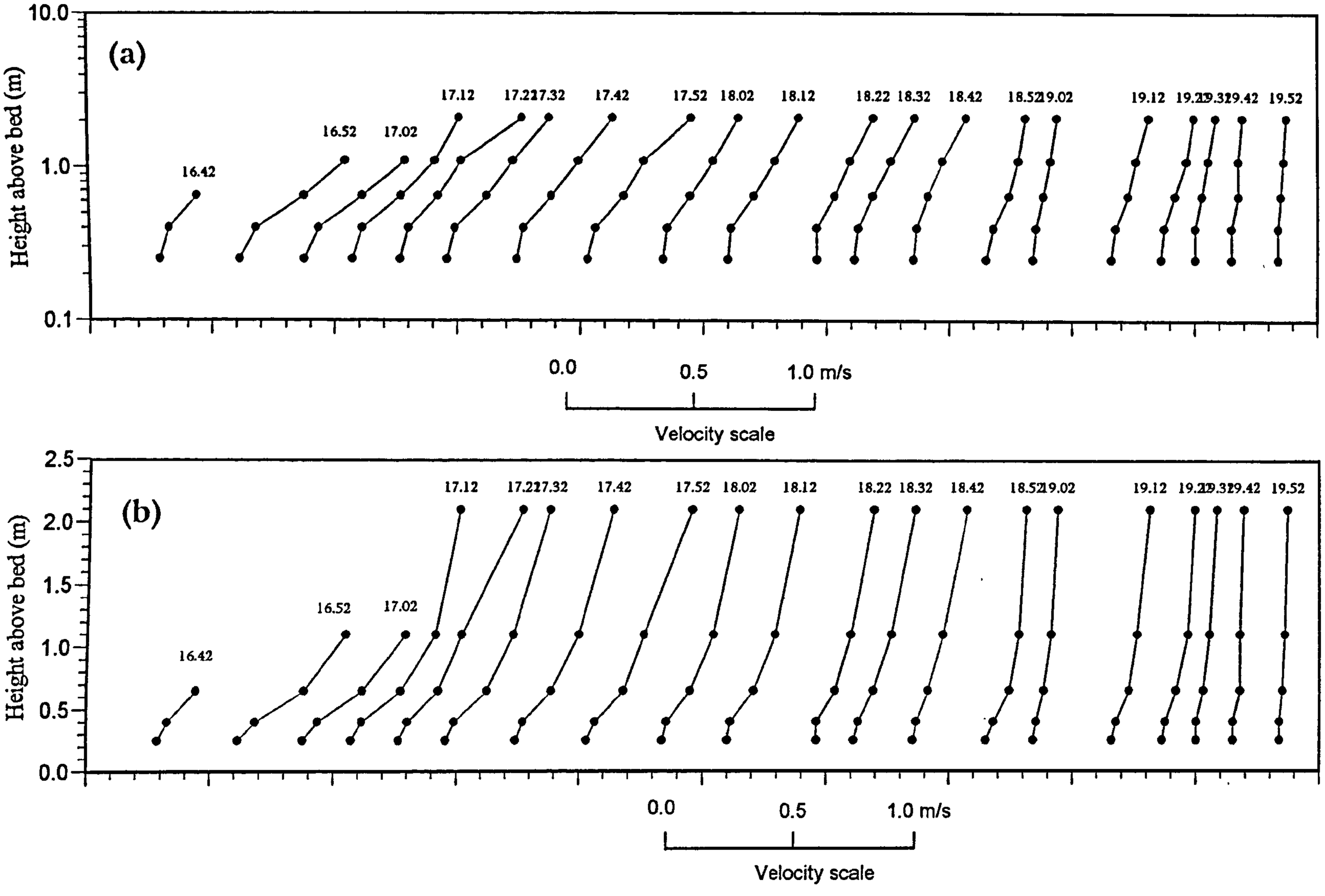

Figure 5.2 Velocity profiles for a spring tidal cycle obtained from the VGU record during flood tide:(a) log scale, and (b) linear scale. The label on top of each profile indicates the time of measurement.

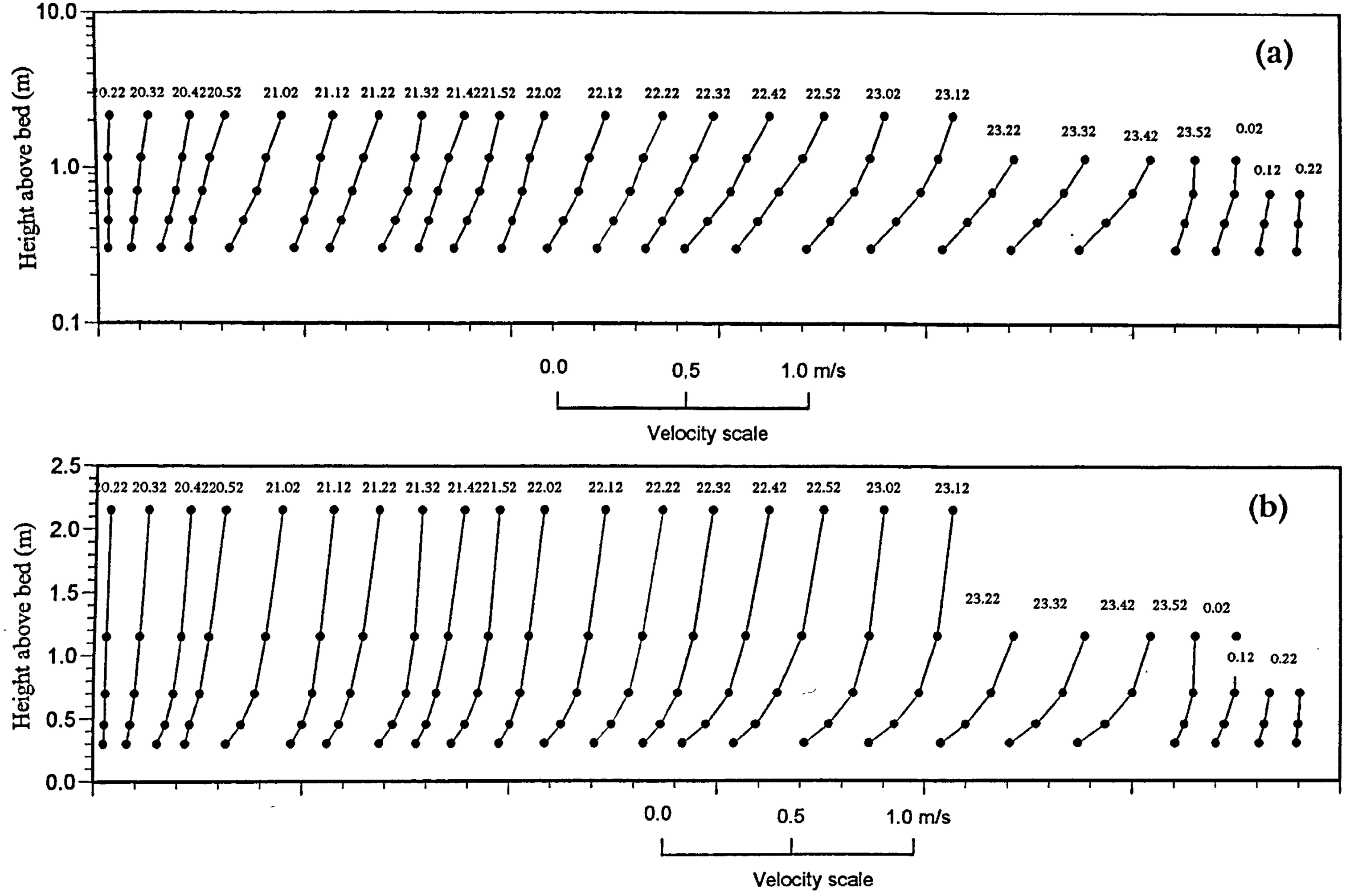

Figure 5.3 Velocity profiles for a spring tidal cycle obtained from the VGU record during ebb tide:(a) log scale, and (b) linear scale. The label on top of each profile indicates the time of measurement.

flood, the deviations from the logarithmic profiles occur at the top and at the bottom of the profiles (Figure 5.2a), while for the ebb the deviation occurs only at the top of the profiles (Figure 5.3a). The upward curvatures of the log-profiles are seen during the early stage of the flood and at the end of the ebb where there are large increases in current velocities within a short period (i.e. currents were accelerating). Unexpectedly during the flood, the profiles are convex downward at the bottom which are most noticeable during the early and middle parts the flooding stage when the currents are very strong (u_{100} > 0.75 m/s); the downward curvature diminishes approaching high water. During the diminishing currents towards high water and accelerating currents in the early part of the ebb, the velocity profiles indicate 'steady' flows for much of the time.

For the neap tidal cycle, the flood and the ebb velocity profiles show some degree of upward curvature at the top around the maximum flow velocity on the accelerating currents (Figure 5.4). However, during the accelerating currents in the early flood, velocity profiles do not show the downwards curvature at the bottom of the profiles (Figure 5.4a) as seen for the spring tide. Either sides of high water, the velocity profiles indicate 'steady' flows, as observed in spring tides.

The break of the slope for the upward curvatures of the spring and the neap velocity profiles generally occur at a depth greater than about 1.0 m above the bed. Due to these curvatures, the flood logarithmic profiles are better expressed by the middle three current meters, while the ebb logarithmic profiles are better expressed by the bottom four current meters. Therefore only these current meters should be used for any sediment transport calculation.

The velocity profiles for the whole water column can be studied from current measurements made in the main channel. These measurements were made from a moored boat using a single current meter profiling through the total water depth. An example of these velocity profiles are plotted in Figures 5.5 and 5.6 using linear and log scales respectively. Most profiles during the flood tide deviate from the logarithmic model; however, most of the profiles during the ebb tide are more or less logarithmic. The deviation from the straight log line in particular for flood stage profiles is most noticeable near the surface where the profiles curve upward.

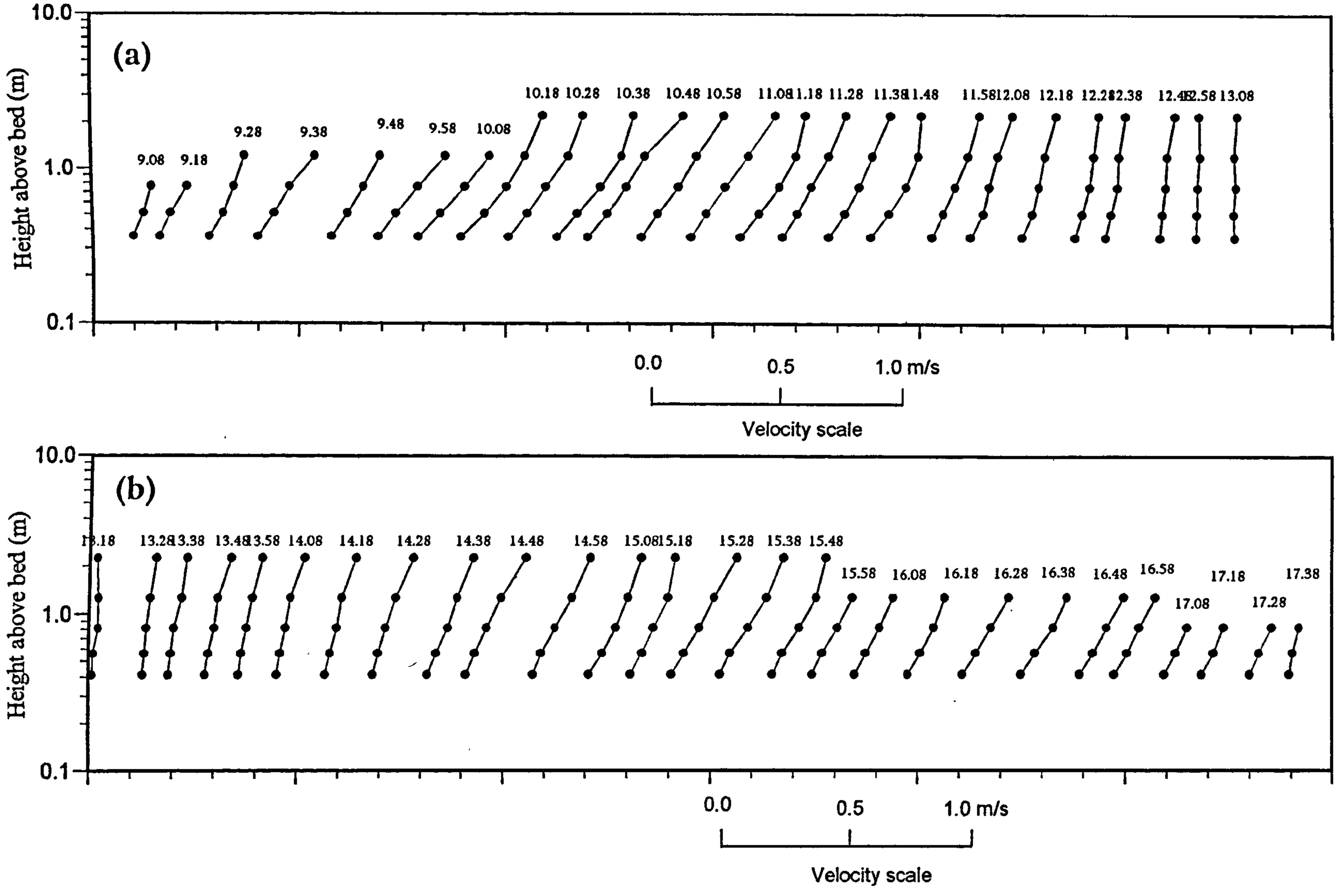

Figure 5A Velocity profiles for a neap tidal cycle obtained from the VGU record : (a) flood stage, and (b) ebb stage. The label on top of each profile indicates the time of measurement.

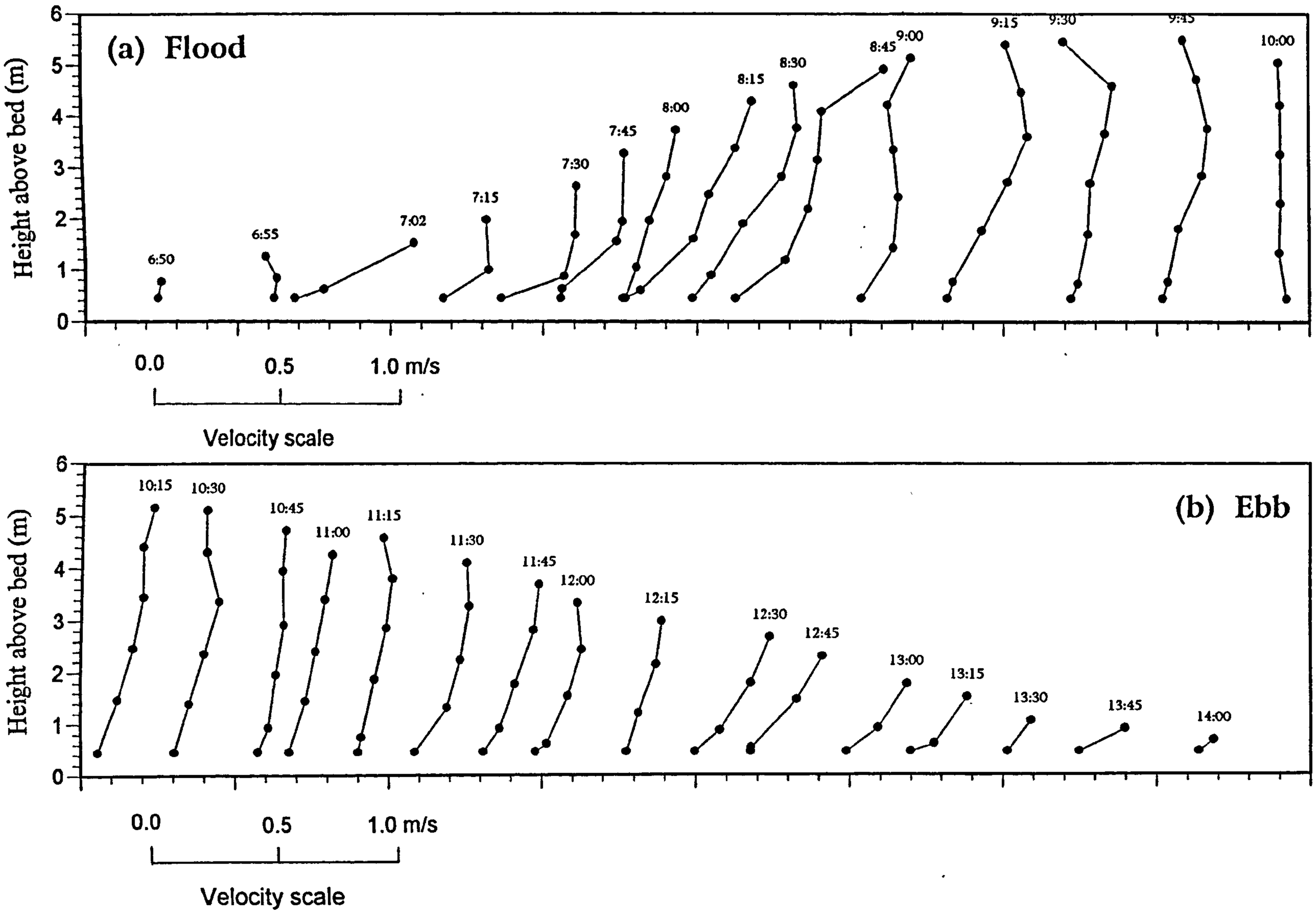

Figure 5.5 Velocity profiles for the whole water column plotted using linear scale: (a) flood stage, and (b) ebb stage. The profiles are for 16 July 1995. The label on top of each profile indicates the time of measurement.

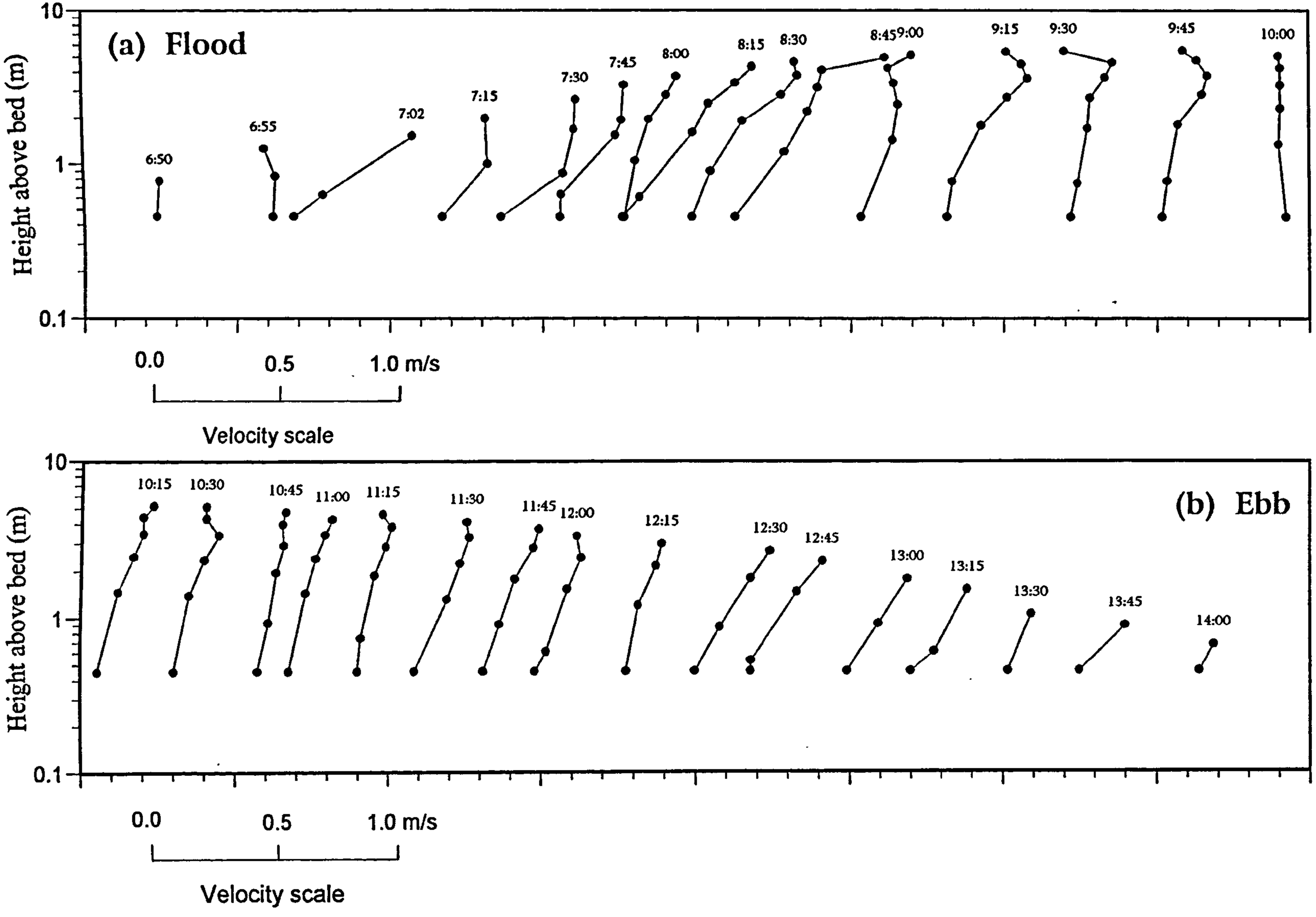

Figure 5.6 Velocity profiles for the whole water column plotted using log scale: (a) flood stage, and (b) ebb stage. The profiles are for 16 July 1995. The label on top of each profile indicates the time of measurement.

The change in slope generally occurs at water depth less than 2 m. Thus, for these profiles, only the bottom two (or three) measurements in depths less than 2 m conform to the logarithmic model, and should be used for any calculation related to the sediment transport.

5.3 Discussion

5.3.1 Current velocity profiles

Most of the velocity profiles of the study area can be adequately explained by the logarithmic law conforming to the form described by the Karman-Prandtl equation. Correlation coefficients greater than 0.9 were maintained throughout the tidal cycles, except around high water. Lack of correlation during high water is most probably due to the unsteadiness of the flow as the current reverses. At this period, the ebb flows begin at the upper layers of the water column as the flood current diminishes near the bottom. It is also partly caused by the poorer resolution of the current meter readings for a flow velocity below 0.03 m/s (see Chapter 3).

Mahamod (1989) argued that high values of the correlation coefficient may also be obtained by assuming a linear model and are not necessarily an indication of logarithmic profiles. Our measurements showed that this is only true during high current velocities in the early flood stage when the readings of the bottom current meter is higher than the expected value. When this occurred, a better logarithmic fit could be obtained by disregarding the reading of the bottom-most current meter.

Local scouring around the base of the VGU mast was observed for this data set , therefore there was a chance of assigning incorrect height of each current meter above the bed as an accurate height of each flood current meter above the mean level of the bed was difficult to determine. The error is relatively large for the lowermost rotor, becoming progressively less for the higher rotors. However, the scouring has been shown to have very little effect on altering the shape of the flood velocity profiles; this feature was not repeated during the ebb, and it also did not occur for a neap tide. Even by adding and reducing the depth of each

current meter by 5 and 10 cm, the shape of the velocity profiles was maintained, indicating the profile shape is not due to the incorrect rotor depths above the datum. The other explanation for the downward curvature of the early flood velocity profiles observed for a spring tide is caused by the density stratification. The present of high sediment concentration near the bottom only affects the reading of the bottom most flood current meter. As explained by Coleman (1981), McCutcheon (1981), and Villaret and Trowbridge(1991), a sediment-laden flow typically has a mean velocity profile with a larger gradient than the corresponding profile in a flow of clear water. Experiments made by Vanoni and Nomicos (1959) show that for flows of the same depth and surface slope, the flow with suspended solids has a higher mean velocity than clear water flows, and this implies a lower friction factor, or a drag reduction. The shape of velocity profiles such found in this study and caused by sediment stratification has been modelled by McLean (1991a) who shows that the stratification affecting the profiles by decreasing the stress and reducing the sediment in suspension. This will finally will reduce the integrated product of the mean velocity and concentration to nearly 40 %.

Examinations made on velocity profiles from another VGU (not affected by scouring), located on the intertidal sand flats show a similar feature (Figure 5.7), which also affecting the flood bottom most current meter only, thus supports this explanation. However, experimental data by Coleman (1981) shows that very close to the bed (less than a few centimetres), suspended sediment dampen the turbulence resulting in reduction in flow velocities. Because of density stratification, turbulence is damped, thus limiting the ability of the flow to transport both mass and momentum vertically. This results in a reduction of the drag coefficient and a lessening of the ability of the flow to keep sediment in suspension (McLean, 1991b). This effect is especially important for fine sands such as found in the Taf as more material can be carried into suspension compared to larger sizes material; for smaller sizes the wash-load tendency reduces the concentration gradient. In the Taf, very strong spring tidal currents resuspend the fine sand from the bed in early flood, creating a stable stratification close to the bed. The stratification stays stable for some times, resulting in the apparent increase in the flow velocity in the sediment-laden layer near the bed. Away from the bed, the sediment concentration is much reduced and the velocity profile resemble those of a clear water profiles (lower velocity gradient). During the neap, very little sands are

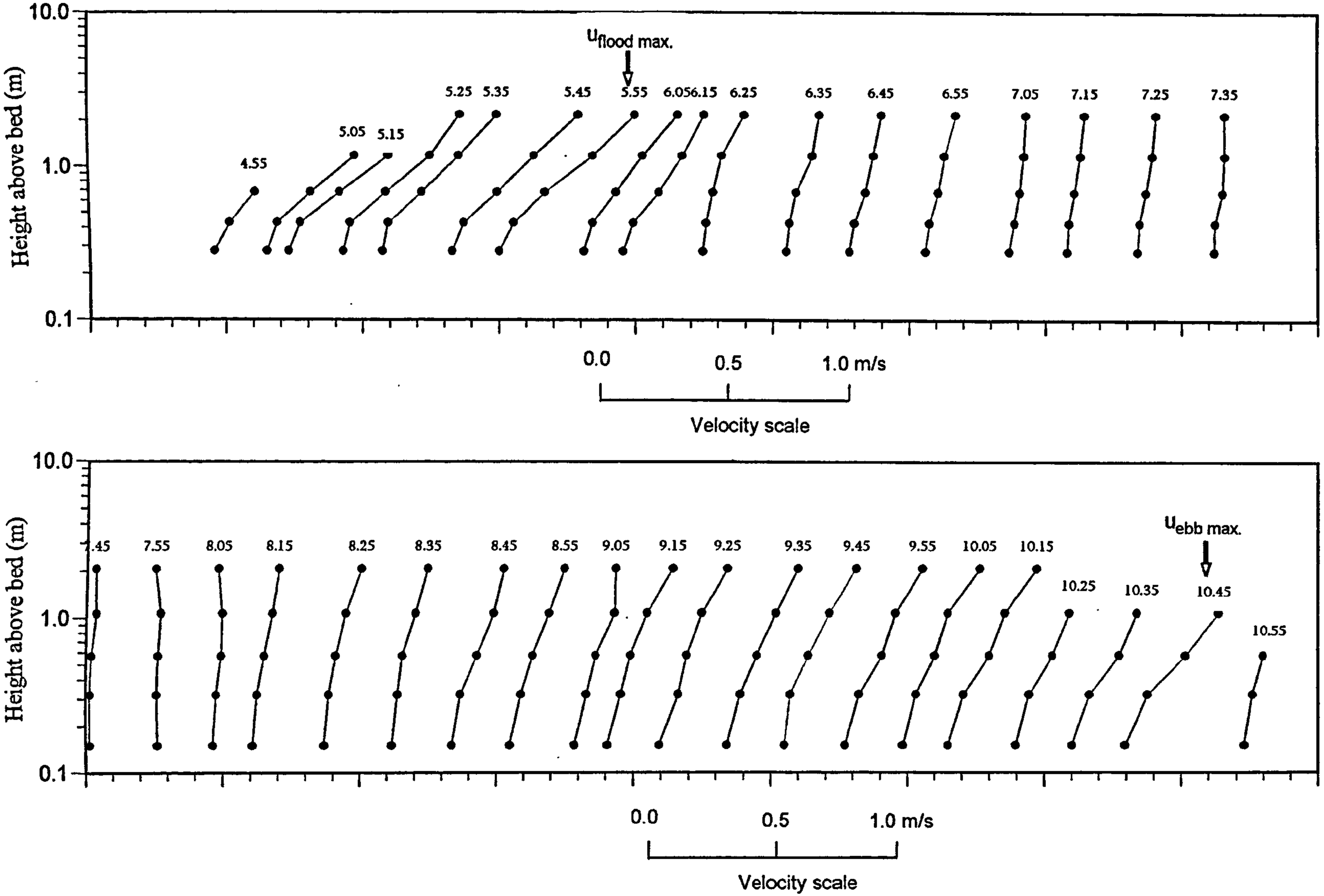

Figure 5.7 Velocity profiles for a spring tidal cycle obtained from the VGU not affected by scouring : (a) flood stage, and (b) ebb stage. The label on top of each profile indicates the time of measurement.

resuspended by the much weaker currents and no density stratification develops. Sediment stratification will have a stronger effect during the spring tide than during the neap as the transport rate is proportional to the cube of the flow velocity (eg. Bagnold, 1963; Heathershaw, 1981; Hardisty, 1983), therefore a lot more sand would be in suspension during springs than during neaps. In the Taf, the flow at the beginning of the flood does not start from zero velocity as in non-intertidal estuaries. During a spring tide, the current is already flowing fast and the water column is heavily laden with suspended sand grains as the tide pours in, and this continues during the first hour of the flood. Due to this density stratification, it is justified to ignore the bottom current meter for calculation of u_* and z_0 from the flood velocity profiles.

The upward curvatures at the top of the velocity profiles are observed during accelerating current flow, in particular during a spring tidal cycle. However, the downward curvatures during the decelerating current flow are less noticeable due to the gradual decrease in the flow velocity. The profiles are concave upwards with an accelerating current because away from the boundary, flow will retain a `memory' of preceding driving forces longer than at the bed (Dyer, 1986). Conversely, the profiles are concave downwards with a decelerating current.

Deviations from the logarithmic model are observed in the profiles taken for the whole water column with a single current meter. The profiles exhibit straight log lines at the bottom and curve upward at the top . This is probably due to the time lapse between the measurement points of each profile. Salinity measurement indicated that the water column was well-mixed both during the spring and the neap (see Chapter 4); thus salinity stratification will have little effect on the velocity profiles.

From the results presented it can be concluded that both flood and ebb profiles are generally logarithmic. An excellent fit of the model was obtained during the ebb tides but a slightly poorer fit during the flood tides. This is in contrast to the finding by Carling (1978) who studied the velocity profiles in the Burry Inlet and found the model fitted the flood profiles better than the ebb profiles. In the Taf, the better logarithmic fit during ebb tides is because

the flows are more steady during a longer ebb period than during a shorter flood period. It is also due to ebb velocity profiles are less affected by the density stratification.

5.3.2 Calculation of roughness length and shear velocity

It has been discussed in the preceding section that the density stratification of the water column by sediment modifies the velocity profile from its usual logarithmic form. This vertical density gradient effects the flow dynamics and the subsequent values of roughness length, z_0 and shear velocity, u_* calculated from these profiles. The velocity profiles are also modified by the accelerating and decelerating flows, particularly on a spring tide when the maximum flood and ebb velocities are at their highest. Due to these modifications, the readings of the bottom and top rotors of flood current meters, and the reading of the top rotor of the ebb current meters have been excluded and the R^2, z_0 and u_* have been recalculated for the velocity profiles measured by the VGU using the VGU.FOR fortran program.

The regression analysis using only three middle rotors for the flood and the bottom four rotors for the ebb have generally improved the correlation coefficient. This improvement is most noticeable for the spring tide on the flood, but less obvious for the neap tide (Figure 5.8).

5.3.3 Roughness length

The mean z_0 for the tidal cycles varies from 0.17 to 3.78 cm for the flood and from 0.48 to 5.39 cm for the ebb (Table 5.3). The mean z_0 for the flood is always lower than the mean for the ebb. The values of z_0 are lowest at spring tides with a general increase towards neaps. The individual values of z_0 calculated for each velocity profile over a tidal cycle however, vary considerably. Figures 5.9 and 5.10 show the variation of z_0 over time during a spring and a neap tidal cycle, respectively. There are two orders of magnitude difference between the minimum and maximum z_0 over a tidal cycle. As observed in both figures, the minimum flood z_0 is an order of magnitude lower than the minimum ebb z_0.

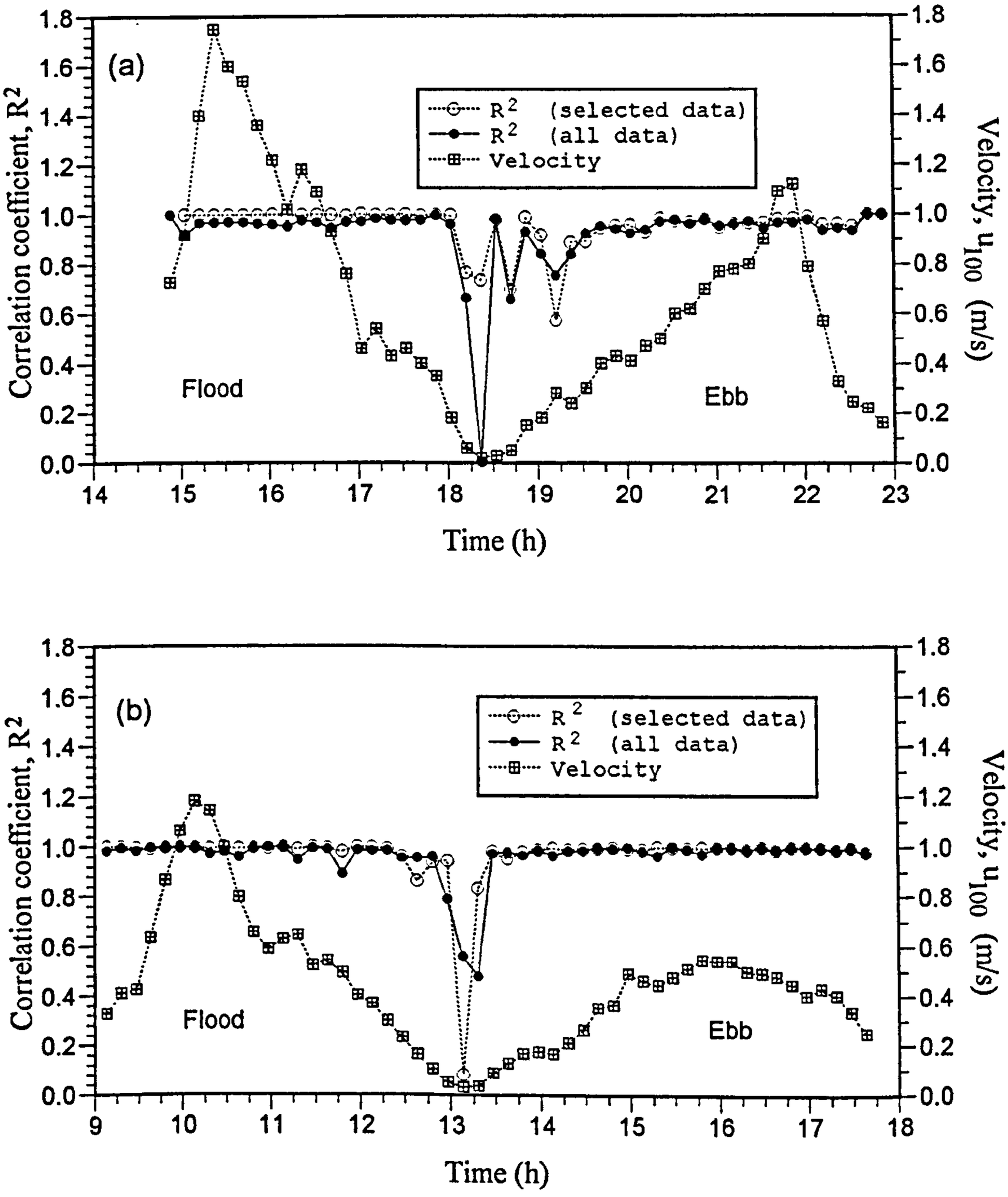

Figure 5.8 Corelation coefficient, R^2 using all data and selected data only, (a) spring tide, and (b) neap tide, (see text for explaination).

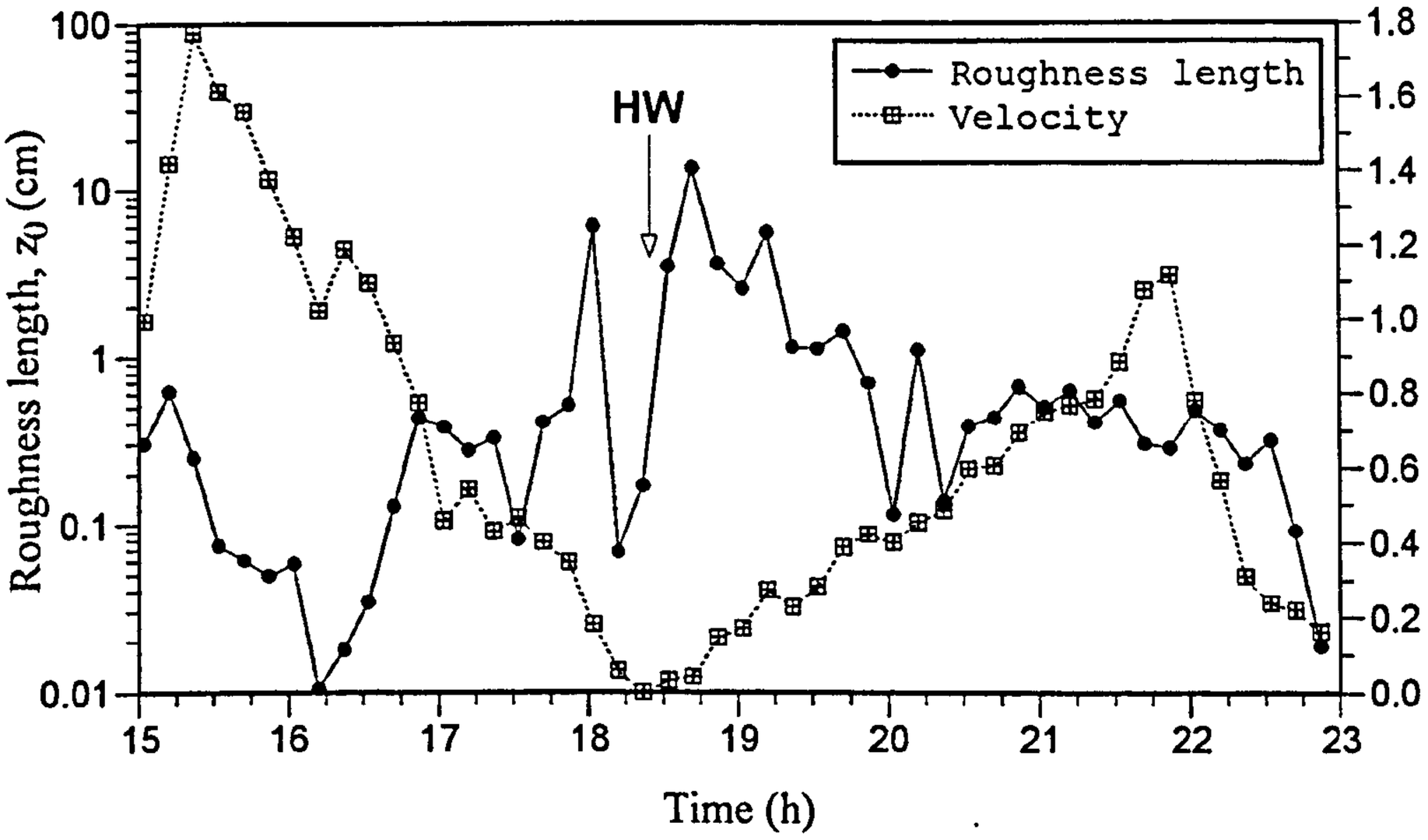

Figure 5.9 Variation of roughness length, z_0 over a spring tidal cycle. The arrow shows the time of high water.

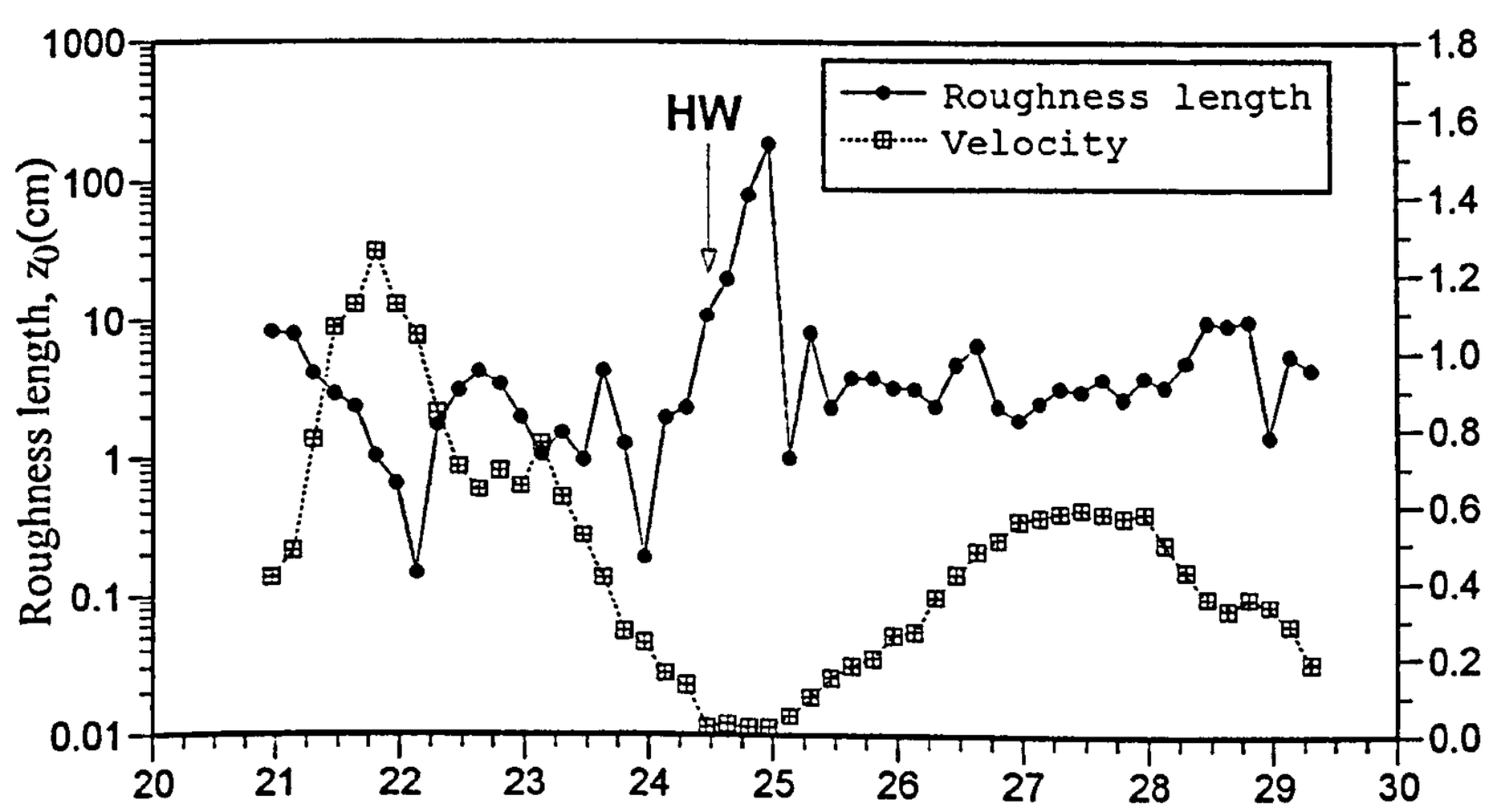

Figure 5.10 Variation of roughness length, z_0 over a neap tidal cycle. The arrow shows the time of high water.

Table 5.3 Mean flood, ebb and the tide roughness lengths, z_0 for 17 tidal cycles.

Tidal cycle	Averaged z_0 (cm)		
	Flood	Ebb	Tide
1	0.22	0.73	0.48
2	0.56	1.24	0.90
3	0.59	1.10	0.85
4	0.66	1.18	0.92
(Spring) 5	0.58	1.81	1.20
6	1.67	1.92	1.80
7	0.50	1.88	1.19
8	0.17	3.33	1.75
9	0.56	2.23	1.40
10	1.02	2.31	1.67
11	0.91	1.04	0.98
12	0.61	2.25	1.43
13	1.00	2.02	1.51
14	2.82	4.29	3.56
15	3.78	3.88	3.83
16	2.68	4.39	3.54
(Neap) 17	3.78	7.00	5.39
Sum	22.11	42.60	32.36
Average	1.30	2.51	1.90

During a spring tide, z_0 varies between 0.01 - 13.43 cm. At the beginning of the flood, there is a rapid drop in z_0 values as the flow accelerates. The minimum z_0 during the flood coincides with a rapid drop in the flow velocity. The minimum z_0 occurs during the flood tide at 1612 hours when the velocity (u_{100}) is about 1.0 m/s, and a second minimum occurs just before high water slack. The maximum z_0 occurs 20 minutes after high water slack when velocity is less than 0.2 m/s. During the ebb, z_0 shows a decreasing trend and reaches a minimum at the end of the ebb flow. Though z_0 is higher during the ebb than the flood, there is less variation of z_0 during the ebb than the flood. The pattern observed in Figure 5.9 is more or less repeated in every tidal cycle.

During a neap tide, z_0 varies from 0.14 - 188.62. In the early flood, there is a rapid drop in

z_0 values as the velocity increases, and z_0 attains a minimum value which corresponds to the maximum flow velocity. This trend during the flood tide is similar to that observed during a spring tidal cycle. The maximum z_0 occurs immediately after high water when the velocity is very small i.e. $u_{100} \approx 0.03$ m/s. z_0 varies very little through most of the ebb indicating that during the neap tides, a bedform remains stable through most of the ebb period. Apart from the points that have been noted, there appears to be no obvious correlation between z_0 and tidal velocity.

As noted in Chapter 2, z_0 is directly related to the nature of the seabed. For a seabed with bedforms, it is the bedforms rather than the sediment grains that determine the roughness length. For the roughness length over ripples , Wooding *et al.* (1973) proposed the following predictive equation:

$$z_0 = 2.0\ d\ (\frac{d}{\lambda})^{1.4} \qquad [5.2]$$

where d is the ripple's height and λ is the ripple's wavelength. The ebb orientated straight transverse ripples with wavelength 6 - 8 cm and height of 1- 2 cm which are commonly observed around the VGU station at low tide would have a roughness length of 0.11 - 0.86 cm . This is comparable to the calculated z_0 values shown in Table 5.3. According to Lettau (1969) z_0 can be approximate from the relationship:

$$z_0 = 0.5dH/\zeta \qquad [5.3]$$

where d is averaged vertical extent (obstacle's height), and H is the cross sectional area seen by the flow per horizontal area ζ. For two dimensional ripples, H/ζ approximates to the ripple's steepness (height/wavelength). Application of this equation to the study area given an averaged $z_0 = 0.16$ cm which is slightly lower than the measured values.

The rapid drop in z_0 seen at the beginning of the flood may be related to the destruction of the

ripples by the accelerating flow and the subsequent decrease in form drag as a plane bed forms. As the flow decreases towards HW, the ripples reestablish, so z_0 increases. At the beginning of the flood, the flow is heavily laden with sediment. During this initial accelerating stage, sediment concentration at the bottom layer can reach 1000 mg/l or higher. This could form a stable interface due to the damping out of turbulence by the present of a high density gradient in the water column (Dyer, 1986). This will modify the velocity profiles so that higher z_0 values are produced by this stable flow stratification. As the sediment-laden flow affects only the readings of the bottom flood rotor, this increase is not clearly seen in the measured z_0 values for the Taf. In the Taf, the decrease in z_0 values is associated with the formation of a plane bed during the maximum flow velocities in the early stage of flood and late ebb on a spring tide, and during the maximum flood velocities on a neap tide. There is less variation of z_0 values during the ebb of a neap tide as the bed is rippled for most of the ebb.

The very high z_0 values observed around high water, and at the beginning of the ebb may not be valid. During this period of flow reversal, the velocity profiles are not logarithmic as shown by low R^2 values. It is also the period when ripple orientation and the flow direction are in opposite directions, thus giving a rougher bed until ebb oriented ripples are fully developed at a higher flow velocity.

The mean z_0 for the flood is smaller than the mean z_0 for the ebb. Similar findings were also obtained by Carling (1978), Mahamod (1989), Larcombe (1992). This is generally related to the strong flow asymmetry between the flood and the ebb in the intertidal environment. Stronger currents means that the higher stage plane bed (very low z_0 values) would remain for a longer period during the flood, while during the ebb this plane bed rarely achieved due to weaker currents, and the beds are rippled for most of the ebb. There is also a general increase in values of z_0 toward the neap tide. This is in agreement with the observations made by Dyer (1980) and Harvey and Vincent (1977). Dyer related the increase to the higher and steeper ripples developed during low tidal ranges, giving a rougher bed. Furthermore the ripples formed during a neap tides would be stable for a longer period of time compared to those formed during a spring tide.

5.3.4 Shear velocity

Shear velocity calculated from the velocity profiles varies over tidal cycles. Figures 5.11 and 5.12 show the typical variation of shear velocity during spring and neap tidal cycles, respectively. The variation of shear velocity during a tidal cycle follows closely the variation of the current velocity. During a spring tide, the flood shear velocity rapidly reaches its maximum value of 0.125 m/s at the early stage of the flood, then decreases and attains its minimum value of 0.004 m/s at HW. As the ebb begins, u_* gradually increases and reaches its maximum value of 0.109 m/s at the end of the ebb tide. The maximum u_* during flood and during the ebb and the minimum at HW more or less coincide with the maximum and minimum flow velocities, respectively. Similar features are observed for the neap tidal cycles, but with slightly lower values of maximum u_* during the flood and ebb. However the ebb maximum shear velocity occurs about an hour after the ebb maximum flow velocity.

In order to study the variation of u_* over a neap-spring tidal cycles, the shear velocities during the maximum flood and ebb flows are plotted against tidal cycles and tidal ranges (Figures 5.13 and 5.14). As expected the maximum u_* is generally highest during the spring tide and decreases toward the neap. This trend is best shown by the ebb phase of the tidal cycles; it is less clearly shown by flood phase of the tidal cycles. This is may be a result of density stratification which alters the shape of the velocity profiles during the maximum flood flows and thus overestimates u_*. There are always uncertainties as to the degrees of stratification occur in each tidal cycle, in particular during the maximum flood velocities. During the ebb, the maximum flow velocities are less and the velocity profiles are less affected by the density stratification.

As mentioned previously (see Chapter 4) the spring-neap tidal cycle is strongly reflected in the peak flood velocities, and to a lesser extent in the peak ebb velocities. Maximum flood and ebb velocities are highest during springs (maximum tidal prism) and lowest during neaps (minimum tidal prism). This is also reflected well in the calculated shear velocity; however the variations of u_* over lunar tidal cycles are also related to bed morphology and the presence of any density stratification in an active sediment transport environment.

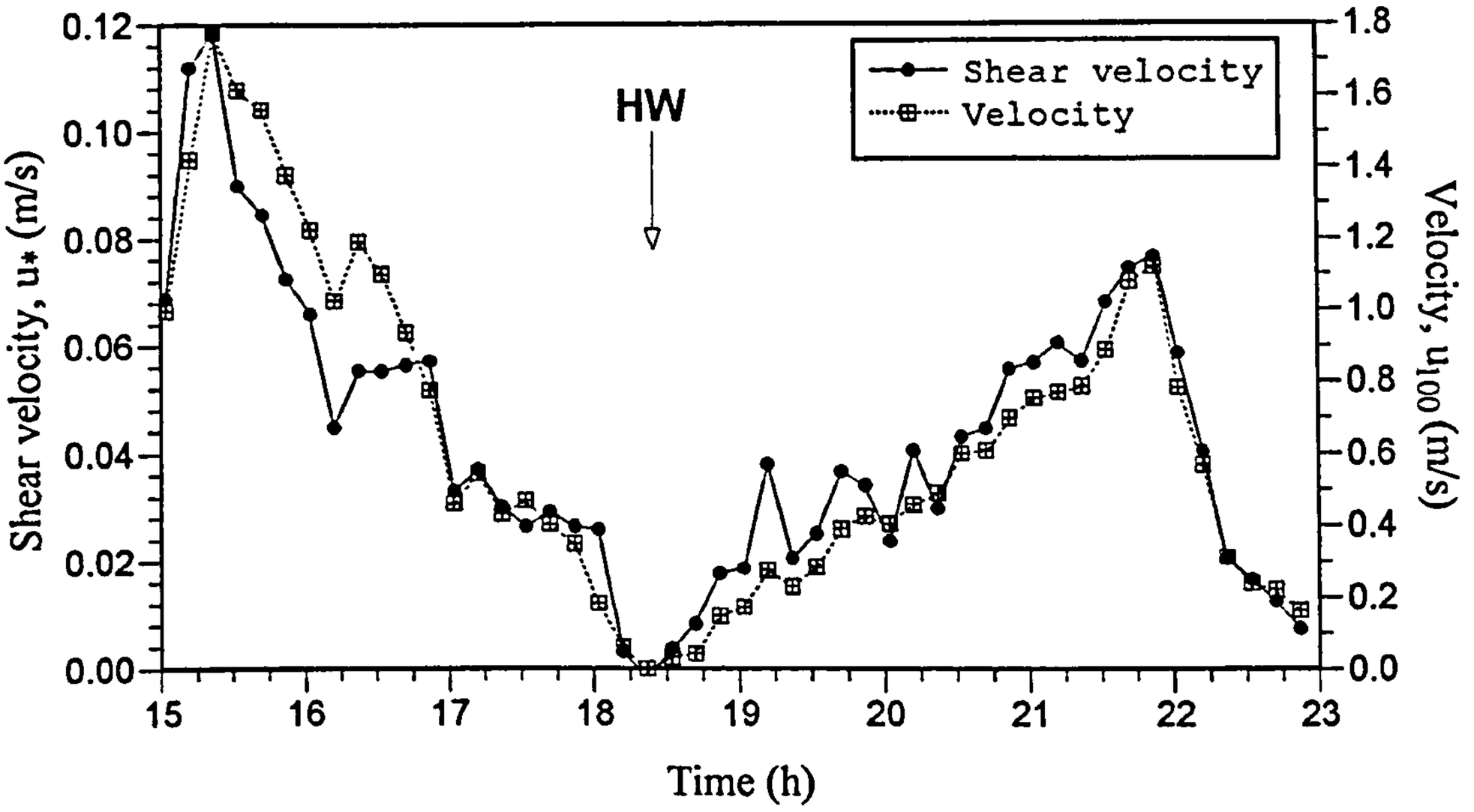

Figure 5.11 Variation of shear velocity, u_* over a spring tidal cycle. The arrow shows the time of high water.

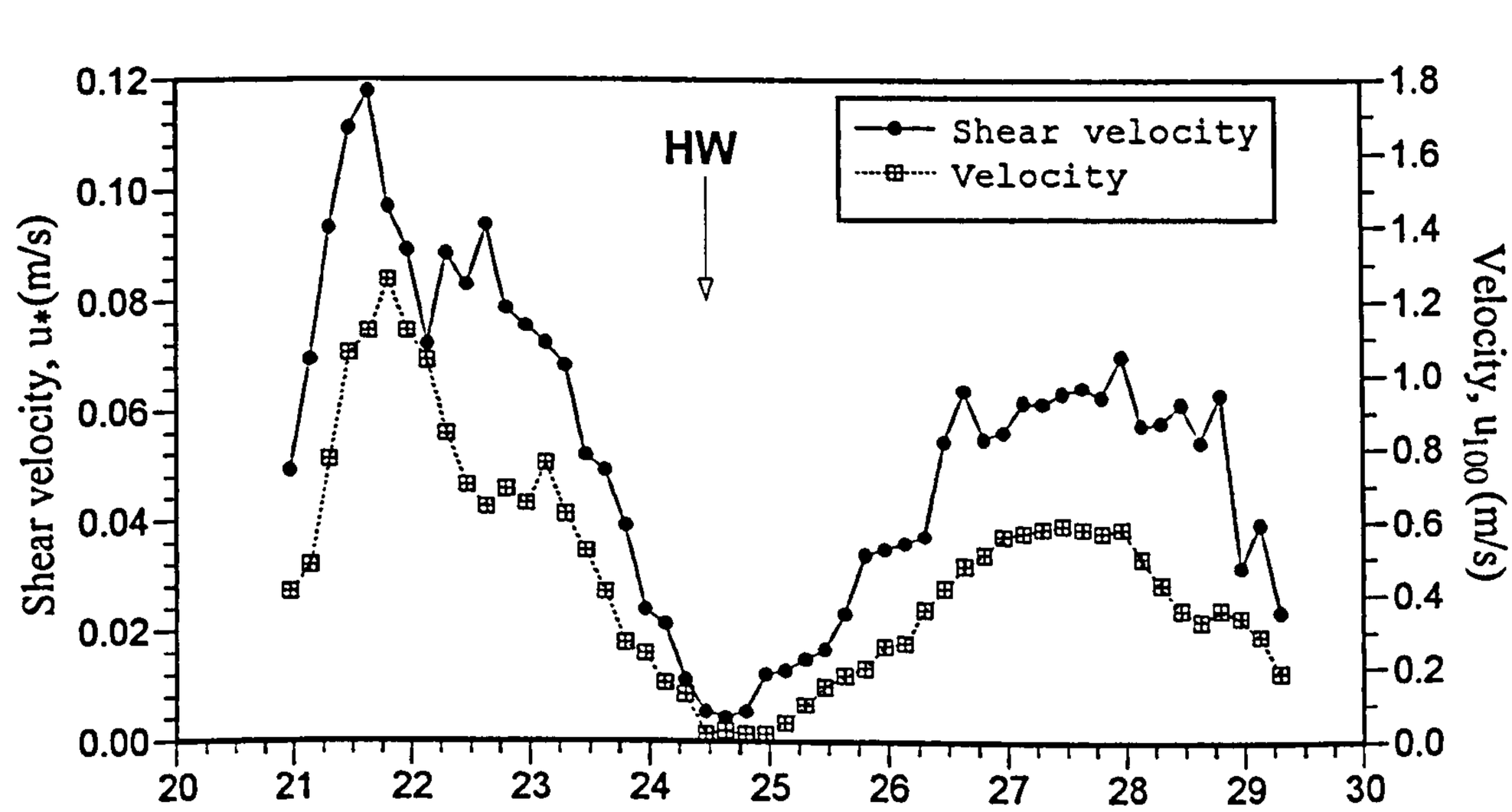

Figure 5.12 Variation of shear velocity, u_* over a neap tidal cycle. The arrow shows the time of high water.

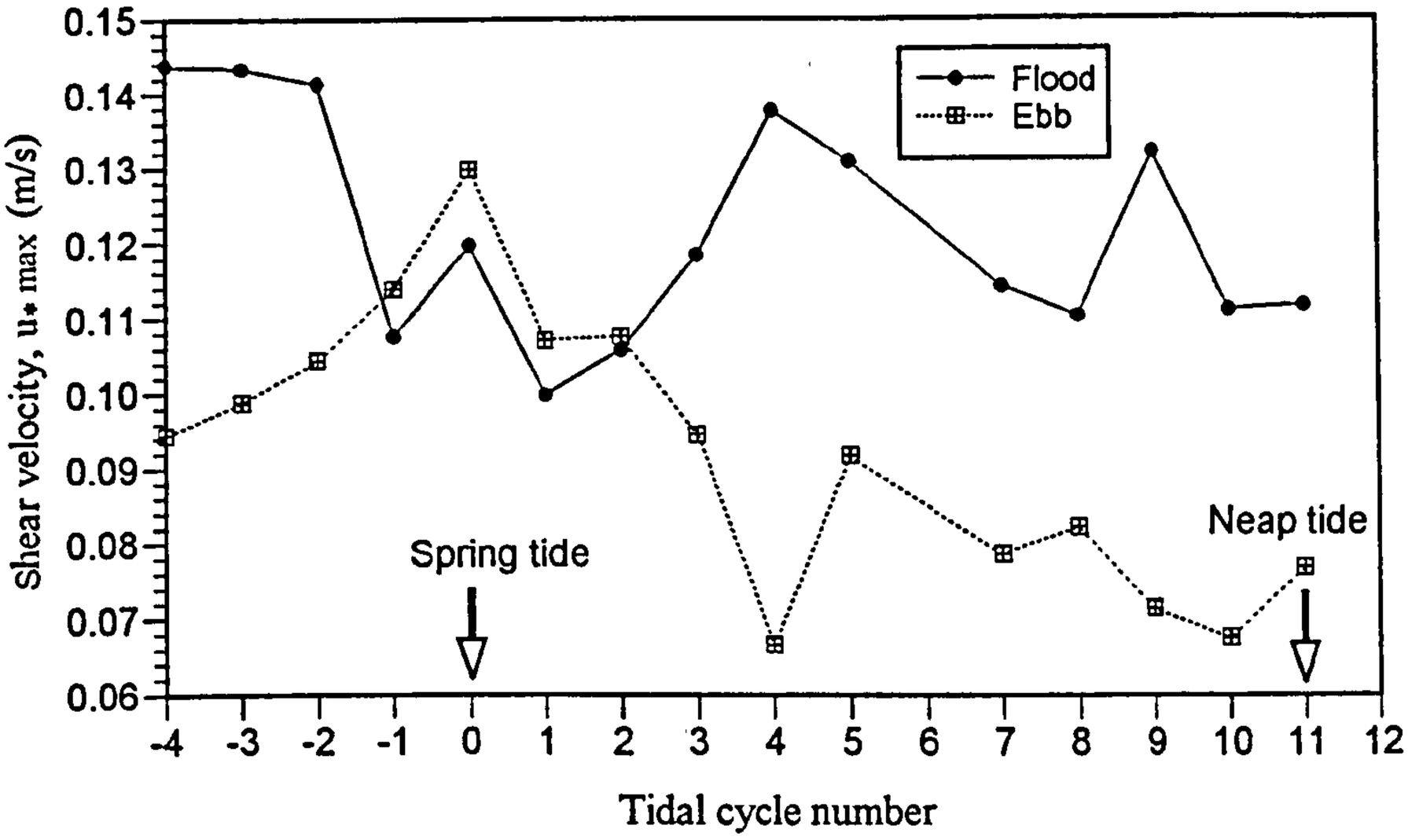

Figure 5.13 Variation of shear velocity, u_* over a lunar tidal cycle for station 2, transect T9, July 1995.

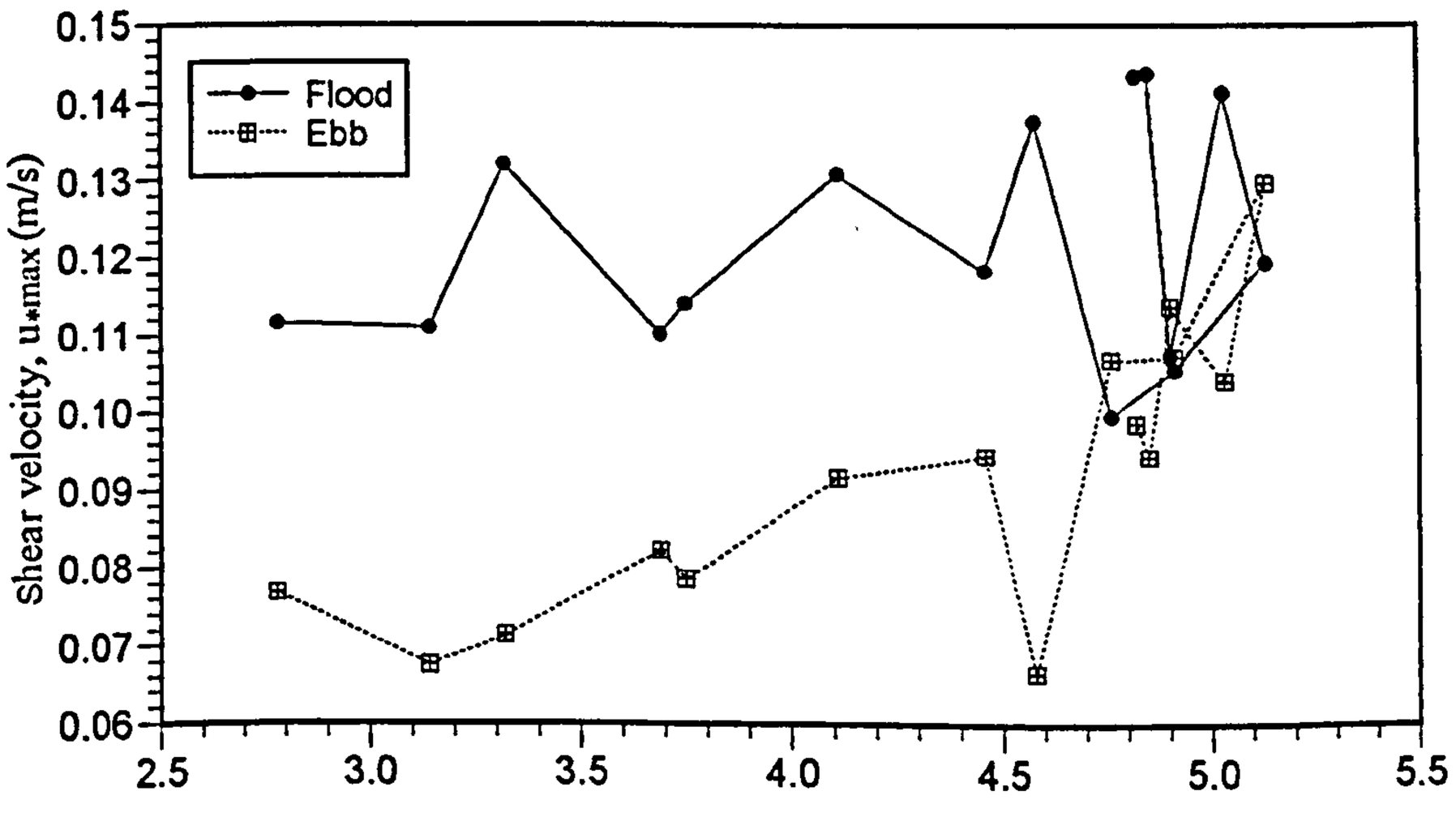

Figure 5.14 Variation of shear velocity, u_* with tidal height, for station 2, transect T9, July 1995.

An estimate of u_* in a sediment-laden flow, but in which the effect of sediment is ignored, would overestimate u_* compared with the true value of u_*. Taylor and Dyer (1977) and Soulsby and Wainwright (1987) present methods for obtaining u_* from velocity profiles which take into account the suspended sediment effects. The graphical approach of Soulsby and Wainwright (1987) is simple and easy to use, and has been adopted here in order to evaluate the effect of sediment stratification on the measured values of u_*. Their graph for obtaining the correct u_* from a sediment-laden flow is shown in Figure 5.15 where u_* can be obtained from the measured flow velocity at 100 cm above the bed, u_{100}. This plot suggests that if u_{100} < 30 cm/s, then the velocity profile is sediment-free, and Equation 5.1 can be used to obtain u_*. Soulsby and Wainwright (*op.cit.*) also publish a diagram that shows the stability of water column when sediment is in suspension (see Figure 5.16). The plots of u_* at the time of peak flood and ebb currents in the Soulsby and Wainwright diagram for 17 tidal cycles for the fine sand (mean diameter 130μm or 2.95 ϕ) generally found in the study area are shown in Figure 5.16a. These values of u_* have been calculated using Equation 5.1 i.e. neglecting the effect

Figure 5.15 Contours of the velocity (cm/s) at 100 cm above the bed for obtaining u_* from velocity measurements made with sediment in suspension. The contours are for quartz sand in sea-water at 10 ^{0}C, 35‰ (Soulsby and Wainwright, 1987)

of sediment stratification. The plot shows that the entire profiles for the spring and neap as well as for the flood and the ebb are stratified, indicating an overestimate of u_*, in particular during a neap, where it is known that little sediment is in suspension (see Chapter 6). It is therefore the entire water column that is affected by density stratification, and not just the near-bed layers as previously postulated. Certainly the near bed layer is more sediment-laden than the layers above it.

Using u_{100} for the same velocity profiles and the mean diameter of the sediment, u_* has been reestimated from Figure 5.15. The new (valid) u_* values are plotted in Figure 5.16b. This shows that the apparent value of u_* obtain if suspended sediment effects are neglected is more than twice that obtained if such effects are allowed for, even though the correlation coefficients for the logarithmic profiles are quite high ($R^2 > 0.95$ for all the selected profiles).

5.3.5 Drag coefficient

By assuming the shear stress is constant within the boundary layer, it has been shown that the bed shear stress can be estimated from velocity profiles; similarly, the stress operating at the boundary layer can also be estimated from known values of the drag coefficient and the mean value of flow velocity.

From Sternberg (1972), the drag coefficient at 100 cm above the bed (C_{100}) can be obtained from the relationship:

$$u_*^2 = C_{100} u_{100}^2 \qquad [5.4]$$

Using this equation, C_{100} has been calculated for the study area from the VGU velocity data. The velocity at 100 cm above the bed has been estimated from the VGU data using cubic

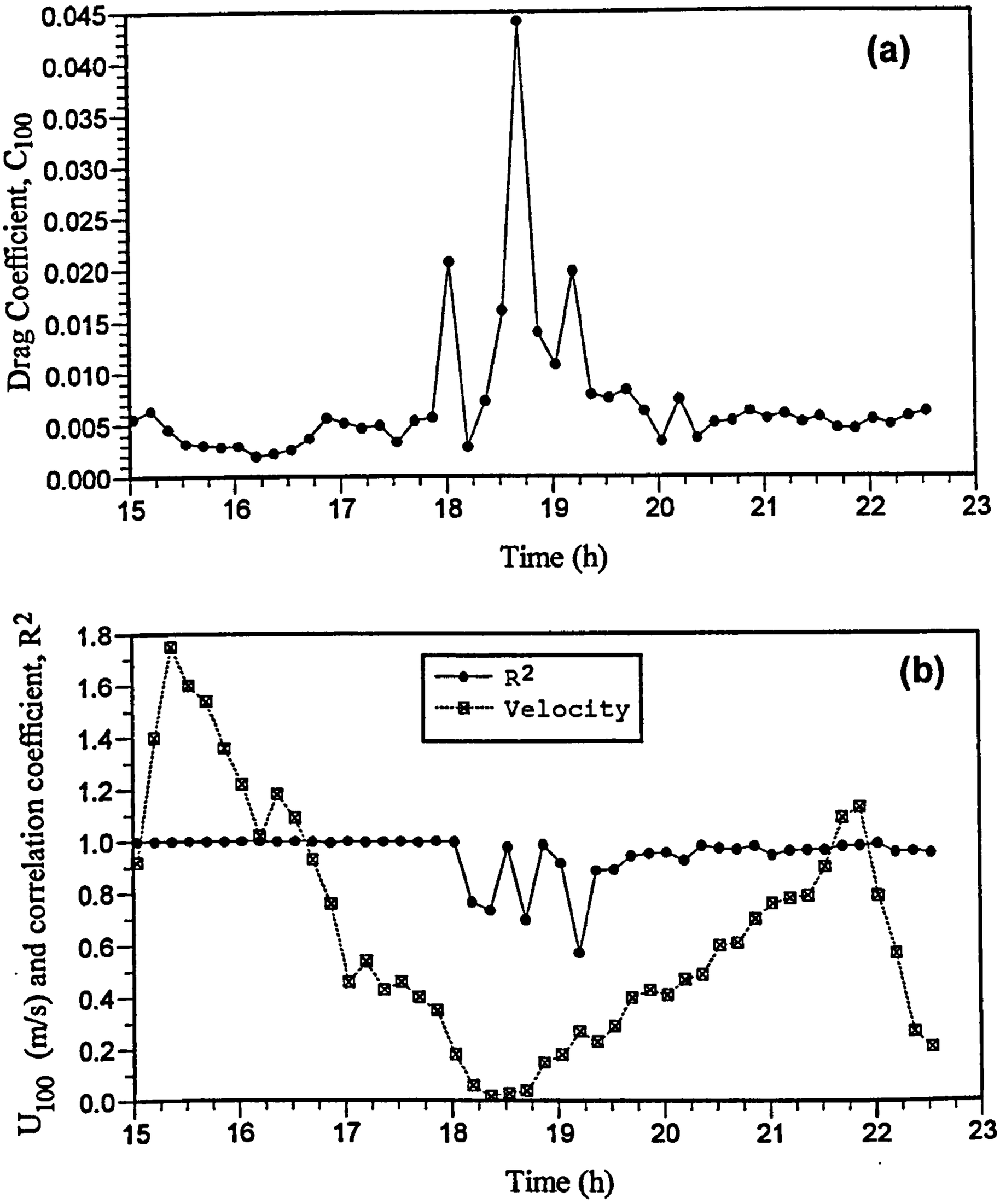

Figure 5.17 Variation of (a) drag coefficient, C_{100} over a spring tidal cycle, and (b) the corresponding tidal velocity, u_{100} and correlation coefficient, R^2.

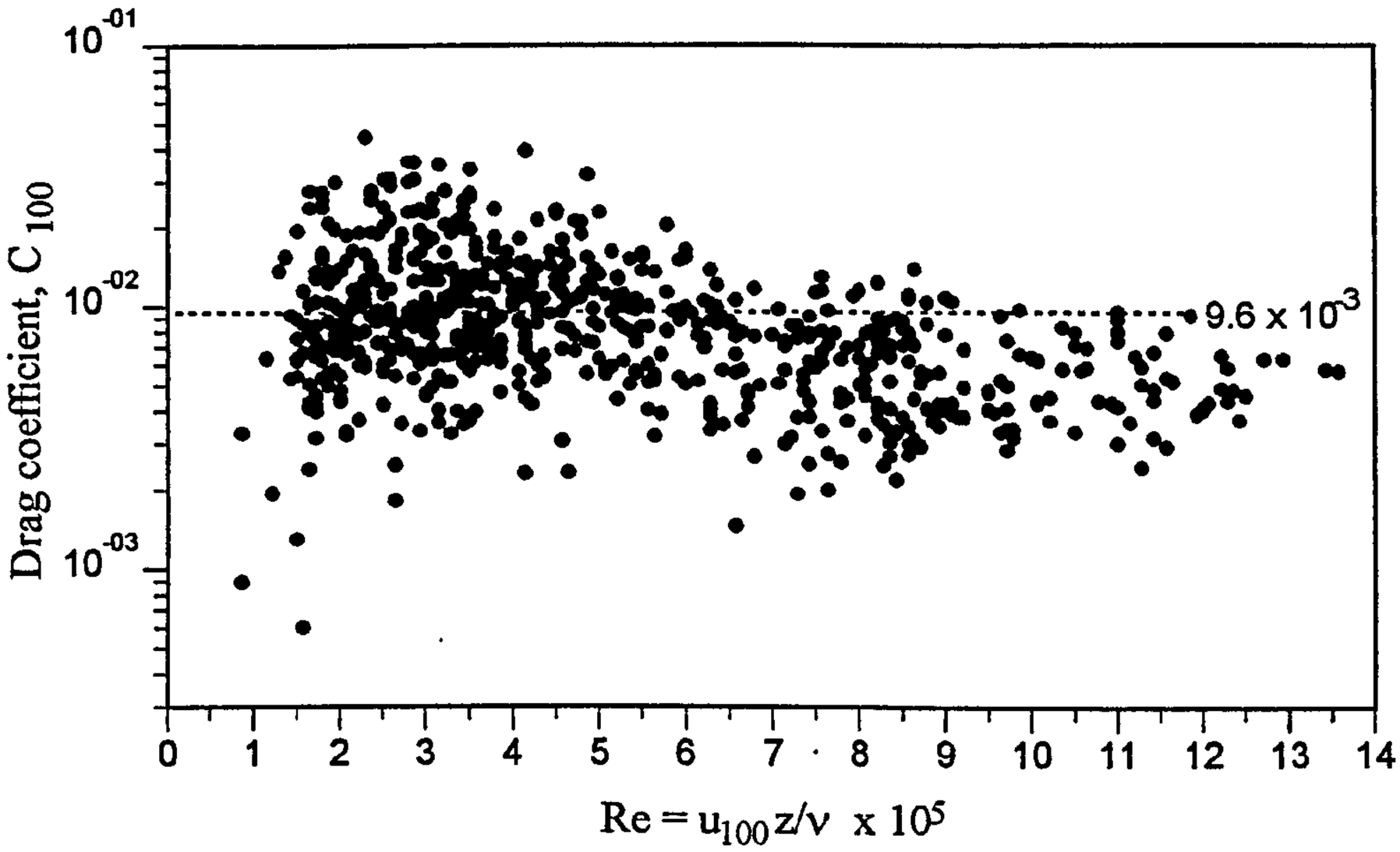

Figure 5.18 Drag coefficient, C_{100} as related to Reynolds number for flow velocity > 0.2 m/s. Also shown is the mean C_{100} for all data.

5.3.6 Velocity at 100 cm above the bed.

The velocity at 100 cm above the bed , u_{100} have been calculated using a cubic spline curve fitting technique for all velocity profiles. The u_{100} during the flood attains a maximum value of 1.80 m/s for springs and 1.18 m/s for neaps. The corresponding values for the ebb were 1.27 m/s and 0.57 m/s, respectively. The spring-neap tidal cycle is reflected strongly in the peak flood and ebb velocities. The regression of peak flood and peak ebb velocities show correlation coefficient greater than 0.86. The relationship between flood and ebb u_{100} maximum velocities and tidal heights can be approximated by:

For the flood: $u_{100\,max} = 0.28$ x Tidal height

For the ebb: $u_{100\,max} = 0.30$ x Tidal height

The current velocity at 100 cm above the bed (u_{100}) can also be calculated using the Karman-Prandtl equation which described the logarithmic profile at the seabed.

$$u_{100} = \frac{u_*}{\kappa} \ln \frac{z}{z_0} \qquad [5.5]$$

Using z = 100 cm, $\kappa = 0.4$, and the calculated z_0 and u_* from the logarithmic profiles, u_{100} has been calculated for each profile. The calculated values can be compared with u_{100} obtained independently by using a cubic spline curve fitting technique for the same velocity profiles. The results from both techniques agree very well for all ranges of flow velocities (Figure 5.19). The correlation coefficient, R^2 obtained for the velocities using two different techniques is 0.9994. This illustrates that the use of $\kappa = 0.4$ is appropriate for an intertidal environment despite some suggestions (eg. Gust and Walger, 1976) that the value of κ may be reduced by the presence of suspended sediment. This is consistent with Coleman (1981) who demonstrates that κ is not affected by the presence of suspended sediment.

5.4 Summary

More than 800 records of individual velocity profiles measured over 17 tidal cycles have been analysed. The logarithmic velocity profiles existed ($R^2 > 0.8$) for 90 - 100 % of the time for individual tidal cycles with an averaged of 95 % of the time for all the profiles. 82 % of the profiles had R^2 values of 0.95 or greater. This indicate that the logarithmic model could adequately describe the velocity profiles in the intertidal zone. It is therefore justified to use the associated shear velocity and roughness length in estimating the potential transport of the bottom sediment. The deviation from the logarithmic model mostly occurred around high water slack when current reverses and velocities were reduced to almost zero (and the potential for sediment transport was a minimum).

The shape of velocity profiles from the study area is affected by the density stratification which effects the readings of the bottom current meter more than the upper ones, and affecting flood rotors more than the ebb rotors. This density stratifications results in apparent increase in flow velocities in the upper layers and the associated z_0 and u_* values calculated from the velocity profiles. Close to the bed, the suspended particles damp the turbulent, thus reducing the

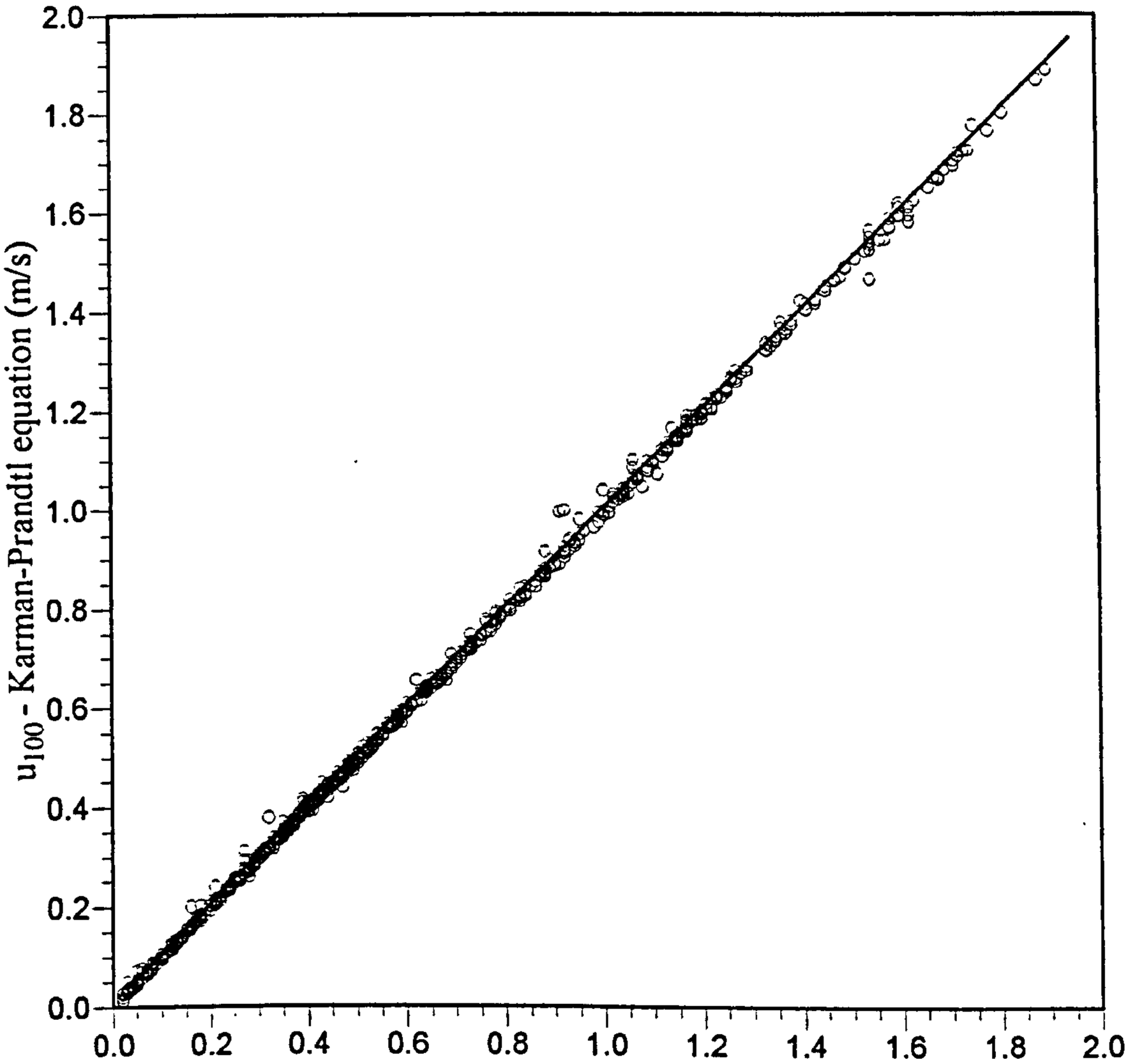

Figure 5.19 Comparison between velocity at 100 cm above the bed, u100 as calculated using Karman-Prandtl equation and by interpolation from a cubic spline curve fitting technique. The straight line is the similar velocity line.

velocity and potential of sediment transport.

The evidence showed that in the area of active sand transport of Taf estuary, z_0 varies considerably both within a tidal cycle and throughout the neap-spring tidal cycles. The mean roughness length for the flood varies from about 0.2 cm during spring tides to 3.8 cm during neaps. For the ebb, these values ranges from 0.7 cm during springs to 5.4 cm during neaps. For flood and ebb phases of the tidal cycle, there are two orders of magnitude difference between the minimum and the maximum z_0. These variations are caused by changes in ripple geometry, sediment stratification, tidal acceleration and deceleration. The observations show that a variable z_0 rather a fixed value should be used for any accurate modelling of bottom friction in areas of active sand transport.

While the variation of z_0 through a tidal is difficult to predict, since it reflects changes in bed morphology with increasing and decreasing flow velocities, the variation of the corresponding u_* is much more predictable. Though the local bed roughness has some influence on the calculated values, u_* generally increases as the velocity increases. The occurrence of maximum and minimum u_* more or less coincide with the maximum and minimum flow velocities. Similarly, u_* is higher during the springs than the neaps. This may be related to the density stratification, causing u_* to be overestimated during springs.

The drag coefficient, C_{100} varies considerably within a tidal cycle and between spring-neap tidal cycles. Within a tidal cycle, averaged C_{100} value for the flood is usually smaller than the averaged value for the ebb. The averaged values of C_{100} generally increase towards neaps. The averaged C_{100} value of 9.6×10^{-3} obtained for the Taf is slightly higher than the published values for similar bed morphologies.

The values of u_{100} calculated using a cubic spline curve fitting technique and those obtained from the quadratic stress law correlation for the same velocity profiles show a very good agreement for all ranges of flow velocities and show a near unity correlation coefficient. This illustrates that the use of $\kappa = 0.4$ is appropriate for sediment transport calculation in an intertidal environment.

CHAPTER SIX

SUSPENDED SEDIMENT DYNAMICS

6.1 Introduction

Evidence of suspended sediment transport in tidal estuaries is shown by the formation of turbidity maxima. They are common features of the upper reaches of estuaries and they occur at the limit of salt water intrusion in both stratified and well-mixed systems. The development of a turbidity maximum needs up-estuary transport of suspended matter by a mechanism which depends on the nature of estuarine dynamics: either landward advection of bottom waters in stratified systems (eg. Postma, 1967; Schubel, 1968, 1971; Feasta and Hansen, 1978; Officer, 1981) or tidal pumping in vertically mixed systems (eg. Allan *et al.*, 1980; Uncles *et al.*, 1985; Uncles and Stephen, 1989). Neither mechanism is applicable to the Taf estuary, a well-mixed system in which all salt water is withdrawn at low tide, so no net landward advection.

In this Chapter, the turbidity maximum found in the Taf estuary, and its variation in response to the fluvial and tidal regimes will be described. The mechanisms responsible for its formation in the Taf is discussed. We also present the results of the suspended sediment measurements made in the lower and in the upper estuary. The variability of SPM concentrations at stations across the measurement transects in the estuary is discussed in the context of variable flow strength during lunar tidal cycles and in relation to the fresh water input.

6.2 Longitudinal SPM variation at HW over a lunar cycle

In this section the results of spatial surveys carried out during three sampling campaigns between September 1994 - September 1996 are presented. During these surveys measurement of salinity, temperature and suspended sediment concentration were made

along the longitudinal axis of the estuary around the time of high water. Contour plots are to illustrate the variability of parameters along this axis (from the estuary mouth to the limit of salt water intrusion) for different tidal ranges and river discharges.

6.2.1 Spatial surveys - September/October 1994

In 1994 the longitudinal surveys were carried out during an average river discharge. The monthly mean discharge rates were 6.7 m^3/s for September and 7.1 m^3/s for October 1994. No turbidity maximum was observed during neap tides on 28 and 30 September 1994 when the tidal ranges were less than 4.0 m (Figures 6.1 and 6.2). The turbidity maximum was first develop on 1st October when a sediment concentration over 20 mg/l was recorded at the upper reach of saline intrusion, compared to a background concentration in the estuary of about 10 mg/l (Figure 6.3). The turbidity maximum became more developed on the subsequent surveys on the 2nd and 3rd October as the tidal range increased (Figures 6.4 and 6.5). The highest concentration reached a value of 52 mg/l on 2nd October and a value of 70 mg/l on 3rd October 1994 which was during the mid-spring tide (Table 6.1). In the last three surveys, when a turbidity maximum developed, the centre of the maximum

Table 6.1 Location of turbidity maximum during HW at different tidal ranges during average discharge. For 28 and 30 September the location of the maximum was inferred from the highest depth averaged SPM concentration.

Date	Tidal Range (m)	Discharge (m^3/s)	TM location (km)	Maximum concentration (mg/l)
28/9/94	3.88	5.59	8.55	17
30/9/94	3.58	4.99	7.83	12
1/10/94	4.40	4.90	9.5	22
2/10/94	5.58	6.37	10.3	52
3/10/94	6.82	4.96	11.2	70

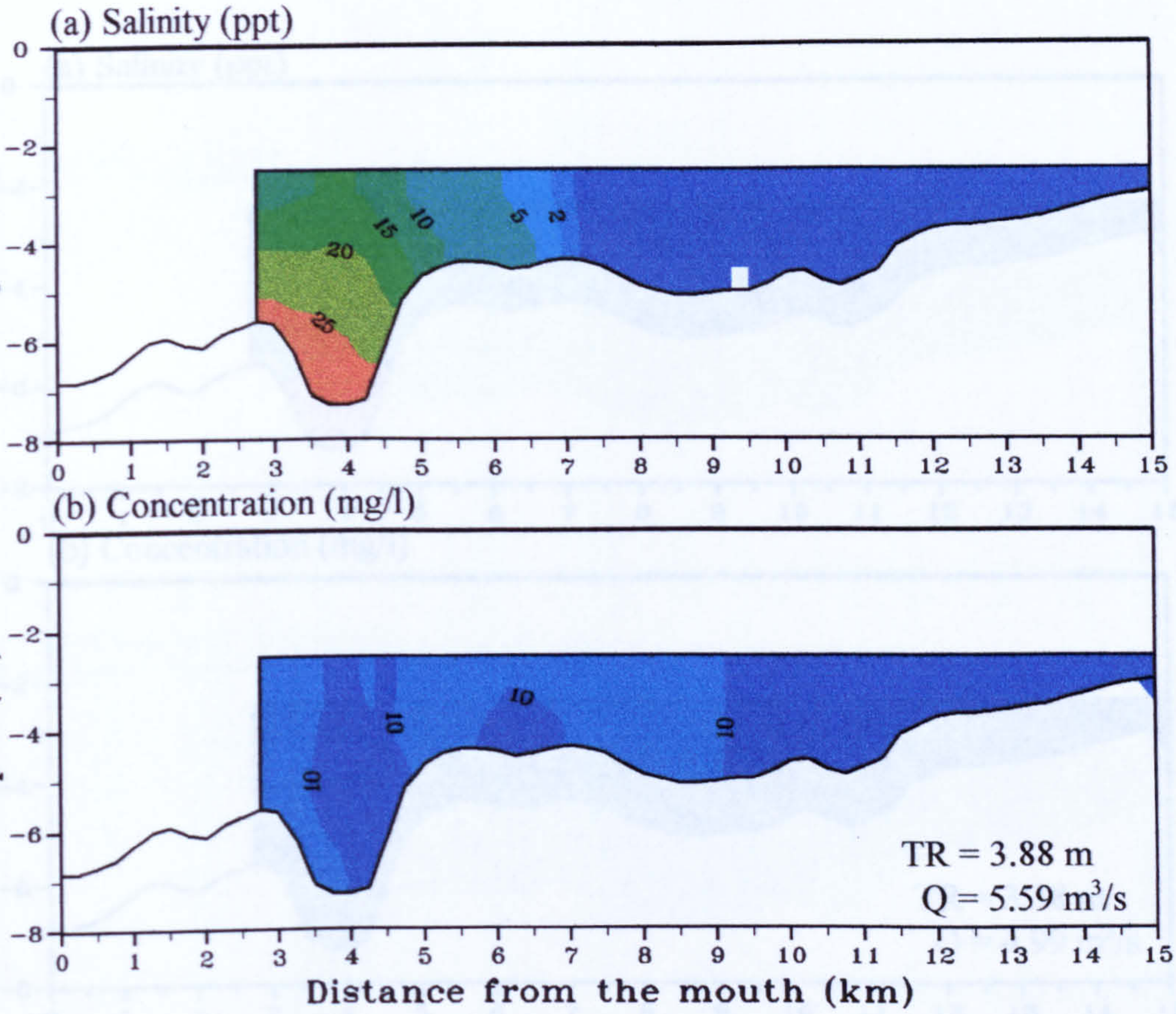

Figure 6.1 Longitudinal variations of salinity and suspended sediment concentration during high water, 28 September 1994, (TR = tidal range, Q = river discharge).

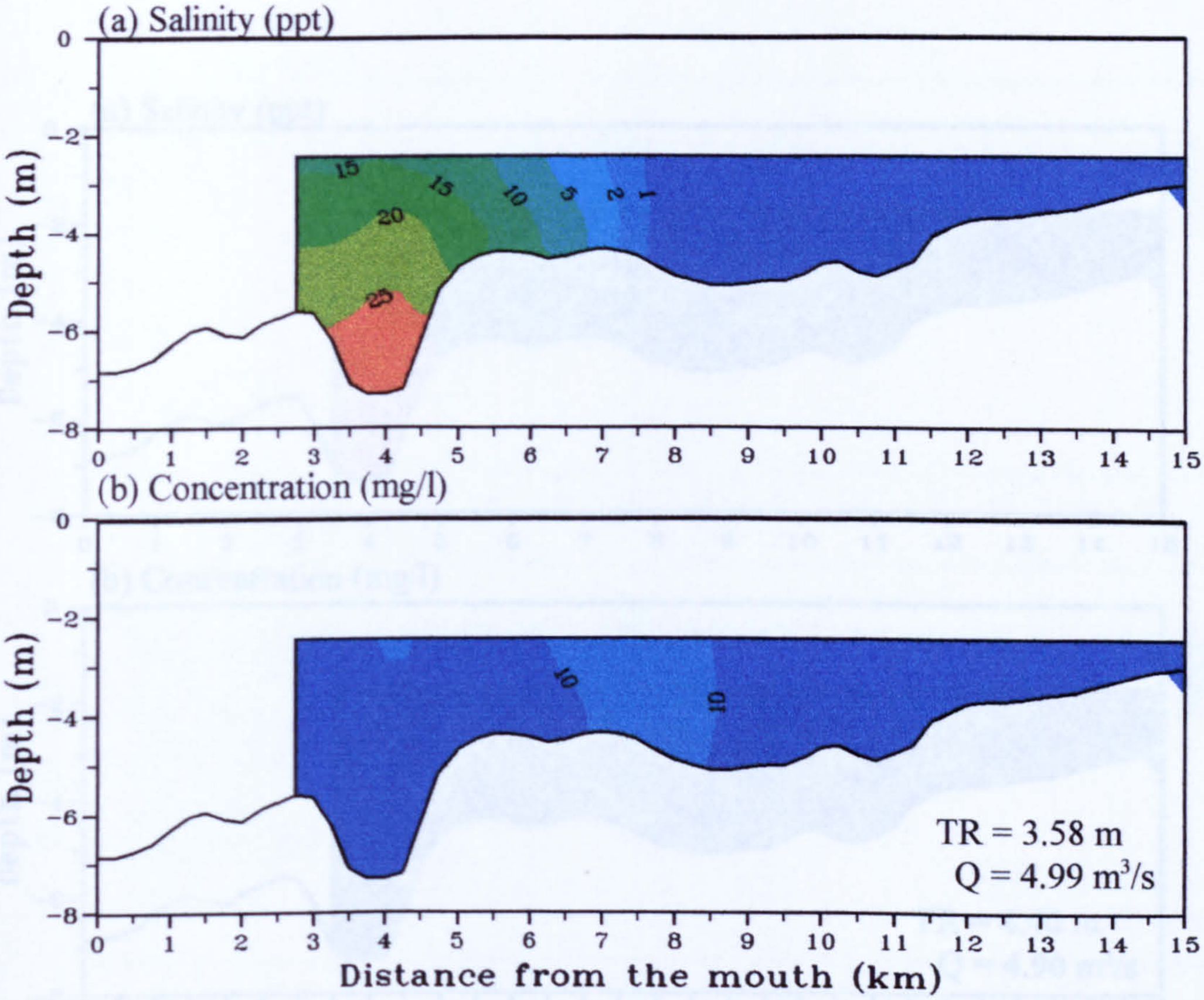

Figure 6.2 Longitudinal variations of salinity and suspended sediment concentration during high water, 30 September 1994, (TR = tidal range, Q = river discharge).

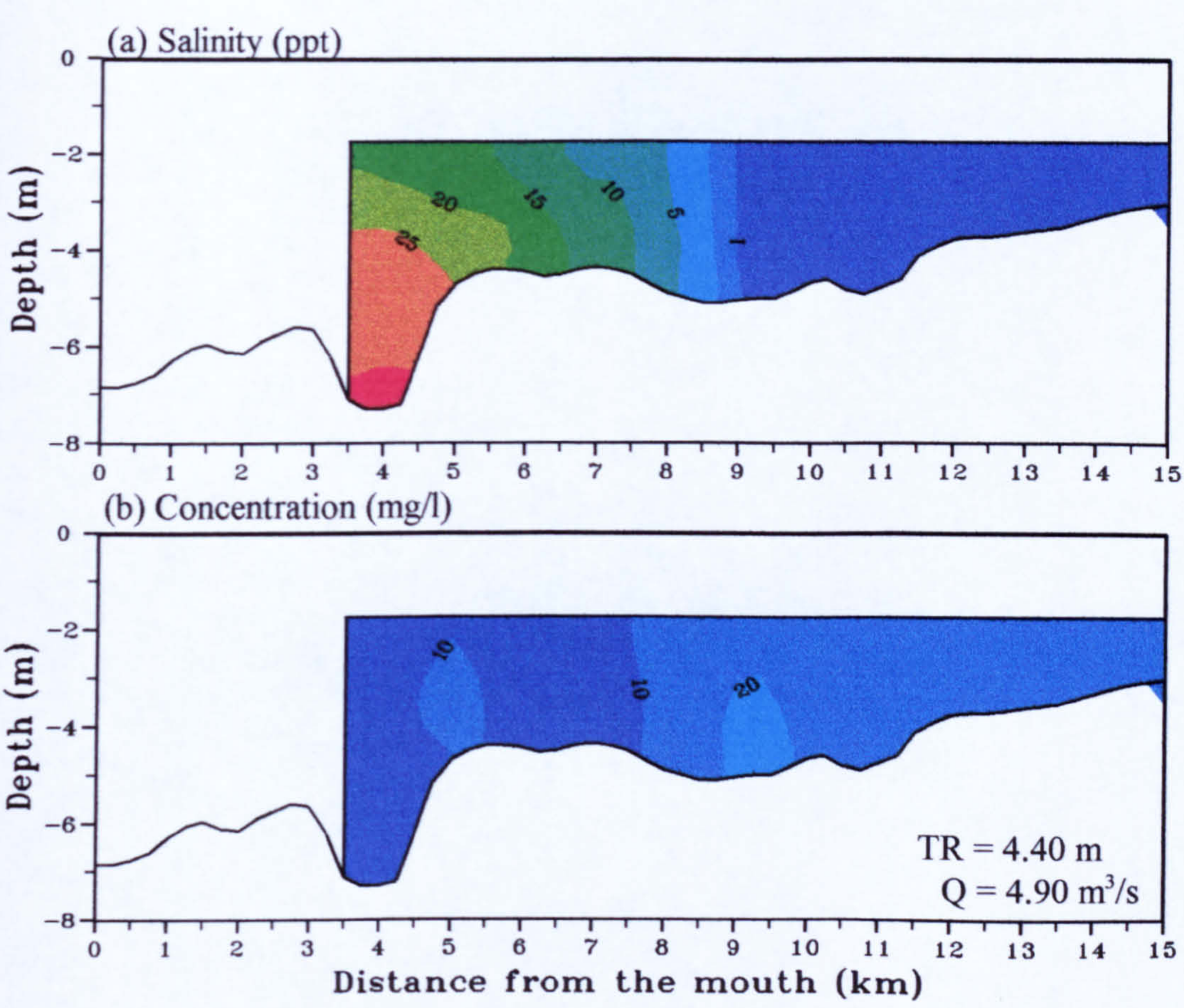

Figure 6.3 Longitudinal variations of salinity and suspended sediment concentration during high water, 1 October 1994, (TR = tidal range, Q = river discharge).

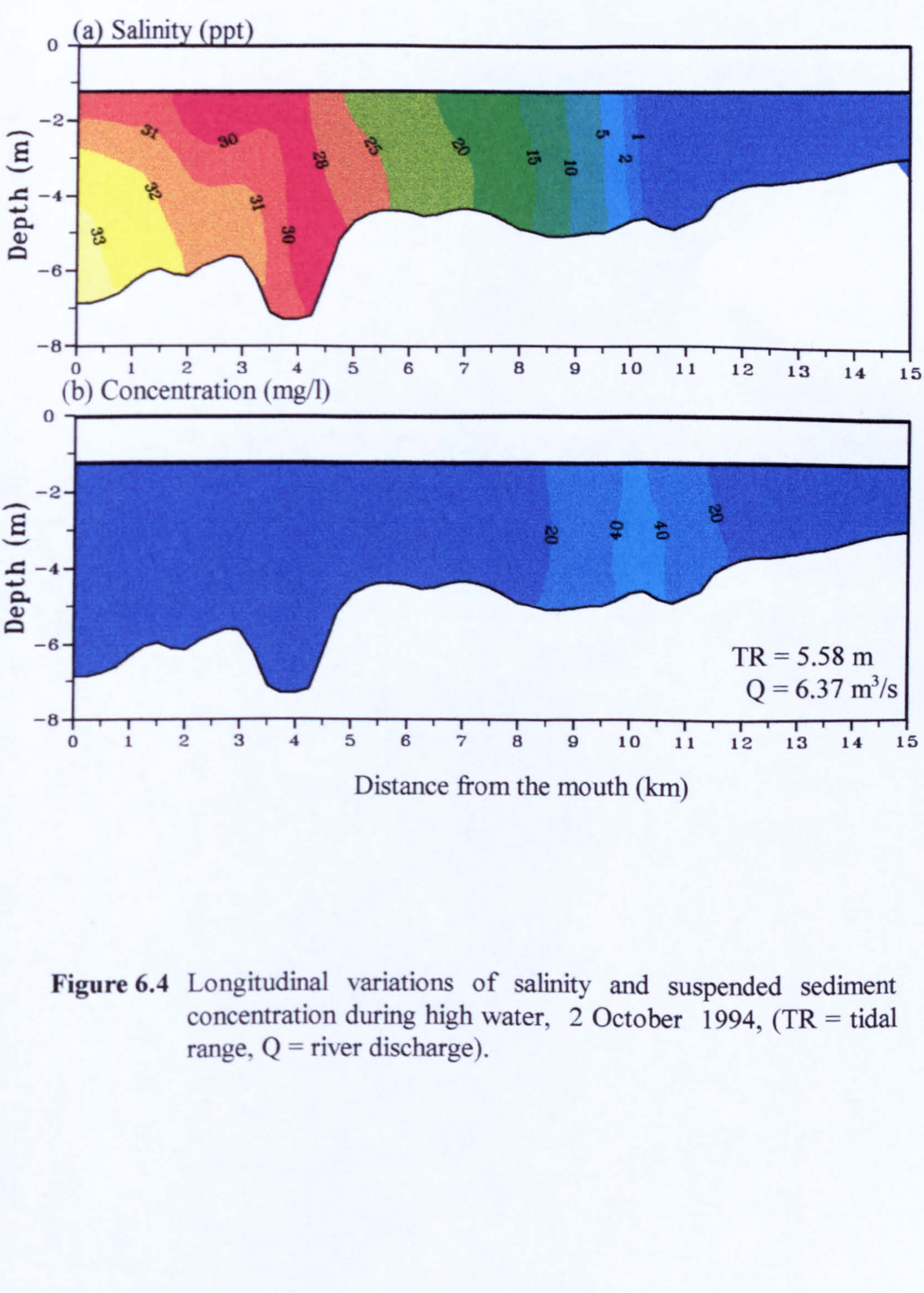

Figure 6.4 Longitudinal variations of salinity and suspended sediment concentration during high water, 2 October 1994, (TR = tidal range, Q = river discharge).

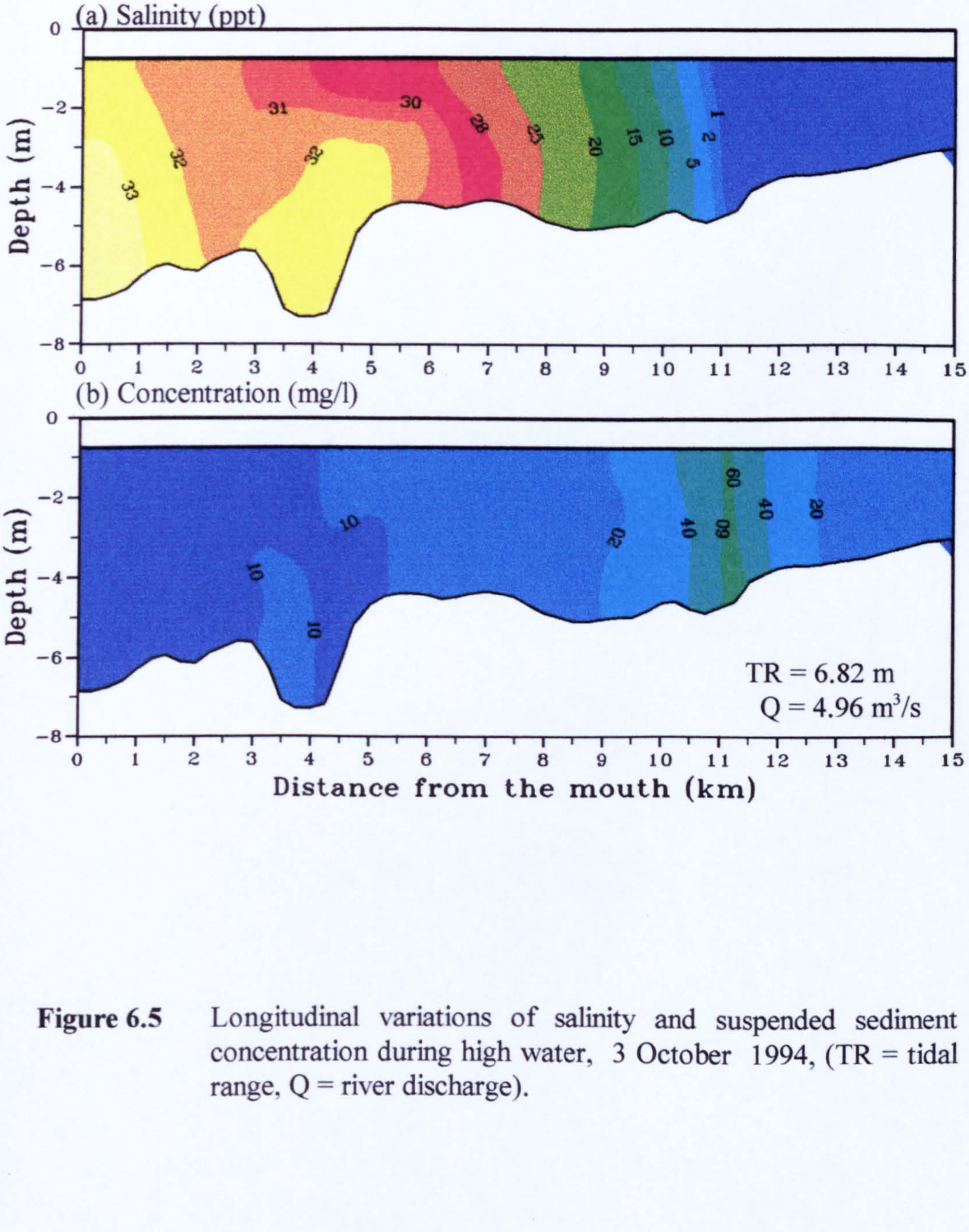

Figure 6.5 Longitudinal variations of salinity and suspended sediment concentration during high water, 3 October 1994, (TR = tidal range, Q = river discharge).

was located around salinity 0.5 - 2 ppt. The location of the turbidity maximum was about 9.5 km from the mouth on 1st October but migrated landward as tides grew; it was about 11.2 km from the mouth on 3rd October.

As all the longitudinal surveys were started at approximately the same time relative to the time of high water at Laugharne, the locations of the turbidity maxima are only relative to each other. In the upper reaches, the water was still flooding at the start of the surveys, therefore the actual locations of the maximum during high water slack would be slightly further up estuary than the distance given in Table 6.1. No attempt was made to correct this position to the time of high water as no current measurements were made during the surveys.

Though in the upper estuary near the limit of salt water intrusion the water was well mixed, the water in the lower estuary was strongly stratified as shown by Figures 6.1 - 6.5. The stratification was strongest when tidal ranges were small during neap tides.

6.2.2 Spatial surveys - July 1995

In July 1995 the river discharge was very low with a monthly average of 0.75 m^3/s. The longitudinal surveys were carried out for three tides from spring to neap . The turbidity maximum was observed in all three surveys (Figures 6.6 - 6.8). The location of this maximum centred around the fresh-salt water interface (salinity 1 ppt) on 13 and 17 July 1995 but on 19 July 1995 its location was slightly upstream of this interface. The maximum SPM concentration at the surface during the neap 19 July 1995 was 148 mg/l against the background concentration of between 10 to 20 mg/l. During the spring tide the SPM concentration reached a maximum value around 224 mg/l at the surface and more than 250 mg/l at the bed. The actual concentration could not be established as the transmissometer readings were saturated above SPM concentrations of 250 mg/l. During the neap tide, the transmissometer was saturated when near the bed, but on the spring tide the saturation occurred immediately below 0.5 m depth. Thus closer to the bed the actual sediment

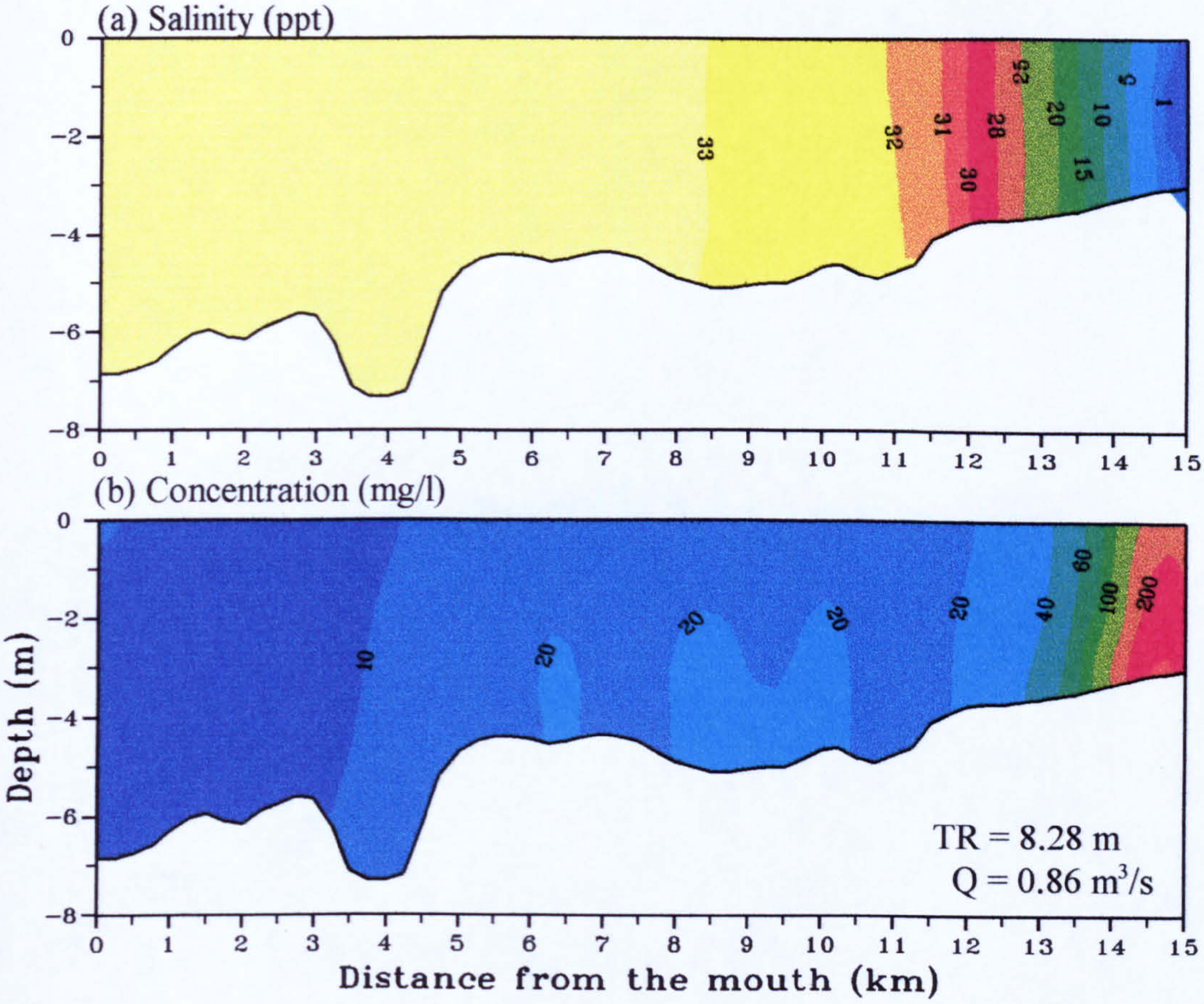

Figure 6.6 Longitudinal variations of salinity and suspended sediment concentration during high water, 13 July 1995, (TR = tidal range, Q = river discharge).

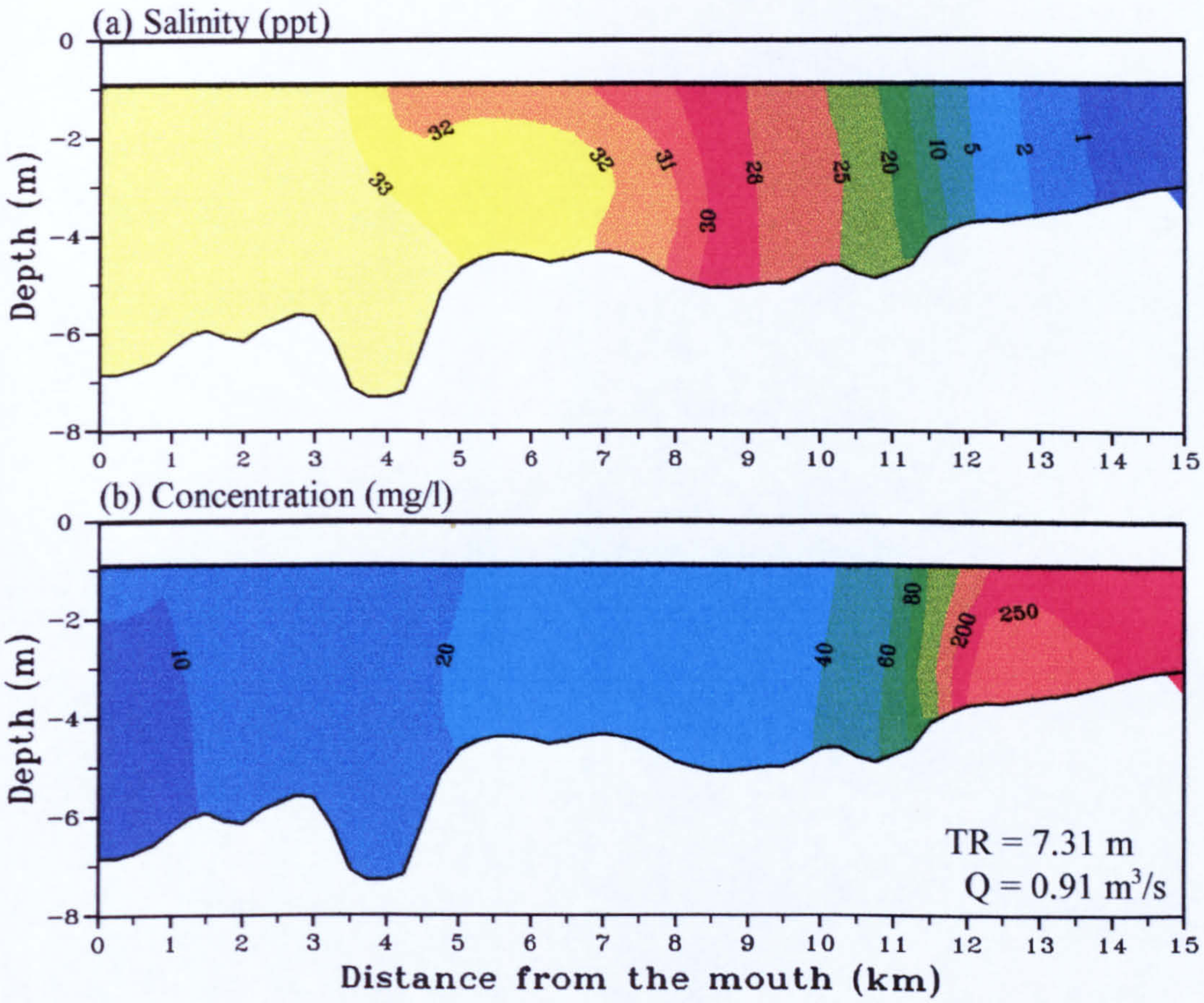

Figure 6.7 Longitudinal variations of salinity and suspended sediment concentration during high water, 17 July 1995, (TR = tidal range, Q = river discharge).

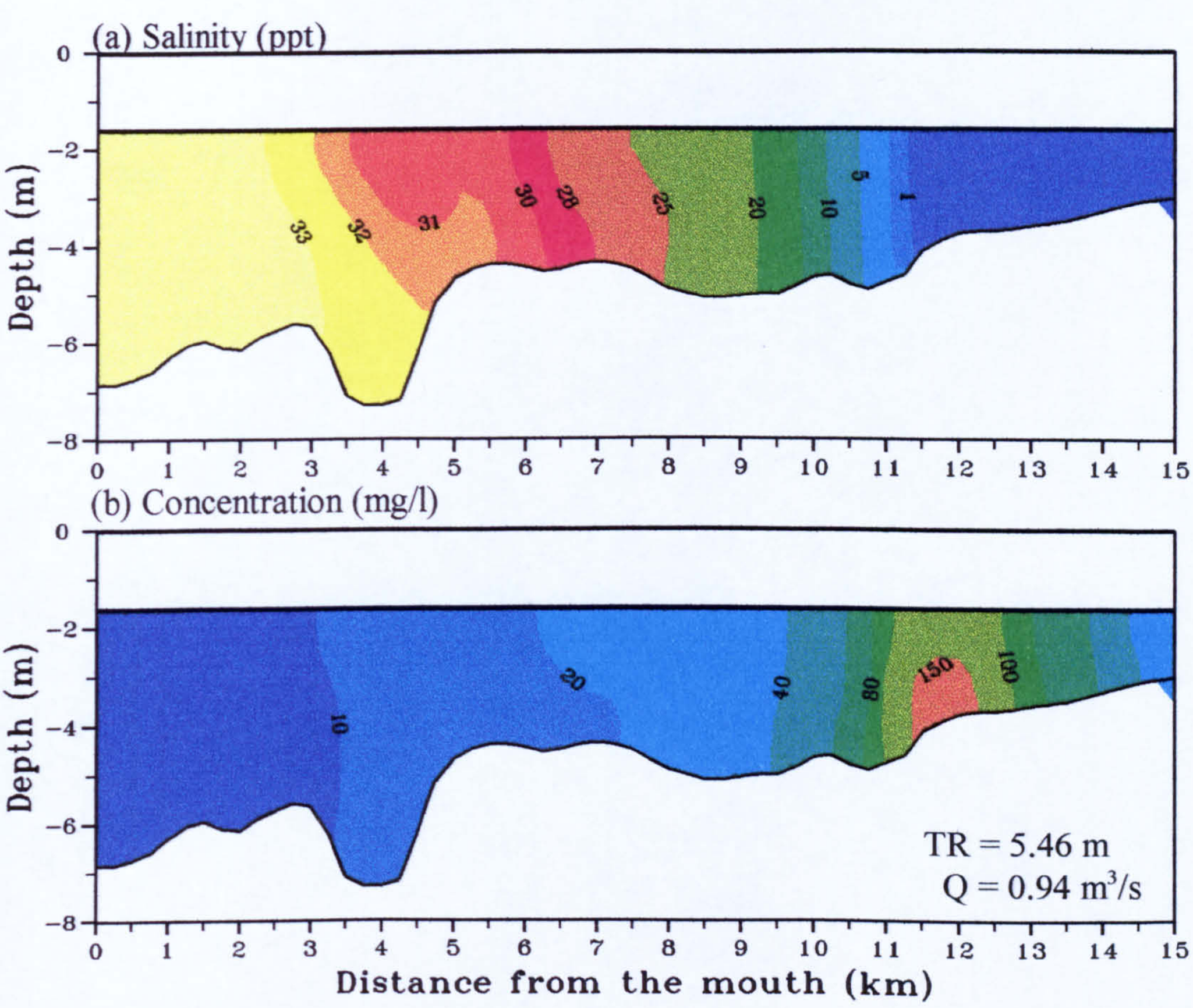

Figure 6.8 Longitudinal variations of salinity and suspended sediment concentration during high water, 19 July 1995, (TR = tidal range, Q = river discharge).

concentration in the turbidity maximum zone was greater than 250 mg/l. A sediment concentration over 600 mg/l was obtained from the discrete surface water samples from the turbidity maximum zone.

During the spring tide on 13 July 1995, the turbidity maximum was located 14.5 km from the mouth but close to the neap tide on 19 July 1995 this maximum migrated down estuary and located roughly at 11.6 km from the mouth (Table 6.2). A slight salinity stratification was observed at the lower estuary on the 17 and 19 July. This stratification was absent during the spring tide on 13 July when the whole section of the water column was fully mixed.

Table 6.2 Location of turbidity maximum during HW at different tidal ranges during low discharge

Date	Tidal range (m)	Discharge (m^3/s)	TM location (km)	Maximum concentration (mg/l)
13/7/95	8.28	0.86	14.5	> 250
17/7/95	7.31	0.91	12.7	> 250
19/7/95	5.46	0.94	11.6	> 250

6.2.3 Spatial surveys - September 1996

The results of spatial surveys for September 1996 are shown in Figures 6.9 - 6.12. A well developed turbidity maximum was observed in all of the four surveys. The centre of this maximum was located slightly upstream of the fresh-salt water interface (salinity = 1 ppt). As with the previous surveys, the location of the maximum migrated upstream with higher tidal ranges (Table 6.3). During these surveys the sediment concentration within the turbidity maximum zone was determined from the gravimetric analysis of the water samples which showed an increased concentration with higher tidal ranges. A surface maximum

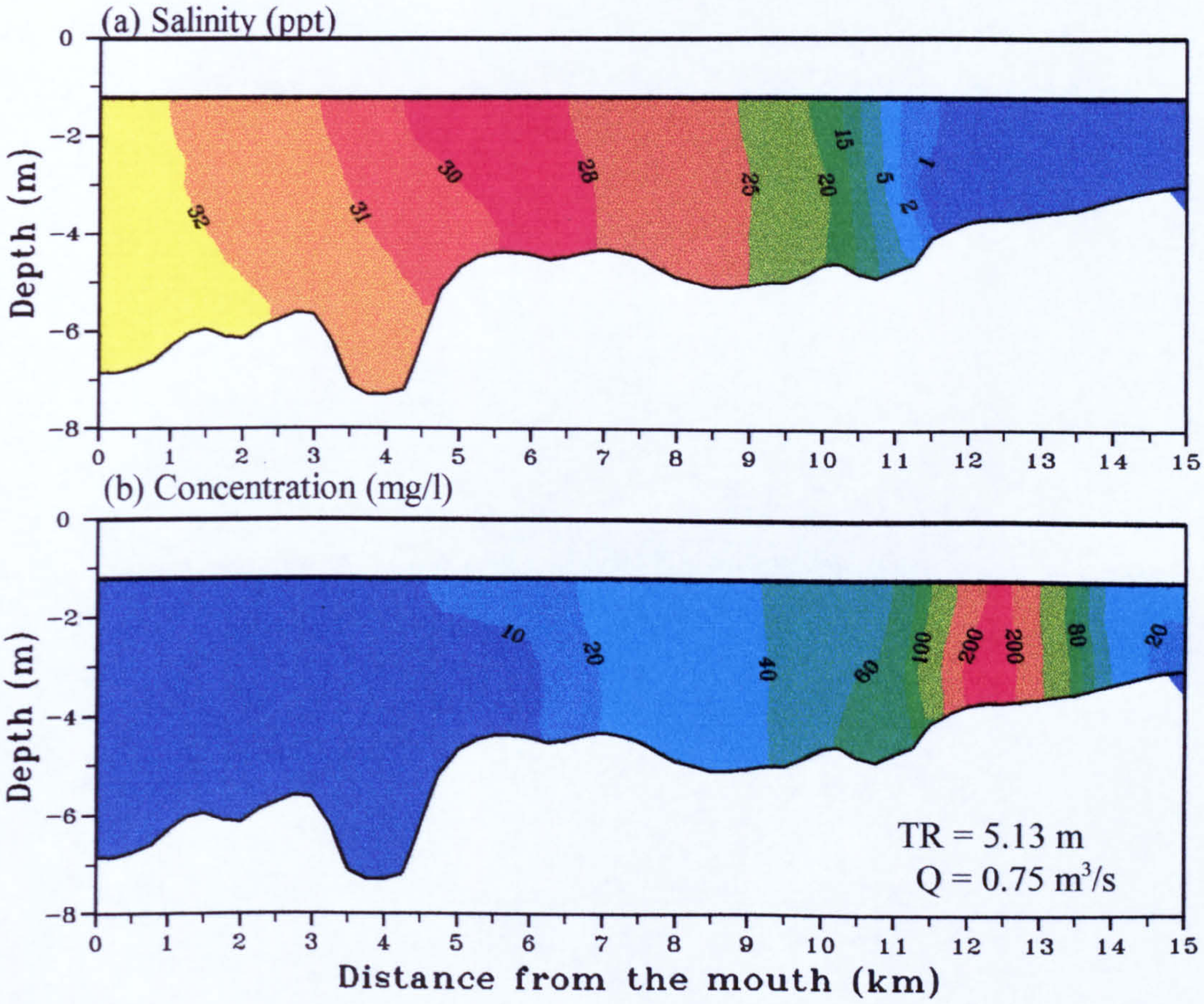

Figure 6.9 Longitudinal variations of salinity and suspended sediment concentration during high water, 10 September 1996, (TR = tidal range, Q = river discharge).

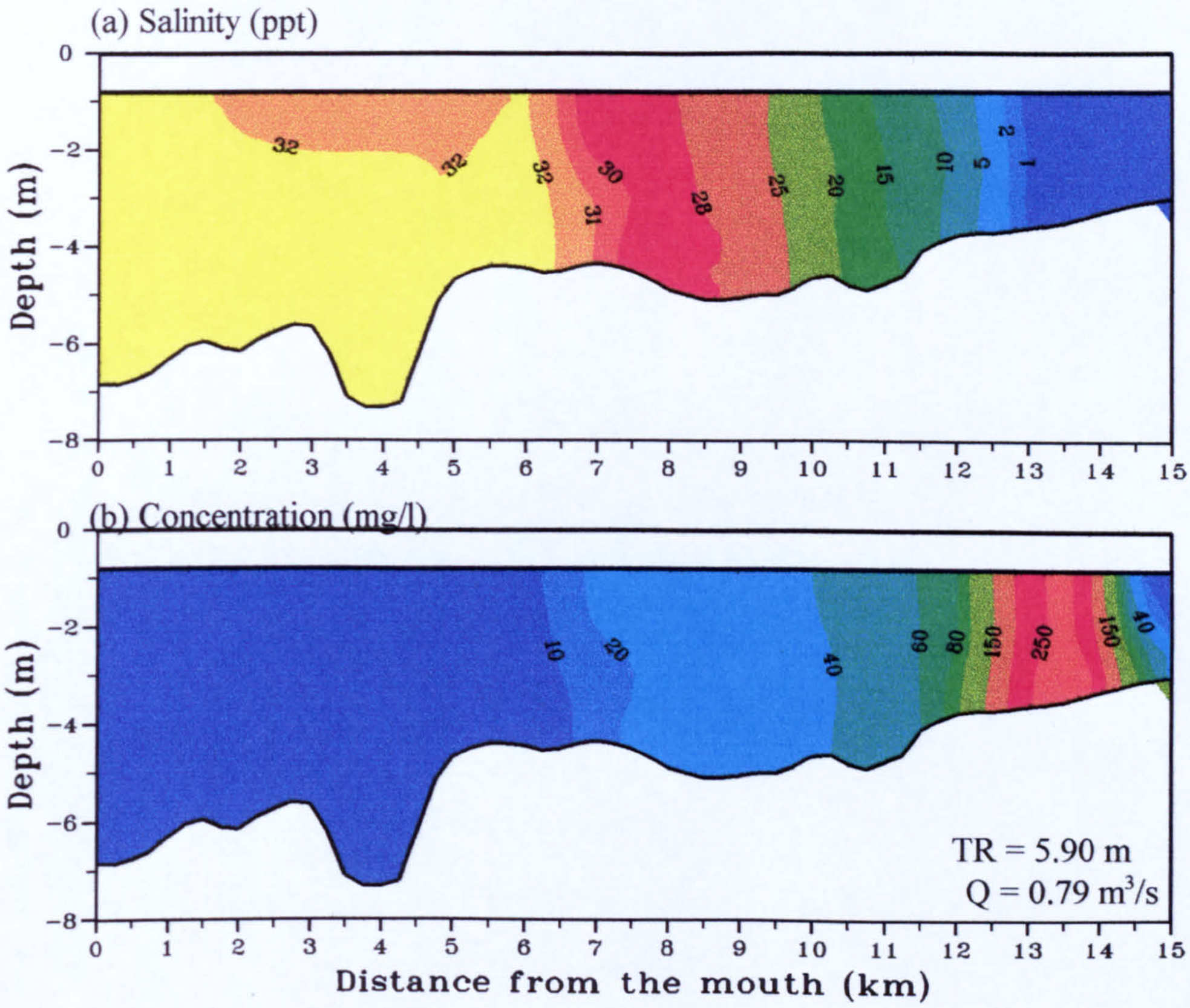

Figure 6.10 Longitudinal variations of salinity and suspended sediment concentration during high water, 11 September 1996, (TR = tidal range, Q = river discharge).

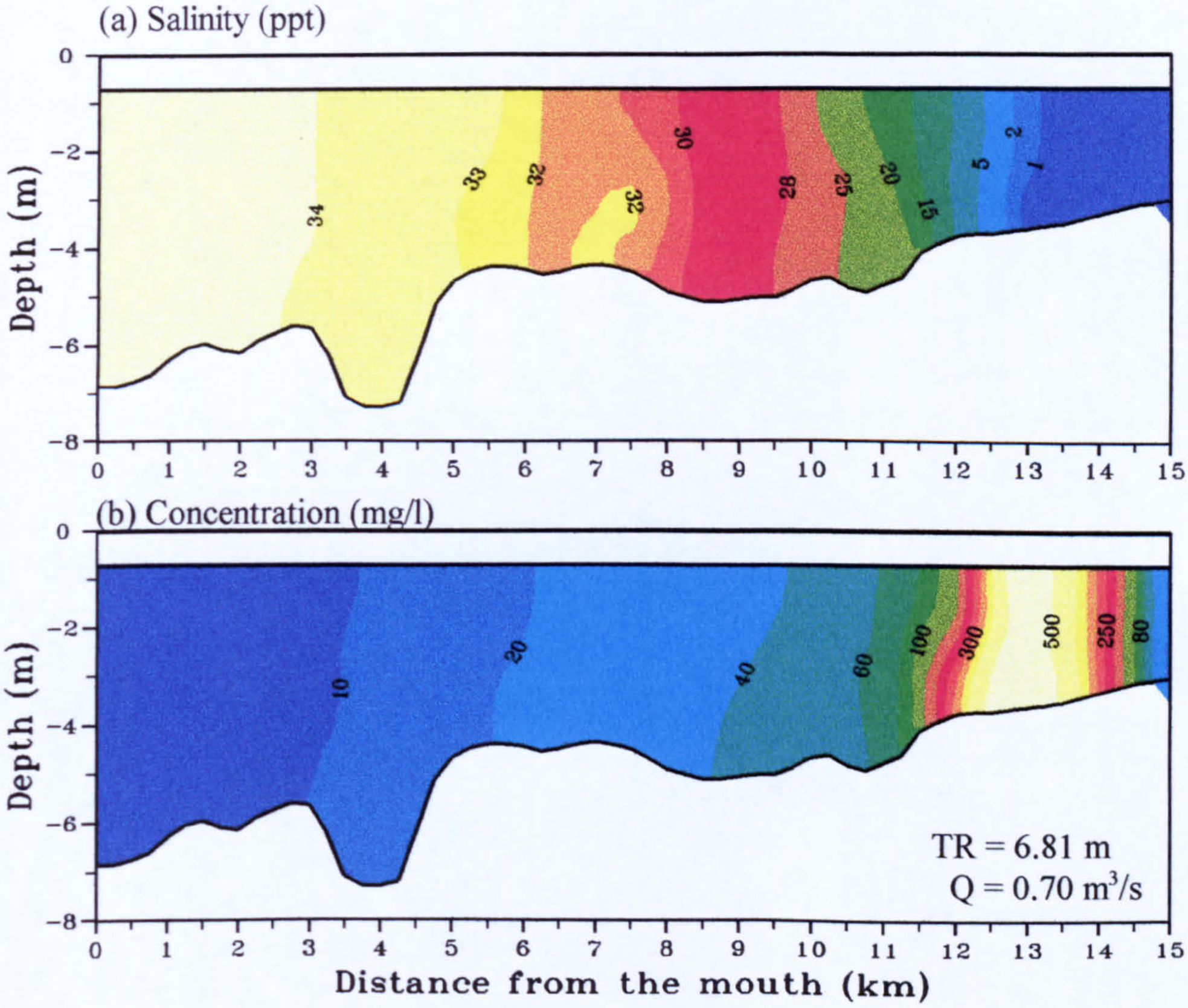

Figure 6.11 Longitudinal variations of salinity and suspended sediment concentration during high water, 13 September 1996, (TR = tidal range, Q = river discharge).

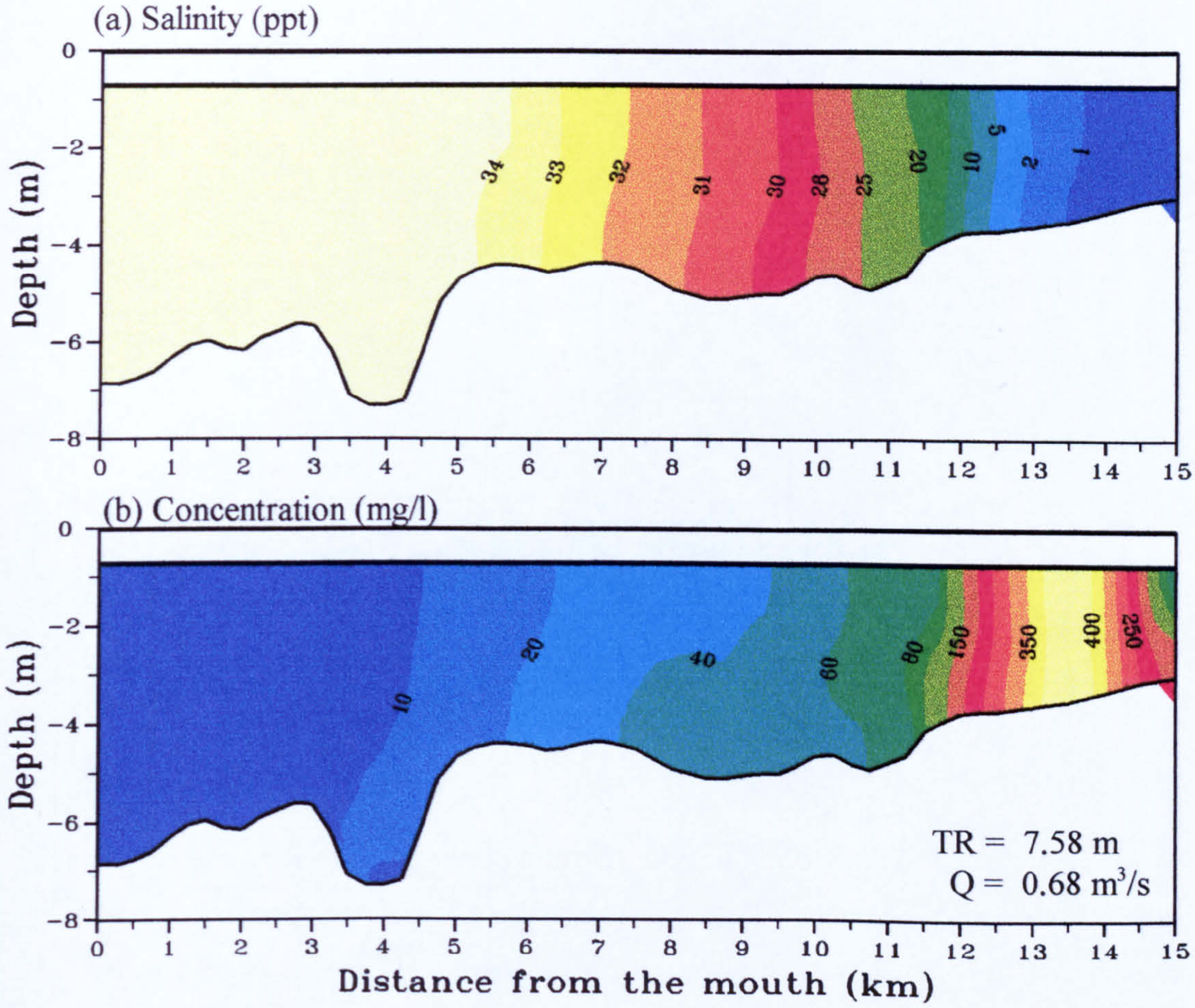

Figure 6.12 Longitudinal variations of salinity and suspended sediment concentration during high water, 15 September 1996, (TR = tidal range, Q = river discharge).

concentration of more than 600 mg/l was obtained from one of these samples.

The salinity contours show the estuary water column was fully mixed, except on the lowest tidal range where there was a slight stratification in the lower estuary.

Table 6.3 Location of turbidity maximum during HW at different tidal ranges during low discharge (September 1996)

Date	Tidal range (m)	Discharge (m^3/s)	TM location (km)	Maximum concentration (mg/l)
10/9/96	5.13	0.75	12.3	247
11/9/96	5.90	0.79	13.7	325
13/9/96	6.81	0.70	13.9	688
15/9/96	7.58	0.68	14.2	506

6.2.4 Depth-averaged results

The data on suspended sediment concentration, salinity and temperature for all the spatial surveys were depth-averaged and are plotted in Figures 6.13 - 6.15; all surveys showed a well developed turbidity maximum except on 28 and 30 September 1994 (Figure 6.13a&b). The peak sediment concentration in the turbidity maximum varied from around 20 mg/l to over 600 mg/l depending on the tidal range and the fresh water discharge. The maximum extended 2-3 km in length from a salinity of about 5 ppt at the seaward limit to salinity 0.3 ppt at the landward limit. At the seaward end, the concentration gradually decreased from its maximum until it reached the background values in the lower estuary. However, at the landward end of the turbidity maximum, there was a sharp boundary where the concentration decreased rapidly to its background value of less than 10 mg/l in the fresh water.

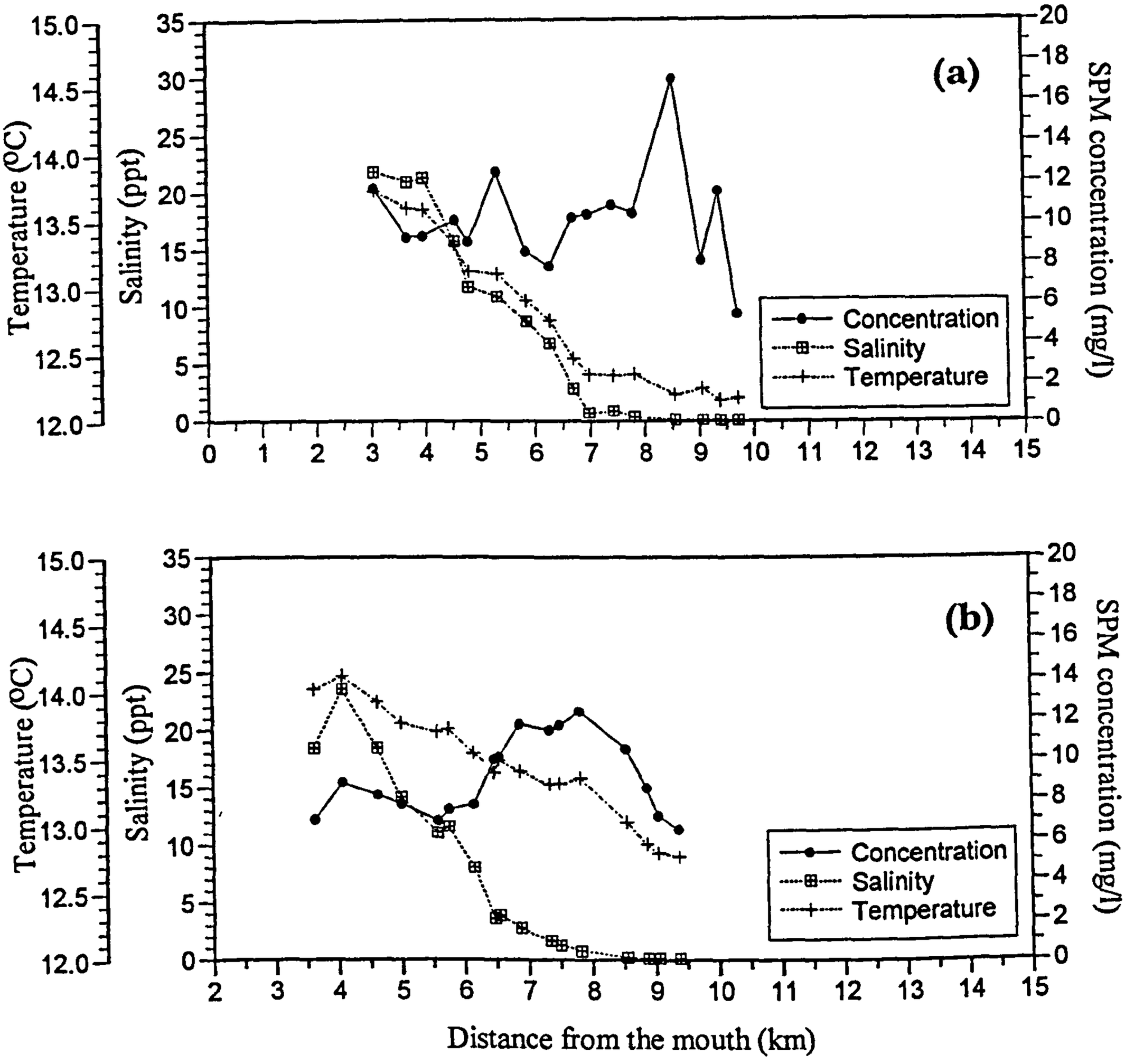

Figure 6.13 Depth-averaged variations of suspended sediment concentration, salinity and temperature along the longitudinal axis during high water for survey carried out in September-October 1994: (a) 28 September 1994; (b) 30 September 1994; (c) 1 October 1994; (d) 2 October 1994; and (e) 3 October 1994.

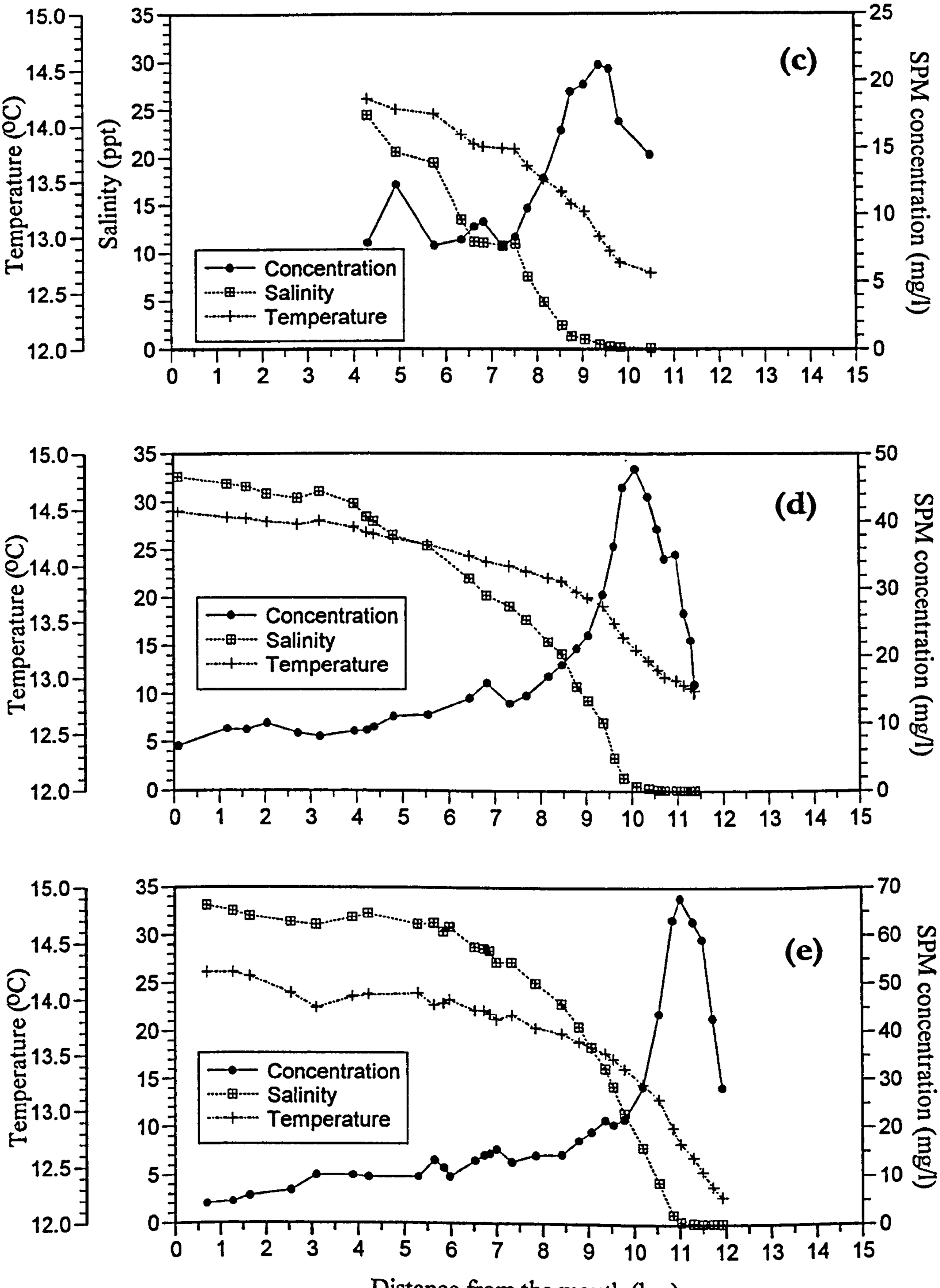

Figure 6.13 (continued)

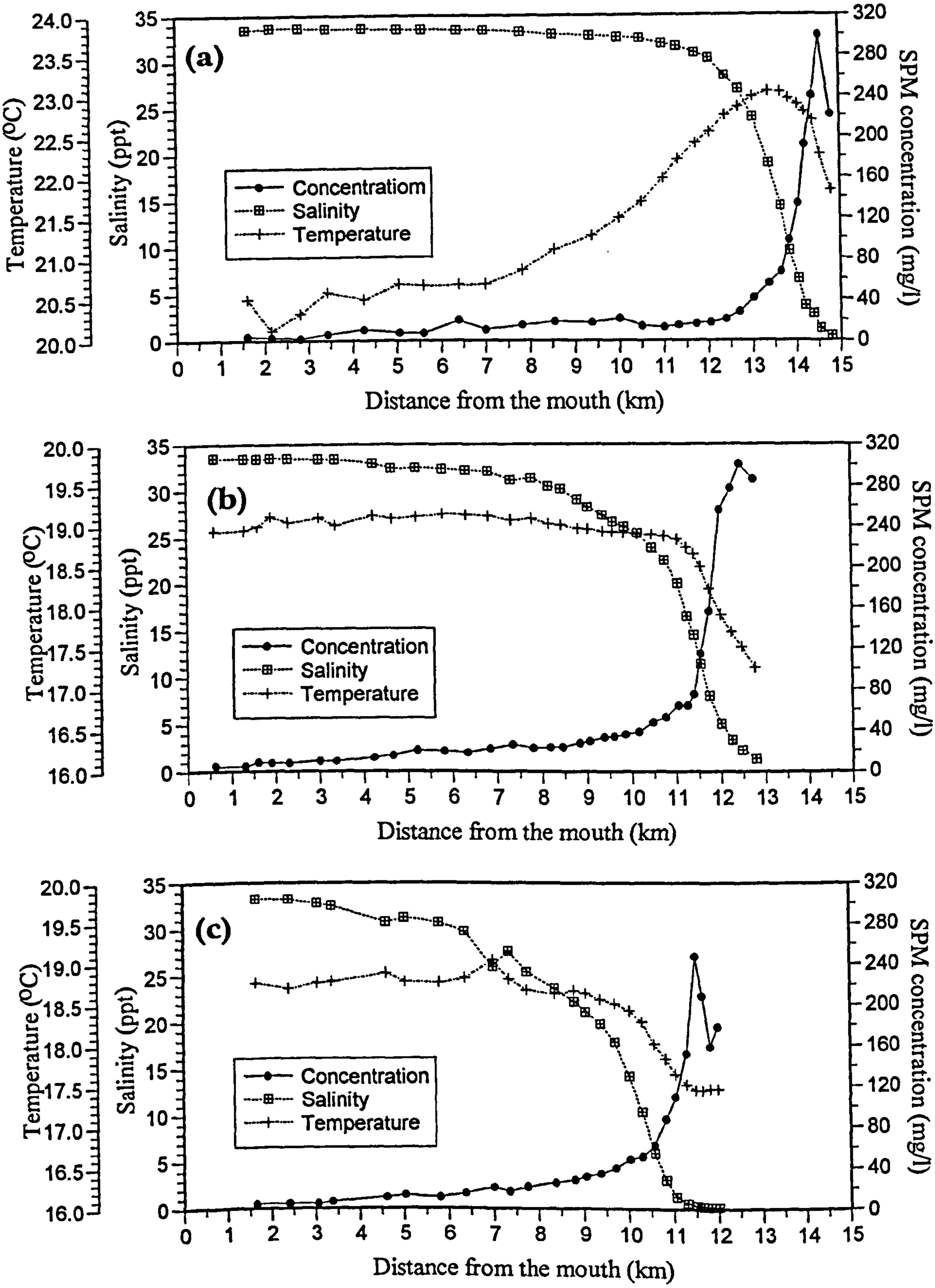

Figure 6.14 Depth-averaged variations of suspended sediment concentration, salinity and temperature along the longitudinal axis during high water for survey carried out in July 1995: (a) 13 July 1995; (b) 17 July 1995; and (c) 19 July 1995.

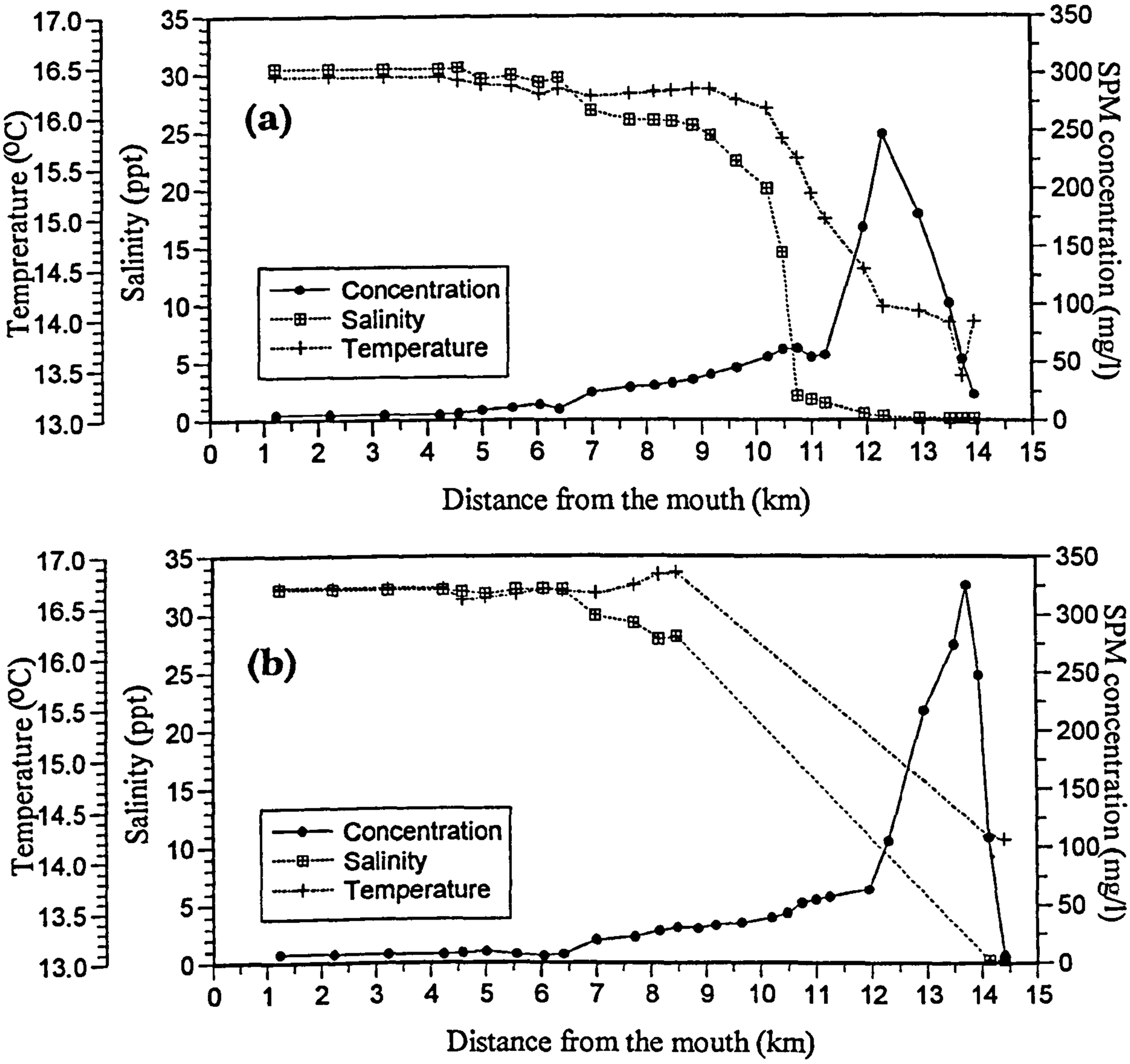

Figure 6.15 Depth-averaged variations of suspended sediment concentration, salinity and temperature along the longitudinal axis during high water for survey carried out in September 1996: (a) 10 September 1996; (b) 11 September 1996; (c) 13 September 1996; and (d) 15 September 1996.

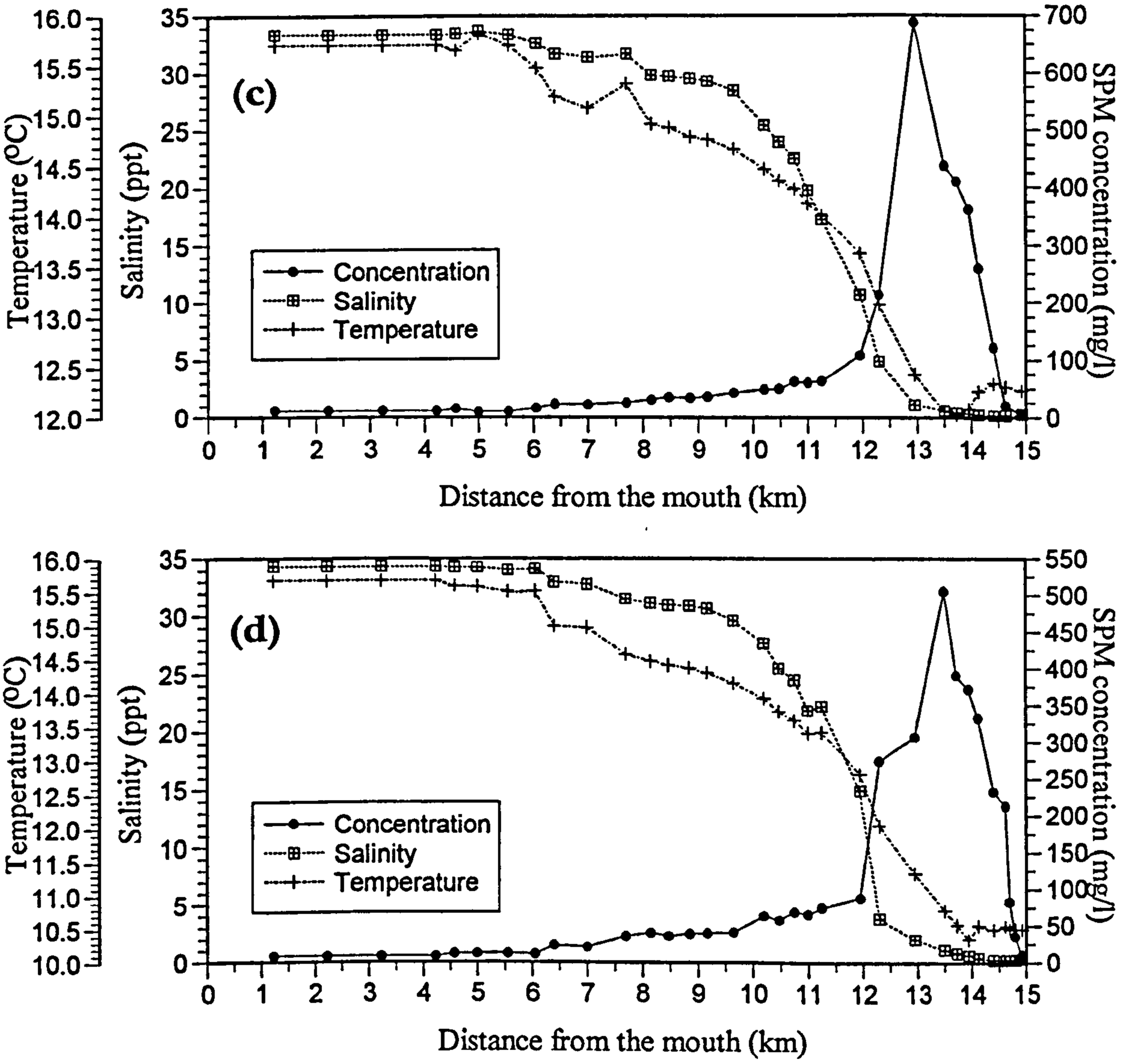

Figure 6.15 (continued)

Figures 6.13 - 6.15 also show the temperature of the estuary water which was warmer at the mouth and cooler near the head as a result of the mixing between a warmer sea water and a cooler fresh water. There was a 3 - 5^{0}C difference between sea water and fresh water temperature. The temperature did not change very much for most parts of the estuary, but close to the head within the turbidity maximum zone the temperature dropped sharply to its minimum value in the fresh water region. The drop in the temperature towards the estuary head was more rapid during higher river discharges and smaller tidal ranges (Figure 6.13a&b). All surveys shows that the occurrence of the turbidity maximum corresponded to the sudden drop of water temperature. On 13 July 1995, however, the reverse occurred when the temperature increased steadily from 20 ^{0}C at the mouth to a maximum of 23 ^{0}C near the head before it dropped at the turbidity maximum zone (Figure 6.14a). The sea water temperature was also slightly higher (about 1 ^{0}C) than on 17 and 19 July 1995. This shows a significant warming as the survey on the 13 was carried out after mid-day.

The limited data suggest that if the river discharge is fairly constant, during a neap-spring tidal cycle, the location of the turbidity maximum depends solely on the tidal range. Correlation coefficients, R^2, of 0.94 and 0.90 were obtained between the predicted tidal range and the location of the turbidity maximum from the estuary mouth for October 1994 and July 1995, respectively. A lower R^2 (0.81) was obtained for the surveys in September 1996. If the data for all the three surveys are combined, the tidal range only explains about 76 % of the variance in turbidity maximum location. A regression of turbidity maximum location against tidal height and river discharge results in a much better correlation i.e. an R^2 of 0.93. The location of the turbidity maximum can be predicted by the equation: $Y = 0.85x_1 - 0.49x_2 + 8.0$, where Y is the distance of turbidity maximum from the mouth (km), x_1 is the predicted tidal range (m), and x_2 is the river discharge (m^3/s).

6.3 Temporal SPM variations

In this section, results of SPM measurements made at anchor stations across transects T9

and T5 in the lower estuary are presented. As SPM dynamics vary according to the spring-neap tidal cycle and to the fresh water discharge, separation will be made between the measurements carried out under different tidal conditions and fresh water discharges. In October 1994, measurements were made during an average river discharge and during spring tides only, while in July 1995 and September 1995, they were made during low river discharges for both spring and neap tides. In addition, SPM measurements were made in the upper estuary near St. Clears for one tidal cycle only, during a low discharge spring tide. No measurements were made near St. Clears during a neap tide as the saline intrusion does not extend that far.

6.3.1 SPM variations over spring tides in the lower estuary - average river discharge

SPM and tidal velocity measurements for spring tides were made on 5 and 6 October 1994 at five anchor stations across transect T9 (see Figure 3.2 for positions). The tidal ranges on 5 October were 8.2 m for the ebb and 8.6 m for the flood, and on 6 October they were 8.8 m for the ebb and 9.0 m for the flood. The fresh water discharges were 4.3 m^3/s and 4.1 m^3/s on the 5 and 6 October, respectively.

Typical contour plots of tidal velocity and SPM concentration over depth and time are shown in Figure 6.16, while Figure 6.17 shows the depth averaged values for SPM and current velocity for the ebb and the flood of the same tidal cycles. These plots are for 6 October, station 1, which was located in the main ebb channel. The flood was characterised by fast currents exceeding 2.5 m/s near the surface with instantaneous resuspension of bed sediment giving SPM concentrations of over 1000 mg/l. At 1600 hours (Figure 6.17), an interesting phenomenon can be seen, where the SPM dropped from 1000 mg/l down to below 100 mg/l over a short period, while the currents were still strong (over 1.4m/s). The SPM concentration reduced to less than 30 mg/l during HW slack. During the ebb the maximum SPM concentration did not coincide with the peak flow which was about 1.4 m/s (Figure 6.17), the maximum SPM concentration lagged the peak flow by about 1 hour when the velocity had reduced to 0.9 m/s. Similar phenomena can be seen on 5 October

explanation: => Concentration dropped to <100mg/l due to the settling of the coarse to sand particles as the the water depth increase, but current still strong.

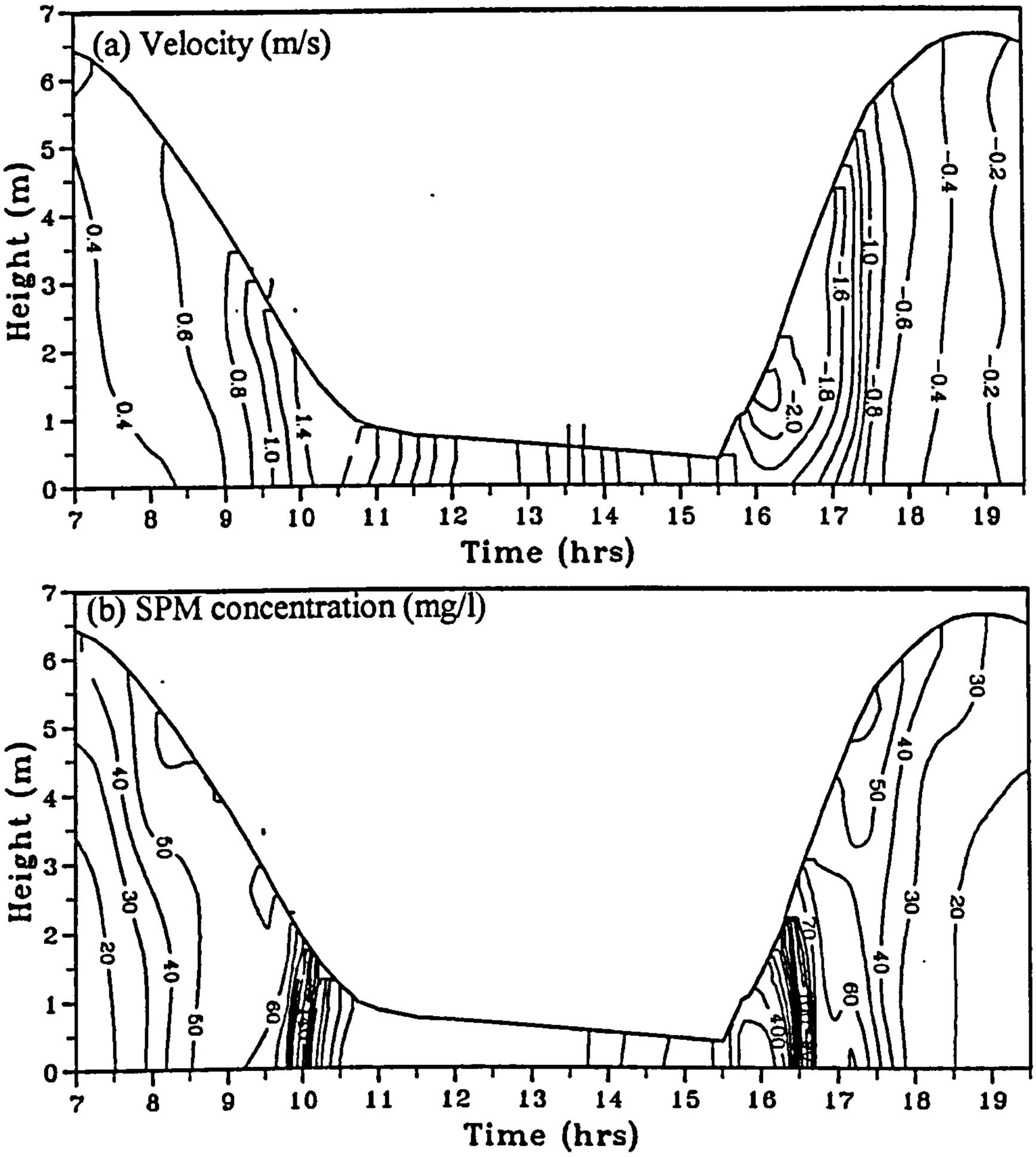

Figure 6.16 Time series contour plots of tidal velocity and suspended sediment concentration during a spring tide at station 1, transect T9, 6th October 1994.

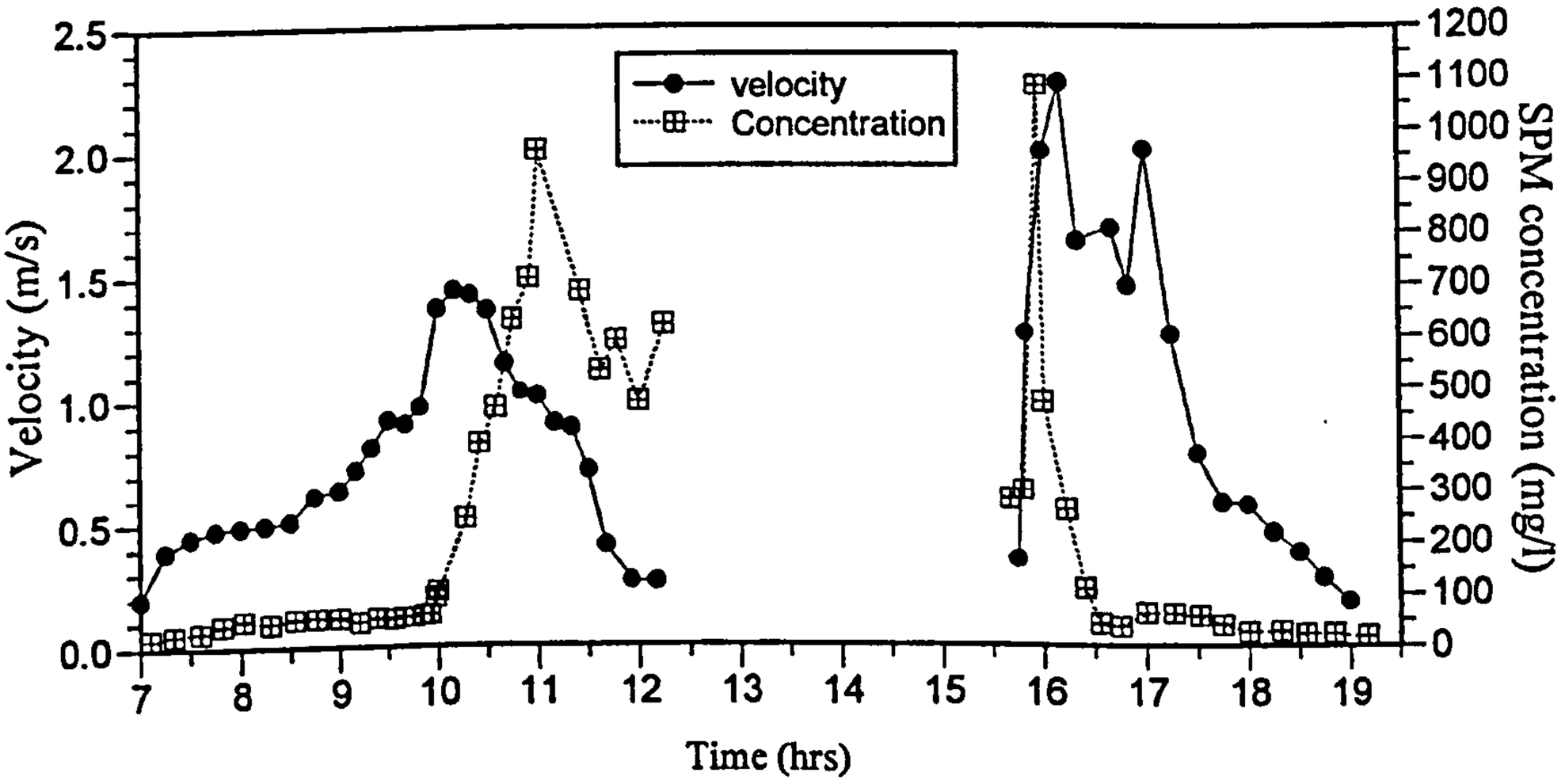

Figure 6.17 Depth averaged velocity and suspended sediment concentration (SPM) during a spring tide at station1, transect T9, 6th October 1994.

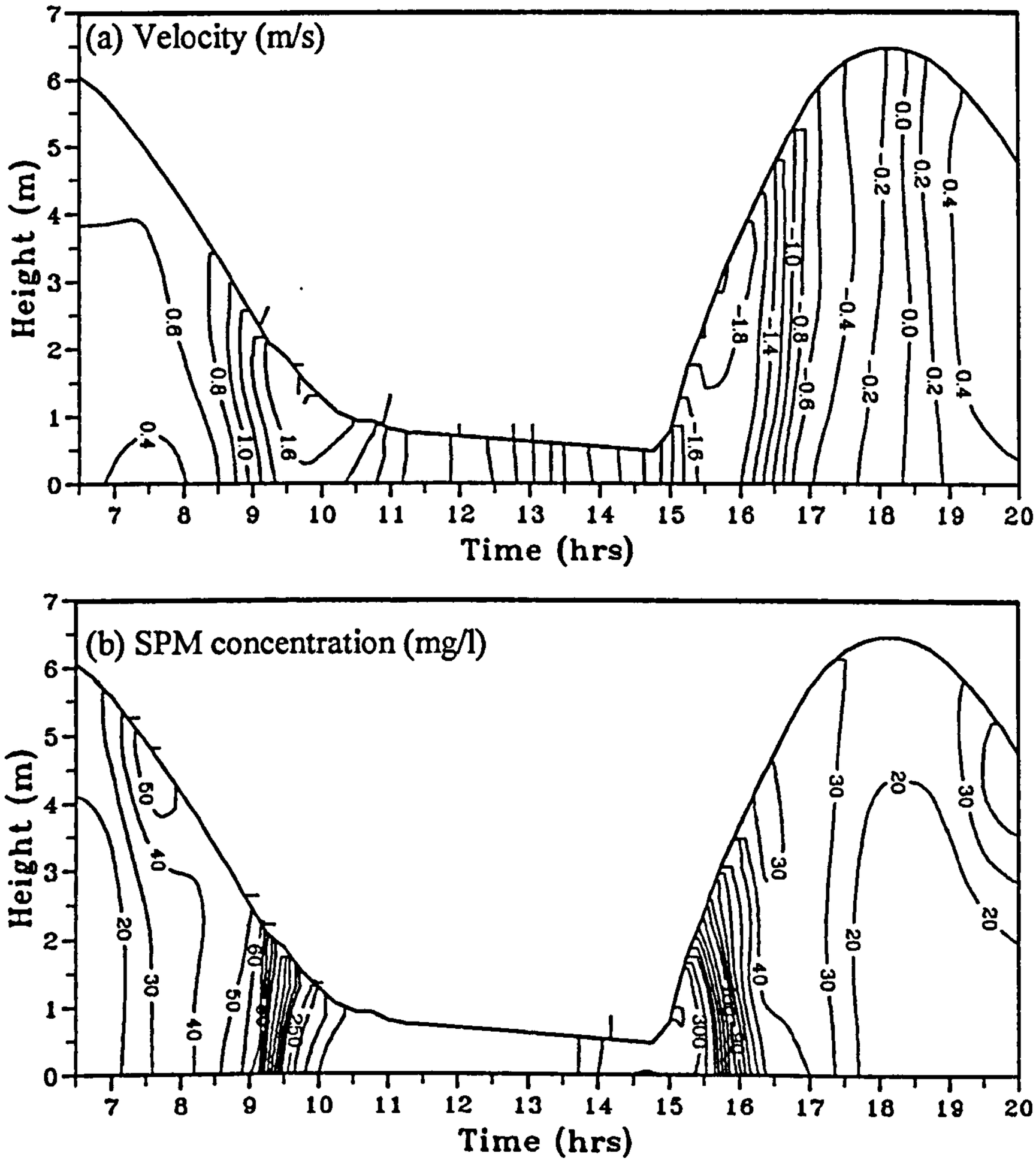

Figure 6.18 Time series contour plots of tidal velocity and suspended sediment concentration during a spring tide at station 1, transect T9, 5th October 1994.

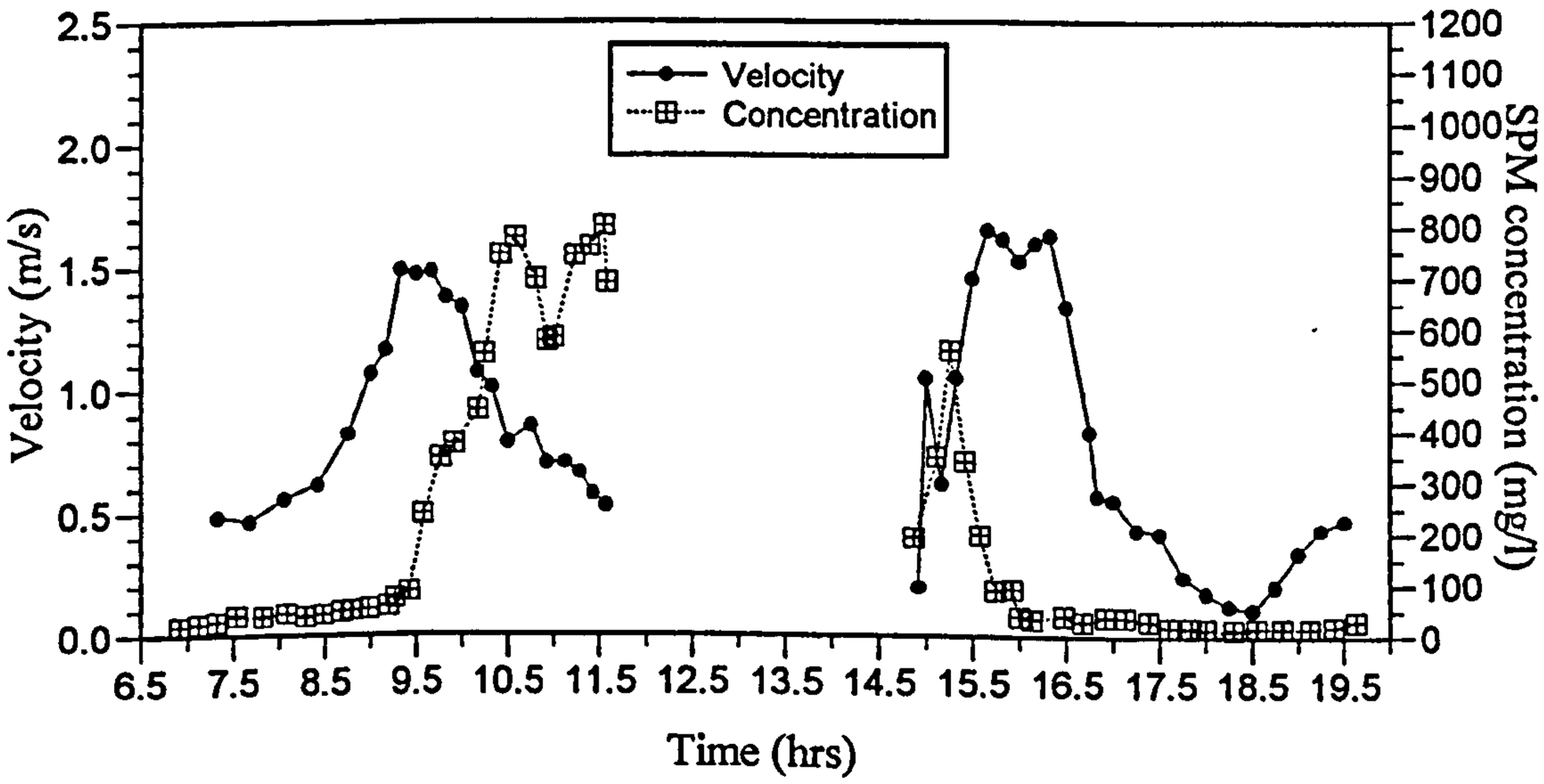

Figure 6.19 Depth averaged velocity and suspended sediment concentration (SPM) during a spring tide at station 1, transect T9, 5 October 1994.

1994 (Figures 6.18 and 6.19) but with smaller values of SPM concentration and current velocity.

One distinctive feature shown by Figure 6.16 is a reversed sediment stratifications whereby the SPM concentrations in the water near the surface are higher then in the water below it. These stratifications occur at about 2/3 of the flood with a concentration near the surface is over 60 mg/l and at the bottom is about 40 mg/l (this stratification is not seen at other stations across the estuary), and again at HW slack with a concentration about 30 mg/l near the surface and less than 20 mg/l at the bottom. On 5 October 1994 at station 1, the reversed sediment stratification was observed only at high water slack (Figure 6.18).

The time series contour plots for other stations across the estuary are shown in Figures C.01 and C.02 in Appendix C. At these stations, which were located on the inter-tidal sand flats, the velocities were less than at station 1 and so were the SPM concentrations. However they all show similar features with highest concentrations recorded in the late ebb just before the stations dried out and in the early stage of the flood tide. The reversed sediment stratification during high water as observed at station 1 was less clearly seen at these stations.

The development of the reversed sediment stratification is more clearly illustrated by Figure 6.20 which shows the cross estuary contour plots for SPM at different stages of the tide for 6 October 1994. The dots in the figure show the measurement points at the five stations across the estuary with station one in the deepest channel on the left hand side (looking down estuary). During the flood, this stratification was first observed at Station 1 at HW - 1.20 hours (Figure 6.20c) when the depth-averaged velocity dropped to below 0.3 m/s, and persisted throughout HW (Figure 6.20d-h). At the beginning of the ebb, the strongest reversed sediment stratification was observed at station one and to a lesser extend at station 2, but stratification was less obvious at other stations across the estuary (Figure 6.20i-l). This stratification continued for almost 2 hours after HW and disappeared at about mid-ebb (Figure 6.20n), by which time the depth-averaged velocity exceeded 0.5 m/s. Thus, there is an asymmetry in the stratification where it persists longer during the ebb than

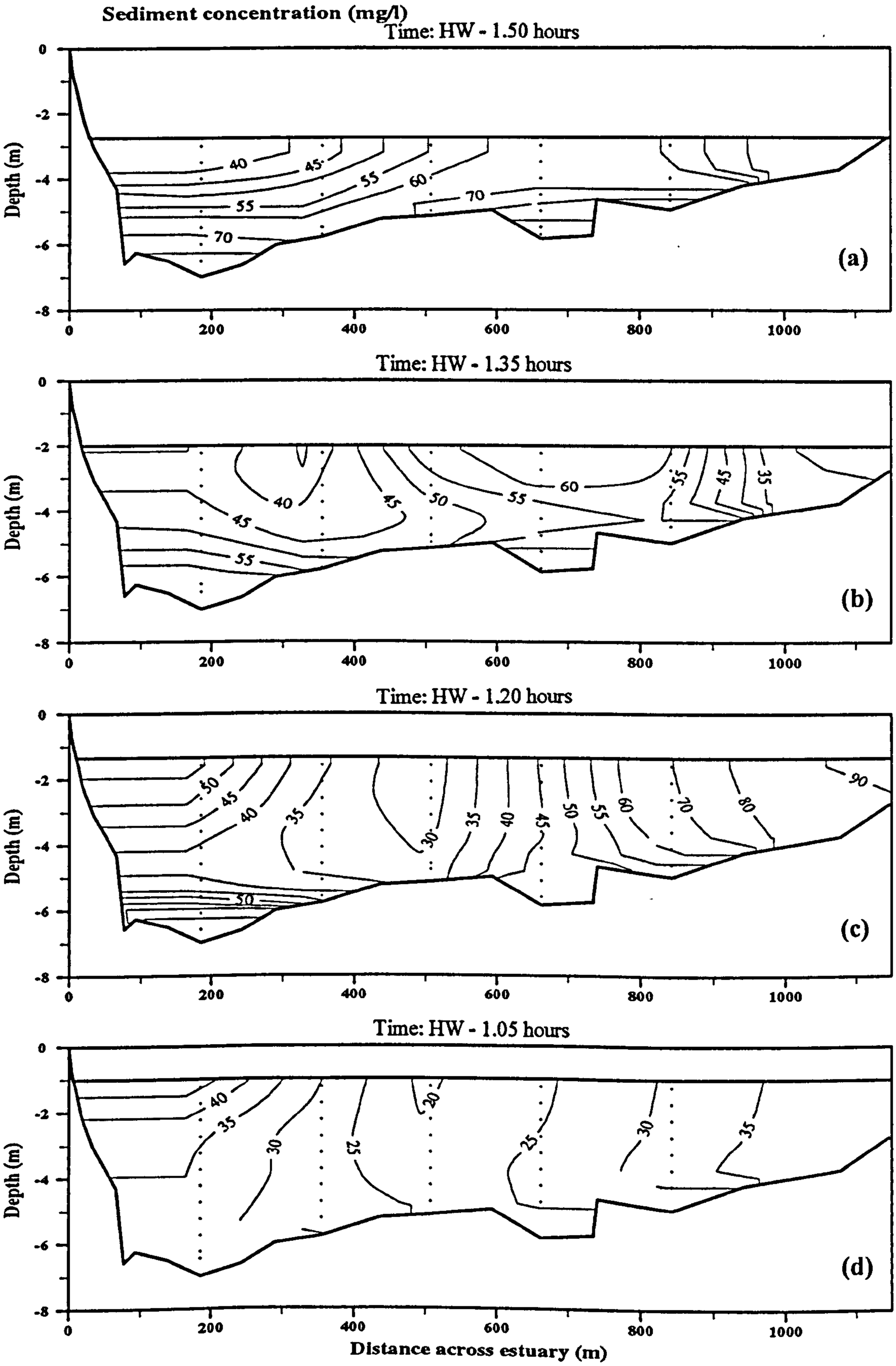

Figure 6.20 Cross estuary contour plots of suspended sediment concentration (mg/l) at different stages of the tide, 6 October 1994.

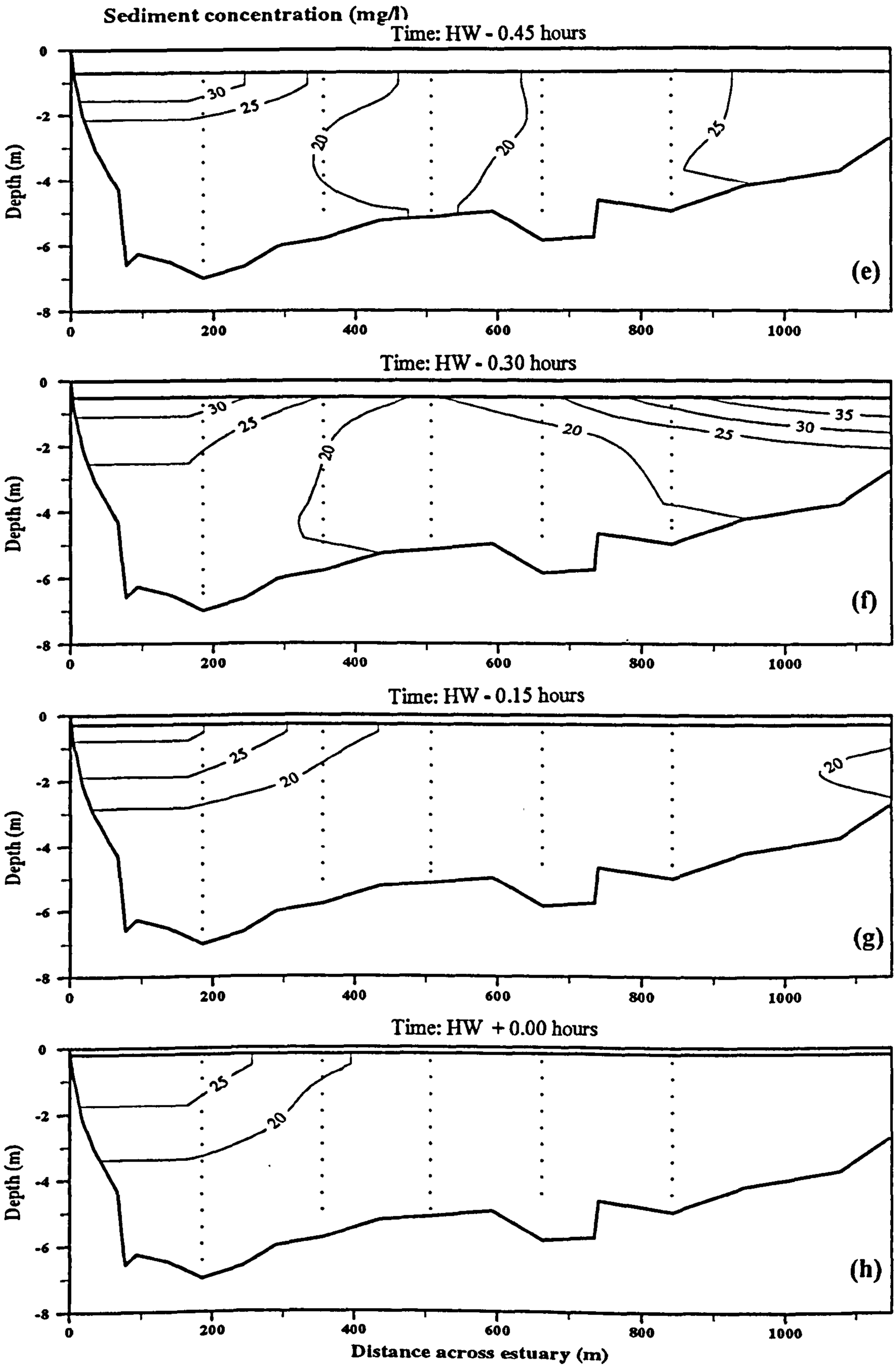

Figure 6.20 (continued)

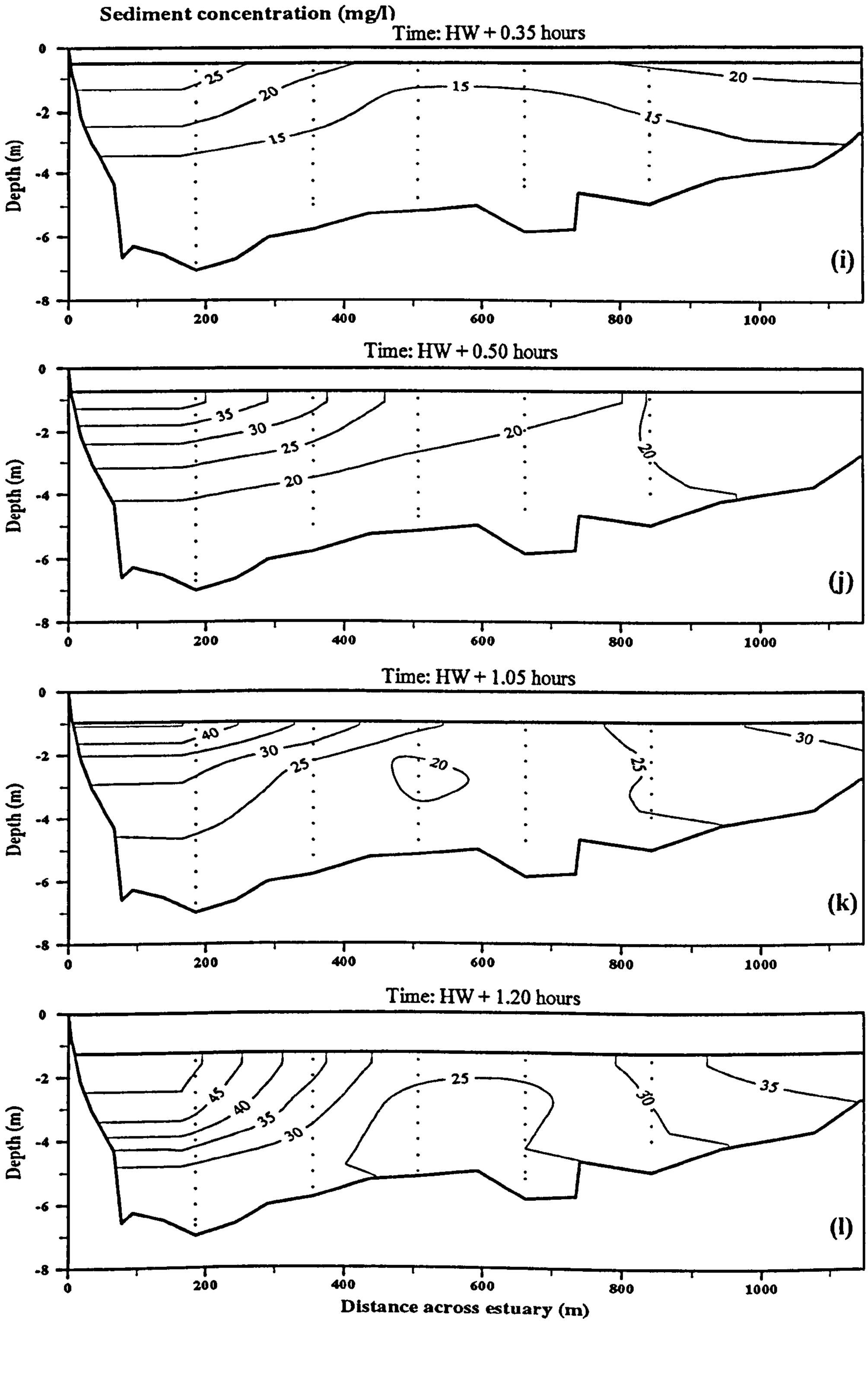

Figure 6.20 (continued)

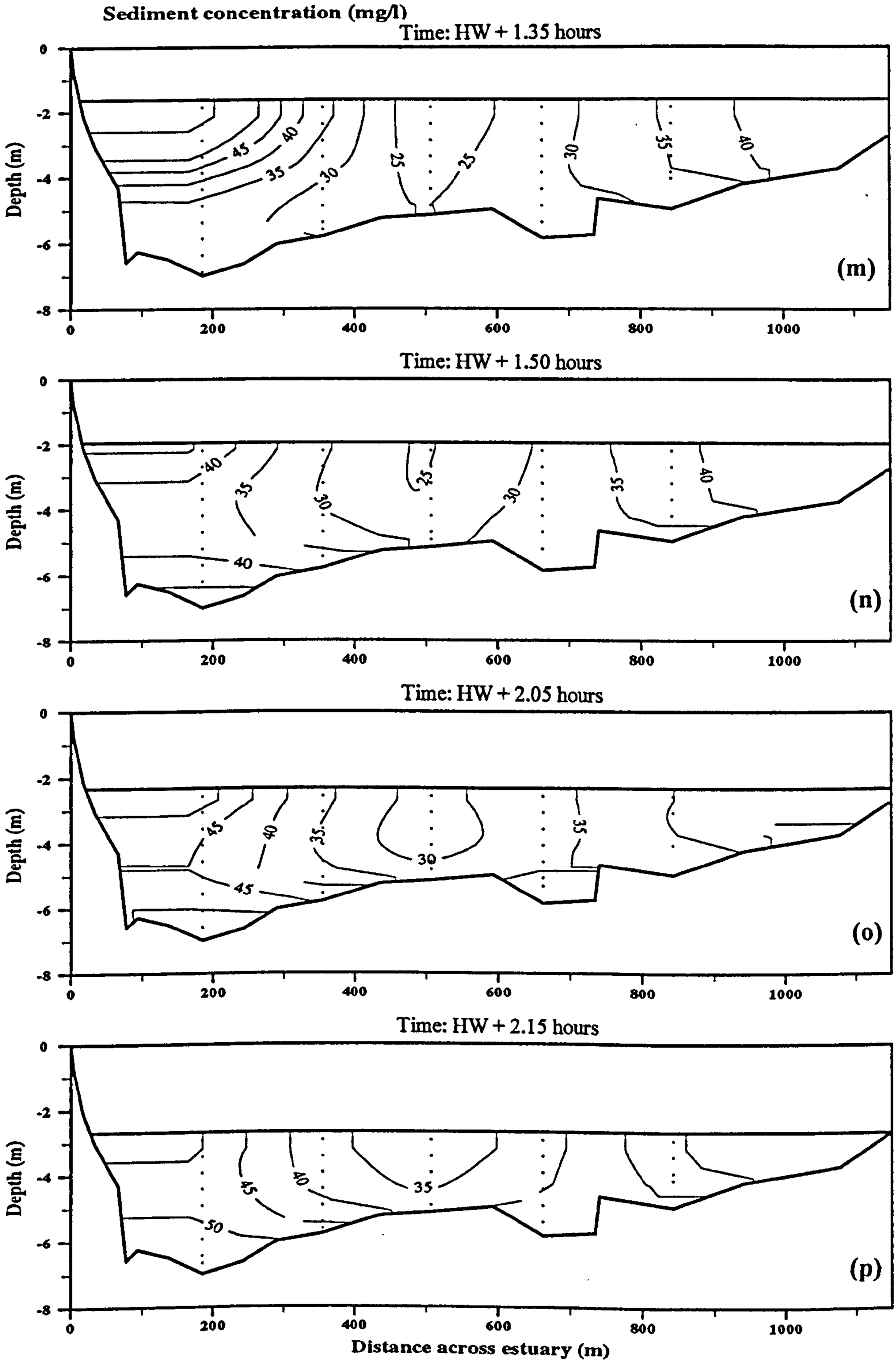

Figure 6.20 (continued)

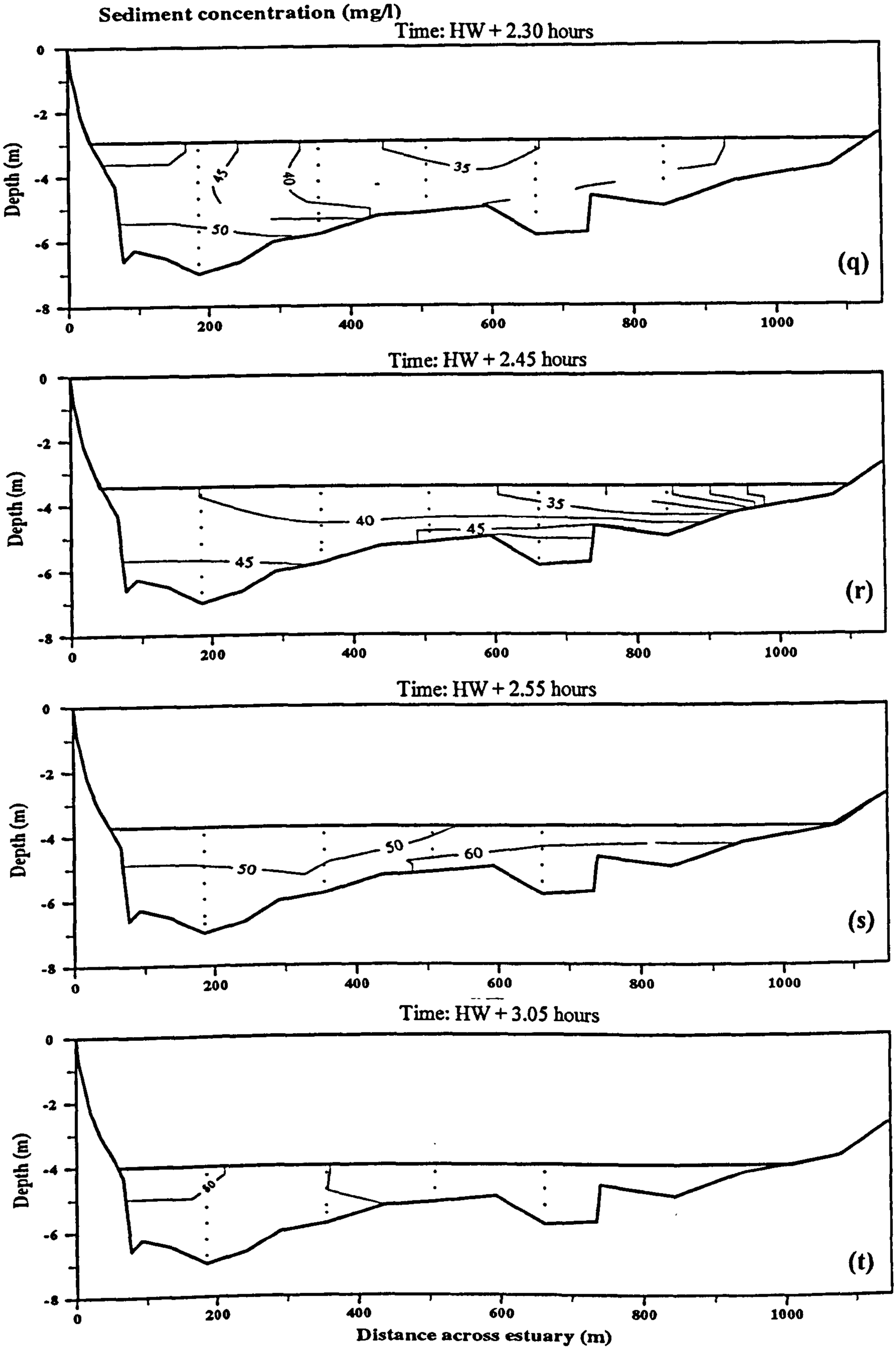

Figure 6.20 (continued)

during the flood. A similar phenomenon but to a lesser degree was also shown by the measurements made on 5 October 1994 (Figure C.03, Appendix C).

6.3.2 SPM variations over spring tides in the lower estuary - low river discharge

The spring tide SPM variation during a low river discharge can be seen from the measurements made at anchor station 1, transect T5 on 13 September 1995 (Figure 6.21). The tidal range was 7.6 m while the river discharge was 0.53 m^3/s. The vertical distributions of tidal velocity and SPM concentration over depth and time show a very fast flood current exceeding 1.8 m/s over a short time period during the early flood, followed by the simultaneous resuspension of bottom sediment with peak SPM concentration over 600 mg/l. The SPM concentration was reduced to less than 20 mg/l at high water slack and gradually increased as the ebb flow became stronger. The maximum SPM concentration of over 600 mg/l was again recorded 4.5 hours after HW (at 1400 hours), but the maximum SPM concentration did not coincide with peak ebb flow (1.0 m/s, Figure 6.22). The concentration lagged the peak flow by approximately 1.5 hours when currents had declined to 0.7 m/s. So local resuspension causes the peak suspended sediment concentration on the flood but not on the ebb. The reversed SPM stratification as observed during the high river discharge was not seen during this measurement.

The time series contour plots of SPM concentrations for other stations across the estuary are shown in Figure C.04 (Appendix C) which show the same features as observed at Station 1. However the peak SPM concentrations for the stations located on the sand flat (Stations 3 and 4 for Transect T5 are much less than at station 1. Similarly on smaller tidal ranges, the concentrations are much reduced at all stations across the estuary (Figures C.05 and C.06, Appendix C). The contour plots for stations 1-7, transect T9 for a spring tidal cycle is shown in Figure C.07, in Appendix C. At this transect the peak SPM concentrations during early flood and late ebb at stations located in the main channels were very low i.e. less 300 mg/l. This may be related to the changes in the channel morphology (which has became wider), thus reduced the flow velocities and the ability of currents to resuspend the

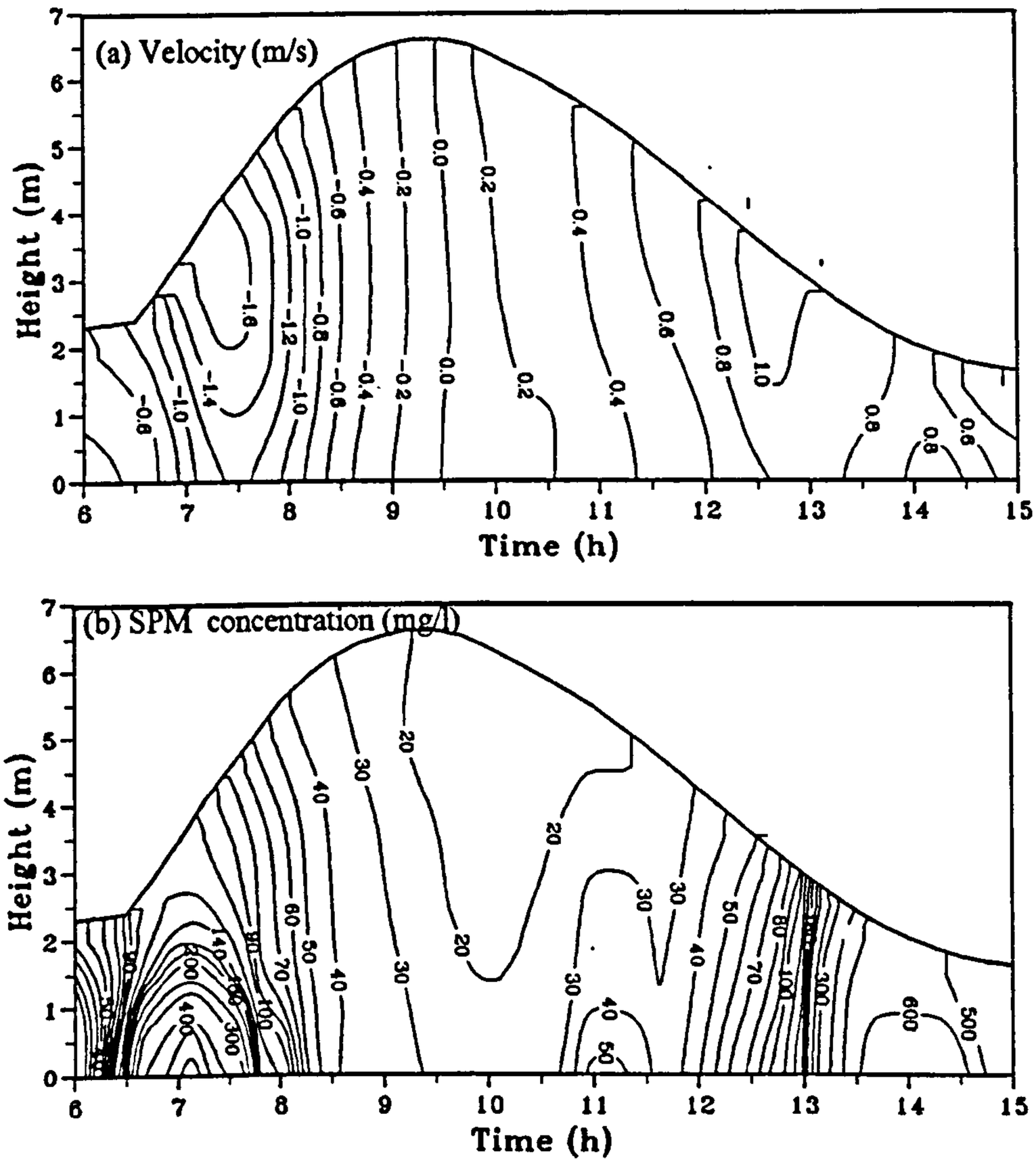

Figure 6.21 Time series contour plots of tidal velocity and suspended sediment concentration during a spring tide at station 1, transect T5, 13th September 1995.

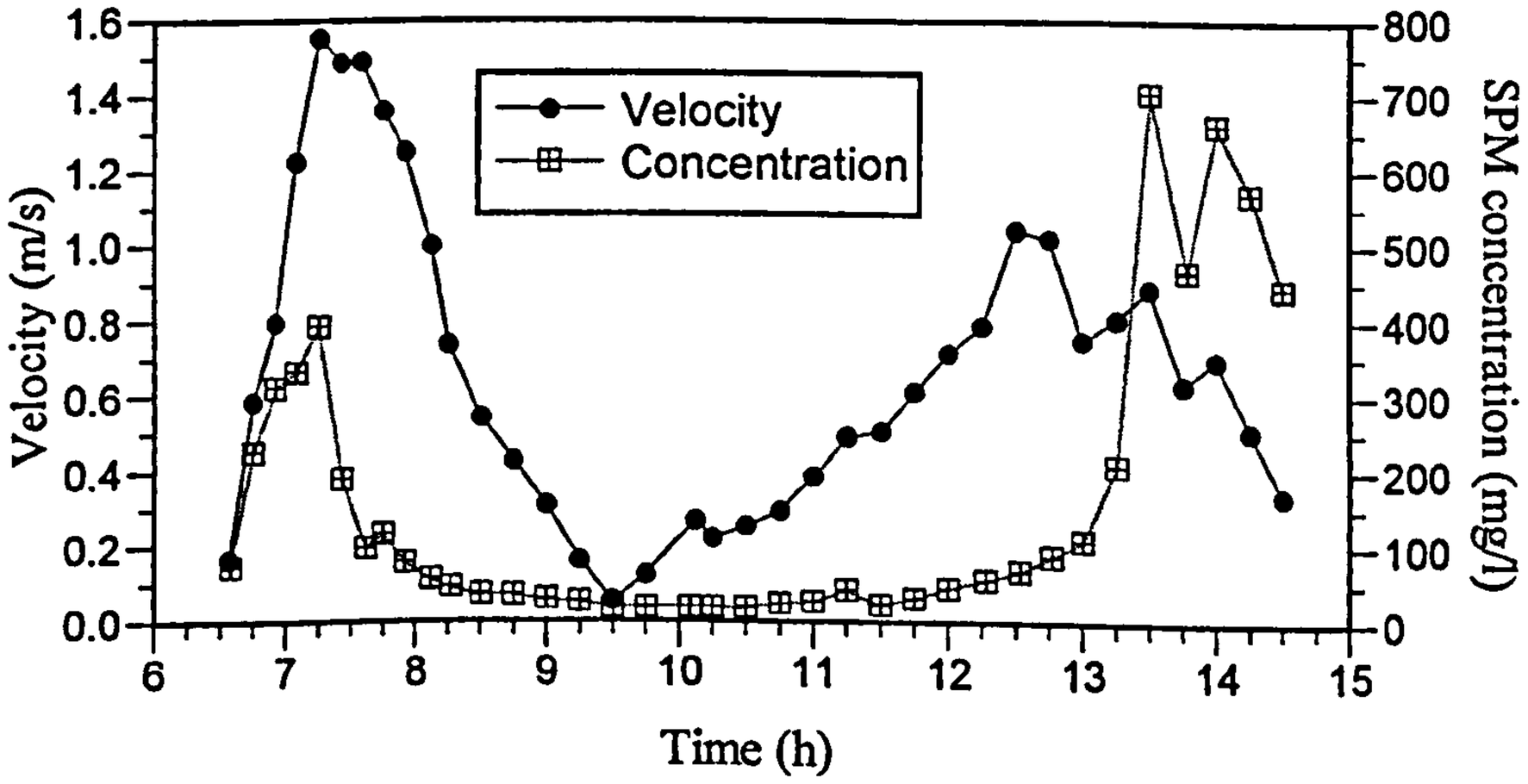

Figure 6.22 Depth averaged velocity and suspended sediment concentration at station 1, transect T5, 13th September 1995.

bed sediments.

Figure 6.23 shows SPM variation across the estuary at different stages of the tidal cycle during a spring tide on 16 July 1995. As expected the concentration increased closer to the bed and decreased away from the bed. There was little variation in sediment concentration across the estuary during the early stage of the flood when flow was concentrated within the main channel (Figure 6.23a-d), concentration then gradually reduced as the flood progressed. As the water level increased and the intertidal sand flat was covered during the mid-flood, a slightly higher concentration was observed at the stations on the sand flat (Figure 6.23e-i). At HW slack, the concentration was the same across the estuary with SPM values around 15 mg/l (Figure 6.23j). As ebbing progressed, the SPM concentration in the main channel gradually increased until all flow was confined within the channel, while stations on the sand flat showed very little increase in SPM concentration up to the stage when it was dried out (Figure 6.23k-r).

6.3.3 SPM variations over neap tides in the lower estuary - low river discharge

For the neap tide, the data are presented for the measurements made on 20 July 1995 (transect T9) and 19 September 1995 (transect T5). On 20 July 1995, the tidal range was 4.5 m and the river discharge was 0.8 m^3/s. The tidal range on 19 September 1995 was 3.0m while the river discharge was 0, 4 m^3/s.

Figure 6.24 shows the time series contour plots of velocities and SPM concentration during a neap tide at anchor station 1, transect T9 on 20 July 1995. The tidal velocities are less than on a spring tide, and less markedly asymmetrical than on springs. The depth-averaged velocities show a maximum value of 0.79 m/s for the flood and 0.66 m/s for the ebb (Figure 6.25). The vertical profiles of SPM concentration show very little variation throughout the tidal cycle with subdued peaks barely exceeding 40 mg/l during the flood and 90 mg/l during the ebb. The peak SPM concentration during the ebb lags the peak velocity by about 1.5 hours, half an hour later than that observed on the spring tide. There

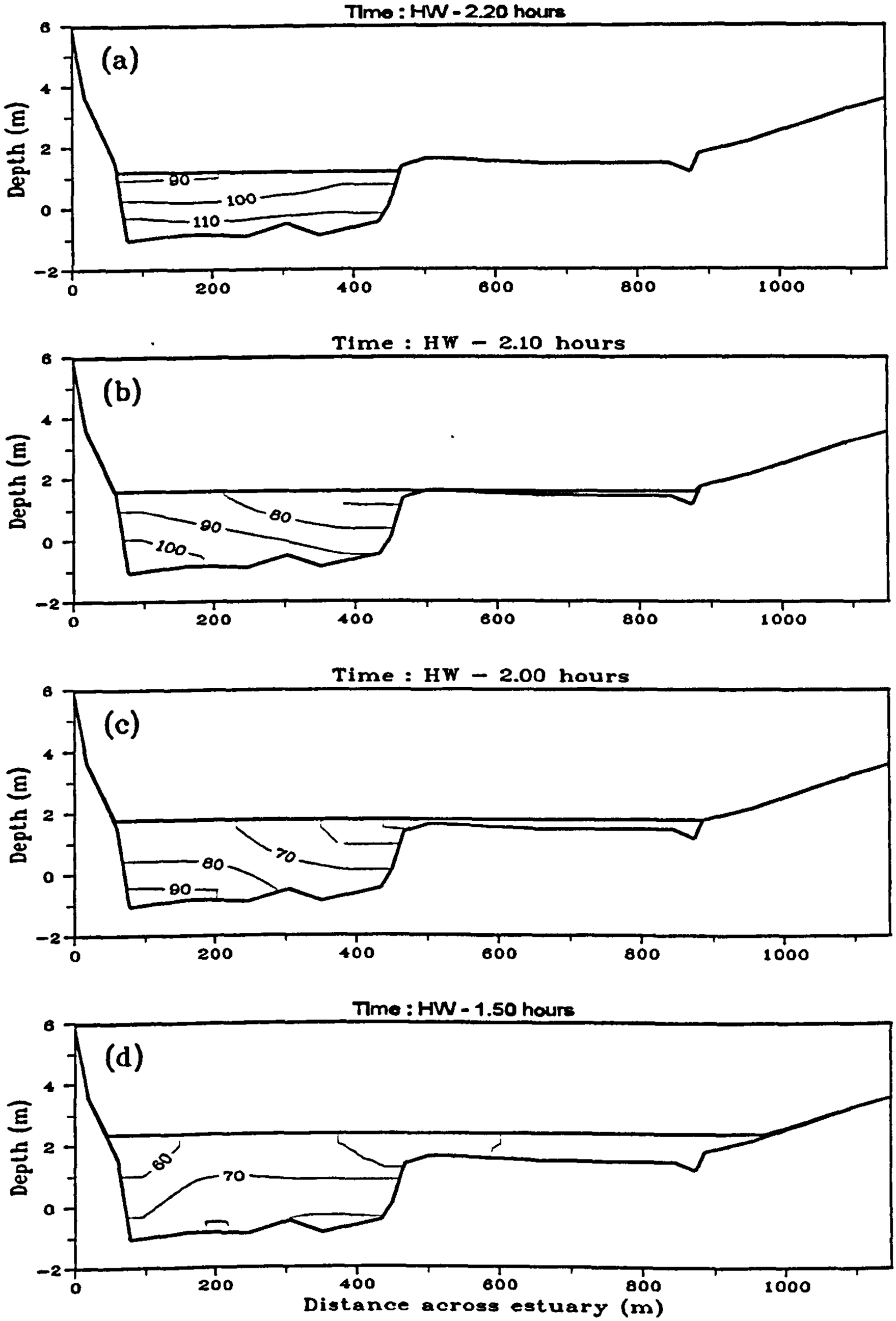

Figure 6.23 Cross estuary contour plots of suspended sediment concentration (mg/l) at different stages of the tide, 16th July 1995.

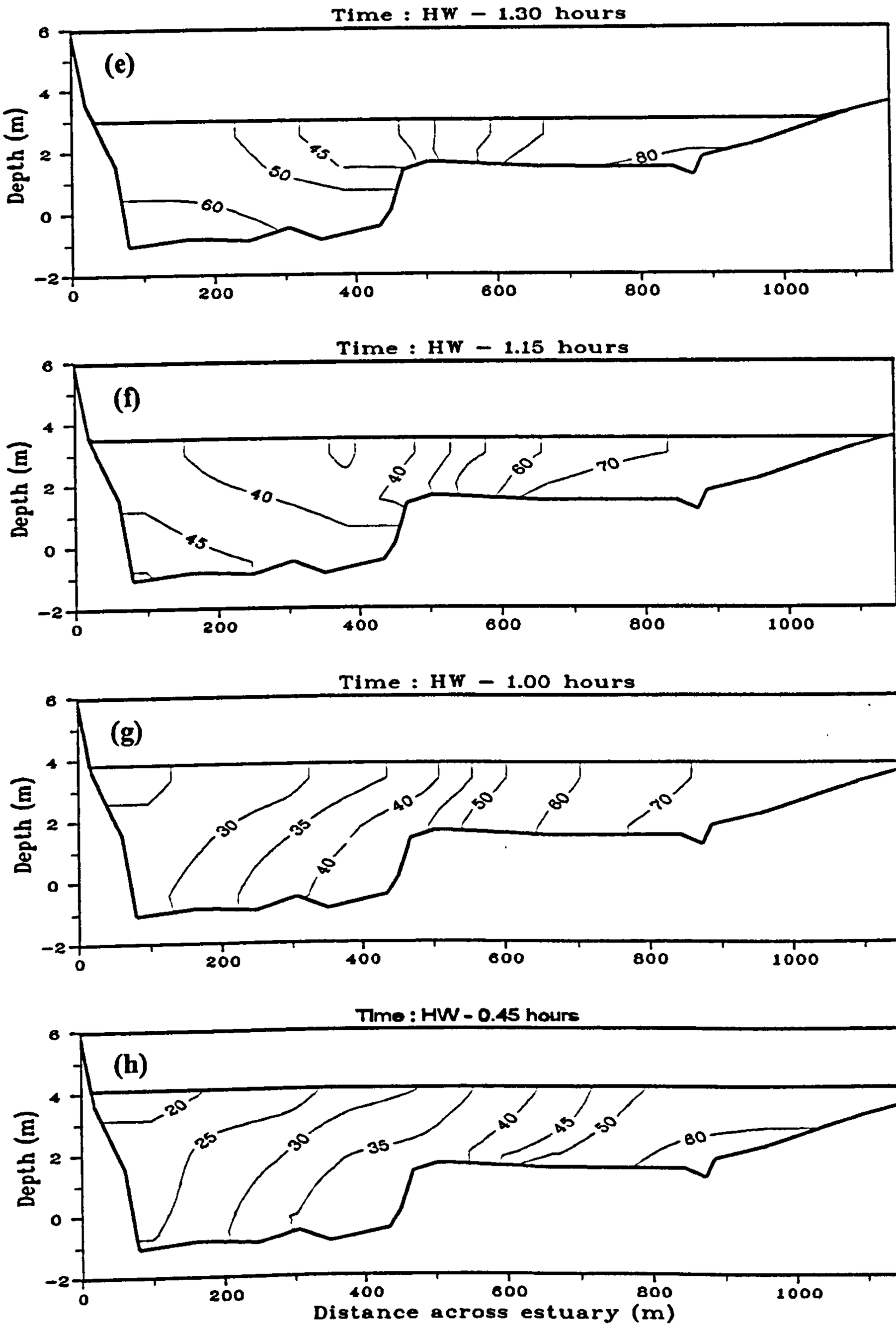

Figure 6.23 (continued)

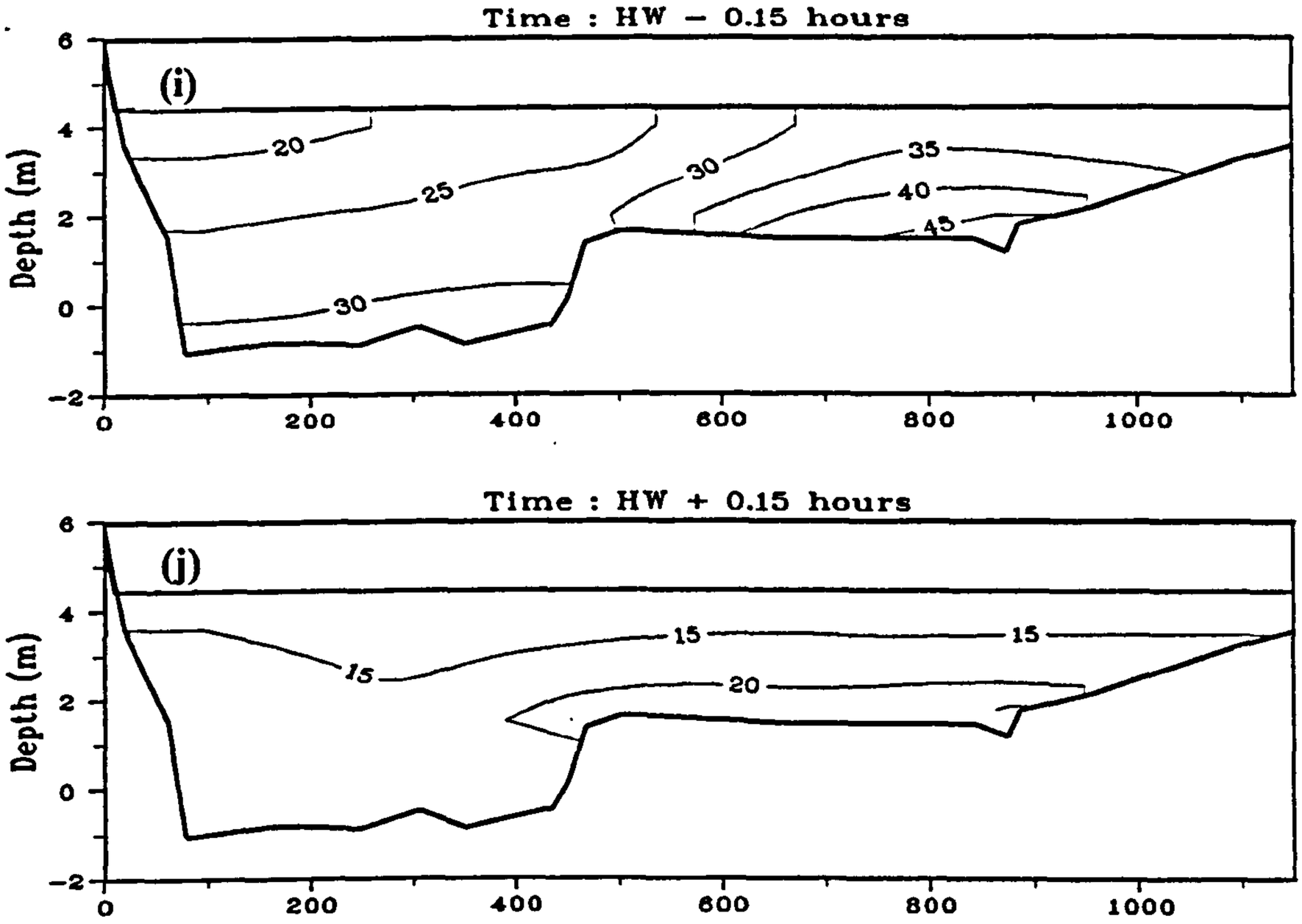

Figure 6.23 (continued)

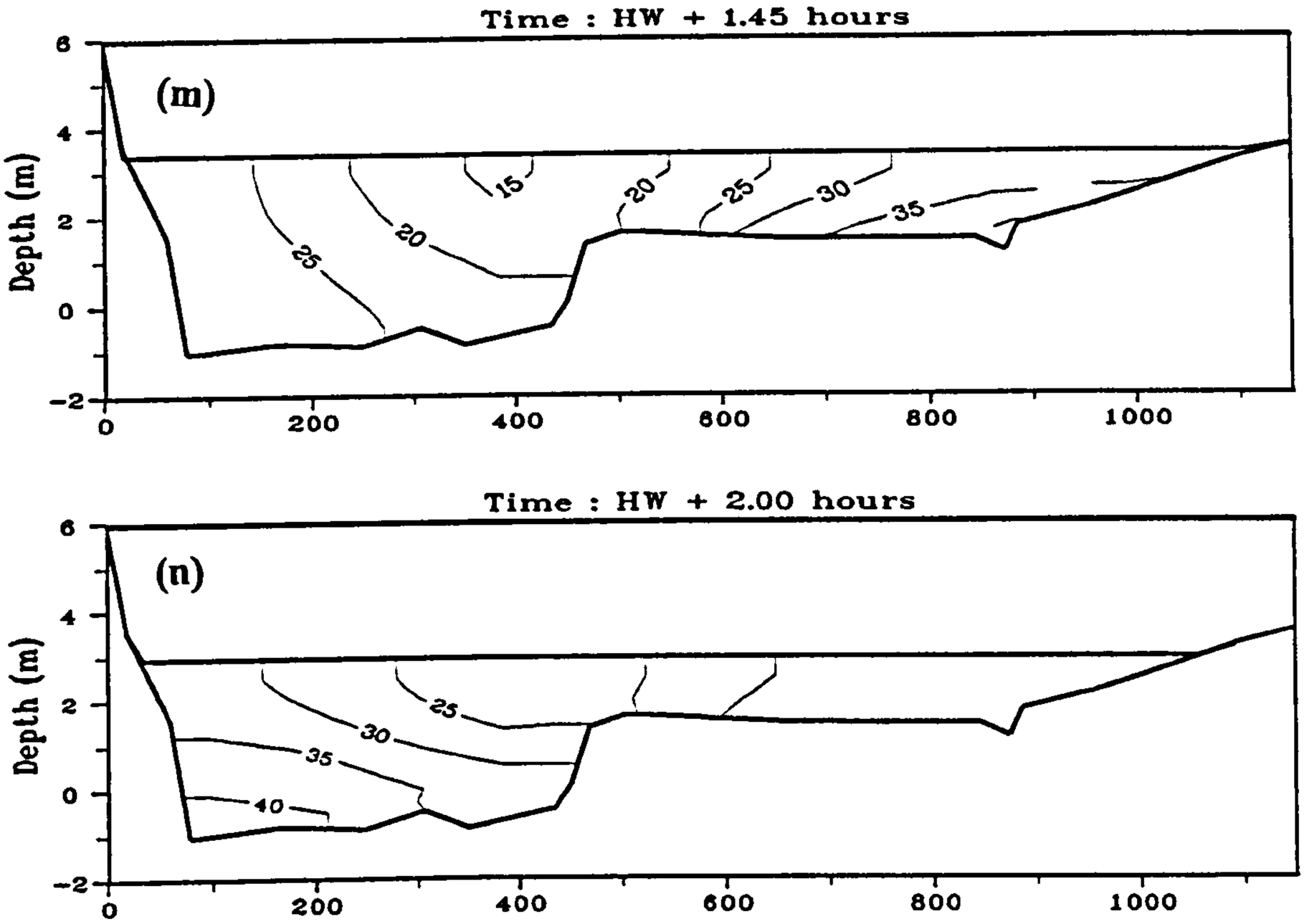

Figure 6.23 (continued)

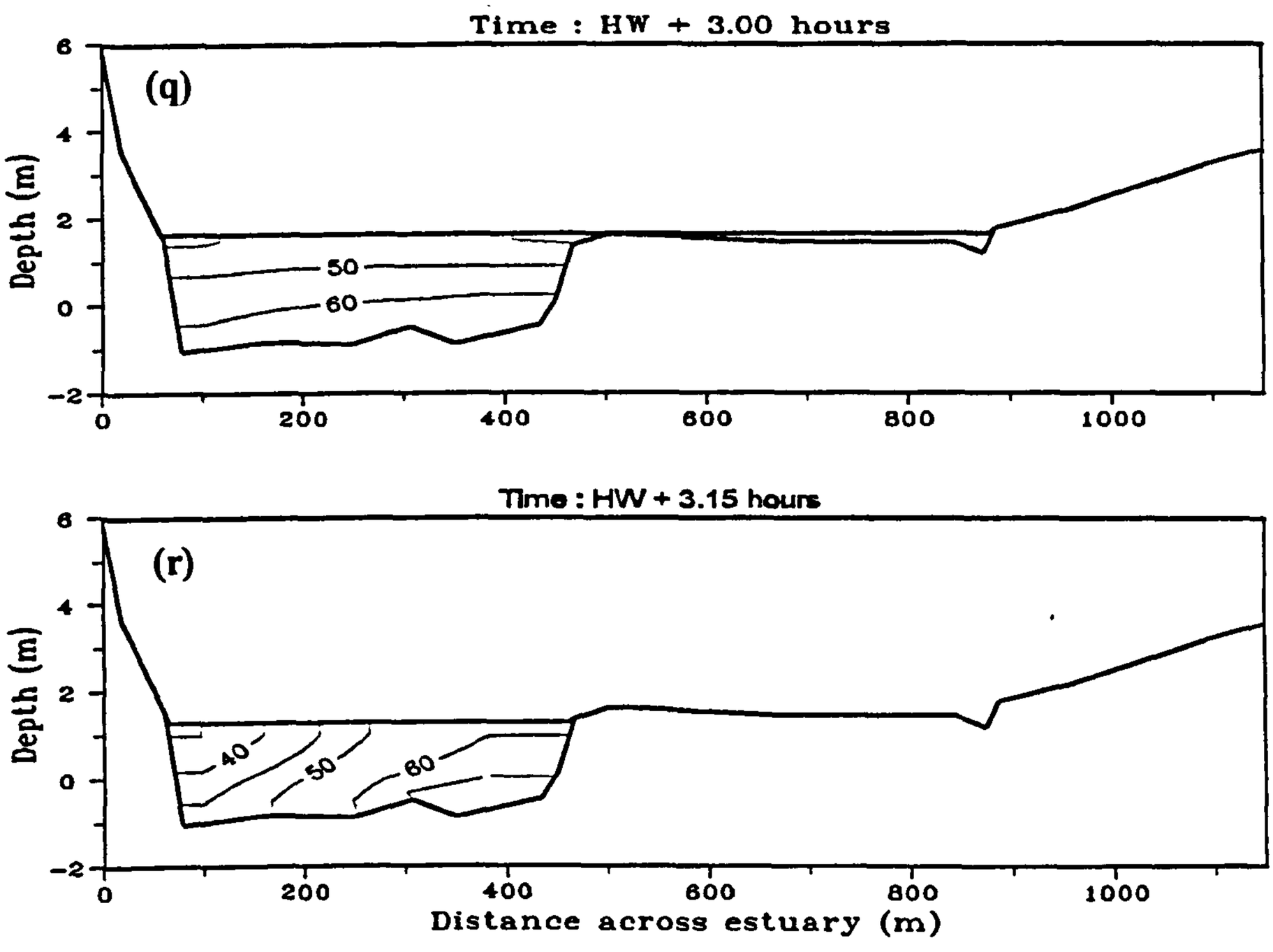

Figure 6.23 (continued)

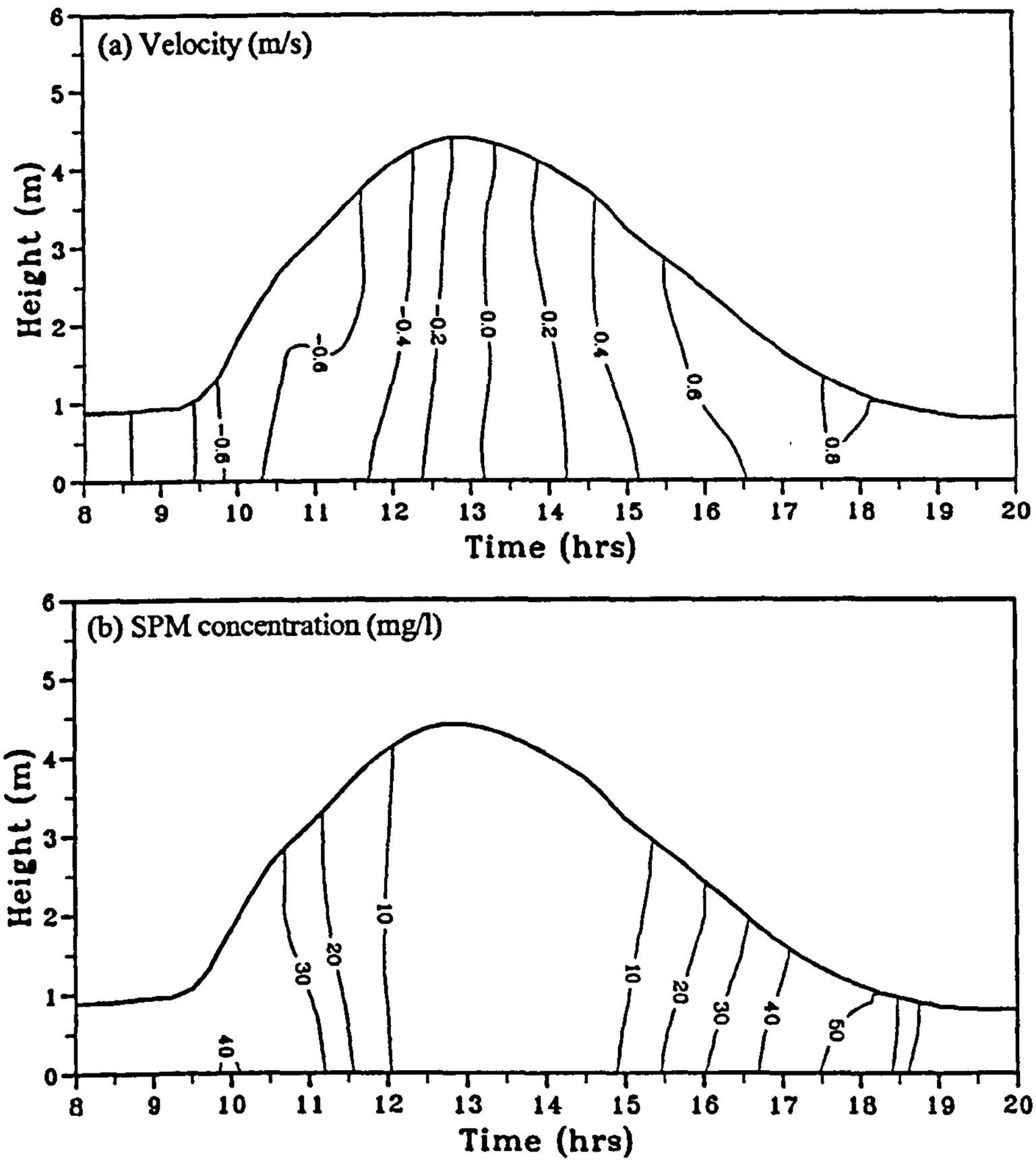

Figure 6.24 Time series contour plots of tidal velocity and suspended sediment concentration during a neap tide at station 1, transect T9, 20 July 1995.

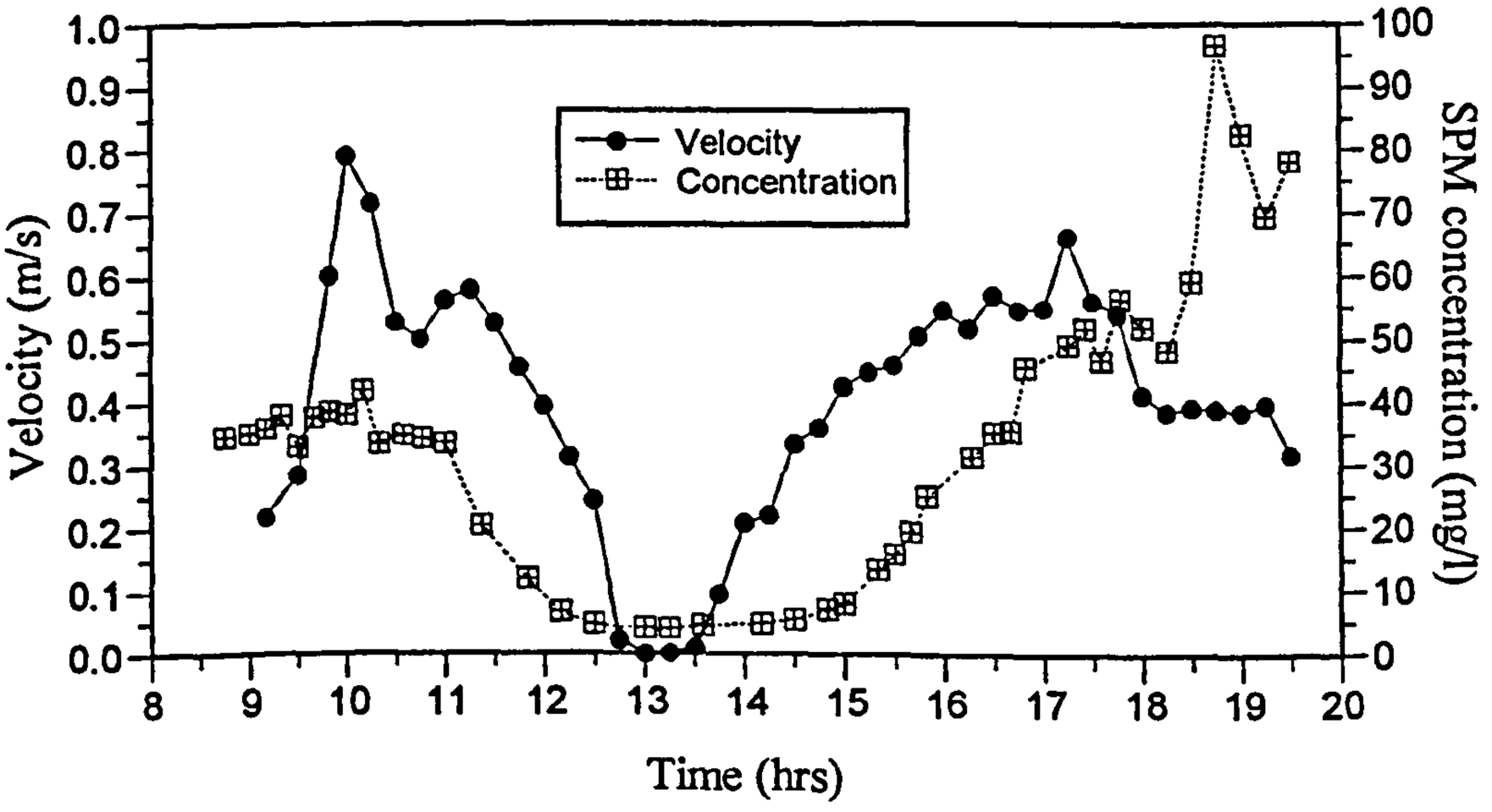

Figure 6.25 Depth-averaged velocity and suspended sediment concentration at station 1, transect T9, 20 July 1995.

is a long period (about 3 hours) from HW - 1 hour to HW + 2 hours, when SPM concentration remains very low (about 10 mg/l) which indicates that very little resuspension takes place during this period. The time series contour plots for other stations at transect T9 (Figure C.08, Appendix C) show similar features. Stations 5-7 which was located on the intertidal sand flats show concentrations less than 30 mg/l throughout the tidal cycle. As the SPM concentration remains very low throughout the tidal cycle, the concentration does not vary significantly across the estuary cross section as shown in Figure 6.26.

For stations 1 and 2, transect T5, a higher concentration, about 100 mg/l was recorded during the early flood and also at the end of the ebb (Figure C.09, Appendix C). No contour plots were prepared for station 3 and 4 of transect T5 as the maximum water depth at these stations barely exceeded 0.5 m. A higher sediment concentration boosted by a higher flow velocities was recorded at T5 than at T9 as the main channel was narrower at T5.

6.3.4 SPM variations at a fixed mooring station during a neap tidal cycle

A detailed measurement of SPM variation over three neap tidal cycles was made on 16 and 17 September 1995 in the lower estuary. A Sea Tech transmissometer attached to an Applied Microsystems CTD probe was fixed to the VGU mast at 0.25m above the bed, at station 2 transect T5. This station was located at the edge of the main channel. The SPM concentration, salinity temperature and water depth were recorded at one minute interval, while the current velocities were logged at every 10 minute interval.

The results of these measurements are plotted Figure 6.27 which also shows the depth-averaged velocities (from the Ott current meters of the VGU). Also shown is the water level during the tidal cycle at the measurement station which varied between 0.45 m and 4.1 m (Figure 6.27b). The figures show similar patterns of SPM variation to those observed at the anchor stations. During the flood on 16 September 1995, the SPM shows two peak concentrations; the first one (100 mg/l) at 0840 hours when the current was still weak (0.4

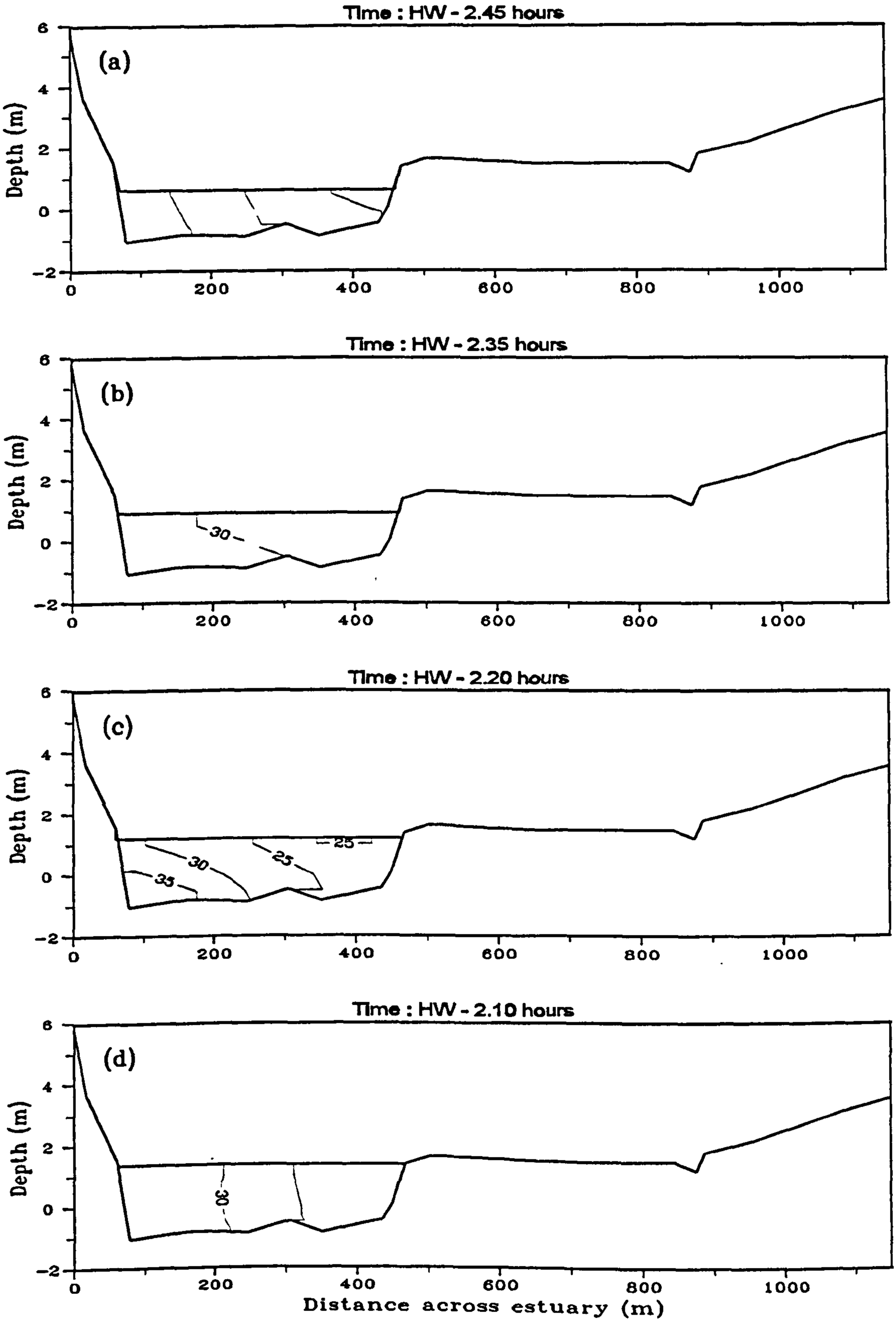

Figure 6.26 Cross estuary contour plots of suspended sediment concentration (mg/l) at different stages of the tide, 20 July 1995.

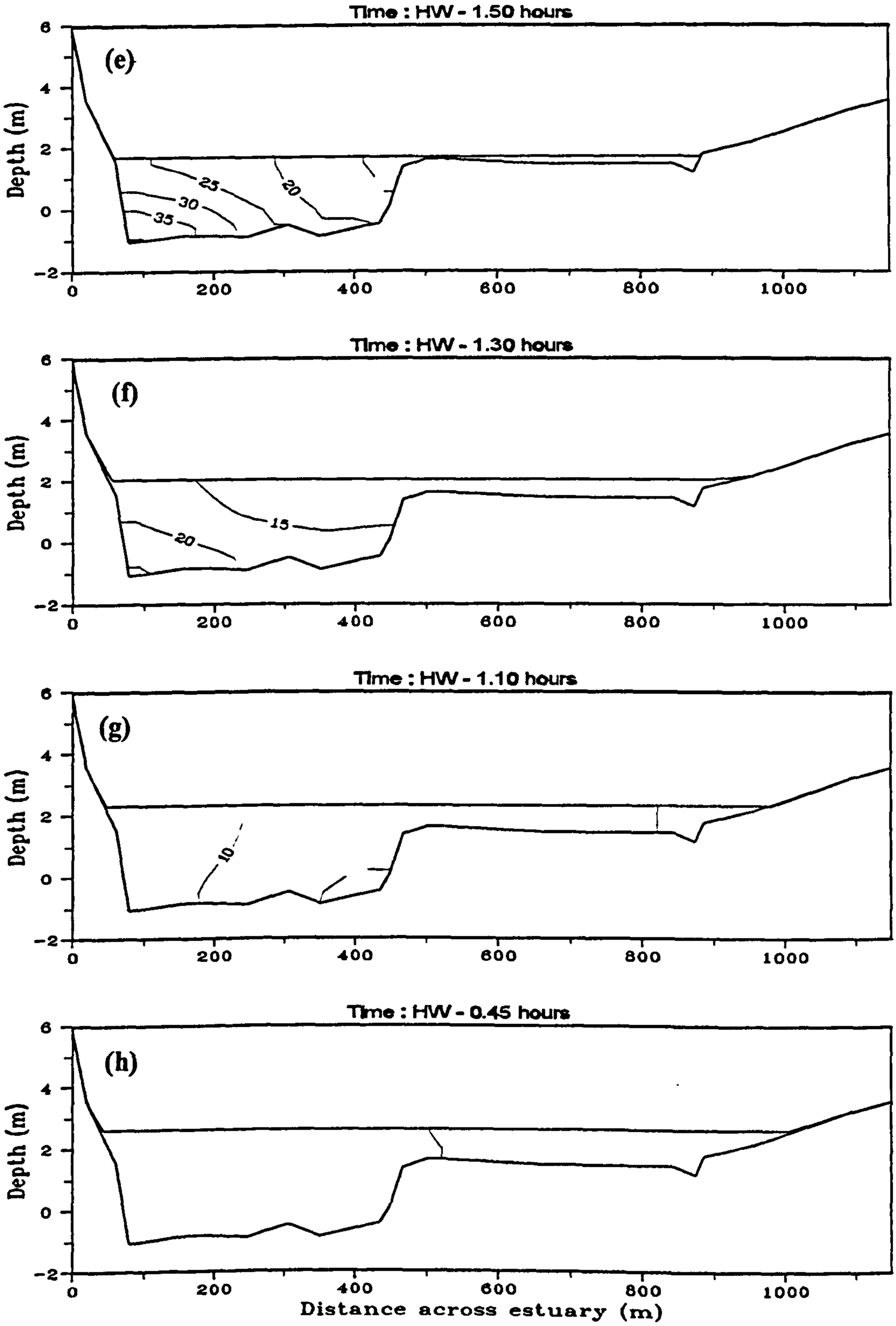

Figure 6.26 (continued)

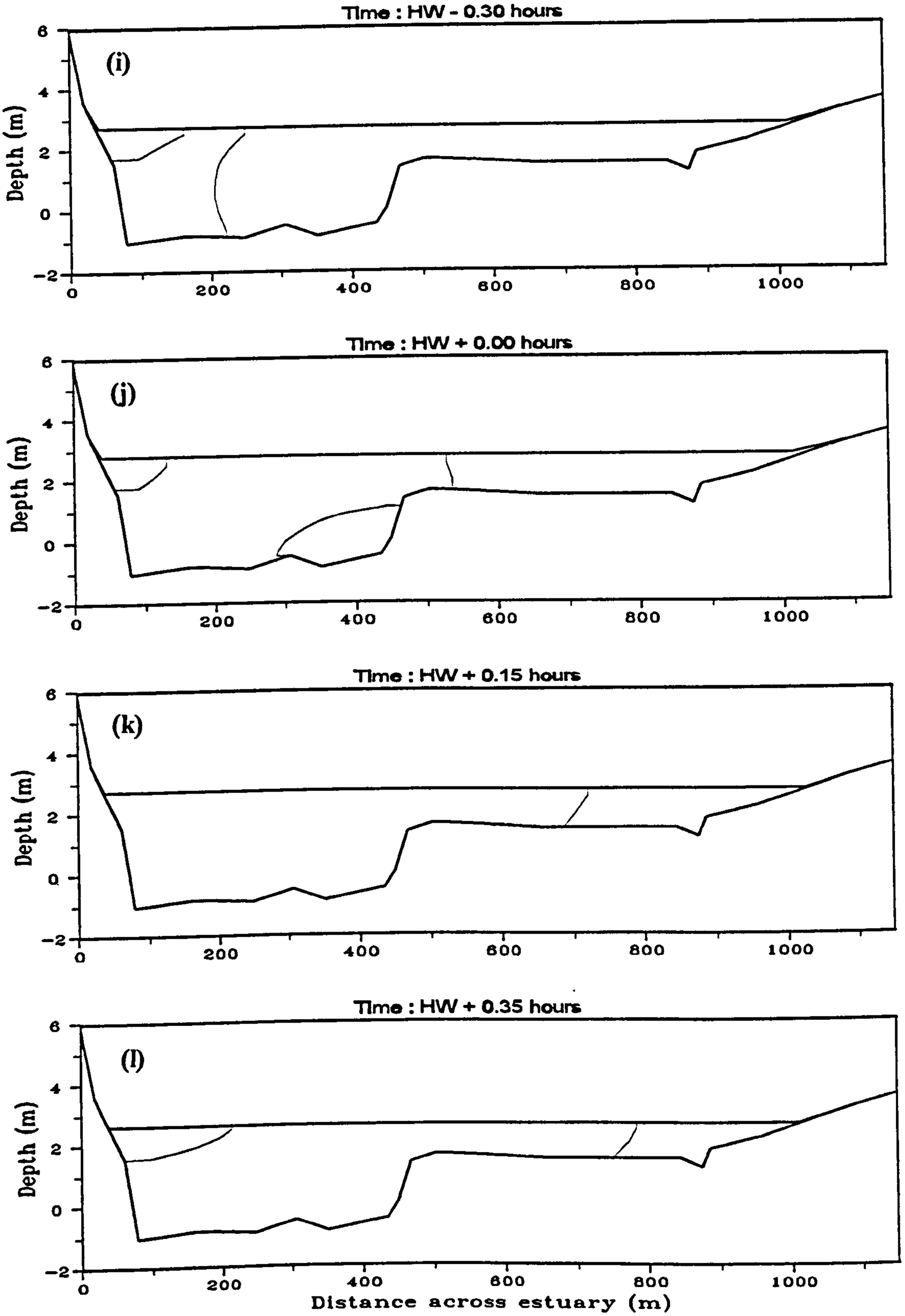

Figure 6.26 (continued)

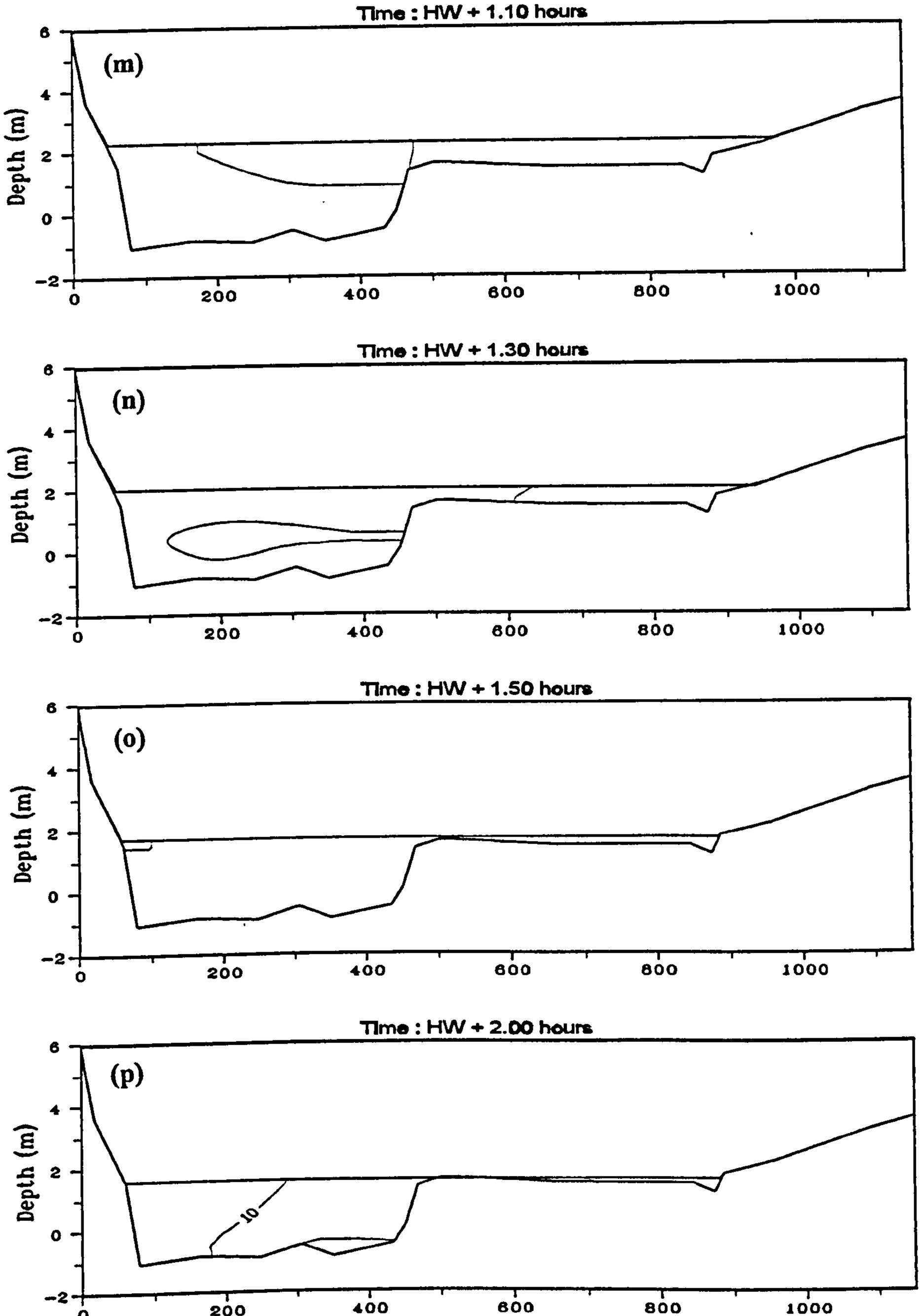

Figure 6.26 (continued)

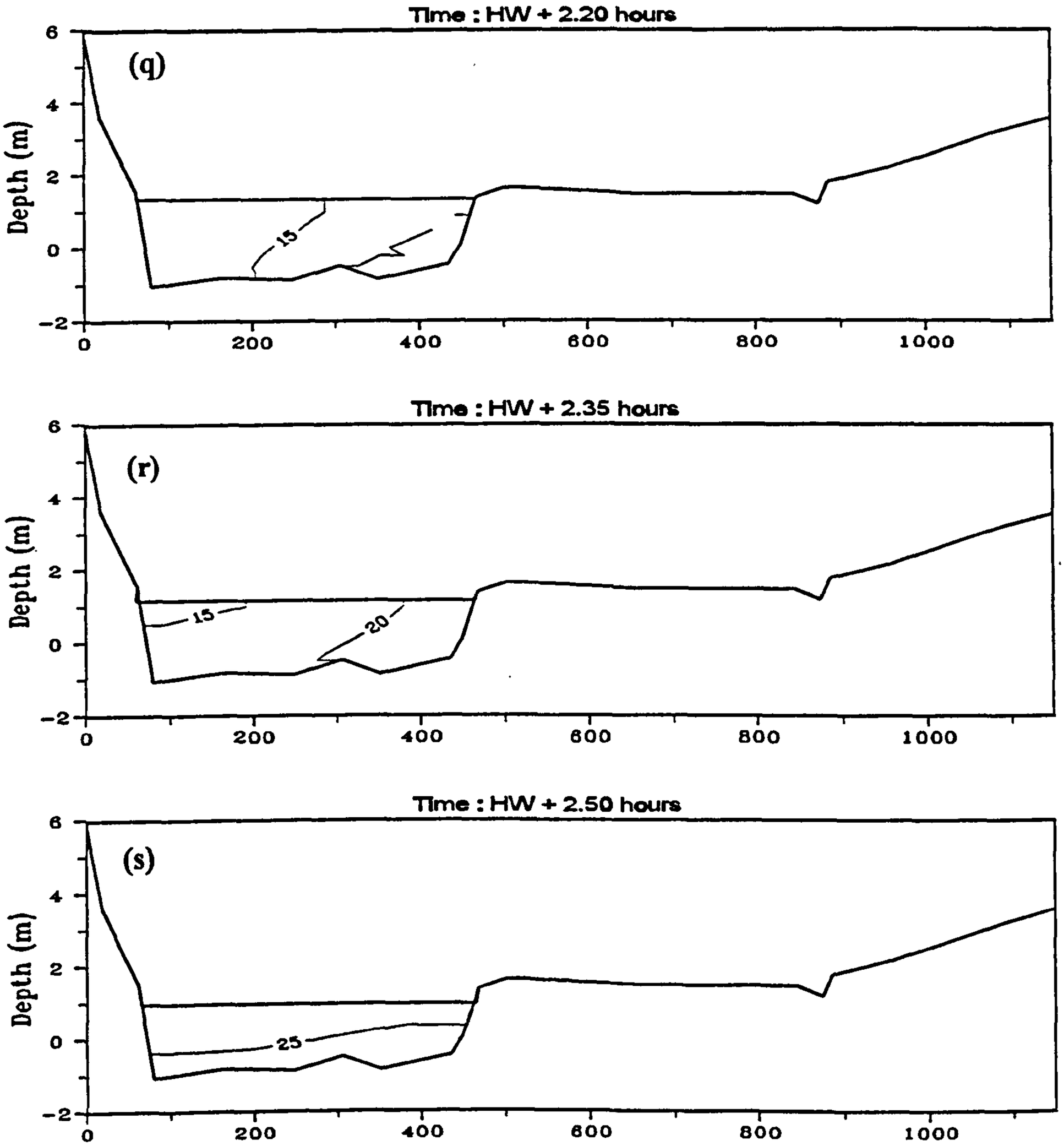

Figure 6.26 (continued)

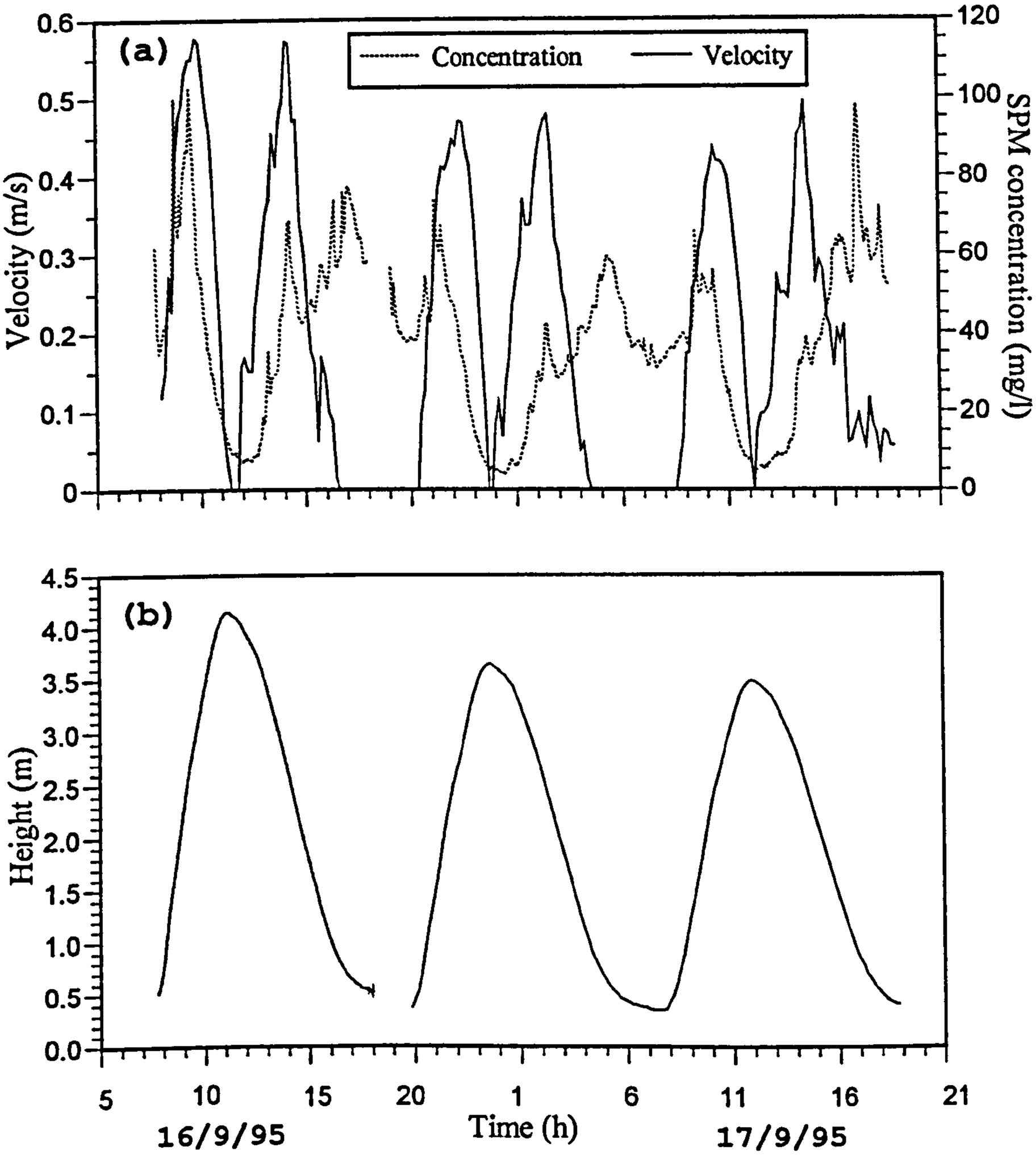

Figure 6.27 Variation of suspended sediment concentration at 0.25 m above the bed at anchor station 2, (T5) for three neap tidal cycles. Also shown in (a) depth averaged current velocity, and (b) tidal height at the measurement station.

m/s) and the other (103 mg/l) at 0930 hours which corresponded to the peak flood velocity (0.6 m/s). The SPM concentration dropped to about 10 mg/l during slack HW but steadily increased as the ebb current became stronger. There was a long period of low concentration during high water slack, and the minimum concentration lagged minimum current velocity by about 0.5 hour. The peak ebb concentration (67 mg/l) occurred at about 1410 hours i.e. when the ebb flow was at its maximum (0.6 m/s). The concentration then dropped as the ebb current decreased; however the concentration increased again to a second maximum after 1500 hours even though the ebb flow was diminishing toward low water. The concentration remained high for more than an hour before dropping again. These features were consistently observed in the two other tidal cycles of the second deployment on 17 September 1995, which all show larger second SPM peaks at the end of the ebb tide. These second ebb SPM peaks occurred after current velocities had diminished towards low water.

6.3.5 SPM variations over a spring tidal cycle in the upper estuary

In the upper estuary, measurements of tidal velocity and SPM concentration were made at St. Clears on 12 July 1995 during a spring tide. The tidal range was 7.8 m but the fresh water discharge was very low (0.6 m^3/s). There was a strong correlation between SPM concentration and the tidal velocity (Figures 6.28 and 6.29). The fast flows exceeded 1.0 m/s and vertically-mixed water on the early flood carried with it a high suspended load of more than 4000 mg/l as a turbidity maximum advected past. This concentration was significantly greater than any measured in the lower estuary. As the flood progressed the concentration and current velocity declined rapidly towards HW, and reached their minima at slack water where SPM concentration in the surface water of around 20 mg/l was recorded. The SPM concentration gradually increased as the ebb current became stronger. At the end of the ebb high turbidity water with surface concentrations over 1000 mg/l again advected past; however the maximum turbidity lagged the maximum velocity by about 0.5 hours. Limited water samples indicate that at the this final stage of the ebb the bottom SPM concentration was at least double the surface concentration. The measurements

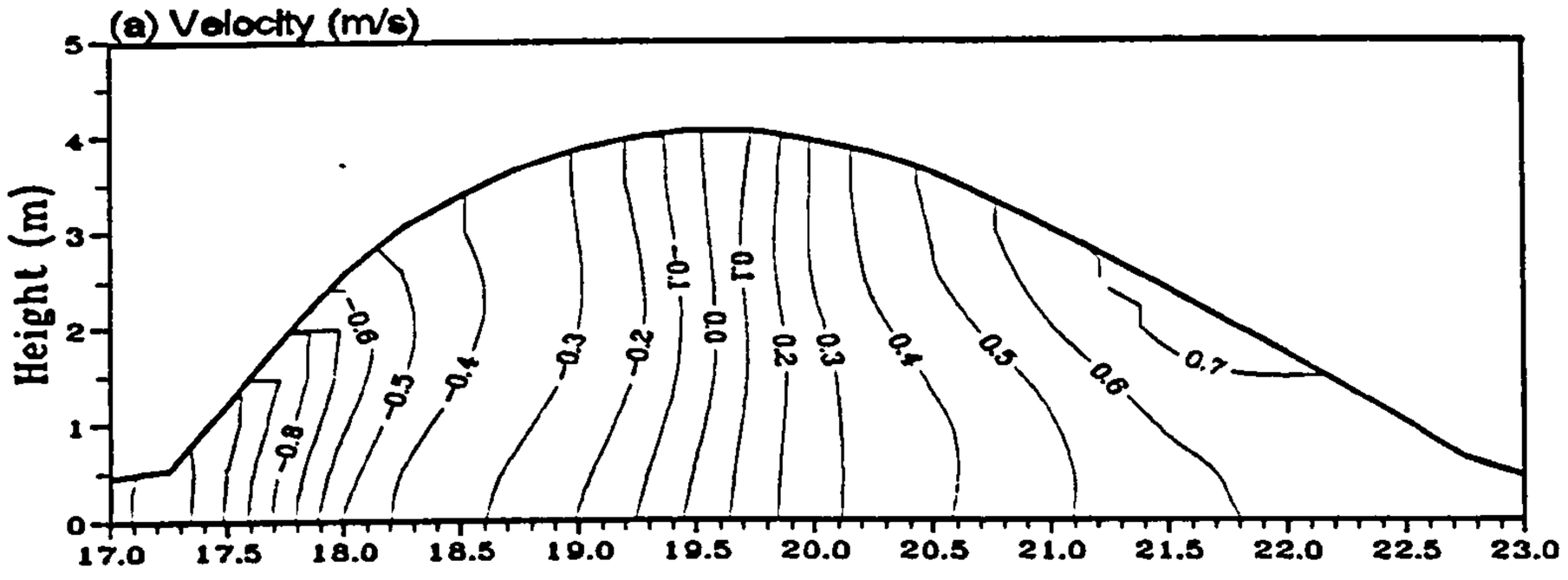

Figure 6.28 Time series contour plots of (a) velocity, and (b) suspended sediment concentration at St Clears, 12 July 1995. The contours for the concentration are in g/l.

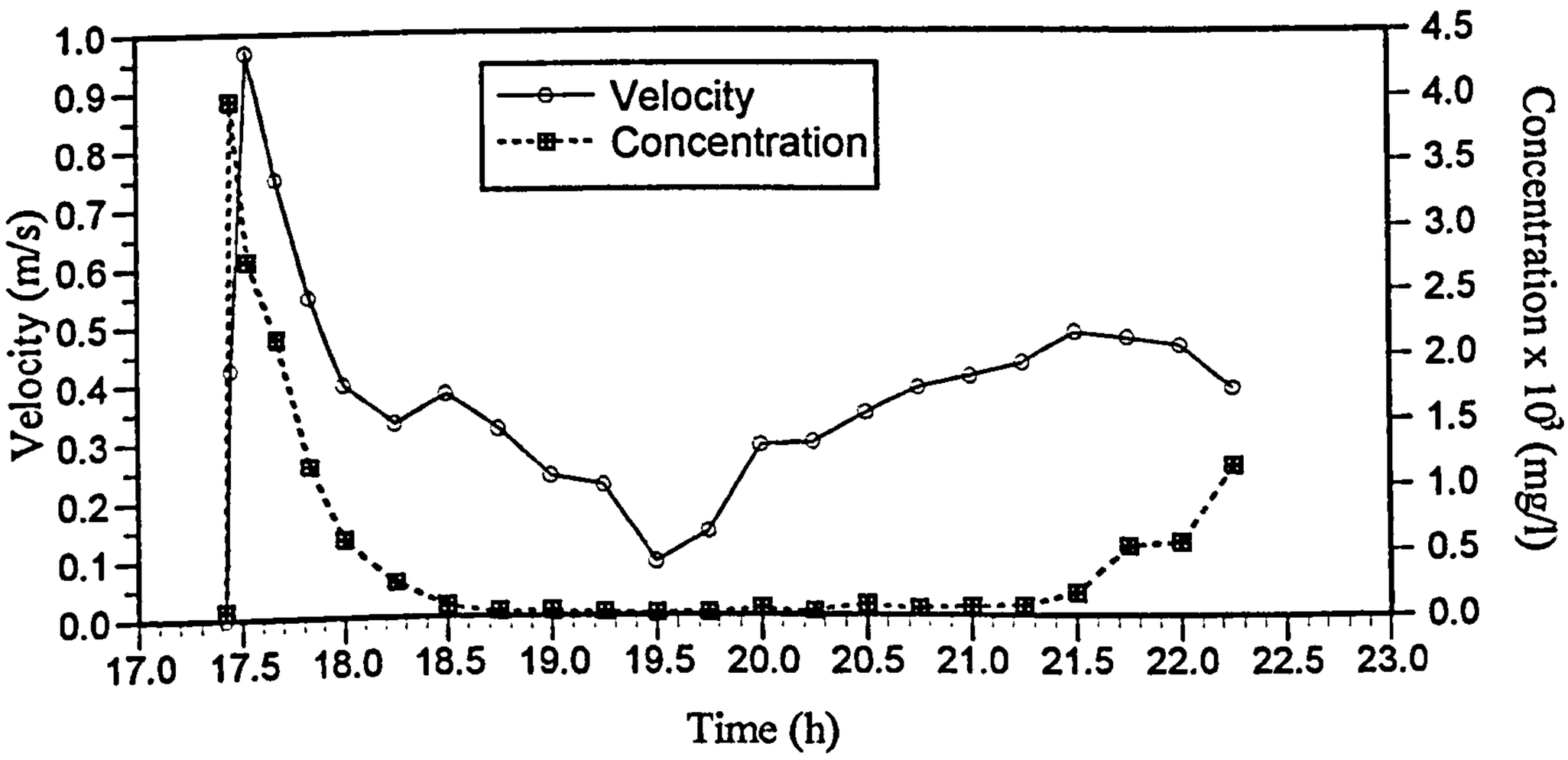

Figure 6.29 Depth-averaged velocity and suspended sediment concentration in surface water at St Clears, 12 July 1995.

showed that the centre of this turbid water was maintained at the 1 ppt salinity line both during the flood and ebb.

6.4 Size distribution of suspended sediment

The grain size of suspended particles in the surface water samples collected during the anchor station surveys has been determined using a Galai-CIS 100 laser particle sizer (see Chapter 3, Sections 3.3.3 and 3.3.4 for the detailed technique and instrumentation). One of the output from this analysis in the form of percentage volume distribution for a range of particle sizes. Figure 6.30 shows typical particle size spectra (given by a probability volume density graph) of suspended sediment at three different tidal stages for a spring tide in the lower estuary. The Figure shows that the suspended sediment is made up of three sub-populations and these can be classified as background; resuspension; and large diameter floc sub-populations. The background sub-population with a particle mode about 17-20 μm represents the background concentration of SPM in the water column. It is a dominant population during high water but a minor component during the early flood and late ebb. The background population has small size, so it settles very slowly; thus remain in suspension. The second sub-population is the sediment being resuspended from the bed by tidal currents and has a particle mode range between 150-200 μm. This sub-population has the same mode as the bed sand. Its proportion varies with the tidal cycle being highest during the early flood and late ebb when the currents are strongest and lowest around high water due to particle settling when the current is at its minimum. The third sub-population is the coarsest of all with grain mode around 350-450 μm. This subpopulation represents mainly particles that have recoagulated and formed high diameter flocs either within the analysis cell or before the particles reaching the cell or both. The very sharp decline in the grain population at the coarser end of this sub-population suggests that there is a limit that flocs can grow. Samples collected around high water showed smaller flocs diameters as the sediment concentration in the water was low, so less particles are available for formation of new flocs and smaller flocs to grow.

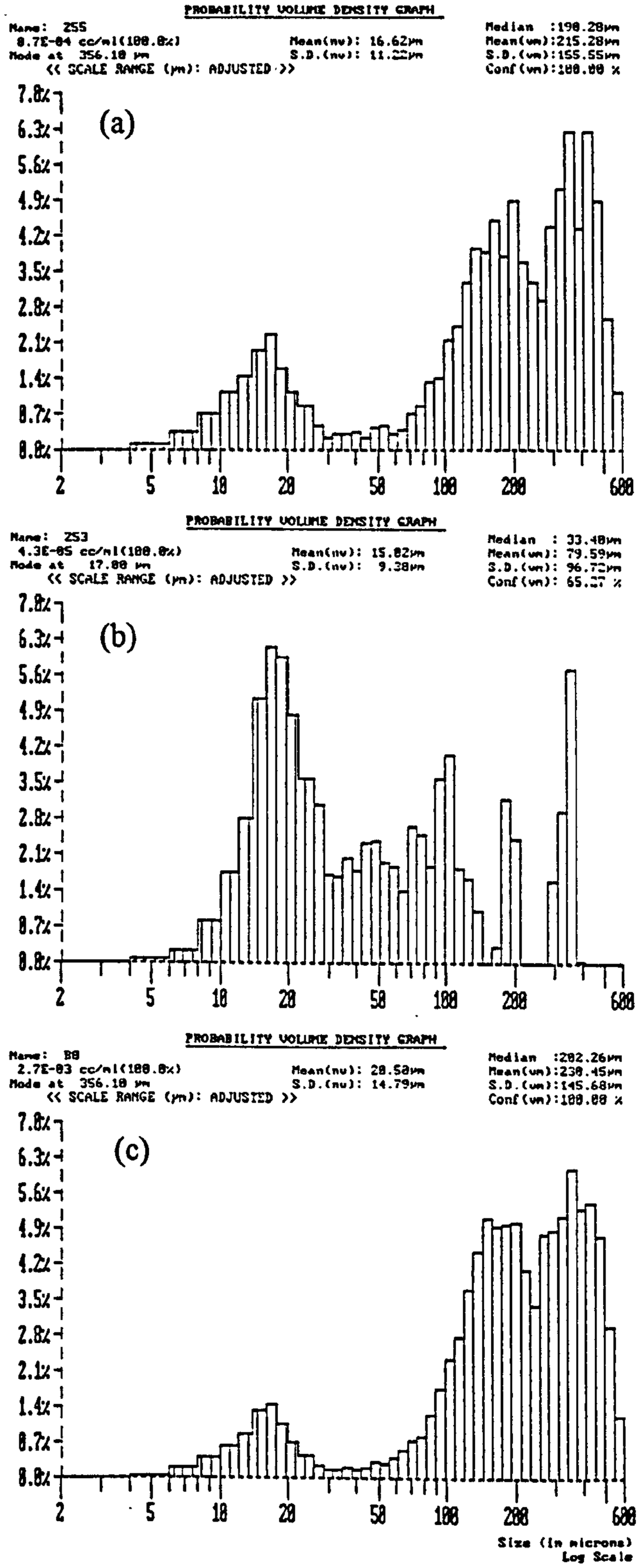

Figure 6.30 Particle size distribution of suspended sediment at three tidal stages, (a) early flood, (b) high water, and (c) late ebb.

As evidenced from Figure 6.30, the background population represents the size range smaller than about 34 μm. The volume percentage of this sub-population of all the water samples collected for whole tidal cycle at station 1 on 14 July 1995 (transect T9) and 13 September 1995 (transect T5) as obtained from the grain size analysis (see Chapter 3, Section 3.3.4) has been converted into mass (mg/l) for size fractions less than 34μm and greater than 34μm, and these are plotted in Figure 6.31. The concentrations of each fraction are relative rather than absolute values as the particles densities of the two fraction would be different. The figure shows that the concentration of the background population fluctuates between 5 - 30 mg/l throughout the tidal cycle, but the resuspension (+ the flocs) populations varies considerably. At the beginning of the flood there is a significant increase in the resuspension population due to remobilization of bed material by the accelerating current; the concentration declined toward high water due to decreasing erosion and increasing particle settling. During the ebb, the concentration of the resuspension sub-population increased when the current increased as the ebb progressed. Very high concentration of suspended sediment was recorded at the very late stage of the ebb tide, when the currents already diminished; thus it represented admixture of resuspension sub-population and contributions from other sediment sources.

6.5 Discussion

6.5.1 The turbidity maximum

General

The formation of a turbidity maximum in the Taf estuary is a result of resuspension of bed sediment by the fast tidal currents. During periods of low river runoff, the turbidity maximum develops on all tide; however during periods of high river runoff, the turbidity maximum exists only when the tidal range is greater than 4.0 m. The turbidity maximum is best developed during times of low river discharge and spring tides. During these times, the turbidity maximum reaches its highest concentration and is located approximately 14 km from the mouth. During times of high river discharge, the spring tides turbidity

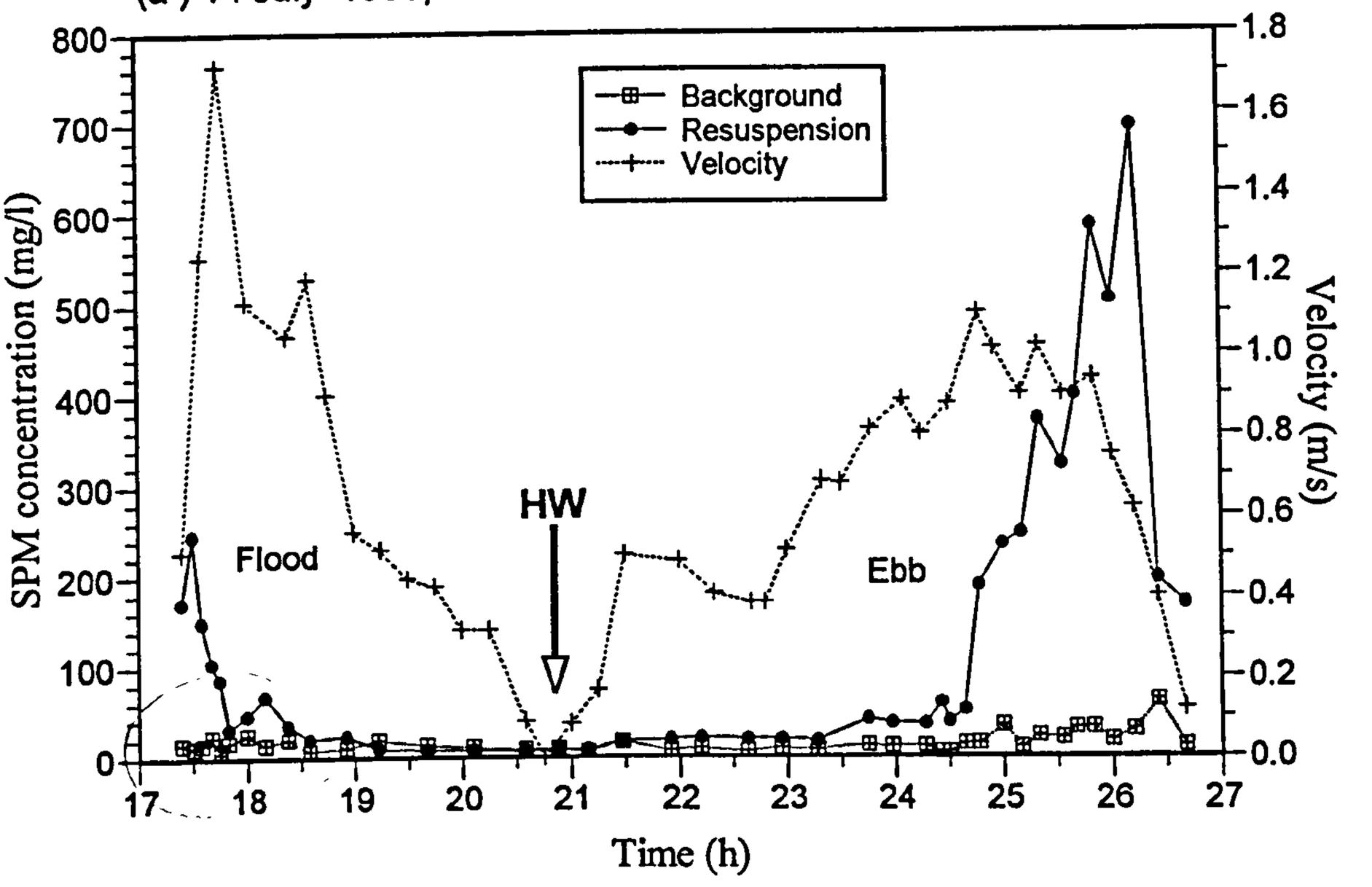

Figure 6.31 Variation of two sub-populations of suspended sediment over a tidal cycle at station 1 on (a) 14 July 1995, and (b) 13 September 1995.

maximum is small and is located about 9 km from the mouth. As the SPM concentration in the turbidity maximum zone is small during times of high river discharge, the existence of a neap tide turbidity maximum during high river discharge could be masked by the background SPM concentration, hence no turbidity maximum seen during these times.

SPM contribution during high river discharge

During times of high river discharge, there is limited supply of fine erodible material on the bed. This is discussed below.

Any suspended sediment deposited in the upper reach of the estuary during high water slack will be resuspended during the ebb, and, together with the fluvial sediment, will be redistributed down estuary and subsequently carried out of the estuary by the fast ebb currents produced by the fresh water flow and also due to the prolonged ebb flow. During times of high river discharge, the mean currents in the upper reaches of the estuary are ebb dominated (see Chapter 4), which removes the sediment from the upper reaches. Therefore during periods of high river runoff, there is very little supply of fine material on the bed. This limited supply of erodible fine sediment in the upper reach of the estuary results in the much smaller turbidity maximum observed during a high river discharge. A similar result was obtained by Uncles and Stephens (1989) in the Tamar which shows a much smaller maximum concentration observed during high river discharges; though the mechanism for the turbidity maximum formation in the Tamar is different from the Taf. As the bed is already deprived of fine erodible material, therefore on much smaller tides during neaps, very little sediment is brought into suspension by the weaker currents, and this can be masked by the background sediment concentration in suspension, thus no turbidity maximum is observed during this period. Furthermore, the location of the fresh-salt water interface would be much further down the estuary (pushed by high fresh water flows) and does not reach the mobile stock of the fine sediment which is located further up estuary.

SPM contribution during low river discharge

During low discharge in the summer, fresh water flows are weaker, and more of the

settled fine sediment would remain on the bed during the ebb. This sediment would be resuspended and transported in suspension to the upper estuary by the stronger flood current to form a turbidity maximum. Even during a neap, there is enough supply of erodible fine sediment on the bed for the formation of turbidity maximum at the limit of salt water intrusion. The narrowing down of the channel at the upper estuary increases flow velocity and enhances SPM concentrations in the turbidity maximum zone. The long period of HW slack as observed in many estuaries (eg. Postma, 1967; Allen *et al.*, 1980; Dronkers, 1986; and Uncles *et al.*, 1994) encourages SPM deposition resulting a tidally-averaged landward transport and accumulation of fine sediment.

General effect of fresh water input

Fresh water input have significant influence on the turbidity maximum. The importance of fresh water discharge is two folds; firstly the river water itself may supply significant amount of suspended sediment whereby an increase river flow implies more suspended sediment is discharge into the estuary, thus increase the mass of sediment in the turbidity maximum; and secondly the river flows directly affect the estuarine circulation pattern for dispersal and trapping of suspended sediment (eg. Meade, 1969; Nichols and Biggs, 1985; Dyer, 1994). Typical suspended concentration in the river Taf during averaged river discharge in September 1994 was between 5 -10 mg/l, similarly during low discharge in July 1995, the concentration in the river was less than 10 mg/l. This is compared to the down estuary values of between 10 - 30 mg/l. Judging from this extremely low value of river sediment concentration, it is unlikely that it will contribute to any measurable amount to the turbidity maximum during the survey periods. The effect of variation of river discharge on the sediment dynamic and water circulation in the inter-tidal estuary is perhaps minimum. This is due to the fact that the turbidity maximum only exists as a ephemeral features in the estuary, i.e. it grows and decays with the tidal prism. Further more the main mechanism for the formation of turbidity maximum in the Taf is the tidal resuspension of the bottom sediment. The main effect of river discharge in this case is to cause the migration of of turbidity maximum to lower down estuary during high river discharge, and further up estuary during low discharge.

The analysis shows that in the Taf, the variation of river discharge accounts for 32 % of the variation in the turbidity maximum location. For a similar tidal range, there is between 1.5 - 2.5 km down-estuary migration of turbidity maximum between a low (about 1.0 m^3/s) and an averaged (about 5.0 m^3/s) river discharges. This is a very small migration as compared to the migration of a turbidity zone in other much bigger estuaries. In the Tamar for example, the turbidity maximum migrates some 12 km down estuary in the summer from it winter location (Bale, 1983), while in Gironde the position of the maximum varies some 40 km with low and high river discharges (Allen *et al.*, 1977; 1980).

Effect of temperature

Generally the temperature of the estuary water gradually decreases toward the head as a result of the tidal mixing between a warmer sea water and a cooler fresh water. This is not always true in a tidal estuary such as the Taf. Solar heating of sandflats and mudflats during low water (when the estuary is dry) can elevate the estuarine water temperature significantly (to a few degrees Celsius) such as shown by Figure 6.14a. High water temperature affect the viscosity of the seawater as well as the settling rates and shear stress exerted by a bottom current in the inter-tidal zones (Taylor, 1974; Young, 1977). It is very unlikely that the small rise in the water temperature will have any significant effect on the resuspension of the bottom sediment in the Taf. Anderson (1980) studied the effect of rising water temperature on the depositional and resuspension processes of intertidal sediments in a tidal cove, New Hampshire but found very little relationship between the water temperature and suspended sediment concentration though the flood-front water temperature was 15 ^0C warmer than in the deeper channel. Changes in the ambient temperature may be important as it influences biological activities that take place within the estuary. The decrease in temperature during winter and autumn period is likely to reduce biological and microbiological activity, making the mud easier to erode both subtidally and intertidally (Dyer, 1986).

Source of fine sediment for turbidity maximum

The major supply of erodible fine sediment for the formation of the turbidity maximum most probably comes from the upper 7.5 km section of the estuary i.e. when the channel narrows down to less than 50 m across. The anchor station measurements made in the upper estuary indicate sediment concentrations six times higher than those measured at the lower estuary for a similar tidal range; however the maximum current speeds are only about half of that at the lower estuary. Thus the turbid front of the turbidity maximum become increasingly concentrated as the flood progresses further up estuary, and it represents the influx of suspended matter stirred up by stronger flows further down the estuary.

No systematic sampling of bottom sediment has been carried out along the upper 7.5 km section of the estuary, but limited samples by Jago (1974) shows that close to St. Clears more than 80 % of the bed sediment is made up of the suspension population (finer than 32 μm). Sediment samples from the channel 6.5 km distance from the mouth (transect T1, Figure 3.1) are made up of well sorted fine sand (Jago 1974; 1980) which could not be the main source of the fine sediment stock for the formation of the turbidity maximum. Thus the main supply of the easily erodible sediment lies between these two points.

Mechanism for the turbidity maximum formation

The formation of the turbidity maximum in the Taf Estuary is caused by resuspension of bottom sediment by fast tidal currents on the advancing flood tides. Progressive resuspension as the flood tide advances across the intertidal flats, and narrowing of the channel, boosts suspended sediment concentrations so that, in the upper estuary, the leading edge of the flood tide is very turbid. Much of this material remains in suspension at high water (and so must comprises of light organic-rich matter rather than fine sand), thus producing a turbidity maximum at the limit of salt water intrusion. Much material remains in suspension during the ebb and progressively retreats down the estuary. The turbidity maximum passes through the lower estuary approximately 5 hours after high water. As the estuary becomes dry towards low tide, all the sediment from the turbidity maximum zone

is flushed out of the estuary into Carmarthen Bay. High river discharge helps to speed up the flushing of the sediment into the bay.

The turbidity maximum is therefore an ephemeral and transient phenomenon that moves through the estuary with the advancing and retreating tidal prism. This is quite distinct from the dynamics of conventional turbidity maxima in stratified and mixed estuaries that are not predominantly intertidal. In many of these estuaries, turbidity maxima can be permanent features that are maintained within the estuaries. The sediment may escape onto the adjacent shelf only during spring low tides combined with high river flow, as in the case of the Gironde river and Aulne river (Castaing and Allen, 1981; Avoine and Larsonneur, 1987).

6.5.2 Formation of reversed sediment stratification

During 6 October 1994, mid-way towards the HW, a front of more turbid water was observed passing station 1. This water was less saline than the water below it, and that measured at the middle of the channel. Its brownish colour and the existence of foam lines with floating detrital material was distinctive from the more bluish coastal water.

The front represents the zone of convergence between the seaward flowing fresh water over the ambient denser coastal waters (Officer, 1981) and is indicative of density-driven secondary circulations in tidal estuaries (Turrell *et al.*, 1996). Nunes (1982) shows the front results from secondary flows directed from either bank, toward the centre of the estuary at the surface; It is present during the flood tide only. This front caused the sediment stratification that was seen at the middle stage of the flood at station 1 on the 6 October 1994 (Figure 6.16b). This front could have been developed in the bay due to higher fresh water volume contributed from the nearby rivers (Towy and Grandewereth), and extends a few kilometres into the Taf during the mid-flood. This front has also been observed in other Welsh estuaries (eg. the Conwy and the Seone, Nunes (1982); Turrel *et al.*, (1996); and the Mawdach, Larcombe (1992)).

The reversed sediment stratification as seen at high water during high river discharges is caused by fresher and more turbid water which begins to ebb at the surface while the more saline and clearer water is still flooding near the bottom. During low river discharge, however, waters are fully mixed and no sediment stratification develops on the spring tide, but it could develop on neap tides. On the flood, after the resuspension event, less turbid seawater is advecting into the estuary. The greater the salinity, the lower the turbidity. Since seawater pushes in faster near the bed (where there is no contrary fresh water flow), the bottom waters are more saline and less turbid. Hence reversed turbidity gradient occurs.

A higher SPM concentration is present on the intertidal sand flats during mid-flood (Figure 6.20). This is due to the combined results of bed erosion (as the bed sediment gets finer closer to the mud flat), but also due to the more turbid water being pushed to the inter tidal area by more saline and low turbidity water.

6.5.3 SPM variability in the lower estuary main channel

In lower estuary during neaps, the flood SPM peak is larger than the ebb peak despite similar maximum current speeds. The flood maximum SPM concentration is associated with the turbid front at the leading edge of the flood. The first ebb peak is related to resuspension , while the second ebb peak is related to turbidity maximum zone which advects past the measurement station and is thus independent of current speed. Anchor station measurements in the lower estuary reveal that this turbid zone reaches the lower estuary approximately 5 hours after HW and is completely flushed out the estuary an hour later. The flushing of the turbid water is slightly delayed during neap tides and is earlier when spring tides coincide with high river discharge.

The advection through the lower estuary and the subsequent flushing out of SPM that form the turbidity maximum zone at the end tidal prism expulsion is reflected both in the concentration profiles from the transmissometer records and from the water samples collected at regular interval during the course of the surveys. The profiles from the water

samples (Figure 6.31) is interesting as it shows a sudden rise in the SPM concentration of resuspension sub-population at the end of the ebb at the time when the currents already diminishes. It shows the time when the very turbid water from the turbidity maximum advected passed, thus it consists of mainly high diameter flocs rather than the mineral grains.

6.6 Conclusions

From the spatial surveys undertaken during neap-spring tidal cycles both in autumn 1994 and 1996 and in summer 1995, a pronounced and well defined turbidity maximum has been observed in the upper reaches of the Taf estuary. The turbidity maximum occupies 2-3 km stretch of the estuary between the 5 - 0.3 ppt isohalines and is generally centred slightly upstream of the interface between saltwater and fresh water (the 1 ppt isohaline). The actual location of this maximum varies between 9.5 km to 14.5 km distance from the mouth depending on the tidal range and river discharge. Its location corresponds to a sharp drop in the estuary water temperature. About 76 % of the variance in turbidity maximum location at high water can be explained in terms of tidal range alone and 93 % by the combination of tidal range and river discharge.

The maximum SPM concentration in the turbidity maximum zone varies fortnightly over neap-spring cycle and seasonally between autumn and summer periods. During high river discharge in the autumn, the concentration is small (less than 100 mg/l) and the turbidity maximum less developed; at this time the neap tide turbidity maximum can be masked by the background SPM concentration which varies between 10 - 20 mg/l, thus no turbidity maximum observed. During low river discharge, the turbidity maximum develops in all tidal cycles and has a much higher concentration i.e more than 600 mg/l on springs. Horizontal concentration gradient in the turbidity maximum zone is greater as sediment concentration become higher toward the springs. There is also a vertical concentration gradient with a maximum concentration near the bed and a lower concentration at the surface.

It appears that the main mechanism that generates and supports the turbidity maximum in the Taf is the erosion and resuspension of bed sediment by the fast currents on the early flood. The fact that the turbidity maximum occurs landwards of the salt intrusion indicates that the gravitational circulation is not a dominant process. Some of suspended material settles during high water but some remains in suspension and is advected back to the lower estuary during the ebb and subsequently flushed into the bay. The mobile stock of this fine erodible sediment that forms the turbidity maximum is thought to come mainly upstream of about 7.5 km distance from the mouth where the estuary channel narrows down to less than 50 m in cross section.

CHAPTER SEVEN

ESTUARINE SEDIMENT FLUX

7.1 Introduction

With the advent of new optical and acoustic technologies, it is now possible to measure suspended sediment concentration and current velocity with high temporal and spatial resolution. It is thus feasible to quantify suspended sediment fluxes in the coastal environment with some confidence. However, it is not always possible to accurately quantify the net flux over a tidal cycle in an estuary where the gross flux is very large. Due to this large number (which also implies a large uncertainties), it has also been difficult to extrapolate such an estimate meaningfully over time to give the net annual flux. The present study indicates that with carefully planned experiments and good instrumentations, it is possible to estimate annual sediment budget for an estuary with some confidence from the flux measurement.

In this Chapter, we will try to estimate the annual sediment budget for the Taf based on short term flux measurements made at two transects (T9 and T5 in Figure 3.1). For each transect, measurements of suspended sediment concentration and current velocity were made through the water column at 15 minute intervals over a selected numbers of tides within neap-spring cycles. At T9 the measurements were made for six tidal cycles at five or seven stations across the transect, while at T5 the SPM concentration and tidal velocity were measured for 4½ tidal cycles at four stations across the transect. From this flux measurements an estimate of the sediment budget and, hence, the accumulation rate will be made. The results are then compared with the sedimentation rates estimated from a long-term measurement of the changes in estuarine sand volume. This volumetric change of estuarine sand has been obtained from the levelling surveys at the eleven transects shown in Figure 3.1 at regular intervals.

7.2 Flux calculations

The residual mass transport of suspended sediment is normally determined by spatially integrating the instantaneous suspended sediment flux over the water column and temporally integrating the resulting instantaneous mass transport for successive casts for the whole tidal cycle. The instantaneous flux for a section of water column in terms of weight per unit width per unit time is simply a depth-integrated product of current speed (u), and suspended sediment concentration (SSC). This calculation is valid if either u or SSC is constant throughout the water column. Our measurements showed that in most cases, u decreases towards the bed due to shearing effects, whereas SSC decreased away from the bed due to settling. Sand is normally concentrated close to the bed and its movement occurs in the lowermost metre or two of the flow, while finer material (silt and clays) remain in suspension and are evenly distributed throughout the water column. Thus the results of a depth-integrated product would not be valid in this case.

In the calculations of sediment fluxes, the water column was divided into 0.5m layers, each had different suspended sediment concentration and current velocity values as determined by the transmissometer and the current meters respectively. For every anchor station of the transect, the instantaneous mass transport (Q_t) for each cast was calculated using the following formula:

$$Q_t = \left(\sum_{i=1}^{n-1} C_i u_i A_i\right) + (C_n u_n A_n)\Delta x \qquad [7.1]$$

where;

C = suspended sediment concentration (g/m^3)

u = current speed (m/s)

A = cross sectional area over which other factors are representative (m^2)

Δx = depth function, is not constant and is given by:

$$\Delta x = (\frac{h}{0.5} - l) \qquad [7.2]$$

where;

h = water depth (measured by the tide gauge) at the anchor station (m).

l = number of 0.5 m depth interval in each cast.

The last term in Equation 7.1 was included to take into consideration the transport associated with the water depth measured by the tide gauge and the depth obtained from the CTD profiler. The two were different due to the boat swinging and the topography of the sea bed. The corresponding current speed for each depth interval of a CTD cast was obtained using spline curve fitting technique (Kjerfve, 1979 and Press *et al.*, 1992). The area of the estuary cross section was determined from levelling surveys at low water. The resulting integration has the unit of g/s.

The total flux for each cast (Q_T) is given by:

$$Q_T = Q_t \Delta t \qquad [7.3]$$

where;

Δt = the time interval between each cast.

By integrating the total flux for each cast over the flooding and the ebbing stages of a tide, yields the mass transport of SPM for the two tidal stages (Equations 7. 4 and 7.5).

$$Q_f = \frac{1}{2}Q_{T_1} + (\sum_{2}^{v-2} Q_{T_v}) + \frac{1}{2}Q_{T_v} \qquad [7.4]$$

and

$$Q_e = \frac{1}{2}Q_{T_1} + \left(\sum_{2}^{w-1} Q_{T_w}\right) \qquad [7.5]$$

where;

v = number of casts over the flood.

w = number of casts over the ebb.

The difference between the flood and the ebb values gives the net mass transport for that particular station, and the difference between the total flood and total ebb values for all the stations across the estuary gives the net mass transport for the tidal cycle.

Replacing the SPM term in Equation 7.1 with the mass of sea water (taken as 1020 kg/m^3) yields the mass water transport for each tidal cycle. This water flux is termed as the 'tidal prism'. Neglecting the river input and evaporation, the net mass transport of water should approach zero in order to conform with the continuity of mass.

7.3 Results

7.3.1 Water flux

The results of tidal prism calculations at Transects T9 and T5 are shown in Tables 7.1 and 7.2, respectively, and plotted in Figure 7.1. The results of the measurements carried out in October 1994 and July 1995 are combined for transect T9. The tables show that for the same tidal cycles, the flood tidal flux is generally slightly bigger than than the ebb tidal flux. However this difference is very small i.e it varies between 0 - 5% for all tides, except on the neap tides where the different is about 8% for transect T9 and 28% for transect T5. This bigger differences between flood and ebb water masses for the neap tides are partly due to the measurement error, whereby the the measurements were stopped prematurely before

Table 7.1 Calculated water flux at transect T9 - October 1994 and July 1995.

Date	Tidal height above O.D. (m)	Calculated water fluxes (m^3)		
		Flood	Ebb	Net
5/10/94	5.17	n.d.	1.5367×10^7	0.2057×10^7 *
5/10/94	5.36	1.7424×10^7	n.d.	n.d.
6/10/94	5.40	n.d.	1.5966×10^7	0.3680×10^7 *
6/10/94	5.46	1.9646×10^7	n.d.	n.d.
14/7/95	5.13	1.8992×10^7	1.7360×10^7	0.16318×10^7
16/7/95	4.46	1.4175×10^7	1.3492×10^7	0.0683×10^7
18/7/95	3.75	1.0651×10^7	1.0684×10^7	-0.0033×10^7
20/7/95	2.78	0.6711×10^7	0.6177×10^7	0.0534×10^7

n.d. = no measurement made; * = different tidal cycle

Table 7.2 Calculated water flux at transect T5, September 1995

Date	Tidal height above O.D. (m)	Water flux (m^3)		
		Flood	Ebb	Net
12 /9/95	4.96	n.d.	0.5212×10^7	-
13/9/95	4.73	0.4553×10^7	0.4433×10^7	0.0120×10^7
14/9/95	4.35	0.4096×10^7	0.4010×10^7	0.0086×10^7
15/9/95	3.74	0.2796×10^7	0.2804×10^7	0.0008×10^7
19/9/95	2.66	0.1269×10^7	0.0912×10^7	0.0358×10^7

n.d. = no measurement made.

the total expulsion of the prism from the estuary. On the neaps, more times are needed for the the tidal prism to be flushed out of the estuary completely, than on the springs. However this was very difficult to judge as the water remained salty during the ebb due to the late drainage of the saline water retained by the salt marshes, until the return of the next tide. Due to this different and the uncertainties of the ebb fluxes, only the food fluxes were

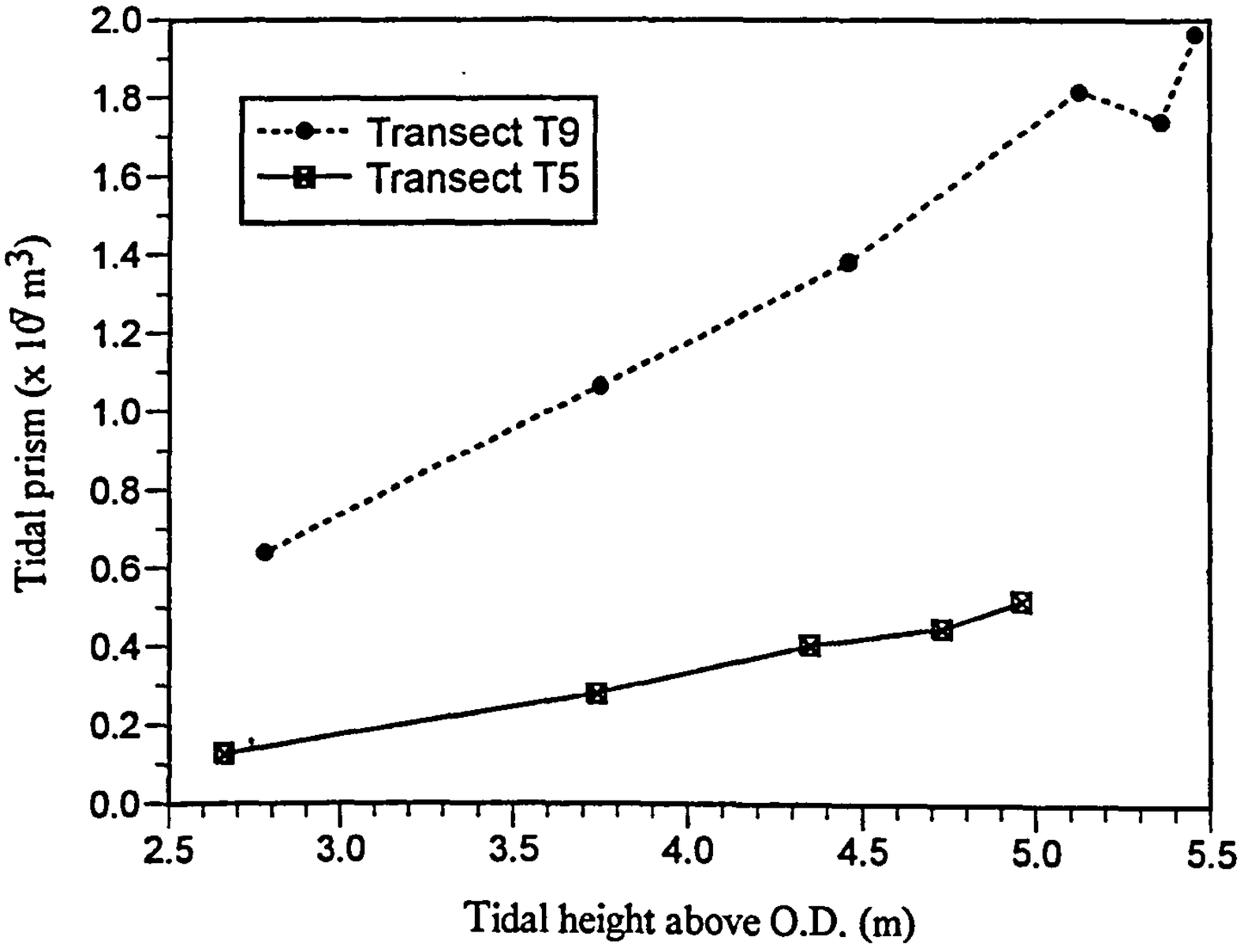

Figure 7.1 Variation of tidal prism with tidal height at transects T9 and T5.

used in the plot shown in Figure 7.1 which shows the tidal prism varies linearly with the tidal height. At T9 the spring tidal prism is 1.9 x10^7 m^3 while the neap tidal prism is 0.7 x 10^7 m^3. Further upstream at T5, these values reduced to 0.5 x 10^7 m^3 for the spring and 0.1 x 10^7 m^3 for the neap.

7.3.2 Sediment flux

The suspended sediment flux calculated at each stations across transects T9 and T5 are plotted in Figures 7. 2-7.4 (the positions of the stations in relation to the bed topography are shown in Figures 3.2). Highest sediment fluxes are recorded at stations located in the main channel (Station 1 in Figure 7.2; Stations 1, 2 and 3 in Figure 7.3; and Station 1 in Figure 7.4). They show that the fluxes calculated from these stations are crucial to the total fluxes for the transects, for each tidal cycle. The lowest sediment fluxes are recorded at stations away from the main channel, and those located in the intertidal sand flats; which are much lower than those for the channel stations. Although the total flood fluxes are greater than the total ebb fluxes (as can be seen later), the ebb fluxes are greater than the flood fluxes at some stations. This is related to the present of ebb dominated channels across the estuary as discussed in Chapter 4.

The sediment fluxes represented by each anchor station across the transects were combined to obtain the total sediment fluxes for the transects. The calculated suspended sediment fluxes for Transects T9 and T5 are tabulated in Tables 7.3 and 7.4, respectively. For Transect T9, the results for measurement in October 1994 and July 1995 are combined. The Tables show that the sediment fluxes measured at both transects increase with increasing tidal height. The sediment fluxes for the flood are higher than the for the ebb for all tidal cycles, resulting in a net landward flux of suspended sediment. At Transect T9, the gross flood flux is around 10 - 30 % higher than the gross ebb fluxes, at Transect T5 it is about 20 - 40 % higher.

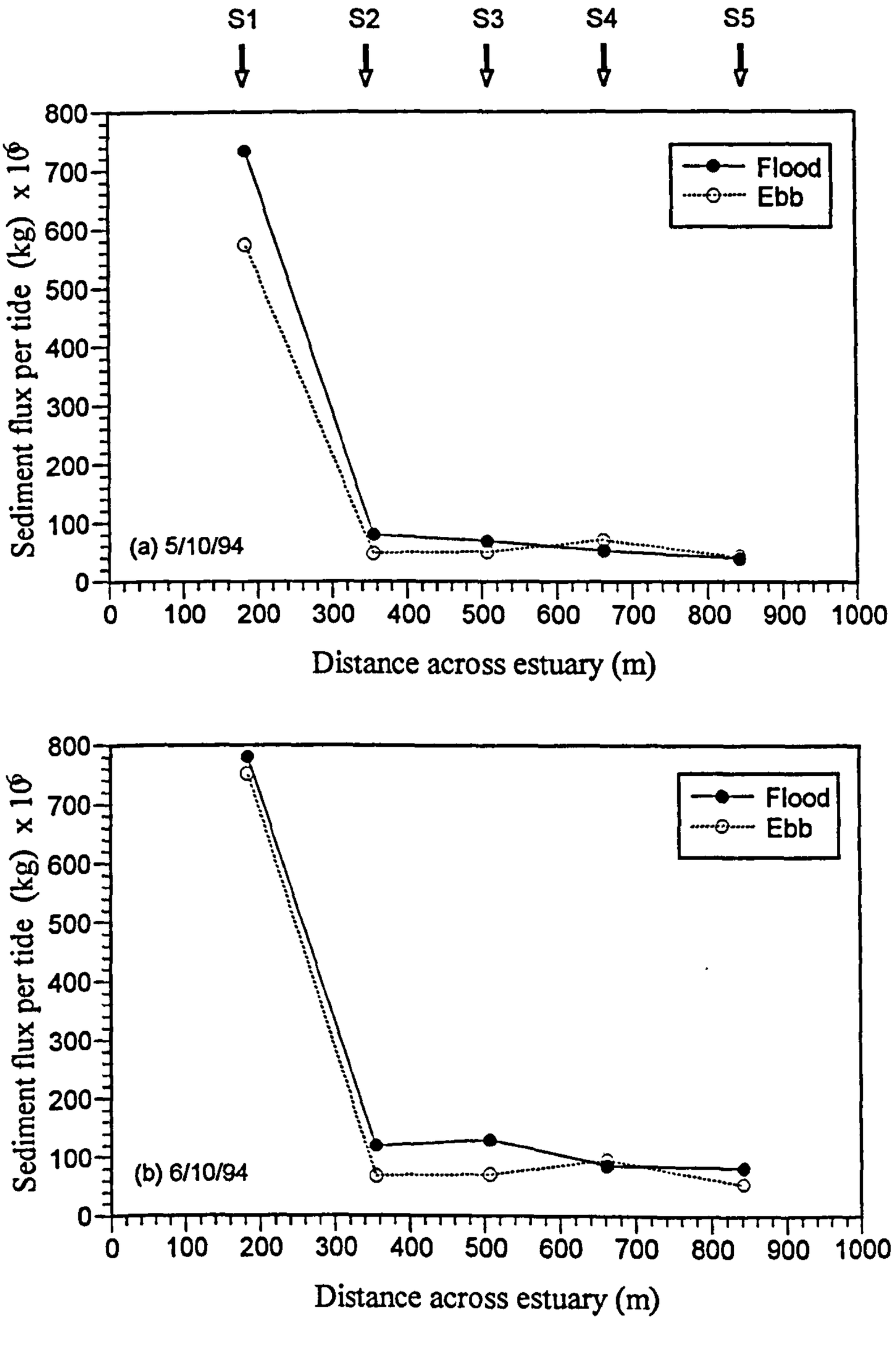

Figure 7.2 Variation of sediment fluxes at five stations across estuary (transect T9) on 5 & 6 October 1994.

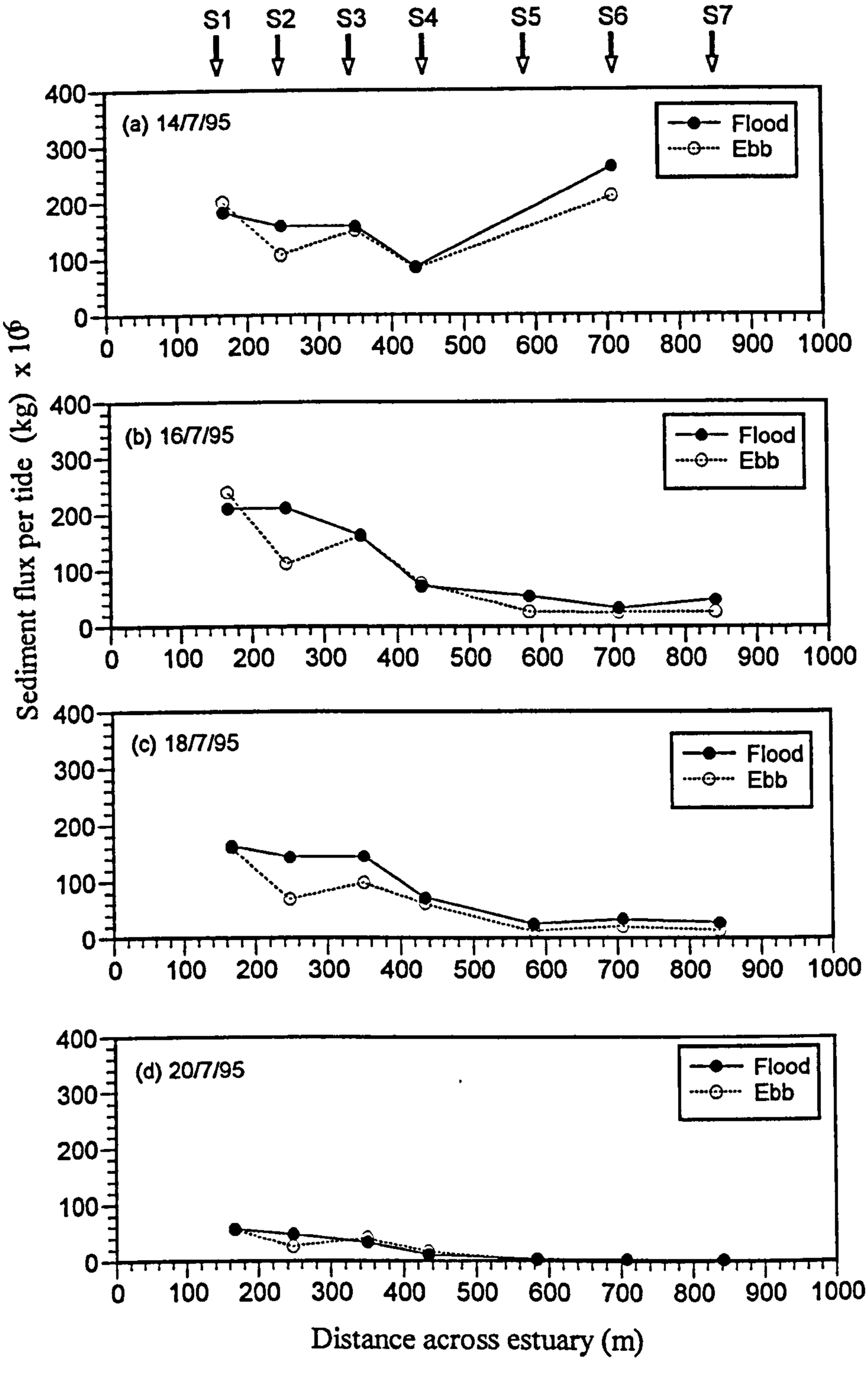

Figure 7.3 Variation of sediment fluxes at seven stations across estuary (transect T9) on 14, 16, 18 & 20 July 1995. The fluxes shown for station 6 on 14 July 1995 were the total for stations 5, 6 & 7 combined.

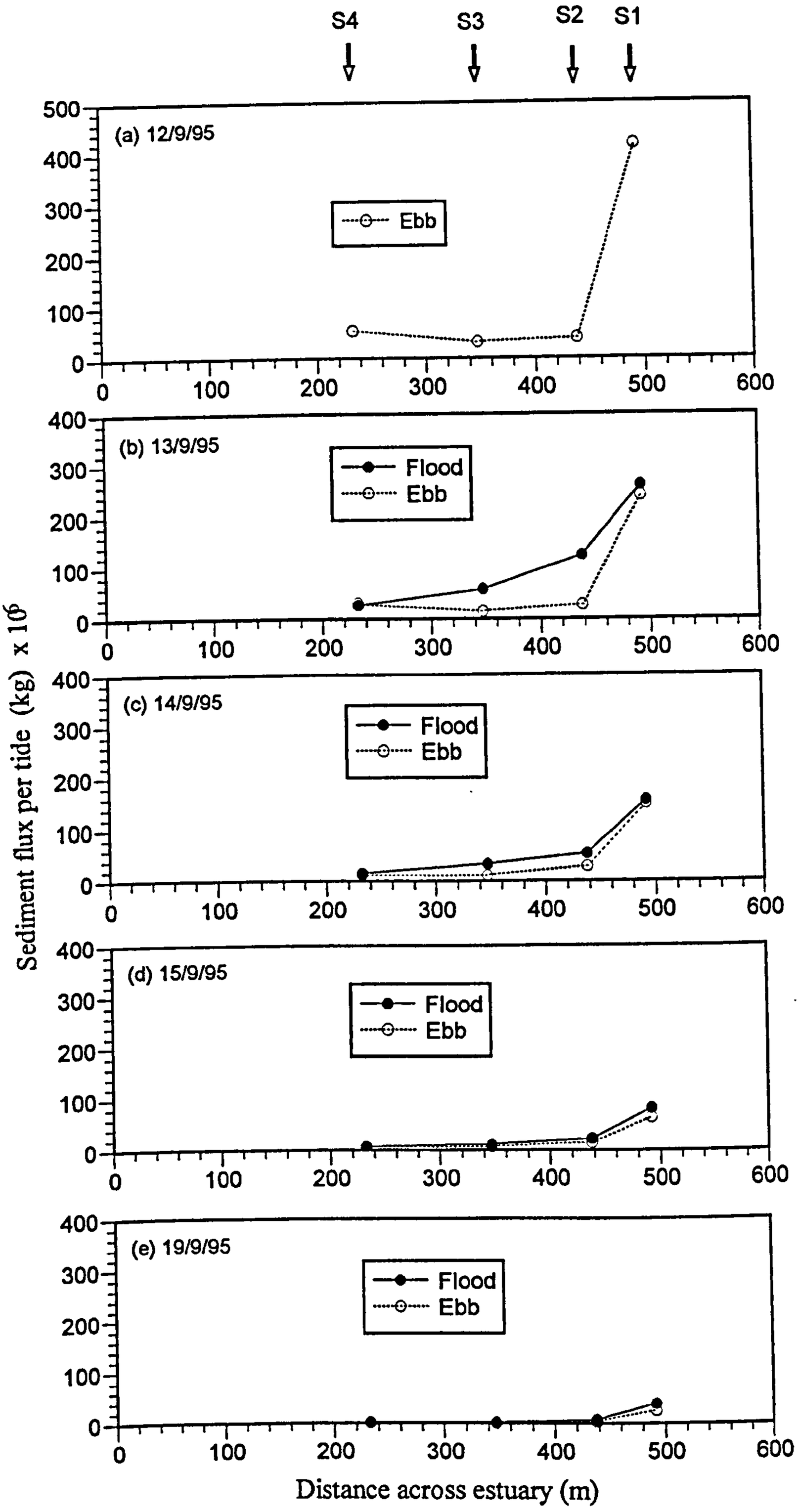

Figure 7.4 Variation of sediment fluxes at four stations across estuary (transect T5) on 12, 13, 14, 15 & 19 September 1995. Fluxes for 12 September 1995 were for ebb tide only.

Table 7.3 Suspended sediment flux across estuary at Transect T9.

Date	Tidal height above O.D. (m)	Calculated sediment fluxes (kg/tide)		
		Flood	Ebb	Net
5/10/94	5.17	n.d.	7.9072×10^5	1.8812×10^5*
5/10/94	5.36	9.7884×10^5	n.d.	-
6/10/94	5.40	n.d.	10.4090×10^5	1.5775×10^5*
6/10/94	5.46	11.9865×10^5	n.d.	-
14/7/95	5.13	8.4495×10^5	7.5275×10^5	0.9219×10^5
16/7/95	4.46	7.8894×10^5	6.6543×10^5	1.2351×10^5
18/7/95	3.75	6.0782×10^5	4.3755×10^5	1.7027×10^5
20/7/95	2.78	1.5736×10^5	1.4347×10^5	0.1389×10^5

n.d. = no measurement made; * = different tidal cycle

Table 7.4 Suspended sediment flux across estuary at Transect T5.

Date	Tidal height above O.D. (m)	Calculated sediment flux (Kg/tide)		
		Flood	Neap	Net
12 /9/95	4.96	n.d.	5.4269×10^5	-
13/9/95	4.73	4.7012×10^5	3.1469×10^5	1.5545×10^5
14/9/95	4.35	2.5988×10^5	2.0427×10^5	0.5564×10^5
15/9/95	3.74	1.2364×10^5	0.9411×10^5	0.2954×10^5
19/9/95	2.66	0.4885×10^5	0.2997×10^5	0.1888×10^5

n.d. = no measurement made.

The data in Tables 7.3 and 7.4 are plotted in Figures 7.5 and 7.6, respectively. At both transects the calculated sediment fluxes vary exponentially with the tidal heights. The results of Transect T5 however show a better exponential relationship than the results of Transect T9. For both transects, the best fit regression lines between tidal height and log of sediment fluxes have been drawn for both flood and ebb components of the fluxes and are shown in Figures 7.7 and 7.8. The regression statistics for T9 and T5 are given in

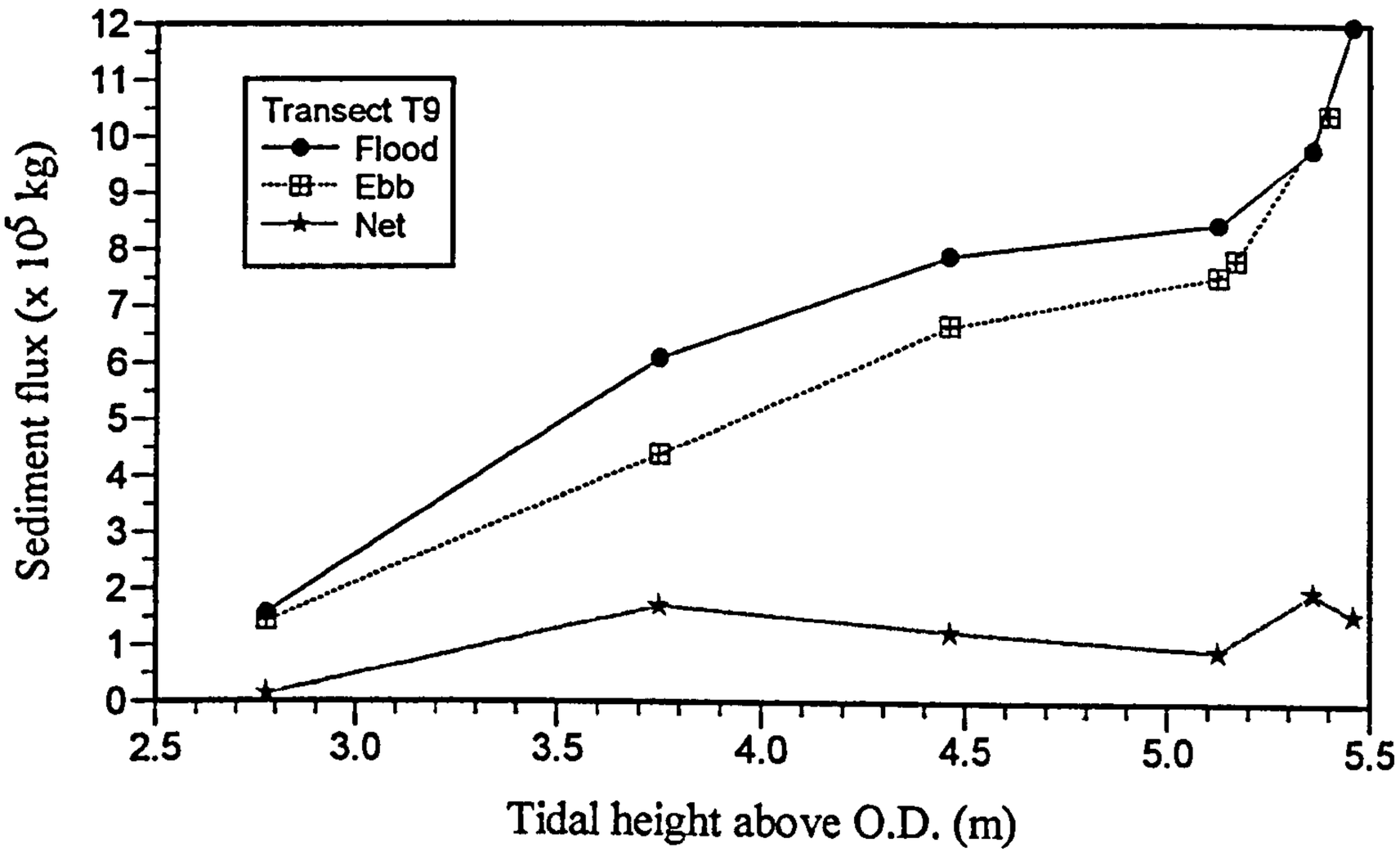

Figure 7.5 Variation of sediment fluxes with tidal height at transect T9.

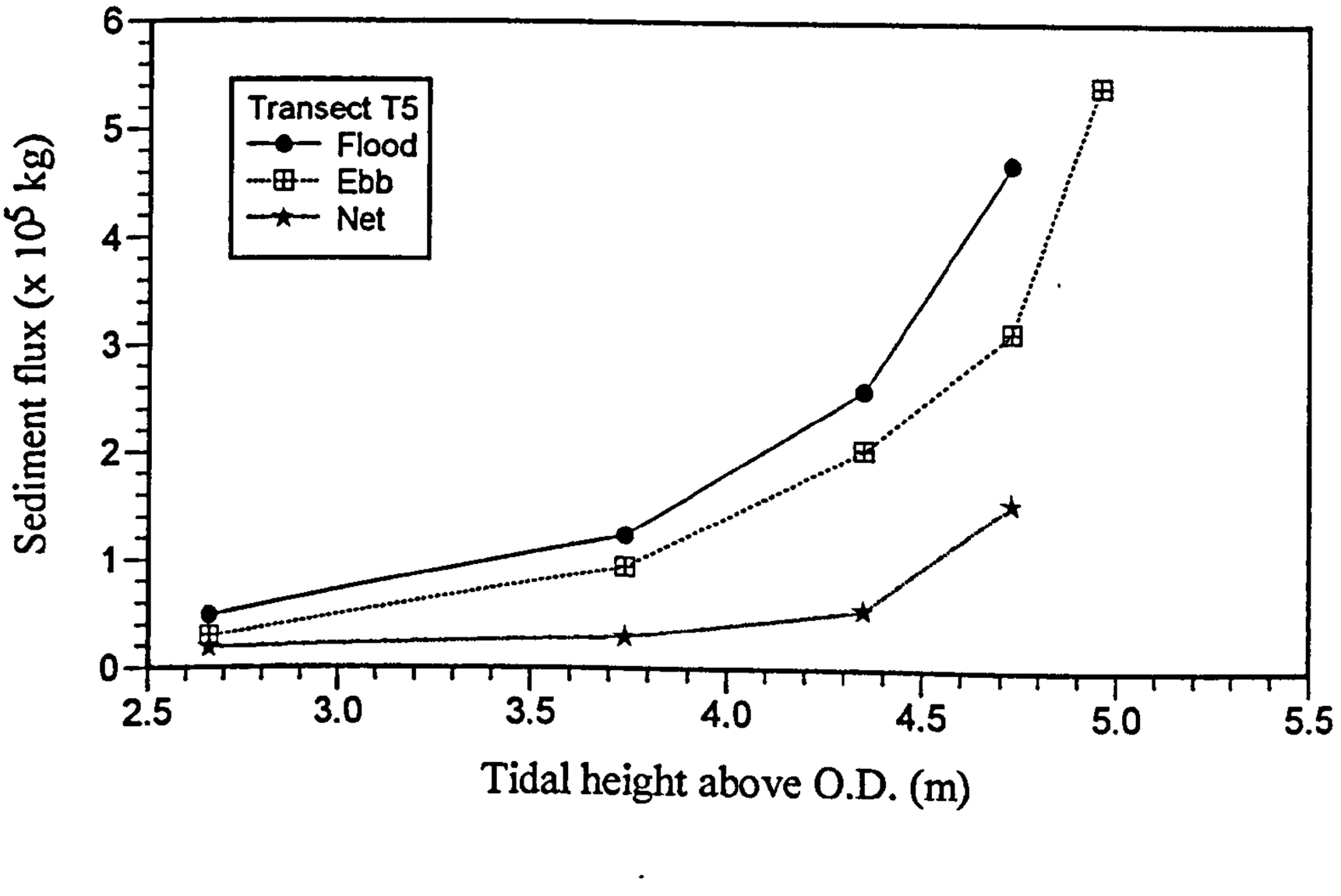

Figure 7.6 Variation of sediment fluxes with tidal height at transect T5.

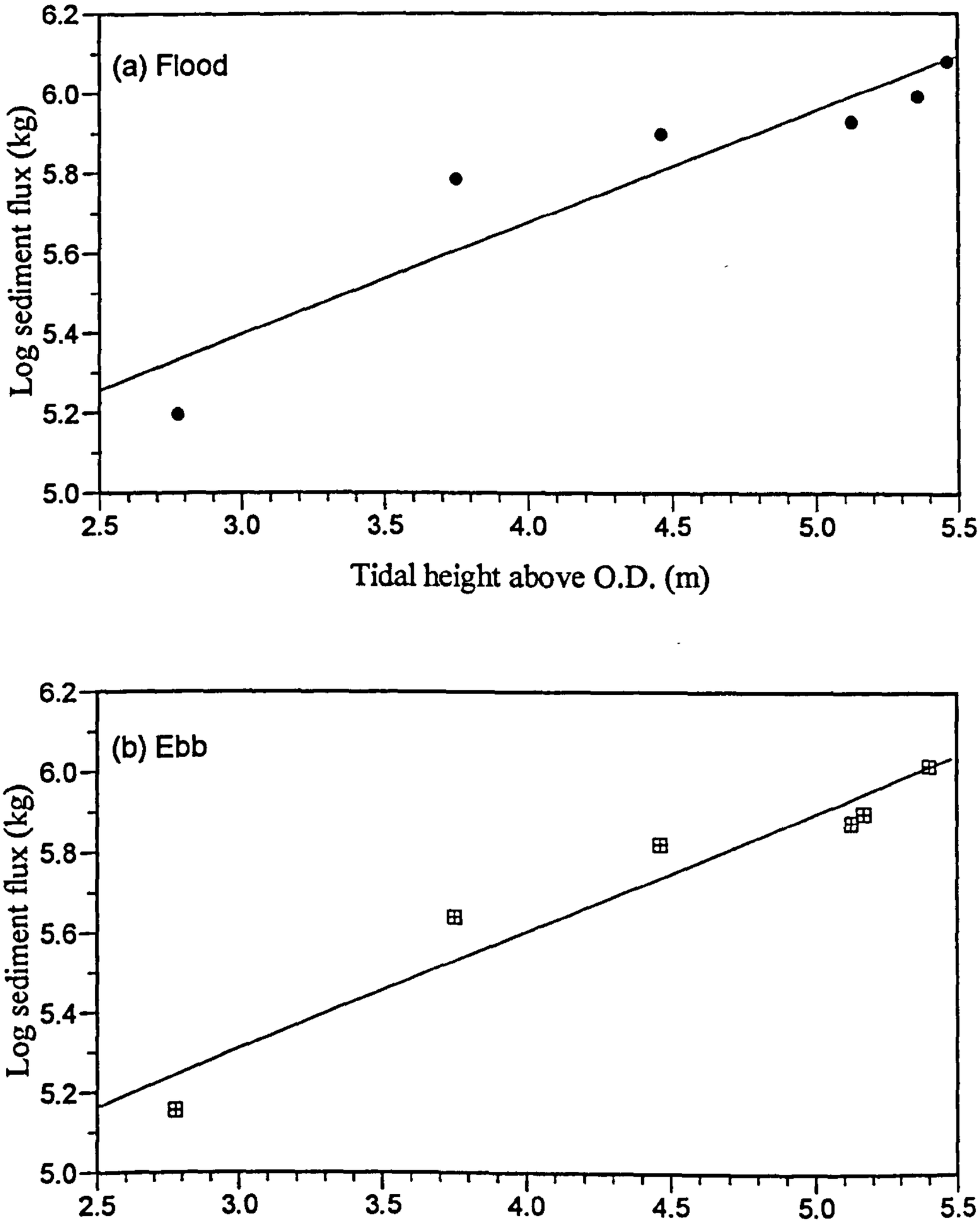

Figure 7.7 Linear regression between log of sediment flux and tidal height at transect T9.

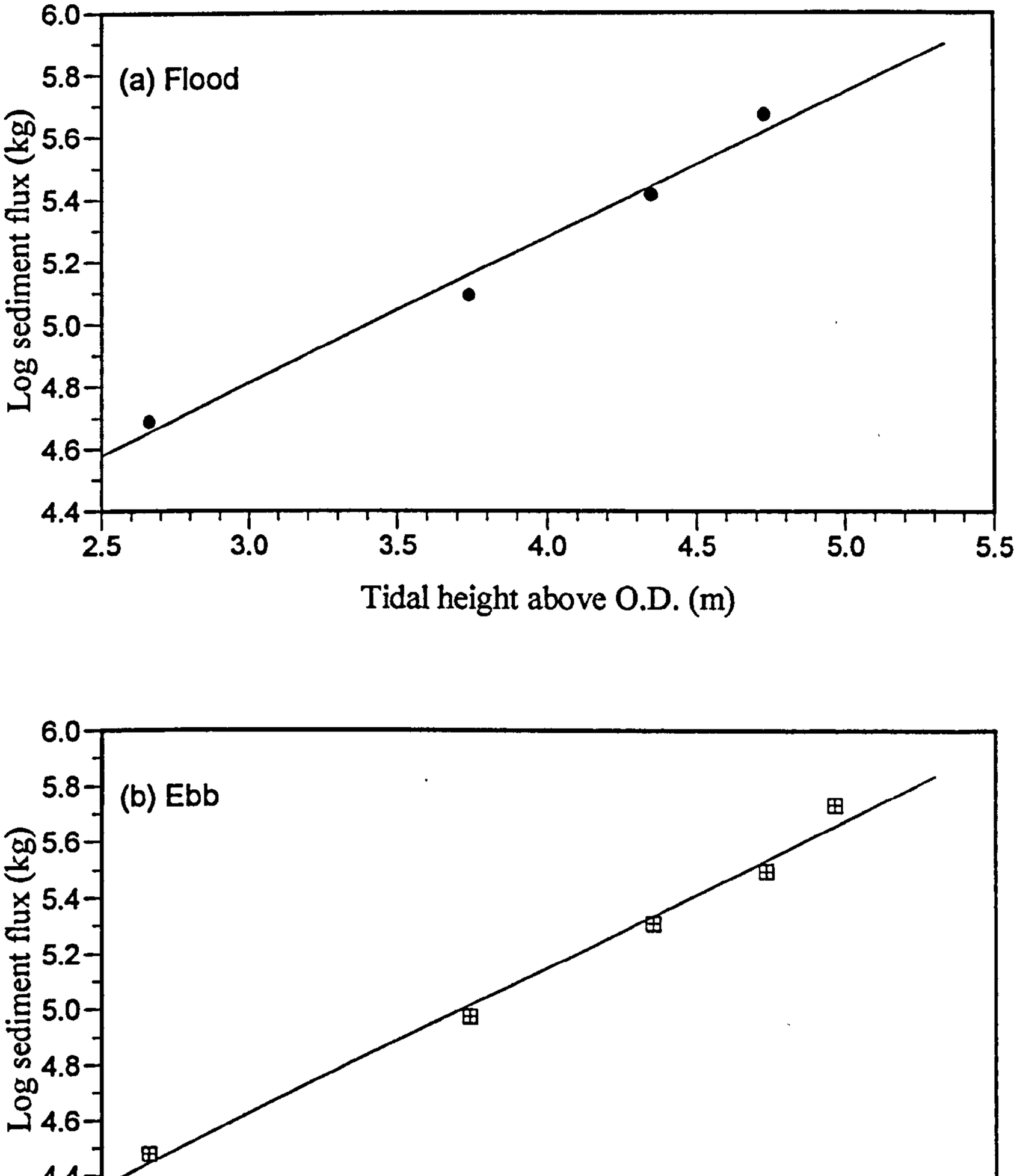

Figure 7.8 Linear regression between log of sediment flux and tidal height at transect T5.

Tables 7.5 and 7.6, respectively. The tables shows the statistical errors of the intercepts and slopes of the regression lines at 95% confidence level. For both transects highly significant correlations between the fluxes and tidal heights were obtained with R^2 values greater than 0.87 for both transects.

Table 7.5 Least square linear regression between tidal height and log of sediment flux for Transect T9.The intercept and slope show the errors at 95% confidence level.

Tidal direction	Intercept	Slope	R^2	n
Flood	4.56 ± 0.70	0.28 ± 0.15	0.867	6
Ebb	4.43 ± 0.50	0.29 ± 0.11	0.932	6

Table 7.6 Least square linear regression between tidal height and log of sediment flux for Transect T5. The intercept and slope show the errors at 95% confidence level.

Tidal direction	Intercept	Slope	R^2	n
Flood	3.41 ± 0.73	0.47 ± 0.18	0.983	4
Ebb	3.04 ± 0.43	0.53 ± 0.10	0.989	5

The gross sediment fluxes during the flood and ebb of each tidal cycle for T9 and T5 were divided by the estuary width at each transects (T9 = 1050 m, and T5 = 430 m) in order to obtain the sediment flux per meter width cross section. The results for both transects are combined, and plotted in Figure 7.9. The figure shows the amount of sediment that passes every metre section of the estuary, during the flood and ebb for a neap-spring lunar cycle. The best fit exponential curves have been drawn for the flood and ebb components of sediment fluxes. These gave the following exponential relationships:

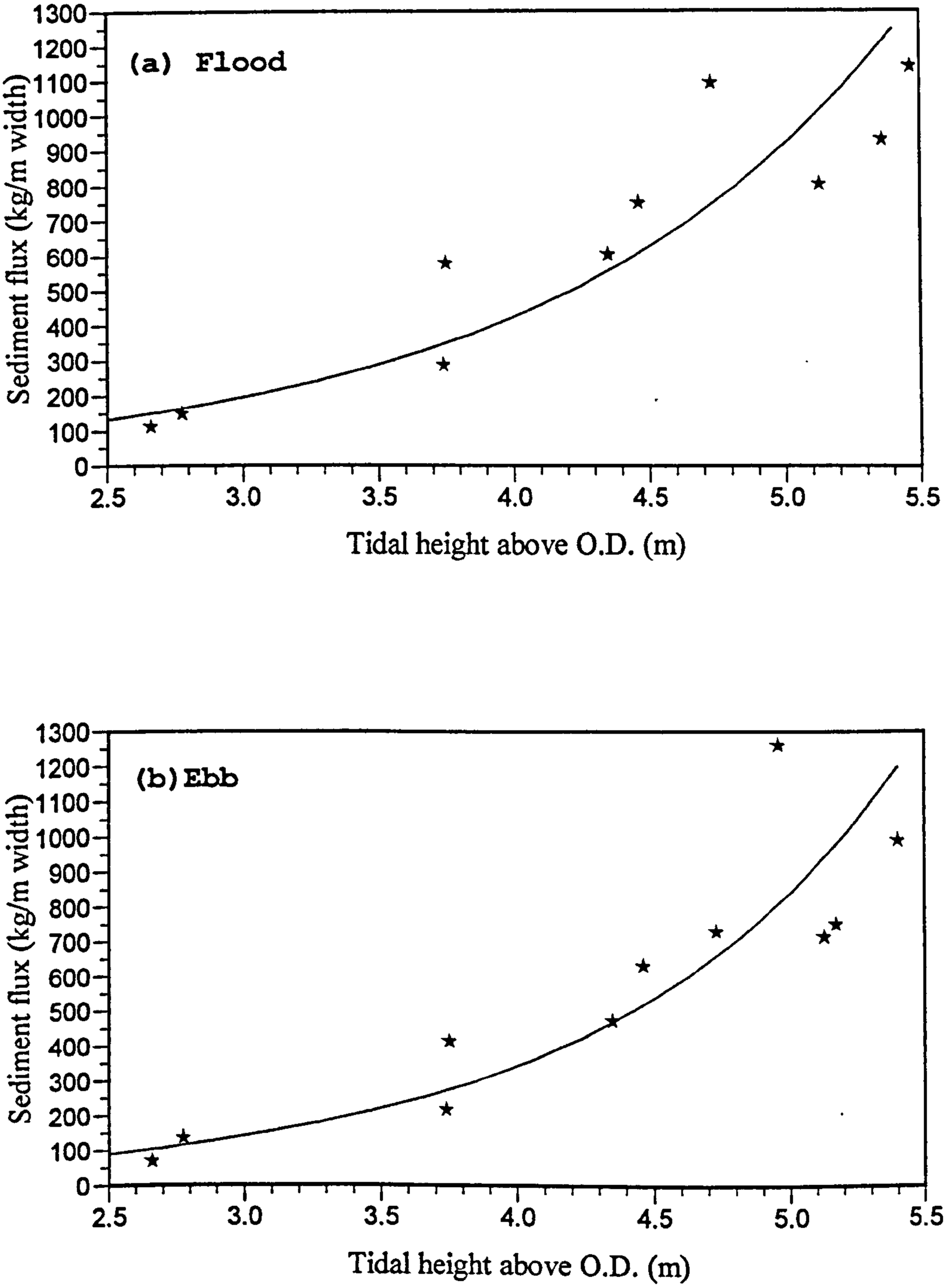

Figure 7.9 Variation of sediment fluxes with tidal height during (a) flood, and (b) ebb, with best exponential fit lines for all data from transects T9 and T5.

$$F_{flood} = 19.20 \times 2.17^{t} \quad [7.6]$$

and

$$F_{ebb} = 9.67 \times 2.44^{t} \quad [7.7]$$

where;

F = sediment flux (kg/m)

t = tidal height above O.D. (m).

For the same data set, the regression statistics for the best fit regression lines between tidal height and log of sediment fluxes has also been calculated and shown in Table 7.7. The table also shows the statistical errors of the intercepts and slopes of the regression lines at 95% confidence level. For both flood and ebb tides, highly significant correlations between the fluxes and tidal heights were obtained with R^2 values greater than 0.88.

Table 7.7 Least square linear regression between tidal height and log of sediment flux for the combined data of Transects T9 and T5. The intercept and slope show the errors at 95% confidence level.

Tidal direction	Intercept	Slope	R^2	n
Flood	1.28 ± 0.44	0.34 ± 0.10	0.882	10
Ebb	0.99 ± 0.44	0.39 ± 0.10	0.895	11

Given the tidal amplitudes, either of the relationships (Equations 7.6 and 7.7, or the values given in Table 7.7) may be used as general equations to predict sediment fluxes across any transect of the Taf estuary.

7.4 Sedimentation rate

From the measurement of sediment flux made across the estuary cross section over the

spring-neap tidal cycles, it has been possible to estimate the sediment budget for the estuary. Using the correlations given in Tables 7.5 and 7.6 i.e. from the regression shown in Figures 7.7 and 7.8, sediment fluxes at both transects have been estimated for 14 tidal cycles i.e. from spring to neap. The tidal heights above Ordnance Datum (O.D.) as measured by the tide gauges were used in this calculation. The results are shown in Tables 7.8 and 7.9 which also show the associated error bars at 95% confidence level calculated from the values given in Tables 7.5 and 7.6. At Transect T9 a total of 7.6361×10^6 kg of sediment were transported into the estuary and 6.5637×10^6 kg of sediment were transported out of the estuary for a complete spring-neap cycle, giving a net transport in favour of the flood of 1.0724×10^6 kg . Assuming the same amount of sediment is transported into the estuary during a neap-spring cycle, the amount of sediment carried into the estuary is 5.5764×10^7 kg/year. The areas of the estuary (i.e. using the mean high water mark) upstream from the transect lines have been measured using a planimeter. The surface area of the estuary

Table 7.8 Sediment flux calculated for 14 tidal cycles at Transect T9.

Tide no.	Tidal height above O.D. (m)	Sediment fluxes (kg)	
		Flood	Ebb
1	4.90	844870±91076	738414±69010
2	5.13	979452±185778	862500±131580
3	4.76	772175±45330	671797±38735
4	4.91	850317±94652	743418±71382
5	4.46	636775±29408	548590±10339
6	4.58	687825±2908	594900±6985
7	4.11	508512±86089	433105±46882
8	4.26	559972±65140	479279±33488
9	3.75	403483±120488	339629±68290
10	3.69	388221±124456	326142±70670
11	3.32	306064±140642	254031±79814
12	3.14	272630±144429	224953±81560
13	2.78	216321±146419	176402±81441
14	2.73	209480±146235	1705054±81133
TOTAL		7636097±1422455	6563705±871309

Table 7.9 Sediment flux calculated for 14 tidal cycles at Transect T5

Tide no.	Tidal height above O.D. (m)	Sediment fluxes (kg)	
		Flood	Ebb
1	5.21	693774±390707	618565±154821
2	4.96	530601±235604	456310±86420
3	5.04	578139±278399	502968±105016
4	4.73	414605±140512	344909±46203
5	4.59	356798±98680	290881±29211
6	4.35	275823±47406	217208±9379
7	3.96	181538±923	135133±6705
8	3.74	143381±12710	103393±10556
9	3.59	122074±18671	86142±11890
10	3.38	97455±23787	66716±12585
11	3.06	69143±26754	45197±12054
12	2.94	60793±26884	39056±11574
13	2.58	41320±25436	25202±9748
14	2.56	40443±25301	24596±9640
TOTAL		3605886±1351773	2956274±515802

landwards of the Transect T9 is 2.96×10^6 m^2. Assuming a sediment density of 1.57 g/cm^3 (40% porosity), this represents a deposition rate of 1.20 cm/year. Similarly, at line T5 a net accumulation of 6.4961×10^5kg of sediment (Table 7.9) has been deposited in the estuary during a spring-neap cycle, giving a total sediment accumulation of 3.378×10^7 kg/year. The surface area landward of the transect line is 1.344×10^6 m^2. With the similar sediment density, this represent an accumulation rate of 1.60 cm/year.

The highest and the lowest possible sedimentation rates at T9 and T5 may be calculated for the same tidal cycles using the error bar estimate at 95% confidence level as given in Tables 7.8 and 7.9, respectively. This will provide the range of errors in the calculated sedimentation rates at the two transects. The difference between the maximum flood flux

Table 7.10 Maximum and minimum sediment flux calculated for 14 tidal cycles at Transects T9 and T5.

Transect no.	Tide	Sediment flux (kg)	
		Maximum	Minimum
T9	Flood	9058552	6213642
	Ebb	7435014	5692396
T5	Flood	4957659	2254113
	Ebb	3472076	2440472

Table 7.11 Sediment fluxes calculated using Equations 7.6 and 7.7 for 14 tidal cycles at Transect T9

Tide no.	Tidal height above O.D. (m)	Sediment fluxes (kg)	
		Flood	Ebb
1	4.90	892239	806372
2	5.13	1065975	990196
3	4.76	800663	711621
4	4.91	899167	813604
5	4.46	634845	544402
6	4.58	696595	605970
7	4.11	484272	398293
8	4.26	543851	455372
9	3.75	366565	288807
10	3.69	349941	273742
11	3.32	262844	196729
12	3.14	228680	167522
13	2.78	173097	121472
14	2.73	166530	116169
TOTAL		7565265	6490269

and the minimum ebb flux, extrapolated over a year, will give the maximum possible sedimentation rate; the difference between the minimum flood flux and the maximum ebb flux, extrapolated over a year will give the minimum possible sedimentation rate (Table 7.10). Thus, for T9 the maximum sedimentation is 3.8 cm/yr and the minimum sedimentation rate is -1.4 cm/yr, and for T5 the maximum and minimum sedimentation rates are 6.2 cm/yr and -3.0 cm/yr, respectively. Therefore, the sedimentation rate estimated for Transect T9 is 1.2 ±2.6 cm/yr, and for T5, the estimated sedimentation rate is 1.6±4.6 cm/yr.

Table 7.12 Sediment fluxes calculated using statistical parameters given in Table 7.7 for Transect T9.

Tide no.	Tidal range above O.D. (m)	Sediment flux per metre width (kg)	
		Flood	Ebb
1	4.90	849 ±109	768 ±92
2	5.13	1015 ±185	943 ±164
3	4.76	762 ±73	678 ±60
4	4.91	856 ±112	775 ±95
5	4.46	604 ±16	519 ±10
6	4.58	663 ±36	577 ±27
7	4.11	461 ±25	379 ±24
8	4.26	518 ±10	434 ±12
9	3.75	349 ±48	275 ±40
10	3.69	333 ±51	261 ±42
11	3.32	250 ±60	187 ±46
12	3.14	218 ±61	160 ±46
13	2.78	165 ±61	116 ±44
14	2.73	159 ±60	111 ±43
TOTAL		7202 ±908	6183 ±744

To demonstrate whether Equations 7.6 and 7.7, and the statistical parameters given in Table 7.7 are valid, the sediment fluxes across the estuary at Transect T9 have been

recalculated for the same tidal amplitudes, and the results are shown in Tables 7.11 and 7.12, respectively. From Table 7.11, the net sediment accumulation in the estuary for the same spring-neap tidal cycles is 1.0750×10^6 kg; this is equivalent to a sedimentation rate of 5.59×10^7 kg/year or 1.2 cm/year. From Table 7.12 the maximum possible sediment accumulation (extrapolated over 1050 m cross section and over a year) is 1.4578×10^8 kg/yr which represents an accumulation rate of 3.1 cm/yr, and the minimum possible sediment accumulation rate of -3.4562×10^7 kg/yr which represents an accumulation rate of -0.7 cm/yr. The sedimentation rate calculated based on the mean values are 5.5637×10^7 kg/yr which gives an accumulation rate of 1.2 cm/yr. Therefore, the sedimentation rate of fine sands in the estuary is 1.2 ± 1.9 cm/yr.

As the measurements were made only for part of the 14 tides for a full spring-neap tidal cycles, several assumption have to be made: a) there is a linear variation of log sediment flux with the tidal height above O.D. between the successive measurements; and b) the measurements represent fair weather conditions.

7.5 Long term measurement of sand budget

The sedimentation rate estimated from the sediment flux measurement may be compared with that estimated from long term measurement of the sand budget. The long term sand budget of the Taf estuary has been determined since 1968 (Jago, 1980; Jago *et al.*, 1996). Eleven transects were set up along the estuary cross section (see Figure 3.2) and periodically surveyed at low tide, thus providing accurate measures of annual volumetric change of estuary sand body. The surveys showed that there has been a net sand accretion in the estuary (Figure 7.10). The annual sand budget calculated from this survey is 6.8×10^4 m^3 which gives an equivalent sedimentation rate of 1.8 cm/yr. The results of the short term measurement of sediment flux and the long term measurement of sand budget are thus very similar.

7.6 Discussion

For a valid sediment flux calculation, the flood water masses should balance the ebb water masses. For the Taf, the ebb tidal prism should include the fresh water contribution which accounts for less than 0.5 % of the total water masses. A very small difference in flood and ebb tidal prisms can be accounted for by evaporation and the water retained by the salt marsh at the end of the ebb tide. Another possible reason for this difference is the calculation was only made up to the measurement time i.e. about five hour after HW, however the ebbing continues for several hours during low water before the next flood tide enters the estuary. The large different (28%) obtained between flood and ebb tidal prisms on the neap tide of 19th September 1995 (Transect T5) is thought to be due to an inaccuracy of the tidal velocity measurement at low flow velocities made at Station 1. As the water depth barely exceeded 0.5 m during high water at other stations, the sediment flux measured at Station 1 accounts for most of the total flux for the tidal cycle. The velocity measurements and the CTD casts were also not made for the full tidal cycle at this station. The measurements ceased after 3.5 hours through the ebb, thus for a few hours of the ebb, the velocity and sediment concentration had to be extrapolated which may not be so accurate for the flux calculation. Though there was a relatively large different in the flood and ebb water masses on the neap tide, this would not invalidate the overall result of sediment flux calculations as the values for neap tides are much smaller than on bigger tides. In general, the residual mass transport of water masses approximate zero for both transects, therefore the results should give a representative picture of the transport of suspended sediment in the Taf estuary.

The values obtained for the sediment fluxes are for fair weather conditions and low- to - average river discharges. It is expected that during storm conditions, more sediments from Carmarthen Bay are entrained and carried into the estuary by the tide. Similarly, high river discharges bring down more suspended sediment into the estuary, and the higher discharge velocity would result in more sediment being transported out of estuary into the bay.

Attempts were made to measure the current speed at the same time as the CTD-

Transmissometer casts were made, but this was not always possible particularly around HW where the water column was the deepest. To complete a CTD cast at a station took less than 2 minutes but it took up to 15 minutes to do a compete profile of current measurements. The intended 15 minutes time interval for current measurement and CTD cast were not always possible due to limited man power and resources to cover all seven anchor stations across the estuary within that period, thus at some times the measurement intervals were up to 30 minutes. Therefore, there was up to 15 minutes time different between a CTD-Transmissometer cast and its corresponding current measurement. This time different resulted in an underestimate of sediment fluxes if the currents were measured later than the transmissometer cast during the rising tide on the flood, and an overestimate of flux if the currents were measured later than the transmissometer cast during the falling tide on the ebb.

Another point to note is that measurements at Transects T9 and T5 were made during falling spring tides. There is definitely some differences in transport mechanism and strength between falling and rising tides. Field observations showed that the intertidal sand bank prograded during rising tides and retreated during the falling tides. Thus the net sediment fluxes at both transects could be slightly underestimated.

The results of the sedimentation rate calculation show that a smaller error was obtained for T9 (1.2 ± 2.6 cm/yr) compared to T5 (1.6 ± 4.2 cm/yr), despite poorer correlation coefficients between sediment fluxes and the tidal heights at T9 than at T5 (see Tables 7.5 and 7.6). This better estimate of sedimentation rate for T9 is due to the fact that T9 has more data points (6 for both flood and ebb) compared to T5 (4 for flood and 5 for ebb). Thus to obtain a statistically good estimate of sedimentation rate based on suspended sediment flux calculation, the measurement of at least 6 different tidal cycles should be made. A similar sedimentation rate (1.2 ± 1.9) but with a smaller error bar was obtained for the combined data set (11 different tidal cycles) from the both transects.

Over spring-neap cycles the gross flood suspended sediment flux is a significant proportion of the gross ebb suspended sediment flux; at T9 it is 16.3 % higher and at T5 it is 22.0 %

more. Thus there is a net deposition of sediment in the estuary.

McCave (1979) questioned the validity of the results of the net sediment flux calculation as the ebb and flood fluxes are often two very large numbers having relatively large uncertainties. A number of similar studies dealing with net flux (eg. Terwindt, 1967 on the Rhine; Fleming, 1970 on the Clyde; Allen and Castaing, 1973 on the Gironde; and Harris and Collins, 1988 in the Bristol Channel, U.K.) were also posed with similar uncertainties. A similar study to the Taf is being carried out in the Humber in eastern England, an estuary 10 times bigger than the Taf. A sediment flux curtain has been established across the 7000 m width of the estuary mouth in order to asses the sediment exchange between the estuary and the sea on daily, monthly, seasonally and yearly time scales (Hardisty and Rouse, 1996). Comparison of some of the physical and measurement parameters in the Humber and the Taf are listed in Table 7.13. The Table shows the difficulties (in terms of sampling frequencies and measurement stations) of doing a detailed measurement of sediment fluxes in large estuaries in order to quantify the sediment budget as highlighted by McCave (1979)

Table 7.13 Comparison of sediment flux study between Humber Estuary and Taf Estuary.

Estuary parameters	Humber	Taf
Catchment area	25,000 km^2	217 km^2
Width	8 km	1.5 km
Tidal influence	120 km	15 km
Spring tidal range	6.5 m	8.5
Spring tidal prism	160 x 10^7 m^3	1.8 x 10^7 m^3
Sampling interval	60 minutes	15 minutes
Number of monitoring station across estuary mouth	5 (3)	5 - 7
Averaged inter-station distance	1400 m	150 - 240 m
Spring sediment flux (flood)	165 x 10^6 kg	1.0 x 10^6 kg

and Dyer (1986). A crucial different between the two estuaries is the percentage of the net to the gross sediment fluxes; for the Taf, the difference is more than 10%; in the Humber, it is less than 1%.

Our measurements in the Taf indicate that the net sediment flux can be quantified with a high degree of confidence using transmissometer casts and an array of current meters across the estuary. The calculated annual sedimentation rates based on sediment flux measurement is 1.2 ± 1.9 cm/yr for T9 and 2.18 ± 1.70 cm/yr for T5. This value is very similar to that obtained from the long term measurements of the volumetric change of the estuarine sands that give an accumulation rate of 1.8 cm/yr as measured by Jones and Jago (1994) and Jago *et al.* (1996). There are several reasons for this success:

(1) the barred estuary is largely protected from waves and it is fed by a smaller river, so most of the sand flux is achieved by tidal currents;

(2) the estuary has a narrow cross section so the tidal flow can be monitored without difficulty; it is therefore easy to achieve balanced flood and ebb water masses, the first prerequisite for a sediment flux estimate;

(3) because of the tidal asymmetry, the net sand flux is a significant proportion (between 10 - 30 %) of the gross sand flux and can be meaningfully quantified by transmissometers over tidal cycles;

(4) the suspended matter is very uniform in composition i.e. a well sorted fine sand and is the same on both flood and ebb, so transmissometer calibration is easy and reliable; and

(5) the high temporal and spatial sampling rates adopted in this study increased the degree of confidence in this tidally active and changing environment.

Without all these conditions it is doubtful whether a reliable estimate of sediment flux can be made.

CHAPTER EIGHT

SEDIMENT TRANSPORT

8.1 Introduction

Sediment transport is of great interest to engineers and sedimentologists as they are of vital importance to many river and marine engineering problems. This is also evidence from many predictive formulae which have been developed to quantify the sediment movement. The sediment transport rate is the total mass of sediment grains passing through a section per unit time. It is a product of the mass of moving grains present in the water over a unit area and the velocity at which they move. The study of sediment transport, whether in rivers, estuaries or along coasts, is a highly complex problem. Prediction of sediment transport rates is often subjected to large uncertainties, while field measurement normally requires extensive manpower and equipment.

In this Chapter the results of sediment transport rate measurements made at two transects (T5 and T9) in the lower estuary will be presented. The measured transport rate is then compared with the transport rate calculated using some of the available transport equations. Many of these equations have been derived elsewhere from flume studies and calibrated using experimental data under laboratory conditions. The predictive capability of these equations are here tested in the field environment.

In order to make this comparison, the same data used for sediment flux calculation (see Chapter 7) are again used here to obtain the transport rate at each anchor station. As the instantaneous transport rate is measured in mass per unit length per unit time (as do the rate given by empirical formulae), the transport rates presented here are specific to each measurement station; they do not represent the transport rate across the compartment represented by each station.

8.2 Measured sediment transport

As described in Chapter Three, measurements of current velocity and suspended sediment concentration were made over spring-neap tidal cycles at anchor stations set up along transect T5 and T9 in the lower estuary. The data available provided a direct measure of the suspended sediment transport at these measurement stations. The instantaneous transport rate over one metre width of the water column at any one station is simply the product of the current speed and the suspended sediment concentration. The total transports for the flood and ebb tide at a particular station can be obtained by integrating the instantaneous transport over the flood and ebb phases of the tidal cycle. These total transports have been calculated for all the stations along the two transects. There were cases however, where no current data were available; thus the total transports were not calculated for these stations.

It is important to note that the measured transport rates were for the suspended load transport, whereas many predictive transport equations with which the measured transport are compared, are either for bedload transport or for total load transport (bedload and suspended load). For the very fine sands found in Taf estuary, only limited bedload transport takes place but suspended sediment load makes up most of total transport, and as noted before (see Chapter 2), for these sands, the suspension occurs at the threshold of movement, so suspended transport equals to total transport. The transport rate is different from the suspended sediment flux as it represents the mass perunit width of a water column at the measurement station, while the flux represents the mass for a cross-sectional area represented by the station.

8.2.1 Transect T9 - October 1994

At this transect, measurements were made over two tidal cycles on 5 and 6 October 1994 which were during a spring tide (6 October was the bigger tide). On both dates, the flood and the ebb sections were not of the same tidal cycles but of the two consecutive tides. As

there was only a very small difference between the maximum tidal heights of the two tides, direct comparison between the ebb and flood transports may be made.

The locations of the five measurement stations across Transect T9 are shown in Figure 3.2a. and the measured sediment transports at these stations are given in Tables 8.1. It shows that across the transect, transport was quite variable. Maximum transport occurred at Station 1 and minimum transport at Station 5, during both the flood and the ebb. Station 1 was located in the main channel where current speed was the strongest, while Station 5 was located at the greatest distance from the main channel on the relatively high level of the intertidal sand flat, where current speed was the weakest. On the flood, a total of 4677 kg/m of the transport occurred at Station 1, but transport rapidly decreased across the estuary toward Station 5 where only 289 kg/m of transport occurred. During the ebb, Station 1 recorded a total transport of 5313 kg/m but only 183 kg/m at Station 5. At Stations 1 and 4, the transport was ebb dominant while Stations 2, 3 and 5 showed a flood dominant transport.

Table 8.1 Measured total transport at Stations 1-5, Transect T9, on 5 - 6 October 1994.

Date	Station number	Transport rate (kg/m)			Net direction
		Flood	Ebb	Net	
5/10/94	1	4207	4609	402	Ebb
	2	567	356	211	Flood
	3	425	312	113	Flood
	4	378	620	242	Ebb
	5	166	148	18	Flood
6/10/94	1	4677	5313	636	Ebb
	2	880	456	424	Flood
	3	806	438	368	Flood
	4	598	829	231	Ebb
	5	289	183	106	Flood

Figure 8.1 shows the variation of the transport rate over the tidal cycle at Station 1. The highest transport rate corresponding to the maximum flow velocity was recorded on the early flood. This maximum (2.2 kg/m/s) was twice that recorded during the ebb. The transport rate then rapidly declined and attained its minimum value (0.02 kg/m/tide) at high water. There was very little increase in transport rate during the first three hours of the ebb. A rapid increase in transport rate occurred in the fourth hour of the ebb when the mean velocity reached a value greater than 1.0 m/s. At the end of the ebb, two peak transports were recorded; the first one corresponded to the maximum flow velocity, but the second peak was recorded after a decline in the flow velocity. The transport rate declined rapidly when velocity reduced to the river flow velocity at the end of the ebb tide.

At Station 3 (Figure 8.2) which was located on the intertidal sand flat, the transport rate was much less, only about 10 % of that observed at Station 1. On the flood tide, peak transport (0.2 kg/m/s) occurred at the early stage of the flood when the current was strongest. This is similar to that observed at Station 1; however the peak concentration was about 10 % of the concentration at Station 1, though the maximum flood velocity at Station 3 was 50% of that at Station 1. At the end of the ebb tide, the transport rate showed only a single peak (0.15 kg/m/s) which corresponded to the maximum flow velocity.

8.2.2 Transect T9 - July 1995

In July 1995, seven anchor stations were set up along Transect T9. The positions of these stations along the transect are shown in Figure 3.2b. Stations 1 - 4 were located in the main channel while Stations 5 - 7 were located on the intertidal sand flat on the right hand side (looking seawards) of the estuary. These stations were occupied over four tidal cycles between 14 and 20 July 1995. Due to the shortage of man power to cover the three stations on the sandflats, no current measurements were made at Stations 5 and 7, on 14 July, thus total transports were not calculated for these stations. On 18 July current data for Stations 6 and 7 were not available during the flood due to the instrument failure, thus at these

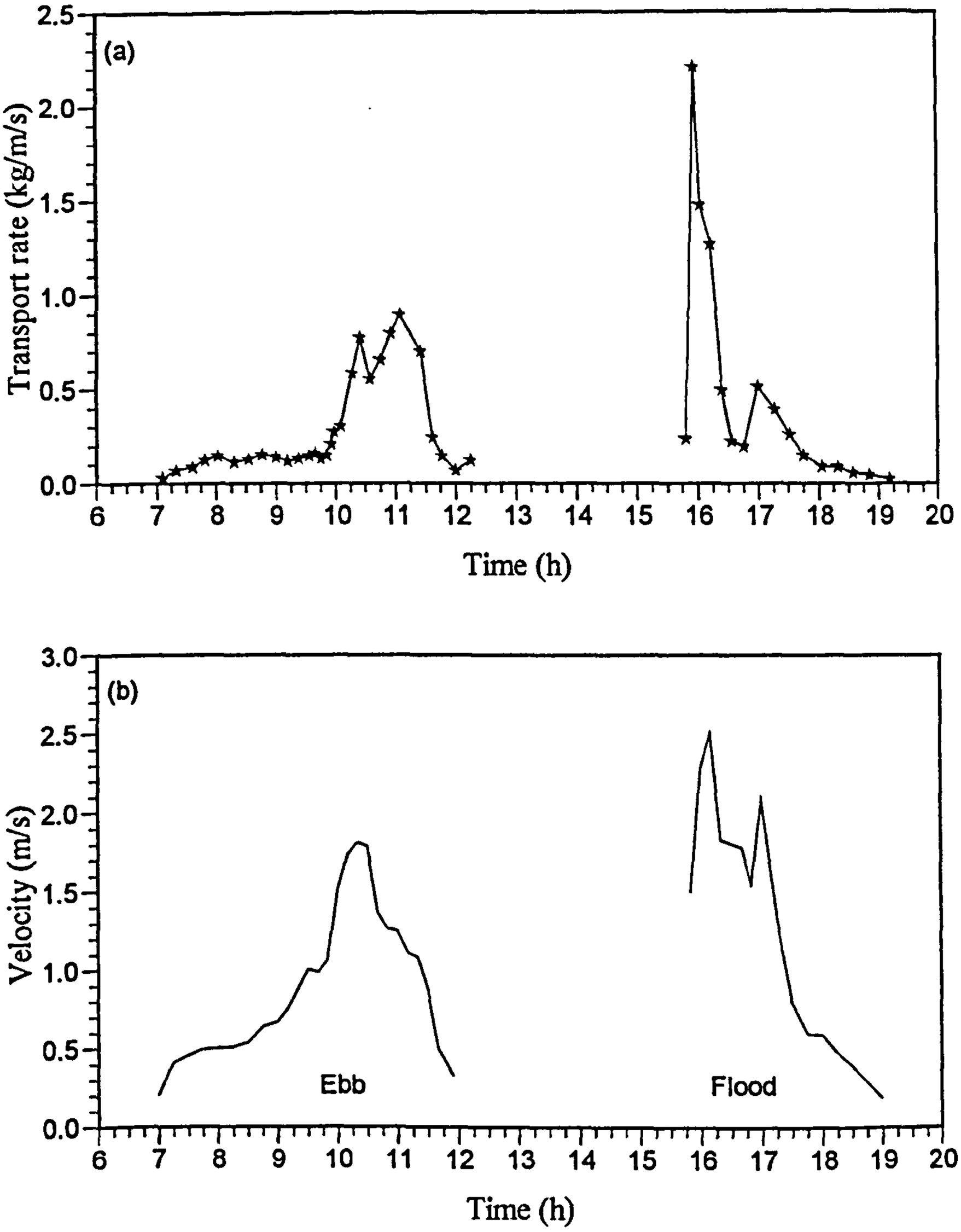

Figure 8.1 The variation of (a) transport rate and (b) depth-mean velocity over a spring tidal cycle as measured at station 1 (in the main ebb channel), transect T9, 6 October 1994.

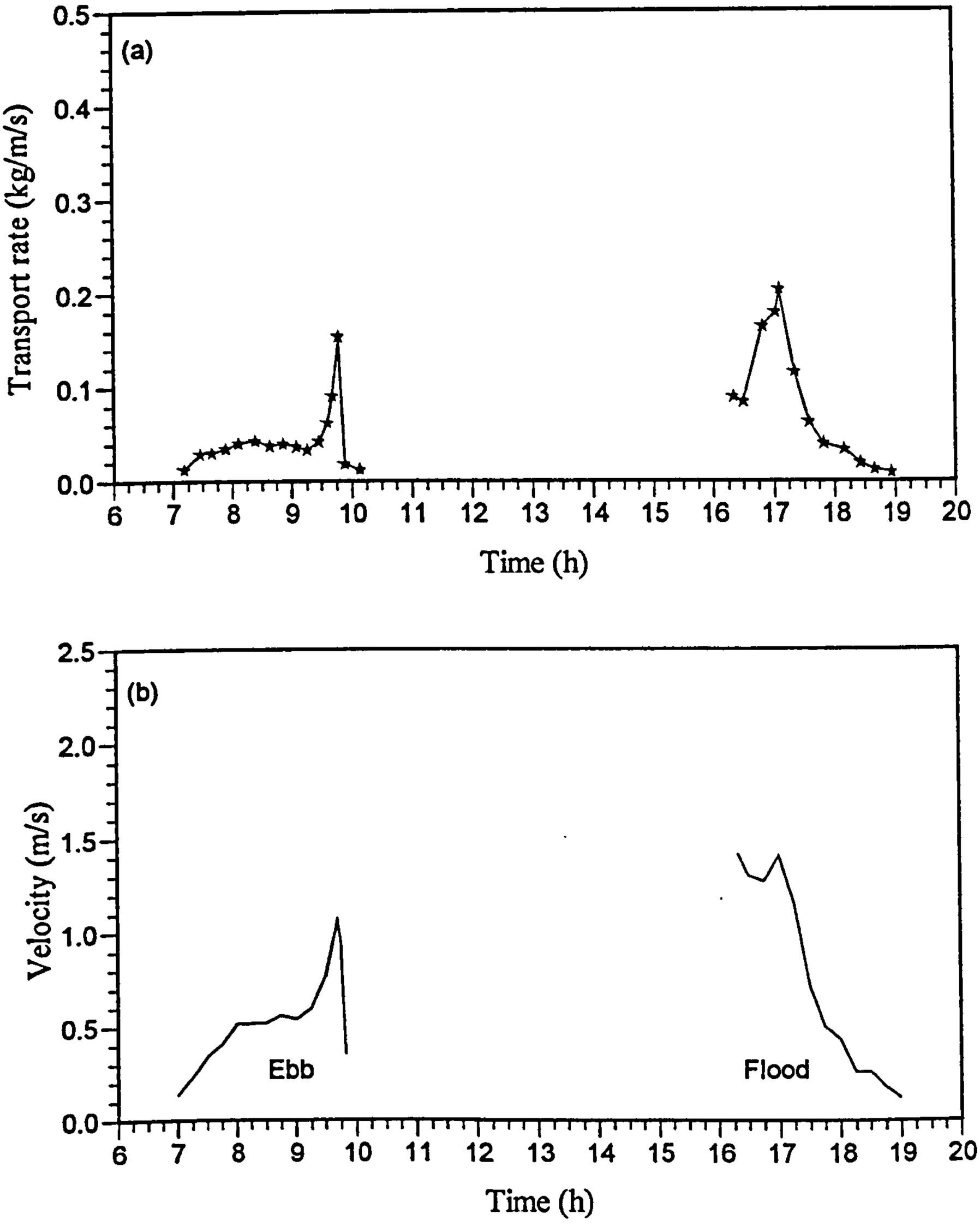

Figure 8.2 The variation of (a) transport rate and (b) depth-mean velocity over a spring tidal cycle as measured at station 3 (on the intertidal sand flat), transect T9, 6 October 1994.

stations, the transports were available only for the ebb.

The measured total transports are presented in Table 8.2. The highest transport rates were recorded at Stations 1-3 which were located in the main channel. During the spring tides (14 July 1995) the transport rates measured at each of these stations varied between 1500 - 2200 kg/m for the flood and between 1100 - 2400 kg/m for the ebb. On the neap tide (20 July 1995) the transport rates were reduced to less than 500 kg/m for both flood and ebb. The flood and ebb transport rates at Stations 5- 7 were much less, about 500 kg/m during the spring tide, and reduced to less than 30 kg/m during the neap tide.

Table 8.2 Measured total transport at Stations 1-7, Transect T9, on 14 - 20 July 1995.

Date	Station number	Transport rate (kg/m)			Net direction
		Flood	Ebb	Net	
14/7/95	1	1446	1704	258	Ebb
	2	1643	1104	539	Flood
	3	1737	1765	28	Ebb
	4	1120	1253	133	Ebb
	5	n.d.	n.d.	-	-
	6	526	429	97	Flood
	7	n.d.	n.d.	-	-
16/7/95	1	1708	2106	398	Ebb
	2	2177	1219	958	Flood
	3	1723	2425	702	Ebb
	4	963	1343	380	Ebb
	5	370	165	205	Flood
	6	235	186	49	Flood
	7	247	135	112	Flood

Table 8.2 (continue)

Date	Station number	Transport rate (kg/m)			Net direction
		Flood	Ebb	Net	
18/7/95	1	1290	1417	127	Ebb
	2	1460	710	750	Flood
	3	1539	1173	366	Flood
	4	1002	1101	99	Ebb
	5	167	86	81	Flood
	6	n.d.	138	-	-
	7	n.d.	76	-	-
20/7/95	1	443	486	43	Ebb
	2	482	259	223	Flood
	3	351	409	58	Ebb
	4	164	299	135	Ebb
	5	28	19	9	Flood
	6	25	28	3	Ebb
	7	19	15	4	Flood

Stations 1 and 4 consistently showed an ebb dominant transport while Stations 2, 5 and 7 constantly showed a flood dominant transport. Station 3 showed an ebb dominant transport except on 18 July which was flood dominant. Except on 20 July 1995, Station 6 show a flood dominant transport.

The variations of sediment transport over spring and neap tidal cycles are shown in Figures 8.3 and 8.4, respectively. On the spring tide, the plot shows a flood dominant transport with

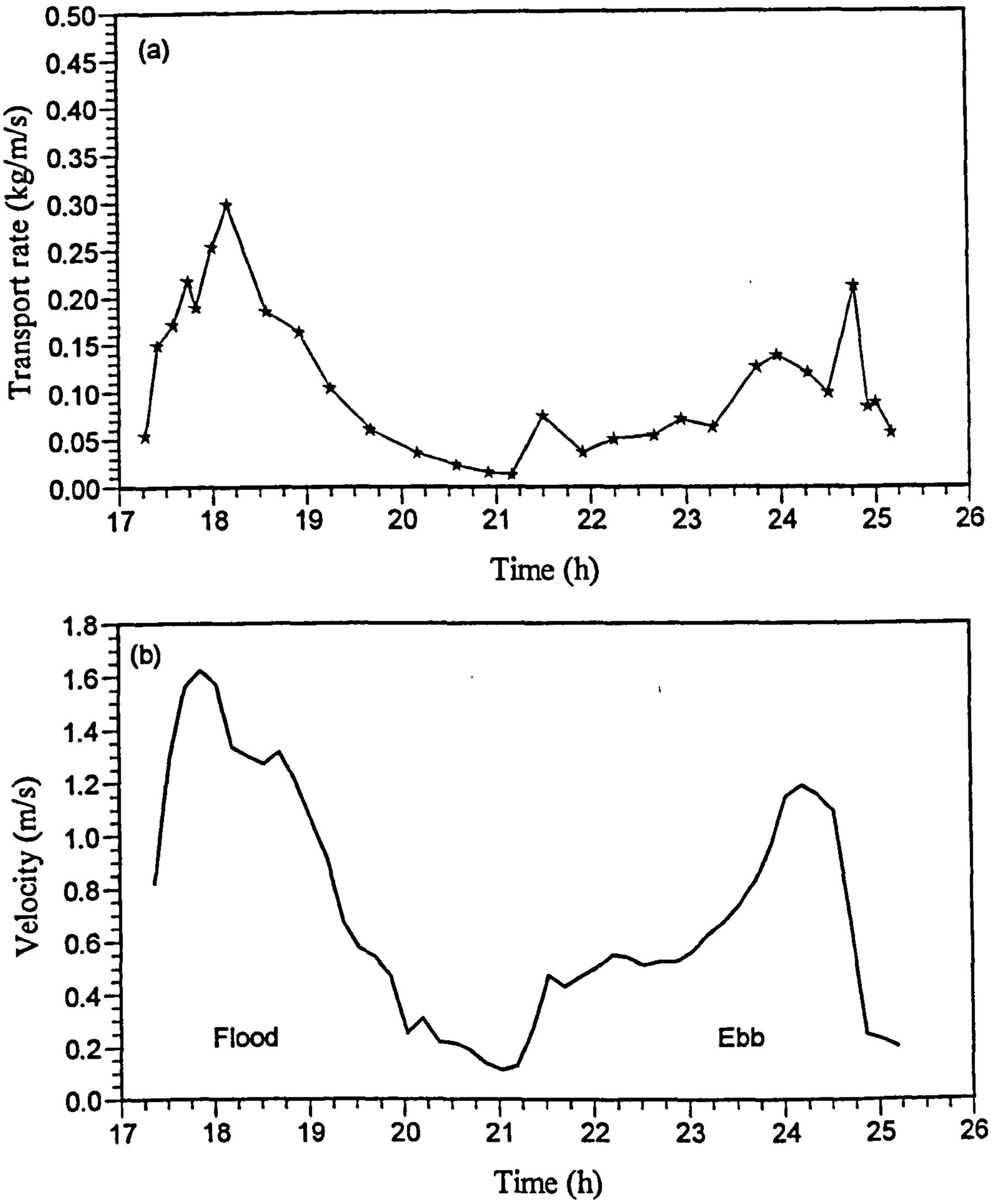

Figure 8.3 The variation of (a) transport rate and (b) depth-mean velocity over a spring tidal cycle as measured at station 2, transect T9, 14 July 1995.

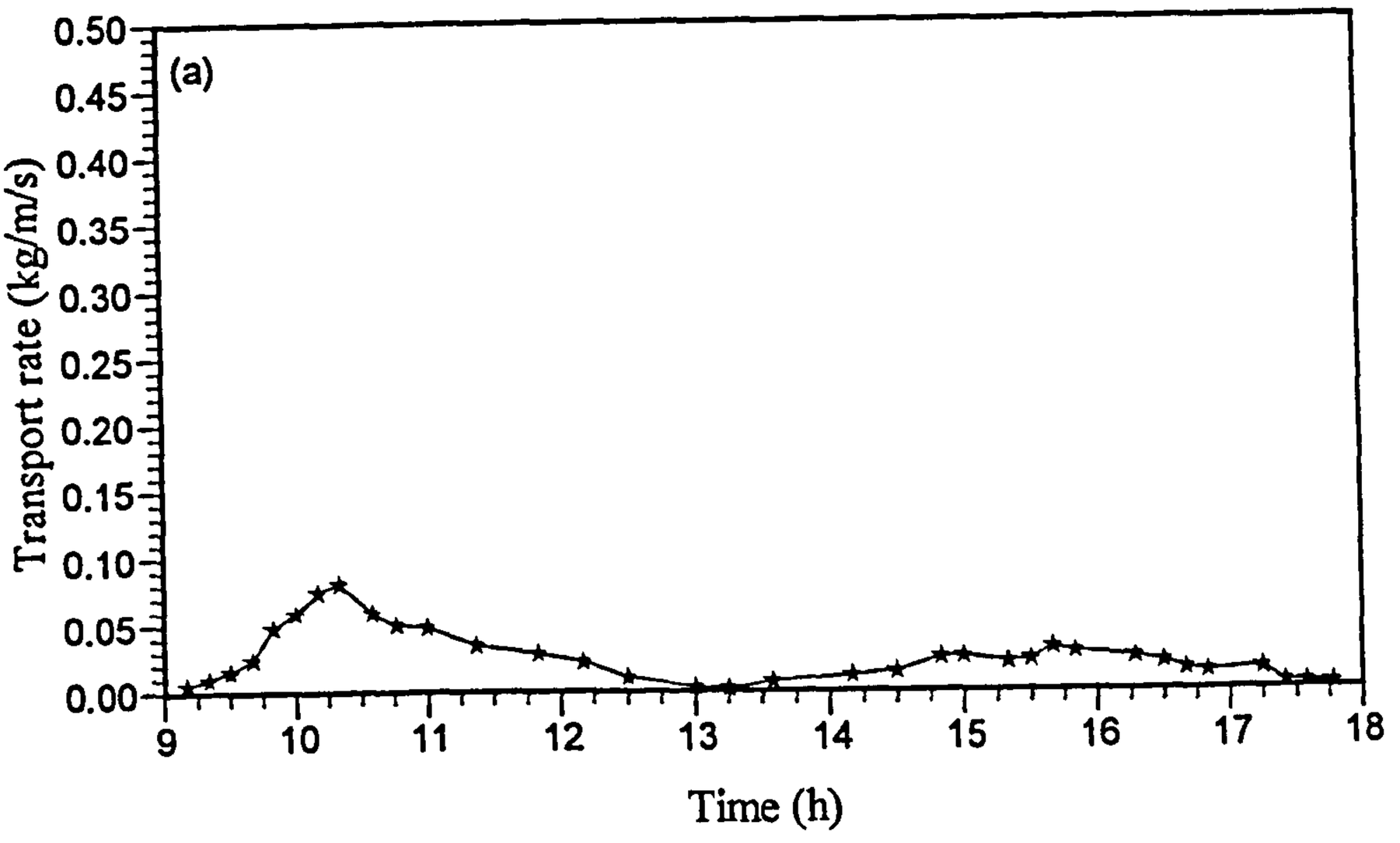

Figure 8.4 The variation of (a) transport rate and (b) depth-mean velocity over a neap tidal cycle as measured at station 2, transect T9, 20 July 1995.

a transport rate up to 0.3 kg/m/s measured on the flood but only about 0.15 kg/m/s measured on the ebb. The peak transports occurred during the early flood and late ebb when the velocities were at their maxima. At the end of ebb of the spring tide, a larger second peak was observed after the velocity had declined from its maximum. On the neap tide, a smaller peak was observed during the flood, there was no obvious peak transport during the neap, and the second ebb transport peak was not present.

8.2.3 Transect T5 - September 1995

At Transect T5 the distance across the estuary is about half of that at Transect T9, therefore only 4 measurement stations were set up along this transect (Figure 3.2c). The stations were occupied over 4½ tidal cycles between 12 - 19 September 1995. The total transport rates at each station are given in Table 8.3. Station 1 which was located in the main channel showed the highest transport rates during both the flood and the ebb. On 13 September which, was 4th tide after the spring tide, a total of 5694 kg/m on the flood and 5485 kg/m on the ebb were measured at Station 1. During the neap on 19 September 1995, the total transport at this station was much less, about 10 % of that measured during the spring tide. Stations 3 and 4 which were located on the sand flat and near the salt marsh boundary, respectively, showed the lowest transport rates. The total transport at Station 3 on 13 September for example was 534 kg/m for the flood and only 138 kg/m for the ebb. During the neap, these values were reduced to 16 kg/m and 5 kg/m, respectively.

Stations 1-3 showed flood dominant transport for all tide. Station 4, however, showed flood dominance only on small tides, but on the bigger tide on 13 September the transport at this station was ebb dominant.

Typical variations of transport rate over spring and neap tidal cycles at this transect are shown in Figures 8.5 and 8.6, respectively, for Station 1. Both figures show similar trends to those at Transect T9; however higher transport rates were measured at T5 than at T9. The flood dominant transport is shown by both figures. During the spring tide, maximum

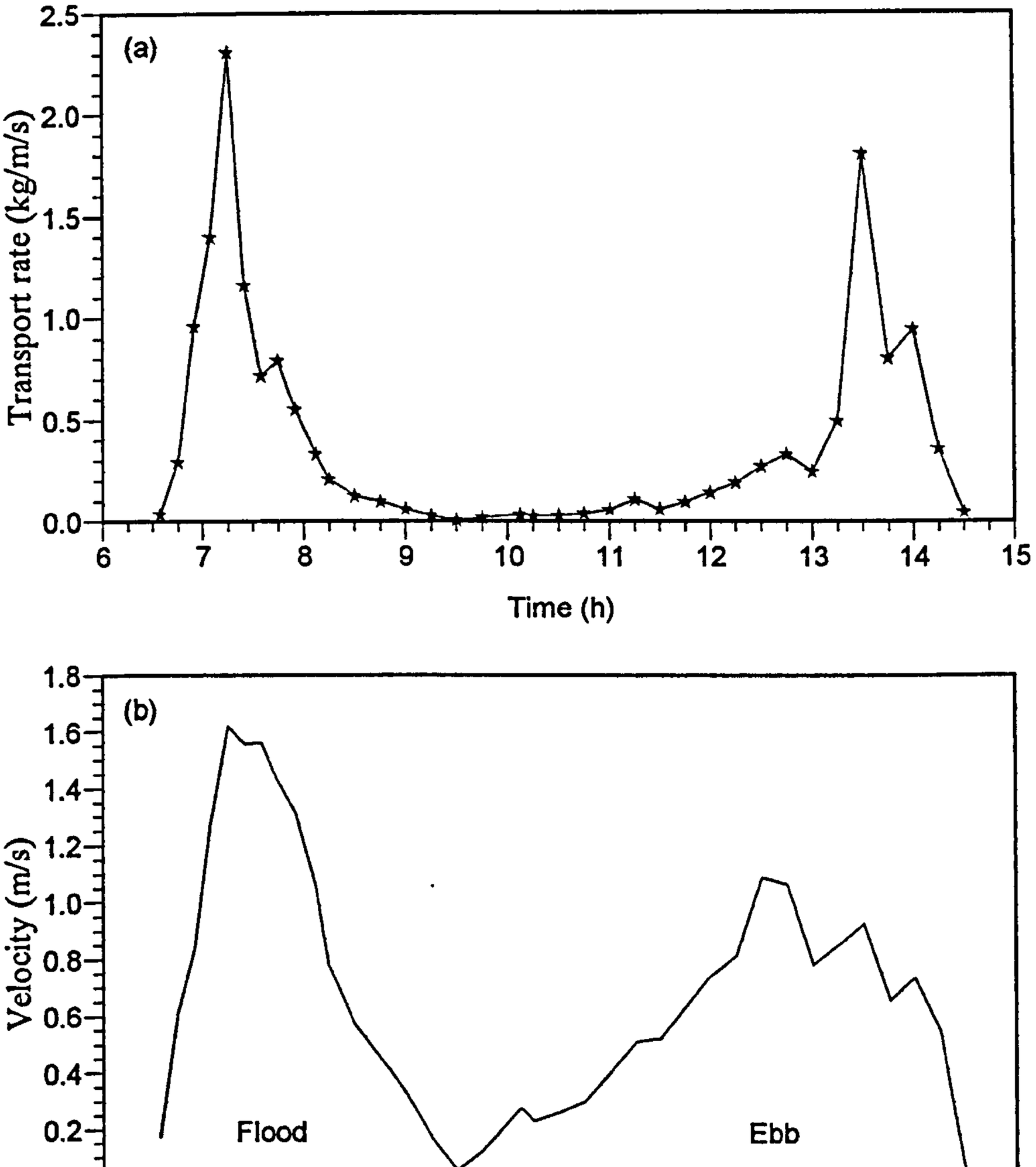

Figure 8.5 The variation of (a) transport rate and (b) depth-mean velocity over a spring tidal cycle as measured at station 1, transect T5, 13 September 1995.

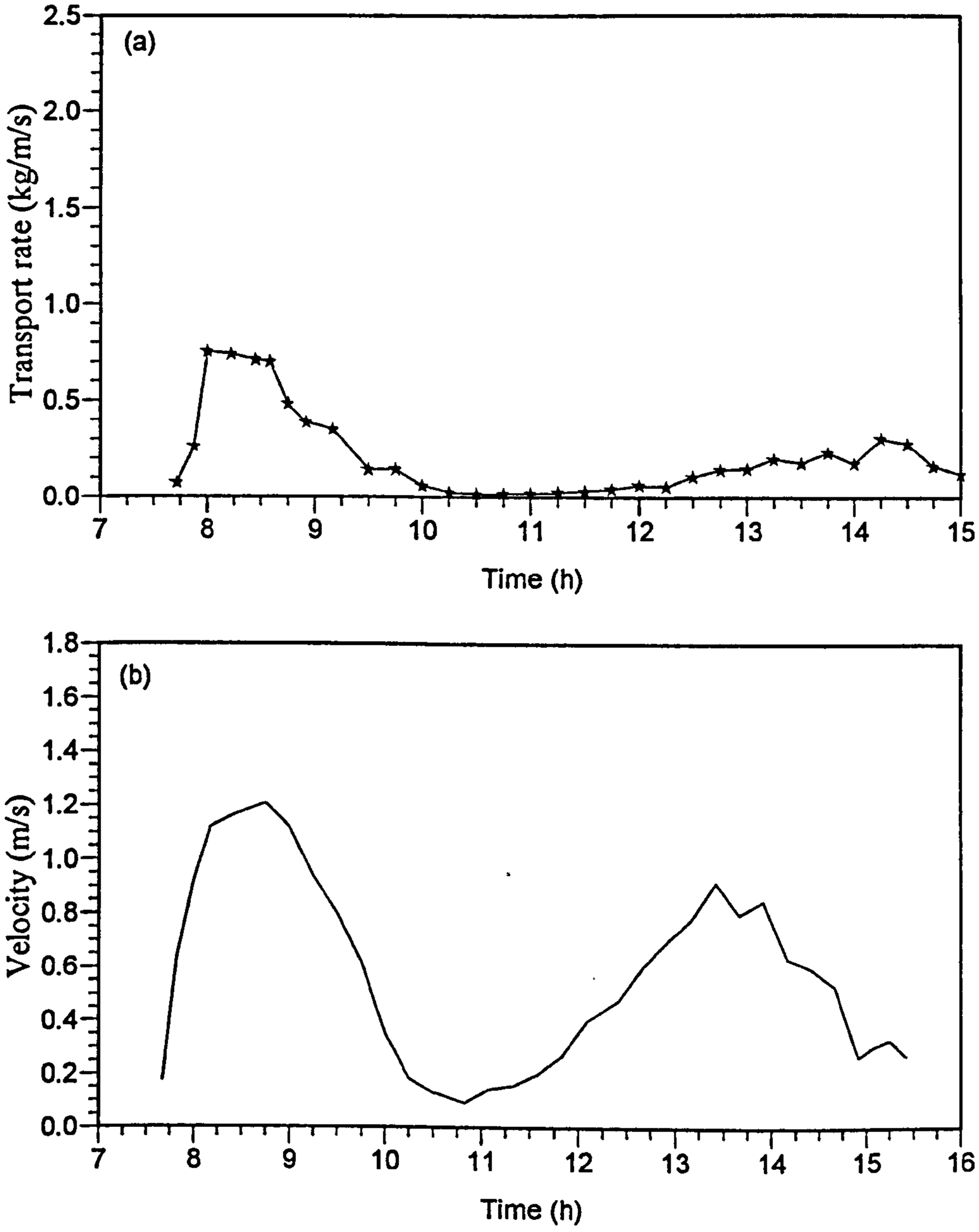

Figure 8.6 The variation of (a) transport rate and (b) depth-mean velocity over a spring tidal cycle as measured at station 1, transect T5, 15 September 1995.

transport on the flood and ebb reached 2.3 kg/m/s and 1.8 kg/m/s, respectively. During the ebb, the maximum transport rate occurred after the flow velocity had reduced from its peak value, but on the neap tide the peak was very much subdued.

Table 8.3 Measured total transport at Stations 1-4, Transect T5, on 12- 19 September 1995.

Date	Station number	Transport rate (kg/m)			Net direction
		Flood	Ebb	Net	
12/9/95	1	-	9481	-	-
	2	-	1432	-	-
	3	-	293	-	-
	4	-	648	-	-
13/9/95	1	5694	5485	209	Flood
	2	3839	871	2968	Flood
	3	534	138	396	Flood
	4	318	395	77	Ebb
14/9/95	1	3535	3223	312	Flood
	2	1930	976	954	Flood
	3	314	108	206	Flood
	4	215	198	17	Flood
15/9/95	1	1693	1331	362	Flood
	2	763	538	225	Flood
	3	105	63	42	Flood
	4	128	113	15	Flood
19/9/95	1	789	437	352	Flood
	2	283	139	144	Flood
	3	16	5	11	Flood
	4	56	17	39	Flood

8.2.4 Discussion

The transport rate measured at stations across the estuary varies considerably. Highest transport rates were recorded at stations located in the main ebb channel while lowest transport rates were measured at stations furthest from the main channel and at those located on higher intertidal sand flats. In the main channel, the tidal currents are strongest but currents are progressively weaker on the intertidal sand flats further away from the channel. Furthermore measurements in the main channel could be carried out for a much longer time, and at other stations the measurements were only possible for a limited time period either side of high water as they were dry at low water. Where only a single ebb channel was present, more than 50% of the total transport occurred within that channel.

More than 50 % of the total ebb transport measured at stations in the main channel occurred during the final 1-1.5 hours of the ebb period. During this time the current was strongest, but the measured transport also included suspended material from the turbidity maximum which advected passed the lower estuary during the late ebb, particularly on spring tides when the maximum was most developed (as shown by a second and larger transport peaks during the ebb in Figures 8.1, 8.3 and 8.5). During neap tides, when there was no turbidity maximum or a less developed maximum, the transport rate followed the pattern of the tidal velocity.

The net transport directions varied from station to station and between transects, and the direction of net transport was not necessarily consistent with the dominant flow direction. At Transect T9, the stations within the main channel normally showed an ebb net transport though the current velocity was flood dominant, while those stations located on the sand flat showed a flood dominant tidal velocity and a flood net sediment transport. In the main channel, the measurement was continued until about 5 hours after high water by which time the water depth in the channel was less than 0.5m. Therefore, though these stations show an ebb net transport, the total transport across the compartment represented by the station during the ebb was still less than the total transport during the flood as

revealed in the calculation of sediment flux. This is because the transport during the final hours of the ebb represents a much smaller channel width and water depth.

At T5 the station in the main channel (Station 1) did not show an ebb dominant transport as expected. The input from the river discharge may be a significant factor. In October 1994, the measurement was carried out during a higher river discharge (monthly averaged = 7.1 m^3/s), while in September 1995, the monthly averaged river discharge was only 0.5 m^3/s. Thus more sediment from alluvial input and channel erosion is carried by the ebb during a high river discharge compared to a low river discharge and this contributed to the ebb dominant transport as observed at Station 1 in the measurement made in October 1994. Similarly for July 1995, the monthly averaged discharged was 0.8 m^3/s which was higher than in September 1995, thus contributed to the apparent ebb dominant transport measured at stations in the main channel at Transect T9 (Table 8.2).

8.3 Calculated sediment transport

It has been a standard practice to estimate sediment transport using one or more of the available transport equations from velocity measurement made within the bottom boundary layers (see Dyer, 1986 for a review). Thought some of these transport equations were calibrated using laboratory data from flume studies, studies (eg. Heathershaw, 1981; Lees, 1983; Van den Berg, 1987) in the natural environment either using sediment tracers or bedform celerity show that the transport predicted by each equation can be up to two orders of magnitude different from the measured transport.

Current velocities and transmissometer measurements made in the present study will be used to test the predictive capability of some of the available sediment transport equations. The transport estimated by these equations will be compared with the measured transport presented before. To demonstrate this capability , only the measurements made along Transect T5 will be used as the data set is more complete and a particularly good transmissometer calibration was obtained for this transect. Furthermore, it represents all

ranges of flow velocities common to the study area.

Transport equations of Engelund and Hansen (1967), Hardisty (1983), and Jago and Mahamod (1997) have been chosen to predict sediment transport. The first two transport equations are most commonly used in intertidal and continental shelf studies (eg. Collins *et al.*, 1981; Mahamod, 1989; Collins *et al.*, 1995), while the last equation is a newly-formulated equation for prediction of sediment transport in fast tidal current environments common to macrotidal estuaries. Engelund and Hansen`s, and Jago and Mahamod`s equations are for total load transport while Hardisty's equation is only for bedload transport.

Where the tidal velocity was measured using a single profiling current meter, only the bottom readings taken within 2.5 m from the bed were used in the calculation of bed shear stress (by fitting the velocity profile to the Karman-Prandtl equation) for input to the appropriate sediment transport equation. Readings taken at a greater distance were found to deviate from the logarithmic profile (see Chapter 5).

8.3.1 Estimation of threshold velocity

The sediment transport predicted by the Engelund and Hansen equation depends on shear stress operates at the bed and it does not require a threshold value, but the formulations of Hardisty, and Jago and Mahamod are based on a power law of velocity measured at a standard height 100 cm above the bed (u_{100}); both equations require the determination of threshold velocity for initiation of sediment transport (see Chapter 2). For the sediment in the Taf estuary, this threshold velocity has been estimated using three different methods: a) from the Shield threshold curve; b) interpolations from Jago and Mahamod's Calibration Table; and c) by direct observation of transmissometer and current velocity records. For the Hardisty and Jago and Mahamod equations, a threshold velocity, u_{100c} of 0.17 m/s has been used. This threshold velocity has been determined from the transmissometer records and current velocity data, and is a direct measure of the threshold velocity for the sediment movement in the study area. As the sands are extremely uniform

in the estuary, one threshold is sufficient and it has been used to calculate sediment transport at all stations across the transect.

Method 1: Using the modified Yalin's Shield threshold curve

The following parameters were used in the estimation of threshold velocity;

Sediment density, $\rho_s = 2650\ kgm^{-3}$

Water density, $\rho = 1020\ kgm^{-3}$

Mean grain size, $D = 0.00013$ m

Gravitational acceleration, $g = 9.81\ ms^{-2}$

Kinematic viscosity of sea water, $\nu = 1.3 \times 10^{-6}\ m^2s^{-1}$

The Yalin parameter, Ξ was calculated using the following formula:

$$\Xi = \frac{Re_*^2}{\theta_c} = \frac{(\rho_s-\rho)gD^3}{\rho\nu^2} \qquad [8.1]$$

which gives Ξ equal to 20.4. From Figure 2.6 i.e. the modified Yalin threshold curve of Miller *et al.* (1977) it was estimated that:

$$\frac{\tau_c}{(\rho_s-\rho)gD} = 0.043 \qquad [8.2]$$

from which τ_c was found to be $0.0894\ Nm^{-2}$. Application of the Sternberg (1972) method and $C_{100} = 0.003$ (mean drag coefficient at 100 cm above the bed), yielded a critical entrainment velocity, $u_{100c} = 0.17\ ms^{-1}$. This value is much lower (about half) of that given by the modified Sundborg curve given in Miller *et al.* (1977) which estimated u_{100c} = 0.35 m/s for the sediment size of the study area.

Method 2: Using Jago and Mahamod calibration curve

Using the published flume data set of Guy *et al.* (1966), Jago and Mahamod (1997) have derived the threshold velocities for four sand diameters (Table 8.4). It shows that for medium to fine sands the threshold velocity does not alter significantly which implies that the sediment is most likely to go into suspension. Thus the threshold velocity can be extrapolated from the values given in Table 8.4. As discussed by Bagnold (1963) and McCave (1971), for fine sand (< 0.19 mm grain diameter) sands are transported in suspension at the threshold of movement. For the Taf estuary sediment which has the mean grain diameter of 0.13 mm, the threshold velocity was estimated to be 0.17 m/s from Table 8.4.

Table 8.4 Threshold velocities (u_c) for four grain diameters derived from flume data set of Guy *et al.* flume data (from Jago and Mahamod; 1997).

Grain diameter (mm)	Threshold velocity (cm/s)
0.19	18
0.28	19
0.45	19
0.93	38

Method 3: From the VGU and transmissometer records

The VGU and three transmissometers deployed side by side in September 1996 provided a direct measure of the threshold velocity for the Taf sediment. Though the transmissometers gave a long record of sediment concentration values (i.e. from 9 -24 September 1996), the current meter data extended only from 9 to 17 September 1996 (16 tidal cycles). The velocity and concentration records were therefore examined for each of the 16 tidal cycles. The threshold velocity was determined from sediment concentration values recorded by the bottom two transmissometers (located at 0.14 m and 0.60 m above bed, respectively);

the third transmissometer was located too higher up above the bed (at 1.5 m above bed) for accurate determination of sediment threshold velocity.

The transmissometer records show that as the water begins to ebb the concentration increases from a minimum value at high water slack . The threshold is reached when the concentration just begins to exceed the background levels (Lavelle and Mofjeld; 1987). i.e.

Table 8.5 Threshold velocities (u_c) for 16 tidal cycles as determined from transmissometer and VGU records.

Date	Tidal cycle no	Threshold velocity, u_{100t} (m/s)
9/9/96	1	0.15
10/9/96	2	0.13
10/9/96	3	0.19
11/9/96	4	0.16
11/9/96	5	0.18
12/9/96	6	0.15
12/9/96	7	0.13
13/9/96	8	0.20
13/9/96	9	0.15
14/9/96	10 (Spring)	0.16
14/9/96	11	0.19
15/9/96	12	0.23
15/9/96	13	0.11
16/9/96	14	0.20
16/9/96	15	0.21
17/9/96	16	0.14
Mean		0.17

the averaged concentration over high water slack. The time was noted and the corresponding current velocity at 1 m above the bed for each tidal cycle was obtained from the VGU record (directly from the ebb rotor of the VGU positioned at 1 m above the bed). A consistently good agreement was shown by the two transmissometers and both showed that the threshold was reached at approximately similar times (± 5 minutes). The threshold velocities obtained varied from 0.11 - 0.23 m/s with a mean value of 0.17 m/s (Table 8.5). A threshold velocity, u_{100t} of 0.17 m/s has been selected and used in the calculation of sediment transport since it was consistent with the threshold velocity determined by the other methods.

8.3.2 Sediment transport at Transect T5.

At this transect, sediment transport at four stations across the estuary have been calculated for the velocity measurements made between 12 - 15 September 1995. For 19 September no calculation was made as with the exception of anchor Station 2, there were inconsistencies in the velocity data which did not warrant any accurate estimates of u_{100}, mean velocity u, or shear velocity u_* that could be used in the transport equations. The measurement on 12 September 1995 was only for ebb tidal cycle at the four anchor stations. The calculated transports have been integrated over the flood and ebb cycles to give the total transport for the flood and the ebb of each tidal cycle.

The measured ebb transport at Stations 1 and 2 of Transect T5 would include the contribution from the turbidity maximum zone which advects through the lower estuary at the end of the ebb tide. Since this is an advection signal, not a resuspension signal, this contribution has been excluded from the measured total ebb transport.

8.3.2.1 Anchor Station 1

This station is located in the deepest part of the main ebb channel and experiences the strongest currents during both flood and ebb. At this station the maximum mean currents during the spring tide was 1.6 m/s for the flood and 1.1 m/s for the ebb, but for the neap these values were reduced to 1.2 m/s and 0.9 m/s, respectively. The variation of sediment transport predicted by different formulae over a spring tidal cycle is shown in Figure 8.7. As expected the transport rate is increased with increased tidal velocity; however the transport rates predicted by different equations vary considerably. As predicted by Jago and Mahamod, the transport rate rises to a maximum of 34 kg/m/s during the flood, and up to 4 kg/m/s during the ebb. The maximum flood transport predicted by Hardisty, and Engelund and Hansen, are 8 kg/m/s and 6 kg/m/s, respectively. Sediment transport predicted for the flood by Hardisty, and Engelund and Hansen, fall within the same order of magnitude but Jago and Mahamod predict an order of magnitude higher for the flood transport. During the ebb, the transport rates predicted by the different formulae are comparable and all fall within the same order of magnitude.

Compared to the measured transport, the formulae of Hardisty, Engelund and Hansen, and Jago and Mahamod overestimate the transport rate at high (> ~ 0.7 m/s) flow velocities but at low flow velocities the transport rates are slightly underestimated by all the formulae. At around slack high water, the measured transport is higher than the calculated transport as during this period most of the sediment is made up of fine particles which remain in suspension and do not represent sediment resuspended by the tidal currents.

The sediment transports over flood and ebb periods for Station 1 are given in Table 8.6. All formulae predict a net landward transport and this is consistence with the measured transport at this station. The total measured transport showed that at higher tidal ranges the flood transport is 3 times greater than the total ebb transport, but at lower tidal ranges, this ratio is reduced to about 1.5. The total flood transport predicted by the different formulae varies between 2 to 9 times greater than the ebb transport. Compared to the measured transport, all the formulae overestimate total flood and ebb transports . Table 8.6 shows

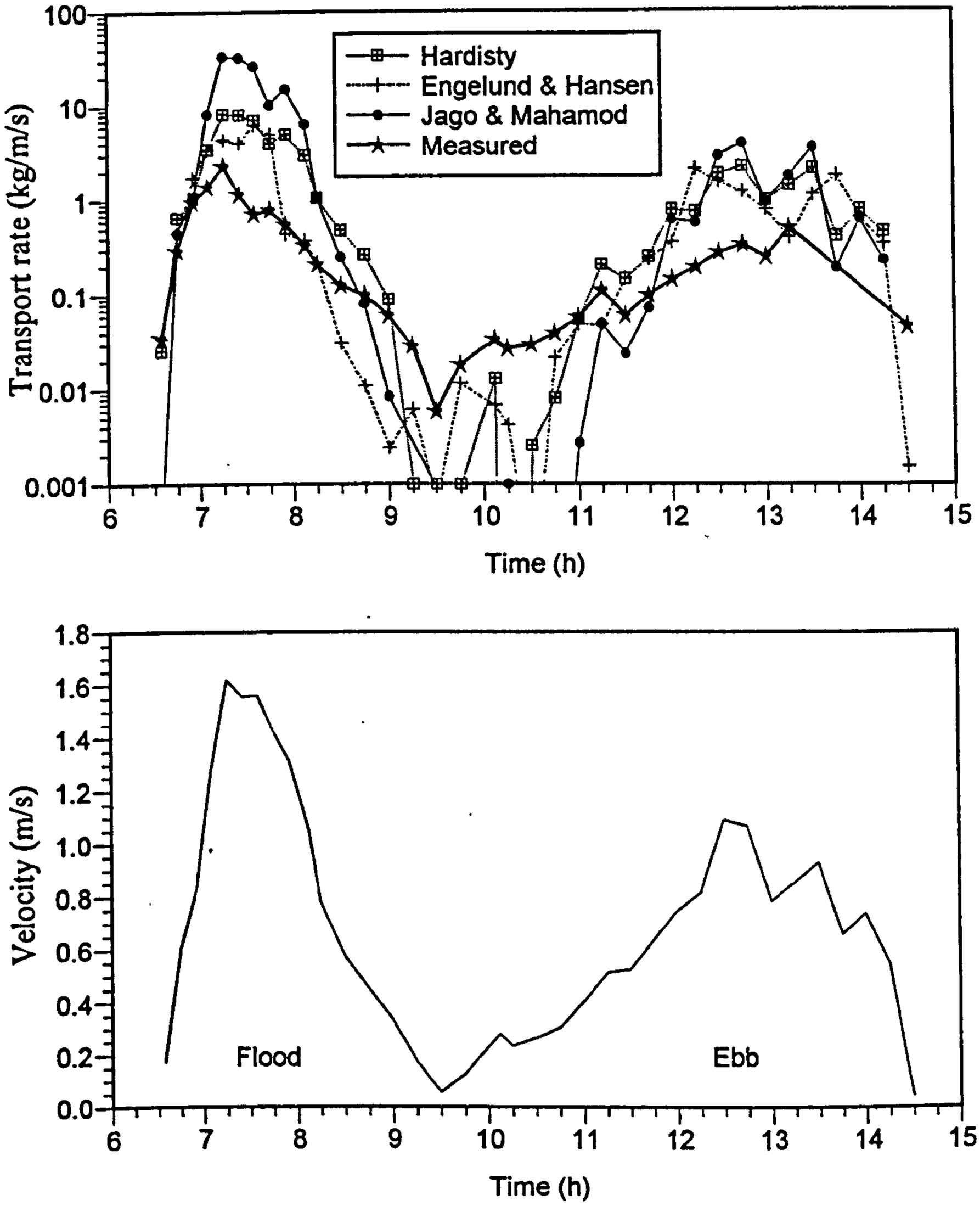

Figure 8.7 The variation of (a) Calculated and Measured transport rates at station 1, and (b) depth-mean velocity at station 1, transect T5, 13 September 1995.

that the formula of Engelund and Hansen gives the best estimate of total transport for flood and ebb tidal cycle, the Hardisty equation overestimates the transport by a factor of 2 on both the flood and ebb, while the Jago and Mahamod equation overestimates by a factor of 11-15 during the flood, and 3-5 during the ebb.

Table 8.6 Calculated and measured total load transport over flood and ebb tidal cycle at anchor Station 1, Transect T5. The values in bracket indicate the ratios between calculated and measured transport.

Date	Tide	Transport rate (kg/m)			
		Hardisty	Engelund & Hansen	Jago & Mahamod	Measured
12/9/95	Flood	n.d	n.d	n.d.	n.d
	Ebb	7078 (2.49)	7328 (2.58)	9074 (3.19)	2842
13/9/95	Flood	26634 (4.70)	15911 (2.81)	84949 (14.98)	5669
	Ebb	7809 (4.03)	6206 (3.20)	9709 (5.01)	1938
14/9/95	Flood	17021 (4.81)	6017 (1.70)	39284 (11.11)	3535
	Ebb	5674 (4.40)	2978 (2.31)	5617 (4.35)	1290
15/9/95	Flood	12767 (7.54) 5402 (5.13)	6549 (3.87)	21333 (12.60)	1693
	Ebb		3275 (3.11)	4271 (4.06)	1052

n.d. = no measurement made

8.3.2.2 Anchor Station 2

This station was located at the edge of the main ebb channel. During the spring tide, the maximum mean currents was 1.54 m/s for the flood but only 0.66 m/s for the ebb. The

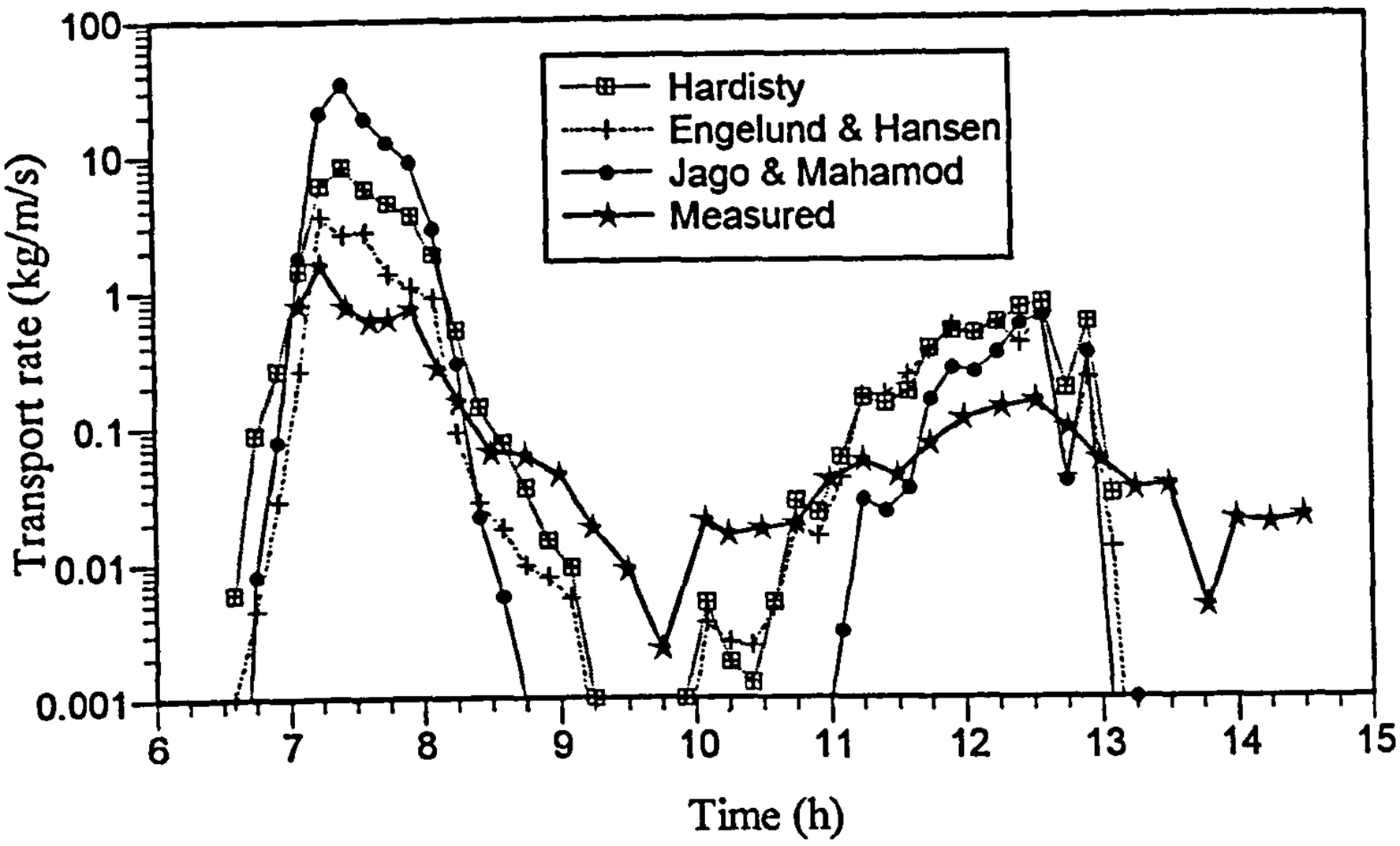

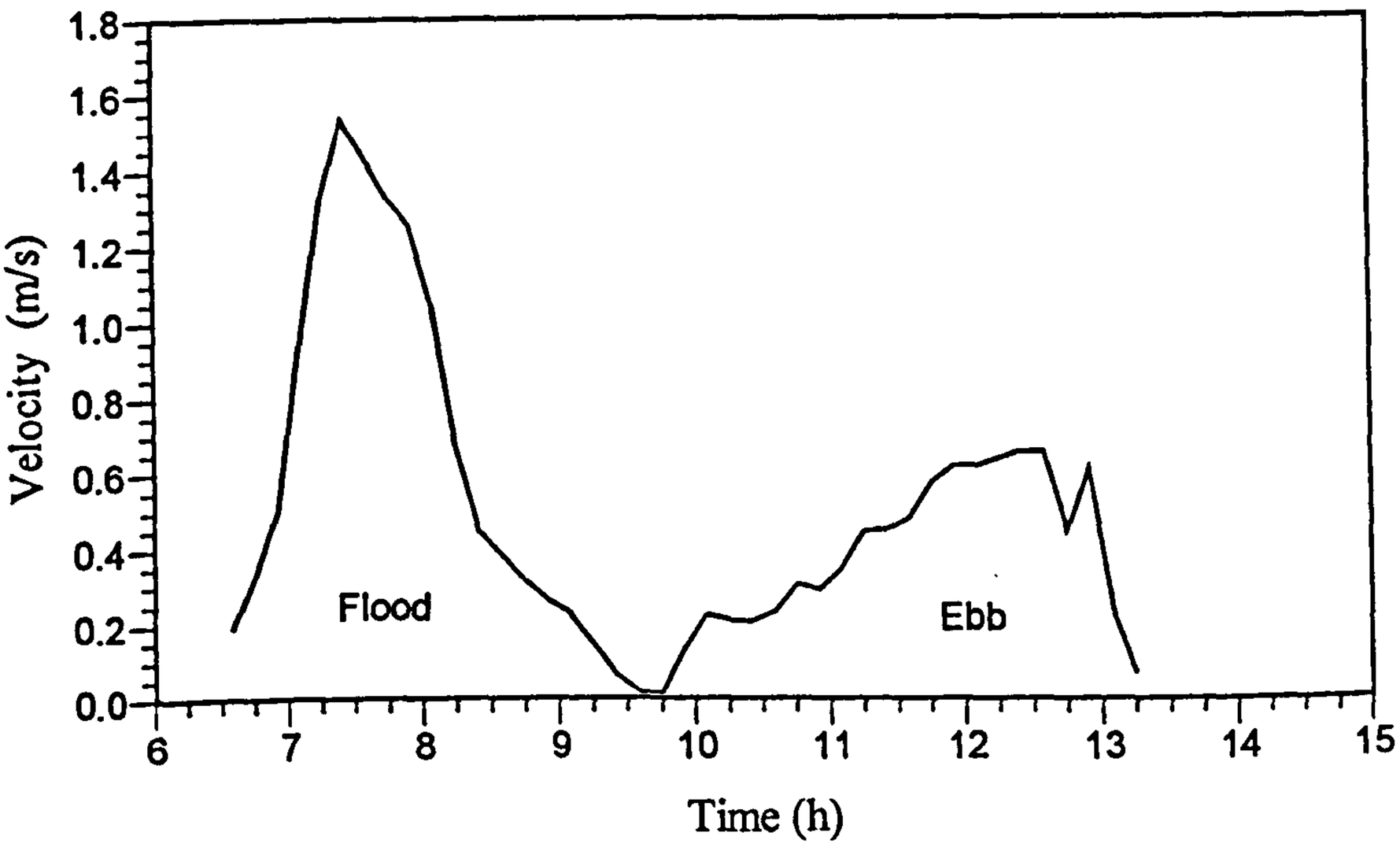

Figure 8.8 The variation of (a) Calculated and Measured transport rates at station 1, and (b) depth-mean velocity at station 2, transect T5, 13 September 1995.

transport rate predicted by the different equations follows a similar pattern to that observed at anchor Station 1 for the flood, but not for the ebb (Figure 8.8). For the flood, Jago and Mahamod predict transport an order of magnitude higher than Hardisty and Engelund and Hansen during the maximum tidal flow. For this station the maximum transport is 34 kg/m/s for Jago and Mahamod, and 8.3 kg/m/s and 2.8 kg/m/s for Hardisty and Engelund and Hansen, respectively. Hardisty and Engelund and Hansen give similar transport rates for the ebb, but Jago and Mahamod give a slightly lower transport rate. At high flow velocities all the formulae overestimate the transport rate particularly during flood period, but only slightly overestimate the ebb transport though they all fall within the same order of magnitude.

Table 8.7 Calculated and measured total load transport over flood and ebb tidal cycle at anchor Station 2, Transect T5. The values in bracket indicate the ratios between calculated and measured transport.

Date	Tide	Transport rate (kg/m)			
		Hardisty	Engelund & Hansen	Jago & Mahamod	Measured
12/9/95	Flood	n.d	n.d	n.d.	n.d
	Ebb	5544 (4.30)	5348 (4.15)	5650 (4.38)	1290
13/9/95	Flood	19716 (5.13)	7640 (1.99)	60492 (15.75)	3839
	Ebb	2856 (3.66)	2321 (2.97)	1578 (2.02)	781
14/9/95	Flood	13744 (7.12)	3040 (1.58)	29879 (15.48)	1930
	Ebb	2584 (3.25)	548 (0.69)	1223 (1.54)	795
15/9/95	Flood	4792 (6.28)	1058 (1.39)	4125 (5.41)	763
	Ebb	2322 (4.59)	771 (1.52)	1093 (2.16)	506

n.d. = no measurement made

As at Station 1, the total load calculation demonstrates that flood transport is dominant over ebb transport as shown in Table 8.7. The flood transport is up to 38 times greater than the ebb transport; the trend is similar with the measured transport, which shows that the flood is up to 5 times greater than the ebb transport, resulting in a net landward transport.

The ratio between predicted and measured total transports indicates the degree of discrepancy of the total transport predicted by the different equations. Again at this station Engelund and Hansen gives the better estimate for flood and ebb transport, where except on 12 September 1995, the ratios fall between 0.3 and 3. Predictions by Jago and Mahamod deviate quite considerably from the measured transport and are the most inconsistence. The ratio varies from 5 to 16 for the flood and from 1.5 to 4.4 for the ebb.

8.3.2.3 Anchor Station 3

This station was located on the intertidal sand flat in the middle of the estuary. The maximum mean velocity was 1.3 m/s for the flood and 0.6 m/s for the ebb. The transport rate calculated at this station follows similar patterns as found in the previous two stations with the Jago and Mahamod equation giving the highest transport rates during the flood i.e. up to 15 kg/m/s (Figure 8.9). This is an order of magnitude higher than predicted by the Hardisty and Engelund and Hansen equations. During the ebb, all the equations predict similar ranges of transport rate. Comparison with the measured transport shows that all the equations overestimate transport rates both during the flood and ebb periods between the one to two orders of magnitude higher than the measured transport rates.

The total transport rates as predicted by the three equations are presented in Table 8.8. As shown, all equations predict a flood dominant transport; however, the total amount is only about one tenth of that measured at Stations 1 and 2. Similar to Stations 1 and 2, the net transport at Station 3 is landwards. The ratios between the calculated and measured transport are quite variable. The ratios are bigger on the bigger tides (up to 37 times higher) but on smaller tides the ratios are reduced to 0.6 to 7. At smaller flow velocities, Jago and

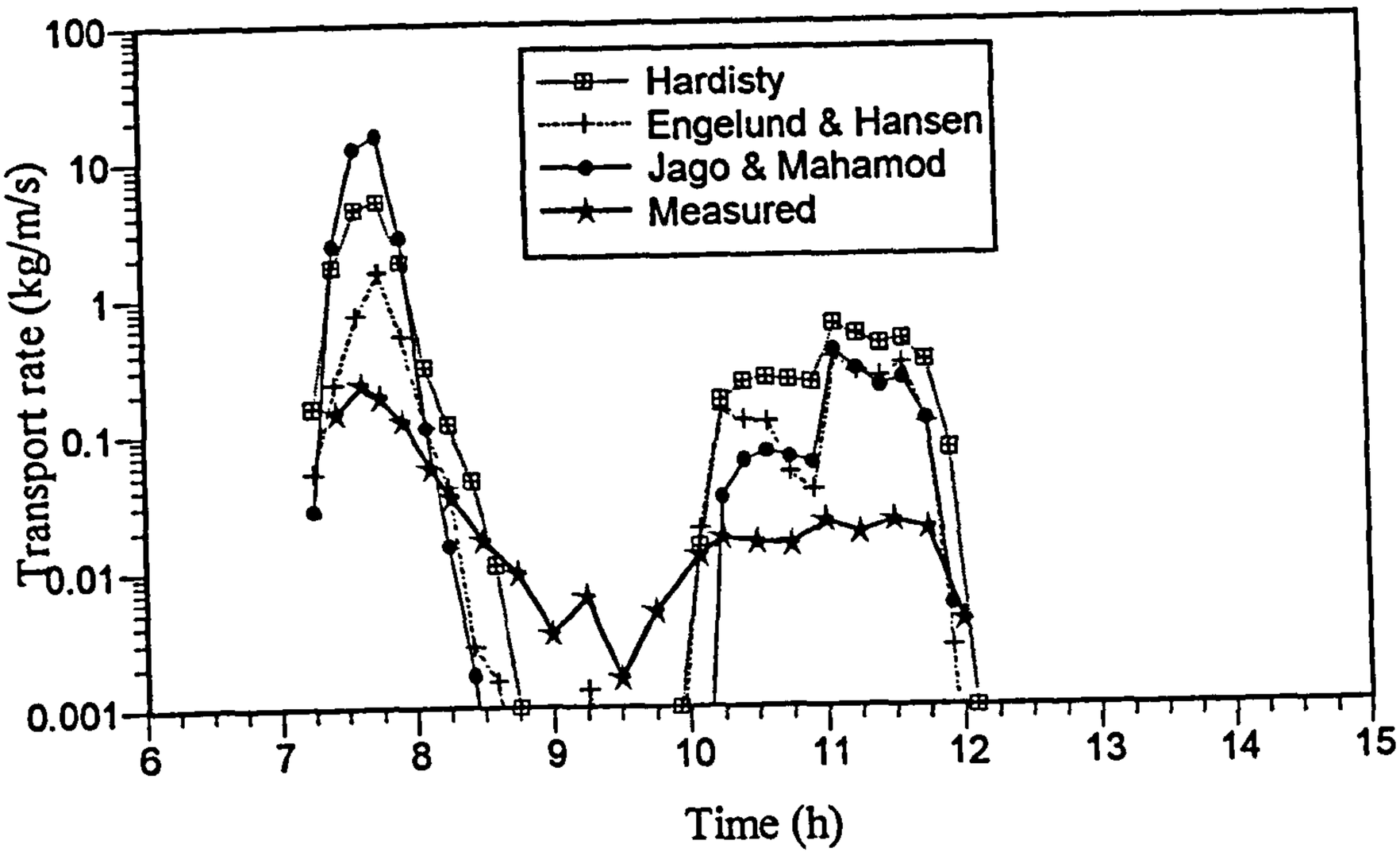

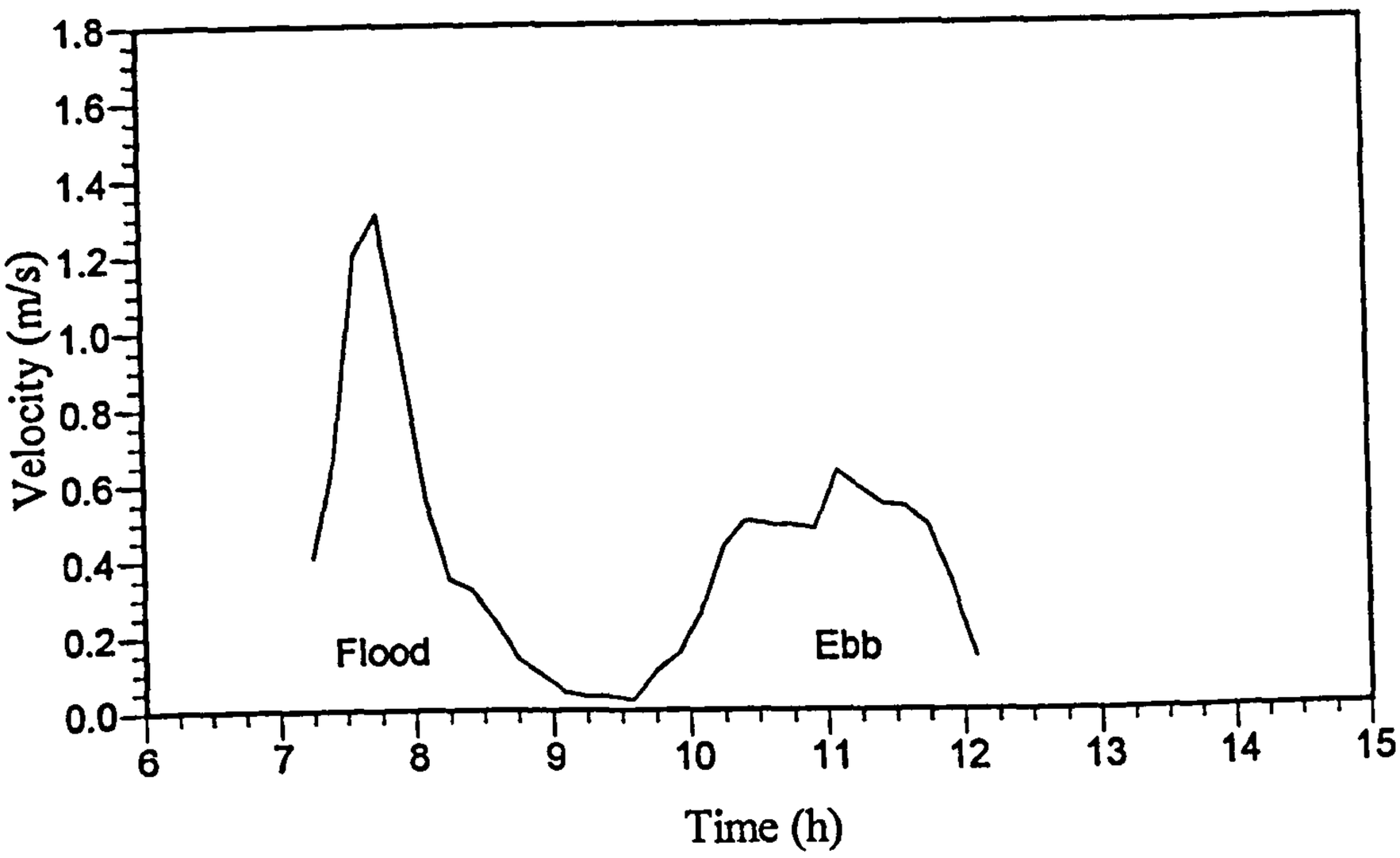

Figure 8.9 The variation of (a) Calculated and Measured transport rates at station 1, and (b) depth-mean velocity at station 3, transect T5, 13 September 1995.

Mahamod and Engelund and Hansen are better predictors than Hardisty.

Table 8.8 Calculated and measured total load transport over flood and ebb tidal cycle at anchor Station 3, Transect T5. The values in bracket indicate the ratios between calculated and measured transport.

Date	Tide	Transport rate (kg/m)			
		Hardisty	Engelund & Hansen	Jago & Mahamod	Measured
12/9/95	Flood	n.d	n.d	n.d.	n.d
	Ebb	1334 (4.55)	385 (1.31)	415 (1.42)	293
13/9/95	Flood	8246(15.44)	8937 (16.74)	19994 (37.44)	534
	Ebb	2148 (15.57)	1080 (7.83)	938 (6.80)	138
14/9/95	Flood	1649 (5.25)	1228 (3.91)	1537 (4.89)	314
	Ebb	571 (5.29)	132 (1.22)	72 (0.67)	108
15/9/95	Flood	625 (5.95)	62 (0.59)	143 (1.36)	105
	Ebb	420 (6.67)	66 (1.05)	37 (0.59)	63

n.d. = no measurement made

8.3.2.4 Anchor Station 4.

This station was located in a shallow depression of an old ebb channel. The elevation down-estuary of the station was greater than up-estuary due to the development of an intertidal sand flat in the middle of the estuary. Current velocity measurement at this station proved to be difficult particularly on the flood. At the early stage of the flood the flow was towards the south (down estuary) until the sand flat was fully covered by the water of the incoming flood tide. During the ebb the flow reversed when the water depth on the sand flat had reached less than 0.5 m. Due to these difficulties, and to the fact that this station was at a higher elevation than the station in the main ebb channel, current measurements could only

be made for a limited time period, generally less than 2 hours during the flood and about three hours during the ebb on a spring tide. The maximum mean currents measured at this station on 13 September 1995 were 0.33 m/s and 0.46 m/s for the flood and ebb, respectively.

The variation of transport rate over a tidal cycle for this station is shown in Figure 8.10. Negligible sediment transport is predicted by all formulae during the flood phase, but there is a significant transport over the ebb phase of the tidal cycle, though the predicted amount is much less than at Stations 1 and 2. Comparison with the measured transport shows that

Table 8.9 Calculated and measured total load transport over flood and ebb tidal cycle at anchor Station 4, Transect T5. The values in bracket indicate the ratios between calculated and measured transport.

Date	Tide	Transport rate (kg/m)			
		Hardisty	Engelund & Hansen	Jago & Mahamod	Measured
12/9/95	Flood	n.d.	n.d.	n.d.	n.d.
	Ebb	2129 (3.29)	2641 (4.08)	793 (1.22)	648
13/9/95	Flood	102 (0.32)	167 (0.53)	6 (0.02)	318
	Ebb	1481 (3.59)	1118 (2.83)	347 (0.88)	395
14/9/95	Flood	197 (0.92)	250 (1.16)	10 (0.05)	215
	Ebb	778 (3.93)	1350 (6.82)	110 (0.56)	198
15/9/95	Flood	44 (0.34)	67 (0.52)	0.3 (0.002)	128
	Ebb	410 (3.63)	474 (4.19)	44 (0.39)	113

n.d. = no measurement made

all formulae underestimate transport during the flood period. The transport rates are more or less comparable for most of the ebb, except toward the end of the ebb. During this time

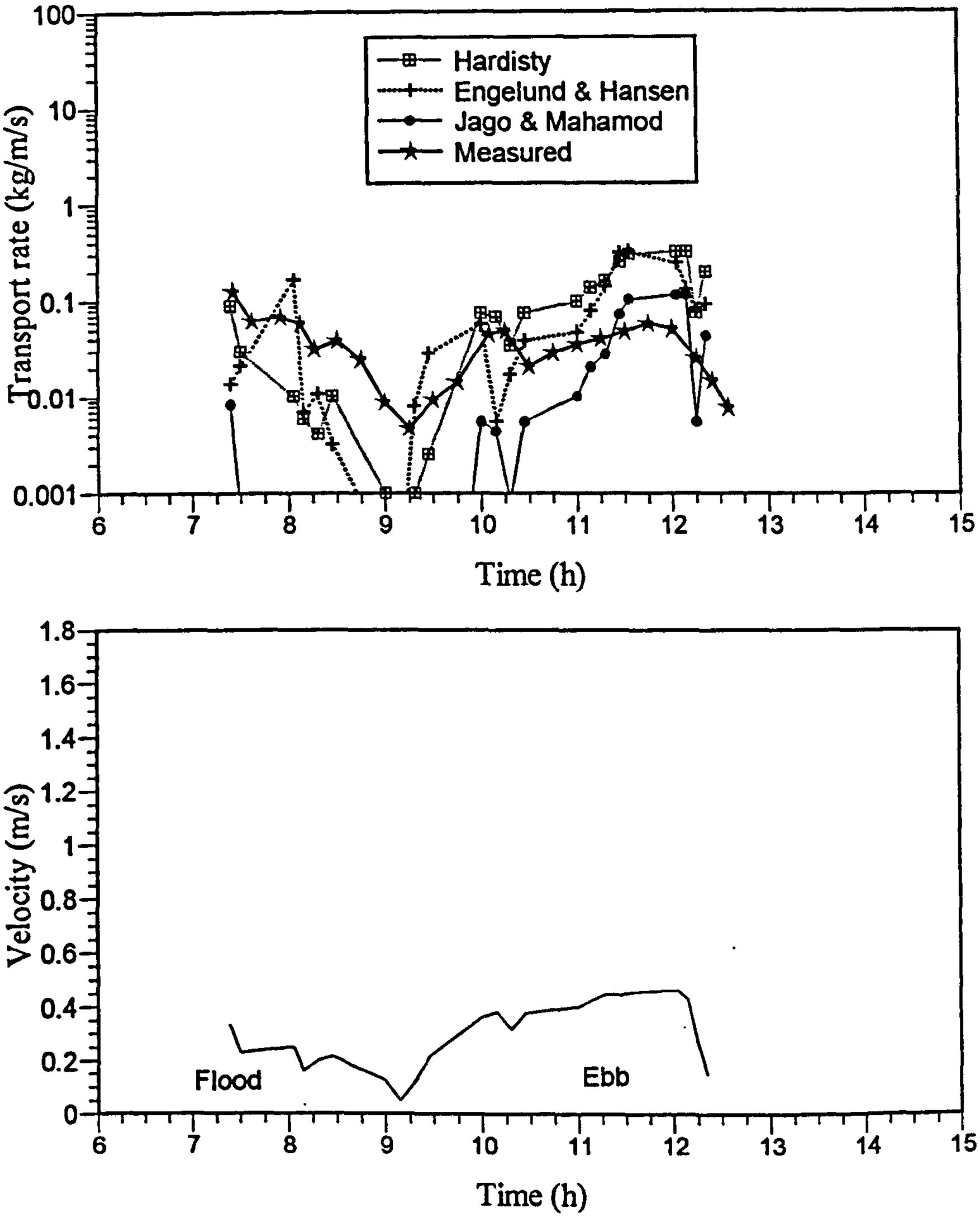

Figure 8.10 The variation of (a) Calculated and Measured transport rates at station 1, and (b) depth-mean velocity at station 4, transect T5, 13 September 1995.

the velocities were higher than 0.4 m/s, and the transport is slightly overpredicted by all of the equations.

Although the equations predict limited transport during the flood, the measurements showed that there was a significant amount of flood transport at this station (Table 8.9). The measured total transport for the ebb showed that on bigger tides the net transport was in the ebb direction, but on smaller tides the flood transport more or less equalled the ebb transport. However, the calculated transport showed an ebb dominance for all tidal ranges. Thus the net sediment transport at this station was in the ebb direction. Again the ratios of calculated to measured transports show a considerable variation. The total flood and ebb transports at this station are underestimated by the Jago and Mahamod equation. Hardisty and Engelund and Hansen underestimate the flood transport but overestimate the ebb transport.

8.3.3. Discussion

Calculated sediment transports show that there is a net landward sediment transport at Stations 1, 2 and 3, and a net seaward transport at Station 4. The amount of seaward transport at Station 4 is small compared to the amount of landward transport at Stations 1 and 2, resulting in the net landward transport across the total transect.

Clearly, there are considerable variations of transport rates predicted by the three different transport equations examined in this study. Even at a single station where calculations were based on the same flow velocities, the predicted transport rates can vary from less than 1 to more than 10 times the measured transport rates. This shows that each equation has limited application. As these equations were calibrated using data from flume or field studies, they will only be as good as the data used to calibrate them, and their use will be restricted to the range of conditions of the calibration data (Dyer , 1986).

Of the three equations tested in this study, the formula of Engelund and Hansen gives the

overall best prediction of the transport rates, with the discrepancy ratio ranging from 0.5 to 17. The Jago and Mahamod equation give the most inconsistent prediction of the transport rates with the discrepancy ratios varying from 0.002 to 38.

The variation of transport rates across the estuary are also reflected in the calculated values. The difference between stations located in the main channel and on the intertidal sand flat can range from 2 to 100 times using the Engelund and Hansen equation, and to more than 1000 times using the Jago and Mahamod equation. This large variation indicates the overall inaccuracy of an estimation of sedimentation rate for the whole estuary from a single station measurement such as in Mahamod (1989) and Larcombe (1992). This single measurement is usually made as much as possible in the fastest flow of the main channel. Thus, a calculation of sediment accumulation rate based on a single station measurement should be viewed with cautious. Mahamod (1989) quotes an accumulation rate of 4.9 cm/year for the Dwyryd Estuary, and Larcombe (1992) gives a value of 8.2 cm/year for the Mawddach Estuary from such measurements. They are higher as compared with sedimentation rates of only 1.0 - 2.2 cm/year for the Taf Estuary (based on the measurement of sediment fluxes made at stations across the estuary as calculated in Chapter 7).

In the natural environment, the measurement of sediment concentration very close to the bed (where high transport may occur) is difficult to make due to the design and setting of the measuring instrument (in this case the transmissometer). The transmissometer only measures the particles that move in suspension at a distance above a few cm from the bed. Although suspension is the main mode of transport for fine sand at high transport stages, the transport by saltation and rolling (bedload) can account for up to 20 % of the total transport (Dyer, 1986). The saltations which occur at maximum height of only a few grain diameters (Francis, 1973; van Rijn, 1984) will not be measured by the transmissometer. Thus, the result of the measured transport would be underestimated.

8.4 Calibration of Jago and Mahamod transport equation

One of the main objective laid out for this chapter was to test the predictive capability of the transport equations. One of these equations was from Jago and Mahamod (1997) which was derived and calibrated against a wide range of flow velocities (up to 1.5 m/s) in a laboratory flume. Thus, it should predict the transport rate reasonably well for the ranges of velocities that exist in this study area. However, as demonstrated in the preceding section, the sediment transport calculated using the Jago and Mahamod equation was the most inconsistent compared to the other equations in predicting the transport rate. At high flow velocities (> about 0.7 m/s), the equation very much overestimated the transport rate and at low flow velocities (< 0.7m/s) the transport rate was very much underestimated. The performance of the Jago and Mahamod equation will be further tested and compared with the measured transport.

As the Jago and Mahamod formula is based on a very high power law for the transport of fine sand, the equation is very sensitive to the choice of the threshold velocity. To illustrate this sensitivity, Station 2 of Transect T5 was selected as it has a wide range of current velocity (up to 1.6 m/s) over the tidal cycles measured. The current velocities at this station were measured using the VGU, thus giving a good record (at 10 minute intervals) of tidal velocities over the complete tidal cycle. At this station, the sediment transport was recalculated using threshold velocities ranging from 0.17 m/s to 0.26 m/s and the results are tabulated in Table 8. 10. The table shows that for a spring tide (13 September 1995), in order to obtain the predicted transport comparable to the measured transport, it is necessary to use a threshold velocity higher than 0.26 m/s for the flood, but for the ebb the threshold velocity required is much lower i.e. 0.22 m/s. On a much smaller tide on 15 September 1995, the predicted transport is comparable to measured transport when a threshold velocity of 0.23 m/s is used for the flood, and 0.19 m/s is used for the ebb.

Table 8.10 Sediment transport calculated using Jago and Mahamod (1997) total load equation with different threshold velocities for station No. 2, transect T5, 12 - 15 September 1995.

Threshold velocity (m/s)	Transport rate (kg/m)							
	12/9/95		13/9/95		14/9/95		15/9/95	
	Flood	Ebb	Flood	Ebb	Flood	Ebb	Flood	Ebb
0.17	-	5650	60492	1578	29879	1223	4125	1093
0.18	-	4137	45558	1128	22331	868*	3000	778
0.19	-	3069	34767	816*	16909	624	2209	560*
0.20	-	2302	26849	597	12955	453	1645	408
0.21	-	1744	20957	441	10031	331	1237	300
0.22	-	1334*	16516	328	7841	245	939	222
0.23	-	1029	13131	246	6183	182	718*	166
0.24	-	800	10528	185	4913	136	553	124
0.25	-	625	8496	141	3933	102	429	94
0.26	-	492	6905*	107	3168*	77	334	72
Measured	-	1290	3839	781	1930	795	763	506

* indicates closest estimate to the measured transport.

This analysis indicates that in order to obtain a predicted transport comparable to the measured transport it is necessary to use different threshold velocities for the flood and for the ebb, and different thresholds are required for spring and neap tides. A higher threshold value is necessary for stronger currents (> 1.0 m/s) while a lower threshold velocity is required for weak current (< 0.8 m/s). As such the Jago and Mahamod equation is difficult to use in such varying tidal conditions. As the threshold velocity for sediment transport depends on the grain diameter, it should remain about the same regardless of tidal condition (unless there is a significant change in bed morphology i.e. ripple geometry and orientation, due to changing in tidal velocity). To resolve this ambiguity, a further test was carried out using different values for the exponent n.

As shown in Figures 8.1- 8.5, the calculated transport overestimates the measured transport when the current speed has reached a certain critical velocity. This critical velocity differs slightly between the flood and the ebb. At T5, the values vary between 0.7 to 0.85 m/s for the flood , and between 0.6 to 0.7 m/s for the ebb. A mean critical velocity of 0.7 m/s has been selected as representative for both tidal phases; therefore a velocity greater than 0.7 m/s is considered as a fast current and a velocity lower than 0.7 m/s as a slow current. Assuming the exponent n derived from the Guy *et al.* (1966) flume data was correct for the slow current, the exponent for the fast current was varied between n = 2.8 to n = 4.2 in order to bring down the predicted transport comparable to the measured transport. Using a variable value of n for the fast current, and a threshold velocity of 0.17 m/s, the transports at station 2 of transect T5 were recalculated for spring and neap tides.

Table 8.11 Sediment transport at station No. 2, transect T5 , 12 - 15 September 1995 calculated using Jago and Mahamod (1997) total load equation with different exponent n for u_{100} greater than 0.7 m/s and u_t = 0.17 m/s

Exponent n	Transport rate (kg/m)							
	12/9/95		13/9/95		14/9/95		15/9/95	
	Flood	Ebb	Flood	Ebb	Flood	Ebb	Flood	Ebb
2.8	-	1067	2852	977*	1943*	1028*	720	635*
2.9	-	1147	3429	991	2288	1034	788*	645
3.0	-	1239*	4132*	1006	2701	1038	865	656
3.2	-	1471	6064	1043	3791	1051	1055	682
3.3	-	1615	7336	1065	4504	1059	1171	698
3.4	-	1783	8913	1090	5360	1067	1304	716
3.6	-	2204	13208	1151	7621	1088	1631	760
3.8	-	2772	19651	1228	10880	1113	2062	819
4.0	-	3539	29323	1326	15583	1144	2627	894
4.2	-	4573	43853	1453	22373	1184	3370	993
Measured	-	1290	3839	781	1930	795	763	506

* indicates closest estimate to the measured transport.

The results are shown in Tables 8.11. For comparison, the transport rates were also recalculated using different exponent n for all ranges of flow velocities (Table 8.12).

The accuracy of the predicted transport using different values of the exponent n for fast velocities and also for all flow velocities is given by the discrepancy ratio, here defined as the total predicted transport over the total measured transport. These ratios are calculated for the transport rates given in Tables 8.11 and 8.12, and the results are plotted in Figure 8.11. The ratios show there is a systematic deviation from the unity value (discrepancy ratio = 1) with increasing and decreasing values of n. A higher exponent n overestimates the total transport, while a smaller n underestimates the total transport. A bigger scatter is obtained when using different a exponent n for all flow velocities (Figure 8.11a);

Table 8.12 Total sediment transport at station No. 2, transect T5 , 12 - 15 September 1995 calculated using Jago and Mahamod (1997) total load equation with different exponent n for all flow velocities and u_t = 0.17 m/s

Exponent n	Transport rate (kg/m)							
	12/9/95		13/9/95		14/9/95		15/9/95	
	Flood	Ebb	Flood	Ebb	Flood	Ebb	Flood	Ebb
2.8	-	636	2669	291	1799*	253	540	223
2.9	-	728	3249	323	2149	280	614	245
3.0	-	834	3960*	359	2566	308	697*	270
3.2	-	1097	5887	444	3667	376	901	328
3.3	-	1259*	7184	495	4387	416	1026	363
3.4	-	1447	8769	551	5249	459	1167	401
3.6	-	1915	13085	684	7526	562	1515	491*
3.8	-	2540	19551	851*	10804	689	1969	603
4.0	-	3375	29252	1060	15530	845*	2562	744
Measured	-	1290	3839	781	1930	795	763	506

* indicates closest estimate to the measured transport.

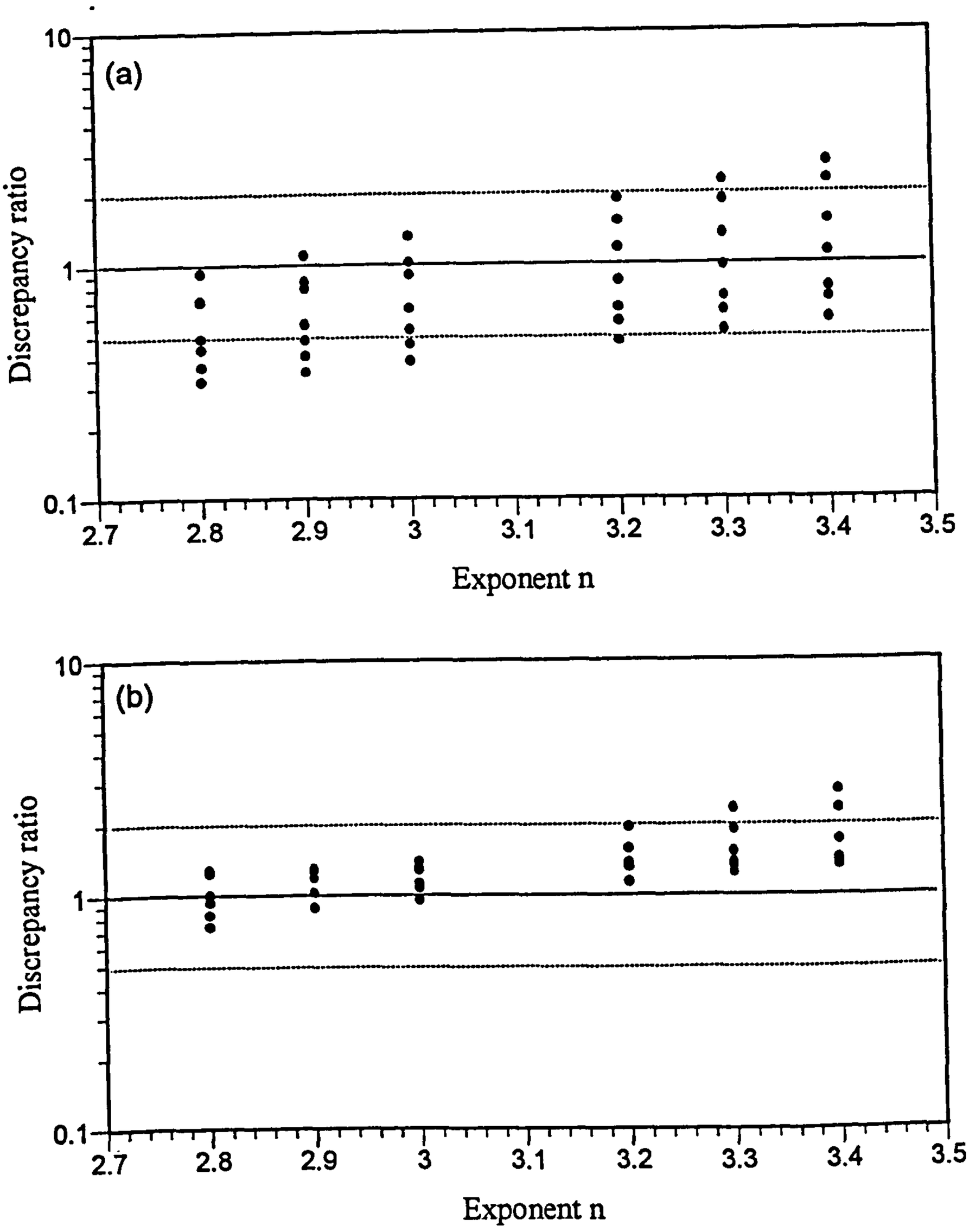

Figure 8.11 Discrepancy ratio (calculated transport rate/measured transport rate) for station 2, transect T5: (a) different values of exponent n for all flow velocities, and (b) different values of exponent n for flow velocities > 0.7 m/s.

however if a different n was applied only to high flow velocities, the scatter is reduced (Figure 8.11b). A better agreement between the predicted and measured transport is obtained when using exponent n = 3.0 for high flow velocities.

Table 8.13 Total transport rate at stations 1-4, transect T5, on 12- 15 September 1995 as calculated using the modified Jago and Mahamod equation. The measured rates is included for comparison.

Date	Station number	Transport rate (kg/m)					
		Calculated		Measured		Difference (%)	
		Flood	Ebb	Flood	Ebb	Flood	Ebb
12/9/95	1	-	2381	-	2842	-	83.8
	2	-	1239	-	1290	-	96.0
	3	-	415	-	585	-	70.9
	4	-	793	-	1296	-	61.2
13/9/95	1	5597	1336	5669	1938	98.7	68.9
	2	4132	1006	3839	781	107.6	128.8
	3	750	413	1067	276	70.3	149.6
	4	3	347	636	790	0.5	43.9
14/9/95	1	3356	908	3535	1290	94.9	70.4
	2	2701	1038	1930	795	139.9	130.6
	3	413	72	628	216	65.8	33.3
	4	10	110	492	395	2.0	27.8
15/9/95	1	2704	1248	1693	1052	159.7	118.6
	2	865	656	763	506	113.4	129.6
	3	143	37	209	125	68.4	29.6
	4	0.3	45	256	225	0.1	20.0

Using n = 4.35 for the slow currents and n = 3.0 for fast the currents, and threshold velocity of 0.17 m/s, the total sediment transport at other stations have been recalculated for Transect T5 and the results are shown in Table 8.13. The table indicates that 71% of the calculated transport rate falls within the discrepancy ratios of 0.5 - 2.0. This is a very significant improvement compared to only 29 % of the calculated transport falling within the discrepancy ratio of 0.5 - 2.0 as predicted using the unmodified equation.

8.4.1 Estimation of sediment flux

By using the modified Jago and Mahamod equation, it is possible to estimate, with increased confidence, the sediment flux across the transect. The calculated flux can then be compared with the measured flux across the same transect; this will demonstrate the accuracy of the modified equation. For this purpose, sediment flux across Transect T5 has been recalculated using the modified equation for measurements made on 13 September 1995.

The sediment flux represented by each measurement station has been recalculated using the modified equation in the same manner as the sediment flux calculation (Chapter 7). For this calculation, the estuary cross section for Transect T5 has been divided into 4 compartments, each represented by the 4 measurement stations. The flux across each compartment at any particular time is a product of the instantaneous transport rate times the averaged width of the compartment cross section. In this case, the width has been obtained by dividing the compartment cross sectional area by the water depth at the measurement station for every 15 minute interval. This averaged width varies with the tidal heights and also with the geometry of the cross sectional area at each measurement station. The instantaneous flux was integrated over time to obtain the mass transport over flood and ebb tidal cycle at each station. The results of this calculation are shown in Table 8.19 which also shows the measured sediment flux from the current velocity and transmissometer casts (Chapter 7). In Table 8.19, the advecting sediment from the turbidity maximum has been omitted from the measured flux at Stations 1 and 2 (the main channel stations).

Table 8.19 Comparison between calculated and measured sediment flux at Transect T5, 13 September 1995.

Station no.		Sediment flux (kg)			Direction
		Flood	Ebb	Net	
1	Calculated	290626	95739	194887	Flood
	Measured	261060	92586	168474	Flood
2	Calculated	147902	30105	117797	Flood
	Measured	124112	25673	98439	Flood
3	Calculated	176786	102176	74610	Flood
	Measured	58020	15050	42970	Flood
4	Calculated	383	16928	-16545	Ebb
	Measured	26930	30740	-3810	Ebb
SUM	Calculated	615697	244948	370749	Flood
	Measured	470122	164049	306073	Flood

The table shows that only the calculated fluxes at Station 2 at which the modification was based, and the calculated fluxes at Station 1 agree with the measured fluxes for flood and ebb periods. For Station 1, the good agreement between the measured and the calculated fluxes are due to the similarity in the flow strength and bed geometry and configuration (both were located within the same channel). For Station 3, the equation overestimates the flood flux by a factor of 3, and the ebb flux by a factor of 7. For Station 4, although the equation predicts correctly the dominant transport direction, it underestimated the flood flux by a factor of 70 and ebb flux by almost double.

The above results indicate how the calculated and the measured flux vary at stations across the estuary. Even after modification and field calibration, the equation does not predict the flux correctly for the all stations across the estuary, except for those at which the calibration has been based, and which have similar flow conditions and bed geometry. In reality, the flow velocity does not entirely depend on the tidal forcing; it also affected by local factors, such as the presence of ebb channels, meanders, bends, intertidal sand bars and sand flats.

Therefore, it seems that for a correct estimate of sediment flux, a separate calibration of the transport equation is required for each station across the estuary; this is cumbersome and unrealistic.

8.4.2 Discussion

A major difficulty in predicting sand transport is the non-linearity of the entrainment and transport processes. For example, for bedload transport, it is related to the shear velocity u_* times the excess shear stress $(\tau - \tau_c)$ at high transport rate and to u_* times $(\tau - \tau_c)^2$ at low transport rates (Heathawshaw, 1981). Other workers have adopted different values of n in their transport equations. Sternberg (1972), Gadd *et al.* (1978) and Hardisty (1983) have suggested $n = 3$ in their bed load equations. Similarly Bagnold (1963) and Yalin (1972) suggest the rate varies as u_*^3. Heathershaw (1981) however suggests that for high velocities, bedload may be proportional to $n = 3$, and at low velocities the transport is proportional to $n = 5$. For total load transport, Jago and Mahamod (1997) found the value of n as a function of grain diameter rather than flow velocity. They proposed $n = 3$ for coarse sand when traction is predominant and $n > 4$ for fine sand where suspension is predominant.

For suspended load, there are considerable uncertainties; the transport rate is related to u_* to the power of n+2, where n is at least 1 (Lees, 1983). Measurement of suspended sediment transport in the Sizewell-Dunwich area by Lees (1983) indicates that the transport rate varies as $u_*^{2.8}$. Dyer (1980) indicates that in certain cases the suspended transport is proportional to u_* to a power between 5 and 7. As concluded by Dyer (1986), at high transport rates, the transport is proportional to u_*^3, but at low rates near the threshold, u_*^5 is possible. This is consistent with the findings of the present study where at high current velocities the transport is proportional to $n = 3$, but for low current velocities a higher exponent n ($n = 4.4$) is required. The value of n however is not consistent over flood and ebb periods which implies that there are other mechanisms responsible for the net suspended load transport in addition to the mean flow. The justification for this reduction in the value of n for high flow velocities is that at fast current, the water is saturated with sediment so

that there is a density stratification exist within the water column. The suppression of turbulent by density stratification reduces the transport rates as discussed before (see Chapter 5); while the formula predicts transport regardless of velocities. All ransport equations do not consider the nature of the fluid (which changes with flow velocities due to the density stratification), and the nature of the bed which also changes depending on the flow strength, so the the threshold also varies throughout a tidal cycle, though the sediment size remains the same.

There are also differences between conditions in the natural environment and in flumes. In an estuary, the sediment supply is effectively unlimited. The concentration measured at a station may not be the result of suspension by tidal currents at immediately upstream of the measurement point. A lot of resuspension may occur well away from the measurement point at high flow velocities and be carried to the measurement point where the flow velocity has already reduced due to the local topography. This may explain why the measured transport is much higher than the calculated transport as seen at station 4.

In a flume the flow is more or less parallel to the wall and once equilibrium is reached, the velocity at any height above the bed is the same if measured at any one point in the flume. However the flow in the natural environment is controlled by the local geometry of the stream cross section, and depends on the relative position of the main ebb channel to the measurement points. Therefore a sediment transport equation which totally depends on the calibration from the flume data may not be truly applicable to the more complicated field conditions.

In the calibration of the Jago and Mahamod equation the mean flow velocity was assumed to be equal to that expected at 1.0 m above the bed. Since the averaged flow depth in the flume was only about 0.3 m, this estimation could lead to a significant underestimation of u_{100}.

In the Taf, the bed material is very uniform spatially and temporally (see Jago 1974, 1980). The uniform grain size across the transects made the condition to verify the various

equations as carried out in this study much simpler. In other estuaries where bed material normally changes across an estuary cross section, the similar exercise could be more complicated.

No consideration was given to the effect of waves on the calculated transport rates. No doubt, as shown by other studies, wave action intensifies transport rates by enhancement of bed shear stress (eg. Larcombe, 1992; Collins *et al.*, 1995). However in the Taf, storm waves may have very little effect on the total transport as a whole. Most transport occurs during the early flood when the water depth in the main channel is quite shallow (less than 2 m). Waves break before entering the estuary. The sand spit at the estuary mouth protects the estuary from large waves. Wave activity in the estuary may be important when water in the estuary reaches a depth greater than 4 m around high water, by which time the transport has almost ceased. Measurements made during a stormy day on 14 July 1995 did not show a significant increase in the sediment concentration in the water column. Wave action may of course be important in more exposed estuaries and bays.

8.5 Conclusion

This study shows that the spring-neap tidal cycle is the primary control of the temporal variation of sediment resuspensions. Measurements made at stations across Transect T5 and T9 show that transport rates vary across the estuary. The main controlling factor of this variability is the local morphology of the estuary channel which, in turn, determines the flow velocity and direction. The maximum transport occurs in the main ebb channels during flood and ebb periods, but the transport is rapidly reduced away from the channel. On the intertidal sandflats and mudflats, the transport rate is only about 10% of that in the main channel. Therefore any estimate of sediment budget based on a single station measurement must be inaccurate. The measurements also indicate that the general transports are flood dominant which gives rise to the net sediment accumulation in the estuary. Locally, however, transport is either flood or ebb dominant due to the local morphology of the channel and sandflats.

Comparison of various sediment transport equations shows that there are considerable differences in predicted transport rates for the same flow velocity and sediment size. Hardisty`s and Engelund and Hansen`s equations give comparable transport rates, but Jago and Mahamod`s equation is very sensitive to the changes in flow velocity and predicts much higher transport rates than the other equations. Provided the velocity profiles are accurately measured, so that bed shear stress can be determined, the Engelund and Hansen's equation gives better agreement with the measured transport than Hardisty`s and Jago and Mahamod`s equations.

The Jago and Mahamod equation is based on a variable power law, and for fine sand the value of the exponent n in the equation can increase up to 4.4. This leads to overestimation of transport rates at high flow velocities. It also means that the equation is very sensitive to the choice of threshold velocities used to calculate the transport, particularly for very fine sand when the exponent n becomes greater than 4. Therefore, it is critical to obtain an accurate value for the threshold velocity for the sediment size in the study area. Comparison with the measured transport showed that for an accurate estimate of transport rate, the exponent n needs to be reduced to n = 3.0 for current velocities above 0.7 m/s while maintaining n = 4.4 for velocities less than 0.7 m/s. Application of this modified equation to the 28 measurement data of Transect T5 (see Table 8.13), shows that 71 % of the predicted transport was found to be within 0.5 - 2.0 times the measured transport rate. However, the modified equation only gives a good estimate of sediment flux at the station where the measured data are used to calibrate the equation. The flux estimates for other stations vary significantly from the measured flux. This discrepancy arises because the flow in the estuary is complicated by the presence of ebb channels, bends, meanders and intertidal sandflats. Even after calibration with field measurement, the application of such a transport formula for flux estimation is still limited. Therefore the sediment flux can be determined correctly only by making measurements of the actual sediment concentration and flow velocity across the estuary cross section.

The results of this study also indicate that an evaluation of a sediment transport formula using flume data is not conclusive and should always be followed by a verification in the

field. Our finding confirms the previous argument that at high velocity the transport rate is proportional to the cube of the measured velocity, but at low velocity the transport rates depends on a higher power of the velocity i.e. between 4 and 5.

CHAPTER NINE

SEDIMENTATION RATES OF THE SALT MARSH

9.1 Introduction

Another independent measurement made in this study was the radiometric dating of sediment cores. These cores were obtained from salt marshes of the Taf estuary and used to estimate accretion rates of the marsh sediment. Although the major effort has so far been concentrated in describing the sedimentary processes in the estuary channel and the sedimentation rates of the estuarine sands, the accretion rates of the marsh sediment are related to some extent to the main processes that are occurring in the estuary channel.

In this chapter the results of ^{137}Cs analysis of sediment cores collected from the different salt marshes areas of the Taf estuary are presented. The profiles of the ^{137}Cs in the cores are used to estimate the accretion rates of the mash sediment based on the occurrence of the peak of ^{137}Cs activity which corresponds to 1963 (the peak ^{137}Cs fallout from the nuclear weapon testing) and 1986 (the ^{137}Cs peak from the Chernobyl nuclear accident). Some general comments are made on the quality of the cores and the associated ^{137}Cs activity. The radioisotope dating will provide an estimate of accumulation rates over longer time periods (10 -30 years) which can then be compared with the accumulation rates estimated from the shorter term study (neap-spring cycle) from the sediment flux measurements, presented in Chapter 7.

9.2 ^{137}Cs dating technique

^{137}Cs is a man-made radionuclide produced from nuclear testings and does not occur naturally. It was first introduced into the atmosphere and globally dispersed with the advent of above ground nuclear weapon testings conducted in the 1950s and early 1960s (Miller

and Heit, 1986; Lynch *et al.*, 1989; Williams and Hamilton, 1995). The fallout of this radioisotope is preserved in sediment layers and has been used extensively for dating purposes (Ritchie and Mc Henry, 1990). The highest fall out occurred between 1963 and 1964 (Milan *et al.*, 1994). This maximum in ^{137}Cs activity is found in sediment records and is used as a marker horizon to calculate sediment accumulation rates. ^{137}Cs has been used as a stratigraphic marker for dating rapidly accreting lake and salt marsh sediments (eg. DeLaune *et al.*, 1978; Sharma *et al.*, 1987; Edgington *et al.*, 1991).

^{137}Cs decays exponentially to ^{137}Ba with a half life of 30.2 years, making it suitable for dating sediment deposited within the last 30 - 50 years. The decay emits γ particles at the energy of 661 KeV which can be counted with a relatively simple and non-destructive procedure.

The ^{137}Cs dating technique relies on the preservation of the ^{137}Cs fallout signal within the sediment. Accretion rates are normally calculated assuming the depth of maximum ^{137}Cs concentration corresponding to 1963, the year of peak ^{137}Cs fallout, and 1954, the first year of significant ^{137}Cs fallout (Pennington *et al.*, 1973; De Loune *et al.*, 1978; Williams and Hamilton, 1995). The atmospheric fall out of ^{137}Cs declined after 1964 due to the Nuclear Test Ban Treaty of 1964. The 1986 Chernobyl nuclear power plant accident provided another spike to the declining ^{137}Cs concentration and can be used as another marker horizon to calculate the accretion rate for the last 10 years, particularly in certain parts of the European continent. The plume of radioactive fallout from this accident however was patchy because it did not get into the upper atmosphere and was deposited most intensely with local rain (Cambray *et al.*, 1987).

Caesium is known to have an affinity for clay particles as well as for organic matter (Robbins *et al.*, 1979; Sharma *et al.*, 1987, Mudge *et al.*, 1994) and is not prone to chemical remobilization under normal condition (Robbins and Edgington, 1975; Francis and Brinkley, 1976). However, under conditions of low PH, low clay and high organic content, and also under conditions of high salinity ^{137}Cs is relatively mobile and readily defuses in the pore water of the sediment (Longmore *et al.*, 1986; and Crickmore *et al.*, 1990). In cases where

some diffusion has occurred at the base of the ^{137}Cs record, resulting in ^{137}Cs extending into pre-1954 sediment, the break in slope in ^{137}Cs profiles corresponding to 1954 may still be identifiable and has been used successfully to calculate sedimentation rates (eg. DeLaune *et al.*, 1978; Oenema and DeLaune, 1988).

9.3 Methods

9.3.1 Field sampling

Sediment cores were collected from salt marsh areas within the lower Taf estuary during 11-14 September 1995 and again on 12 September 1996. In September 1995, 10 cores were collected from three sampling sites; A, B and C (Figure 9.1, cores a1-a10). At Site A, 4 cores were collected; cores a1 and a2 were taken 15 m apart in a low marsh area heavily vegetated by *Spartina anglica*, while cores a3 and a4 were collected at the boundary between the salt marsh and the mud flat where little vegetation was present. Within the vegetated area, penetration was difficult due to the dense roots of *Spartina anglica*, thus only short cores (< 36 cm long) were obtained; however in non-vegetated areas full core lengths (54 cm) were recovered. From Site B, 4 cores (a5 -a8) were obtained from the low marsh. The area was dominated by *Spartina anglica*, *Halimione portulacoides*, *Sueda maritama* and *Puccinellia maritama*. All the cores were collected 15 m inside the marsh area from nearest creeks. The coring sites were chosen so that there was minimum vegetation cover on the surface in order to obtain maximum penetration. Cores a9 and a10 (Site C) were collected 20 m apart from a low marsh area heavily over grown by *Spartina anglica*. The sampling locations were 40 m inside the marsh from the mud flat. The nearest creeks were 30 m distance from a9 and 15 m distance from a10.

All the cores collected in September 1995 were recovered using perspex tubes, 60 cm long by 10 cm inside diameter. The tube was fitted with a sharp brass cutting head to facilitate the cutting of the sediment as well as the plant roots while minimizing compaction during penetration. The tube was inserted into the marsh soil using a gentle twisting motion

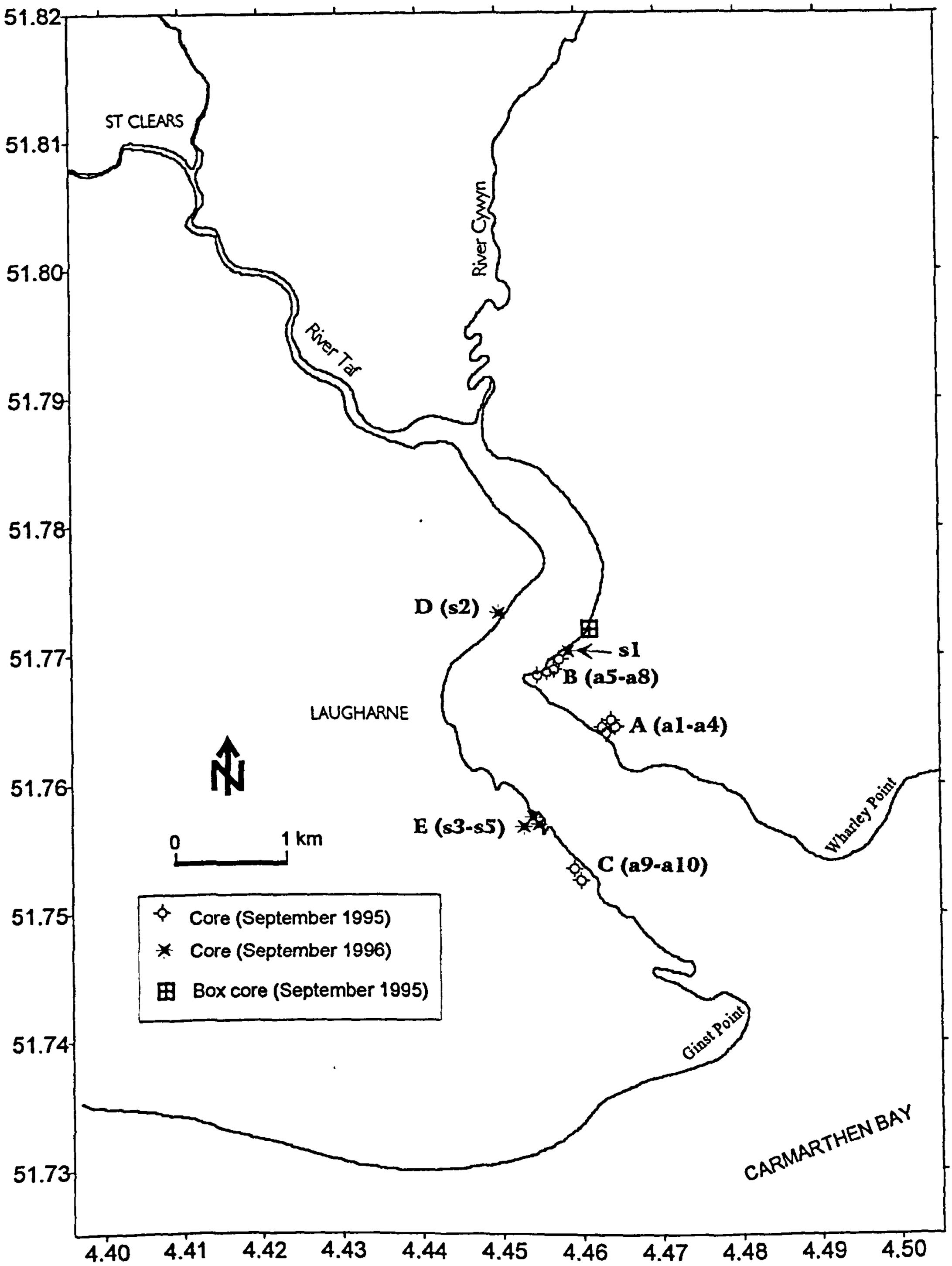

Figure 9.1 Location of sampling sites for sediment cores.

until the top of the core was approximately within 3 cm of the marsh surface or no further penetration could be made. The difference between the top of the core inside the tube and the height of the marsh soil was measured to estimate the degree of compaction. The cores were sealed at both ends with rubber stoppers to stop evaporation, and they were kept in a vertical position both during transportation and storage until the time for sectioning. The exact location of the sediment core was determined by surveying it to the nearest permanent steel pole used for the transect surveys described in Chapter 3.

In addition to the sediment cores, a series of Senckenberg box cores was also taken from an eroding bank which cut through a low marsh area upstream of Site A (Figure 9.1). At the surface the area was densely populated by *Halimione portulacoides*. A total of eight box cores were taken in succession from the top to the base of the erosion cliff, bringing a total core length of 2.40 m. Each box was made up of stainless steel case measuring 30 x 20 x 5 cm that opens and closes at one side to facilitate core recovery and extraction. The cores were kept in a freezer prior to their sectioning.

In September 1996, another five cores were collected from three different salt marsh sites within the lower estuary (Figure 9.1, cores s1-s5). At Site B, a single core (s1) was taken from the low marsh area vegetated by *Spartina anglica* and *Halimione portulacoides*. A single core (s2) was collected at Site D from the high marsh, with dense growth of *Halimione portulacoides;* no low marsh was present at this site. At Site E, three cores were collected; two (s3 and s5) from the low marsh with dense growth of *Spartina anglica* and one core (s4) also from the low marsh, but taken 40 m inland from s3. At s4, the marsh was populated by *Halimione portulacoides*, *Sueda maritama* and *Puccinellia maritama*. All five cores were taken using 15 cm diameter thin wall stainless steel tubes, whose length varied from 55 - 90 cm. The thin wall and larger diameter tubes reduced compaction during coring. The tube was driven into the sediment by gentle twisting followed by tapping the tube using a wooden hammer until the sediment was within 3 cm of the marsh surface or no more penetration could be made. The depth of the core surface inside and outside the tube was recorded during the core collection to determine sediment compaction. The length of the cores varied between 50 - 84 cm. The longest cores were taken from the low marsh

areas in order to get to the base of ^{137}Cs record.

9.3.2 Sample preparation

The sectioning of the cores was carried out within two months of their collection for cores collected in September 1995 but within two weeks for the cores collected in September 1996. The cores were extruded from the tubes using a wooden plunger and the length of the cores were measured after extrusion to evaluate compaction during transportation and storage. Prior to sectioning the core was split along its longitudinal axis. X-radiography was carried out on one of the half cores using an HP faxitron cabinet x-ray machine, in order to determine any evidence of bioturbation and mixing in the cores. Both sides were then sectioned into 2 cm intervals and combined and placed into pre-labelled and pre-weighted PVC evaporating dishes. The core sections were then dried in an oven for 48 hours at 60°C to a constant weight (Bricker-Urso *et al.*, 1989). This procedure allowed for the determination of both wet and dry bulk densities of the sediment. The sediment bulk density (g/cm^3) was calculated from the sediment dry weight and the known volume of each sediment section (2 cm section and 10 cm or 15 cm diameter). For the box cores, the samples were also X-radiographed and sectioned at 2 cm interval.

The dried sections were ground and homogenised using a mortar and pestle; then sieved through a 20-mesh (840 μm) screen to achieve a uniform particle size. The organic content by loss-on-ignition was determined on each ground section by weighing one gram of subsample and combusted it in a muffle furnace at 550°C for 12 hours (Sharma *et al.*, 1987; Williams and Hamilton, 1995). The loss-on-ignition was not determined on the box cores as the ^{137}Cs activity concentration in these cores was very low and erratic; thus it will not help in the interpretation of ^{137}Cs results.

9.3.3 ^{137}Cs Analysis

A sub-sample of 80 g in weight was obtained from the homogenised sample and placed in a 65 x 55 mm diameter plastic counting pot with a tight fitting lid. A constant weight was used so that the same counting geometry was maintained for all the samples. Depending on the proportion of coarser fraction (mainly sand) present in each section, the sample thickness in the counting pots varied between 28- 30 mm, being thicker with a higher silt fraction..

The ^{137}Cs activity concentrations were determined by counting the samples on an EG&G Ortec hyperpure germanium (HPGe) detector (Model No. GMX-20195-P). The detector was interfaced to an EG&G Ortec 918 MCB as part of an integrated gamma-spectroscopy system. Data were acquired and analysed using EG&G Maestro II software. The counting time varied between 4 to 12 hours per sample. A longer counting time was used for sandy samples, in order to obtain better counting statistics. Typical counting errors (based on counting statistics) varied between 5-30% for all sediment sections. Counting errors for samples around 1963 and 1986 peaks were less than 10% and 15% respectively. Longer counting times would have yielded better counting error statistics but would not alter the values of peak concentration and its position within the core. ^{137}Cs activity concentrations were reported as Becquerel per kilogram (Bq/kg) of dry sediment.

The HPGe detector was calibrated for respective geometry and samples matrix using a liquid, mixed radionuclides standard (NPL R08-3, supplied by National Physical Laboratory) containing 12 gamma emitting radionuclides. Solid geometry counting efficiencies were determined for various sample thicknesses by mixing a volume of the mixed radionuclide standard with various depths of table salt in the counting pots. This standard was also counted in various depths of kaolin to investigate the effects of different densities on the calculated efficiencies. No significant difference was detected between the efficiencies calculated in the table salt and the kaolin (see Bourne, 1991; and Mudge *et al.*, 1994).

9.4 Results

9.4.1 Core description

Some colour variation was observed between cores collected from different areas of the marsh where the sediment varied from light to dark grey. The colours reflected the proportion of sand/mud as well as the amount of organic material present in each core. Near the surface, the sediment was of lighter colour and loosely-consolidated but became darker and increasingly compacted with depth. Dead rhizomes were found in most cores and normally extended the whole length of the cores. The dead rhizomes left empty holes of a few millimetres diameter, and in some cores these holes were filled with sandy, lighter colour material. In cores a1 and a2 live roots and rhizomes were found in the upper 15 cm of the cores.

The X-radiograph taken for each core showed that for sandy cores, lamination of deposited material was well preserved, with no or very little bioturbation affecting the cores. In silty cores, no lamination was observed; the X-radiographs showed a lot of small worm-like holes in the core. Due to the poor quality of the X-radiograph pictures, it was difficult to ascertain whether this structure was caused by burrowing animals or were the hollows left by decayed plant rhizomes.

9.4.2 Sediment properties

The variations of organic and water content in the sediment cores collected in September 1995 and September 1996 are shown in Figures 9.2 and 9.3 respectively. The organic content as measured by weight loss-on-ignition varied between 4-14%. Except for cores a1 and a2 which showed a decreasing organic content with depth, other cores showed no particular trend but varied randomly with depth. For cores a1 and a2, live plant roots and rhizomes increased the organic content at the surface layers. Organic content was generally less than 10% in the sandy cores (cores a5-a8) but in other cores which were muddy, the

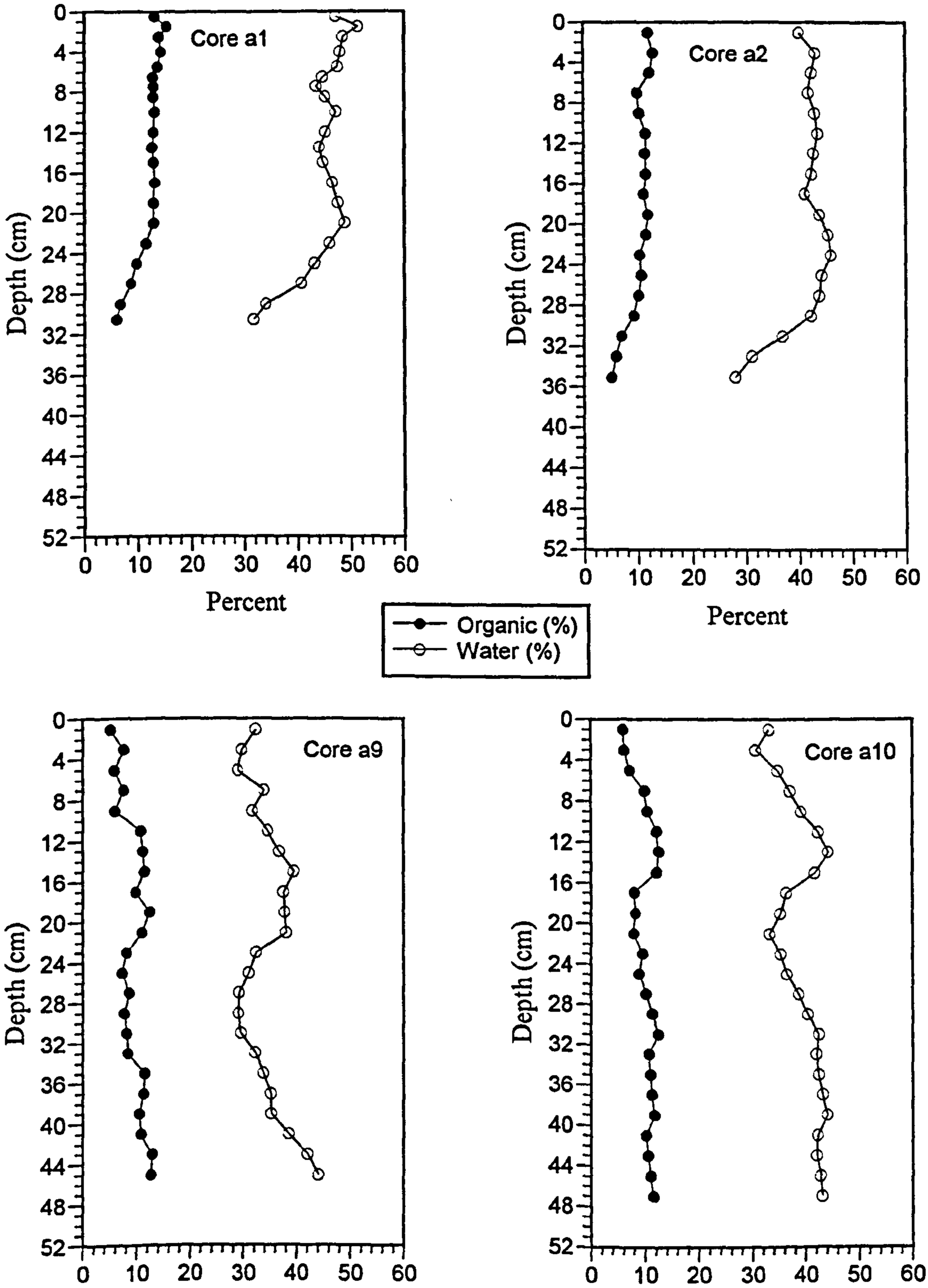

Figure 9.2 Organic and water content profiles in sediment cores collected in September 1995.

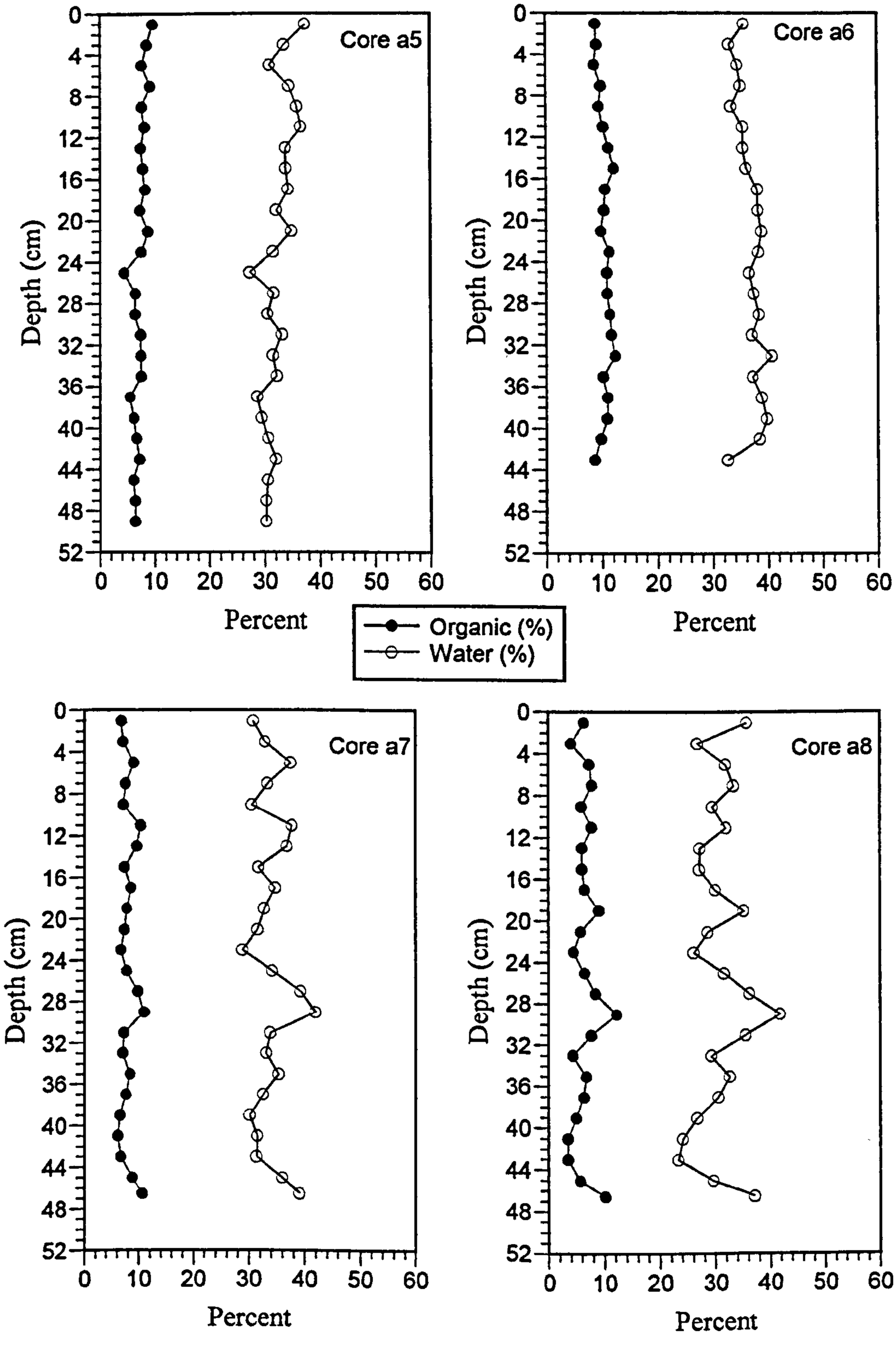

Figure 9.2 (continued)

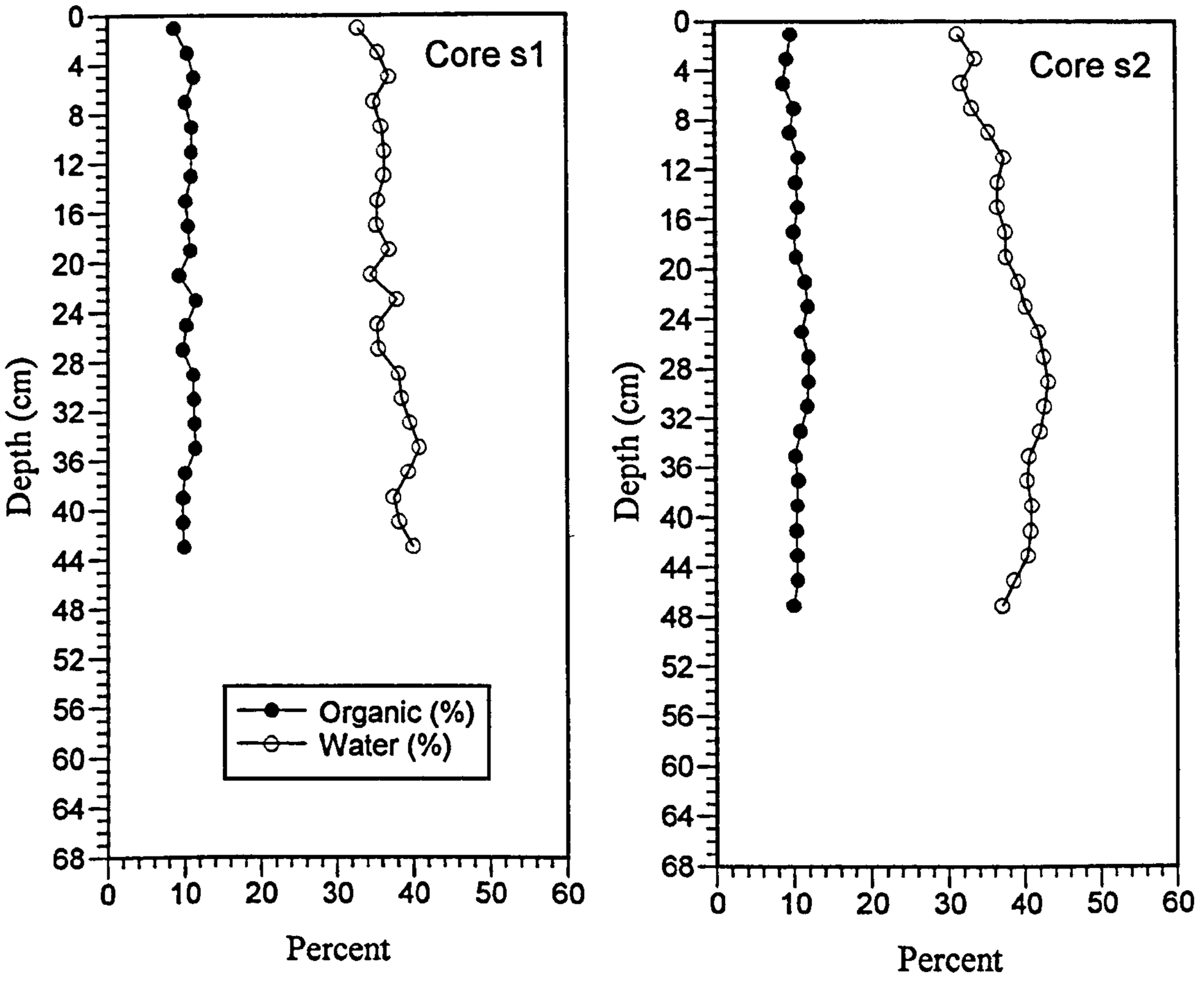

Figure 9.3 Organic and water content profiles in sediment cores collected in September 1996.

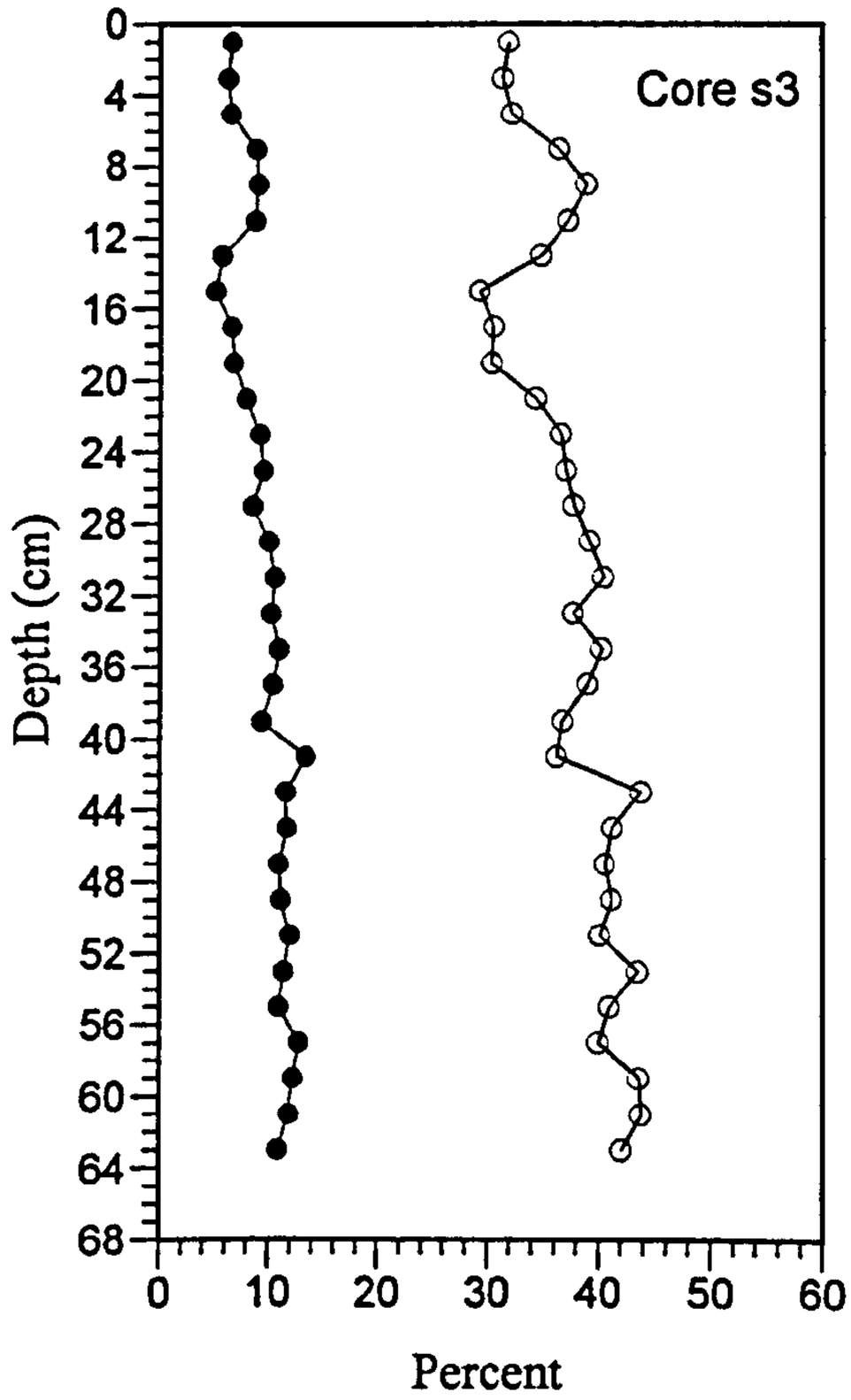

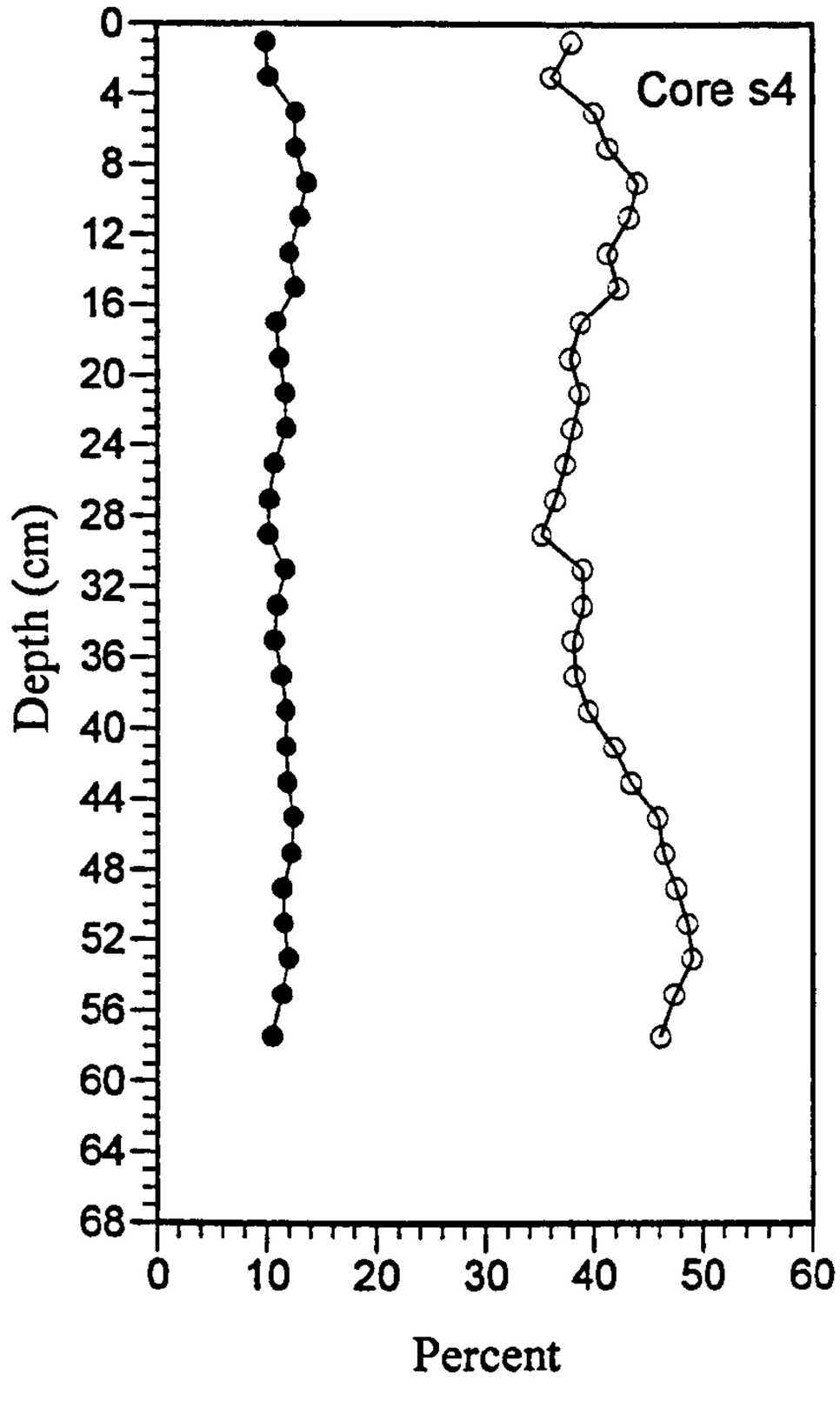

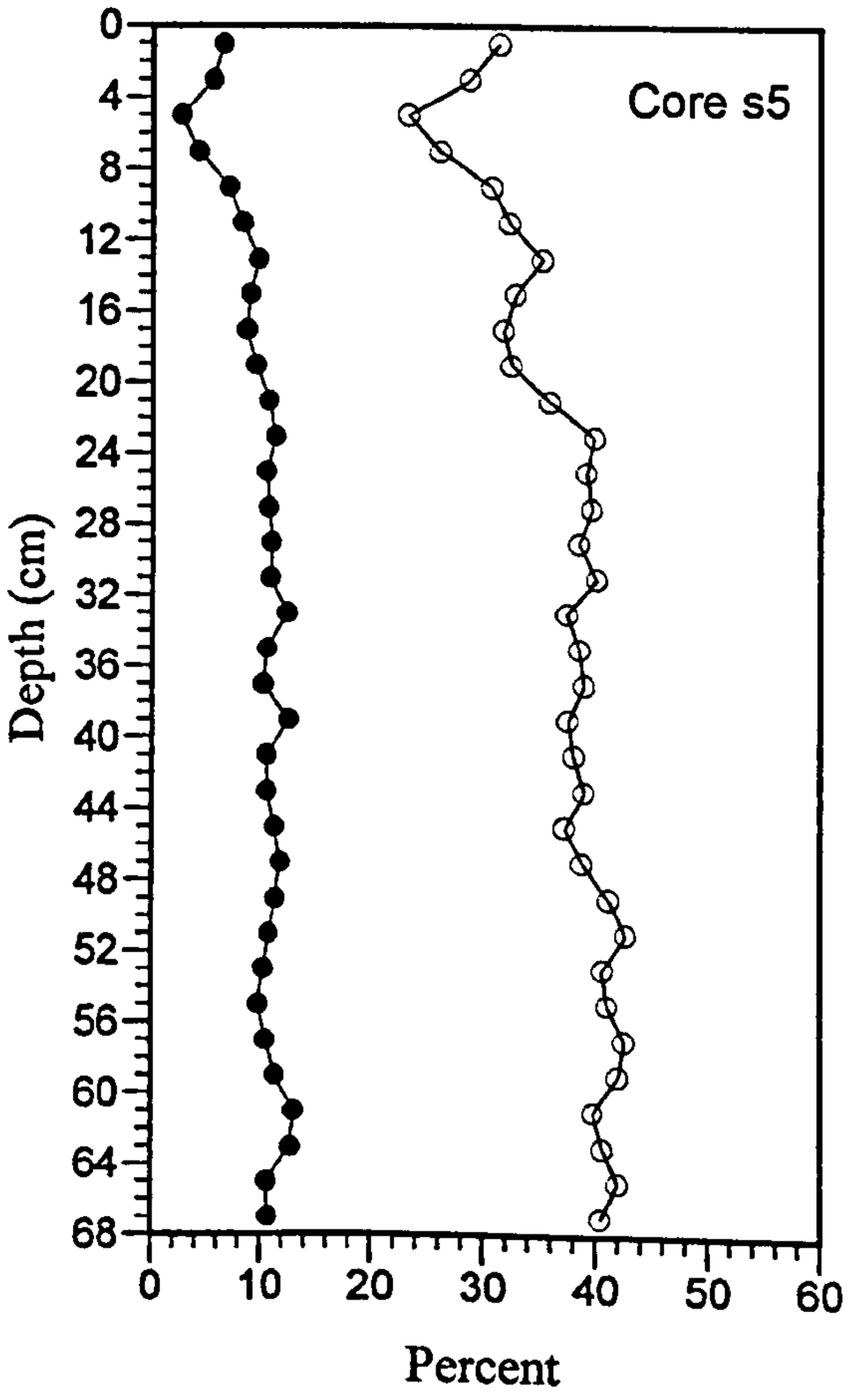

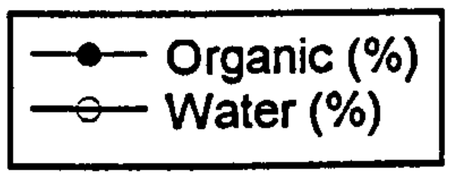

Figure 9.3 (continued).

organic matter constituted between 10-14% of the core material. This general relationship with core material is also reflected in the water content of the cores. Sandy cores contained 25-40% water; in muddy cores it varied between 35-50%. There was a general increase in water content with an increase in organic content.

The densities of the core sediment varied between 0.8 - 1.3 g/cm^3 (Figure 9.4 and 9.5). An increase in core density was associated with a decline in organic and water content of the cores; therefore sandy cores had a higher density than the muddy cores. This reflected the change in the nature of material in the cores and the change of the depositional environment.

9.4.3 Sediment compaction

Compaction during core recovery varied between 0 - 14 %, being generally greater in the longer cores. Only 3 of the 16 cores recovered had compaction greater than 10%, this is not unreasonable owing to the unconsolidated nature of the salt marsh environment. The transportation and storage resulted in another 2-5% compaction for the core collected in September 1995, but no further compaction was observed in the five cores collected in September 1996 prior to sectioning of the cores.

In the calculation of sediment accumulation rates, it was assumed that compaction was uniform throughout the sediment column. The sediment profiles were dated based on the 1963 and 1986 Chernobyl peaks. Average vertical accretion rates were obtained for 1963-1995/6, 1963-1986 and 1986-1995/6 periods. The amount of compaction was added into the total centimetres above the 1963 and 1986 depths. For example if the depth to the 1963 peak was 30 cm and the compaction was 10%, a value of 33 cm was used to calculate the accumulation rates.

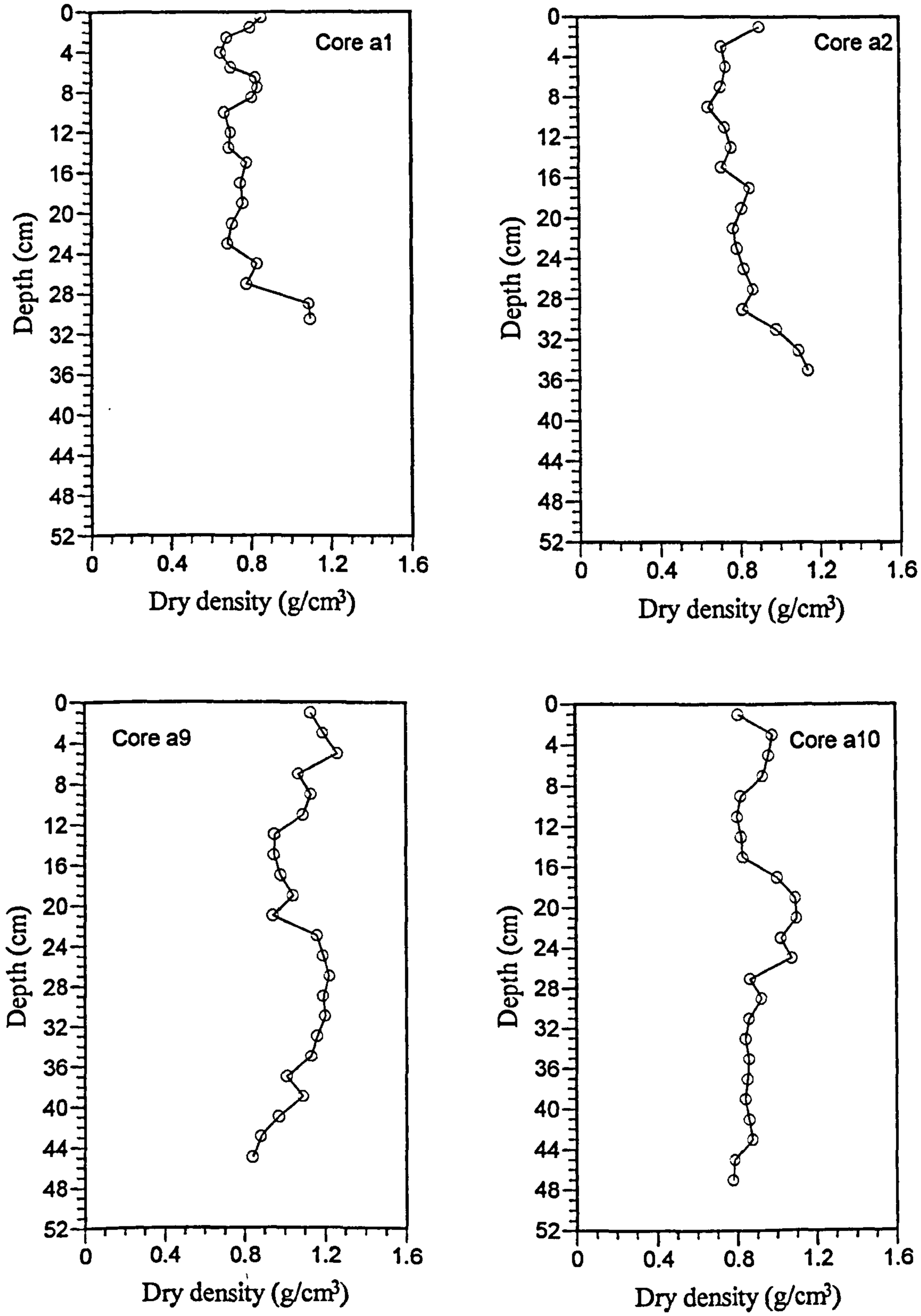

Figure 9.4 Dry bulk density profiles of sediment cores collected in September 1995.

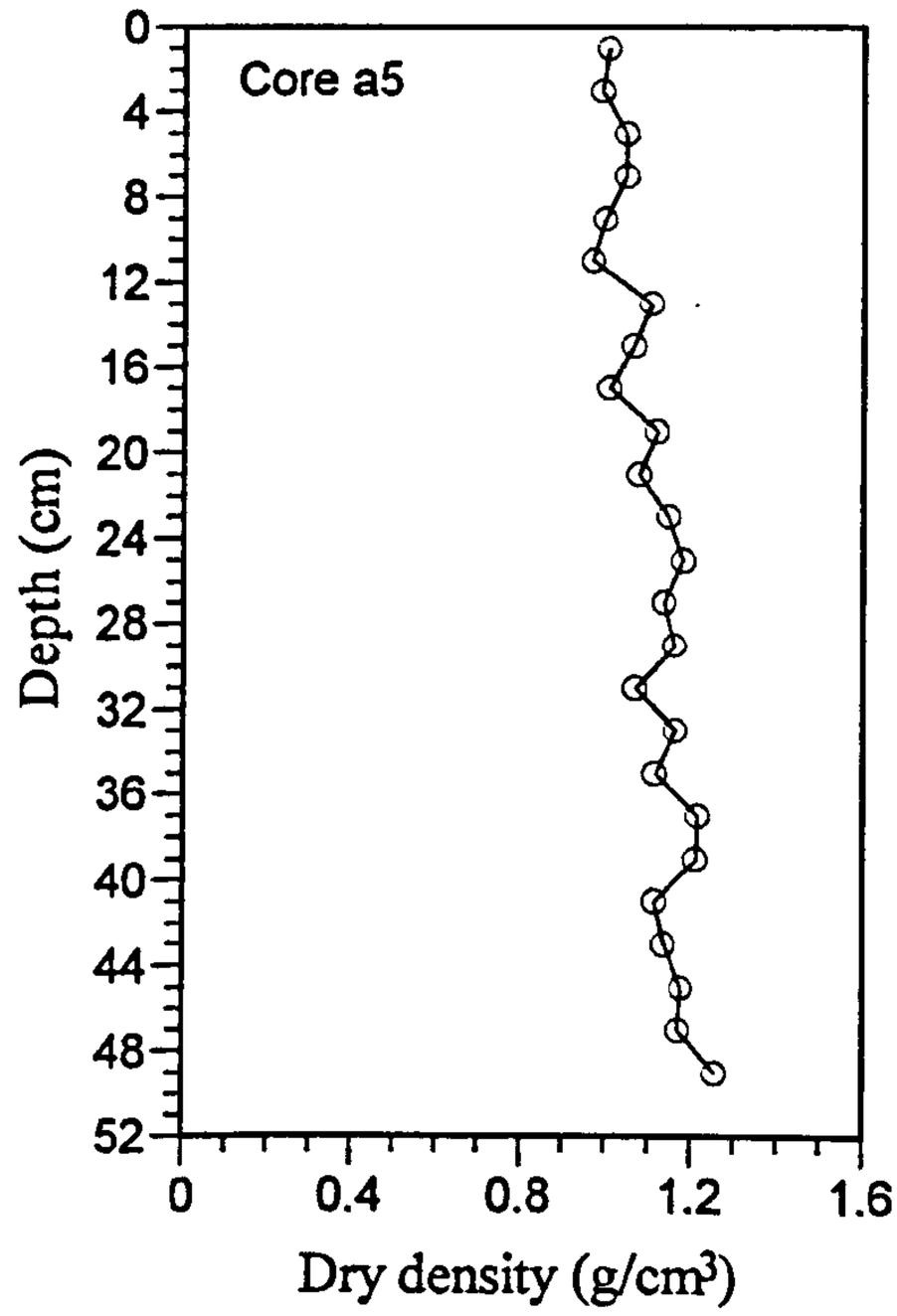

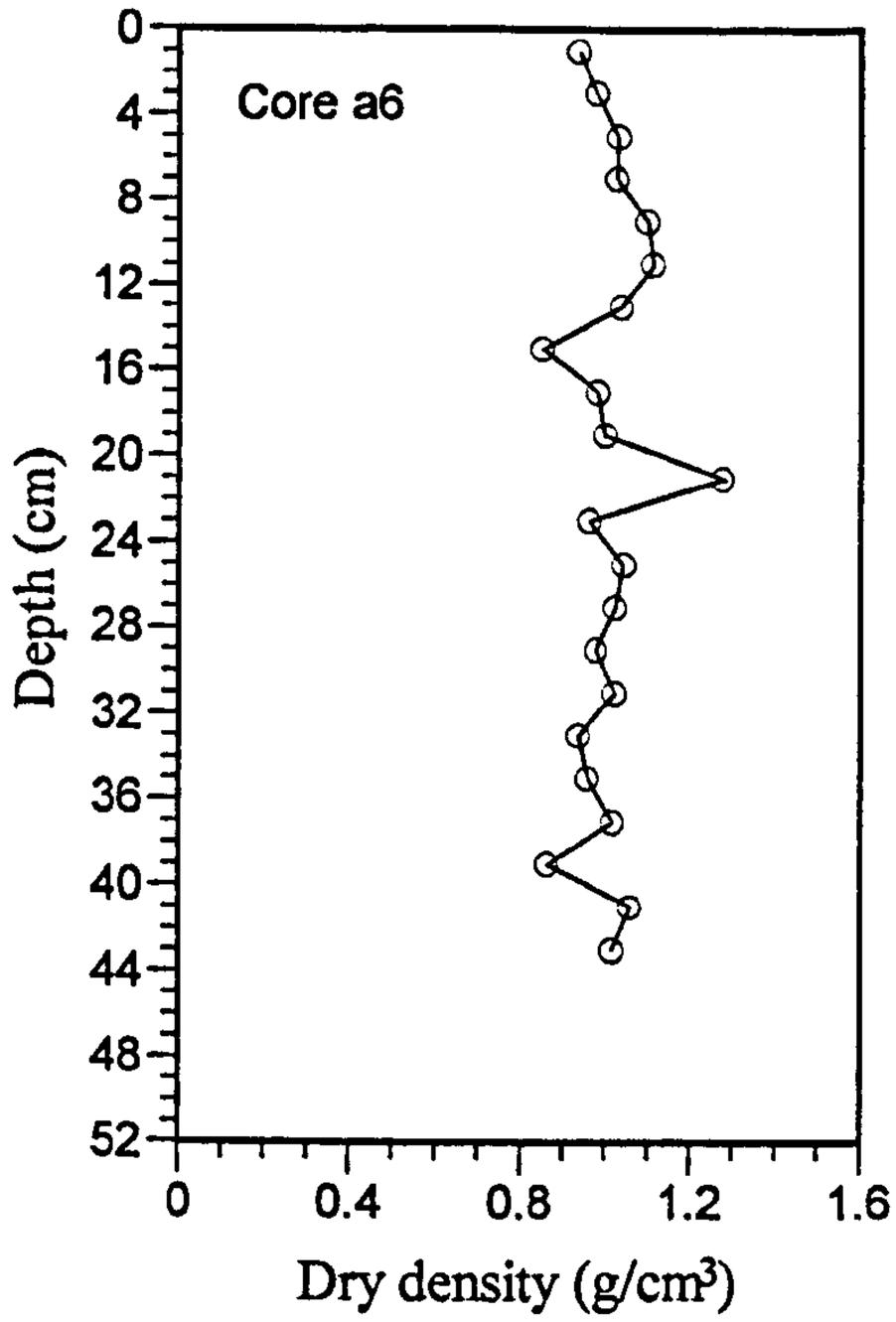

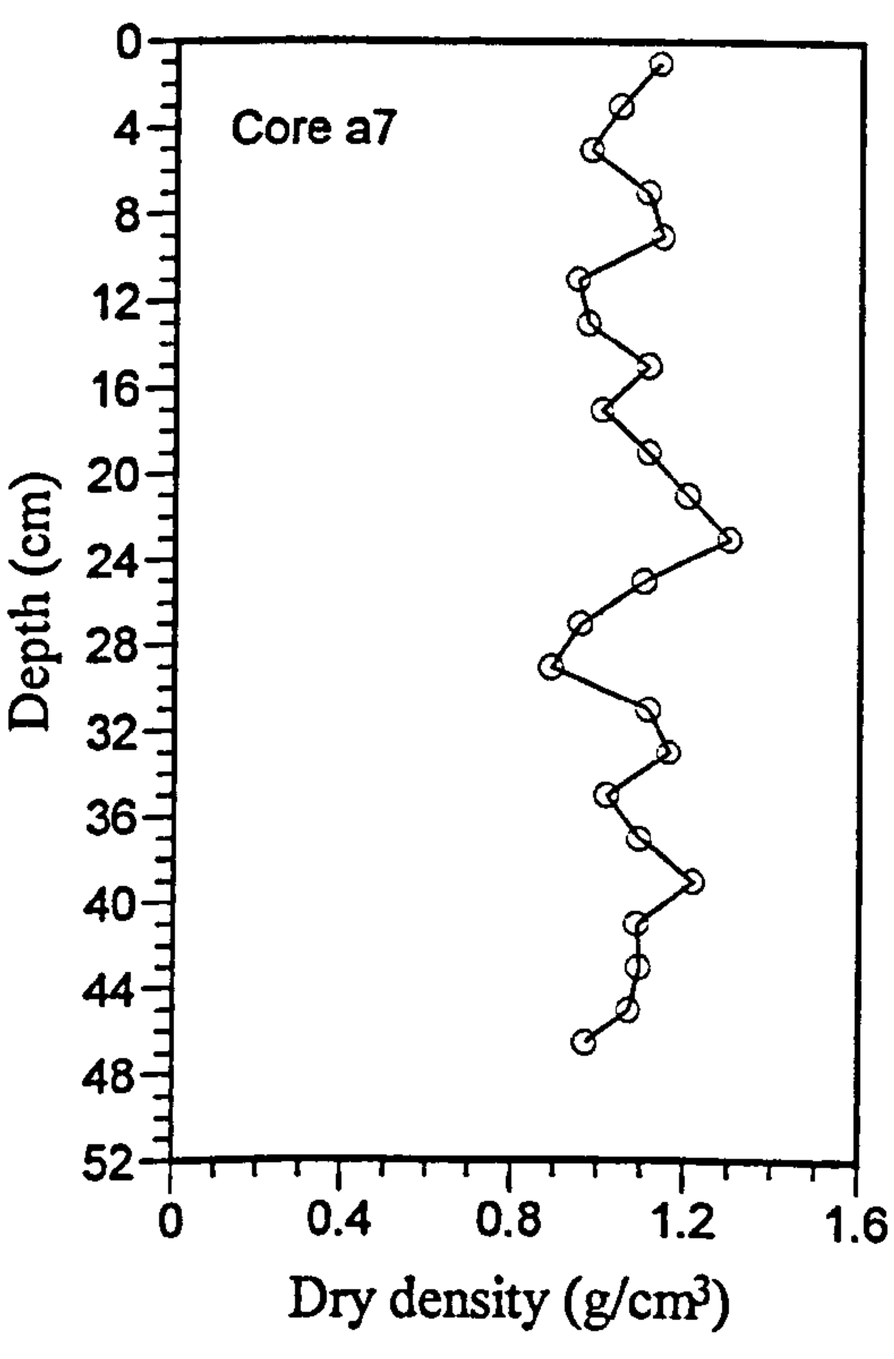

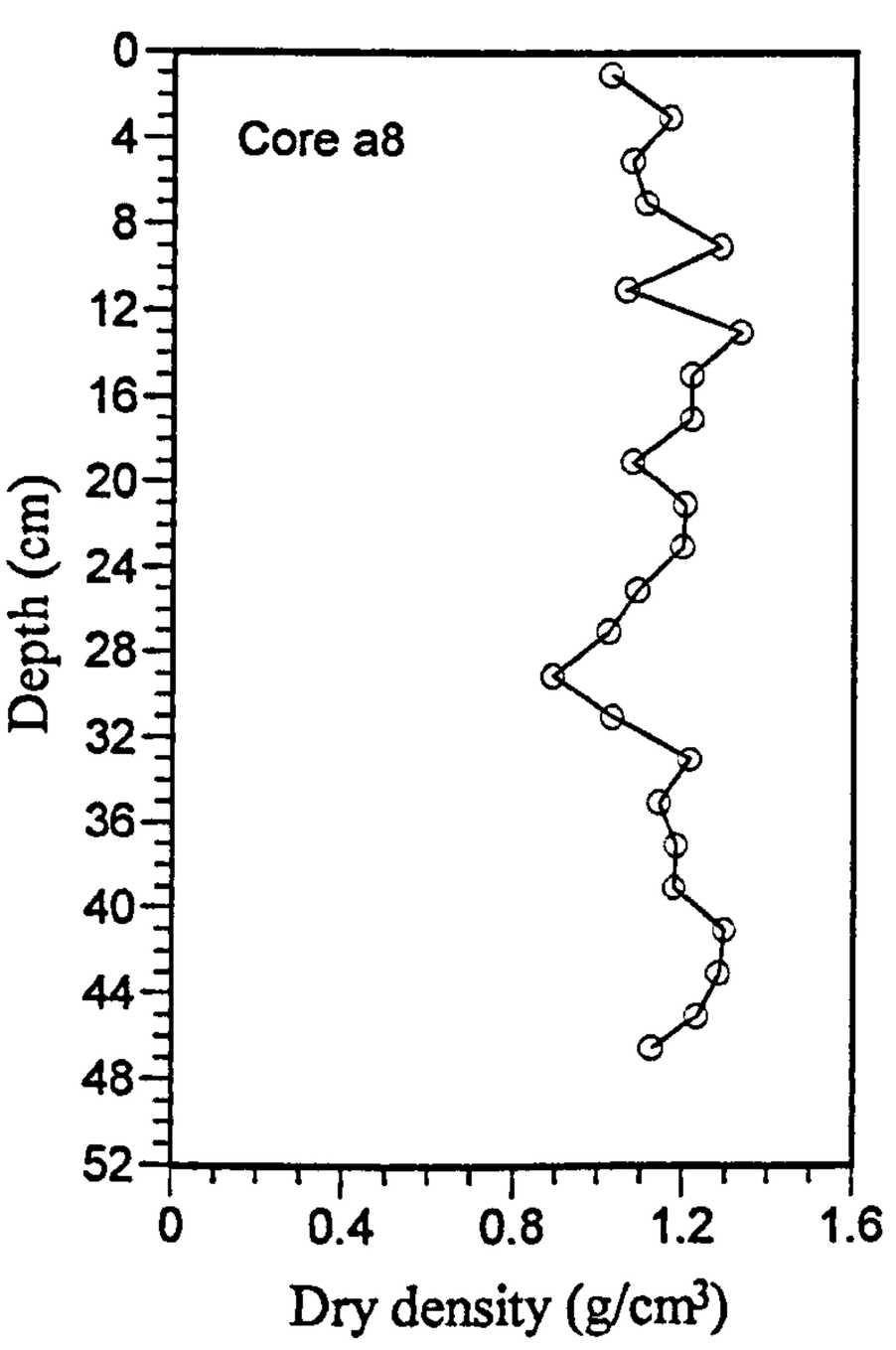

Figure 9.4 (continued)

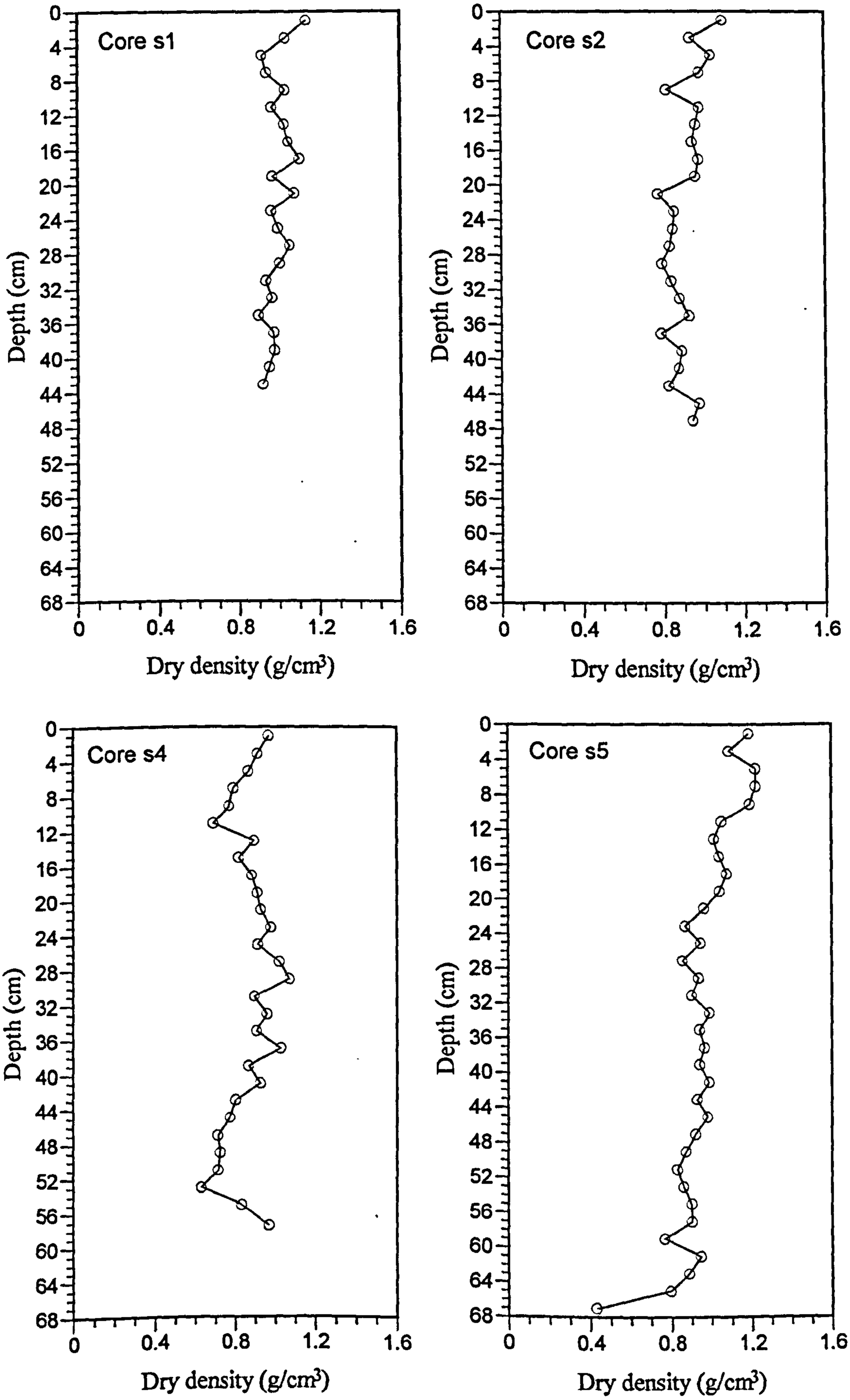

Figure 9.5 Dry bulk density profiles of sediment cores collected in September 1996.

9.4.4 ^{137}Cs profiles and sedimentation rates

The results of ^{137}Cs analysis for the cores collected in September 1995 are presented in Figure 9.6. The ^{137}Cs profiles show that there are some problems in obtaining suitable cores for dating purposes. Only 4 of the 10 cores collected showed the presence of ^{137}Cs peaks (Cores a1, a2, a9 and a10) which can be related to the Chernobyl accident (1986) and the nuclear weapon testing (1963) peaks. In core a9 there was no obvious peak of 1963, but the bottom reading was interpreted as the fallout peak based on the ^{137}Cs activity which was similar to that measured in Core a10 where the 1963 ^{137}Cs peak was present. Where both peaks were present in the cores, the 1963 fallout peaks were generally sharper than the 1986 Chernobyl peaks; however the ^{137}Cs activity in the 1986 peak was less i.e. approximately half of the ^{137}Cs activity in the 1963 peak.

Cores a5-a8 showed no ^{137}Cs peaks that can be associated with either Chernobyl or the fallout from nuclear weapon testings. Core a8 however shows a sharp peak with quite high ^{137}Cs activity (28.7 Bq/kg) at a depth of 19 cm but this high ^{137}Cs activity was associated with the presence of higher organic and muddy section of the core (see Figure 9.2). Cores a3 and a4 (not shown) contained very low ^{137}Cs activity i.e. less than 10 Bq/kg in all sections and ^{137}Cs was only found in the upper 14 cm section of the cores.

The base of the ^{137}Cs record which corresponds to 1954 could not be determined from all the cores collected in September 1995. The obvious reason for this shortcoming was that the sampling was insufficiently deep to reach the base of the ^{137}Cs fallout record.

The profiles of ^{137}Cs activity in sediment cores collected in September 1996 are shown in Figure 9.7. Sharp ^{137}Cs peaks which correspond to 1963 were found in cores s1, s2, s4 and s5 but not in core s3. In cores s1, s2, and s5 much broader ^{137}Cs peaks of 1986 were also present but ^{137}Cs activities were less i.e. about half of the 1963 peak. The 1986 ^{137}Cs peak was not found in core s4. In cores s1, s2, s4 and s5, ^{137}Cs was present down to the base of the cores with generally declining activity below the 1963 peak. In core s5, the tail of ^{137}Cs record continued for at least 38 cm below the 1963 marker but the

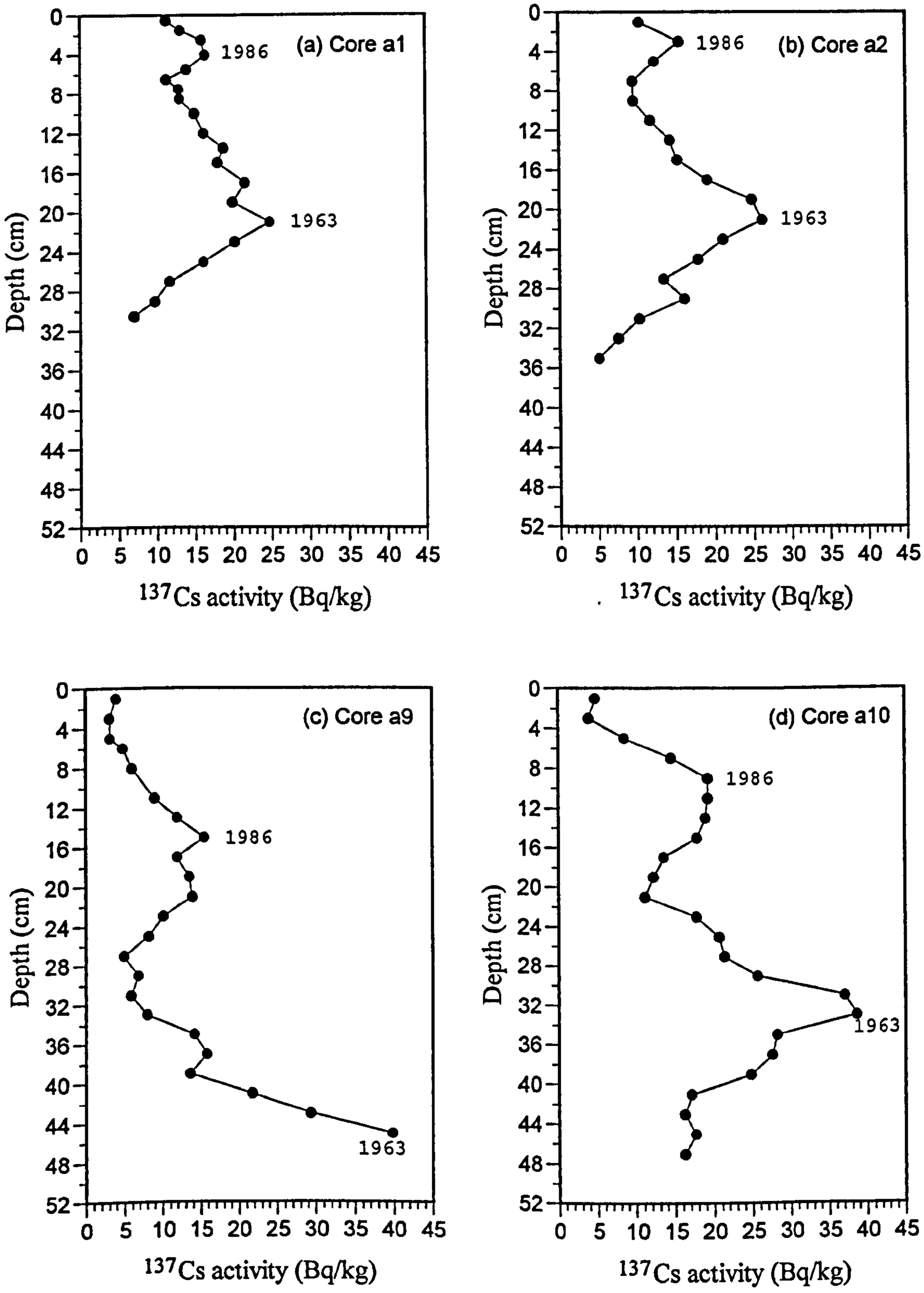

Figure 9.6 Profiles of ^{137}Cs activity for sediment cores collected in September 1995.

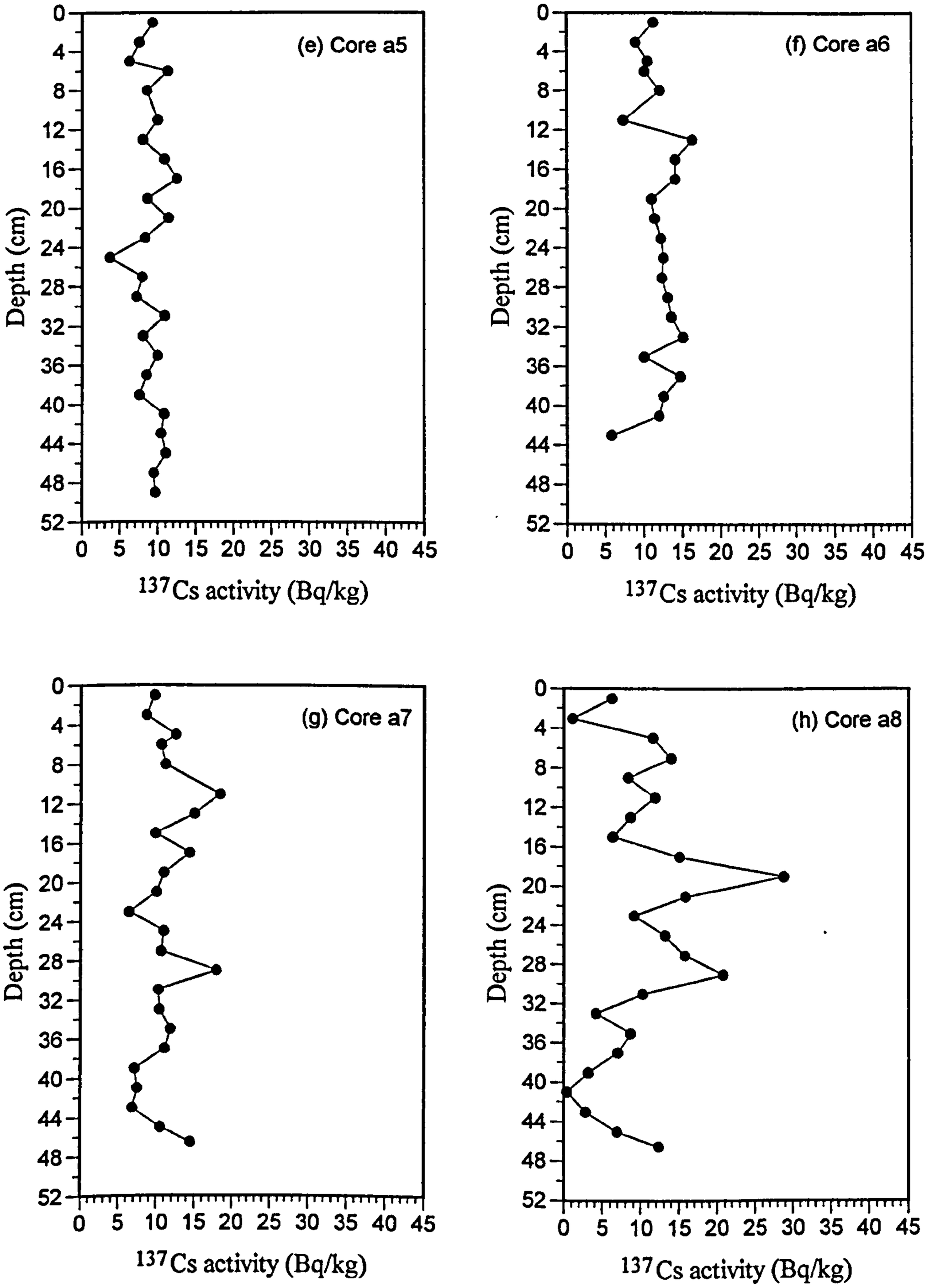

Figure 9.6 (continued)

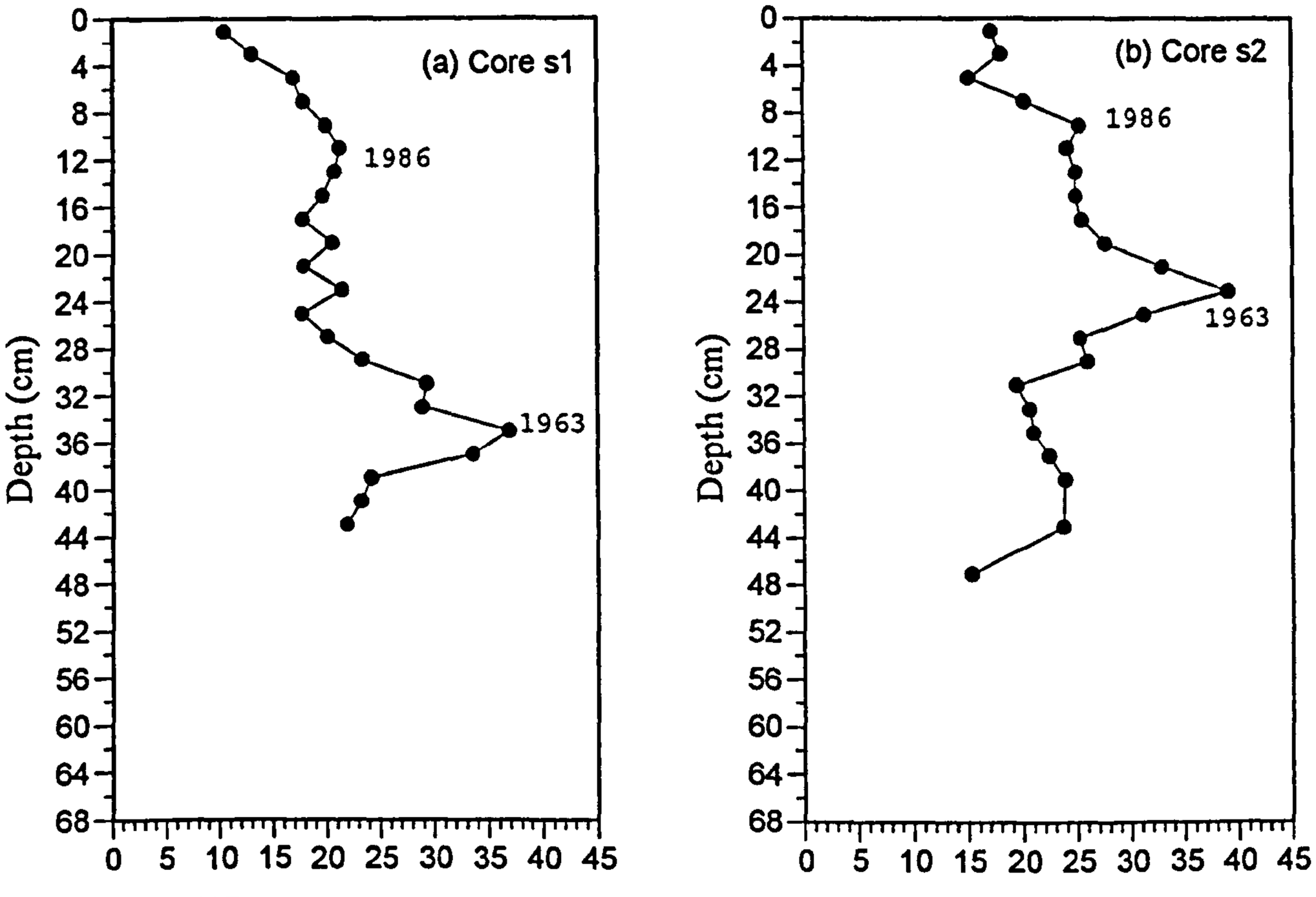

Figure 9.7 Profiles of ^{137}Cs activity for sediment cores collected in September 1996.

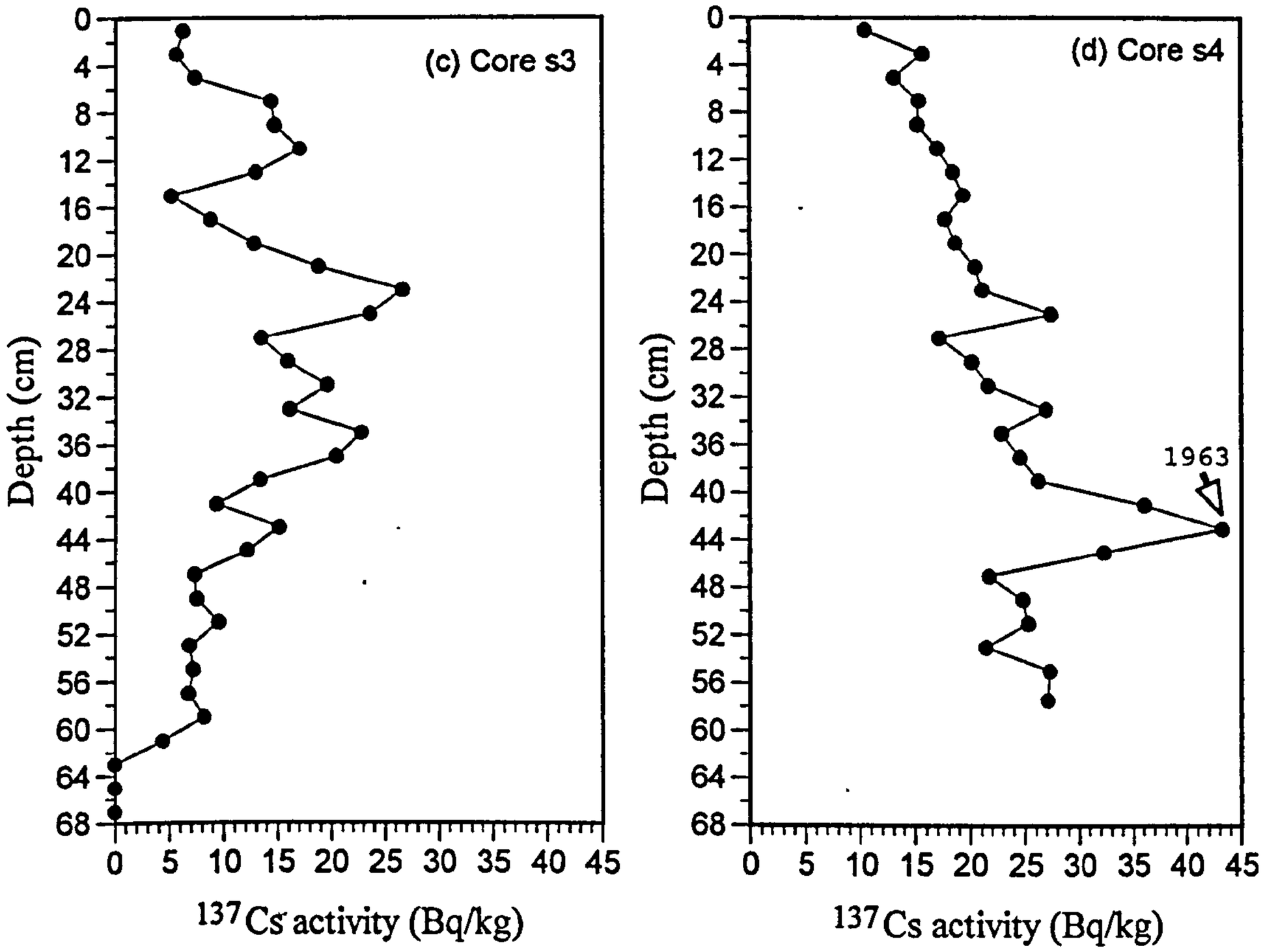

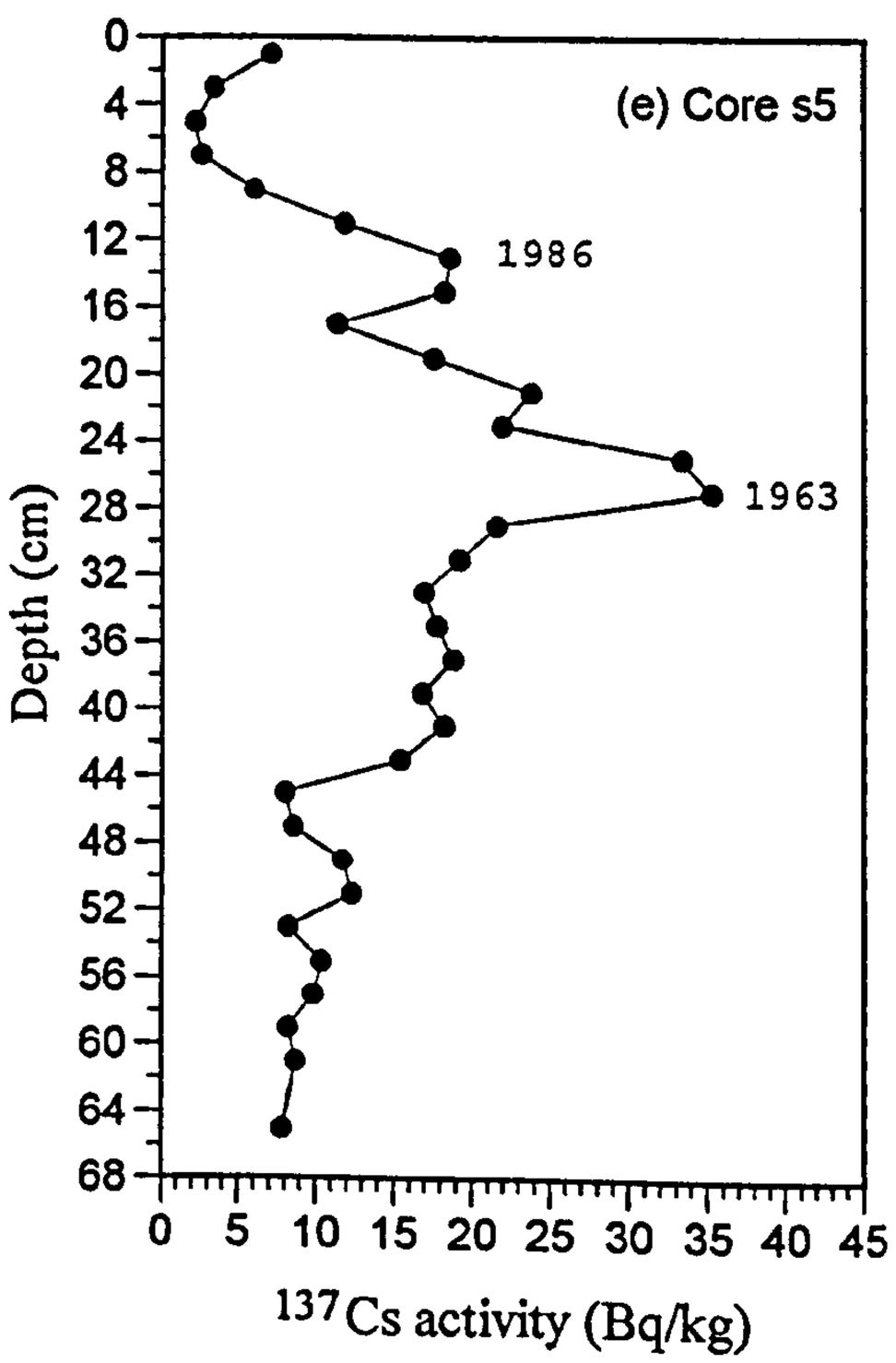

Figure 9.7 (continued).

identification of the base of the fallout record (1954 marker) from this core was difficult as there was no abrupt change of ^{137}Cs activity to mark this onset.

Core s3, which was the longest core collected from the salt marsh area, showed several peak activities, but there were no strong peaks that can be related to the maximum fallout or to the Chernobyl peaks (Figure 9.7c). The ^{137}Cs profile shows a broad maximum between depth 21 - 37 cm, but the identification of the 1963 peak within this maximum was difficult as there was no prominent peak. ^{137}Cs activity declined below 40 cm depth and continued to exist until 61 cm depth i.e. the base of ^{137}Cs record. It is uncertain however if this base represents the 1954 marker or if it is caused by ^{137}Cs migration through plant roots and rhizomes.

To compare the maximum ^{137}Cs of the 1986 and 1963 peaks, the original ^{137}Cs activity of the section containing each peak was calculated based on decay since the time of deposition. The original maximum activity of the 1986 peak (after decay correction) was between 23 - 39 % of the original maximum activity of the 1963 peak (Table 9.1).

Table 9.1 Relative maximum activities of ^{137}Cs peaks (Bq/kg) from 1963 and 1986. Maximum activities were corrected for decay to original activities.

Core	1986	1963	1986:1963
a1	20.0	51.6	0.39
a2	19.1	54.6	0.35
a9	19.0	83.0	0.23
a10	23.7	80.4	0.29
s1	26.9	78.6	0.34
s2	31.8	83.3	0.38
s4	-	92.2	-
s5	23.4	75.3	0.31

The ^{137}Cs profile of the box cores is presented in Figure 9.8. The ^{137}Cs activity was relatively very low throughout the sediment column. Again the ^{137}Cs activity shows no prominent peaks that can be correlated to the fallout but the peak at 25 cm depth was interpreted as the Chernobyl peak based on the ^{137}Cs activity present in the core section. Furthermore the sediment profile showed it was relatively muddy and homogenous from the surface down to a depth of 45 cm ; thus any anomaly in the ^{137}Cs can be regarded as related to a particular nuclear event. Between 45 - 145 cm, the sediment was sandy with some interbedded mud layers. The ^{137}Cs activity in this section of the core was quite variable and related to the composition of the sediment layers. Apart from two ^{137}Cs peaks at 49 cm (27.1 Bq/kg) and at 57 cm (25.4 Bq/kg) which correspond to mud layers, the ^{137}Cs activities were very low and varied between 6 and 14 Bq/kg. Below 100 cm depth, there was a steady decrease in ^{137}Cs activity and no ^{137}Cs was found below a depth of 143 cm, which may be regarded as the base of the ^{137}Cs record.

Recognition of the 1963 fallout peak and the 1986 Chernobyl nuclear accident peak of the ^{137}Cs activity profiles in the sediment column allowed the mean vertical accretion rates between these periods and the sampling period to be calculated (Table 9.2). Mean sedimentation rates are quite variable both between marsh sites and at the same sites over time. The sedimentation rates for the period of 1963 - 1995/6 vary between 0.66 - 1.48 cm/year with a mean value of 1.01 cm/year. The highest sedimentation rate is shown by core a9 (1.71 cm/yr) and the lowest rate is shown by core a2 (0.35 cm/yr) which both occur during the post 1986 period. Except for cores a1 and a2, which show a decline in sedimentation rate, other cores show an increase in sedimentation rate since 1986. There is an overall increase in the mean accretion for 1986-1995/6 (1.04 cm/year) compared to 1963-1986 (0.89 cm/year). The sedimentation rates for the box cores are not included in Table 9.2 as they showed much higher rates than the other cores. The sedimentation rates obtained for the box core are 2.78 cm/year based on the 1986 marker horizon, and 3.49 cm/year if the base of the ^{137}Cs record (at 143 cm depth) is regarded as the 1954 marker horizon.

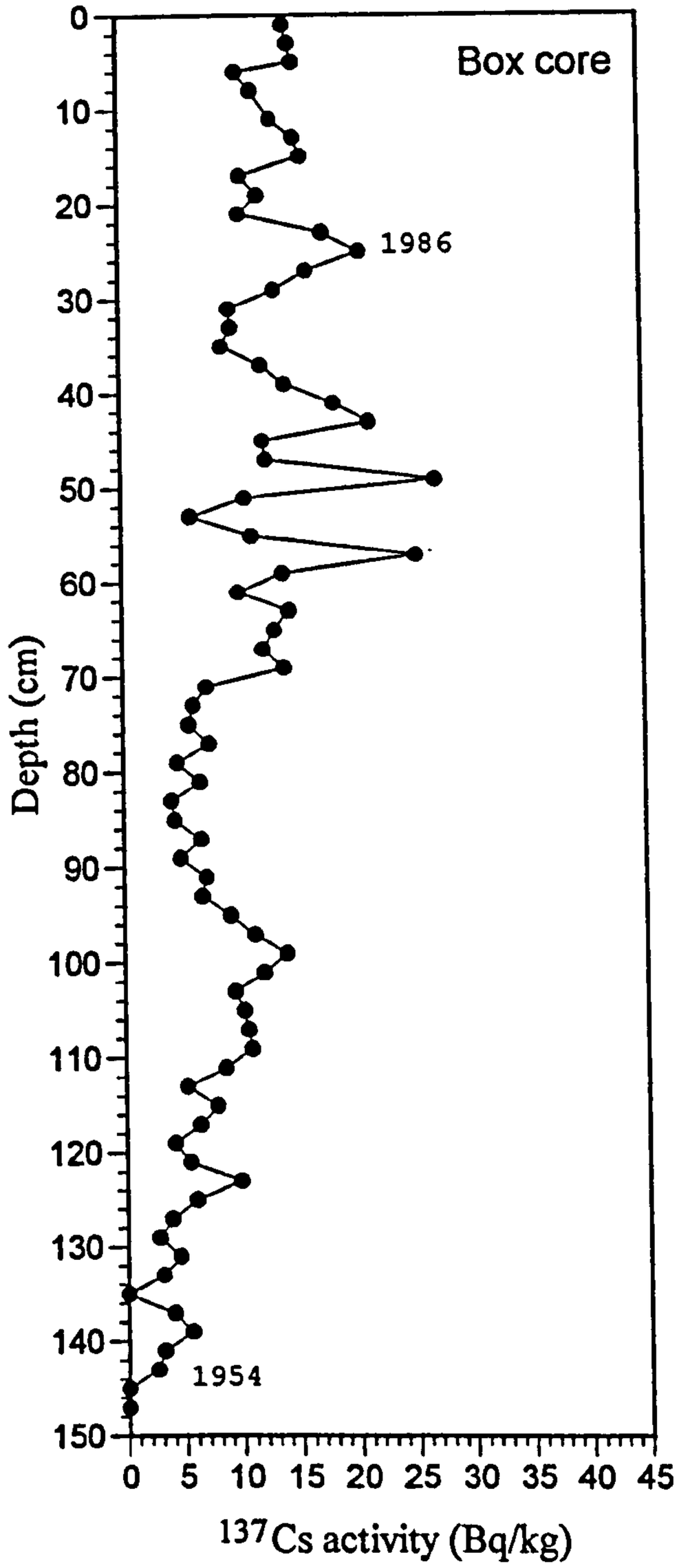

Figure 9.8 Profile of ^{137}Cs activity for box cores.

Table 9.2 Vertical accretion rates determined using ^{137}Cs peaks for sediment cores collected in September 1995 and September 1996. Averages are presented as mean ± 1 standard deviation.

Core	Accretion rate (cm/year)			
	1963-1986	1986-1995/6	Change in accretion rate	1963-1995/6
a1	0.74	0.44	- 40.5 %	0.66
a2	0.82	0.35	- 57.3%	0.69
a9	1.34	1.71	27.6%	1.44
a10	0.99	1.27	28.3%	1.07
s1	1.09	1.15	5.5%	1.11
s2	0.61	0.90	47.5%	0.70
s4	-	-	-	1.48
s5	0.67	1.43	113.4%	0.90
Average	0.89 ± 0.26	1.04 ± 0.50	17.8%	1.01 ± 0.33

9.5 Discussion

The marsh in the study site shows a very high mineral content and a very low organic content. This marsh resembles the salt marshes of other parts of the British Isles (eg. Stoddart *et al*,. 1989; Williams and Hamilton, 1995; and Callaway *et al.* 1996), and is of the minerogenic type (Allen and Pye, 1992). The immediate source of sediment supply for the marsh is from the tidal waters which provide the mineral matter and from the marsh plants themselves which supply the organic matter. These marshes rely on net accretion of allochthonous sediment inputs for maintenance and growth; thus, they are vulnerable to changes in sediment supply and to other changes which cause a shift in the balance of incoming and outgoing sediment fluxes. The effect of mineral matter is to reduce or dilute the ^{137}Cs concentration in the sample because it smears out the fallout signal over a

greater thickness. The coarse mineral sediments have the greatest diluting effect. This may reach a point where the ^{137}Cs concentration in the sediment column is so low that no prominent peaks exist in the concentration profile.

The results of this study show that the 1986 Chernobyl peak found in the sediment cores is less pronounced than the 1963 peak. Its activity concentration is only between 30 - 50% of the 1963 concentration. This is in contrast to the findings in other studies where both peaks are present in the sediment cores, and where the Chernobyl ^{137}Cs concentration far exceeds and produces sharper peaks than that of the fallout peaks from nuclear weapon testings (eg. Ehlers *et al.*, 1993; Callaway *et al.*, 1996). The reported studies were carried out in north western Europe, closer to the place where the Chernobyl accident took place. The smaller concentrations found in this study are partly due to the increasing distance from the caesium source and partly to the possible migration of the radionuclide within the cores. Furthermore the fallout from the Chernobyl accident was erratic and geographically unevenly distributed throughout Northern Europe (Callaway *et al.*, 1996), compared to the global distribution and fallout from the nuclear weapon testing. Ehler *et al.* (1993) also show that ^{134}Cs occurred in the same sediment units where ^{137}Cs was found; ^{134}Cs characterises young fallout because of its short half life (2.06 years). There was no ^{134}Cs present in sediment cores from the study area as the caesium activity was much lower than found in the northern Europe, and the ^{134}Cs activity would have decayed out after about 5 half-lives since the Chernobyl accident.

The original ^{137}Cs activity of the Chernobyl peaks from the study area may be compared to that found in other salt marsh areas (Table 9.3). The ^{137}Cs activity found in the study area is less than those from the continent Europe and from Stiffkey marsh in east coast of England. The table shows a lower ^{137}Cs activity to the west as would be expected based on measurement of fallout immediately after the accident (Cambray *et al.*, 1987).

Beside the contributions from nuclear fallout and the Chernobyl nuclear accident, the ^{137}Cs deposited in Taf estuary may also come from other sources. One of the possible sources of ^{137}Cs is from the BNFL (British Nuclear Fuels PLC) reprocessing plants of used

nuclear fuels at Sellafield on the Cumbrian Coast, NW England. The discharge of ^{137}Cs into coastal waters reached its peak levels in 1970s, with a maximum in 1975 (BNFL, 1995). The discharge has declined since then and from 1986 onwards, the ^{137}Cs discharge from this plant has remained very low i.e. less than 1% from its 1975 level. Therefore the post 1986 contribution from these plants to the ^{137}Cs activity in the study area would be negligible. In the sediment cores where peak ^{137}Cs activities of 1963 and 1986 were present there was no intermediate peak present that could be interpreted as the contribution from the Sellafield discharge in the mid 1970s. The caesium discharged from BNFL is transported through the Irish Sea in a northerly direction, so that it leaves the area via the

Table 9.3 The maximum ^{137}Cs activity from the Chernobyl accident in salt marsh cores obtained from different location of Europe.

Location	Marsh site	^{137}Cs activity (Bq/kg)	Reference
Wales Taf estuary marsh	low low low low low high low	20 19 19 24 27 32 23	This study
England Stiffkey marsh	high	65	Callaway *et al.*, (1996)
Nertherlands St. Annaland marsh	low high	64 36	Callaway *et al.*, (1996)
Germany Sylt Island marsh	low low low	88 67 54	Ehlers *et al.* (1993)
Poland Order river	low high	204 201	Callaway *et al.*, (1996)
Poland Vistula river	low high	572 273	Callaway *et al.*, (1996)

Northern Channel and then moves northwards along the west coast of Scotland and enters the North Sea from the north-west (M.A.F.F., 1981). This means that the ^{137}Cs discharged from the Sellafield in the mid 1970s and carried with this water circulation would never reach into the Taf estuary either from the from the south or from the north, therefore no 1970s peaks were observed even in a well preserved core from the study area.

Another possible source of ^{137}Cs, closer to the study area, is from a French Nuclear Power plant at Cap de la Hague which discharges into the English Channel near Cherbourg. But effluent from Cherbourg too is transported northwards, first into southern North Sea then to central North Sea towards the entrance to the Baltic Sea (M.A.F.F., 1981).

There are also sources of ^{137}Cs from the Berkeley and Oldbury power stations which discharge radioactive waste into the Bristol Channel. A mean ^{137}Cs activity concentration of 37 Bq/kg has been reported in sediment samples obtained 1 km south of Oldbury (Camplin, 1995). This concentration represents the combined effect of discharges from the stations, other nuclear establishments discharging into the channel, fallout and possibly a small Sellafield derived component (Camplin, 1995). It has not been possible to apportion various sources due to the very low level detected. Due to its very low concentration, it is unlikely that the radioactive discharge from these power stations would have any effect on the ^{137}Cs activity profiles observed in the Taf estuary.

It is difficult to avoid any compaction during the recovery of the sediment core. This compaction should be determined even if it is relatively small for a better estimate of sedimentation rates. Beside the compaction of core during sampling, a correction for sediment compaction due to consolidation should also be made (Christensen, 1982; Lynch *et al.*, 1989).

In the second core sampling, where a few long cores were obtained (s3 and s5), the ^{137}Cs was found to extend to some distance below the 1963 peak. Therefore the limit of the ^{137}Cs record in the cores could not be used to indicate the 1954 marker horizon for the calculation of sedimentation rates. Some migration of ^{137}Cs has taken place most probably

through holes left by dead rhizomes which were present from near the surface to the base of the cores or through adsorption by the plant roots. The extended tails of ^{137}Cs activity are not unique to the cores taken from the study area. Delaune *et al.*, (1978) found that tails of ^{137}Cs activity from salt marsh cores of Louisiana, Southern U.S.A. extended below the 1954 marker. This marker corresponds to the rooting depth of *Spartina alterniflora*, probably as a result of plant adsorbtion of ^{137}Cs. In Dengie marsh, England which is dominated by *Spartina anglica*, the ^{137}Cs activity extends at least 25 cm below the 1963 marker (Callaway *et al.*, 1996); no 1954 marker was identified from the ^{137}Cs profiles of the Dengie marsh.

The general increase in recent sedimentation rates obtained in this study may be related to the ability of marsh vegetation to filter and entrap suspended sediment from incoming tidal waters. At the lower estuary, where samples a9, a10 and s3-s5 were taken, new plants of *Spartina anglica* are growing on the mud flats which indicates that the area is steadily accreting.

The decline in the sedimentation rates post 1986 as shown by cores a1 and a2 may be linked to the erosion of the marsh surface. Evidence of erosion in this area was observed during sampling. Numerous erosion scarps were present in non-vegetated patches of the marsh. At the transition between the marsh and the mud flat, isolated blocks of marsh sediment with evidence of recent undercutting are a common feature. Some of these isolated blocks still support healthy vegetation. The fact that the erosion occurred above the 1986 marker horizon indicates that it is a recent phenomenon. The salt marsh as a whole is however accreting at a mean rate of 1.01 cm/year as shown in Table 9.3.

The shift of the main channel may also contribute to the different accretion and erosion rates of the marsh land and mud flats; and the composition of the marsh sediment. Before 1974, the main channel ran close to the left bank of the estuary (Jago, 1974). But since 1986 the main channel has remained on the right bank of the estuary (Jago, pers. com.). The main channel has been the main source of the sediment supply (see Chapter 7); therefore sedimentation rates may be expected to increase if the channel runs close to the marsh;

sedimentation will be reduced if the channel shifts away from the marsh. Likewise the marsh sediment will change from sandy to muddy with the shift of the channel away from the marsh.

The average accretion rate of 1.01 cm/year obtained from this study is similar to the accretion rates of other salt marshes of the British Isles. Stoddart *et al.* (1989) reported rates of vertical accretion up to 1.5 cm/year in the low marsh at Scolt Head Island, Norfolk. Pethick (1981) studied the accretion rates of the tidal marshes of the North Norfolk coast, and found net accretion rates of 1.7 cm/yr for the recent sediment (less than 10 years old). In the Dengie marsh, Essex, Reed (1988) estimated the mean vertical accretion to be 1.1 cm/year near the shoreline and 0.65 cm/year along the most inland transects. Callaway *et al.*, (1996) measured accretion rates of 0.46 cm/year for the Dengie marsh and 0.39 cm/year for the Stiffkey marsh, near Norfolk. The Dovey marsh was studied by Richards (1934) and he reported the accretion rates ranges from 0.1 -1.7 cm/year.

The accretion rate of salt marsh sediment is generally keeping pace with the rising in the sea- level. Estimates of global sea-level rise during the past 100 years range from 0.5 to 3.0 mm/yr, with most estimates within the range 1.0 to 2.0 mm/yr (Warrick and Oerlemans, 1990; Tooley, 1992). Sea level across the region is rising at a rate close to the global average, at about 1.5 - 2.0 mm/yr (Evans, 1995). This is very small as compared to the averaged acreation rate for the marsh sediment of 1.01 cm/yr as determined in the present study for the Taf salt marshes. Therefore within this estuary, the accretion rates of the marsh sediment is determined not only by the general sea level rises, but is also determined by other local factors. These factors include the cyclic migration of the estuary channel from left to right banks as already discussed before, where salt marshes located closer to the main channel will have greater accretion rates due the increased sediment supply, while those away from the main channel will have a lower sedimentation rates. Another factor is the net landward transport of the estuarine sand (Chapters 7 and 8), increases the overall level of sand in the estuary. This increase sand level causes the water level to increase higher than the average sea level rise, resulting in a higher sedimentation rates of the salt marshes sediment. The increased rise of salt marsh sedimentation rates may also caused by

reclamation-related changes in tidal regimes (Woodworth *et al.*, 1991).

9.6 Conclusions

The peaks of ^{137}Cs activity from the fallout (1963) and from the Chernobyl accident (1986) provide two useful markers which can be used to study sedimentation processes in the study area. Although the 1986 peak is much smaller and less well defined than the 1963 peak, its presence can be used to study recent changes in sedimentation patterns. The sedimentation rates calculated using these two markers show there has been an overall increase in recent sedimentation rates. Based on the 1963 marker, the salt marsh of the Taf estuary has been accreting at an average rate of 1.01 cm/year.

The identification of the 1954 marker as the base of ^{137}Cs record was found to be difficult. Even in cores where the base of the ^{137}Cs record could be identified, this base does not necessarily represents the 1954 marker. Some downward migration of ^{137}Cs is believed to have occurred through the holes left by dead rhizomes of *Spartina anglica* causing the tail of ^{137}Cs activity to continue below the 1954 level. Thus future core sampling for ^{137}Cs dating purposes should be aimed at obtaining only the two top sediment markers (1986 and 1963 peaks) which may be found in the first 50 cm of the sediment column.

The results of ^{137}Cs analysis showed that sampling sites should be carefully chosen in order to obtain suitable sediment cores for dating purposes. Cores taken too close to the main channel or at the fringe of the mud flat are normally very sandy and have very low clay and organic contents. As a result these samples contain very low ^{137}Cs activity and make the interpretation of the marker horizon very difficult as no prominent peaks are present in ^{137}Cs activity profiles. The non-homogeneity of the sediment column adds to the problem due to caesium's strong affinity to clay and organic particles. A well preserved record of ^{137}Cs profiles was obtained from cores taken well inside the marsh land where the environment was more constant and less affected by changes in channel migration and morphology.

The reliability of the ^{137}Cs dating technique depends on factors such as the quality of sediment cores, bioturbation and the migration of caesium down the cores. Inhomogeneity of the sediment column caused by rapid changes in depositional environment degrades the quality of the cores. Bioturbation can be determined through X-radiography and it should also be used to asses the non-homogeneity of the sediment column. Other radioisotope dating techniques such as ^{210}Pb should be used in conjunction with the ^{137}Cs dating to obtain accurate accumulation rates of the marsh sediments. Unfortunately, due to the time and financial constrains, this could not be carried out in the present study.

CHAPTER TEN

SUMMARY AND CONCLUSIONS

10.1 Introduction

This concluding chapter briefly summarises the main findings of this study. Emphasis is given to the hydrodynamics of the estuarine water circulation, the measurement of sediment fluxes, and the transport of fine and coarse sediment. Comparison of sedimentation rates as inferred from the flux measurement, sediment budget estimates and from caesium dating of sediment cores, are also made. The chapter concludes with some suggestions for future work.

10.2 Hydrodynamics

The estuary is characterised by fast tidal currents accompanied by strong turbulence on the early stage of the flood tide and also to a lesser extent, at the end of the ebb. Strong flood currents exceeding 2.0 m/s during a spring tide are associated with the asymmetry of the tidal wave as the tide entered the estuary. This asymmetry is produced mainly by sedimentation which has elevated the estuary profile relative to the mean sea level rather than by tidal wave deformation due frictional effects. Frictional effects are importance after the tide has entered the estuary and on smaller tides when the tidal wave is less asymmetrical at the mouth. During the ebb, fast currents are produced as the sand flats emerge and the flow is confined to the main channel. Throughout the tidal cycle, the strongest currents occur in the main channel and currents are slower on the tidal flats and away from the channel. The velocity of the current is greatly affected by channel morphology, particularly when water is shallow and the flow is restricted to the narrow channel during the early flood and late ebb. The swift inundation of the tidal water onto tidal flats and salt marshes results in a sudden decrease in the flow velocity.

The flood velocities are dominant over ebb velocities during both springs and neaps; however locally there exist ebb dominated channels. The velocity asymmetry is greater during springs, but during neaps the velocity is less and less markedly asymmetrical than on springs. The degree of tidal wave asymmetry increases in the landward direction with the flood duration becoming shorter towards the head of the estuary; for example, on a spring tide, the time for the flood rise is about three hours near the mouth, but this is reduced to just over two hours near at the estuary head at St. Clears.

The estuarine circulation can be classified on the basis of Hansen and Rattray circulation-stratification model and varies from a well-mixed type to a partially mixed type with slight stratification. However, application of this classification model for a tidal estuary is limited as the estuarine circulation is dominated by the changing water depth over the short period of tidal cycles and over neap-spring cycles, and interaction between fresh and saline waters is of secondary influence. The estuary is well-mixed during spring tides when there is less than 1‰ difference between surface and bottom salinities, but it can change to partially mixed to stratified during neap tides. Stratification is strongest when neap tides coincide with inflated river flows when at the mouth the surface waters may be 14‰ fresher than the bottom waters.

Although the water body is usually vertically homogenous, there is some lateral salinity variation particularly during the early stages of flood tides and the late ebb of neap tides. During the flood, the more saline water tends to flow in the deeper part of the channel, while during the ebb fresher water occupies the channel. This lateral salinity gradient is controlled by the local channel morphology rather than by the geostrophic force (the cross section of the estuary is too narrow for the latter to be important).

The tidal prism for the estuary varies during the neap-spring cycle from 0.67 x 10^7 m^3 to 1.86 x 10^7 m^3. This variation, together with the variation in river discharge (which varies from 1-50 m^3/s), causes significant changes in flow ratios. Flow ratios, which vary from 0.001 - 0.08 on springs to 0.004-0.26 on neaps, suggest that the estuary is relatively well-mixed during springs but can change to partially mixed during neaps.

The relative magnitudes of tidal range (i.e. tidal prism) and river flow also determines the landward penetration of saline water. For this reason the interface between saline and fresh water is push furthest inland, i.e. at some 15 km distance from the mouth, during spring tides and low river discharges. The interface is just 7 km distance from the mouth during neap tides and high river discharges.

Vertical velocity profiles in the bottom 2 m of the water column are generally logarithmic; therefore, the associated roughness length and shear velocity may be used in estimating the potential transport of the bed sediment. However, the shape of the velocity profiles is affected by density stratification particularly at times of maximum tidal currents during the early flood on spring tides. This density stratification damps turbulance and reduces the potential of sediment transport.

The roughness length shows considerable variation over a tidal cycle as well as over the spring-neap cycle. Over a tidal cycle, the variation is greater during the flood than during the ebb; however the mean roughness length for the flood is always smaller than the mean for the ebb. The roughness length is greater during neaps than during springs, probably due to the formation of plane beds on springs and the formation of steeper and more stable ripples on the smaller tides. The mean value of roughness length varies from 0.2 - 3.8 cm for the flood tide and between 0.70 - 5.4 cm for the ebb tide. These values are comparable to values calculated using the theoretical formula of Wooding *et al.*, (1973), but higher than those calculated using Lettau`s (1963) relationship.

The shear velocities calculated from the velocity profiles affected by the density stratification tend to be over estimated from their true values. Methods are available to deal with such a problem, and it has been shown that the shear velocities are less than half of their apparent values if such effect is allowed for.

10.3 Turbidity maximum

A prominent feature of suspended sediment dynamics in the Taf estuary is the development of a pronounced and well defined turbidity maximum in the upper reaches of the estuary. The maximum is most developed during spring tides and at low river discharges but it is absent when neap tides coincide with high river flows. The suspended sediment concentration in the turbidity maximum exceeds 600 mg/l compared to background concentrations in the river of 10 mg/l. The centre of this maximum is located upstream of the saltwater-freshwater interface (1‰ isohaline) and occupies a 2-3 km stretch of the estuary between salinities 5 - 0.3‰. Its location at high water varies between 9.5 - 14.5 km distance from the mouth, depending on tidal range and river discharge.

The turbidity maximum is developed as a result of erosion and resuspension of bottom sediment by fast tidal currents on the early flood. The narrowing down of the channel increases the suspended sediment concentration so that the leading edge of the flood tide is very turbid producing the turbidity maximum just above the limit of salt water intrusion. Some of the material remains in suspension at high water and progressively retreats down the estuary with the ebb tide. During low water, the turbidity maximum is flushed out of the estuary into the bay by the fresh water flow. The Taf turbidity maximum is therefore a transient and ephemeral phenomenon that grows and decays during the spring-neap cycle and moves through the estuary with the advancing and retreating tidal prism.

10.4 Sediment flux

Short terms measurement of sediment flux at two survey transects (T5 and T9) show that gross sediment flux increases exponentially with tidal range. On all tides, the gross flood flux exceeds the gross ebb flux, thus there is a net landward movement of suspended sediment (mostly fine sand) with each tide. At T9, the net flux was 16% of the gross flux and at transect T5 it was 29 % of the gross flux. From the relationship between sediment flux and the tidal range, the annual gross and net sediment fluxes through the two transects have been

estimated and these are summarised in Table 10.1. The annual sedimentation rates calculated from the net sediment fluxes at each transect are 1.2 ± 2.6 cm/yr for T9 and 1.6 ± 4.6 cm/yr for T5.

Table 10.1 Annual gross and net sediment fluxes at two survey transects.

Transect	Sediment flux (tonnes/yr)			Sedimentation rate (cm/yr)
	Flood	Ebb	Net	
T9	397077	341313	55764	1.2 ± 2.6
T5	187506	153726	33780	1.6 ± 4.6

The sediment fluxes through the transects may be predicted using the following general equations:

$$F_{flood} = 19.20 \times 2.17^{t} \text{ , and}$$

$$F_{ebb} = 9.67 \times 2.44^{t}$$

where;

F = sediment flux (kg/m cross section)

t = tidal height above O.D. (m).

For T9, the sedimentation rate recalculated using the above general equations is 1.2 cm/yr; a similar value (1.2 ± 1.9 cm/yr), was obtained from the log-linear relationships of sediment flux and tidal height.

The sedimentation rate estimated from the sediment flux measurement may be compared with that estimated from long term measurement of the sand budget which has been determined since 1968 (Jago, 1980; Jago *et al.*, 1996). The annual sand budget calculated from this survey is 6.8×10^4 m^3 which gives an equivalent sedimentation rate of 1.8 cm/yr. The results of the short term measurement of sediment flux (Table 10.1) and the long term measurement of sand budget are very similar.

The sedimentation rate of salt marsh sediment has been determined using caesium dating of the sediment cores. Despite the poor quality of some of the cores, two marker horizons with pronounced ^{137}Cs peaks have been recognised and could be used with some confidence to estimate sedimentation rates of the marsh sediment. These ^{137}Cs peaks correspond to 1986 (the Chernobyl nuclear accident) and 1963 (nuclear weapon testing fallout) peaks. The identification of the 1954 marker horizon which is the base of ^{137}Cs record was difficult to make as most cores were insufficiently deep. In cores where a full ^{137}Cs record was obtained, the ^{137}Cs activity show a long tail which indicates either mixing or ^{137}Cs migration down the cores. The sedimentation rate estimated using the 1986 and 1963 peaks varies from 0.4 - 1.7 cm/yr. The mean sedimentation rate of salt mash sediment based on the 1963 fallout peak is 1.0 cm/yr. This rate is very similar to the sedimentation rates obtained for the estuarine sands.

10.5 Sediment transport

Sediment transport rates across estuary cross sections have been calculated using the suspended sediment concentration and the velocity data. The measured transport rates show great spatial and temporal variability both over a tidal cycle and over the spring-neap cycle. Transport is greatest in the main channel where transport rates up to 2.2 kg/m/s occur; this is compared to just 0.2 kg/m/s over the tidal flats. During neap tides transport is much less amounting to just 0.08 kg/m/s in the main channel and 0.01 kg/m/s on the tidal flats. These variabilities reflect the strength of the tidal currents operative in different parts of the estuary cross section.

The predictive capability of three commonly-used transport equations (Hardisty (1983); Engelund and Hansen (1967); and Jago and Mahamod (1997)) have been evaluated in this study by comparing the transport rates predicted by these equations with the measured rates. All equations predict correctly the net direction of sediment transport but each equation predicts quite different transport rates for the same flow velocity. The differences are greatest at high flow velocities (>1.0 m/s) when most transport occurs. Of the three equations, the Engelund and Hansen equation gives the best agreement with the measured transport rate,

while the Jago and Mahamod equation shows the most inconsistent results compared to the measured transport. All equations overestimate transport at high flow velocities.

The Jago and Mahamod equation has been modified by using different threshold velocities for the initiation of sediment grain and also by modifying the exponent value, n, in the equation. The results show that for fast currents the equation should assume a lower power law than for slow currents. For the sediment in the study area, which has a mean grain diameter of 0.13 mm, the following modification can be made:

for $u_{100} < 0.7$ m/s

$$q = 2.72 \cdot 10^{-3} \left(\frac{u_{100} - u_{100c}}{u_{100c}} \right)^{4.4}$$

and for $u_{100} > 0.7$ m/s

$$q = 2.72 \cdot 10^{-3} \left(\frac{u_{100} - u_{100c}}{u_{100c}} \right)^{3.0}$$

Where u_{100} and u_{100c} are the current velocity and the threshold current velocity, respectively, at a standard height 100 cm above the bed. The modified equations significantly improve the predictive capability of the equation. Using the modified equations, 71% of the transport rates fall within 50 - 200 % of the measured rates, compared to 29% using the unmodified equation.

10.6 Future work

This study has concentrated on the hydrodynamics and transport processes that are operative in the estuary proper and no consideration has been given to the physical processes occurring in Carmarthen Bay. Since the estuary and the bay are closely related, future studies should include parts of the bay in order to define this link.

Caesium dating has proved to be a useful technique to estimate the accumulation rate of salt marsh sediment. So far, only sediment from the low marsh has been dated. The full potential of using the 1986 peak should be fully explored by dating both sediment from the low and high marshes. ^{210}Pb dating should also be used in conjunction with ^{137}Cs dating for accurate estimate of sedimentation rates.

Measurement of suspended sediment flux depends on the accurate calibration of transmissometers used to estimate the concentration profiles. A major disadvantage of this instrument is that no information is given regarding the grain size of the suspended particles on which the beam attenuation of a transmissometer depends on. Since in the Taf, the suspended sand is very homogenous in grain size, an improvement in the calibration may be made by having a more controlled water sampling and measurement of the water transmittance i.e. simultaneous measurement and having them side-by-side. The results obtained in this study could be used as guidelines if a similar study is to be made in bigger estuaries. It is very important to have as many measurement stations as possibly can across the measurement transect and that represent different flow regimes and hydrodynamic environments if the flux and budget to be meaningfully estimated.

The next step forward would be to apply the gathered information to a model that will predict the dynamics and fluxes of water and sediment. Instruments capable of providing grain size distribution *in-situ* are now available and should be used in the future studies to provide information on sediment settling velocity which is an important parameter in any model of sediment transport. However, modelling a tidal estuary where the tidal prism is absent at low water is a new challenge.

REFERENCES

Abbot, J. E. and Francis, J. R. D., 1977. Saltation and suspension trajectories of solid grains in a water stream. *Phil. Trans. R. Soc. London*, **A284**, 225-254.

Ackers, P. and White, W. R., 1973. Sediment transport: new approach and analysis. *J. Hydraul. Div., Proc. ASCE*, **99**, 2041-2060.

Allen, G. P. and Castaing, P., 1973. Suspended sediment transport from the Gironde estuary (France) onto the adjacent continental shelf. *Mar. Geol.*, **14**, M47-M53.

Allen, G. P., Sauzay, G., Castaing, P. and Jouanneau, J. M., 1977. Transport and deposition of suspended sediment in the Gironde Estuary, France. In: Wiley, M. (Ed.), *Estuarine Processes. Vol. II, Circulation, Sediments, and Transfer of Material in the Estuary*. Academic Press, New York, p 63-81.

Allen, G. P., Salomon, J. C., Bassoullet, P., DuPenhoat, Y. and De Grandpre, C., 1980. Effects of tides on mixing and suspended sediment transport in macrotidal estuaries. *Sedimentary Geology*, **26**, 69-90.

Allen, J. R. L., and Pye, K., 1992. Coastal saltmarshes: their nature and importance. In; Allen, J. R. L., and Pye, K. (Eds.), *Saltmarshes: Morphodynamics, Conservation and Engineering Significance*. Cambridge University Press. p 1-18.

Althausen Jr, J. D. and Kjerfve, B., 1992. Distribution of suspended sediment in a partially mixed estuary, Charleston Harbour, South Carolina, U.S.A. *Estuarine, Coastal and Shelf Sci.*, **35**, 517-531.

A.S.C.E. (American Society of Civil Engineers), 1975. *Sedimentation Engineering*. Vanoni, V. A., (Ed.), New York, 745 p.

Amos, C. L., 1987. Fine-grained sediment transport in Chicago Bay, Bay of Fundy, Canada. *Continental Shelf Res.*, **7**, 1295-1300.

Anderson, F. E., 1972. Resuspension of estuarine sediments by small amplitude waves. *J. Sed. Petrol.*, **42**, 602-607.

Anderson, F. E., 1980. The variation in suspended sediment and water properties in the Flood-water front traversing the tidal flat. *Estuaries*, **3**, 28-37.

Anderson, F. E., 1983. The northern muddy intertidal; a seasonally changing sources of suspended sediment to estuarine waters - a review. *Can. J. Fish. Aquatic Sci.*, **40**, Supplement I, 143-159.

Avoine, J. and Larsonneur, C., 1987. Dynamics and behaviour of suspended sediment in macrotidal estuaries along the south coast of the English Channel. *Continental*

Shelf Res., 7, 1301-1305.

Bagnold, R. A., 1963. Beach and nearshore processes. Part I: Mechanics of marine sedimentation. In: Hill, M. N. (Ed.), *The Sea, Vol.3*. Wiley-Interscience, New York, pp.507-528.

Bagnold, R. A., 1966. *An Approach to the Sediment Transport Problem from General Physics*. U.S. Geol. Surv. Prof. Paper, 422-I

Bagnold, R. A., 1973. The nature of saltation and bedload transport in water. *Proc. R. Soc. London*. A332, 473-504.

Bale, A. J., 1983. *The characteristics, Behaviour and Heterogenous Chemical Reactivity of Estuarine Suspended Particles: An Interim Report*. Inst. for Marine Enviromental Reseach, Plymouth.

Baker, E. T. and Lavelle, J. W., 1984. The effect of particle size on the light attenuation coefficient of natural suspension. *J. Geophys. Res.*, 89, 8197-8203.

Biggs, R. B., 1969. Sources and distribution of suspended sediment in Northern Chesapeake Bay. *Mar. Geol.*, 9, 187-201.

BNFL, 1995. Annual Report on Radioactive Discharge and Monitoring of the Environment, 1995.BNFL Safety, Health and Environment Directorate, Warrington, Cheshire.

Bourne, G. S., 1991. *Actinide and Fission Product Activity Variations in Inter-tidal Marine Macrophytes*. Ph.D Thesis, University of Wales, Bangor.

Bowden, K. F., 1978. Physical problems of the benthic boundary layer. *Geophys. Surv.*, 3, 255-296.

Bowden, K. F., 1980. Physical Factors: Salinity, Temperature, circulation, and mixing processes. In: Olausson, E. and Cato, I. (Eds.), *Chemistry and Biochemistry of Estuaries*. John Wiley, Chichester, pp. 37-70.

Bowen, D.Q., 1970. South-east and central South Wales. In: Lewis, C.A. (Ed). *The Glaciations of Wales and Adjoining Regions*. Longman, London, 177-228.

Bowen, D.Q., 1981. The South Wales end-moraine: fifty years after. In: Neale, J. and Flenley, J. (Eds.) *The Quaternary of Britain*. Pergamon Press, Oxford, 60-67.

Bricker-Urso, S., Nixon, S. W., Cochran, J. K., Hirschberg, D. J., and Hunt, C., 1989. Accretion rates and sediment accumulation in Rhode Island salt marshes. *Estuaries*, 4, 300-317.

Bridge, J. S., 1981. Hydraulic interpretation of grain-size distribution using a physical

model for bedload transport. *J. Sed. Petrol.*, **51**, 1109-1124.

Buller, A. T., Green, C. D. and Mc Manus, J., 1975. Dynamics and sedimentation: the Tay in comparison with other estuaries. In: Hail, J. and Carr, A. P.(Eds.), *Nearshore Sediment Dynamics and Sedimentation*, John Wiley, Chichester, 201-249.

Caillot, A., 1973. Tracers techniques in sediment transport. IAEA Tech. Rep. Series No. 145, 170 pp.

Caillot, A., 1983. Bedload Transport. In: *Guidebook on Nuclear Techniques in Hydrology.* IAEA Tech. Rep. Series No.91, 103-128.

Callaway, J. C., DeLaune, R. D. and Patrick Jr, W. H., 1996. Chernobyl ^{137}Cs used to determine sediment accretion rates at selected northern European coastal wetlands. *Limnol. Oceanogr.*, **41**, 444-450.

Cambell, D. E. and Spinrad, R. W., 1987. The relationship between light attenuation and particle characteristics in a turbid estuary. *Estuarine, Coastal and Shelf Sci.*, **25**, 53-65.

Cambell, S. and Bowen, D. Q., 1989. *Geological Conservation Review: Quaternary of Wales*. Nature Conservancy Council, **A4.1**, 237 pp.

Cambray, R. S. and Others, 1987. Observations on radioactivity from the Chernobyl accident. *Nucl. Energy*, **26**, 77-101.

Camplin, W. C., 1995. Radioactivity in Surface and Coastal Waters of the British Isles, 1994. *Aquat. Environ. Monit.* Rep.45, MAFF. Direct. Fish. Res., Lowestoft, 111 pp.

Carling, P. A., 1979. *The Influence of Creek Systems on Intertidal* Sedimentation. Ph.D. Thesis, University College of Swansea, Wales.

Castaing, P. and Allen, G. P., 1981. Mechanisms controlling seaward escape of suspended sediment from the Geronde: a microtidal estuary in France. *Mar. Geol.*, **40**, 101-118.

Christensen, E. R., 1982. A model for radionuclides in sediments influenced by mixing and compaction. *J. Geophy. Res.*, **87**, 566-572.

Collins, M. B., Amos, C. L. and Evans, G., 1981. Observations of some sediment transport processes over intertidal flats, the Wash, U.K.. *Spec. Publs. int. Ass. Sediment.*, **5**, 81-98.

Collins, M. B., Shimwell, S. J., Gao, S., Powell, H., Hewitson, C. and Taylor, J. A., 1995. Water and sediment movement in the vicinity of linear sandbanks: the Norfolk Banks, southern North Sea. *Mar. Geol.*, **123**, 123-142.

Coleman, N. L., 1981. Velocity profiles with suspended sediment. *J. Hydr. Res.*, 19, 211-229.

Conner, C. S. and De Visser, A. M., 1992. A laboratory investigation of particle size effects on an optical backscatterence sensor. *Mar. Geol.*, 108, 151-159.

Crickmore, M. J. and Lean, G. H., 1962a. The measurement of sand transport by means of radioactive tracers. *Proc. Royal Soc. London,* A266.

Crickmore, M. J. and Lean, G. H., 1962b. The measurement of sand transport by time integration method with radioactive tracers. *Proc. Royal Soc. London*, A270

Crickmore, M. J., Tazioli, G. S., Appleby, P. G. and Oldfield, F., 1990. *The Use of Nuclear Techniques in Sediment Transport and Sedimentation Problems*. IHP, Unesco, Paris, 170pp.

D & A Instruments, 1988. *Instruction manual: Optical Backscatterance Turbidity Monitor*. D & A Instruments and Engineering. Washington, D. C., 32 p.

D & A Instruments, 1989. *Optical Methods for Measuring Turbidity and Suspended Particles in Water: Some Notes for Users of OBI Sensors*. Technotes (3/89). D & A Instruments and Engineering. Washington, D.C., 9 p.

Dade, W. B., Nowell, A. R. M. and Jumars, P. A., 1992. Predicting erosion resistance of muds. *Mar. Geol.*, 105, 285-297.

Davies, J. L., 1973. *Geographical Variation in Coastal Development*. Hafner, New York, 204pp.

Davison, A., 1984. A predredging sand mobility study using a radioisotope tracer. *Coastal Engineering Conf.* Chapter 138, 2063-2076.

Delaune, R.D., Patrick,W. H., and Buresh,R. J.,1978. Sedimentation rates determined by 137Cs dating in a rapidly accreting salt marsh. *Nature*, 257, 532-533.

Delaune, R. D., Whitcomb, J. H., Patrick, Jr W. H., Pardue, J. H., and Pezeshki, S. R., 1989. Accretion and canal impacts in a rapidly subsiding wetland. *Estuaries*, 12, 247-259.

Dronkers, J., 1986. Tide-induced residual transport of fine sediment. In: van de Kreeke (Ed.), *Physics of Shallow Estuaries and Bays*. Springer-Verlag, Berlin, p. 228-244.

Duff, P. M. D. and Smith, A. J. (Eds.), 1992. *Geology of England and Wales.* The Geological Society, London, 651 p.

Dyer, K. R., 1970. Current velocity profiles in a tidal channel. *Geophys. J. R. Ast. Soc.*, 22, 153-161.

Dyer, K. R., 1972. Sedimentation in estuaries. In: Barnes, R. S. K. and Green, J.(Eds.), *The Estuarine Environment*. Applied Science Publishers Ltd., London, p. 10-32.

Dyer, K. R., 1973. *Estuaries: A Physical Introduction*. John Wiley & Sons, London, 140pp.

Dyer, K. R., 1977. Lateral circulation effects in estuaries. In: *Estuaries, Geophysics and the Environment*. National Academy of Sciences, Washington, D.C., 22-29.

Dyer, K. R., 1980. Velocity profiles over a rippled bed and the threshold of movement of sand. *Estuarine and Coastal Mar. Sci.*, 10, 181-199.

Dyer, K. R., 1986. *Coastal and Estuarine Sediment Dynamics*. John Wiley & Sons, Chichester, 342pp.

Dyer, K. R., 1988. Fine sediment particle transport in estuaries. In: Dronkers, J. and Van Leussen, W. (Eds.), *Physical Processes in Estuaries*. Springer-Verlag, Berlin, p. 295-310.

Dyer, K. R., 1989. Sediment processes in estuaries: Future research requirements. *J. Geophys. Res.*, 94, 14,327-14,339.

Dyer, K. R., 1994. Estuarine sediment transport and deposition. In: Pye, K. (Ed.) *Sediment Transport and Deposition Processes*. Blackwell, Oxford, 193-218.

Edgington, D. N., Val Klump, J., Robbins, J. A., Kosner, Y. S., Pampura V. D., and Sandimirov, I. V., 1991. Sedimentation rates, residence times and radionuclide inventories in Lake Baikal from ^{137}Cs and ^{210}Pb in sediment cores. *Nature*, 350, 601-604

Ehlrers J, Nagorny, K., Schmidt, P., Stieve, B., and Zietlow, K., 1993. Storm surge deposits in North Sea salt marshes dated by ^{134}Cs and ^{137}Cs determination. *J. Coastal Res.*, 9, 698-701.

Eisma, D., 1986. Flocculation and de-flocculation of suspended matter in estuaries. *Netherlands J. Sea Res.*, 20, 183-199.

Eisma, D., 1993. *Suspended Matter in the Aquatic Environment*. Springer-Verlag, Berlin. 315p.

Eisma, D., Bernard, P., Cadee, G. C., Ittekkot, V., Kalf, J., Laane, R., Martin, J. M., Mook, W. G., van Put, A. and Schuhmacher, T., 1991. Suspended-matter particle size in some west-European estuaries; Part II: A review on floc formation and break-up. *J. Sea Res.*, 28, 215-220.

Einstein, H. A., 1950. The bed load function for sediment transportation on open channels. *U.S. Dept. of Agriculture, Soil Conservation Serv., Tech. Bull.* 1026. 78 p.

Engelund, F. and Hansen, E., 1967. *A Monograph of Sediment Transport in Alluvial Streams*. Teknish Forlag, Copenhagen. 62pp.

Evans, C. D. R., 1995. Chapter 2.5 See-level rise and flooding. *In*: Barne J. H., Robson, C. F., Kaznowska S. S., and Doody, (Eds.). *Coasts and Seas of the United Kingdom, Region 12 Wales: Morgan to Little Orme*. Joint Nature Conservation Committee, Peterborough.

Fairbridge, R. W., 1980. The estuary: Its definition and Geodynamic cycle. In: Olausson, E. and Cato, I. (Eds.), *Chemistry and Biochemistry of Estuaries*. John Wiley, Chichester, p. 1-35.

Festa, J. F. and Hansen, D. V., 1978. Turbidity maxima in partially mixed estuary: A two-dimensional numerical model. *Estuarine Coastal Mar. Sci.*, 7, 347-359.

Flemming, G., 1970. Sediment balance of Clyde estuary. *J. Hydraul. Div. Proc. Amer. Soc. civil Eng.*, 96, 2219-2230.

Francis, C. W. and Brinkley, F. S., 1976. Preferential adsorption of ^{137}Cs to micaceous minerals in contaminated fresh water sediment. *Nature*, 260, 511-513.

Francis, J. R. D., 1973. Experiments on the motions of solitary grains along the bed of a water stream. *Proc. R. Soc. Londo*n, A332, 443-471.

Fredsoe, J. and Deigaard, R., 1992. *Mechanics of Coastal Sediment Transport*. World Scientific Publ. Co., Singapore. 369pp.

French, J. R. and Stoddart, D. R., 1992. Hydrodynamics of salt-marsh creek system: implications for marsh morphological development and material exchange. *Earth Surface Processes Landforms*, 17, 235-252.

Gadd, P. E., Lavelle, J. W. and Swift, D. J., 1978. Estimates of sand transport on the New York shelf using near-bottom current meter observations. *J. Sed. Petrol.*, 48, 239-252.

Gameson, A. L. H. (Ed.), 1973. Mathematical and Hydraulic Modelling of Estuarine Pollution. H.M.S.O., London.

Gibbs, R. J., 1987. Sources of estuarine sediments and their coagulation. In: *Proc. Sedimentation Control to Reduce Maintenance Dredging of Navigational Facilities in Estuaries*. Rpt. Natl. Res. Counc., Washington, D.C., p. 32-52.

Glasgow, L. A. and Leucke, R. H., 1980. Mechanisms of deaggregation for clay-polymer flocs in turbulent systems. *Ind. Eng. Chem. Fundam.*, 19, 148-156.

Graf, W. H., 1971. *Hydraulics of Sediment Transport*. McGraw Hill, New York. 513p.

Griffiths, J. C., 1939. The mineralogy of glacial deposits of the region between the rivers Neath and Towy, South Wales, *Proceedings of the Geologists Association*, **50**, 433-462.

Griffiths, J. C., 1940. *The Glacial Deposits West of the Taff.* Ph.d Thesis, University of London.

Gust, G. and Walger, E., 1976. The influence of suspended cohesive sediments on boundary-layer structure and erosive activity of turbulent seawater flow. *Mar. Geol.*, **22**, 189-206.

Guy, H. P., Simmons, D. B. and Richarson, E. V., 1966. Summary of alluvial channel data from flume experiments, 1956-1961. *U.S. Geol. Surv., Prof. Paper* **462-I**, 96pp.

Hansen, D. V. and Rattray, M. Jr., 1966. New dimensions in estuarine classification. *Limnol. Oceanog.*, **11**, 319-326.

Hardisty, J., 1983. An assessment and calibration of formulations for Bagnold's bedload equation. *J. Sed. Petrol.*, **53**, 1007-1010.

Hardisty, J. G. and Rouse, H. L., 1996. The Humber Observatory: Monitoring, modelling and management for the coastal environment. *J. Coastal Res.*, **12**, 683-690.

Harris, P. T. and Collins, M., 1988. Estimation of annual bed load flux in a macotidal estuary: Bristol Channel, U.K. *Mar. Geol.*, **83**, 237-252.

Harvey, J. G. and Vincent, C. E., 1977. Observations of shear in near-bed currents in the Southern North Sea. *Estuarine and Coastal Mar. Sci.*, **5**, 715-731.

Hayes, M. O., 1975. Morphology of sand accumulations in estuaries. In: Cronin, L. E.(Ed.), *Estuarine Research, Vol.2, Geology and Engineering*. Academic Press, New p. 3-22.

Haynes, J. G. and Dobson, M. R., 1969. Physiology, Foraminifera and sedimentation in the Dovey estuary (Wales). *Geol. J.*, **6**, 217-256.

Heathershaw, A. D., 1981. Comparison of measured and predicted sediment transport rates in tidal currents. *Mar. Geol.*, **42**, 75-104.

Heathershaw, A. D. and Simpson, J. H., 1978. The sampling variability of the Reynolds stress and its relation to boundary shear stress and drag coefficient measurements. *Estuarine and Coastal Mar. Sci.*, **6**, 263-274.

Heathershaw, A. D. and Thorn, P. D., 1985. Sea-bed noises reveal role of turbulent bursting phenomenon in sediment transport by tidal currents. *Nature*, **316**, 339-342.

Heinzelmann, C. H. and Wallisch, S., 1991. Benthic settlement and bed erosion. A review.

J. Hydraul. Res., **29**, 355-371.

Howard, J. D. and Frey, R. W., 1980. Physical and biogenic processes in Georgia Estuaries. I. Coastal setting and subtidal facies. In: McCann, S. B. (Ed.), *Sedimentary Processes and Animal-Sediment Relationships in Tidal Environments*. Geol. Assoc. Can. Short Course No. 1, p. 153-220.

Hunt, J. N., 1954. The turbulent transport of suspended sediment in open channels. Proc. *R. Soc. London*, **A224**, 322-335.

Hunt, J. R., 1986. Particle aggregate breakup by fluid shear. In: Mehta, A. J. (Ed.), *Estuarine Cohesive Sediment Dynamics*. Springer-Verlag, Berlin, p. 85-109.

Huntley, D. A., 1982. Canadian Coastal Study- *in-situ* sediment monitoring techniques: A survey of the state of the art in the U.S.A. *Natl. Res. Counc. Can., Ottawa. Rep.* **C2S2-1**, 35pp.

Inman, D. L., 1963. Sediments: Physical properties and mechanics of sedimentation. In: Shepard, F. D. (Ed.), *Submarine Geology*. 2nd. Edition, Harper and Row Publishers, New York, p. 101-151.

Ippen, A. T., 1966. Sedimentation in estuaries. In: Ippen, A. T. (Ed.), *Estuary and Coastline Hydrodynamics*. McGraw Hill Book Com. Inc., New York, p. 648-672.

Jago, C.F., 1974. *The Sedimentology of Estuarine and Coastal Plain Deposits Between Pendine and Wharley Point, Carmarthen Bay*. Ph.d Thesis, Imperial College of Sciences and Technology, University of London, 718 p.

Jago, C. F., 1980. Contemporary accumulation of marine sand in a macrotidal estuary, Southwest Wales. *Sedimentary Geology*, **26**, 21-49.

Jago, C. F., Ishak, A. K., Jones, S. E., and Reid, G. R., 1996. Can suspended sediment budget and flux measurements be reconciled? *UK Oceanography '96*, Bangor, 2-6 September, 1996.

Jago, C. F. and Mahamod, Y., 1997. A total load algorithm for sand transport by fast steady currents (in preparation).

Jenkins, A., 1976. *Circulation and Salinity in the Conwy Estuary*., M.Sc. Thesis, University of Wales, Bangor.

Johnson, R. G., 1974. Particulate material at the sediment-water interface in coastal environments. *J. Mar. Res.*, **33**, 313-330.

Johnson, R. G., 1976. Vertical variation in particulate matter in the upper twenty centimetres of marine sediments. *J. Mar. Res.*, **35**, 273-282.

Jones, S. E. and Jago, C. F., 1994. Sediment flux and budget in a small macrotidal estuary. In: *Shallow Water Sedimentary Processes: Transport, Fluxes and Budgets.* The Marine Studies Group of The Geological Society of London, 11-12 October, 1994.

Jones, S. E., Jago, C. F., Prandle, D. and Flatt, D., 1994. Suspended sediment dynamic: Measurement and modelling in the Dover Strait. In: Beven, K. J., Chatwin, P. C. and Millbank, J. H. (Eds.), *Mixing and Transport in the Environment.* John Wiley. p. 183-201.

Jonys, C. K., 1976. Acoustic measurement of sediment transport. Dep. of Fisheries and the Environment, *Can. Sci. Ser.* No. **66**. 140p.

Kachel, N. B. and Sternberg, R. W.,1971. Transport of bedload as ripples during an ebb current. *Mar. Geol.*, **10**, 229-244.

Kapdasli, M. S., 1990. Threshold condition of sand particles under codirectional combined wave and current flow. *Geo-Marine Lett.*, **10**, 45-49.

Kapdasli, M. S. and Dyer, K. R., 1986. Threshold conditions for sand movement on a rippled bed. *Geo-Marrine Letters*, **6**, 161- 164.

Kjerfve, B., 1979. Measurement and analysis of water current, Temperature, Salinity and Density. In: Dyer, K. R. (Ed.), *Estuarine Hydrography and Sedimentation.* Cambridge University Press, p. 186-226.

Komar, P.D., 1978. Boundary layer flow under steady unidirectional currents. In: *Marine Sediment Transport and Environmental Management.* Swift, D. J. and Stanley, D. J. (Eds.), Wiley, N. York, pp91-106.

Komar, P. D., 1981. The applicability of Gibbs equation for grain settling velocities to conditions other than quartz grains in water. *J Sed. Petr.*, **51**, 1125-1132.

Komar, P. D. and Reimers,C. E., 1978. Grain shape effects on settling rates. *J. Geol.*, **86**, 193-209.

Krank, K., 1981. Particulate matter grain-size characteristics and flocculation in a partially mixed estuary. *Sedimentology*, **28**, 107-114.

Krank, K., 1984. The role of flocculation in the filtering of particulate matter in estuaries. In: Kennedy, V. S., (Ed.), *The Estuary As a Filter*. Academic Press, p. 159- 175.

Krause, G. and Ohm, K., 1984. A method to measure suspended load transport in estuaries. *Estuarine Coastal Shelf Sci.*, **19**, 611-618.

Krone, R. B., 1972. A field study of flocculation as a factor in esturial shoaling processes. *U.S. Army Corps of Engineers, Tech. Bull.* no. **19**., 62pp.

Krone, R. B., 1978. Aggregation of suspended particles in estuaries. In: Kjerfve, B. (Ed.), *Estuarine Transport Processes*. University South Carolina Press, Charleston, 177-190.

Krone, R. B., 1986. The significance of aggregate properties to transport processes. In: Mehta, A. J. (Ed), *Estuarine Cohesive Sediment Dynamics*. Springer-Verlag, Berlin, p. 66-84.

Langhorne, D. N., 1982. A study of the dynamics of a marine sandwave. *Sedimentology*, **29**, 571-594.

Larcombe, P., 1992. *The Post-Glacial Evolution and Present Day Processes of the Mawdach Estuary, Wales*. Ph.d Thesis, University of Wales, Bangor.

Lavelle, W. and Mofjeld, H. O., 1987. Do critical stresses for incipient motion and erosion really exist? *J. Hydraul. Eng.*, ASCE, **113**, 370-393.

Leeder, M. R., 1982. *Sedimentology: Process and Product*. George Allen and Unwin, London. 344 p.

Leeder, M. R., 1983. On the dynamic of sediment suspension by residual Reynolds stress-conformation of Bagnold's theory. *Sedimentology*, **30**, 485-491.

Lees, B. J., 1981. Sediment transport measurements in Sizewell-Dunwich Banks area, East Anglia, UK. *Spec. Pub. Int. Assoc. Sediment.* **5**, 269-281.

Lees, B. J., 1983. The relationship of sediment transport rates and paths to sandbanks in tidally dominated area off the Coast of East Anglia, U.K. *Sedimentology*, **30**, 461-483.

Lessa, G. and Masselink, G., 1995. Morphodynamic evolution of a macrotidal barrier estuary. *Mar. Geol.*, **129**, 25-46.

Lettau, H., 1969. Note on aerodynamic roughness parameter estimation on the basis of roughness-element description. *J. Applied Meteorology*, **8**, 828-832.

Longmore, M. E., Torgersen, T. and O'Leary, B. M., 1986. ^{137}Cs redistribution in the sediment in the Playa, Lake Tyrell, North-Western Victoria. II. Patterns of ^{137}Cs and pollen redistribution. *Paleogeography, Paleoclimatology and Paleoecology*, **54**, 197-218.

Ludwick, J. C., 1989. Bedload transport of sand mixtures in estuaries: A review. *J. Geophys. Res.*, **94**, 14315-14326.

Lynch, J. C., Meriwether, J. R., McKee, B. A., Vera-Herrera, F. and Twilley, R. R, 1989. Recent accretion in Mangrove ecosystems based on ^{137}Cs and ^{210}Pb. *Estuaries*, **12**, 284-299.

M.A.F.F. (Ministry of Agriculture, Fisheries and Food), 1981. *Atlas of the Seas Around the British Isles.*

Mahamod, Y. B., 1989. *Sedimentary Processes in the Dwyryd Estuary.* Ph.d Thesis, University of Wales, Bangor. 476p.

Mantz, P. A., 1977. Incipient transport of fine grains and flakes by fluids: an extended Shields diagram. *J. Hydraul. Div., ASCE,* **103**, 601-615.

Markofsky, M., Lang, G. and Schubert, R., 1986. Suspended sediment transport in rivers and estuaries. In: van de Kreeke, J. (Ed.) *Physics of Shallow Estuaries and Bays.* Springer-Verlag, Berlin. 210-217.

McCann, S. B., 1980. Classification of tidal environments. In: McCann, S. B. (Ed.), *Sedimentary Processes and Animal-Sediment Relationships in Tidal Environments.* Geol. Assoc. Can. Short Course No. 1, p. 1-24b.

McCave, I. N., 1971. Sand waves in the North Sea off the coast of Holland. *Mar. Geol.*, **10**, 199-225.

McCave, I. N., 1979. Suspended sediment. In: Dyer, K. R. (Ed.), *Estuarine Hydrography and Sedimentation.* Cambridge University Press, p. 131-185.

McCave, I. N. and Langhorne, D. N., 1982. Sandwaves and sediment transport around the end of a tidal sand bank. *Sedimentology*, **29**, 95-110.

McCutcheon, S. C., 1981. Vertical velocity profiles in stratified flows. *J. Hydraul. Div., ASCE,* **107**, HY8, 973-988.

McLean, S. R., 1983. Turbulence and sediment transport measurements in a North Sea tidal inlet (The Jade). In: Sundermann, J. and Lenz, W. (Eds.), *North Sea Dynamics.* Springer-Verlag, Berlin, p. 436-452.

McLean, S. R., 1991a. Important considerations in suspended load calculations when waves and currents are present. In: Soulsby, R. L. and Betters, (Eds.), *Euromech 262- Sand Transport in Rivers, Estuaries and Sea.* Balkema, Rotterdam, p 103-110.

McLean, S. R., 1991b. Depth integrated suspended load calculations. *J. Hydr. Eng.*, **117**, 1440-1458.

Meade, R. H., 1969. Landward transport of bottom sediments in estuaries of the Atlantic Coastal Plain. *J. Sed. Petrol.*, **39**, 222-234.

Mehta, A. J. and Dyer, K. R., 1990. Cohesive sediment transport in estuarine and coastal waters. In: Le Mehaute, B. and Hanes, D. B., (Eds.). *The Sea, Vol.9. Part B.* John Wiley, New York, p. 815-839.

Meyer-Peter, E and Muller, R., 1948. Formulae for bed-load transport. *Proc. 2nd. Cong. Int. Assoc.. Hydraul. Res.*, Stockholm.

Middleton, G. V., 1980. Physical Processes. In: McCann, S. B. (Ed.), *Sedimentary Processes and Animal-Sediment Relationships in Tidal Environments*. Geol. Assoc. Canada, Short Cause Notes No.1, p. 25-58.

Millan, C. S., Swenson, E. M., Turner, R. E. and Lee, J. M., 1994. Assessment of the ^{137}Cs method for estimating sediment accumulation rates: Louisiana salt marshes. *J. Coastal Res.*, **11**, 296-307.

Miller, K. M. and Heit, M., 1986. A time resolution methodology for assessing the quality of lake sediment cores that dated by ^{137}Cs. *Lim. Oceanog.* **31**, 1292-1300.

Miller, M. C., Mc Cave, I. N. and Komar, P. D., 1977. Threshold of sediment motion under unidirectional currents. *Sedimentology*, **24**, 507-527.

Montague, C. L., 1986. Influence of biota on the erodibility of sediments. In: Mehta, A. J. (Ed.), *Estuarine Cohesive Sediment Dynamics*. Springer-Verlag, Berlin, p. 251-268.

Moody, J. A., Butman, B. and Bothner, M. H., 1987. Near-bottom suspended matter concentration on the continental shelf during storms: Estimates based on *in-situ* observations of light transmission and a particle size dependent transmissometer calibration. *Continental Shelf Res.*, **7**, 609-628.

Morris, A. W., 1983. Strategy for practical estuarine studies. In: Morris, A. W. (Ed.), *Practical Procedures for Estuarine Studies*. Estuarine Ecological Group, Institute for Marine Environmental Research, Plymouth, 1-17.

Mudge, S. M., Assinder, D. J. and Bourne, G. S., 1994. *A Survey of Radioactivity in the Ribble Estuary. Part 1: Activity Concentrations and Estuarine Dynamics.* Environment Series Report No. 2, H.M.S.O., 67 p.

Neill, C. R., 1968. *A Re-examination of the Beginning of Course Granular Bed Materials.* Hydraulic Research Station, Wallingford. Rep. INT 68.

NERC- (Natural Environment Research Council), 1983. *Practical Procedures for Estuarine Studies*. Estuarine Ecological Group, Institute for Marine Environmental Research, Plymouth.

NERC- (Natural Environment Research Council), 1994. *Land-Ocean Interaction Studies* (LOIS): *Implementation Plan for a Community Research Project*, 61pp.

Neville George, T., 1970. *British Regional Geology: South Wales* (3rd Edition). HMSO, London. 152pp.

Nichols, M. N., 1986. Effects of fine sediment resuspension in estuaries. In: Mehta, A. J.,

(Ed.) *Estuarine Cohesive Sediment Dynamics.* Springer-Verlag, New York, p. 5-42.

Nichols, M. M. and Biggs, R. B., 1985. Estuaries. In: Davis Jr, R. A. (Ed.) *Coastal Sedimentary Environments*. Springer-Verlag, New York, p. 77-186.

Nikuradse, J., 1933. Stromungsgesetze in glatten und rauhen rohren. *Ver. Deut. Ing., Forschungsheft*, V **361**, Berlin.

Nunes, R. A., 1982. *The Dynamics of Small Scale Fronts in Estuaries*. Ph.D. Thesis, University of Wales, Bangor.

Odd, N. V. M., 1988. Mathematical modelling of mud transport in estuaries. In: Dronkers, J and van Leussen, W. (Eds.), *Physical Processes In Estuaries*. Springer-Verlag, Berlin, 503-531.

Oenema, O. and DeLaune, R. D., 1988. Accretion rates in salt marshes in the Eastern Scheld, South-west Netherlands. *Estuarine Coastal Shelf Sci.*, **26**, 379-394.

Officer, C. B., 1976. *Physical Oceanography of Estuaries (and Associated Coastal Waters)*. John-Wiley, New York, 465pp.

Officer, C. B.,1981. Physical dynamics of estuarine suspended sediments. *Mar. Geol.*, **40**, 1-14.

Osborne, P. D., Vincent, C. E. and Greenwood, B., 1994. Measurement of suspended sediment concentrations in the nearshore: Field intercomparison of optical and acoustic backscatter sensors. *Cont. Shelf Res.*, **14**, 159-174.

Owen, M. W., 1971. The effect of turbulence on the settling velocities of silt flocs. *14th Cong. Int. Ass. Hydraul. Res.*, p. 27-32.

Owen, M. W., 1977. Problems in the modelling of transport, erosion, and deposition of cohesive sediments. In: Goldberg, E. D., McCave, I. N., O'Brien, J. J. and Steele, J. (Eds.), *The Sea, Vol.6*, John Wiley , New York, p. 515-537.

Partheniades, E., 1986. A fundamental framework for cohesive sediment dynamics. In: Mehta, A. J. (Ed.), *Estuarine Cohesive Sediment Dynamics*. Springer-Verlag, Berlin, p. 219-250.

Pejrub, M., 1988. flocculated suspended sediment in a micro-tidal environment. *Sedimentary Geology*, **57**, 249-256.

Pennington, W., Cambray, R. S. and Fisher, E. M., 1973. Observations on lake sediments using fallout 137Cs as a tracer. *Nature*, **242**, 324-326.

Pethick J. C., 1981. Long-term accretion rates on tidal salt marshes. *J. Sediment. Petrol.*, **51**, 571-577.

Pethick, J. C., 1984. *An Introduction to Coastal Geomorphology*. Edward Arnold, London. 260p.

Philpott, S., 1993. *The Suspended Sediment Flux in the Taf Estuary: The Flood Tide*. B. Sc. Project, University of Wales, Bangor. 23 p.

Postma, H., 1961. Transport and accumulation of suspended matter in the Dutch Wadden Sea. *Neth. J. Sea Res.*, **1**, 148-190.

Postma, H., 1967. Sediment transport and sedimentation in the marine environment. In: Lauff, G. H.(Ed.), *Estuaries*. Amer. Assoc. Adv. Sci., Publ. 83, Washington D.C., 158-179.

Postma, H., 1980. Sediment transport and sedimentation. In: Olausson, E. and Cato, I. (Eds.), *Chemistry and Biochemistry of Estuaries*. John Wiley, Chichester, p. 154-186.

Press, W. H., Teukolsky, S. A., Vettering, W. T. and Flannery, B. P., 1992. *Numerical Recipes in Fortran: the Art of Scientific Computing* (2nd. edition). Cambridge University Press, Cambridge, 963 p.

Pritchard, D. W., 1955. Estuarine circulation patterns. *Proc. Amer. Soc. civil Eng.*, **81**, 717/1-717/11.

Pritchard, D. W., 1967. Observations of circulation in coastal plain estuaries. In: Lauff, G. H.(Ed.), *Estuaries*. Amer. Assoc. Adv. Sci., Publ. 83, Washington D.C., 3-5.

Reid, I. and Frostick, L. E., 1994. Fluvial sediment transport and deposition. In:Pye, K. (Ed.) *Sediment Transport and Deposition Processes*. Blackwell, Oxford, 89-155.

Raudkivi, A. J., 1976. *Loose Boundary Hydraulics*. Pergamon Press, Oxford. 331p.

Reed, D. J., 1988. Sediment dynamics and deposition in a retreating coastal salt marsh. *Estuarine Coastal Shelf Sci.*, **26**, 67-79.

Richards, F. J., 1934. The salt marshes of the Dovey Estuary: IV, the rates of vertical accretion, horizontal extension and scarp erosion. *Annal. Botany*, **48**, 235-259.

Ritchie, J. C. and McHenry, J. R., 1990. Application of radioactive fallout cesium-137 for measuring soil erosion and sediment accumulation rates and patterns: A review. *J. Environ. Qual.*, **19**, 215-233.

Robbins, J. A. and Edgington, D. N., 1975. Determination of recent sedimentation rates in Lake Michigan using Pb-210 and Cs-137. *Geochim. Cosmochim. Acta*, **39**, 285-304.

Robbins, J. A., McCall, P. L., Fisher, J. B. and Krezoski, J. R., 1979. Effect of deposit feeders on migration of ^{137}Cs on lake sediments. *Earth and Planetary Science Letters*, **42**, 277-287.

Schultz, E. A. and Simmons, H. B., 1957. Fresh water-salt water density currents, a major cause of siltation in estuaries. *Tech. Bull. No.2, Comm. Tidal Hydraulics, U.S. Army, Corps of Engineers*. 28 p.

Self, R. F. L., Nowell, A. R. M. and Jumars, P. A., 1989. Factors controlling critical shears for deposition and erosion of individual grains. *Mar. Geol.*, **86**, 181-199.

Sharma, P., Gardner, L. R., Moore, W. S. and Bollinger, M. S., 1987. Sedimentation and bioturbation in a salt marsh as revealed by ^{210}Pb, ^{137}Cs and ^{7}Be studies. *Limnol. Oceanogr.*, **32**, 313-326.

Shields, A., 1936. Application of similarity principles and turbulence research to bed-load movement. (Translated by: Ott, W. P. and van Uchelen, J. C., California Ins. Tech., W. M. Keck Lab. of Hydraulics and Water Resources, Rep. No.167, 42 p.

Schubel, J. R., 1968. Turbidity maximum of the northern Chesapeake Bay. *Science*, **161**, 1013-1015.

Schubel, J. R., 1969. Size distributions of the suspended particles of the Chesapeake Bay turbidity maximum. *Neth. J. Sea Res.*, **4**, 283-309.

Schubel, J. R., 1971a. Tidal variation of the size distribution of suspended sediment at a station in the Chesapeake Bay turbidity maximum. *Neth. J. Sea Res.*, **5**, 252-266.

Shubel, J. R., 1971b. Estuarine circulation and sedimentation. In: Shubel, J. R. (Ed.), *The Estuarine Environment: Estuaries and Estuarine Sedimentation*. Short Course Lecture Notes, Amer. Geol. Inst., Washington DC.

Shubel, J. R. and Carter, H. H., 1984. The estuary as a filter for fine-grained suspended sediment. In: Kennedy, V. (Ed.) *The Estuary as a Filter*. Academic Press, New York. p 81-105.

Sleath, J. F. A., 1984. *Seabed Mechanics*. John Wiley, New York.

Soulsby, R. L., 1977. *Sensors for the Measurement of Sand in Suspension*. Institute of Oceanographic Science, Taunton. Rep. No.27 (unpublished manuscript), 23p.

Soulsby, R. L., 1983. The bottom boundary layer of shelf seas. In: Johns, B. (Ed.), *Physical Oceanography of Coastal and Shelf Seas*. Elsevier, Amsterdam, p 189-266.

Soulsby, R. L., 1990. Tidal-current boundary layers. In: Le Mehaute, M. and Hanes, D. M. (Eds.). *The Sea Vol.9*. John Wiley, New York, p. 523-566.

Soulsby, R. L., Davies, A. G. and Wilkinson, R. H., 1983. *The Detailed Processes of Sediment Transport by Tidal Currents and by Surface Waves*. Institute of Oceanographic Sciences, Taunton. Rep. No. 152, 80 p.

Soulsby, R. L., and Wainwright, B. L. S. A., 1987. A criterion for the effect of suspended sediment on near-bottom velocity profiles. *J. Hydr. Res.*, **25**, 341-355.

Spinrad, R. W., 1986. A calibration diagram of specific beam attenuation. *J. Geophys. Res.*, **91**, 7761- 7764.

Sternberg, R. W., 1966. Boundary layer observations in a tidal current. *J. Geophy. Res.*, **71**, 2175-2178.

Sternberg, R. W., 1968. Friction factors in tidal channels with differing bed roughness. *Mar. Geo*l., **6**, 243-260.

Sternberg, R. W., 1971. Measurement of incipient motion of sediment particles in marine environment. *Mar. Geol.*, **10**, 113-119.

Sternberg, R. W., 1972. Predicting initial motion and bedload transport of sediment particles in the shallow marine environment. In: Swift, D. J. P., Duane, D. B. and Pilkey, O. H. (Eds.), *Shelf Sediment Transport : Processes and Pattern*. Dowden, Hutchison and Ross, Stroudsberg, 61-82.

Sternberg, R. W., 1989. Instrumentation for estuarine research. *J. Geophys. Res.*, **94**, 14289- 14301.

Sternberg, R. W., Shi, N. C. and Downing, J. P., 1989. Suspended sediment measurements. In: Seymour, R. J. (Ed.), *Nearshore Sediment Transport*. Plenum, New York, 231-257.

Stoddart, D. R., Reed, D. J. and French, J. R., 1989. Understanding salt-marsh accretion, Scolt Head Island, Norfolk, England. *Estuaries*, **12**, 228-236.

Sunborg, A., 1956. The River Klaralven: a study in fluvial processes. *Geog. Ann. Stockholm*, **38**, 125-316.

Taylor, B. D., 1974. Temperature effects in flows over non planar beds. *J. Hydraul. Div. ASCE*, **100**, HY12, 1785-1807.

Taylor, P. A. and Dyer, K. R., 1977. Theoretical models of flow near the bed and their implications for sediment transport. In: Goldberg, E. D., McCave, I. N., O'Brien, J. J. and Steele, J., H. (Eds.), *The Sea, Vol. 6*. Wiley-Interscince, New York, 579-601.

Terwindt, J. H. J., 1967. Mud transport in the Dutch Delta area and along the adjacent coastline. *Neth. J. Sea Res.*, **3**, 505-531.

Thorne, P. D., 1986. An intercomparison between visual and acoustic detection of seabed gravel movement. *Mar. Geol.*, **72**, 11-31.

Thorne, P. D., Williams, J. J. and Heathershaw, A. D., 1989. *In-situ* acoustic measurements of marine gravels threshold and transport. *Sedimentology*, **36**, 61-74.

Tooley, M. J., 1992. Recent sea-level changes. In: Allen, J. R. L., and Pye, K. (Eds.). *Saltmarshes: Morphodynamics, Conservation and Engineering Significance*. Cambridge University Press. p 19-40.

Turrell, W. R., Brown, J. and Simpson, J. H., 1996. Salt intrusion and secondary flow in a shallow, well-mixed estuary. *Estuarine Coastal and Shelf Sci.*, **42**, 153-169.

Tywoniuk, N. and Warnock, R. G., 1973. Acoustic detection of bedload fluvial processes and sedimentation. *Proc. 9th. Canadian Hydrology Symp., Ottawa*, 728-749.

Uncles, R. J., Elliott, R. C. A. and Weston, S. A., 1985. Observed fluxes of water, salt and suspended sediment in a partly mixed estuary. *Estuarine, Coastal and Shelf Sci.*, **20**, 147-167.

Uncles, R. J. and Stephens, J. A., 1989. Distribution of suspended sediment at high water in a macrotidal estuary. *J. Geophy. Res.*, **94**, 14,395-14,405.

Uncles, R. J. and Stephens, J. A., 1993. Nature of turbidity maximum in the Tamar Estuary, U.K.. *Estuarine, Coastal and Shelf Sci.*, **36**, 413-431.

Uncles, R. J., Barton, M. L. and Stephens, J. A., 1994. Seasonal variability of fine-sediment concentration in the turbidity maximum region of the Tamar estuary. *Estuarine, Coastal and Shelf Sci.*, **38**, 19-39.

Unsold, G. and Walger, E., 1987. Critical entrainment conditions of sediment transport. In: Rumohr, J. and Walger, E. (Eds.). *Seawater-Sediment Interactions in Coastal Waters : An Interdisciplinary Approach*. Springer-Verlag, Berlin, 210-219.

Vanoni, V. A. and Nomicos, G. N., 1959. Resistance properties of sediment-laden streams. *J. Hydraul. Div., ASCE*, **85**, HY5, 77-107.

Van den Berg, J. H., 1987. Bedform migration and bed-load transport in some rivers and tidal environments. *Sedimentology*, **34**, 681-698.

Van Leussen, W., 1988. Aggregation of particles, settling velocity of mud flocs: A review. In: Dronkers, J and van Leussen, W. (Eds.), *Physical Processes In Estuaries*. Springer-Verlag, Berlin, 349-403.

Van Rijn, L. C., 1984. Sediment transport part I: Bed load transport. *J. Hydrol. Eng, ASCE*, **110**, 1431-1456.

Van Rijn, L. C., 1986. Evaluation of measuring instruments for suspended sediment. In: *International Conference of Measuring Techniques of Hydraulic Phenomena in Offshore, Coastal and Inland Waters*. (London, England, 9-14 April, 1986), 401-423.

Van Straaten, L. M. J. U. and Kuenen, P. L. H., 1957. Accumulation of fine grained sediment in the Duthcd Wadden Sea. *Geol. Mijnb.*, **19**, 329-354.

Van Straaten, L. M. J. U. and Kuenen, P. L. H., 1958. Tidal action as a cause of clay accumulation. *J. Sed. Petrol.*, **28**, 406-413.

Villaret, C. and Trowbridge, J. H., 1991. Effects of stratification by suspended sediments on turbulent shear flows. *J. Geophys. Res.*, **96**, 10,659-10,680.

Vincent, C. E., Young, R. A. and Swift, D. J. P., 1981. Bedload transport under waves and currents. *Mar. Geol.*, **39**, M71-M80.

Walley, S. S., 1996. *Holocene evolution of a Coastal Barrier Complex, Pendine Sands.* University of Wales Bangor, Ph.D Thesis, 228 p.

Warrick, R. A. and Oerlemans, J., 1990. Sea level rise. In: Houghton, J. T., Jenkins, G. J., and Ephraums, J. J. (Eds.). *Climate Change: The IPCC Scientific Assessment.* Cambridge University Press, Cambridge, 257-281.

Wells, J. T. and Kim, S. Y., 1991. The relationship between beam transmission and concentration of suspended particulate materials in the Neuse River Estuary, North Carolina. *Estuaries*, **14**, 395-403.

Wells, J. T., 1989. *In-situ* measurement of large aggregates over a fluid mud bed. *J. Coastal Res.*, Special Issue, **5**, 75-86.

West, J. R., 1994. Cohesive sediment transport in estuaries. In : Bewen, K. J., Chatwin, P. C., and Millbank J. H. (Eds.). *Mixing and Transport in the Environment*. John Wiley, Chichester, 306-323.

West, J. R., Oduyemi, K. O. K., Bale, A. J. and Morris, A. W., 1990. The field measurement of sediment transport parameters in estuaries. *Estuarine, Coastal and Shelf Sci.*, **30**, 167-183.

Wiberg, P. L. and Smith, J. D., 1985. A Theoretical model for salting grains in water. *J. Geophys. Res.*, **90**, 7341-7354.

Wilkinson, R. H., 1984. A method foe evaluating statistical errors associated with logarithmic velocity profiles. *Geo-Marrine Letters*, **3**, 49-52.

Wilkinson, R. H., Salkield, A. P. and Moore, E. J., 1984. Photogrammetry in sediment transport studies. In: George, D. (Ed.), *Underwater Photogrammetry and Television*

for Scientists. Clarendon Press, Oxford.

Williams, H .F. L. and Hamilton, T. S., 1995. Sedimentary dynamics of an eroding tidal marsh derived from stratigraphic records of ^{137}CS fallout, Frazer Delta, British Columbia, Canada. *J. Coastal Res.*, **11**, 1145-1156.

Williams, J. T., Thorne, P. D. and Heathershaw, A. D., 1989. Comparison between acoustic measurements and predictions of bedload transport of marine gravels. *Sedimentology*, **36**, 973-979.

Wimbush, M. and Munk, W., 1970. The benthic boundary layer. In: Maxwell, A. E.(Ed.), *The Sea Vol.4*. John Wiley, New York.

Wooding, R. A., Bradley, E. F. and Marshall, J. K., 1973. Drag due to regular arrays of roughness elements of varying geometry. *Boundary Layer Meteorology*, **5**, 285-308.

Woodworth, P. L., Shaw, S. M. and Blackman, D. L., 1991. Secular trends in mean sea tidal range around British Isles and along the adjacent European coastline. *Geophys. J. International.*, **104**, 593-609.

Wright, L. D., 1985. River delta. In: Davis Jr, R. A. (Ed.) *Coastal Sedimentary Environments*. Springer-Verlag, New York, 1-76.

Yalin, M. S., 1963. An expression for bed-load transportation. *J. Hydraul. Div., Proc. ASCE.*, **HY3**, 221-250.

Yalin, M. S., 1972. *Mechanics of Sediment Transport*. Pergamon, Oxford. 290 p.

Yang, C. T., 1973. Incipient motion and sediment transport. *J. Hydraul. Div., Proc. ASCE.* **HY10**, 1679-1704.

Young, R. A., 1977. Seaflume: a device for *in-situ* studies of erosion velocity and erosional behaviour of undisturbed marine muds. *Mar. Geol.*, **23**, M11-M18.

Zabawa, C. F., 1978. Microstructure of agglomerated suspended sediments in the northern Chesapeake Bay estuary. *Science* , **202**, 49-51.

APPENDIX A

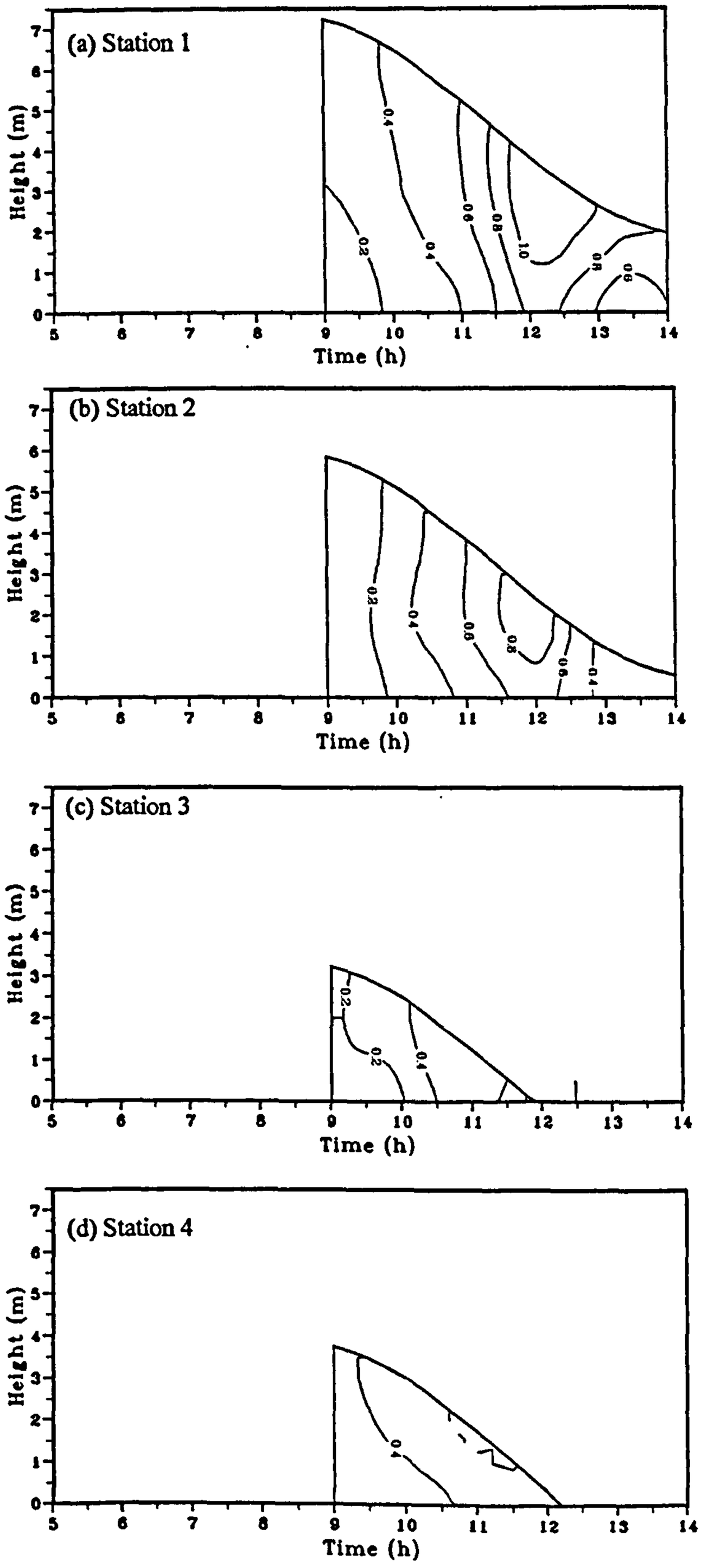

Figure A.01 Time series contour plots of current velocity (m/s) at stations 1-4, 12 September 1995.

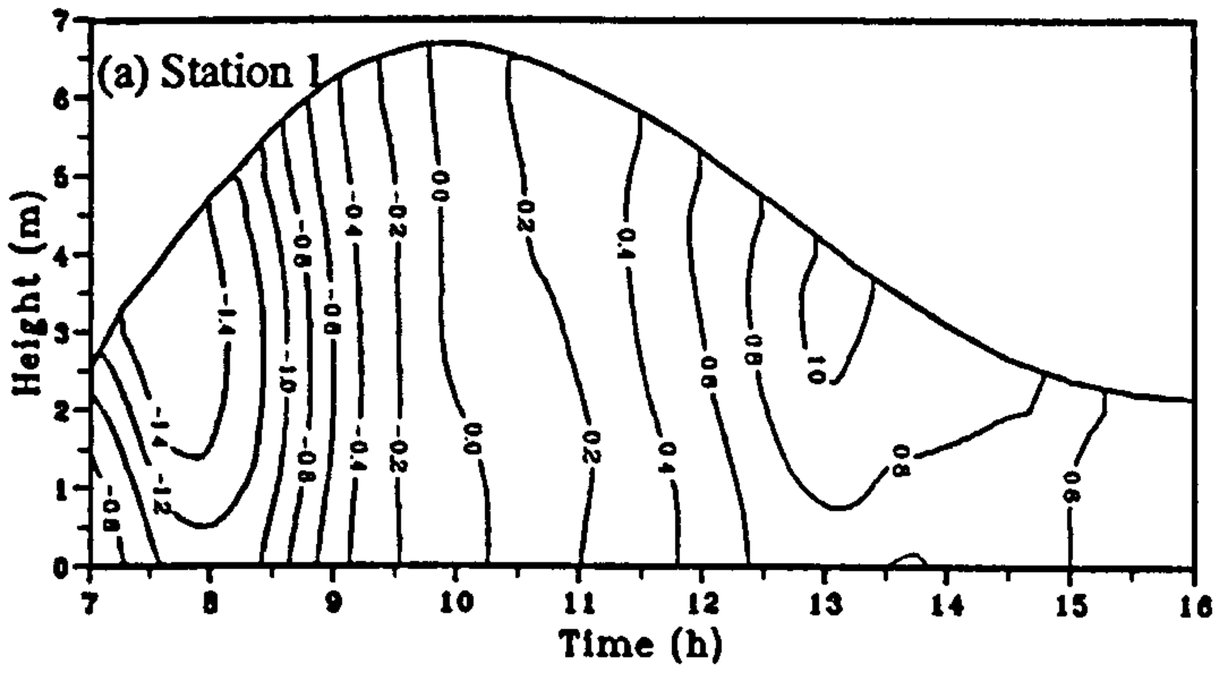

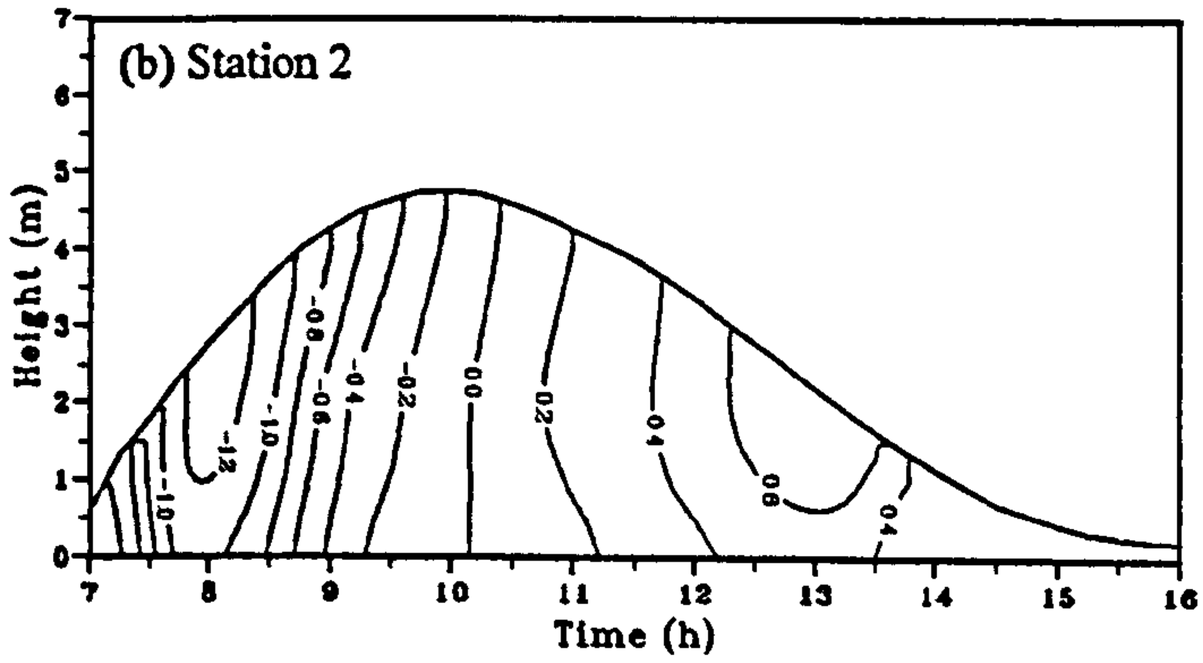

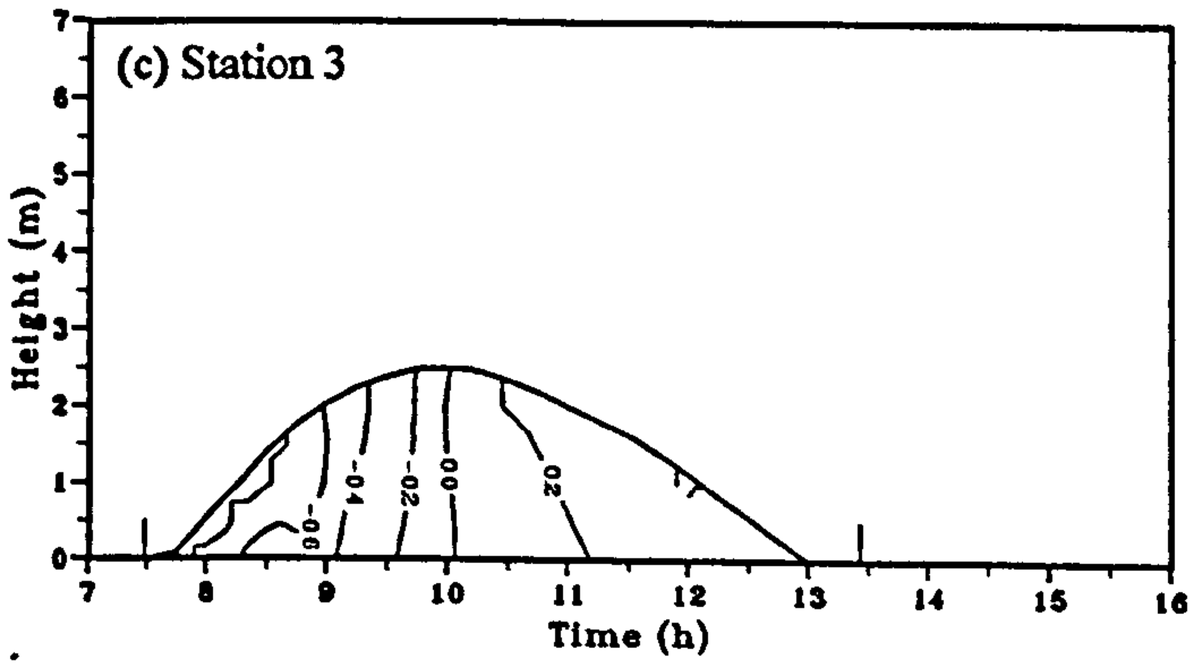

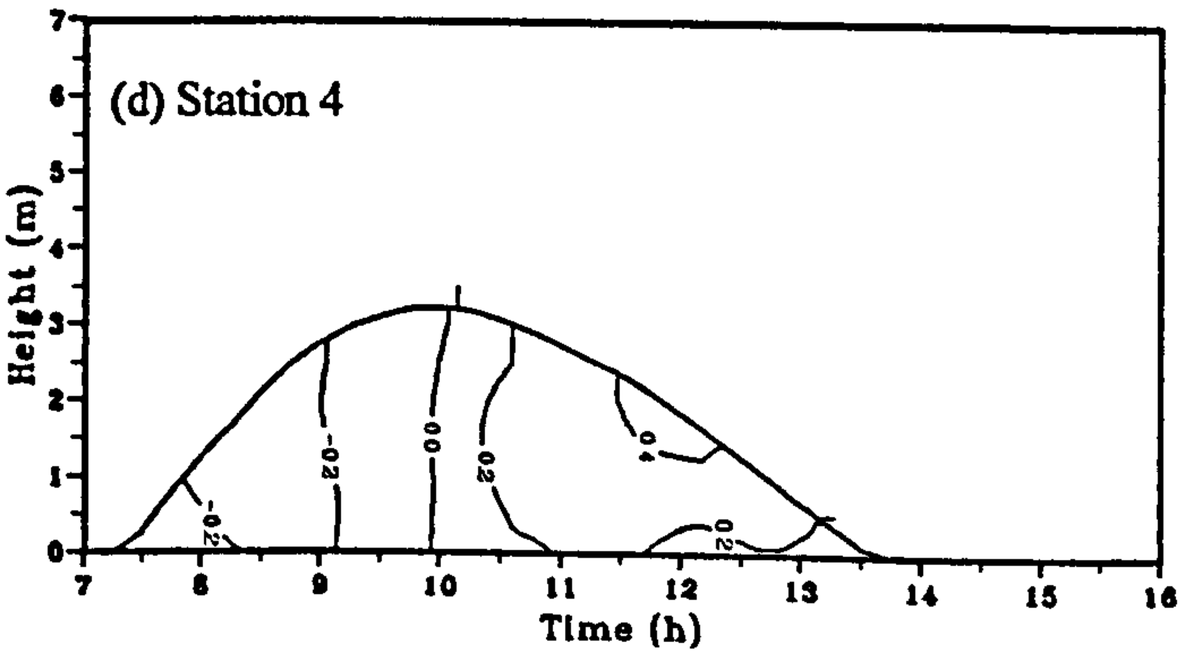

Figure A.02 Time series contour plots of current velocity (m/s) at stations 1- 4, 14 September 1995.

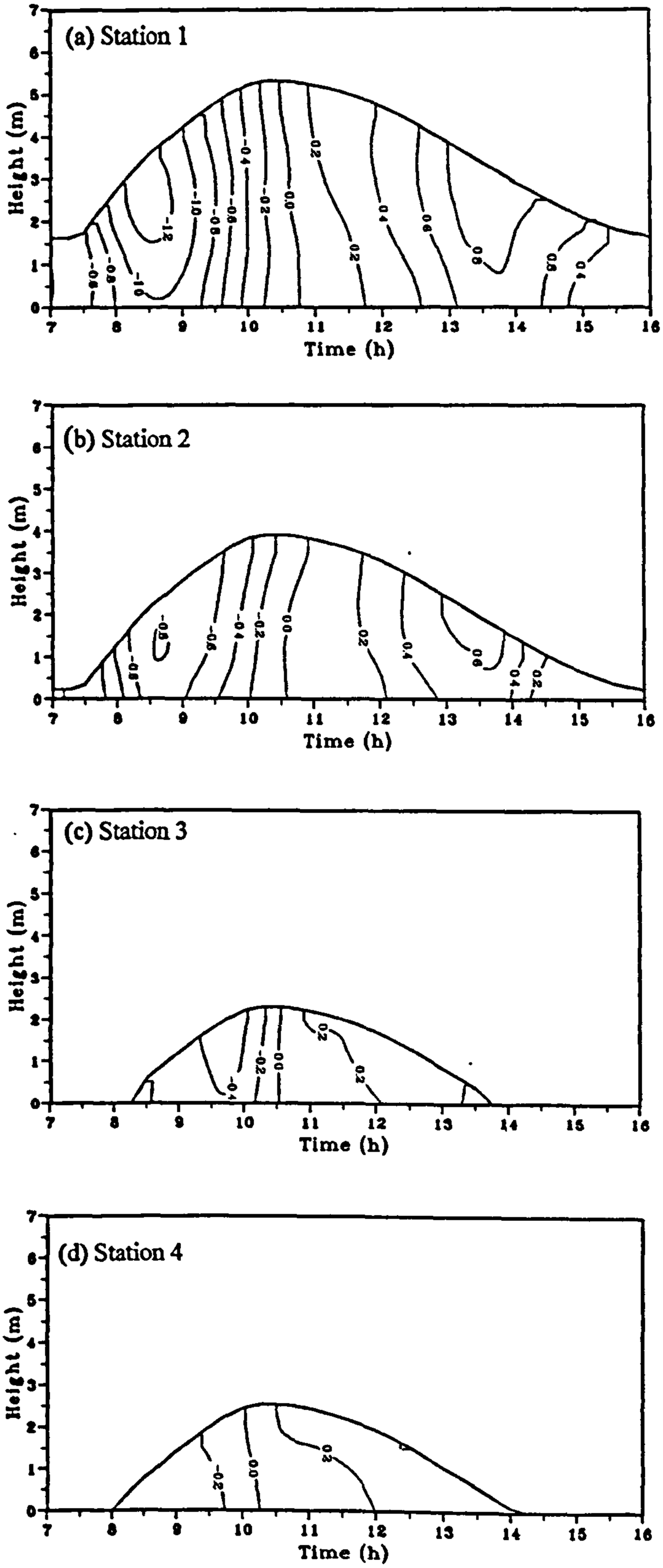

Figure A.03 Time series contour plots of current velocity (m/s) at stations 1-4, 15 September 1995.

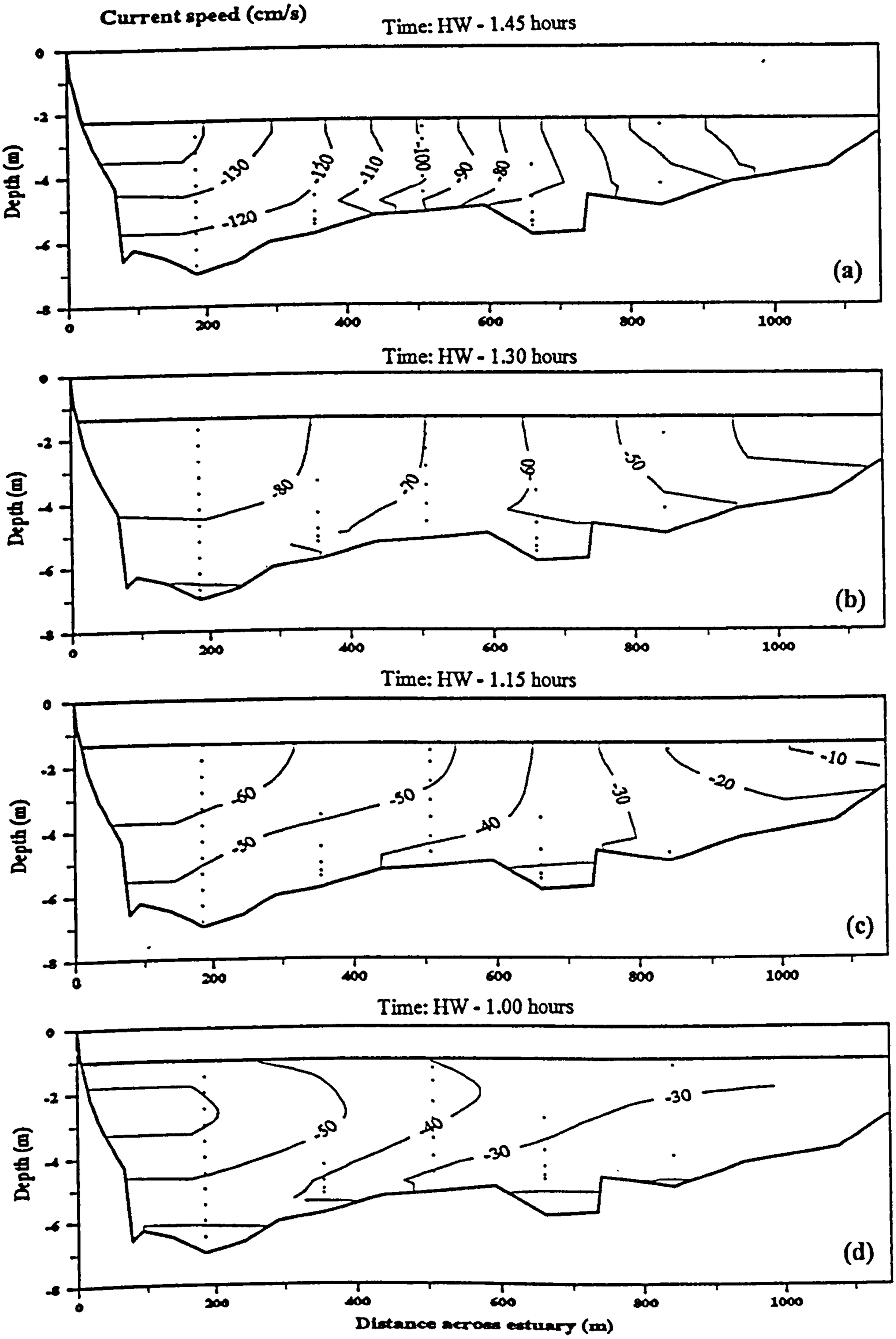

Figure A.04 Cross estuary contour plots of current velocity (cm/s) at different stages of the tide, 6 October 1994.

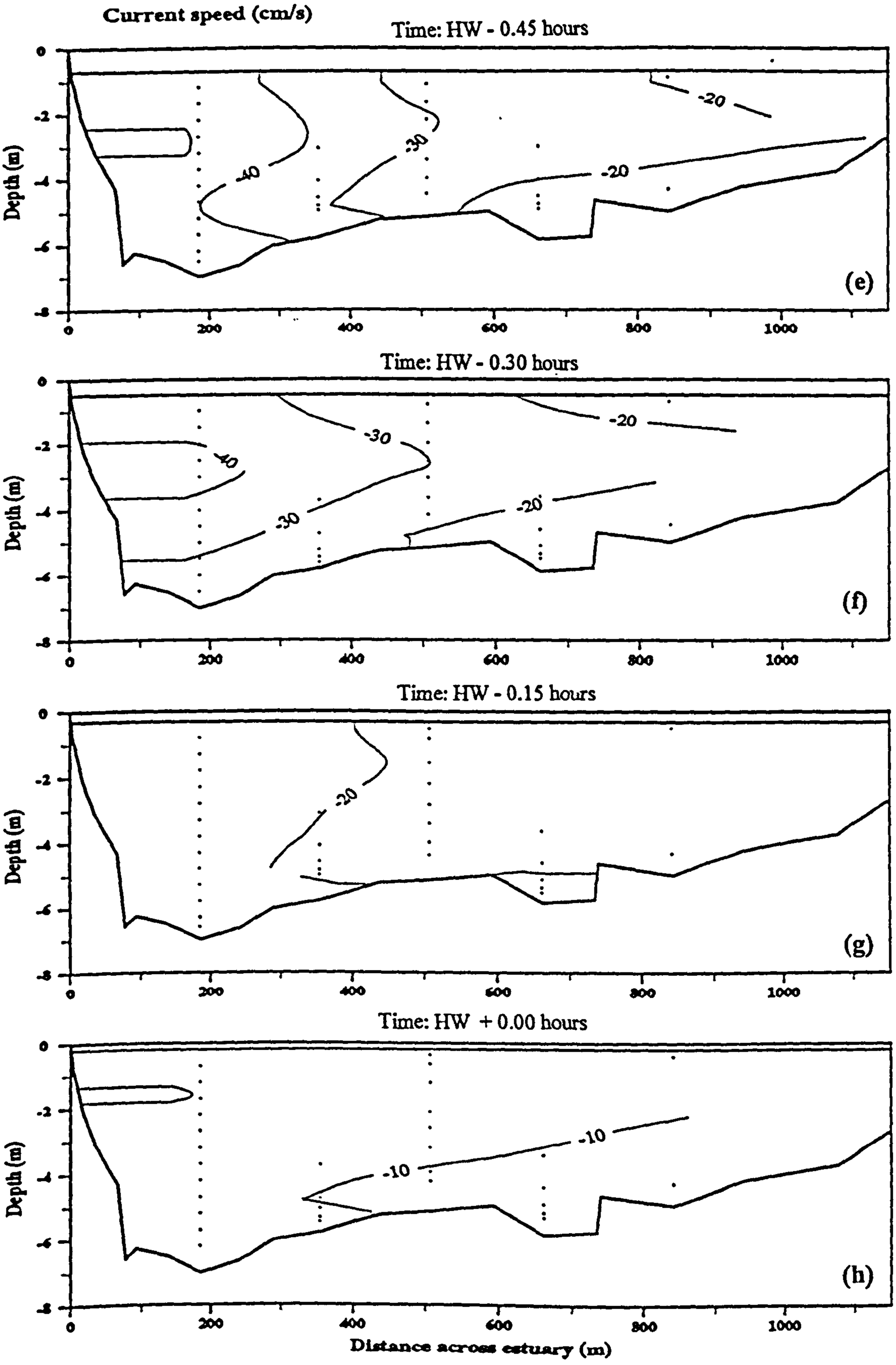

Figure A.04 (continued)

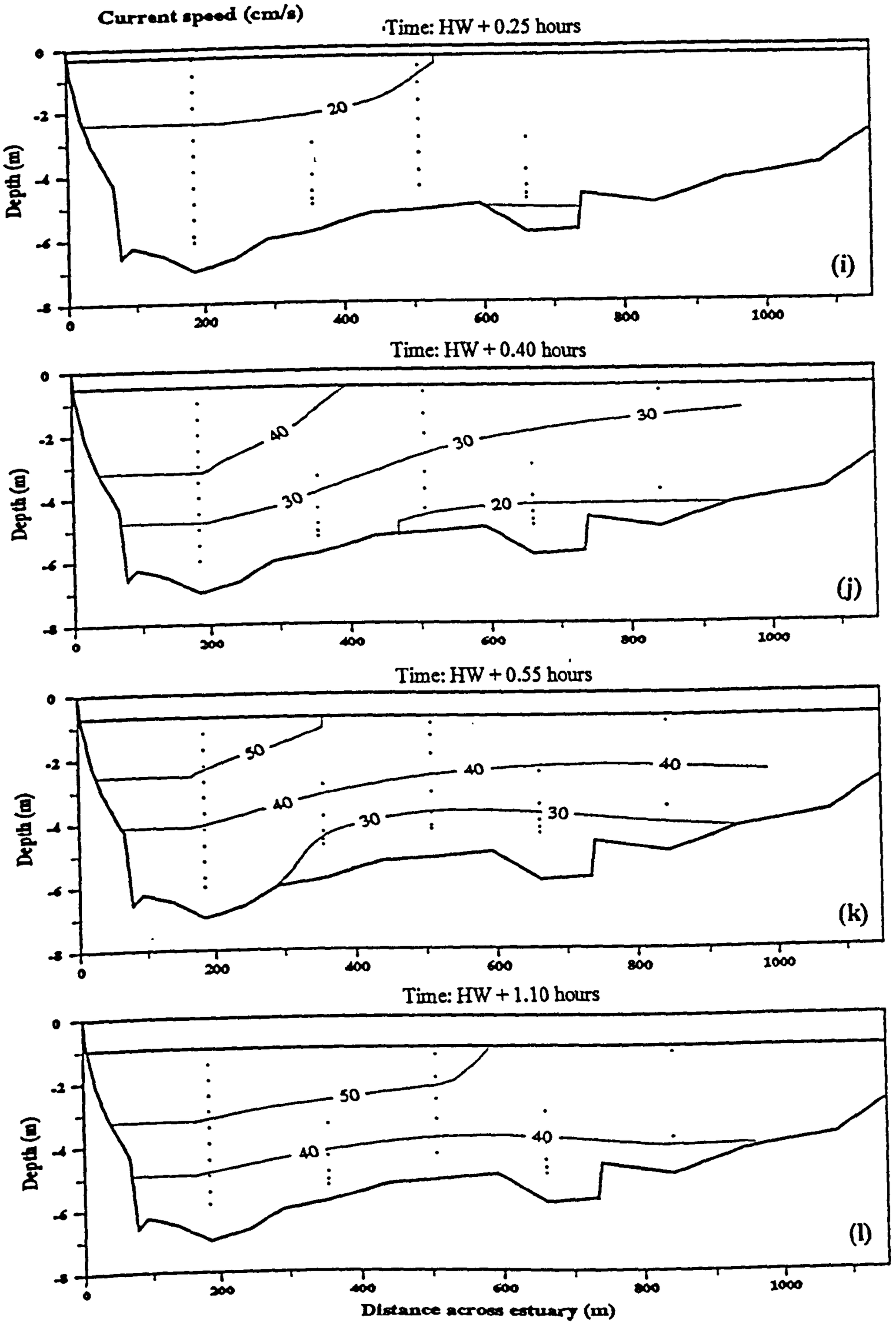

Figure A.04 (continued)

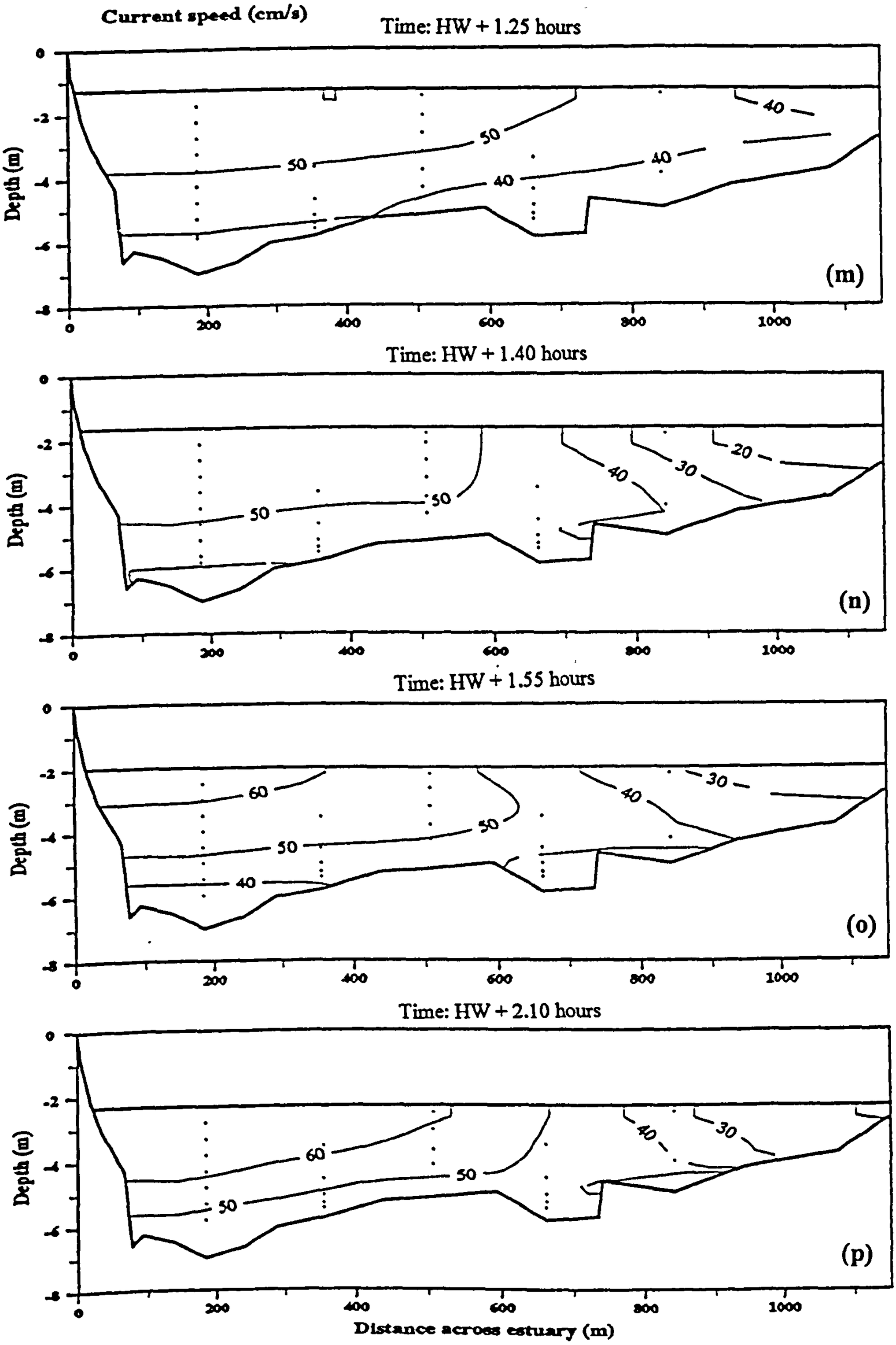

Figure A.04 (continued).

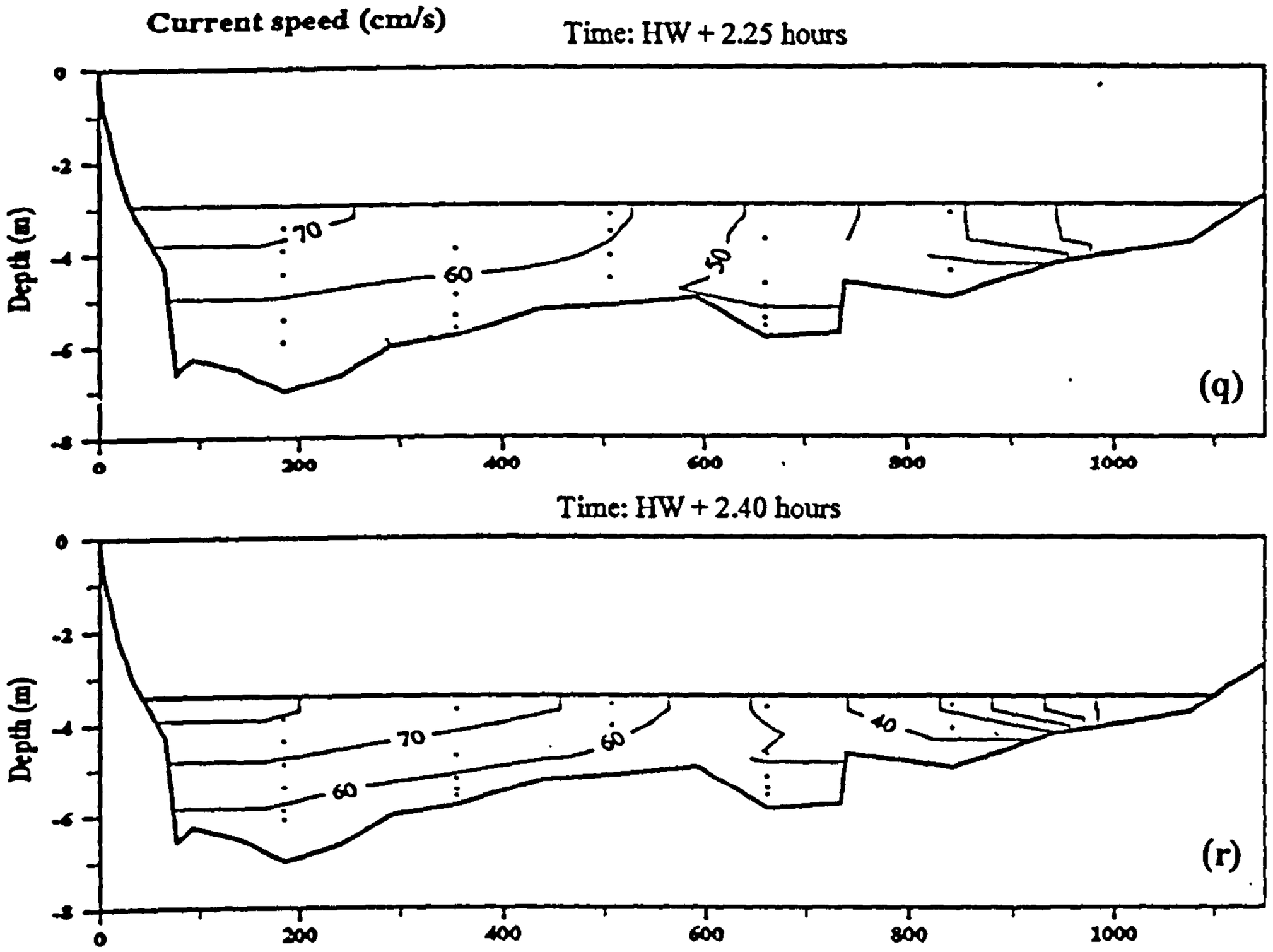

Figure A.04 (continued)

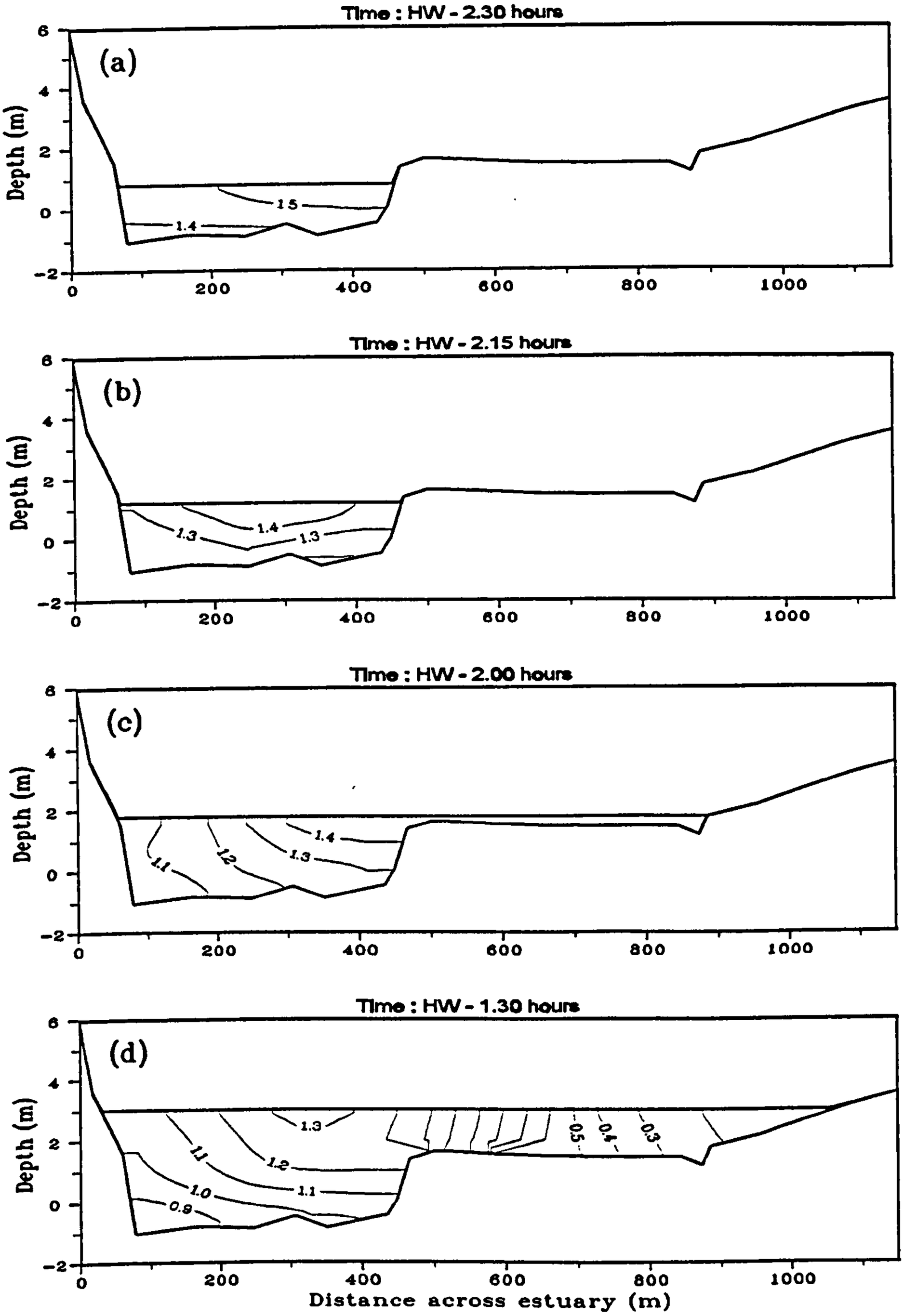

Figure A.05 Cross estuary contour plots of tidal velocity (m/s) at different stages of the tide, 16 July 1995.

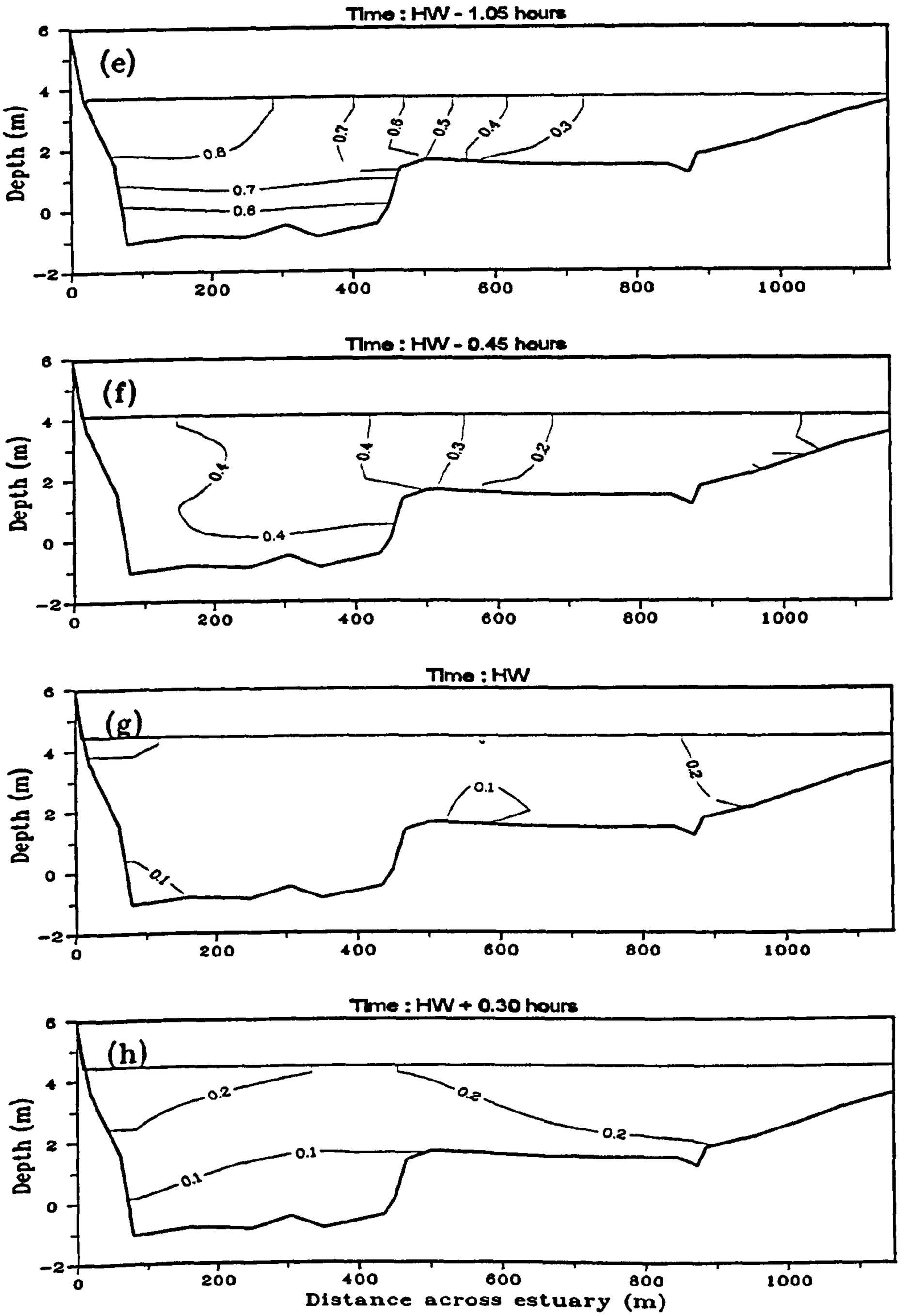

Figure A.05 (Continued).

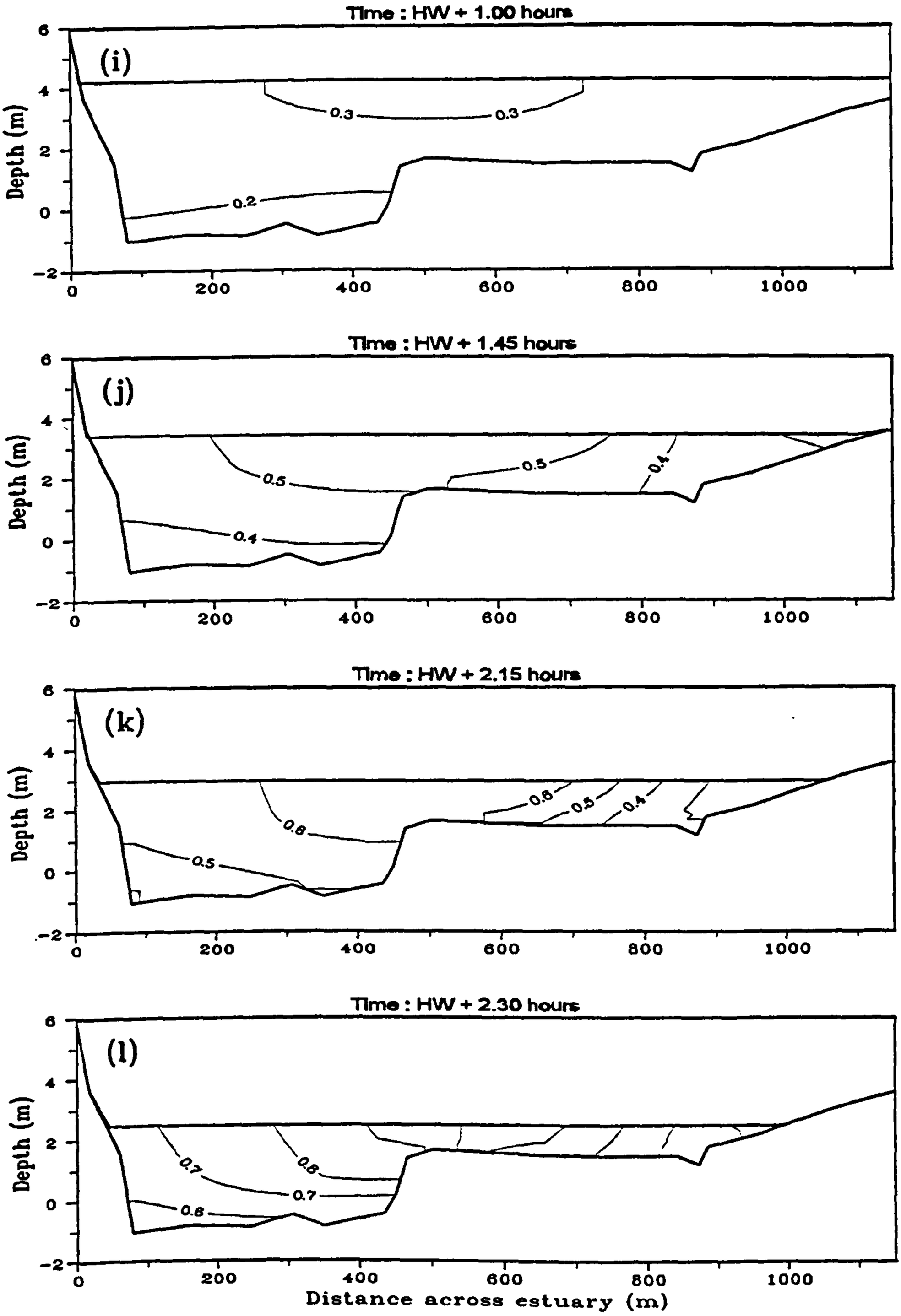

Figure A.05 (Continued).

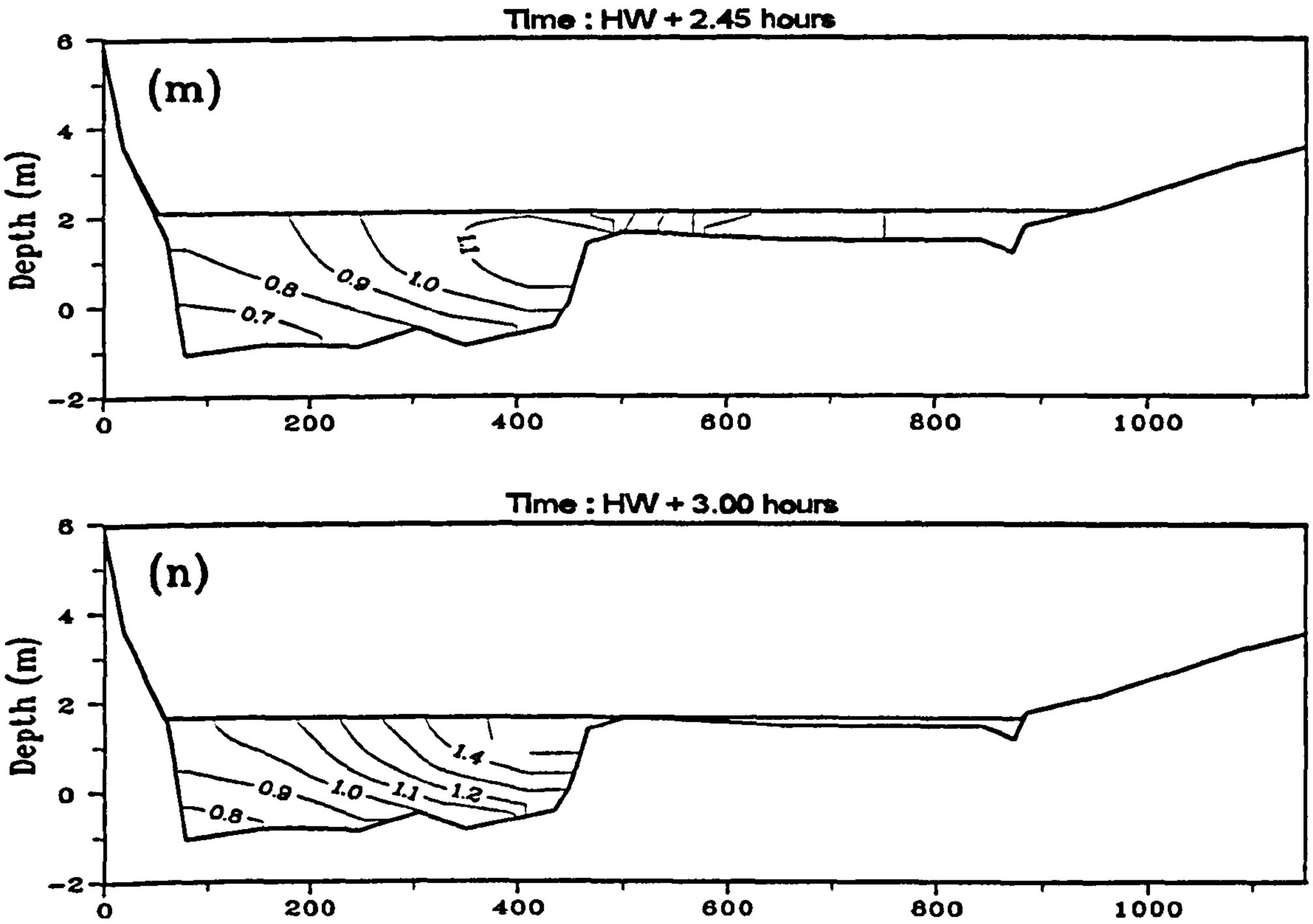

Figure A.05 (Continued).

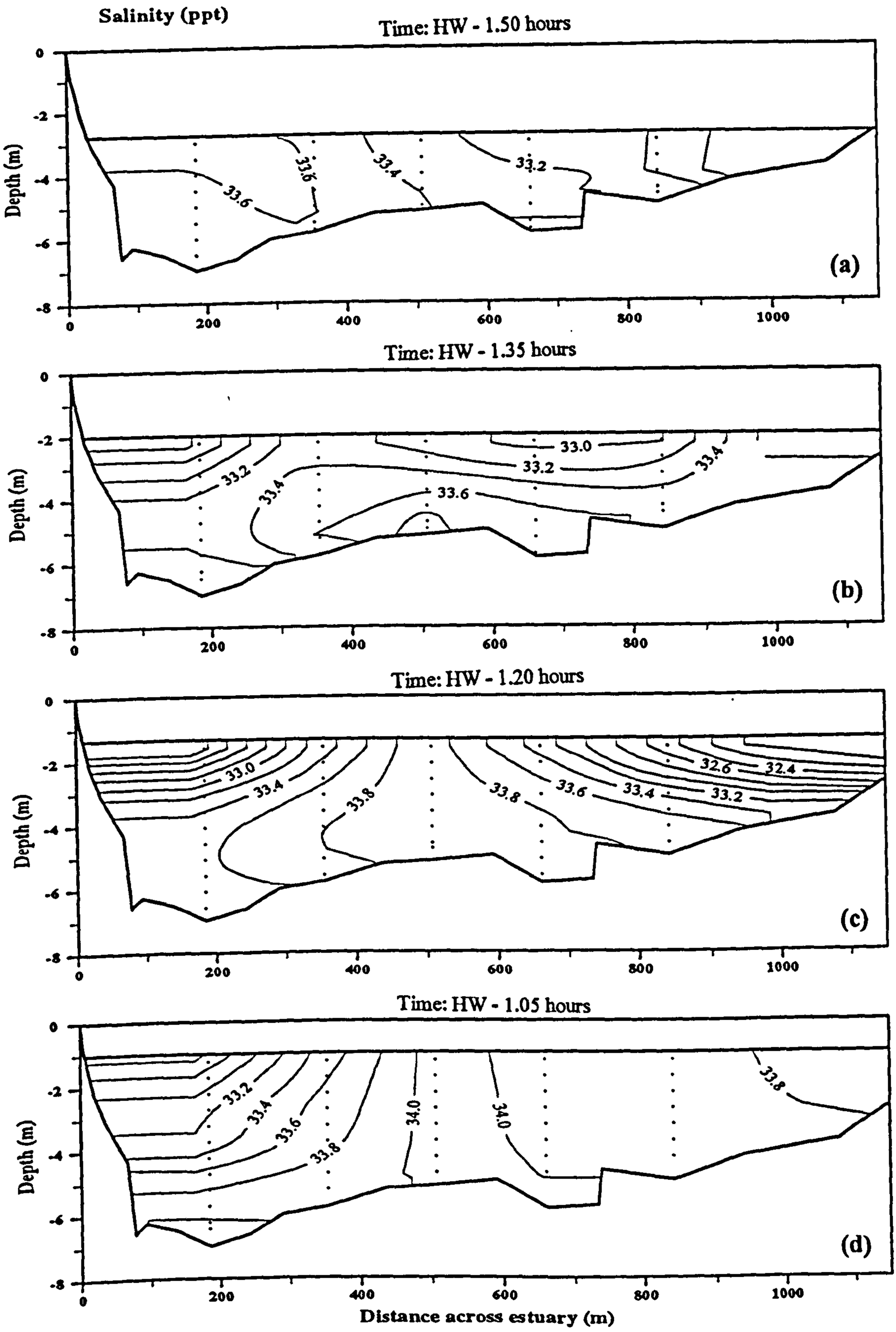

Figure A.06 Cross estuary contour plots of salinity (ppt) at different stages of the tide, spring tide, 6 October 1994.

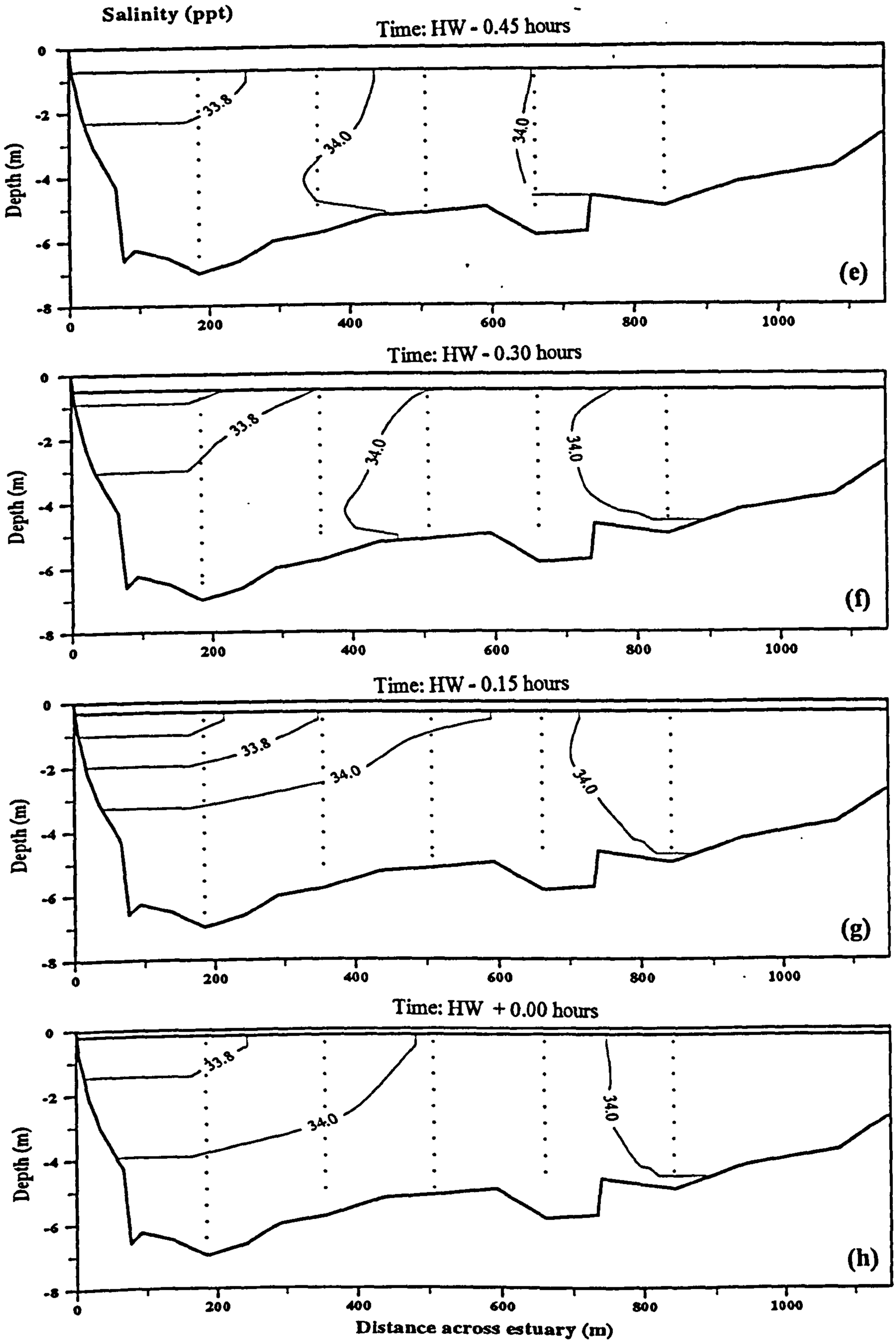

Figure A.06 (continued).

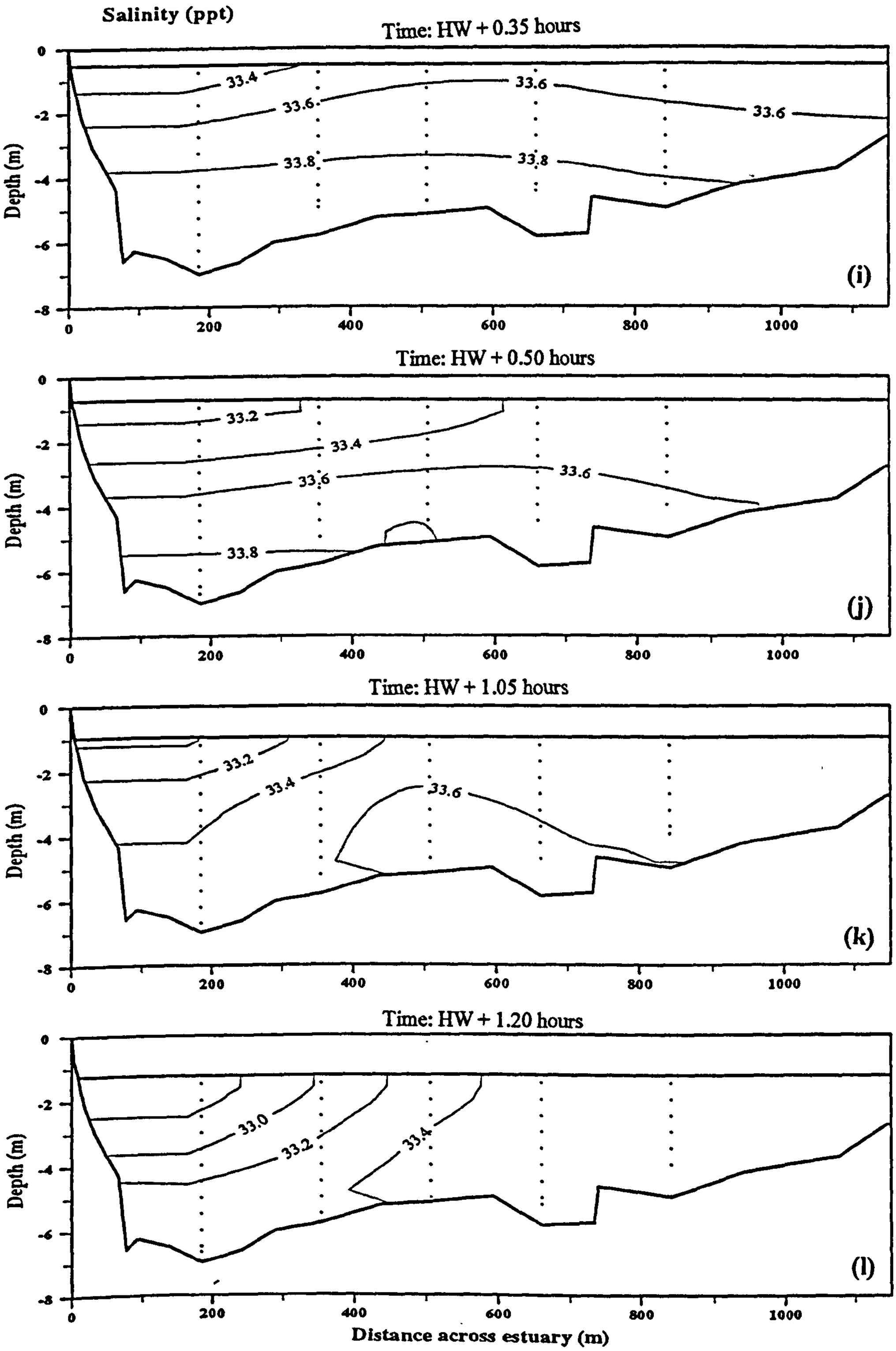

Figure A.06 (continued).

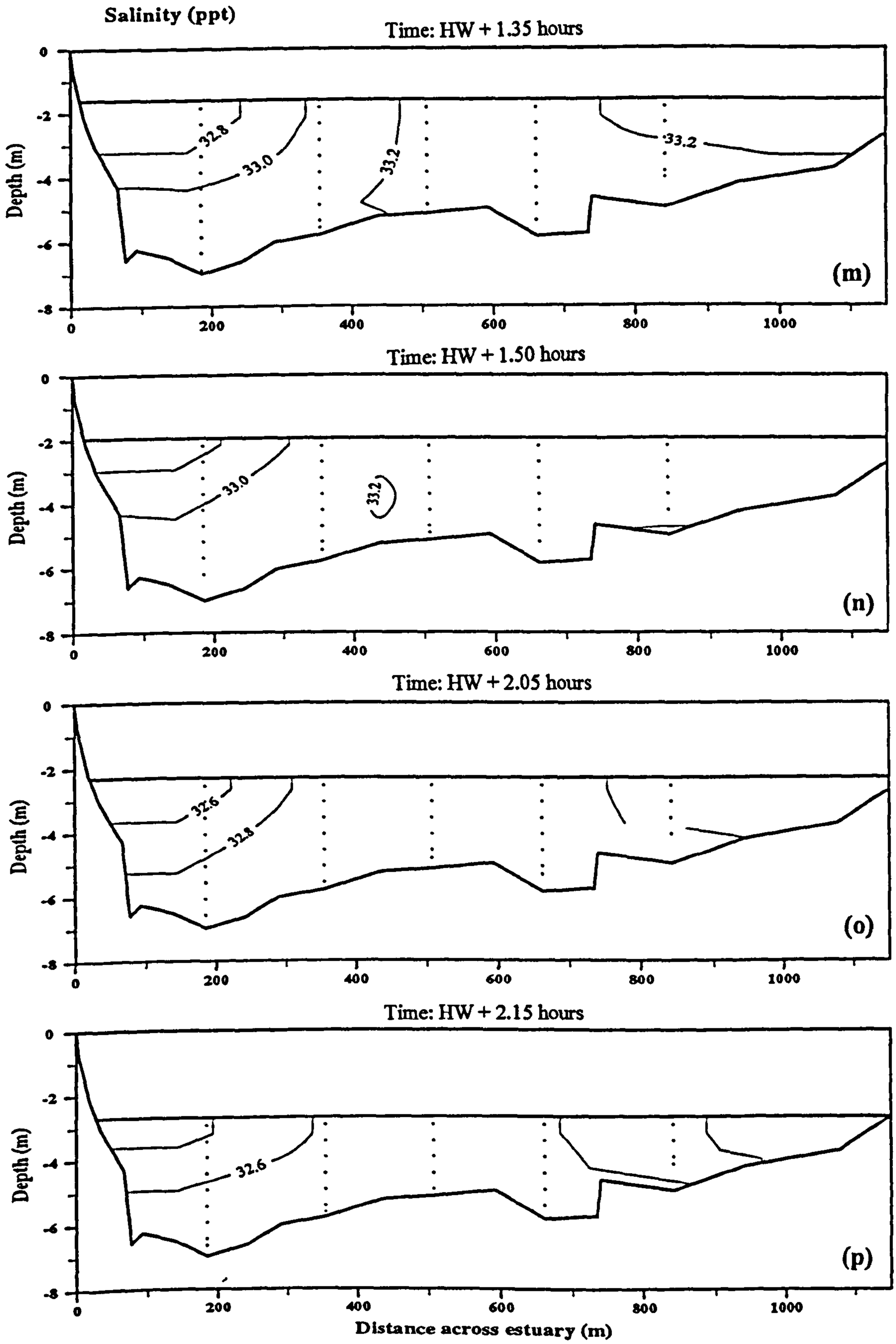

Figure A.06 (continued).

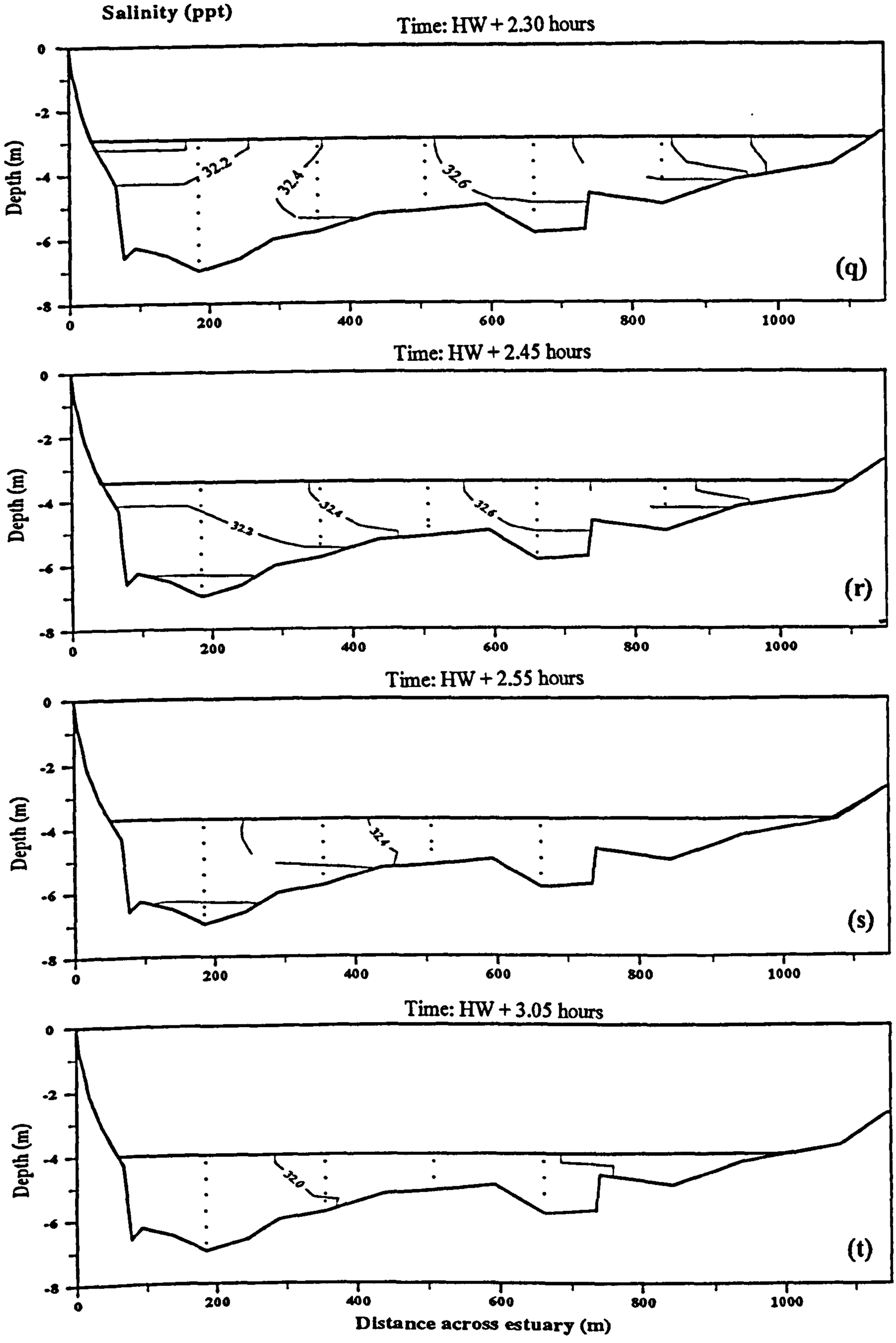

Figure A.06 (continued).

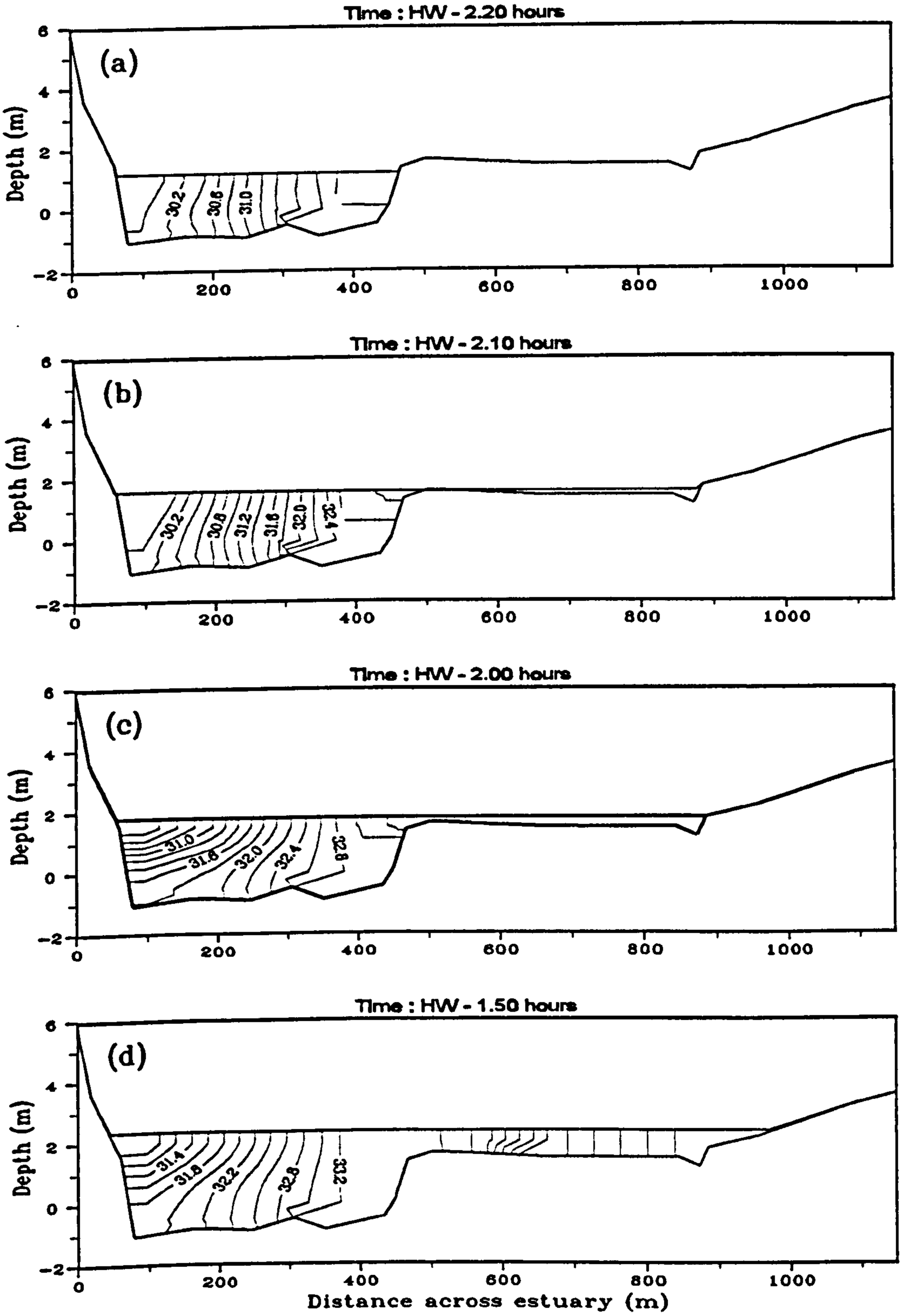

Figure A.07 Cross estuary contour plots of salinity (ppt) at different stages of the tide, spring tide, 16 July 1995.

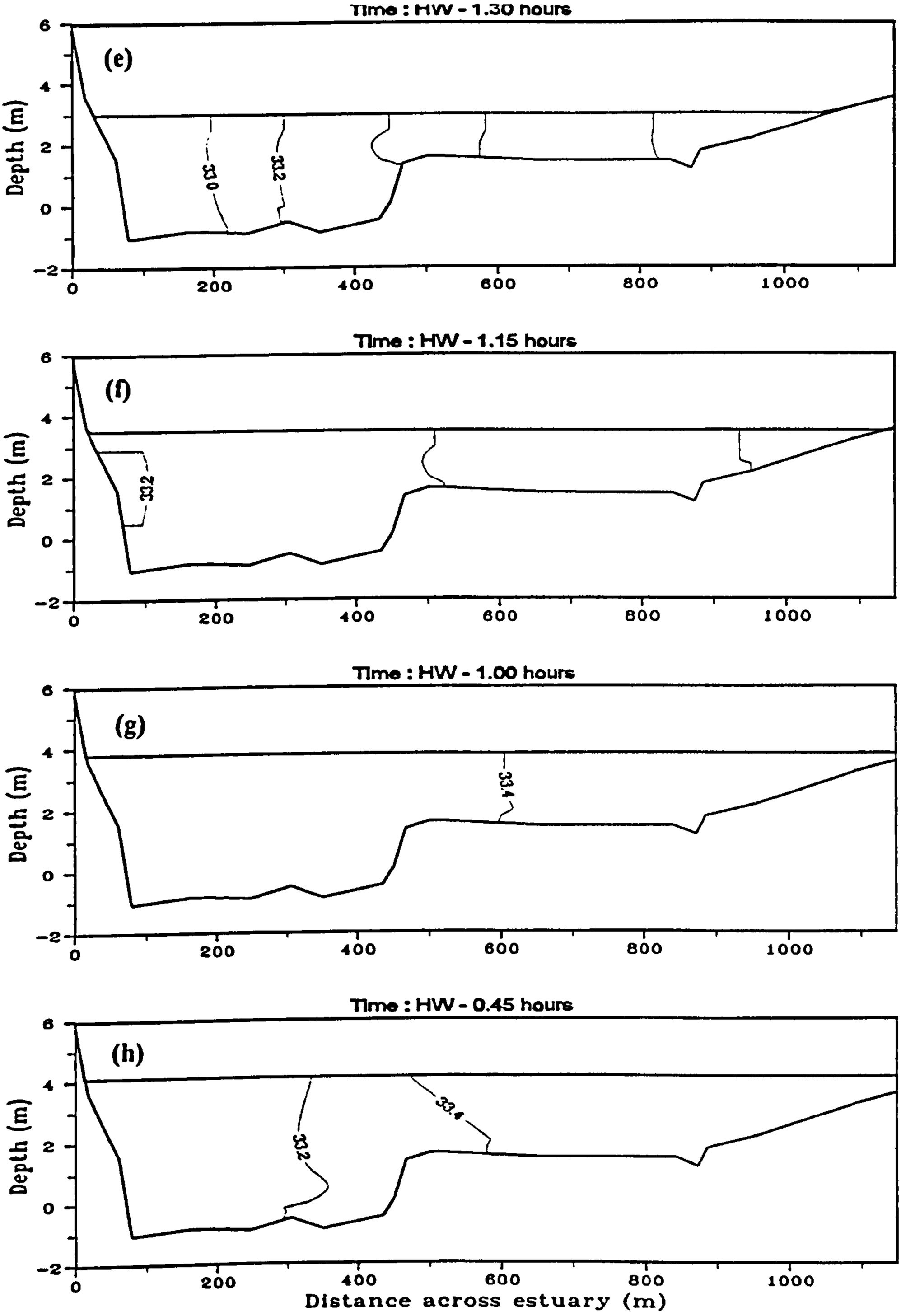

Figure A.07 (continued).

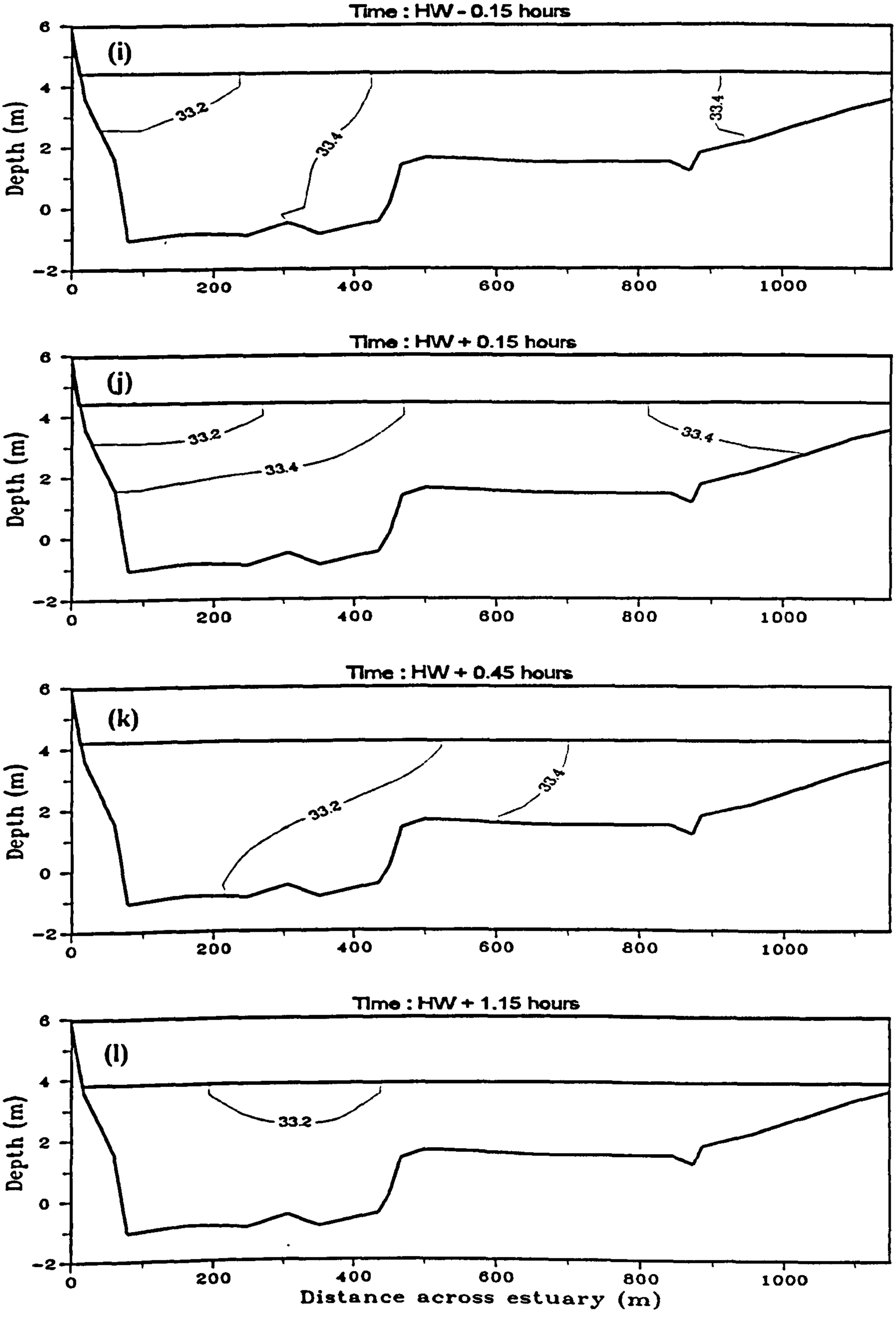

Figure A.07 (continued).

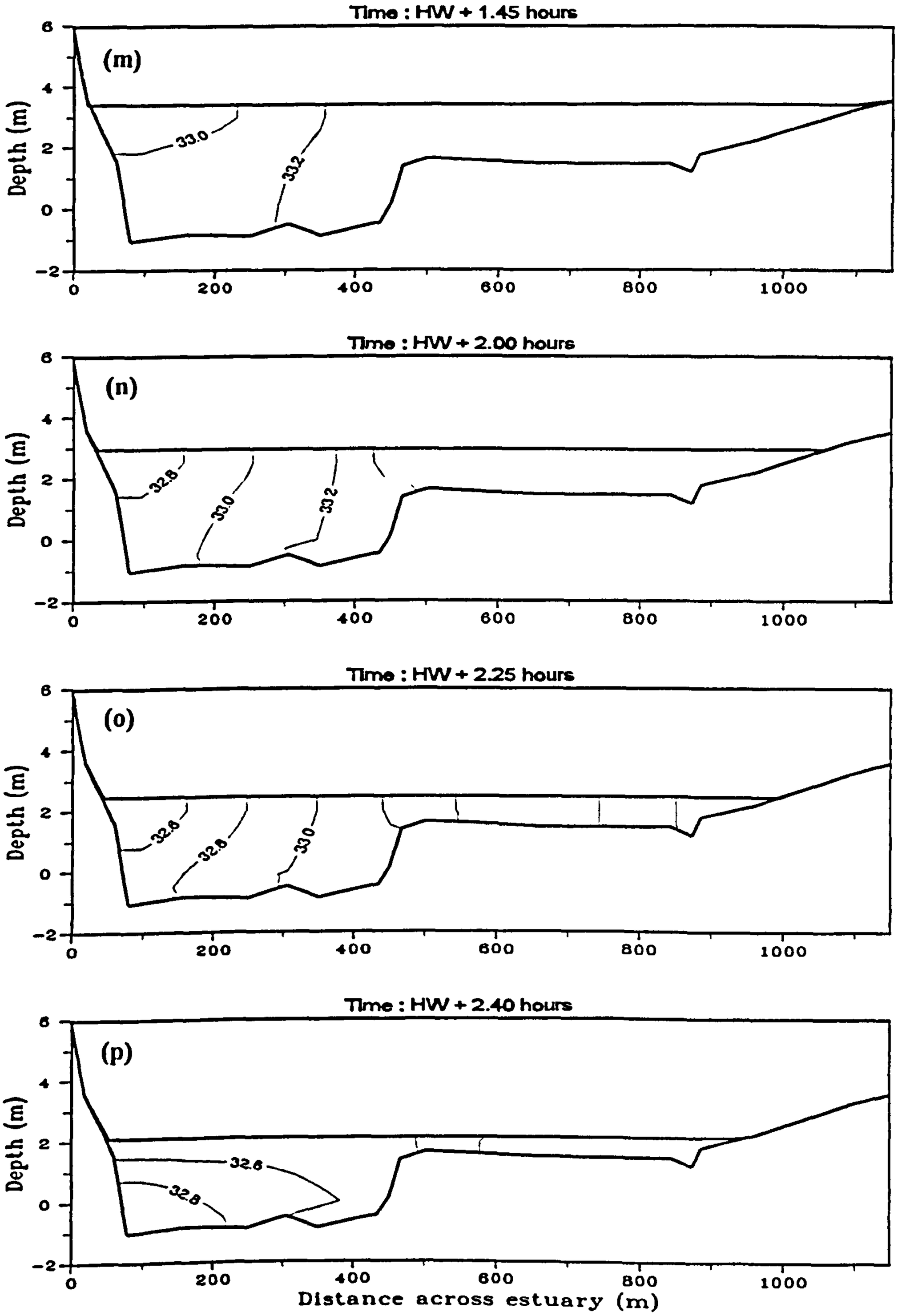

Figure A.07 (continued).

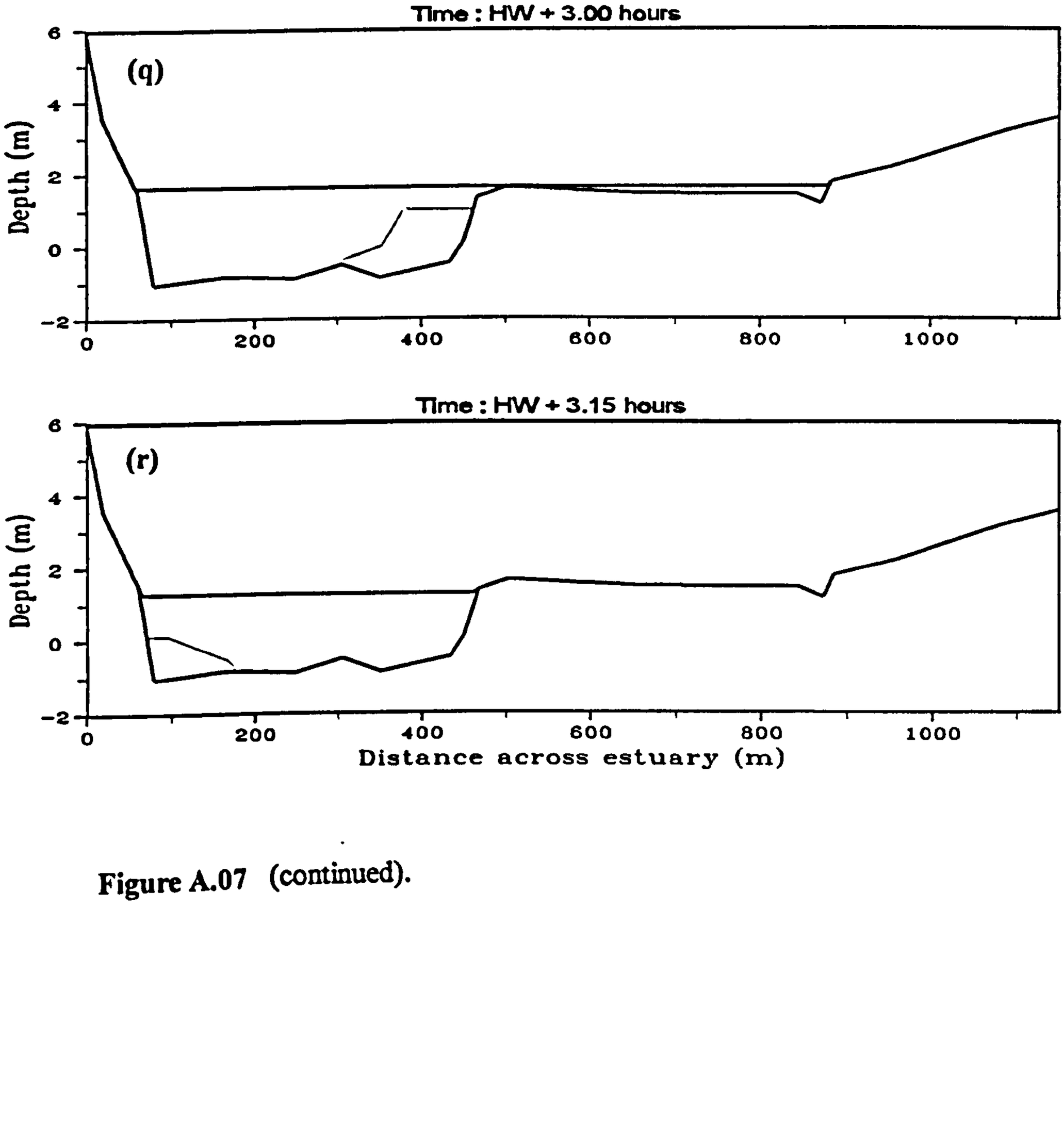

Figure A.07 (continued).

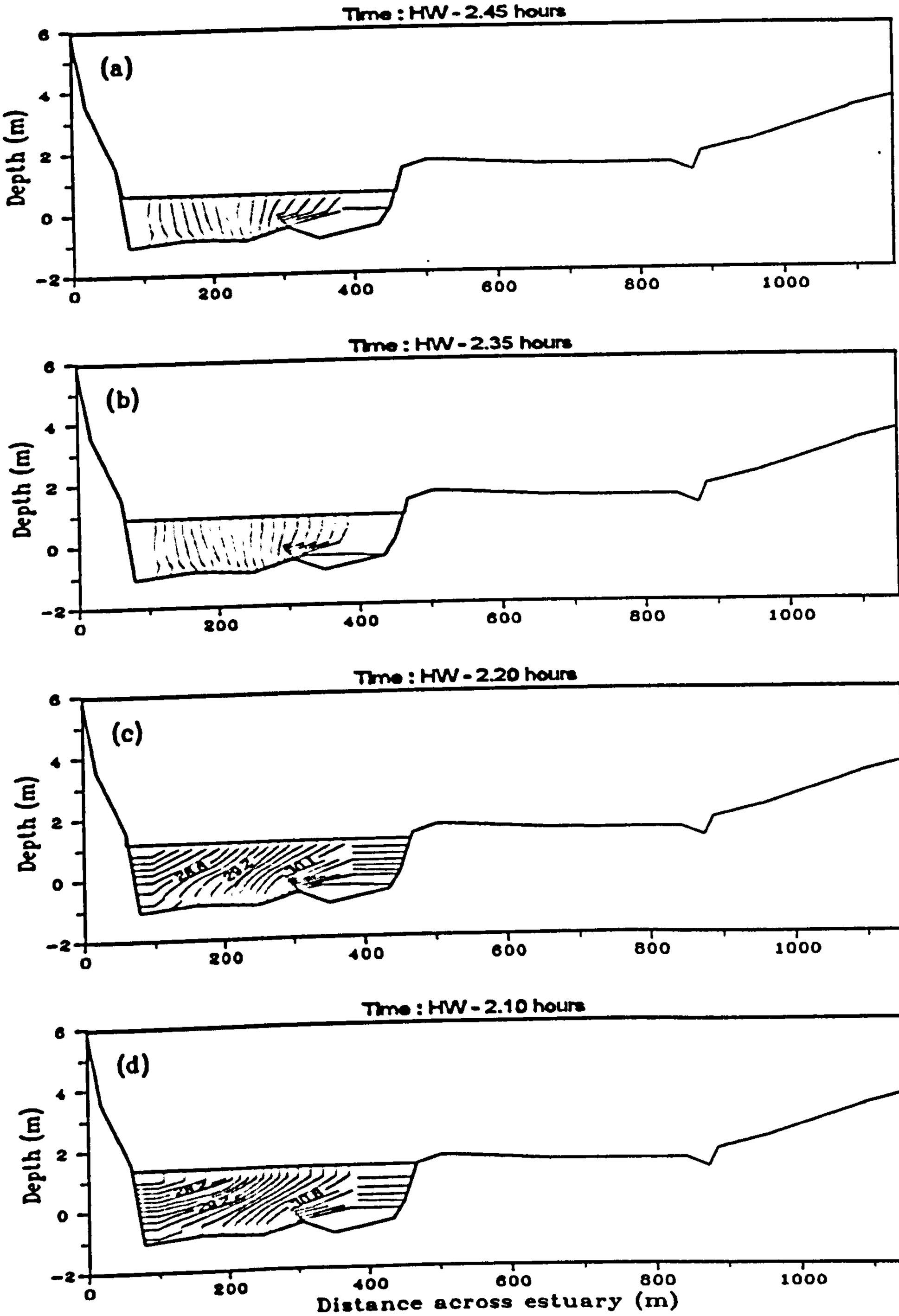

Figure A.08 Cross estuary contour plots of salinity (ppt) at different stages of the tide, neap tide, 20 July 1995.

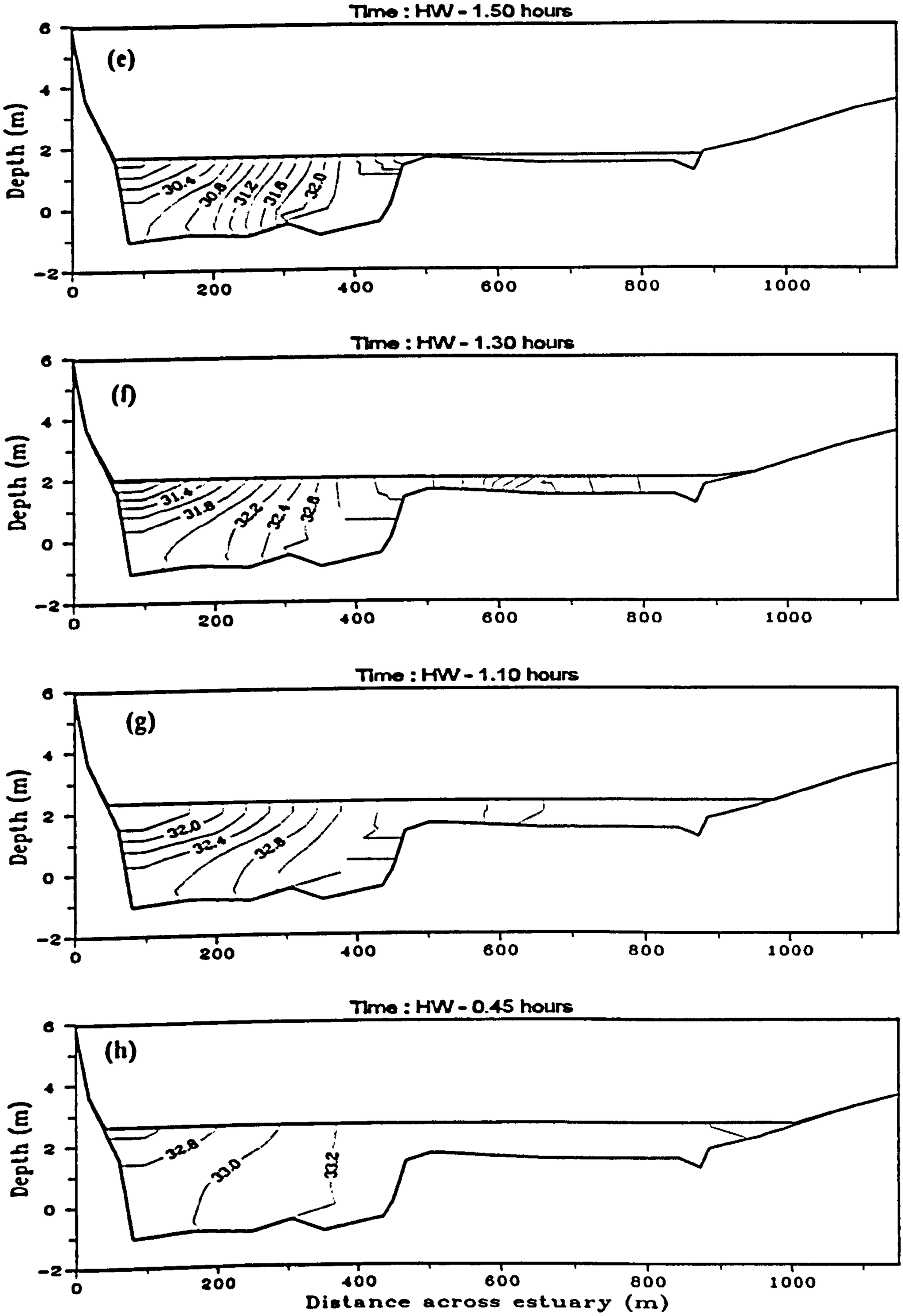

Figure A.08 (continued).

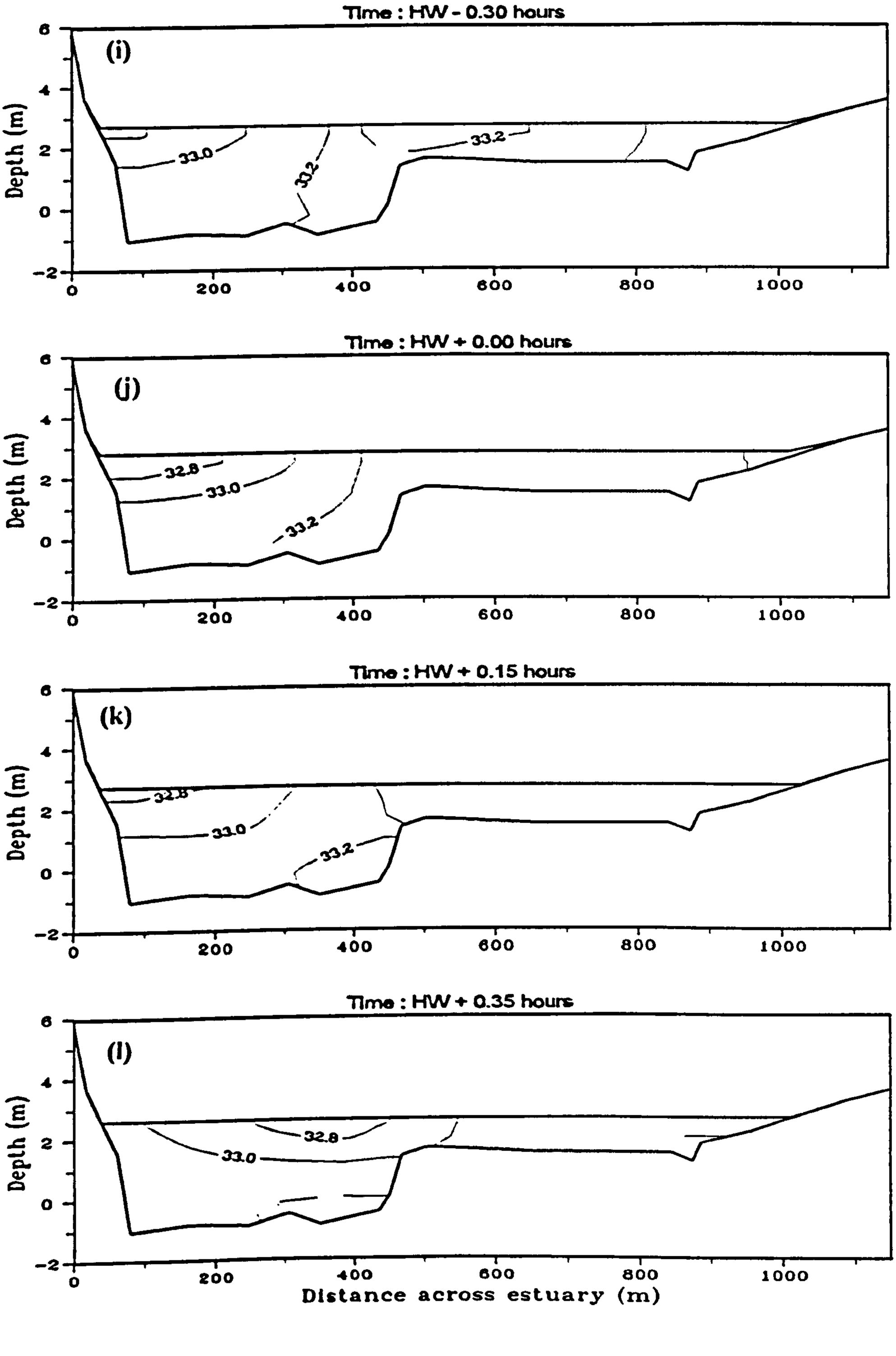

Figure A.08 (continued).

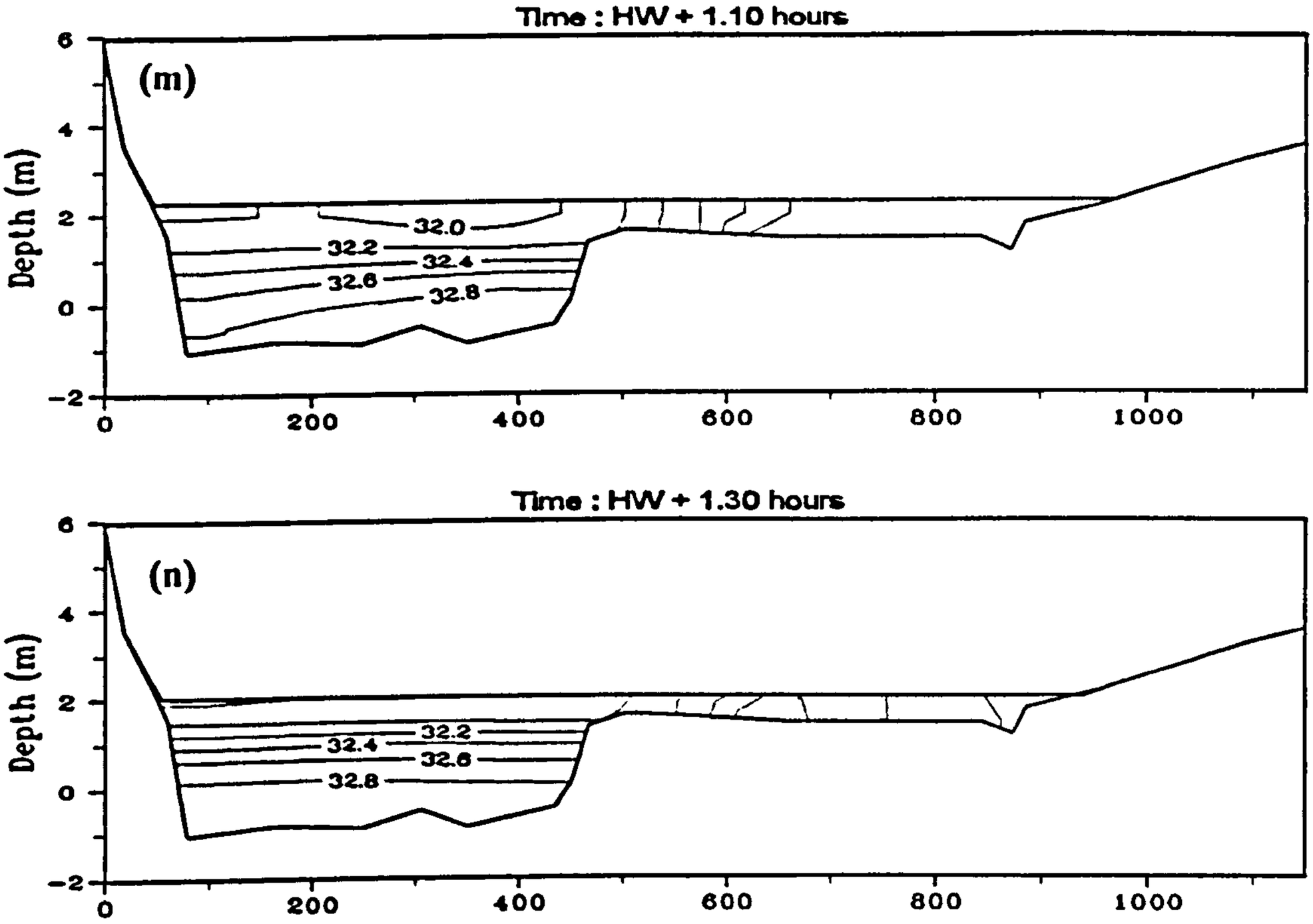

Figure A.08 (continued).

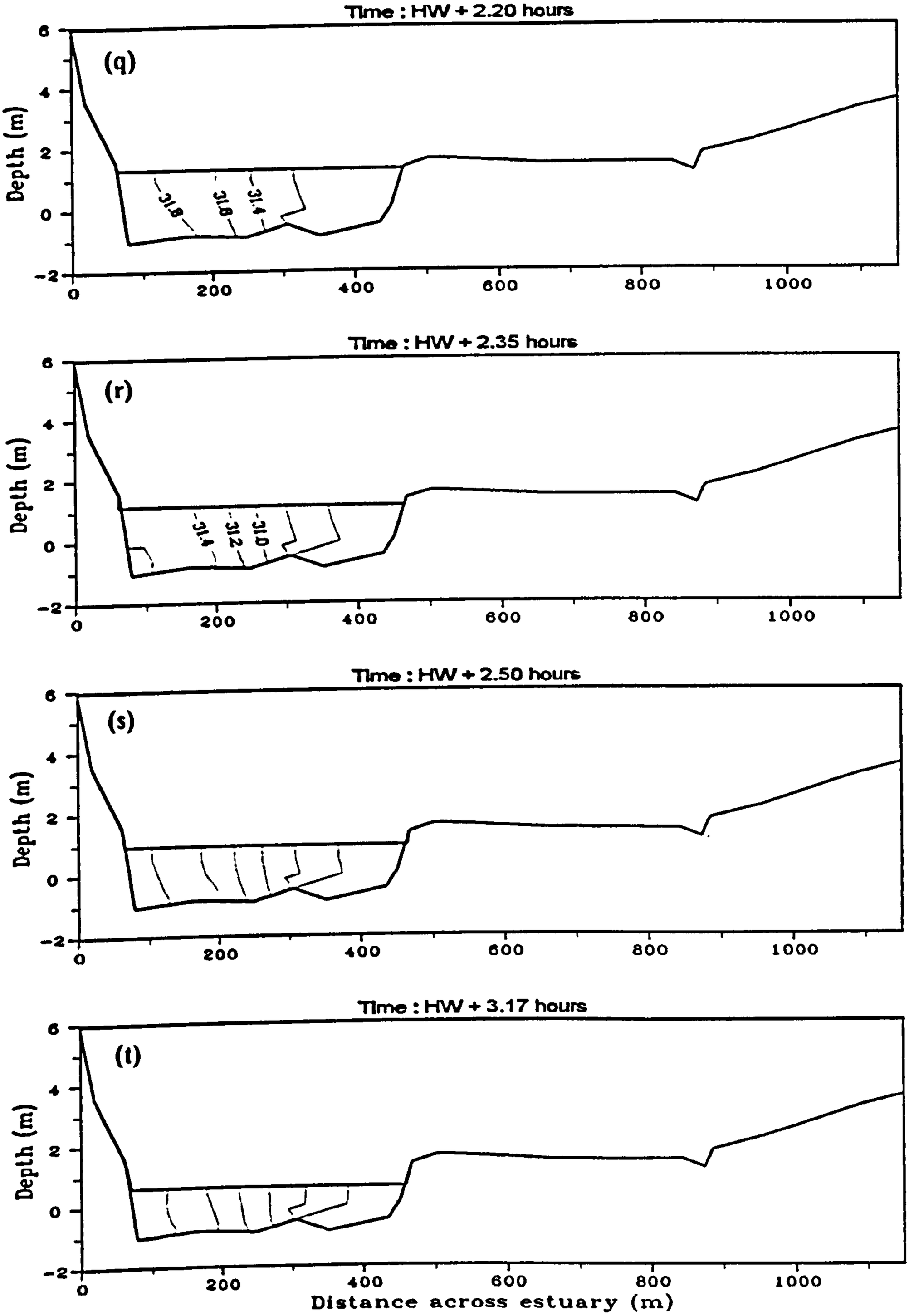

Figure A.08 (continued).

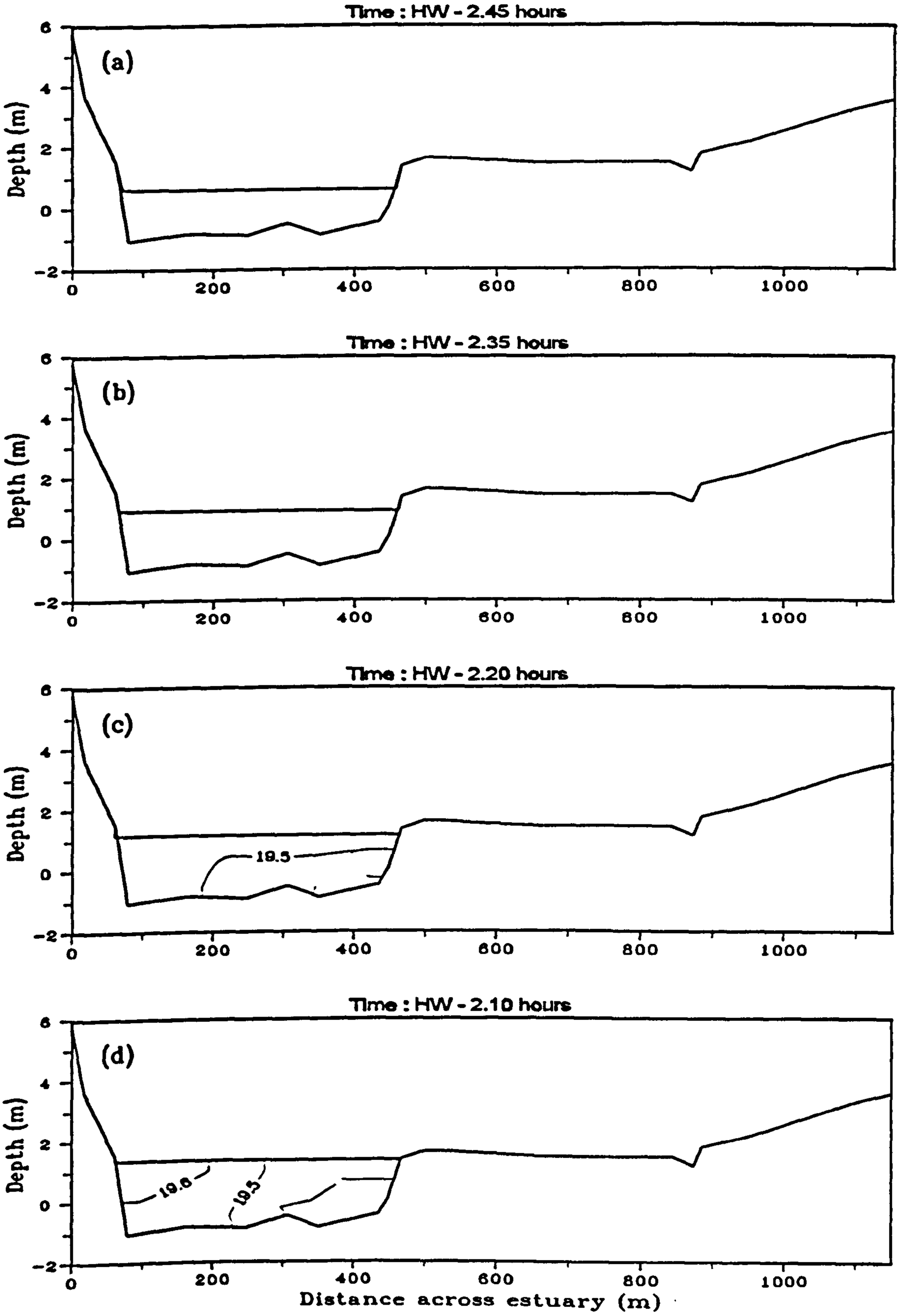

Figure A.09 Temperature (°C) profile across the estuary at different stages of the tide, neap tide, 20 July 1995.

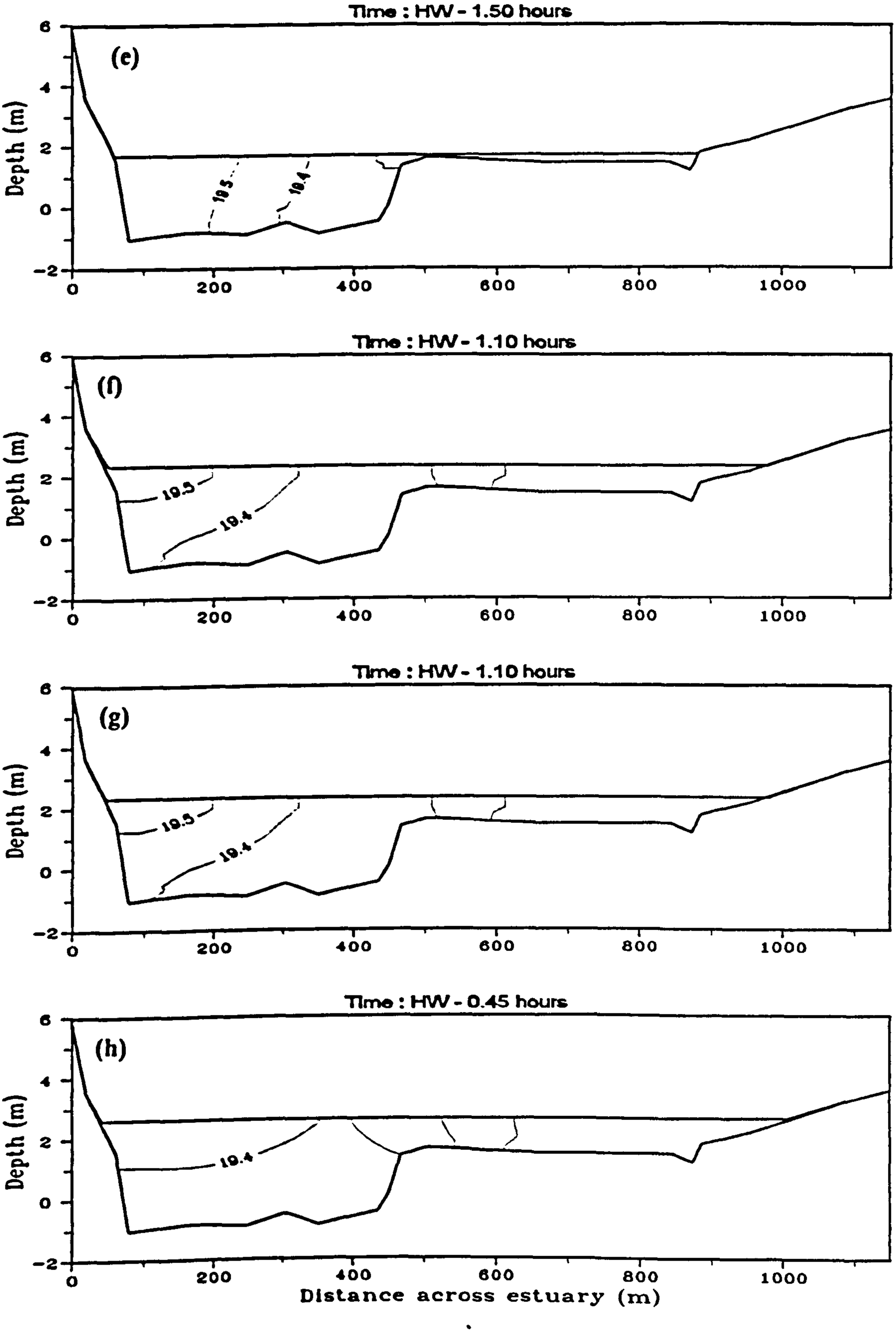

Figure A.09 (continued).

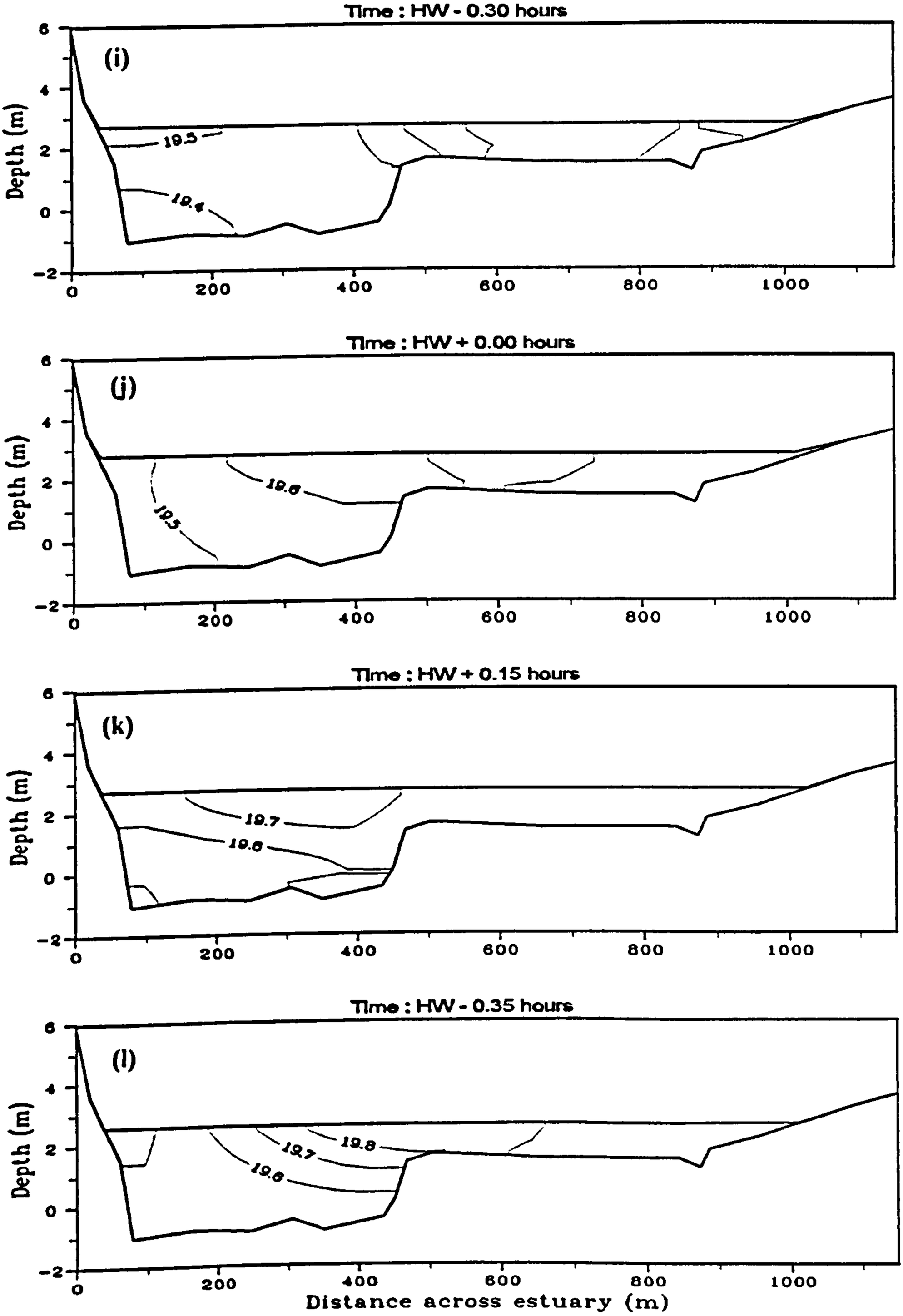

Figure A.09 (continued).

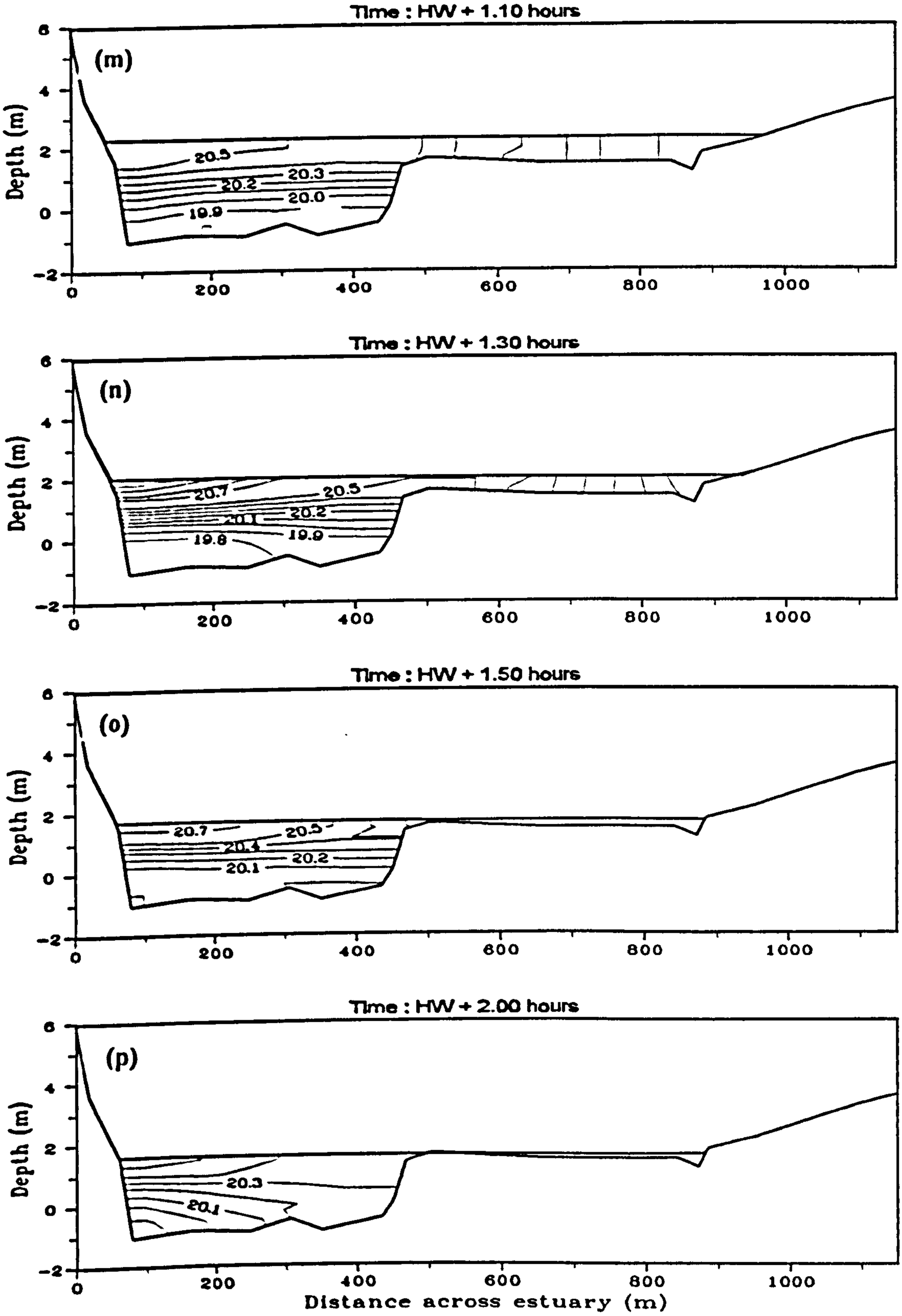

Figure A.09 (continued).

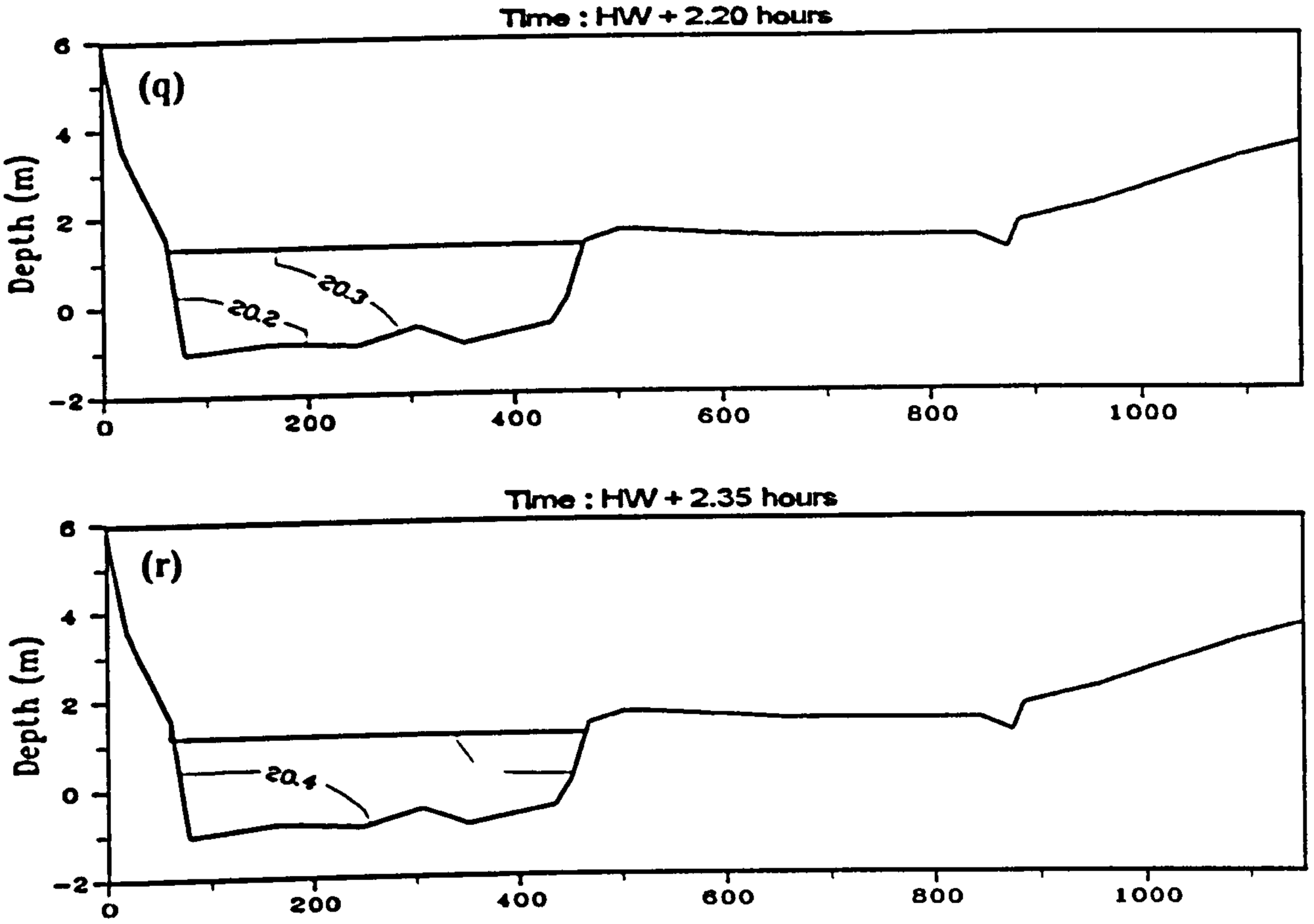

Figure A.09 (continued).

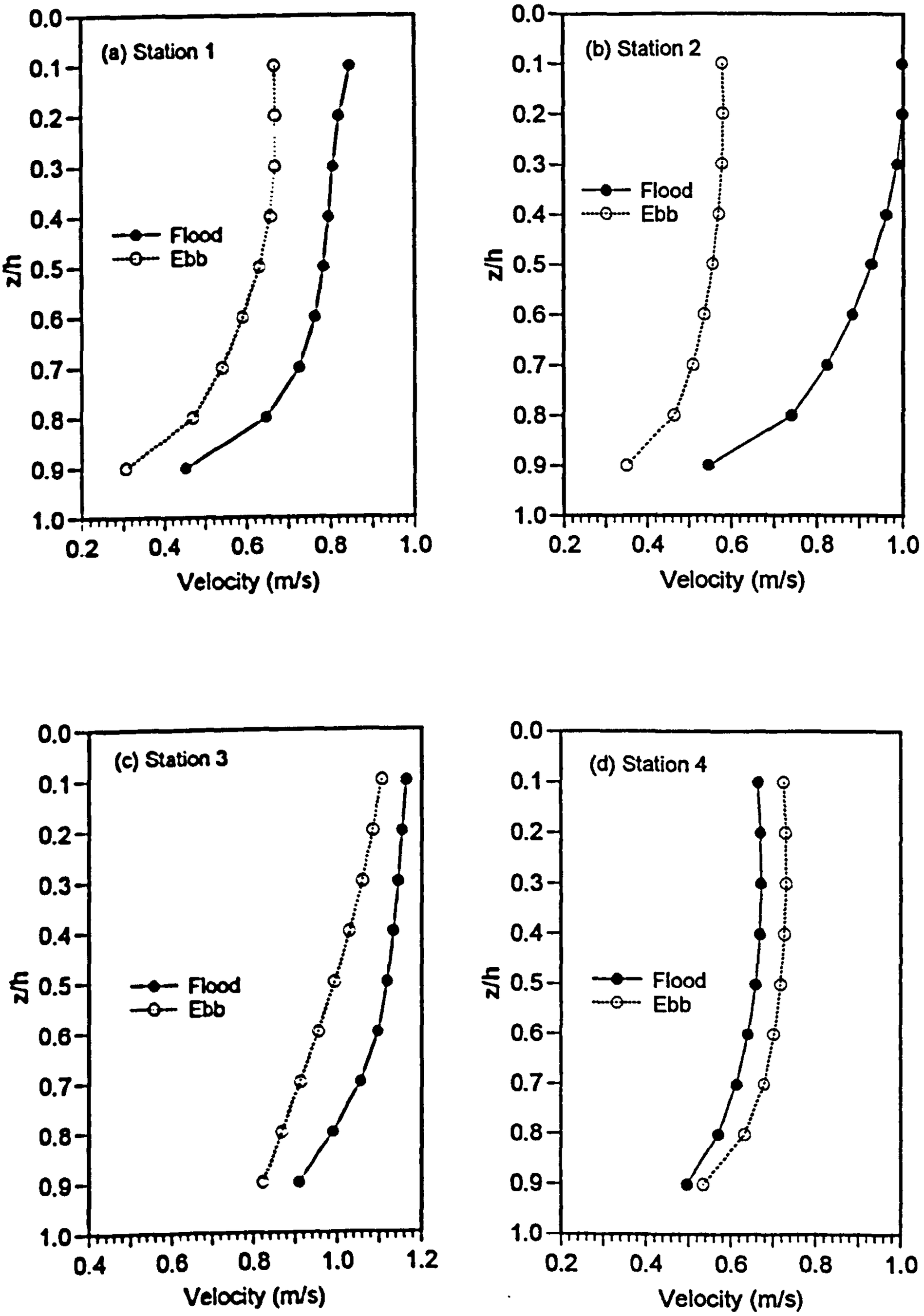

Figure A.10 Vertical profile of mean flood and mean ebb velocity at stations 1 - 7, 16 July 1995.

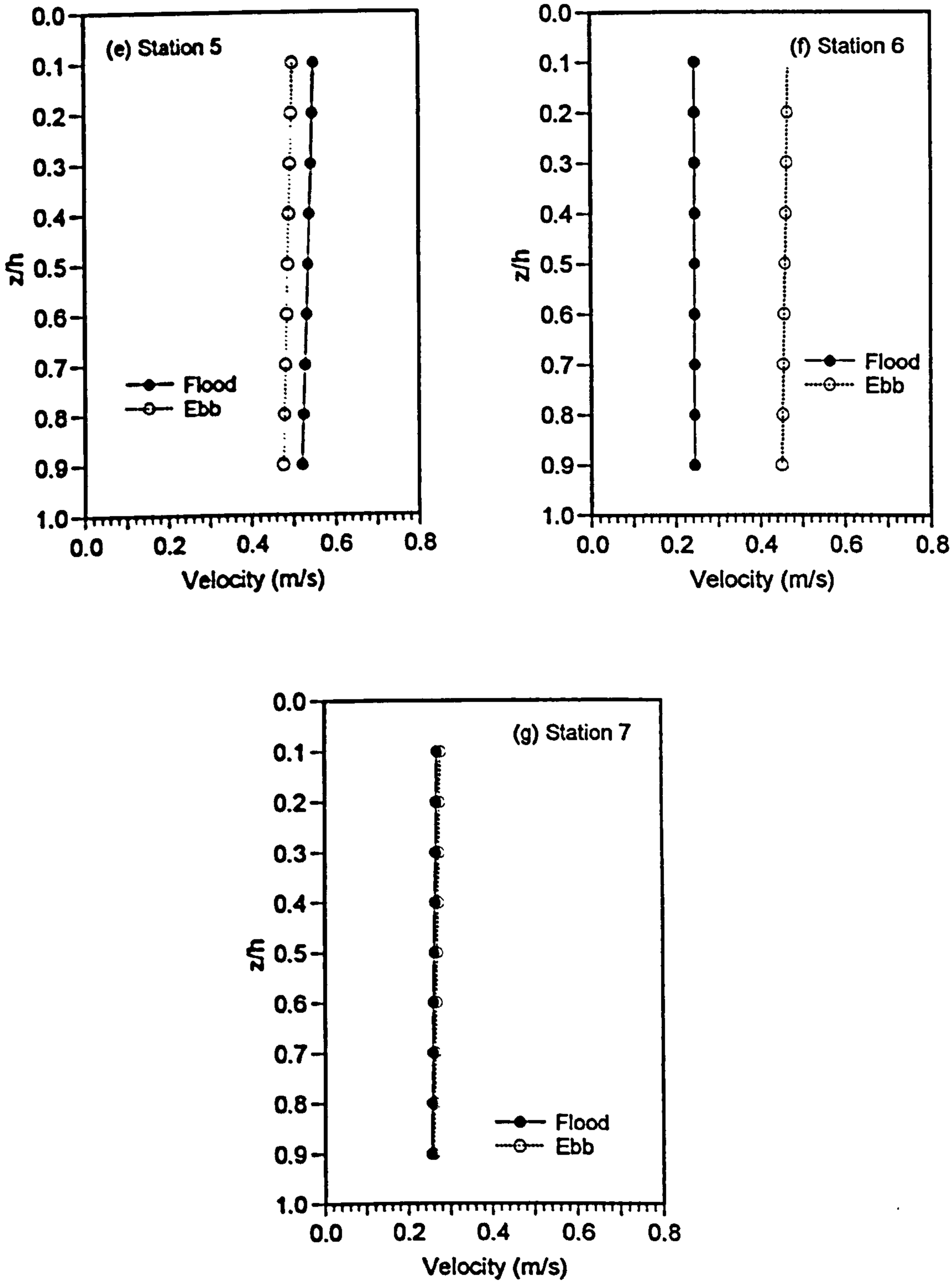

Figure A.10 (continued).

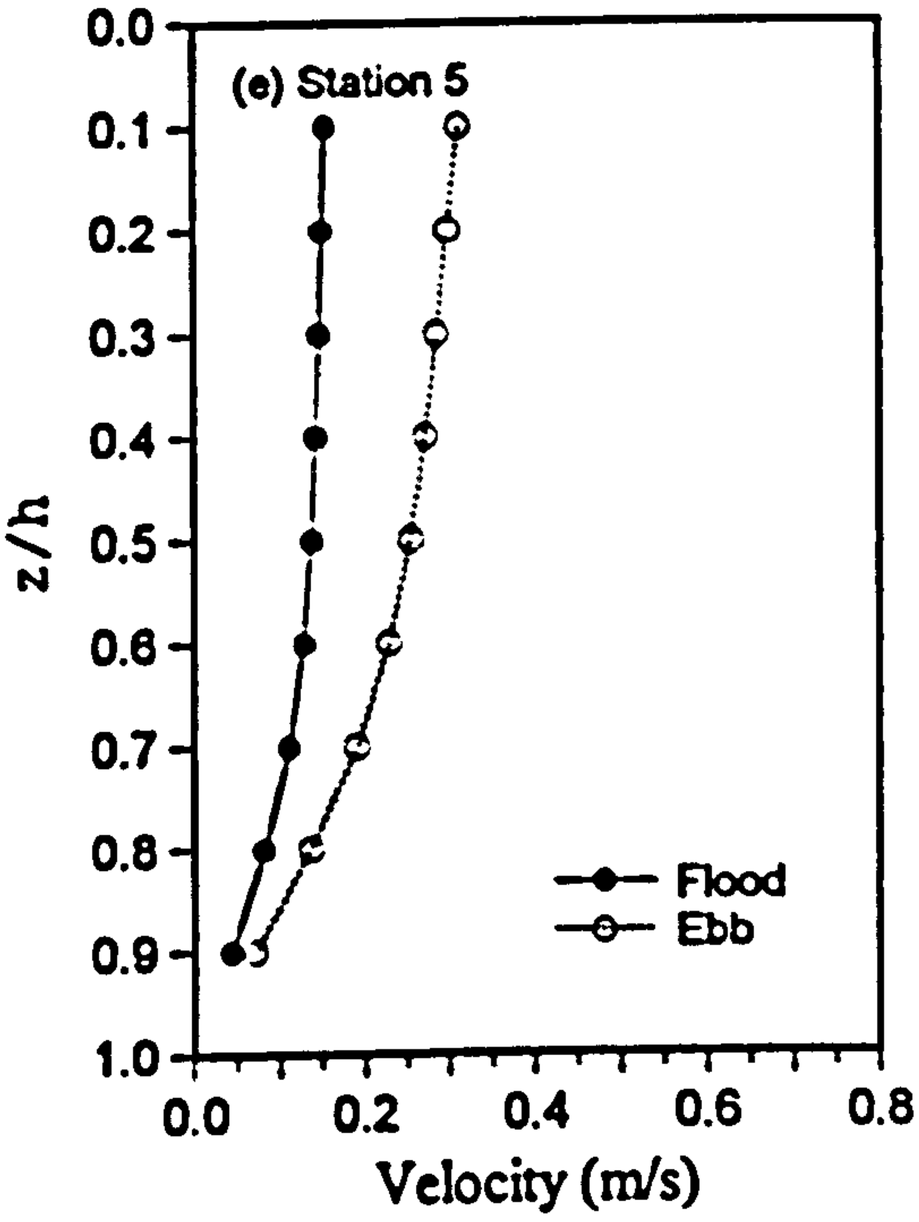

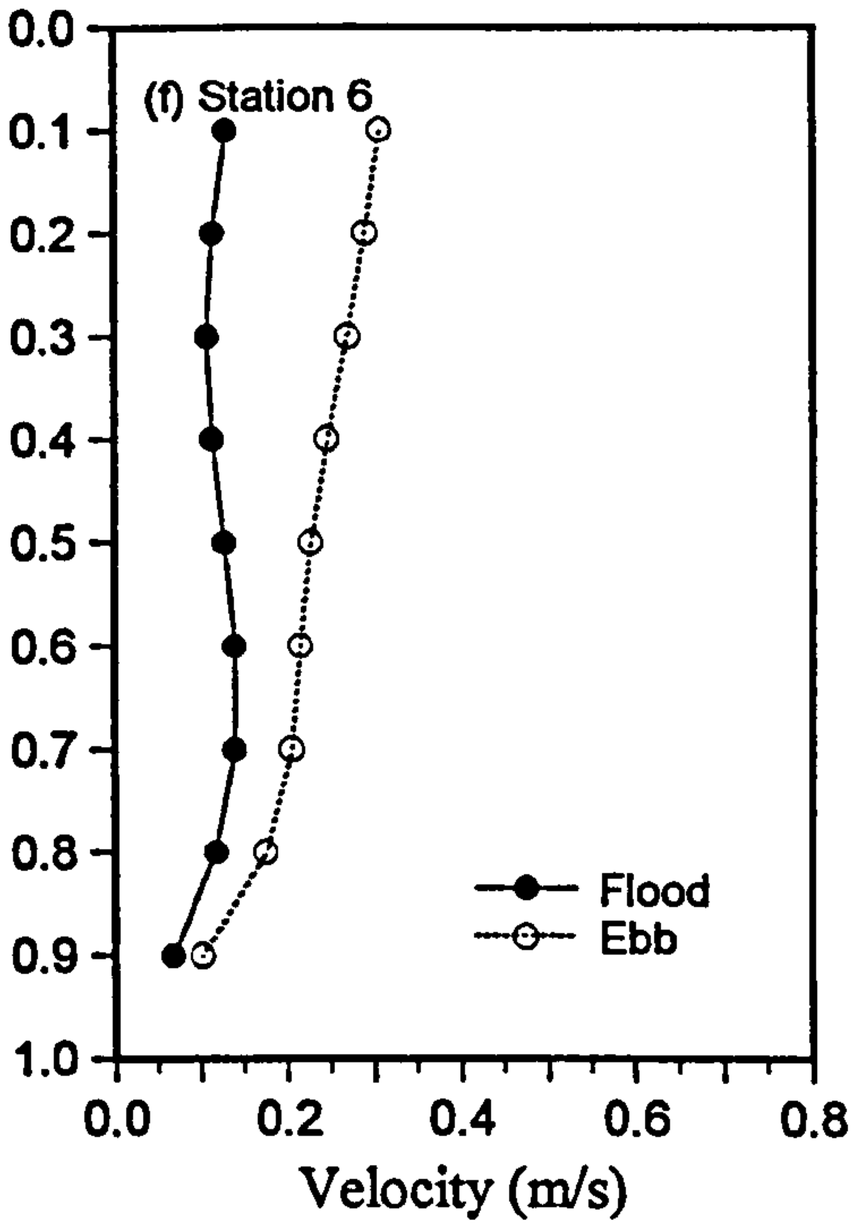

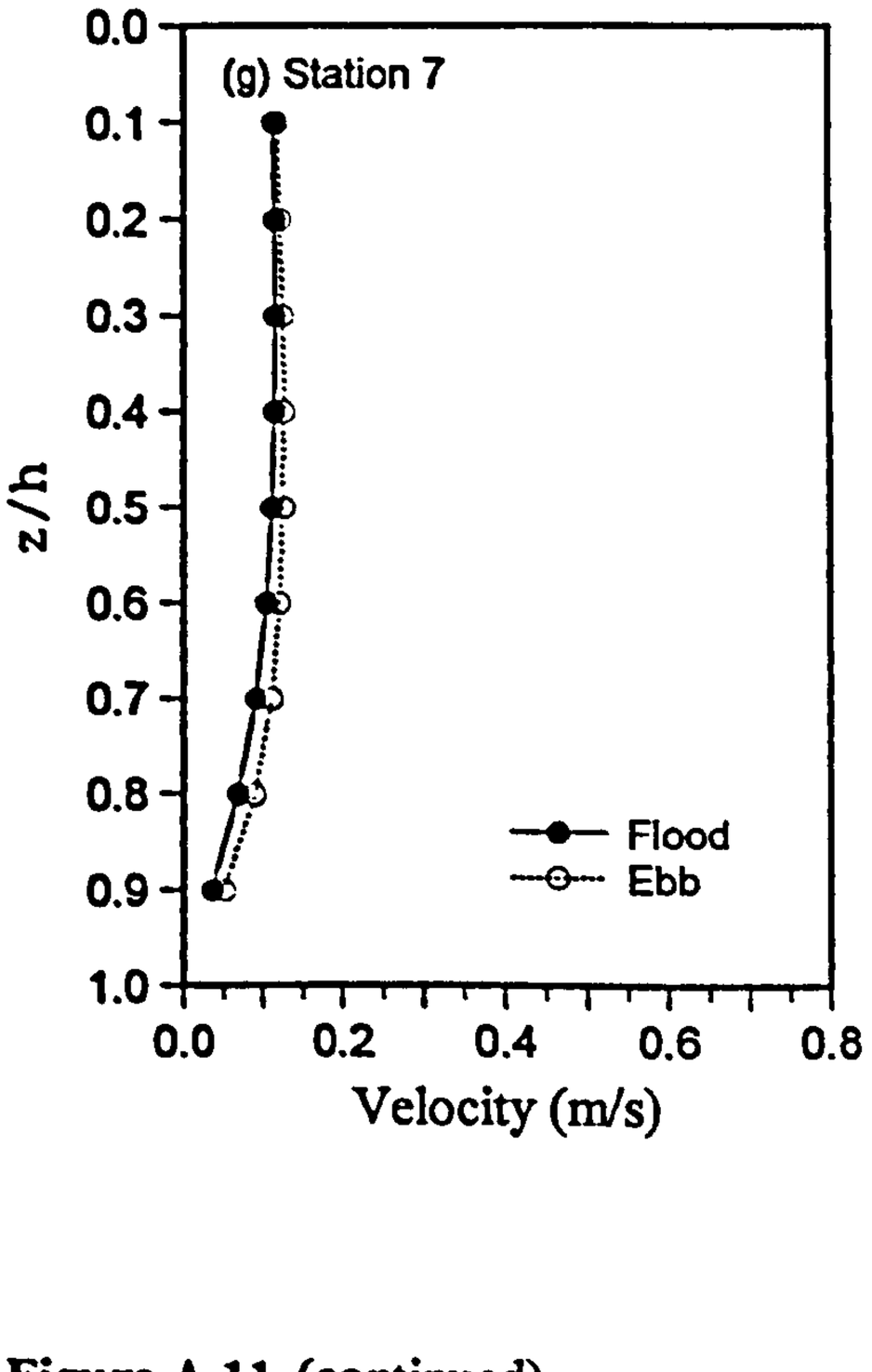

Figure A.11 (continued).

APPENDIX B

```
C       THIS PROGRAMME CALCULATES ROUGHNESS LENGHT Z0,
C       SHEAR VELOCITY U*,AND R SQUARED FOR VGU DATA
C       USING 'LEAST SQUARE METHOD'.

C       DECLARATION

        real date(820),time(820),r(820,5),depht(820)
        real z(5)
        real rmean(820),b1(820),b2(820),rsq(820)
        real rmeansq(820),slope(820),slope1(820),zz(820)
        real rsq3(820)
```

```
C       OPENFILES

        open(1,file='file name',status='old')
        open(2,file='file name',status='new')

C       INPUT

        Do 66 i = 1,820 ! read rest of lines
           read(1,*,end=30) date(i),time(i),(r(i,j), j=1,5),
     +     depht(i)

66      continue
```

```
C       OUTPUT

30      Do 40 i=1,820


         z(1) = log10(depht(i))        ! distance rotor 1 above bed
         z(2) = log10(depht(i)+0.15)    ! distance rotor 1 and 2
         z(3) = log10(depht(i)+0.40)    ! distance rotor 1 and 3
         z(4) = log10(depht(i)+0.85)    ! distance rotor 1 and 4
         z(5) = log10(depht(i)+1.85)    ! distance rotor 1 and 5

         n = 0
         sum = 0.0
         zsum = 0.0
         sqsum = 0.0
         zsqsum = 0.0
         b1sum = 0.0
         do j = 1,5
         if (r(i,j) .ne. 99.999 ) then
           n = n + 1
           sum = sum + r(i,j)
           sqsum = sqsum + r(i,j)**2
           zsum = zsum + z(j)
           zsqsum = zsqsum + z(j)**2
           b1sum = b1sum + z(j)*r(i,j)
endif
enddo
```

```
C       TAKING AVERAGE OF N

        zmean = zsum/real(n)
        zsq = zsqsum
        zmeansq = real(n)*zmean**2
        rmean(i) = sum/real(n)
        RSQ(i) = sqsum
        RMEANSQ(i) = real(n)*rmean(i)**2

        B1(i) = b1sum
        B2(i) = real(n) * zmean * rmean(i)
```

```
C       CALCULATE THE SLOPE

          SLOPE(i) = (B1(i) - B2(i))/(RSQ(i) - RMEANSQ(i))
          Slope1(i) = 1.0/SLOPE(i)

C         "CALCULATE SHEAR VELOCITY, U*"

          ustar = slope1(i)/5.75

C         "CALCULATE INTERCEPT, zz"

          zz(i) = zmean - SLOPE(i)* rmean(i)
          z0 = (10**zz(i))*100.0

C         "CALCULATE R SQUARED"

          rsq1 = ((b1(i) - b2(i))**2)
          rsq2 = (rsq(i) - rmeansq(i))*(zsq - zmeansq)
          rsq3(i) = rsq1/rsq2

        Write(2,99) date(i),time(i),rsq3(i),ustar,z0

40      continue

99      format(2(f8.2),3(f10.4))
        stop
        end
```

APPENDIX C

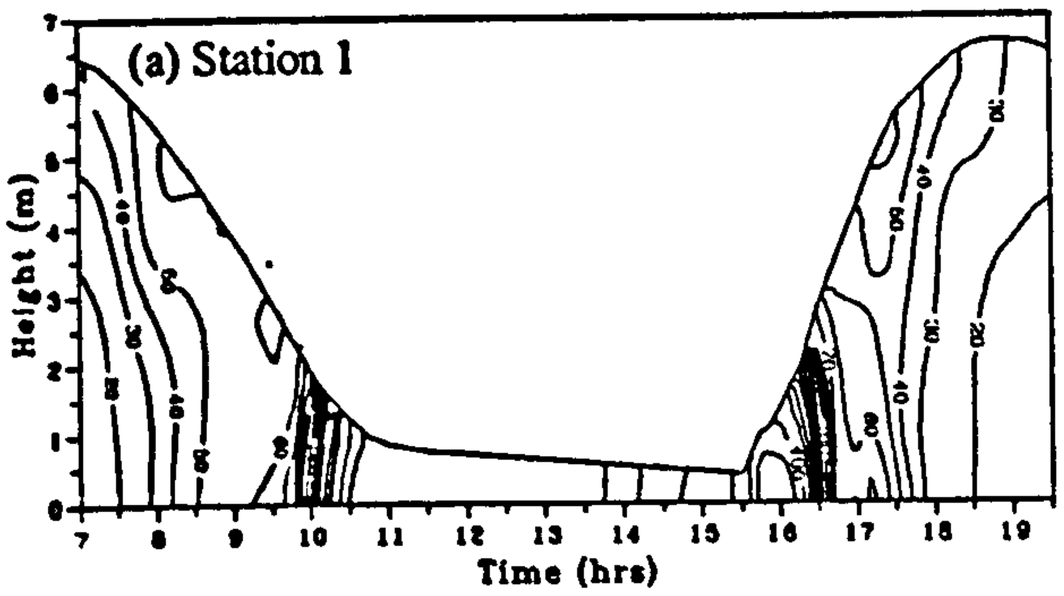

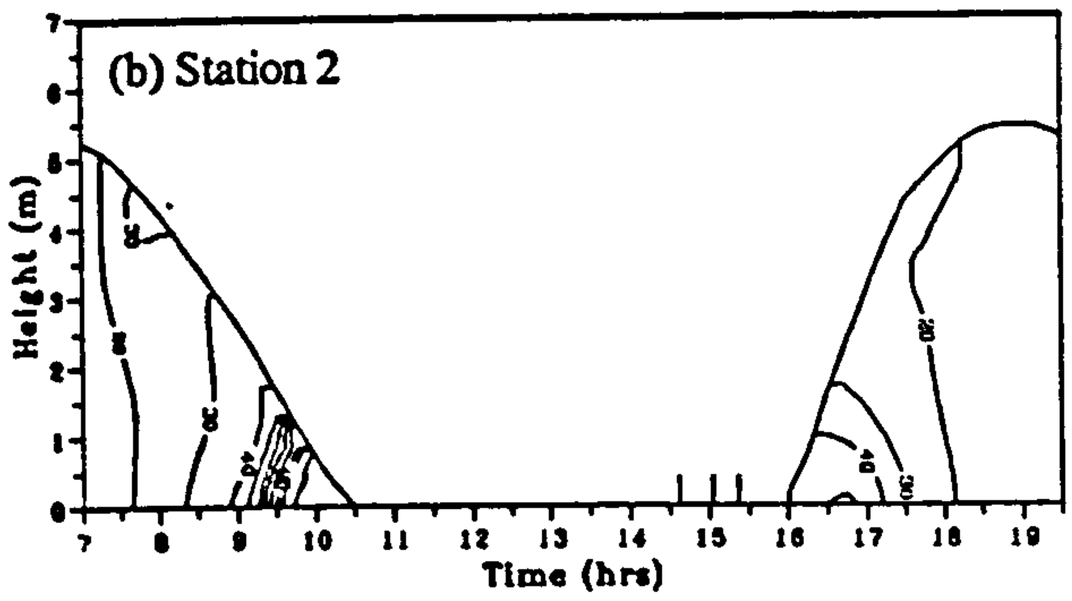

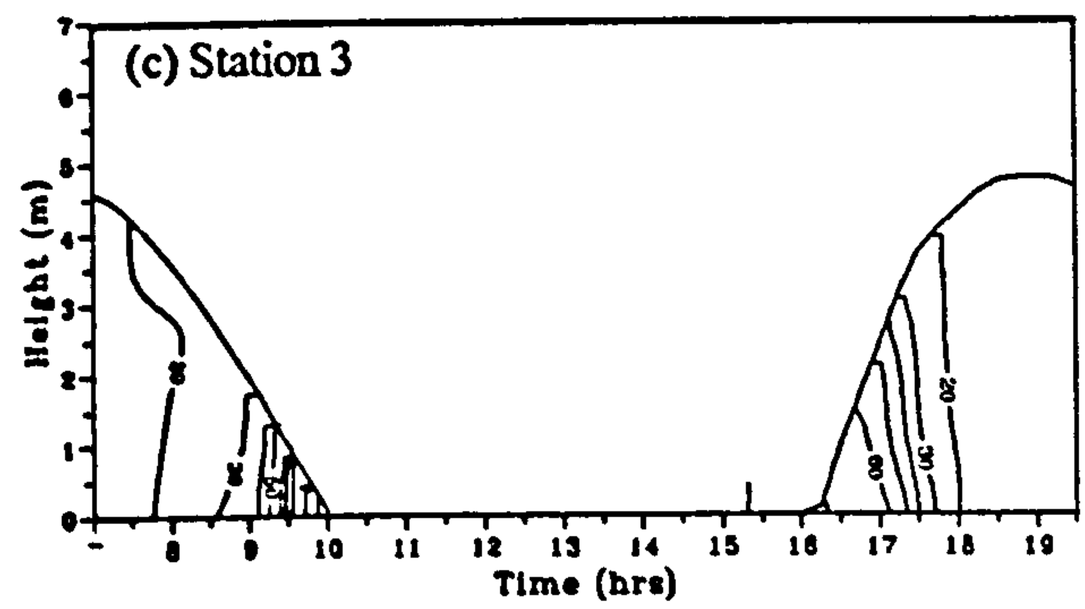

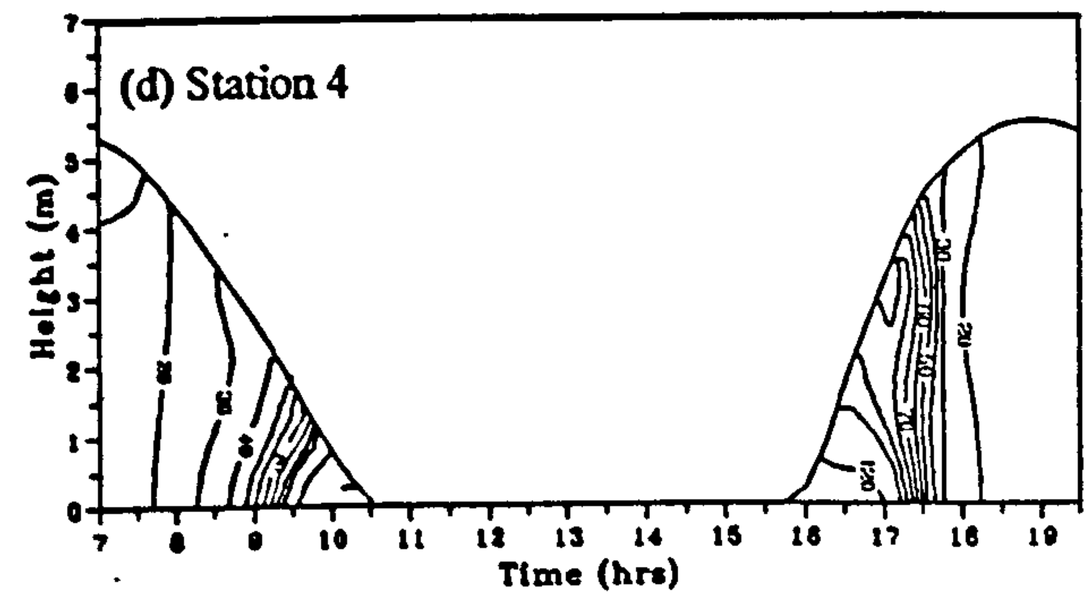

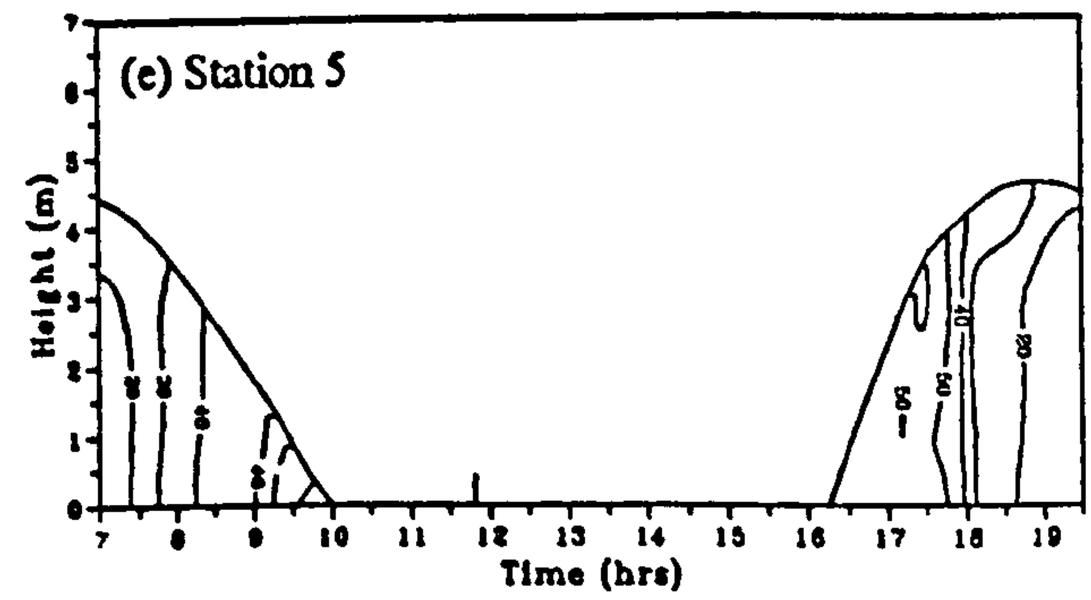

Figure C.01 Time series contour plots of suspended sediment concentration (mg/l) at stations 1-5, 6 October 1994.

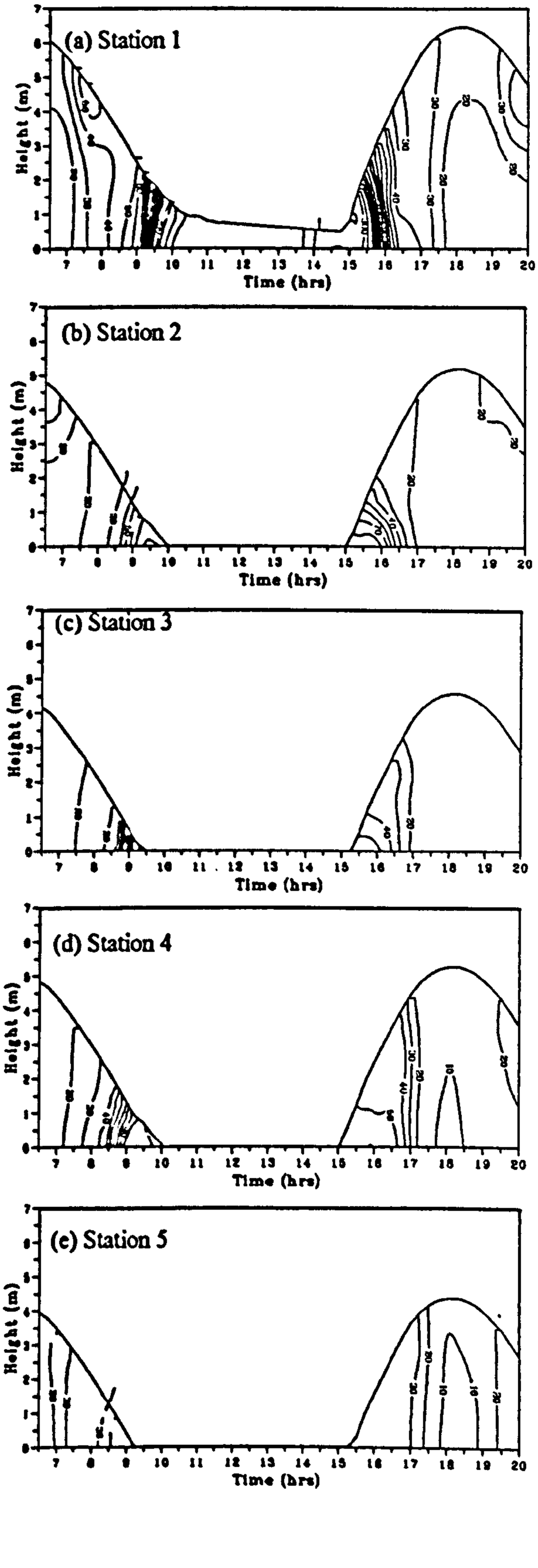

Figure C.02 Time series contour plots of suspended sediment concentration (mg/l) at stations 1-5, 5 October 1994.

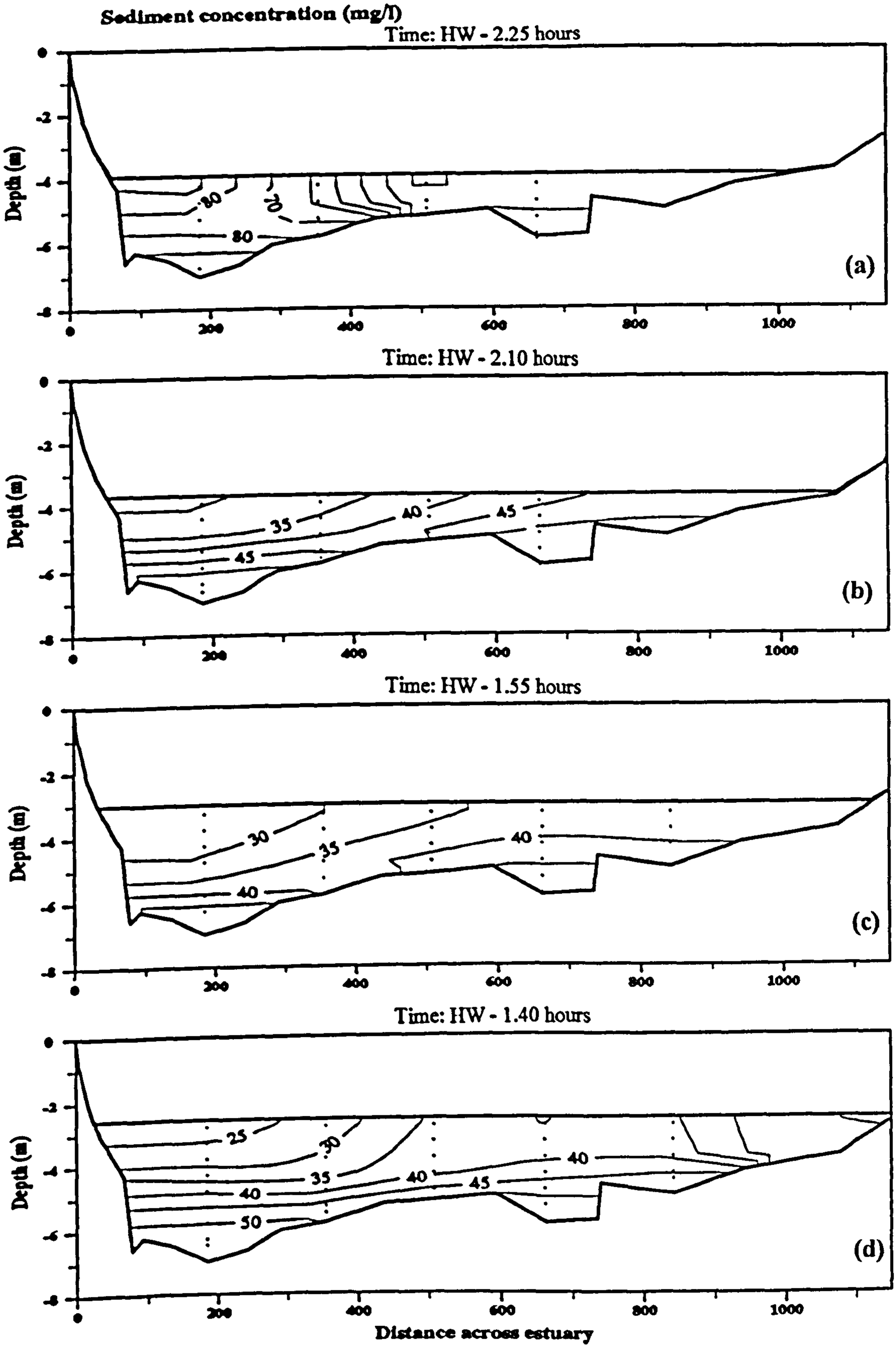

Figure C.03 Cross estuary contour plots of suspended sediment concentration (mg/l) at different stages of the tide, 5 October 1994.

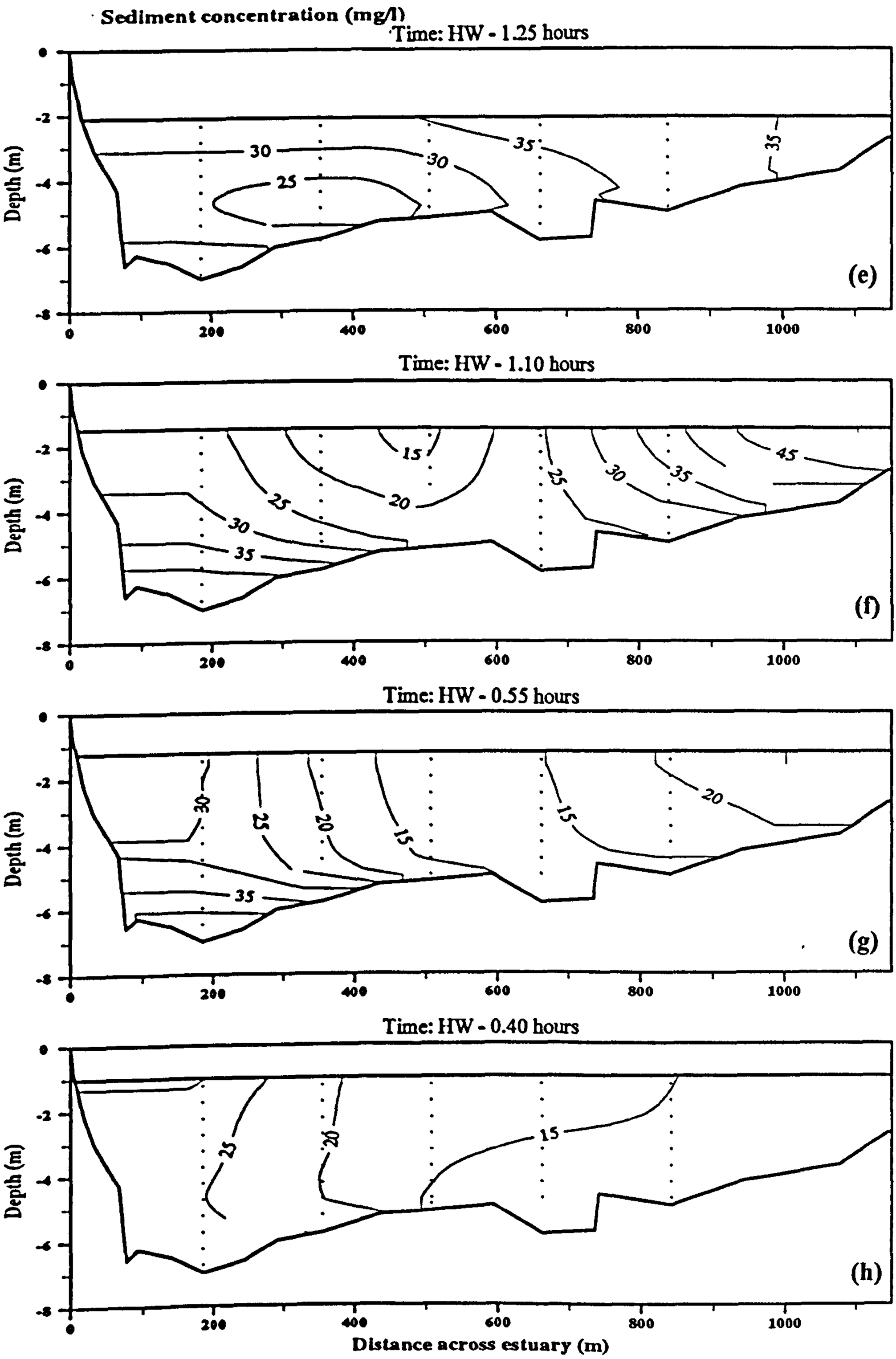

Figure C.03 (continued)

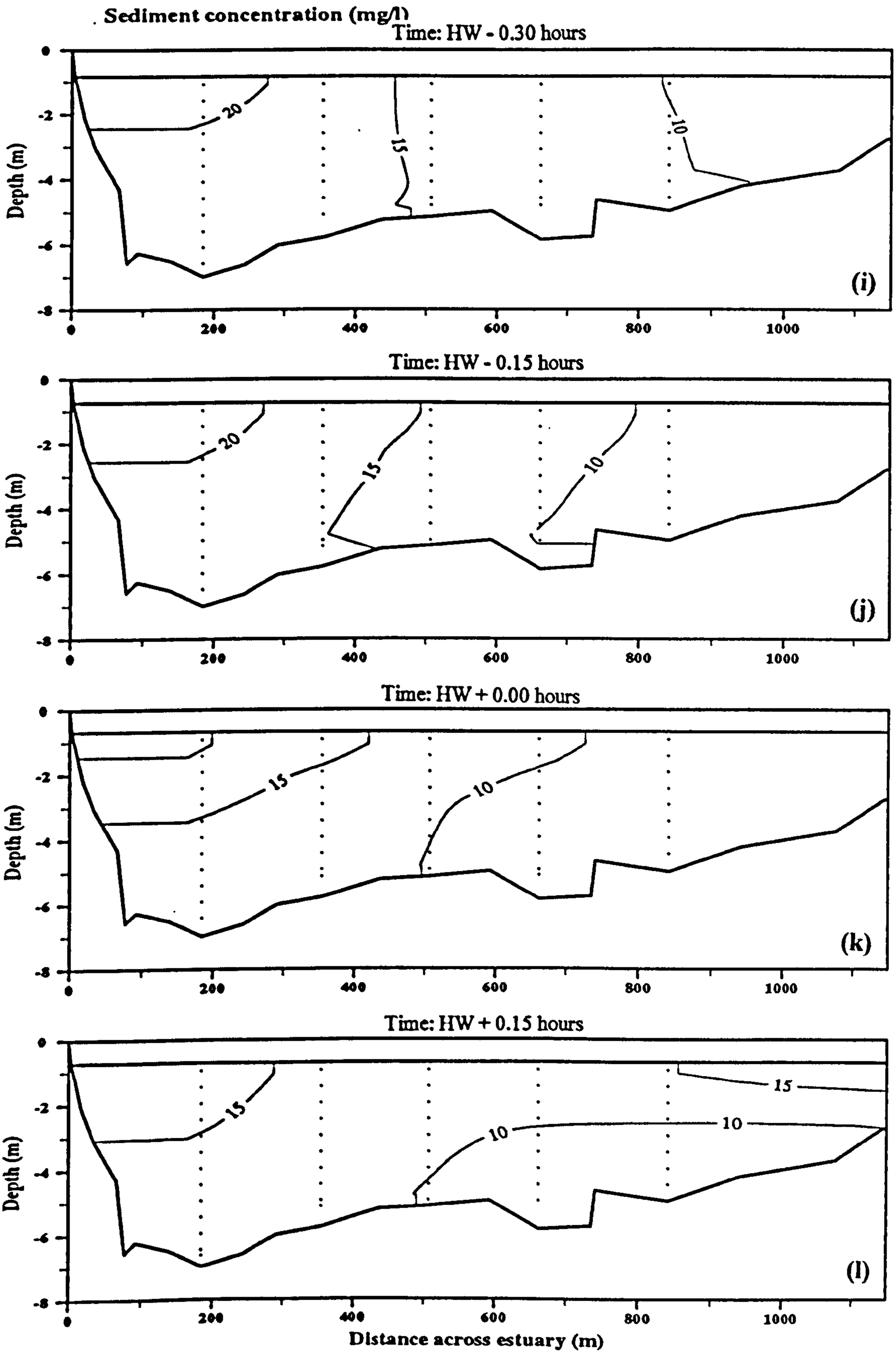

Figure C.03 (continued)

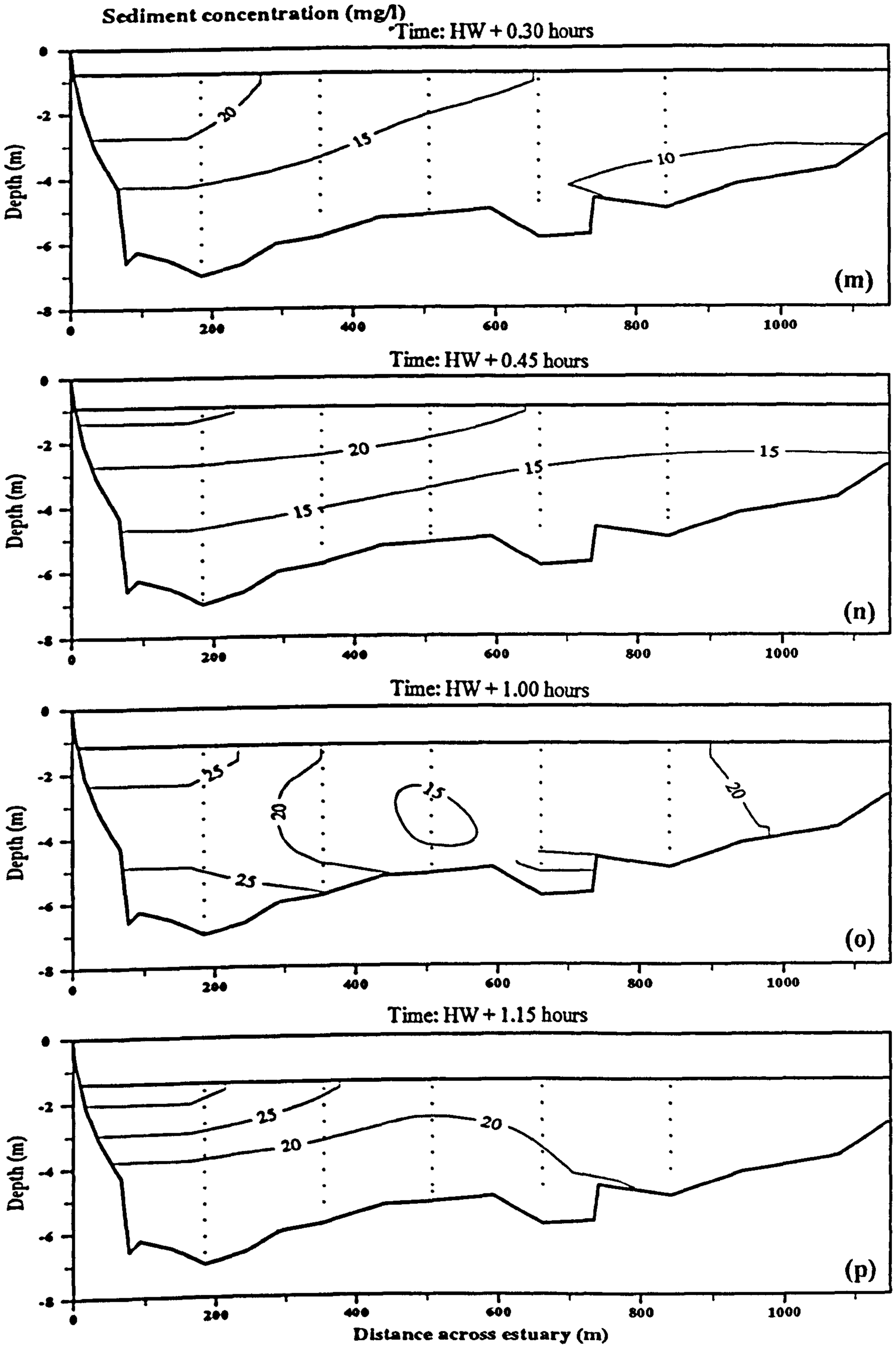

Figure C.03 (continued)

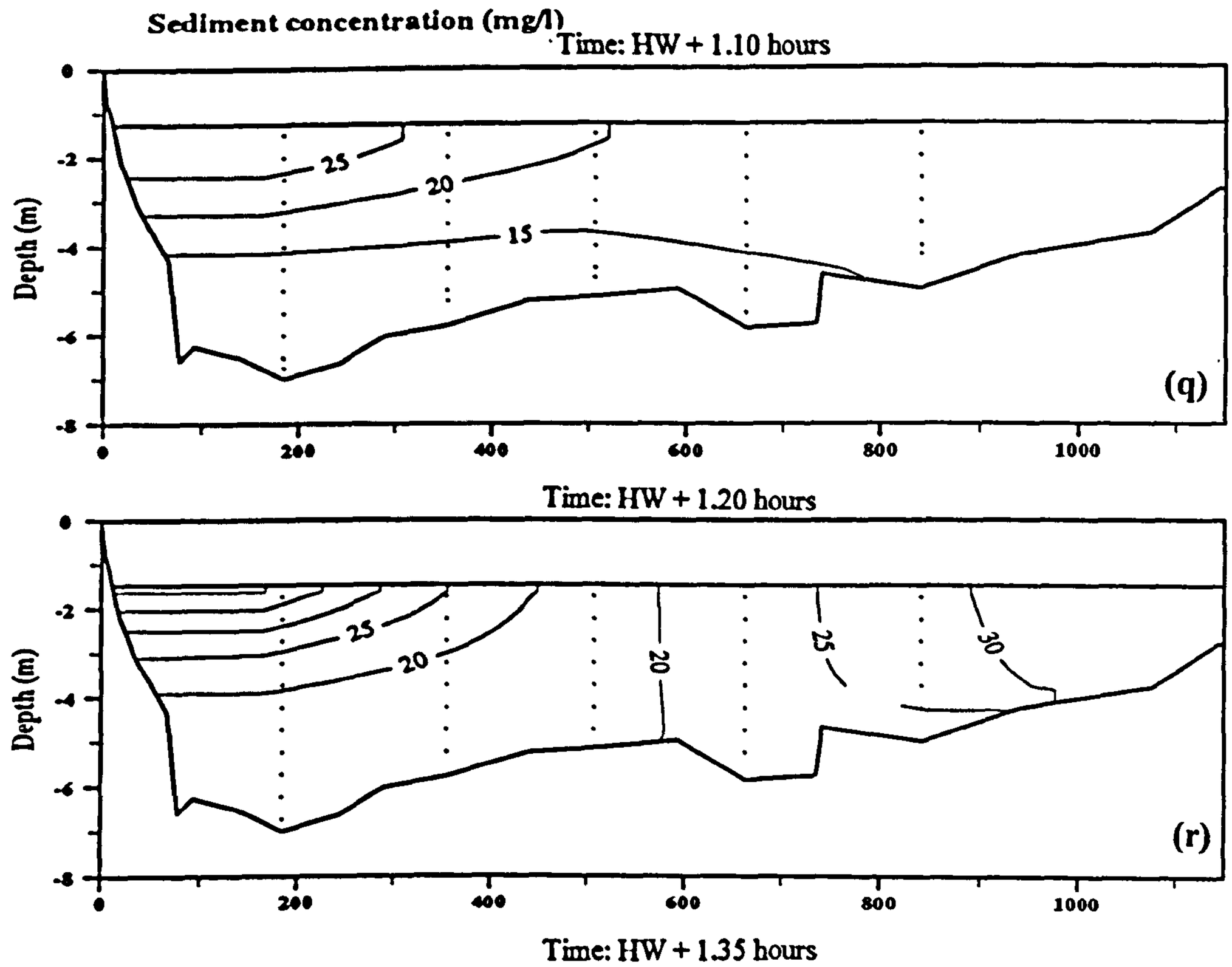

Figure C.03 (continued)

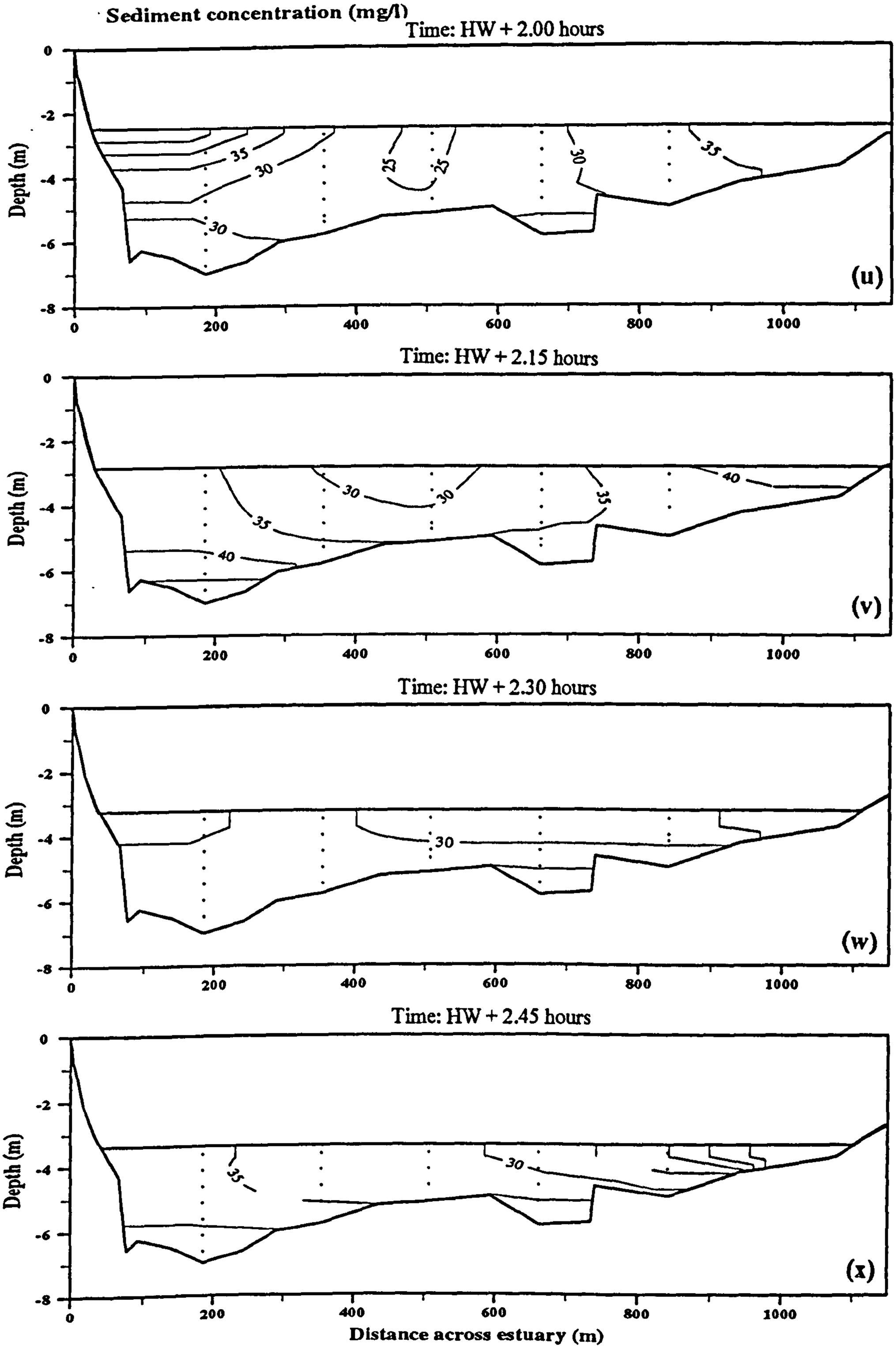

Figure C.03 (continued)

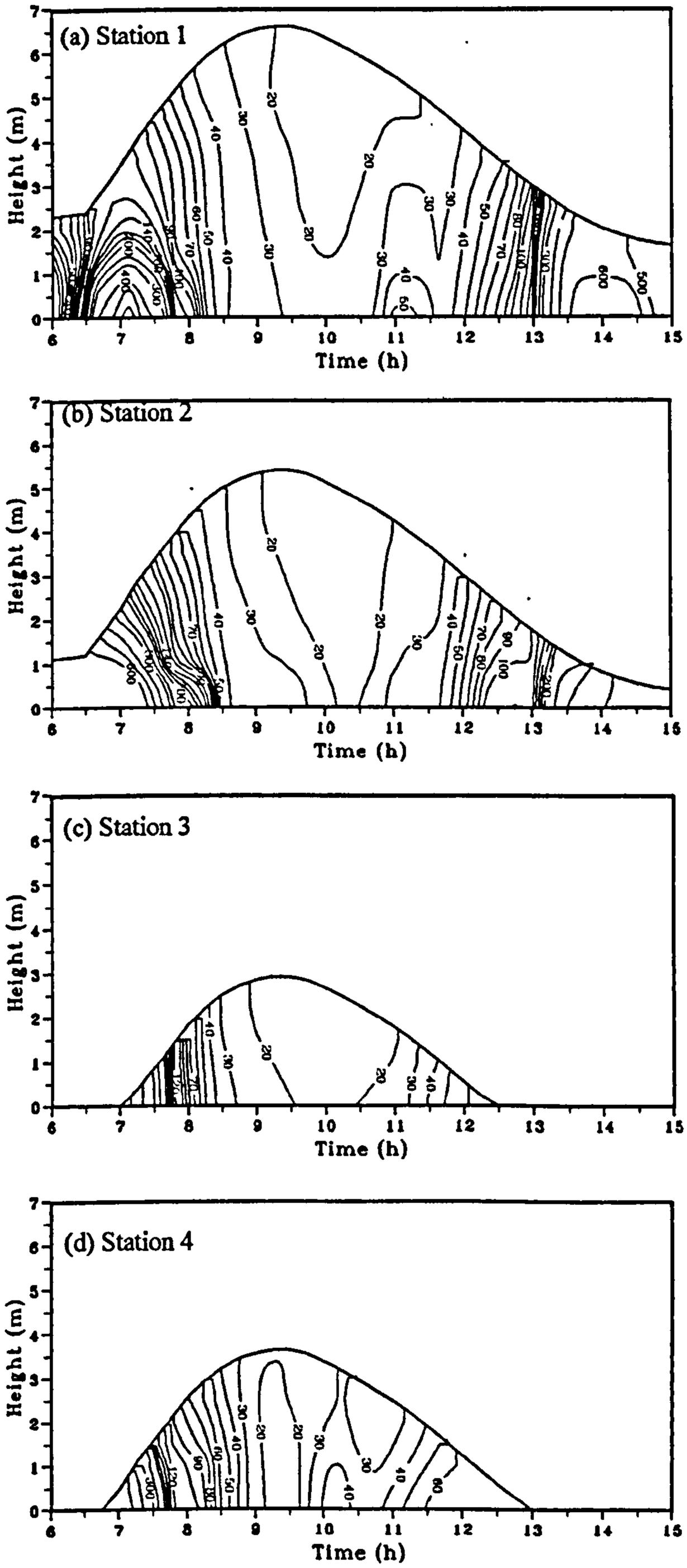

Figure C.04 Time series contour plots of suspended sediment concentration (mg/l) during a spring tide, at stations 1-4, 13th September 1995.

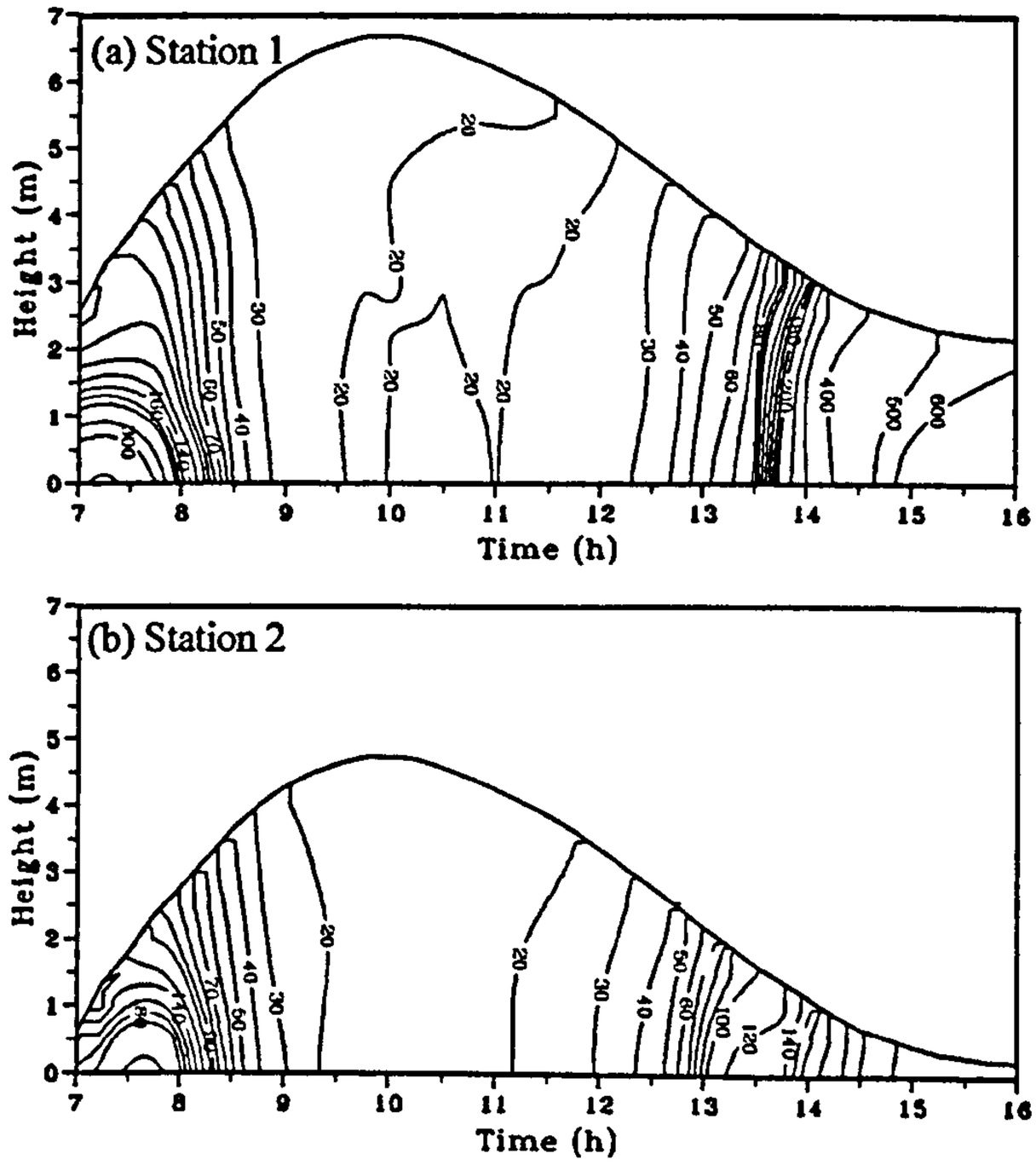

Figure C.05 Time series contour plots of suspended sediment concentration (mg/l) during a mid-tide at stations 1-4, 14th September 1995.

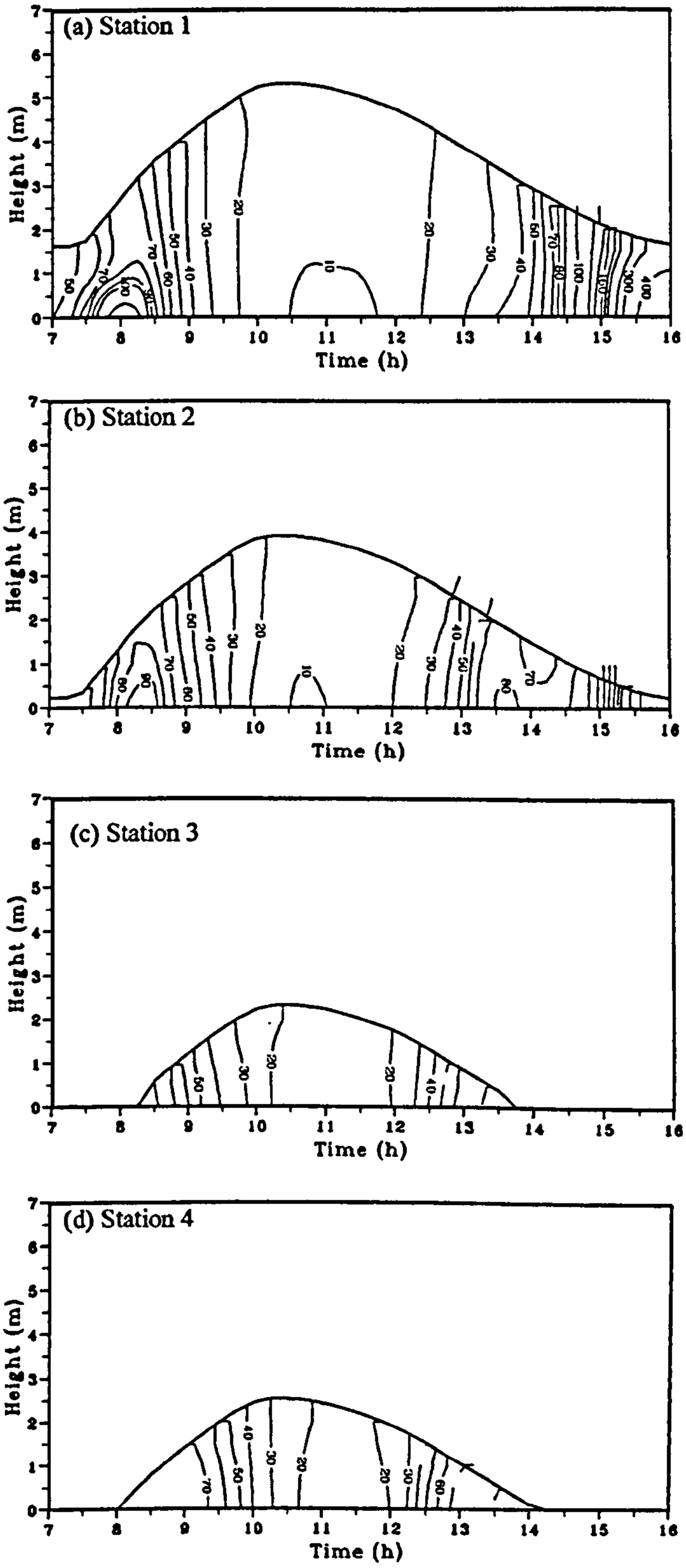

Figure C.06 Time series contour plots of suspended sediment concentration (mg/l) during a mid-tide at stations 1-4, 15th September 1995.

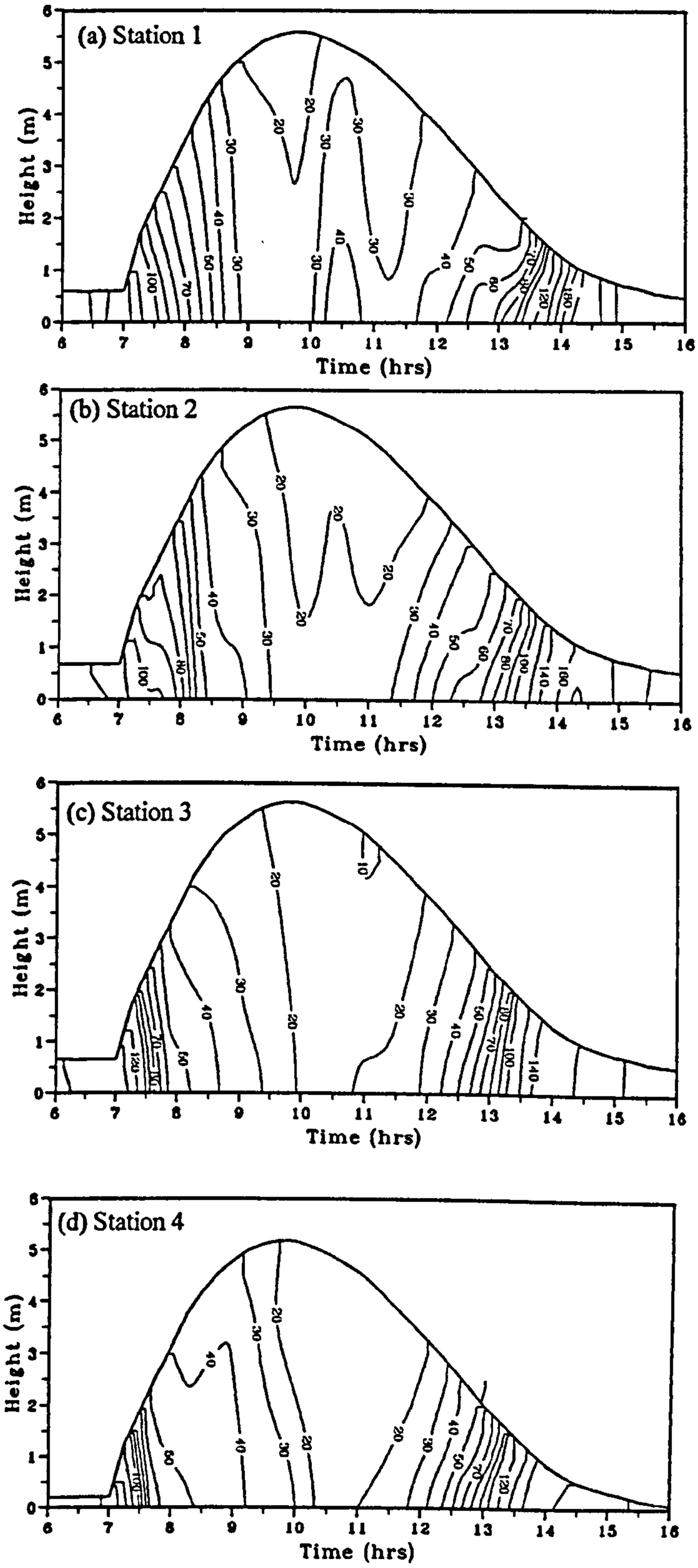

Figure C.07 Time series contour plots of suspended sediment concentration (mg/l) during a spring tide at stations 1-7, transct T9, 16th July 1995.

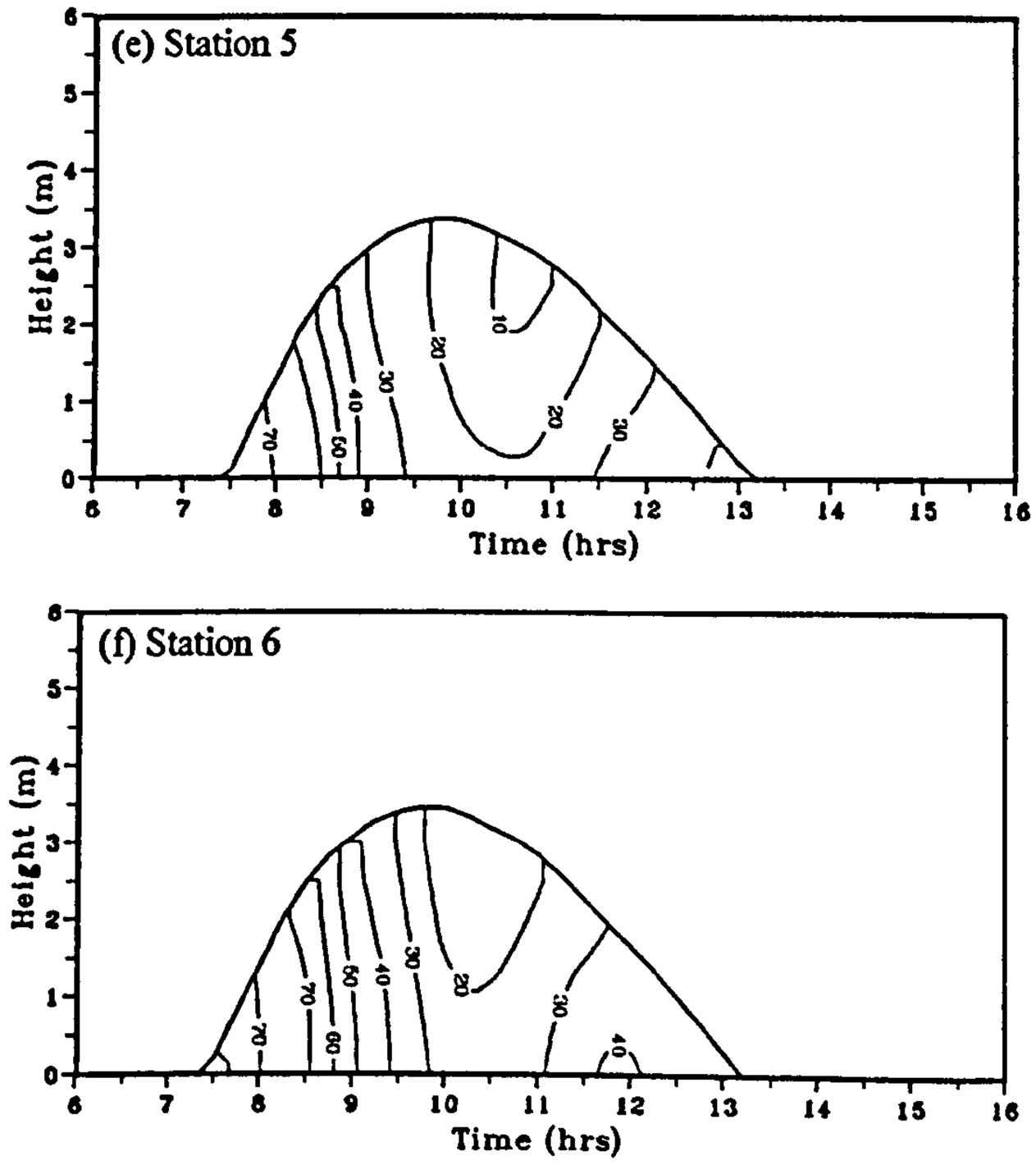

Figure C.07 (continued)

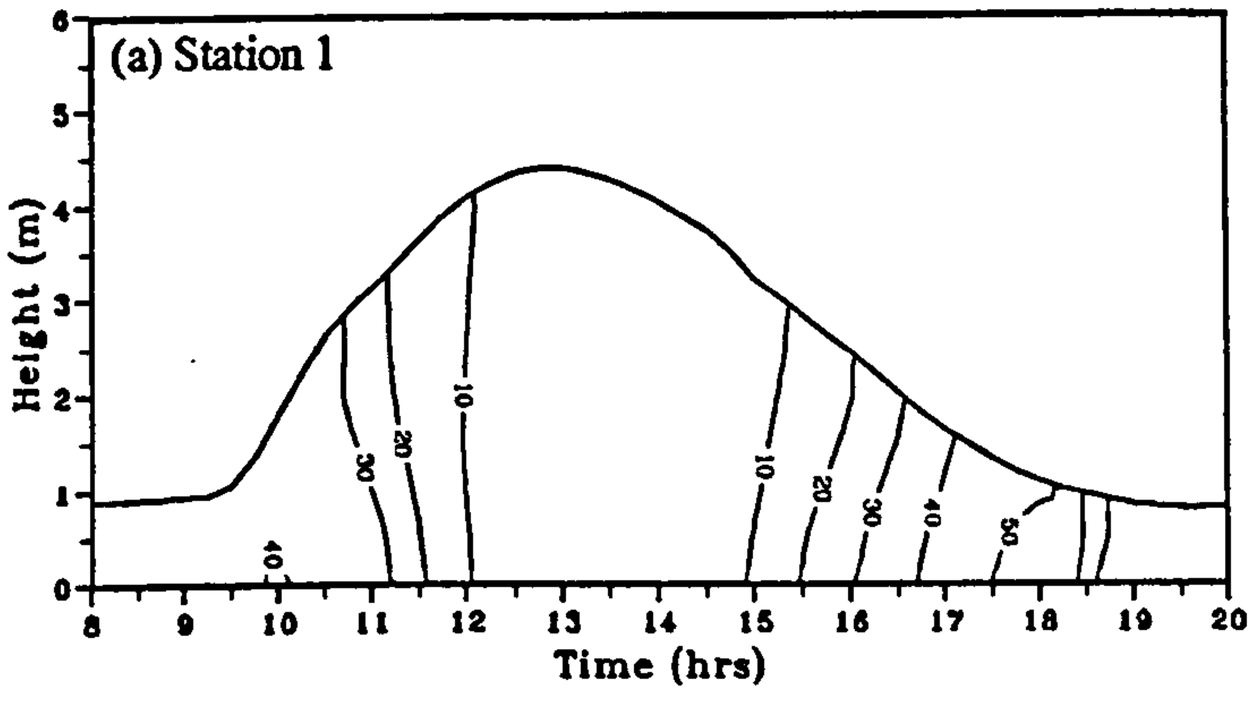

Figure C.08 Time series contour plots of suspended sediment concentration (mg/l) at stations 1-7, 20th July 1995.

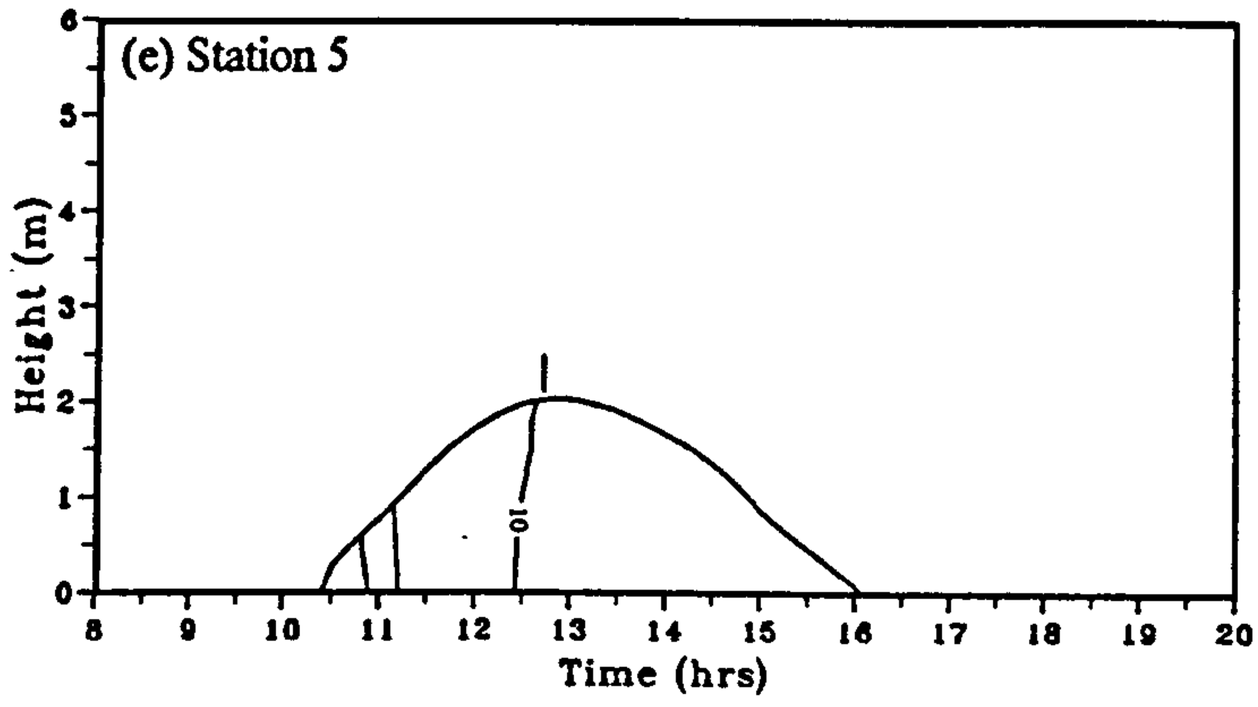

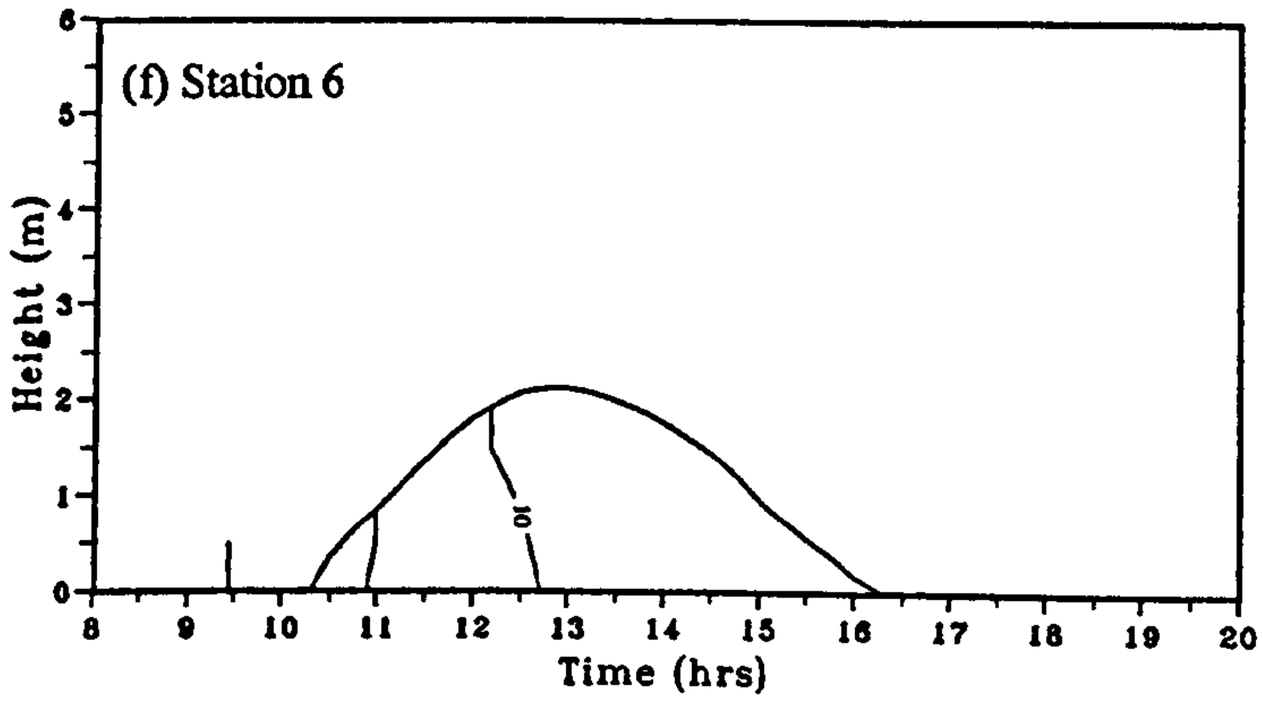

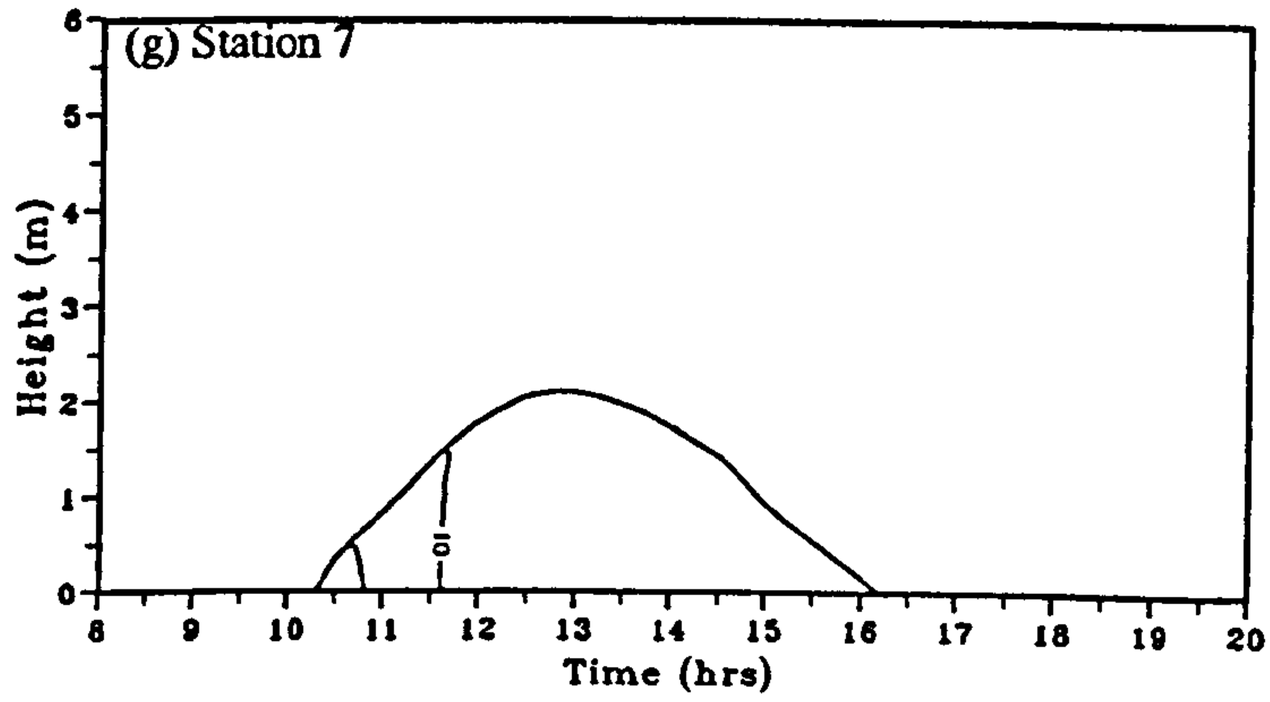

Figure C.08 (continued)

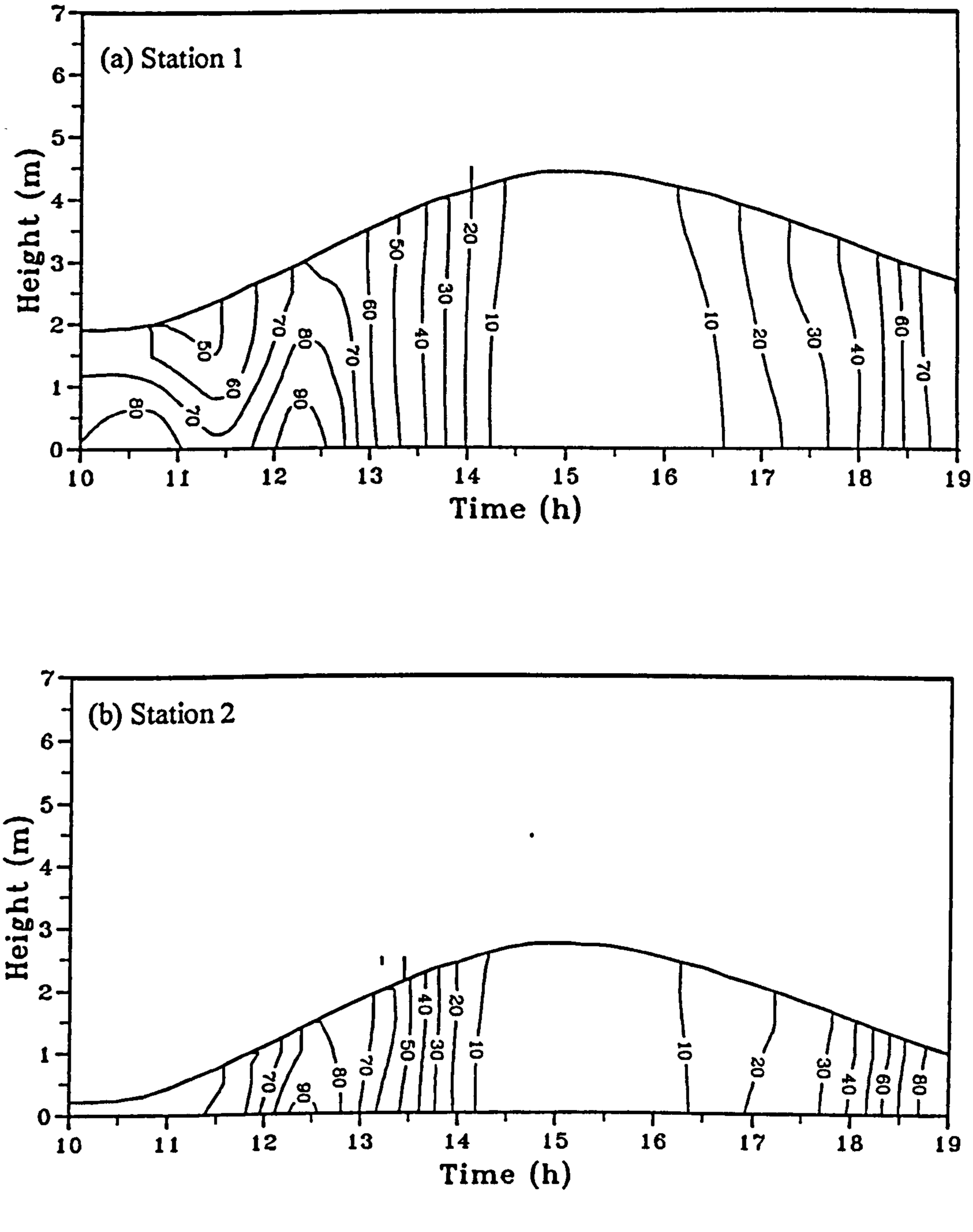

Figure C.09 Time series contour plots of suspended sediment concentration (mg/l) at stations 1 and 2, transect T5, 19 September 1995.